UNIVERSITY OF CAMBRIDGE

Proteolysis targeting chimeras for the directed ubiquitination of the androgen receptor

Elaine Fowler

Darwin College

University of Cambridge

March 2020

Supervised by Professor David R. Spring

This dissertation is submitted for the degree of Doctor of Philosophy

Declaration

This thesis is the result of my own work and includes nothing which is the outcome of work done in collaboration except as declared in the preface and specified in the text. It is not substantially the same as any work that has already been submitted before for any degree or other qualification except as declared in the preface and specified in the text. It does not exceed the prescribed word limit for the Physics and Chemistry Degree Committee.

Elaine Fowler
March 2020
Darwin College, University of Cambridge

Proteolysis targeting chimeras for the directed ubiquitination of the androgen receptor

Elaine Fowler

Abstract

Proteolysis targeting chimeras (PROTACs) are an emerging field of therapeutics and promising potential drug candidates. PROTACs consist of a target protein binder connected *via* a linker to an E3 ligase binder. PROTACs hijack the ubiquitin proteasome system to degrade the target protein in a cellular environment. This work focuses on the androgen receptor (AR) protein, a key nuclear receptor for healthy prostate development. Hence, AR inhibition and degradation are well-established strategies for treatment of prostate cancer. First, in this work stapled peptide PROTACs recruiting E3 ligase MDM2 for AR degradation were investigated. MDM2 has been underexploited as an E3 ligase for PROTACs, despite a beneficial ability to modulate the p53 protein, a vital tumour suppressor, in additional to inducing protein degradation. Using a two-component peptide stapling strategy, stapled peptide PROTACs were developed for AR degradation *via* recruitment of MDM2. Stapled peptides are commonly used to target challenging protein-protein interactions, such as MDM2-p53. Peptides are capable of emulating elements of protein structure, offering significant advantages over small molecule alternatives. Second, a series of small molecule MDM2 recruiting PROTACs were synthesised to establish a novel ligand capable of expanding the PROTAC toolbox. Finally, photoswitchable AR-degrading PROTACs were synthesised. The photophysics and biological activity of the PROTACs were analysed. These PROTACs integrated *ortho*-fluoroazobenzene for light-induced conformational change. Incorporating photoswitchable moieties in pharmaceutical entities has been demonstrated to mitigate off-target toxicity, a promising strategy to reduce attrition rates in drug discovery. Improved selectivity, efficacy, and overall safety profiles could be delivered by dosing an inactive drug and using light to modulate its biological activity at the site of action.

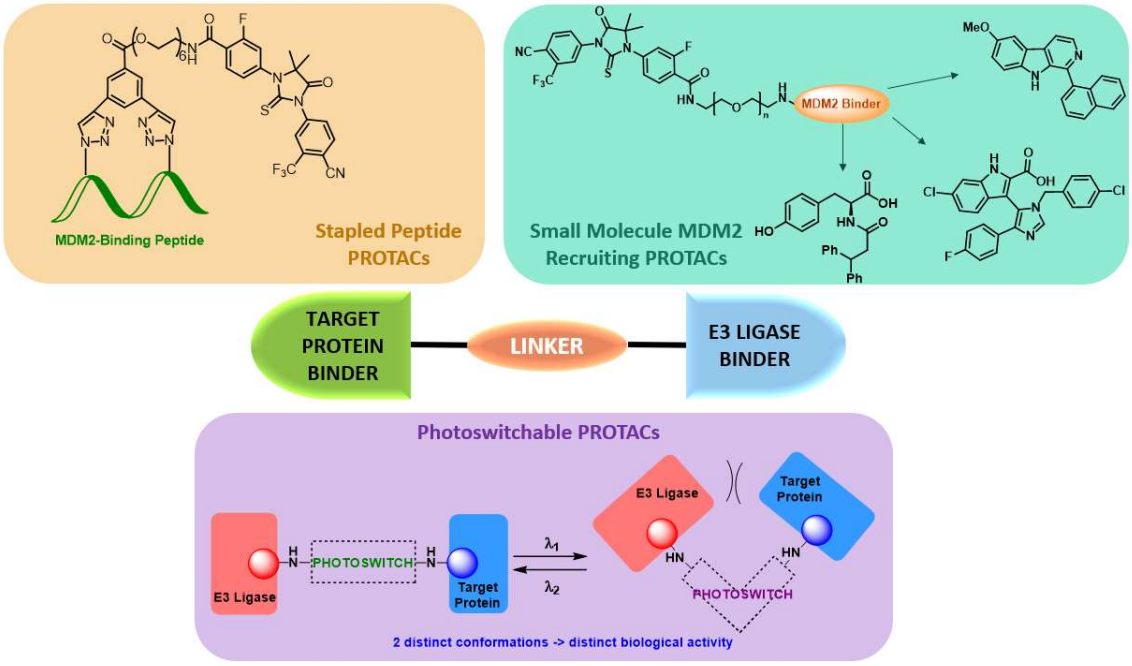

Figure 1: Summary of novel PROTAC technologies development

Acknowledgements

I would like to express my gratitude to Prof. David Spring for providing me with the opportunity to work on exciting chemistry at a great university! Thanks to the EPSRC for funding and to AstraZeneca for their support throughout my PhD.

I also wish to thank my AZ supervisor Dr Daniel O'Donovan for his extremely helpful guidance, putting me in touch with biologists, and for general inspiration. I greatly enjoyed my time working at AZ and the perspective I gained greatly inspired me to develop interesting new ideas.

Thanks to the many collaborators who supported this work throughout, including Dr Daniel O'Neill, Dr Joseph Shaw, and Dr Andreas Hock at AZ for helping me run some assays and for running and processing some of my compounds for me. Thanks to Rohan Eapen and the Itzhaki group for MDM2 assay support.

Massive thanks to Dr Yuteng Wu for supervising me when I started and setting me up with PROTACs. I am grateful to Dr Gabri Fumagalli for all his chemistry advice, memes, and general support. Additional thanks go to Josie Gaynord, Dr Sarah Kidd, Jeffrey Gorman, and Dr Naomi Robertson for proof-reading this thesis, and to all Spring group members (past and present) who have made the group a pleasure to work in!

Finally, thanks go to my family and friends for all their support and to my best friend, Jeffrey for providing me with lasers and UV-vis, answering my dumb questions about light, and being perfect!

Abbreviations

A	Alanine
Ac	Acetyl
AcOH	Acetic acid
ADT	Androgen deprivation therapy
APF	ATP-dependent proteolysis factor
aq	Aqueous
AR	Androgen Receptor
ATP	Adenosine triphosphate
ATR	Attenuated total reflectance
Boc	*tert*-butyloxycarbonyl
BET	Bromodomain and extra terminal
BRD	Bromodomain
ca.	Approximately
CAN	Cerium (IV) ammonium nitrate
CETSA	Cellular thermal shift assay
$CHCl_3$	Chloroform
^{13}C NMR	Carbon nuclear magnetic resonance
CRPC	Castration resistant prostate cancer
CuAAC	Copper-catalysed alkyne-azide cycloaddition
CuI	Copper iodide
DBU	1,8-Diazabicyclo[5.4.0]undec-7-ene
DC_{50}	Concentration required to degrade protein levels to half initial
DCC	*N*,*N*'-dicyclohexylcarbodiimide
DCE	Dichloroethane
DCM	Dichloromethane
DHT	Dihydrotestosterone
DIAD	Diisopropyl azodicarboxylate
DIPEA	*N*,*N*-Diisopropylethylamine
DMAP	4-Dimethylaminopyridine
DMF	*N*,*N*-Dimethylformamide
DMSO	Dimethylsulfoxide

DOS	Diversity-Oriented Synthesis
DSF	Differential scanning fluorimetry
DUBs	Deubiquitinating enzymes
E	Glutamic acid
eq	Equivalents
ER	Estrogen Receptor
EtOAc	Ethyl acetate
EtOH	Ethanol
F	Phenylalanine
FDA	Food and drug administration
Fmoc	Fluorenylmethyloxycarbonyl
FP	Fluorescence polarisation
FRET	Förster resonance energy transfer
g	Grams
GPCR	G protein coupled receptor
h	Hours
H_2	Hydrogen
HATU	*N*-[(Dimethylamino)-1*H*-1,2,3-triazolo-[4,5-*b*]pyridin-1-ylmethylene]-*N*-methylmethanaminium hexafluorophosphate *N*-oxide
HCl	Hydrochloric acid
^{1}H NMR	Hydrogen nuclear magnetic resonance
HOAt	1-Hydroxy-7-azabenzotriazole
HPLC	High performance liquid chromatography
HRMS	High resolution mass spectrometry
HSP	Heat shock protein
IC_{50}	Concentration required to reduce response by a half
IAPs	Inhibitor of Apoptosis Proteins
*i*PrOH	Isopropanol
IR	Infrared
ITC	Isothermal calorimetry
K_d	Dissociation constant
L	Leucine
LBD	Ligand binding domain

LC-MS	Liquid chromatography mass spectrometry
LED	Light emitting diode
Lit.	Literature
LNCaP	Lymph node carcinoma of the prostate
M	Molar
M.p.	Melting point
MDM2	Murine double minute 2
MeCN	Acetonitrile
MeI	Iodomethane
MeOH	Methanol
mins	Minutes
NBS	*N*-bromo succinimide
NCI	National cancer institute
NMP	*N*-Methyl-2-pyrrolidone
Orn	Ornithine
PAL	Photoaffinity label
PDT	Photodynamic therapy
PE	Petroleum ether
PEG	Polyethylene glycol
PMP	*Para*-methoxyphenyl
PPI	Protein-protein interaction
ppm	Parts per million
PROTAC	Proteolysis targeting chimera
PSA	Prostate-specific antigen
PSS	Photostationary state
PyAOP	(7-Azabenzotriazol-1-yloxy)tripyrrolidinophosphonium hexafluorophosphate
Q	Glutamine
qAC50	Concentration required to reduce activity by a half
RCM	Ring-closing metathesis
R_f	Retention factor
r.t.	Room temperature
S	Serine

SAHB	Stabilised α-helix of BCL-2 domain
SARDs	Selective Androgen Receptor Degraders
sat.	Saturated
SCF	Skp, Cullin, F-box
SDS-PAGE	Sodium dodecyl sulfate-polyacrylamide gel electrophoresis
SERDs	Selective estrogen receptor degraders
SERM	Selective estrogen receptor modulator
SM	Starting material
S_NAr	Nucleophilic aromatic substitution
SNIPERs	Specific and Non-genetic Inhibitor-of-Apoptosis proteins-dependent Protein Erasers
SPAAC	Strain-promoted azide alkyne cycloaddition
SPPS	Solid phase peptide synthesis
T	Threonine
t	time
*t*BuOH	*tert*-butanol
TCI	Thiocarbonyl-diimidazole
TFA	Trifluoroacetic acid
THF	Tetrahydrofuran
THPTA	Tris(3-hydroxypropyltriazolylmethyl)amine
TIPS	Triisopropylsilyl ether
TLC	Thin layer chromatography
T_m	Melt temperature
TosMIC	Tosyl-methyl isocyanate
TPSH	2,4,6-Triisopropylbenzenesulfonohydrazide
Ts	Tosyl
TSA	Thermal shift assays
UPS	Ubiquitin proteosome system
UV-vis	Ultraviolet-visible
VHL	Von Hippel-Lindau
W	Tryptophan
Y	Tyrosine

Table of Contents

1. Chaper 1: Introduction

1.1 Proteolysis Targeting Chimeras (PROTACs)

1.1.1 Ubiquitin Proteasome System (UPS)

Selective cellular degradation of proteins is mediated by the ubiquitin proteasome system (UPS), and is a vital process for cell survival.[1] Early studies of protein degradation were published by Hershko *et. al.* in 1971, who found that the process was ATP-dependent.[2] Following this, Hershko went on to discover an ATP-dependent proteolysis factor (APF-1) found to be vital for protein degradation.[3] APF-1 was later identified as ubiquitin, a polypeptide universally observed in nature.[4] Subsequent experimentation gave an understanding of the role ubiquitin played in proteolysis. Initially, ubiquitin molecules are enzymatically linked to a protein, leading to the attachment of a polyubiquitin tag which is then recognised by the proteasome resulting in protein degradation.[5]

Three key enzymes involved in the UPS were elucidated in subsequent years (figure 2). Firstly, the ubiquitin activating enzyme E1[6] activates the ubiquitin molecule by adenylating the *C*-terminus[7] and forming a thioester bond at a surface cysteine residue. The activated ubiquitin is then transferred to a second key enzyme E2, known as the ubiquitin carrier protein[8] before finally being transferred to a surface lysine residue of the target protein mediated by the E3 ligase.[8] This enzyme is responsible for recruiting the target protein, thus is vital for the high specificity of the UPS.[9,10] This process is then repeated to form a polyubiquitin chain. Ubiquitin can also be removed from the protein by various deubiquitylating enzymes (DUBs).[11] A protein is targeted for degradation by the 26S proteasome when it acquires a chain of at least four ubiquitin molecules. The 26S proteasome removes and recycles the ubiquitin units and degrades the target protein into short peptide fragments. The UPS process has been comprehensively reviewed by Hershko and Ciechanover.[12]

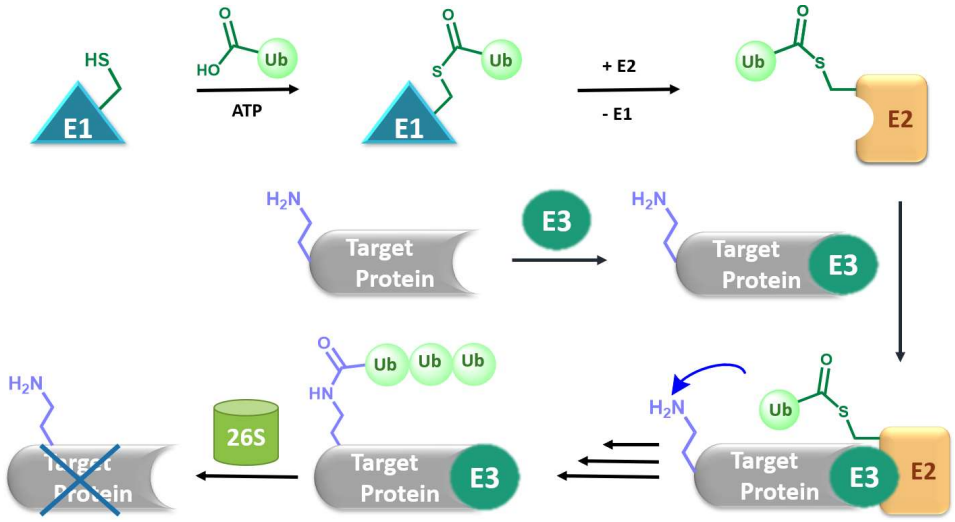

Figure 2: Diagram of the UPS mediated degradation of target proteins

1.1.2 Principles of PROTACs

PROTACs (PROteolysis TArgeting Chimeras) are an interesting new area of medicinal chemistry. These molecules were designed to recruit the UPS for the degradation of therapeutically relevant proteins.[11]

PROTACs are heterobifunctional molecules containing a ligand for an E3 ligase, a linker motif, and a second ligand to bind a target protein.[11] The E3 ligase and the target protein bind to the PROTAC, forming a ternary complex (figure 3). The proximity of the E3 ligase to the target protein facilitates its polyubiquitination, labelling the protein for degradation within the cell.[11] PROTACs have great potential due to their ability to theoretically target any protein within the cell, providing a binding molecule is available.[11]

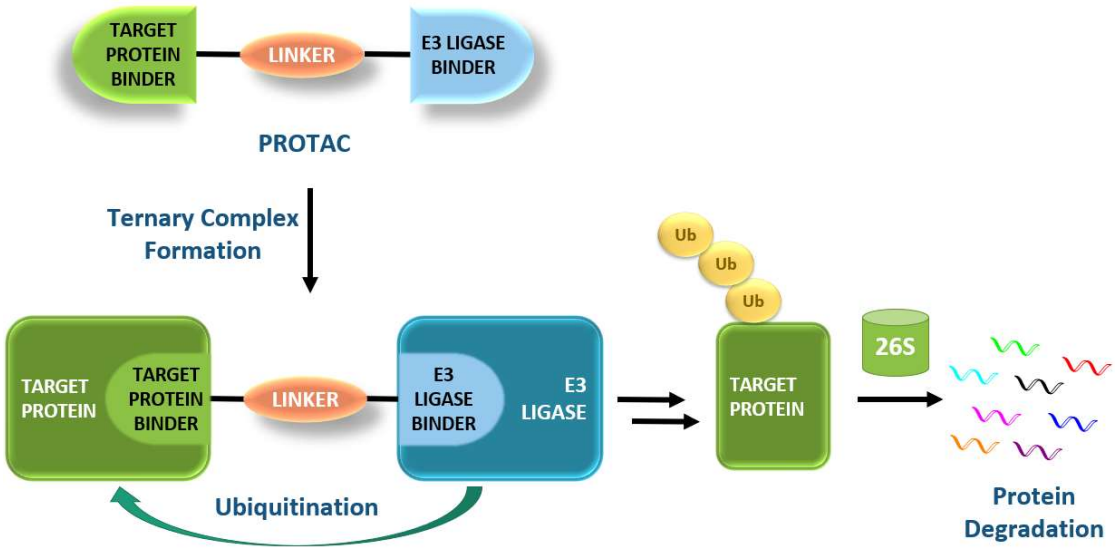

Figure 3: Diagram of PROTAC mechanism of action

There are many benefits associated with the use of PROTACs. Theoretically, PROTACs are catalytic in nature, hence they can be dosed at a very low level and still achieve a high therapeutic effect.[13] This low dose potential should reduce side effects, improving quality of life. Another key benefit for the use of PROTACs is their alternative mechanism of action to standard drugs, which generally inhibit or activate target proteins. In diseases where drug resistance can occur this is particularly useful, provided the PROTAC is still capable of binding the protein partners, key proteins may still be degraded using the UPS completely knocking out their activity.[11]

PROTACs also have immense potential in protein research and genomic elucidation. To understand a proteins function, generally it is deactivated in the cell and phenotypical changes are observed.[14] There are many ways to achieve this result, such as genetic knockout methods, post-transcriptional inactivation, and post-translational modification interference.[14] PROTACs could be very useful for the

simplification of these knockout methods, as any protein could be targeted for complete degradation using cheap and easily synthesised chemicals.[14]

1.1.3 History of PROTAC development

This method of 'hijacking' the UPS was first carried out by Sakamoto et. al. in 2001,[15] with the synthesis of PROTAC-A (figure 4). PROTAC-A contained a phosphopeptide to bind to E3 ligase Skp, Cullin, F-box (SCF) and a small molecule binder of protein MetAP2; ubiquitination was observed *in vitro.* To establish binding affinity and specificity at intracellular concentrations, PROTAC-A was applied to egg extracts where degradation was observed. Although this discovery was a highly significant proof of concept, it was known PROTAC-A would be unable to penetrate the cell due to the impermeable peptide sequence.[15]

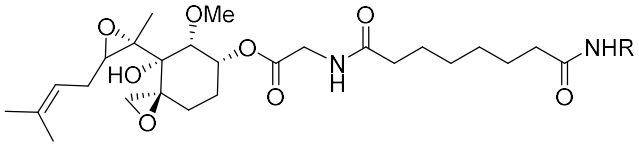

R = GGGGGGDRHDS*GLDS*M
S*: Phosphorylated Serine

PROTAC-A

Figure 4: PROTAC-A developed by Sakamoto et al.[15]

Further work targeted the estrogen receptor and the androgen receptor with PROTAC-B (figure 5).[16] These peptidic PROTACs did not solve the permeability issues, as microinjection into the cells was required for activity.

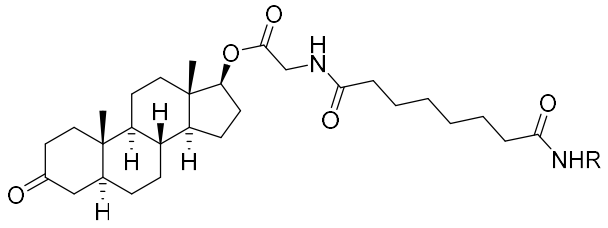

R = DRHDS*GLDSM
S*: Phosphorylated Serine

PROTAC-B

Figure 5: Structure of androgen receptor targeting PROTAC-B

To address the issue of cell permeability, an FKBP12 targeting PROTAC was developed, incorporating an eight-amino acid poly-*D*-arginine chain to the peptide-based von Hippel-Lindau (VHL) binder (figure 6).[17] Sufficient degradation was observed at 25 µM concentration in cells.[17]

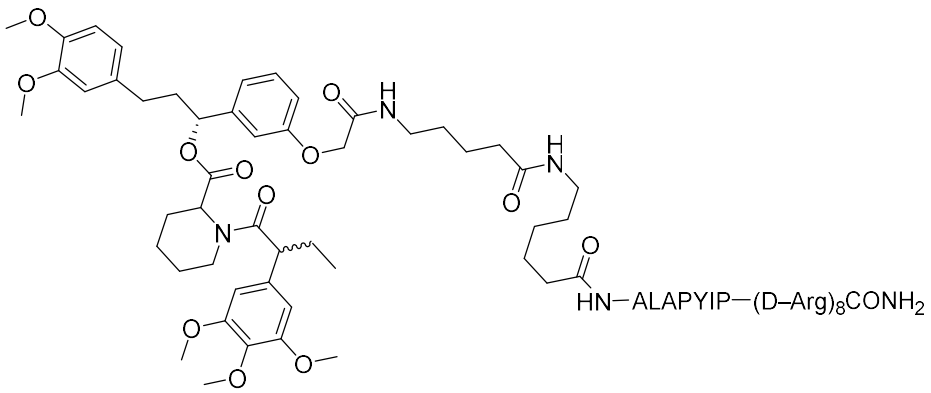

PROTAC-C

Figure 6: First developed cell permeable PROTAC-C

Initial results for peptide based PROTACs were promising, with proof of concept studies showing successful target protein degradation; however, the inherent limitations of peptides including poor permeability and pharmacokinetic properties limited their efficacy. To address these issues, PROTAC development was shifted toward the field of small molecules. The first new generation PROTAC was developed by Schneekloth *et al.* in 2008 (figure 7).[18] PROTAC-D targeted AR using E3 ligase MDM2, and although cell permeability was improved, potency was poorer compared to previous peptidic results.[18]

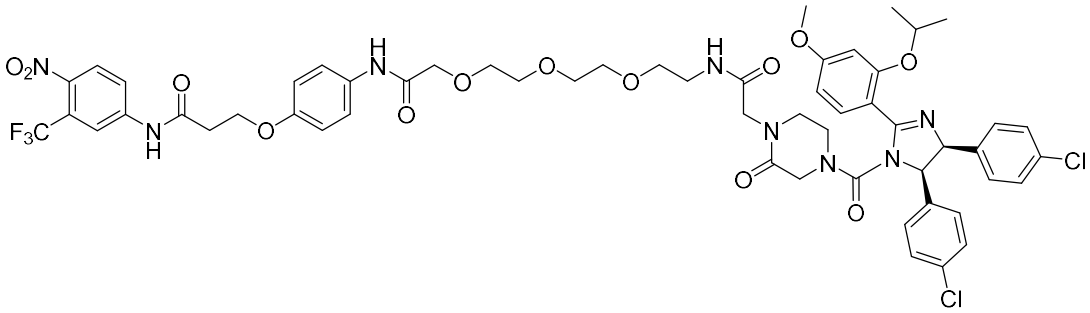

PROTAC-D

Figure 7: First small molecule PROTAC-D

Following this discovery, new small molecule binders for alternative E3 ligases have been identified, leading to significant advances in the potency and permeability of PROTACs.[11,13,19,20]

HaloTag fusion proteins were targeted by Buckley *et al.* utilising the E3 ligase VHL (figure 8).[21] HaloPROTAC3 was found to be particularly potent with a DC_{50} of 19 nM. HaloTag fusion proteins are non-endogenous but are commonly used in chemical genetic studies. This study demonstrated the importance of optimal linker length, as PROTAC activity was vastly reduced at short length likely due to negative steric interactions.[21]

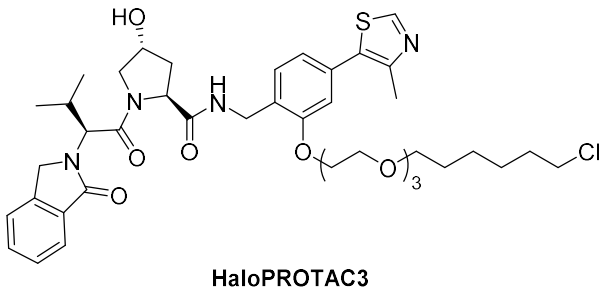

HaloPROTAC3

Figure 8: PROTAC targeting the HaloTag fusion protein developed by Buckley et al. [21]

Studies targeting bromodomain BRD4 using E3 ligase cereblon were published simultaneously by both Winter *et al.*[22] and Lu *et. al* [23] (figure 9). Winter's dBET1 showed rapid BRD4 cellular degradation at 100 nM concentration with complete degradation after 2 h. Unfortunately, stability of these phthalimide-based compounds was found to be limiting, and partial BRD4 recovery was observed 24 h post treatment. Consequences of dBET1 on cellular protein abundance were also assessed. Of the 7429 proteins screened, 3 were markedly depleted: BRD2, BRD3, and BRD4, highlighting selectivity limitations. dBET1 attenuated tumour progression, and reduced BRD4 levels in tumour-bearing mice. Lu's ARV-825 also showed BRD4 protein degradation, with a sub-nM DC_{50}. The efficacy of the PROTAC was shown to be more extensive and longer lasting than the BRD4 binder alone. Interestingly, a bell-shaped dose dependence curve was observed known as the hook effect, rationalised by the formation of dimer protein-PROTAC complexes at higher concentration which compete with the active trimer complex formation. Selectivity issues were also observed for ARV-825.[23]

A

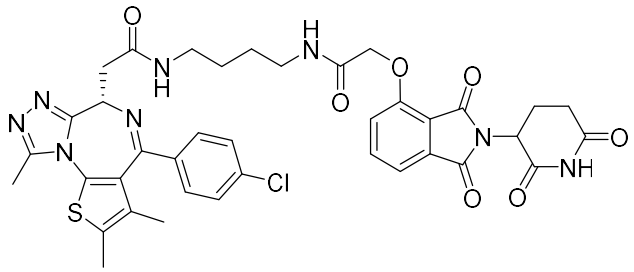

dBET1

B

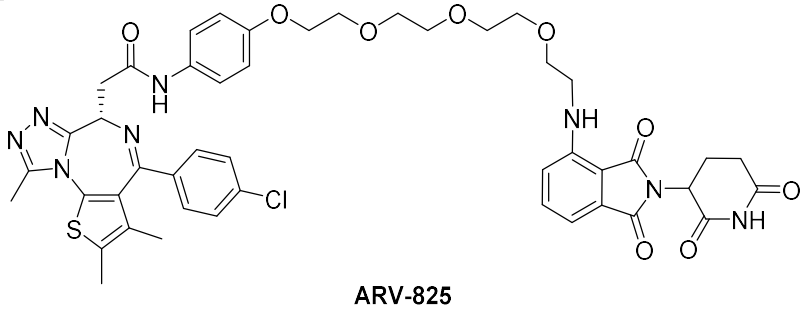

ARV-825

Figure 9: A) dBET1 developed by Winter et al.[22] *B) ARV-825 developed by Lu et al.*[23]

Bondeson *et al.* used PROTACs to target the RIPK2 protein, a serine-threonine kinase which mediates immune signalling (figure 10).[24] The PROTAC designed gave a DC_{50} of 1.4 nM in cellular studies. In this study, the sub-stoichiometric catalytic nature of the PROTAC was evaluated by comparing the absolute quantity of PROTAC to that of ubiquitinated RIPK2 *in vitro*. Depending on molarity, stoichiometry values of 2.0 – 3.4 were observed as evidence for catalysis. These numbers are thought to be a significant underestimation due to experimental limitations. In addition, at high concentrations of PROTAC efficacy was considerably reduced due to the hook effect.

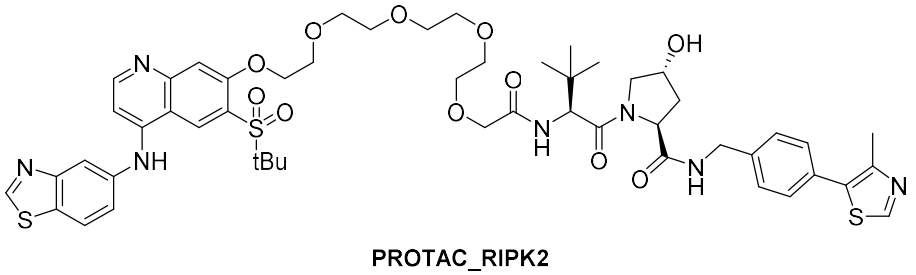

Figure 10: PROTAC targeting RIPK2 developed by Bondeson et al.[24]

Recently, a small molecule BRD degrader has been developed by Zhou *et al.* (figure 11A).[25] This PROTAC was highly potent, with an IC_{50} of 51 pM in leukaemia cells, and showed rapid tumour regression *in vivo*. The PROTAC linker was extensively optimised, establishing the substantial and unpredictable effects linker type and length have on the degradation efficiency (figure 11B).[25] They found that even minor changes in linker nature (e.g. ester to amide bond) resulted in major shifts in potency. They also reported that an optimal linker length (in their case a five-carbon linker) exists.

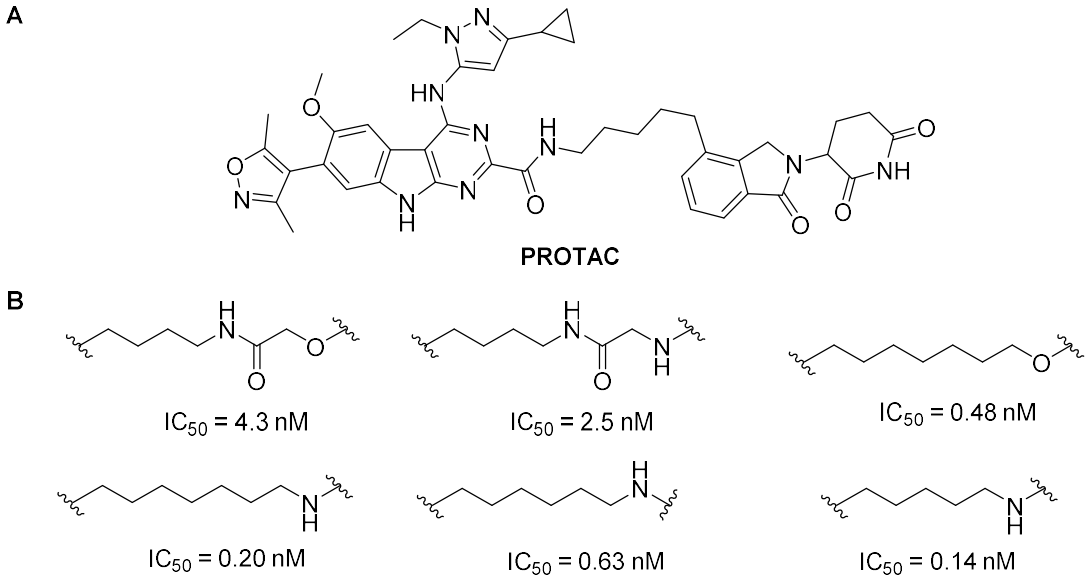

Figure 11: A) PROTAC targeting BET proteins found to have pM activity; B) Different linkers synthesised with IC_{50} values of resultant PROTACs

Since these developments, there has been a surge in publication of PROTACs targeting a huge range of different proteins, including covalent PROTACs,[26,27] macrocyclic PROTACs,[28] homo-PROTACs for self-degradation[29] and dual VHL cereblon targeting PROTACs.[30] Many extensive reviews on these exist,[31–33] hence only a few significant cases will be discussed further.

1.1.4 Recent PROTAC developments

An interesting model was recently reported describing how the cooperative recruitment of a protein target into a ternary complex by a PROTAC can effect both selectivity and efficacy.[34] Isothermal calorimetry (ITC) and x-ray crystallography were used to better understand the complex interactions dictating ternary complex formation. A crystal structure of PROTAC MZ1 bound to BRD4 and VHL was reported, which showed the ligand folding promoted additional intermolecular interactions between the two proteins resulting in cooperative binding (figure 12). The concept of ligand-induced protein-protein interactions was validated and quantified through ITC studies, surface mutagenesis and proximity assays. In addition, Gadd *et al.* were then able to use this understanding for the structure-based-design of a new PROTAC which showed highly selective BRD4 degradation in cells.

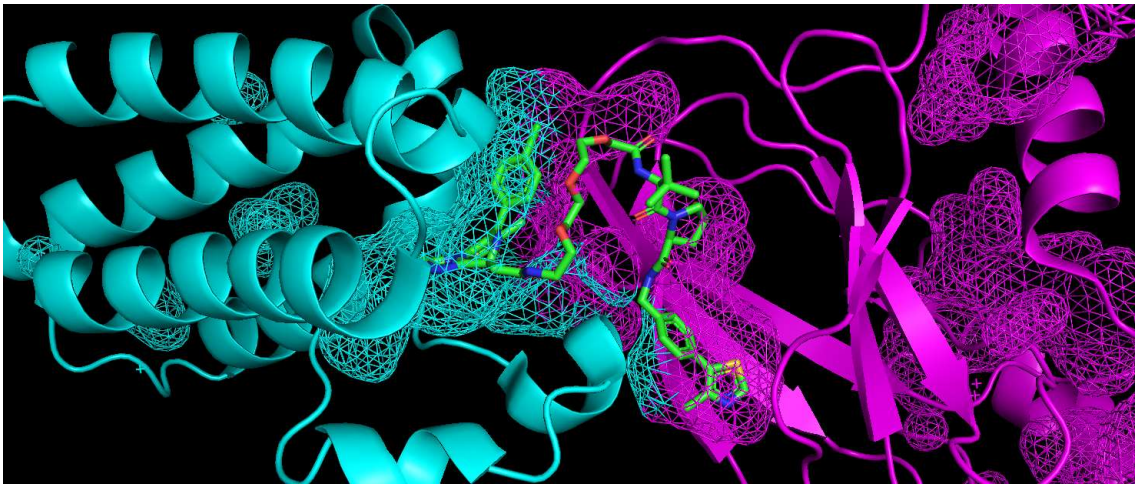

Figure 12: Crystal structure of BRD4 (blue) and VHL (purple) bound to PROTAC MZ1 generated from PDB: 5T35 [34]

An interesting approach was taken by Bondeson *et al*. who generated a PROTAC using a promiscuous kinase warhead.[35] By synthesising highly promiscuous cereblon and VHL-recruiting PROTACs capable of binding >50 kinases, they showed only a subset of the bound targets were degraded. PROTAC-E was derived from kinase inhibitor Foretinib (figure 13) which binds to 133 kinases with little control. The VHL-recruiting PROTAC degraded 9 of these proteins compared to the cereblon-recruiting PROTAC which degraded 14. This is significantly lower than the 133 possible kinases which could have been targeted and highlights the high levels of specificity which can be attained using the PROTAC

technology. Interestingly, the affinity of the kinase to the PROTAC was not a robust predictor of activity. Instead, ability to induce a stable ternary protein complex was more predictive with highly effective degradation observed when protein-protein interactions stabilised the ternary complex.

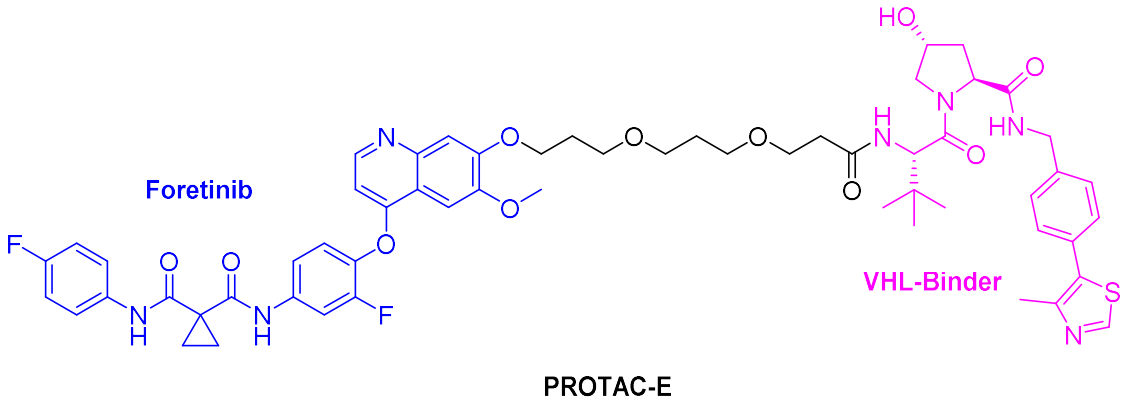

Figure 13: Structure of kinase inhibitor Foretinib derived PROTAC

Interesting comparisons between protein inhibition and degradation have recently been published on CDK9 using cereblon-recruiting PROTACs[36] and RTK using VHL-recruiting PROTACs[37]. Both studies found the PROTAC approach to have superior activity over inhibition alone. The PROTAC activity observed was longer-lasting than the inhibition approach. Activity was dependent on rate of protein re-synthesis instead of clearance rates.

Despite the many benefits of PROTACs described above, there are also considerable challenges which accompany the future development of PROTACs. It is well-known that efficacy can now be achieved at low nM and pM concentrations.[22–25] However, delivery and bioavailability remains a challenge due to the high molecular weight of the molecules (700 – 1000 Da)[20] which can limit their scope. There has recently been a surge in interest in 'beyond rule of 5' compounds and many of these exhibit reasonable oral bioavailability and drug-like properties.[38] Indeed, oral delivery of PROTACs has already been validated as an effective administration method.[39] For clinical applications, there are additional complications of dosing brought on by the hook effect where at high concentrations, formation of dimer complexes dominates rather than the therapeutically active ternary complexes. Achieving the appropriate therapeutic index for maximum effect is difficult in these cases as systemic drug concentrations often fluctuate *in vivo.* This requires further data to overcome.[40] PROTAC metabolism can also complicate further developments due to potential losses in binding to either protein partner. This may result in inactive metabolites which compete with the PROTAC for protein binding. Another aspect of PROTACs which is not well-understood is their off-target toxicity, which could damage healthy cells alongside the disease. Finally, although numerous PROTACs have shown exceptional activity against many targets, this doesn't mean that resistance to PROTACs won't ultimately emerge

following extended PROTAC usage. A recent study on BET-targeting PROTACs found chronic exposure to these PROTACs led to drug resistance in cancer cell lines, and further treatment of these cell lines with BET-PROTACs failed to induce degradation. The cause of this resistance was not loss of binding to the target proteins, but instead determined to be genomic alterations in core components of E3 ligase complexes.[41]

1.2. Prostate Cancer

Prostate cancer (CaP) is the second most prevalent cancer in men worldwide, and in developed regions such as the UK, it is the most prevalent.[42] In 2012 alone, *ca*. 1.1 million cases were diagnosed globally with *ca*. 307,000 deaths.[42]

The androgen receptor (AR) is a nuclear receptor which controls gene expression, depending on ligand binding.[43] The normal development and function of the prostate is moderated by the interactions between the AR and binding androgens, most notably testosterone and the more potent metabolite 5α-dihydrotestosterone (DHT) (figure 14).[43] These hormones bind to the AR ligand binding domain (LBD), and induce transcriptional activity through a conformational change in the protein, which allows it to recruit cofactor proteins and transcriptional machinery.[43]

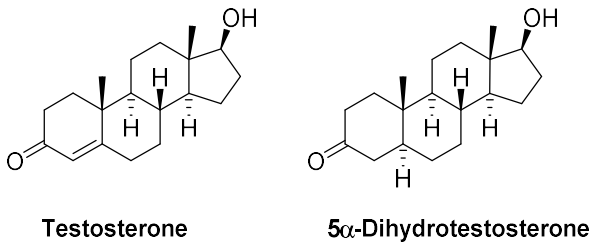

Figure 14: Structures of endogenous androgens, testosterone and 5α-dihydrotestosterone

Prostate cancer is intrinsically dependent on androgen signalling, as these interactions are responsible for stimulating proliferation and inhibiting apoptosis. Due to its significance, androgen deprivation therapy (ADT) is commonly the first line treatment for advanced hormone-sensitive prostate cancer.[44]

Antiandrogens antagonise the endogenous androgens by competitive inhibition of the LBD,[43] and are therapeutically useful in the treatment of prostate cancer. By blocking the endogenous androgens and possessing no intrinsic AR activity when bound, cell proliferation is terminated, leading to apoptosis.[43] One prevalent class of antiandrogens are the substituted toluidides (figure 15). Bicalutamide is the most frequently prescribed due to its reduced hepatotoxicity and 6 day half-life.[45]

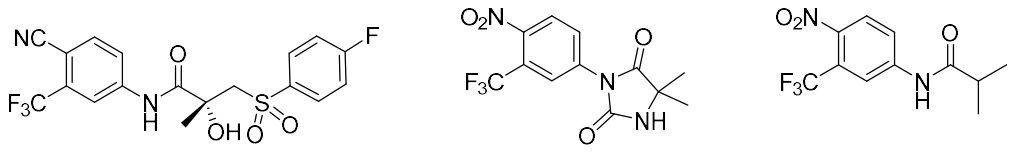

Figure 15: Non-steroidal antiandrogens used for treatment of prostate cancer

Although most prostate cancer diagnoses are androgen-dependent, this often progresses to castration resistant prostate cancer (CRPC) after 2-3 years of ADT. CRPC has little to no response to anti-androgen inhibition, however, AR expression remains crucial for tumour progression.[46] There are multiple mechanisms leading to CRPC, including AR amplification/hypersensitivity, mutations in the AR, and androgen-independent AR activation.[47] A key pathway is AR amplification/hypersensitivity where cells become sensitive to the low androgen concentrations following ADT. This can occur either from AR overexpression or mutations allowing promiscuous AR activation from molecules other than androgens, and lead to the progression of prostate cancer.[48] Ligand-independent AR activation is also a vital mechanism, where various growth factors and proteins increase AR signalling pathways.[49]

When antiandrogens such as bicalutamide are present in CRPC, they can still bind to the AR, however typically there is a switch in their activity from antagonist to agonist, associated with differences in coactivator and corepressor recruitment to AR target genes.[50]

Although understanding of CRPC has substantially developed in the past decade, it is still not comprehensive. Due to the high mortality rates of this late-stage cancer, more effective treatments for the disease are urgently required.

Second-generation antiandrogens have been developed to show activity in CRPC. A key new drug, enzalutamide (figure 16) was approved in the US in 2012 for the treatment of CRPC.[44] Enzalutamide was identified following a screen for compounds that retain AR activity in cells with increased AR expression. This orally available drug was developed by Medivation and in Phase I/II clinical trials 43% of the 30 patients showed >50% decline in prostate-specific antigen (PSA), a key prostate cancer biomarker.[51]

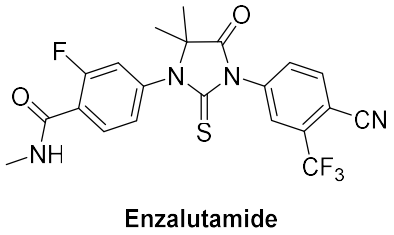

Figure 16: Chemical structure of enzalutamide

Enzalutamide is an AR signalling inhibitor able to target the AR by inhibiting endogenous androgen binding, inhibiting nuclear translocation of activated AR, and through reduced binding of AR to DNA (figure 17).[52,53] The binding affinity of enzalutamide to the AR in CRPC cell lines was found to be five- to eight- fold greater than bicalutamide,[51] and when gene-expression was studied it was found not to have agonist activity in most resistant cells, unlike bicalutamide.[51]

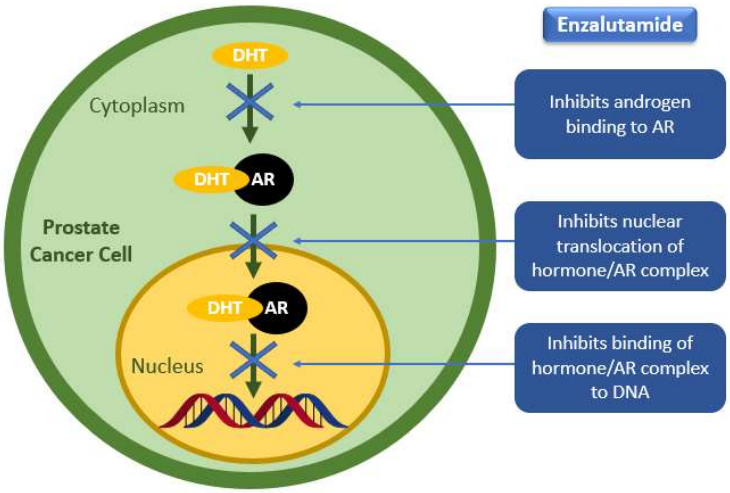

Figure 17: Diagram showing the different AR signalling pathways that enzalutamide inhibits, adapted from Schalken et al.[52]

Unfortunately, resistance to enzalutamide can still occur, thought to be due to a mutation in the AR ligand binding domain. Similarly to the first-generation antiandrogens, activity can be switched from antagonist to agonist.[54] Research has been done to simulate the antiandrogen-AR complex to provide rationale for future third-generation antiandrogens able to bypass the agonist mechanism.[55] Finding new drugs to target CRPC is hugely important, since drug resistance is developing rapidly in prostate cancer.

1.3. Strategies for degradation of the androgen receptor

1.3.1. Selective Androgen Receptor Degraders (SARDs)

Degradation of hormone receptors has been a valid therapeutic strategy prior to the development of PROTACs. Selective estrogen receptor degraders (SERDs) downregulate ER and have been highly effective treatments for breast cancer, for example approved drug Fulvestrant (figure 18).[56] Upon binding, SERDs induce a conformational change to ER which exposes hydrophobic residues synonymous to misfolded ER, which is recognised by the cell leading to degradation. There are a limited number of known scaffolds for generation of SERDs. Fulvestrant is currently the only clinically approved example and only one other scaffold is in clinical trials.[57] Recently, a novel class of SERDs

was discovered with a modular design strategy to expand the degradation toolbox.[58] This strategy involves attachment of a linker with a synthetic handle to an ER binder which can then be conjugated with a variety of different degrons to rapidly screen numerous candidates.

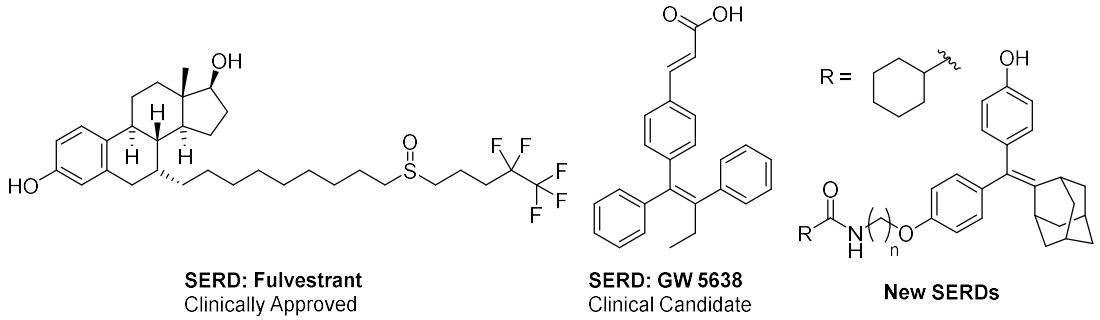

Figure 18: Examples of reported SERDs from clinically approved Fulvestrant to newly developed scaffolds

This hydrophobic tagging approach to protein degradation has also been applied to AR. However, development of selective androgen receptor degraders (SARDs) has been considerably slower than SERDs, and currently no SARDs have been clinically approved.[59] The first reported SARD was published in 2011 (figure 19). This compound was able to down-regulate AR in AR-dependent cell-lines, however adverse cardiovascular effects were predicted due to hERG ion channel potentiation.[60] Further developments were able to bypass this hERG activity, leading to first-in-class SARD AZD3514.[61] This compound showed significant disease stabilisation and PSA reduction in clinical trials, despite notable side effects including nausea and vomiting.[62] Niclosamide is an FDA-approved treatment for anti-helminthic therapy also able to reduce AR levels. Despite its strong activity in preclinical models, the drug exhibited unacceptably high toxicity for clinical studies.[63] Recently, SARD279 demonstrated the potential to overcome some resistance mechanisms, despite showing a modest DC_{50} of 2 μM.[64] More effective SARDs have also been reported, including UT-69[65,66] and next-generation candidate UT-34, which had improved properties and was more efficacious *in vivo*.[67]

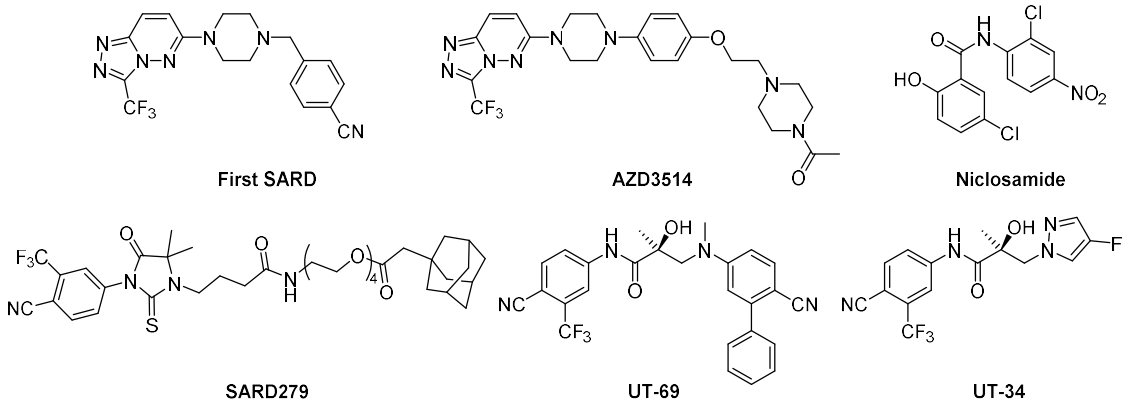

Figure 19: Examples of recently reported SARDs

Compared with PROTACs, one advantage of the new generation of SARDs is their smaller molecular weights which translates to improved pharmacological characteristics and oral bioavailability which are vital factors in drug development.[68] Currently, SARD development is at an early stage and potential side effects are unknown. Fundamentally, PROTAC technology is considerably more generalisable than SERDs/SARDs demonstrated by the single clinically approved example of this technology compared to numerous proteins targeted by PROTACs.

1.3.2. Specific and Non-genetic Inhibitor-of-Apoptosis proteins-dependent Protein Erasers (SNIPERs)

Another way to degrade AR is using a SNIPER approach. SNIPERs are a specific type of PROTAC which use inhibitor-of-apoptosis proteins (IAPs) as the ubiquitin ligase.[69] The first SNIPER targeting AR was AR SNIPER 1, reported by Itoh *et al.* (figure 20A). This SNIPER was demonstrated to reduce AR levels in cells at 30 μM concentration through Western blot analysis.[70]

A further example of a SNIPER approach to AR degradation was reported in 2017 by Shibata *et al*. (figure 20B).[71] AR SNIPER 2 incorporated higher binding affinity ligands and was shown to potently degrade AR in AR-dependent prostate cancer cell lines *via* a proteasome-dependent pathway, resulting in inhibited AR-mediated gene expression, and reduced cell proliferation.

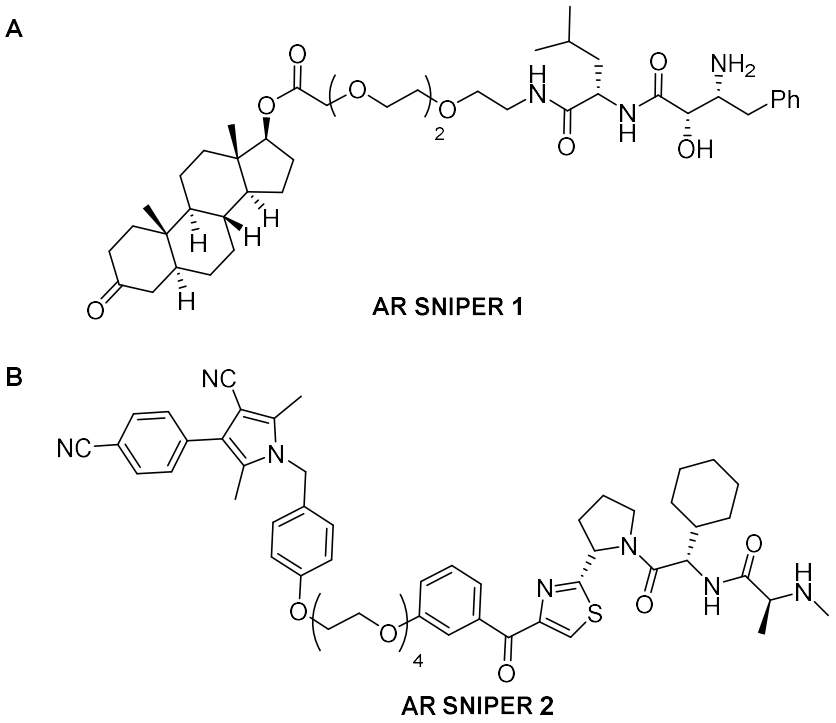

Figure 20: SNIPER structures for degradation of AR via IAPs; A: AR SNIPER 1, B: AR SNIPER 2

In contrast to PROTACs, SNIPERs induce degradation of both the target protein as well as the cIAP1 ubiquitin ligase. This may limit the use of this technology for target protein knockdown, as lowering levels of ligase would in turn lower the rate of target protein degradation.[72] Further research on how this additional degradation pathway will affect SNIPER activity is needed, in particular a comprehensive study on IAP cellular concentrations and re-synthesis rates. For effective SNIPER use, E3 ligase levels would need to be equal or greater than target protein levels. However, it is worth noting that cIAP1 is frequently overexpressed in tumour cells and related to drug resistance. Inhibition of the IAP protein family has been established as a valid treatment for cancer, and several examples are currently under clinical development.[73] Hence, the dual activity of SNIPERs for target protein and cIAP1 degradation may offer additional benefits for treatment of various cancers.

1.3.3. PROTACs targeting AR

Over the past 10 years, there has been a surge of interest in PROTACs targeting AR since the first AR-targeting peptidic PROTAC (figure 5) and the first small molecule AR targeting PROTAC (figure 7).

A head-to-head biological comparison between enzalutamide and a PROTAC derivative of enzalutamide, ARCC-4 (figure 21) was recently reported. This PROTAC was found to degrade ~95% of cellular AR at low nanomolar potencies.[74] ARCC-4 was also found to inhibit prostate tumour cell proliferation and exhibited activity on AR point mutant variants. Enzalutamide loses its anti-proliferative effects in high androgen environments, whilst ARCC-4 overcomes this major limitation and offers significant benefits as an alternative prostate cancer treatment. In addition, ARCC-4 was found to be *ca.* 10-fold more potent than enzalutamide despite its lower intracellular concentrations which stem from poorer permeability.

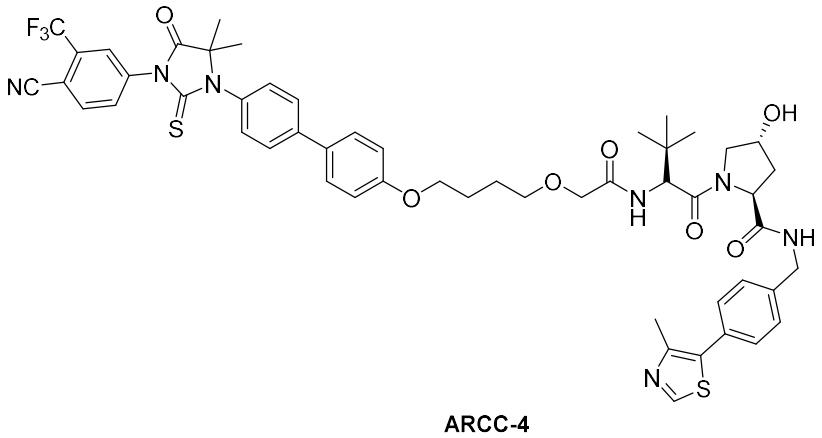

ARCC-4

Figure 21: Structure of AR targeting PROTAC ARCC-4

Another AR-targeting PROTAC was reported in 2019 (figure 22). ARD-69 uses an AR antagonist connected *via* a rigid linker to a VHL ligand.[75] This PROTAC was found to be highly potent, with a sub-nanomolar DC_{50} and over 95% AR degradation in prostate cancer cell lines. This high potency was achieved following an extensive screen of different AR and VHL binders, in addition to linker types and lengths. This highlights a significant challenge in PROTAC development, with huge numbers of compounds required to establish activity and little predictability in design. Typical linker types used in PROTACs are highly flexible, and generally consist of ether connections or alkyl chains. The linker for ARD-69 is very different, it is made up of piperidine rings and an alkyne linkage which imparts rigidity to the drug. Increasing the rigidity through the linker is a potential strategy to improve the pharmacological properties of a PROTAC, and in this case high efficacy was observed in mouse models. Further studies from the same group also showed that highly potent AR PROTACs could be prepared using a weak binding VHL ligand with a K_i of 2.8 μM.[76] This once again highlights the importance of the ternary structure of a PROTAC over the individual binding affinities of its substituents.

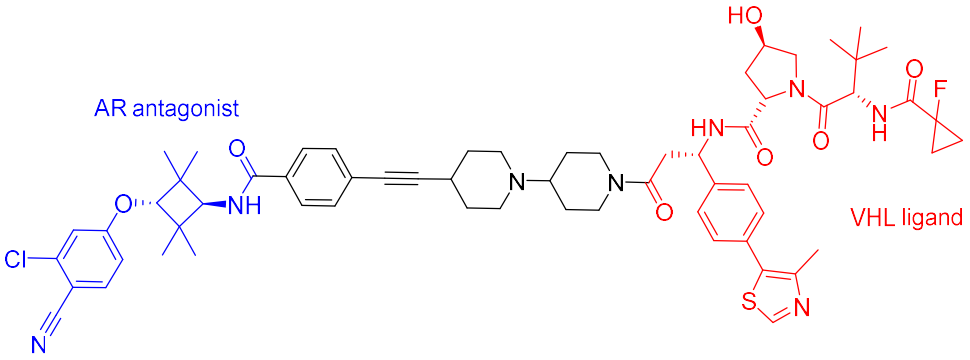

Figure 22: Structure of AR degrader ARD-69

Recently, ARV-110 an oral PROTAC developed by Arvinas, has been reported for the degradation of AR for prostate cancer treatment. The preclinical data on this compound was extremely promising, with *in vivo* efficacy demonstrated in CRPC and enzalutamide resistant tumour models.[77] ARV-110 was progressed into phase 1 clinical trials in March 2019, followed by an ER degrader ARV-471, which entered clinical studies in August 2019 with initial read-outs looking encouraging.[78] It is still too early to judge the pharmacokinetic and safety profiles of these PROTACs from these initial trials, however the rapid development of these PROTACs is indicative of their promise as therapeutic candidates.

2. Chapter 2

2.1. Chapter 2: Introduction

2.1.1. Protein-Protein Interactions (PPIs)

Protein-protein interactions (PPIs) are responsible for regulating numerous cellular processes such as replication, signal regulation, and protein synthesis.[79] Despite the integral role PPIs play in cellular function, they are underexploited in therapeutics due to the difficulties involved in targeting them.[80]

Historically, there has been a large focus on developing small molecules to treat diseases due to their general ease of synthesis and good pharmacokinetic properties.[80] With recent developments leading to FDA approvals of numerous biologic therapeutics, designing Lipinski's 'ideal' drugs is no longer crucial.[81,82] Despite these developments, targeting PPIs is still a formidable challenge. The surface area of the PPI interface typically varies between 600 and 6000 Å for heterocomplexes,[83] hence, to selectively and potently disrupt the PPI an inhibitor must have many binding contacts (figure 23A). Achieving this using small, 'drug-like' molecules is challenging. Protein binding sites are often non-contiguous, which presents additional targeting challenges and selectivity is difficult to achieve due to the often featureless interfaces.[80] This is in direct contrast to typical 'druggable' targets such as receptors or enzyme active sites which generally have well-defined binding pockets (figure 23B).[84]

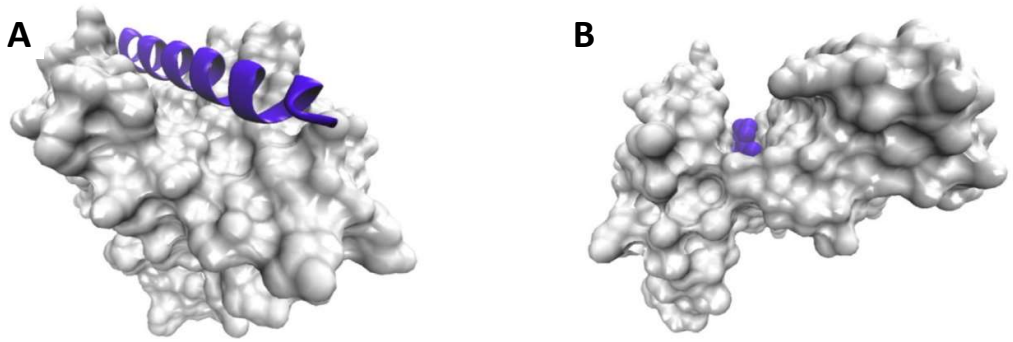

Figure 23: Adapted from Tsomaia[85] with permission from Elsevier; A) shows the PPI interface between BCL-2/BID proteins; B) shows a small molecule kinase inhibitor

Designing small molecule PPI inhibitors can be daunting. One strategy used to design inhibitors is to elaborate the structure-activity relationship of the natural ligand to increase potency and selectivity.[80] It is challenging to directly apply this method to protein-based ligands due to their size, complexity, and generally poorly characterised interface. Conventional high throughput screening often leads to few, weakly potent hits, which can be difficult to develop into potent lead compounds.[86]

The development of PPI inhibitors has garnered great interest in recent decades, thus the field has experienced rapid growth. One reason being the greater understanding of interfaces and key binding interactions.[87] Methods to study binding have been developed which enhance understanding of PPIs,

particularly where no crystal structure can be obtained. One well-established method relies on identifying key binding hot spots through alanine scanning, where amino acid residues are substituted with alanine and the change in binding energy recorded.[88] This identifies key binding residues, known as hot spots. Following this, screening libraries can be designed for identification of potent drugs.[89]

Another relevant technique for rational drug design is computational docking, where a ligand and binding site are conformationally modelled to establish binding modes and key interactions.[90] This technique enables virtual screening, which indicates scaffolds likely to bind to a target protein.[90] The utility of docking is debated due to difficulties predicting accurate 3D protein structures; however, techniques have been refined, and *de novo* design has successfully predicted binding modes.[91]

The discovery of small molecule PPI inhibitors has progressed greatly in recent years. Despite the challenges discussed, there are examples of inhibitors able to potently bind at the PPI interface.[92] The cytokine interleukin-2 (IL-2) is a protein responsible for T cell activation and rejection of tissue grafts.[93] The potent small molecule binder SP4206 (figure 24), was developed using fragment-based approaches.[94] The PPI interface bound to an initial fragment was characterised, and tethering experiments were conducted to elucidate key binding positions. Following this, compound assembly combined key fragments and indicated valuable combinations to synthesise and test. Compound SP4206 was shown to be highly potent, with an IC_{50} of 60 nM and a K_d of 100 nM.[93–95]

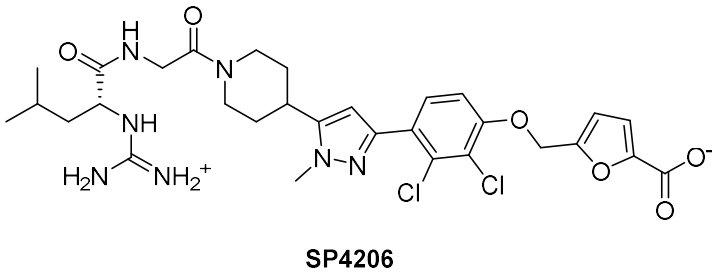

SP4206

Figure 24: IL-2 small molecule inhibitor SP4206 developed by Sunesis Pharmaceuticals

2.1.2. p53-MDM2 PPI

One relevant PPI commonly targeted is p53-MDM2.[96,97] The tumour suppressor p53 protein is thought to be the 'guardian of the genome', as its key functions involve inducing cell cycle arrest, senescence, and apoptosis in response to various stress signals.[98] The levels of functioning p53 in tumours is low, due to either inactivation of the gene encoding p53 (TP53) through mutation, or direct p53 inactivation through binding to cellular proteins.[99] One such protein, MDM2 (murine double minute 2) was discovered to form a tight complex with p53, regulating its function.[100] The autoregulatory

feedback loop of these two proteins is vital for their function, with p53 inducing MDM2 expression which in turn promotes p53 inhibition and degradation.[101] The level of p53 in healthy cells is minimised, then, in response to stress, high p53 levels are rapidly achieved resulting in cell cycle arrest and apoptosis. A key aspect of MDM2 functionality is its ability as an E3 ligase to cause ubiquitination of bound p53, which targets p53 for cellular degradation.[102] Many tumours overexpress MDM2 causing p53 functionality to be lost and continued tumour cell proliferation.[103] Hence, reactivating p53 is a method for treatment of cancer and there are many approaches which can achieve this.

A key strategy to reactivate the p53 pathway is through MDM2 inhibition.[104] A significant study showed p53 activation through MDM2 inhibition supressed tumour formation in mice.[105] However, side effects of targeting this pathway, such as lymphopenia and intestinal apoptosis, were observed by Mendrysa *et. al.*[106] Dosing *ca*. 80% of MDM2 levels gave positive tumour suppressing results, whilst maintaining the integrity of the intestine. Lymphopenia was a more significant issue and *ca*. 20-50% reduction in MDM2 activity was required to prevent this condition.[105]

An early success story in small molecule PPI inhibitors are the nutlin family of compounds (figure 25), which are inhibitors of the p53-MDM2 PPI. Interestingly, these *cis*-imidazoline analogues were identified through library screening methods and gave high IC_{50} values in the range of 100 – 300 nM.[107] From crystal structure analysis of bound nutlin-3, it is thought that the rigid imidazoline scaffold directs three of the attached groups into pockets where vital p53 amino acid residues normally bind.[107]

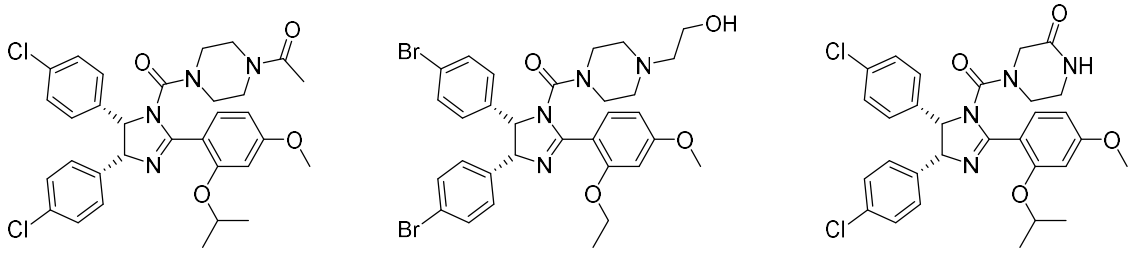

Figure 25: Small molecule p53-MDM2 inhibitors

Nutlin-3 was found to be the most potent MDM2 inhibitor. Further optimisation of its binding, cellular potency, and pharmacokinetics yielded RG7112 (figure 26). This molecule is the first MDM2 inhibitor to reach the clinic,[108] and recently published Phase I data was promising.[109]

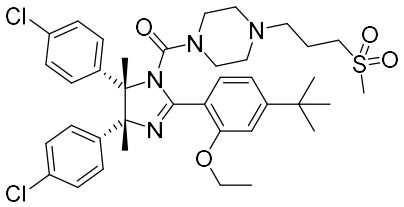

RG7112

Figure 26: RG7112 (Roche) Drug Candidate

Degradation of MDM2 through PROTAC mechanisms has also been validated as an effective strategy for cancer treatment.[110] Li *et al.* have recently reported a first-in-class MDM2 degrader, MD-224 which employed E3 ligase cereblon for MDM2 degradation (figure 27).[111] This PROTAC rapidly degraded MDM2 at sub-nanomolar concentrations and cell proliferation assays gave an IC_{50} of 1.5 nM. This PROTAC was 10 – 100 times more potent than MDM2 inhibition alone, and *in vivo* studies showed long-lasting tumour regression at well-tolerated doses.

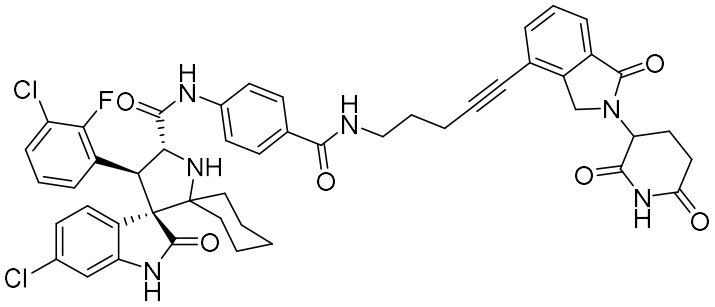

MD-224: MDM2 Degrader

Figure 27: Structure of MD-224, a degrader of MDM2 via E3 ligase cereblon

2.1.3. Introduction to peptides

Peptides are another class of therapeutics commonly used to target PPIs. Peptides consist of a short sequence of amino acids, generally fewer than 50 residues.[112] There are many peptide drugs on the market, examples include 26 amino acid, chronic pain drug ziconotide,[113] and 39 amino acid type 2 diabetes drug exenatide.[114]

The intermediate size and molecular weight of peptides gives them many useful properties. Peptides can be applied to a wide range of PPI targets, due to their ability to mimic elements of a proteins structure, and inherent similarity to the natural binding proteins.[115] Physiologically, peptides also have low tissue accumulation due to their size, and can have lower toxicity than small molecules, as a result of their higher biocompatibility, specificity, and fewer off-target effects.[116] Peptides can also be

synthesised relatively easily compared to numerous biologics. Compared to small molecules however, peptide synthesis entails high production costs due to long synthetic routes and purification challenges.[112]

The secondary structure of a peptide is vital to its function, as the shape largely determines binding specificity. One prevailing element of this is the α-helix (figure 28). The number of amino acids per turn is 3.6, optimal for stabilisation through hydrogen bonding between backbone residues on adjacent coils (*i*,*i*+4).[117,118] Unfavourable steric clashes between side chains are minimised through the torsion angles of the backbone, contributing to the stabilisation of the α-helix.[119] Additional stability can also be imparted through salt bridges between oppositely charged side chains, such as lysine and glutamate residues.[120] The combination of these favourable interactions promotes formation of α-helices in peptides; however, without the structural rigidity of high molecular weight proteins, the conformational flexibility results in poor helicity in water.[121]

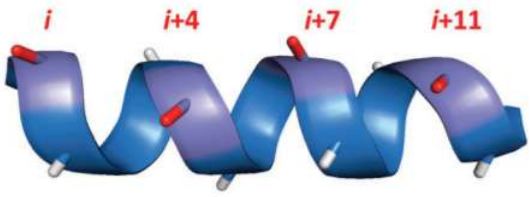

Figure 28: Peptide α-helix, reproduced from Ref. 44 with permission from The Royal Society of Chemistry.[122]

The major drawbacks of peptide-based therapeutics are the poor proteomic stability and lack of conformational rigidity.[115] Another challenge facing peptides is their poor membrane permeability – making it difficult to target intracellular PPIs.[85] These issues can be linked to the lack of defined secondary structure, hence improving peptide helicity can improve peptide properties.[123] These problems have been addressed in two major ways: backbone modifications, and peptide cyclisation.[115]

Backbone modification involves changing atoms on the amino acid backbone to impart greater stability to physiological conditions, these compounds are generally referred to as peptidomimetics.[124] One example of this is β-peptides, where the altered amino acid backbone (figure 29) favours hydrogen bonding with more distal neighbouring groups, for example the 10-helix hydrogen bond.[125] This induces a secondary structure with improved helicity and pharmacological properties.[126]

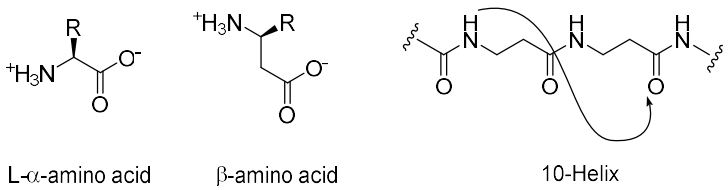

Figure 29: Peptidomimetics with altered backbone giving β-peptides

2.1.4. Peptide cyclisation

Peptide cyclisation is a well-developed area of research. Macrocyclisation rigidifies the peptide conformation which generally enhances stability to proteolysis,[85] and cell permeability.[127] Cyclosporin A is a head-to-tail cyclic peptide and a potent immunosuppressive drug isolated from fungi in 1984 (figure 30).[128] The cyclic and *N*-methylated backbone of this orally administered peptide was thought to impart better pharmacokinetic properties and improved stability over the unmodified peptide.[85]

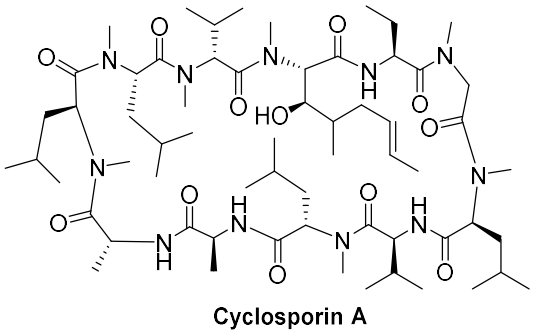

Figure 30: Structure of immunosuppressant cyclosporin A

Stapled peptides are an emerging class of macrocyclised peptides, where covalent linkage of two amino acid residues positioned in *i,i*+3, *i,i*+4, *i,i*+7, or *i,i*+11 positions forms a 'staple' between helical coils.[115] Peptide stapling can be categorised as either one-component, where the two modified amino acid residues directly react with each other, or as two-component, where the two amino acid residues react with a bridging molecule (figure 31).[122]

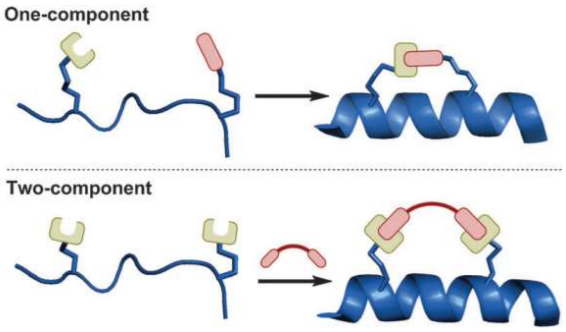

Figure 31: One-component vs two-component i,i+7 peptide stapling[122] reproduced with permission from the RSC

Early examples of cyclisation of amino acid side chains involved lactam formation between proteogenic Lys and Glu/Asp residues.[129] One of the major benefits of lactamisation is its use of natural amino acids, which are cheap and commercially available. However, the requirement of additional orthogonal protecting group strategies for solid phase peptide synthesis (SPPS) can be complex.[130]

Cyclisation through disulfide bridges has promoted helicity and improved stability at elevated temperatures.[131] This also benefits from use of natural amino acids, however poor stability of disulfide bonds in reducing environments limits their therapeutic potential.[122]

One of the most established stapling methods is hydrocarbon stapling, initially developed in the Grubbs group.[132–134] Their early work incorporated olefinic amino acids into a peptide sequence, which were then cyclised using ring-closing metathesis (RCM). [52,53] This work was extended to longer peptides where RCM of *i,i*+4 unnatural residues was performed (figure 32A).[134] Following this, Schafmeister *et. al.* first introduced the term 'stapled peptides' applied to hydrocarbon stapling using RCM of *α,α*-disubstituted amino acids (figure 32B).[135] The optimal *i,i*+7 stapled peptide had increased helicity and stability to proteolysis by trypsin compared to native and unstapled alternatives.

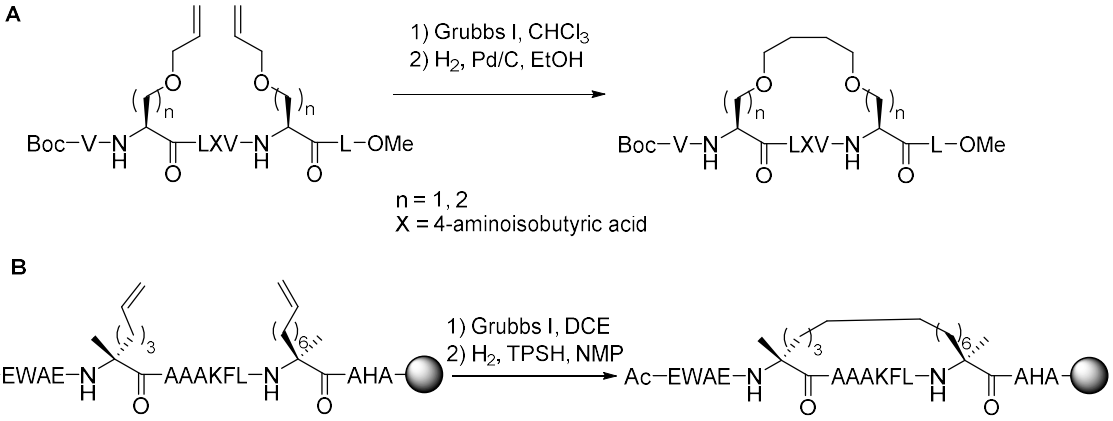

Figure 32: A) RCM hydrocarbon stapling by Grubbs,[134] B) Verdine's all-hydrocarbon RCM stapling[135];

These initial successes allowed further development by Walensky *et. al.*, applying the concept of stapled peptides to PPI targets including BCL-2.[136] BCL-2 is a protein critical for regulation of apoptosis, and an appealing target for therapeutics.[136] Using stabilised α-helix of BCL-2 domains (SAHBs), which are stapled peptides able to mimic a vital part of the binding domain, the apoptosis pathway could be activated.[136] These stapled peptides had high specificity and improved stability to proteolysis, and were shown to kill leukaemia cells. The study showed SAHBs were also effective *in vivo,* with growth of leukaemia inhibited in mice.[136]

There have been many other examples of using hydrocarbon stapled peptides to target challenging proteins, such as the inhibition of the NOTCH transcription factor,[137] and β-catenin.[138] An interesting recent development in this field extends methodology to the synthesis of bicyclic peptides, using orthogonal ring-closing alkyne and olefin metathesis.[139]

Copper catalysed azide-alkyne cycloaddition (CuAAC) click chemistry was first used to staple peptides by Cantel *et. al.* (figure 33).[140,141] There are many benefits to using CuAAC approaches to staple

peptides, such as the high yields, biocompatibility, and low cost reagents.[142] Following this work, click chemistry peptide stapling was applied to the BCL-9/β-catenin PPI, generating a helical peptide with improved binding affinity and stability compared to linear and wild-type peptides.[143]

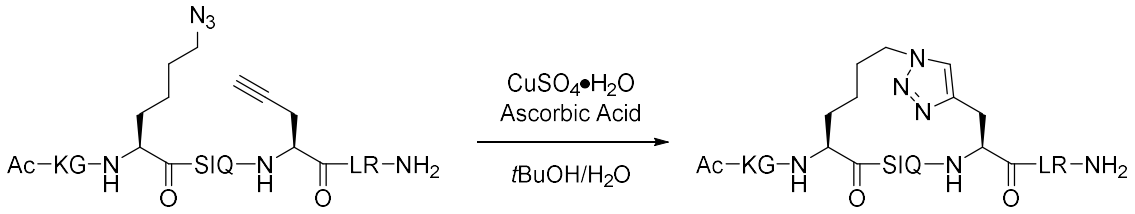

Figure 33: Copper catalysed azide-alkyne cycloaddition synthesis of stapled peptides[140,141]

The second category of peptide stapling is known as two-component peptide stapling, where a bifunctional linker able to react with the complementary amino acids is used as a 'staple'. Two-component stapling enables introduction of complex and diverse staples, which can be used to improve the properties of the peptide or introduce new functionality. Synthesis of these stapled peptides is theoretically more challenging than the one-component equivalent due to the side reactions possible, for example the double coupling by-product (figure 34).[122] Oligomerisation may also be a problem, hence solution phase reactions at low concentrations are generally required.[122]

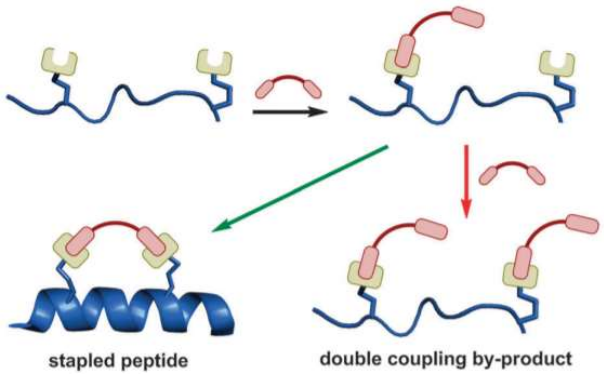

Figure 34: Potential side reactivity found in two-component stapling;[122] *Reproduced from Ref. 44 with permission from The Royal Society of Chemistry*

There have been many examples of two-component peptide stapling strategies which have been comprehensively reviewed elsewhere.[144]

2.1.5. p53-MDM2 binding stapled peptides

Previous work in the Spring group has applied two-component CuAAC peptide stapling to the development of p53-MDM2 PPI inhibitors.[123,145] The peptide sequence used (SP), was developed through point mutations of the wild-type p53 sequence to establish a potent MDM2 binder. This

peptide sequence was then stapled with different diyne linkers in an attempt to improve cell permeability (figure 35).[123]

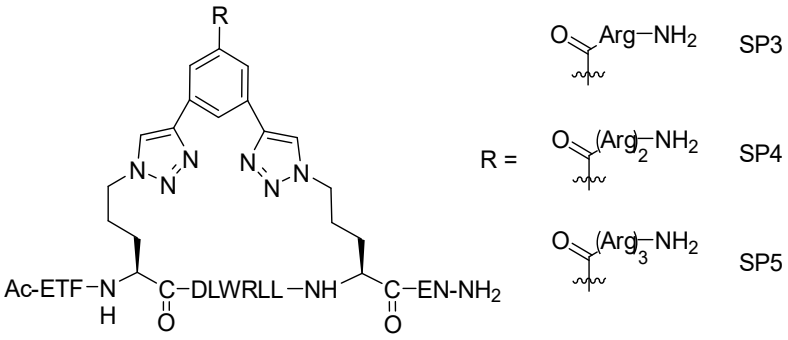

Figure 35: Two-component stapled peptides with varied R-groups

Stability of the peptides was improved upon stapling. The IC_{50} values varied between 90 and 149 nM and K_i varied between 3.7 – 11.7 nM. The cell permeability was assessed using a cellular reporter assay. Activity of each peptide was measured at 25, 50, and 100 µM concentrations (figure 36). Dose-dependent p53 activation was observed for SP5, with little activation observed for the remaining peptides, likely due to poor cell permeability.[123] This study highlighted the benefits of two-component peptide stapling, as optimised stapling gave significantly improved properties.

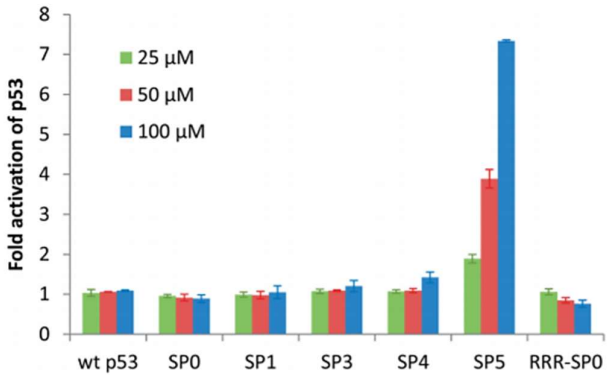

Figure 36: where SP0 is the unstapled peptide residue, SP1: R = H, SP2: R = -NH-TAMRA, RRR-SP0: linear peptide with three arginine residues at N-terminus; taken from Lau et al. with permission from the Royal Society of Chemistry [123]

Further studies were undertaken extending the two-component stapling methodology to the copper-free synthesis of stapled peptides.[145] This strategy used the Sondheimer diyne, which reacted with the peptide *via* a double strain-promoted azide alkyne cycloaddition (SPAAC) reaction. The biocompatible stapling was carried out in the presence of cells in 96-well plates before evaluating in a p53 reporter assay (table 1).[145]

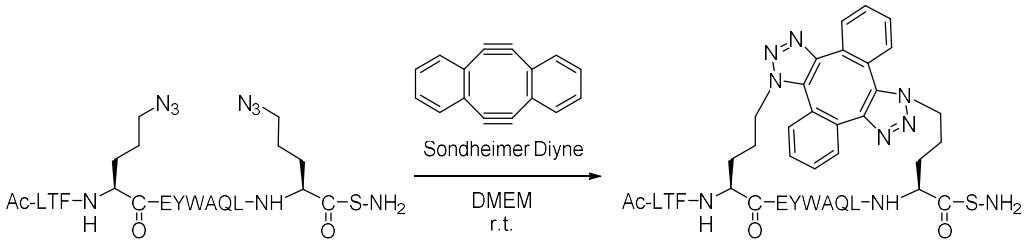

Peptide	Sequence	*In vitro* binding affinity for MDM2 (K_d, nM)		Fold p53 activation of stapled peptide (50 µM)
		Unstapled	Stapled	
A	Ac-ETFXDLWRLLXEN-NH_2	16 ± 1	3.1 ± 0.4	1.03 ± 0.03
B	Ac-LTFXHYWAQLXS-NH_2	36 ± 3	14 ± 1	1.5 ± 0.3
C	Ac-TSFXEYWALLX-NH_2	9 ± 1	7.6 ± 0.7	1.5 ± 0.2
D	Ac-LTFXEYWAQLXSAA-NH_2	6.0 ± 0.6	2.5 ± 0.3	2.3 ± 0.2
E	Ac-LTFXEYWAQLXS-NH_2	6.5 ± 0.6	7.5 ± 0.7	2.9 ± 0.2

Table 1: Stapled peptide sequences with measured binding affinities for MDM2 and cellular p53 activation

Peptide A is based on the SP sequence used previously and gave poor cellular activity. Peptides B – E are based on phage-derived peptides PMI,[146,147] and PDI,[148] and exhibited improved cellular activity. A crystal structure of peptide E complexed with MDM2 shows the α-helical conformation of the stapled peptide interacting with MDM2 (figure 37), with defined hotspot binding triad (F3, W7, L10).[145] The staple motif interacts with the protein,[145] however due to the open face of the MDM2 surface and the staple orientation, structural elaborations of the staple should not significantly affect MDM2 binding.

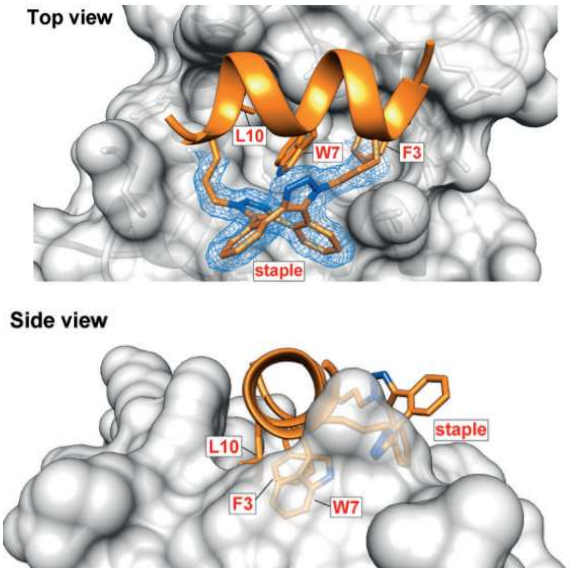

Figure 37: Stapled peptide E bound to MDM2, 1.9Å resolution; taken from Lau et al.[145] permission from John Wiley and Sons

2.1.6. Advantages of the recruitment of MDM2 as an E3 ligase in PROTACs

Overall, exploitation of MDM2 as an E3 ligase for PROTAC generation has many potential benefits over the other commonly used E3 ligases, cereblon and VHL. Importantly, MDM2 is upregulated in many cancers hence could be more selective in degrading target proteins in these cancer phenotypes.[149] This additional selectivity could also lead to a more targeted therapy with reduced side effects, since protein degradation would be more pronounced in the MDM2-overexpressing cancerous cells.

Moreover, MDM2 recruiting PROTACs may unlock the potential to harness a dual mechanism of action.[150] Indeed, MDM2 inhibition is a valid strategy for the treatment of cancers, due to its autoregulatory feedback loop with p53. As a result, MDM2 recruiting PROTACs would not only degrade AR through the PROTAC mechanism, but also inhibit MDM2 to promote p53 levels.[151] This dual effect may lead to improved potency and selectivity for cancer, whilst potentially providing additional protection against resistance.

There are over 600 identified E3 ubiquitin ligases,[152] however, investigation into alternative E3 components remains an underexplored area within the PROTAC field. Accordingly, the development of additional ligands to enable the recruitment of different E3 ligases is an important line of research that would further expand the PROTAC toolbox. Currently, it is very challenging to design highly potent PROTACs without substantial optimisation and as such, increasing the number of available E3 ligases for degradation may simplify this procedure, enabling exploitation of the inherent biases of a given E3 ligase to a subset of proteins. Accordingly, the validation of a novel ligand for MDM2-mediated degradation could instigate degradation of additional protein targets.

2.2. Chapter 2: Aims and Objectives

The objective of this project was to develop a novel PROTAC, which incorporated a stapled peptide using two-component CuAAC click methodology. The key benefit of using 2-component stapling was the ability to introduce additional functionality through the staple and improve the peptide's properties, including cell permeability and solubility. As MDM2 is an E3 ligase able to polyubiquitinate p53, it follows that stapled peptide PROTACs could be developed through staple elaboration.

The generation of 'drug-like' PROTACs is a major challenge in this field due to difficulties in achieving high permeability and bioavailability resulting from their high molecular weight. Stapled peptides are known to have the advantage of high cellular stability, permeability and good biocompatibility over their linear counterparts. Due to the catalytic nature of PROTACs, high cellular stability is vital for a long-lasting therapeutic effect without requiring high or frequent dosing. The stapled peptides developed in the Spring group targeting the p53-MDM2 PPI were demonstrated to achieve low nM binding affinities and good cellular activity. This stapled peptide approach was hypothesised to extend the PROTAC toolbox and further investigate the utility of E3 ligase MDM2 for UPS-mediated protein degradation. Additionally, the two-component stapling strategy was envisaged to be applicable to the degradation of a wide range of proteins through simple staple modification, enabling rapid and efficient PROTAC investigation.

Targeting AR with PROTACs has enormous potential for the development of more effective CRPC therapeutics. Rather than inhibiting AR, like first generation antiandrogens, PROTACs induce degradation which is vital for their applicability to CRPC. Using an alternative mechanism of action to directly deplete AR levels, causing reduced proliferation and enhanced apoptosis, is thought to be a promising strategy for the development of next generation CRPC treatment.[11]

Novel stapled peptide PROTACs were designed, which used a peptide sequence to recruit MDM2 as an E3 ligase and an enzalutamide-based binder to recruit AR (figure 38). Enzalutamide does not display agonist behaviour in cell lines with overexpressed AR and has high affinity for AR making it an ideal PROTAC component (Section 1.2.2). The peptide could be macrocyclised with a staple which is conjugated to enzalutamide using CuAAC approaches. With an initial PROTAC in hand, biological assays could be performed to establish activity in AR-positive cell lines.

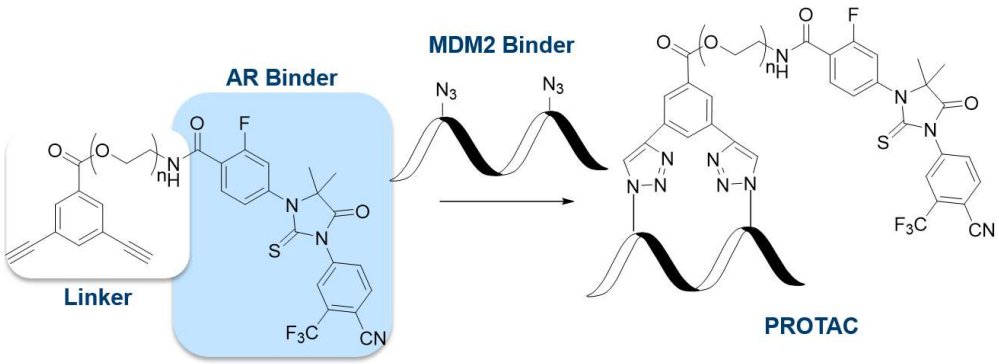

Figure 38: Synthesis of stapled peptide PROTAC

Research in the field of PROTACs has established huge activity differences based on varying linker type and lengths, hence further studies will be done to optimise the properties and activity of the PROTAC. The investigation will initially employ a six-unit poly-ethylene glycol (PEG) linker, due to its high flexibility allowing the ternary complex to adopt favourable conformations, and solubility. From literature precedent,[21] the strategy for linker length optimisation will involve using a long, six-unit PEG chain for initial studies then reducing the length in further work to improve efficacy.

Ideally the target protein would be varied in future studies, as a major benefit of PROTACs is their applicability to multiple targets with just minor alterations of linkers and target protein binders. A proof of concept experiment would involve swapping the enzalutamide-based fragment for an alternative binder, for example using an estrogen receptor binder for the application to breast cancer.

2.3. Chapter 2: Results and Discussion

2.3.1. Synthesis of 1st generation PROTAC staples

The synthesis of staple **1** was designed based upon the retrosynthesis outlined in figure 39. Initially, the complex staple was disconnected into the carboxylic acid **2**, and PEG linker **3** which could be joined through an amide coupling. PEG linker **3** could be synthesised through esterification of benzoic acid **6** with **7**. Carboxylic acid **2** could be synthesised using an isothiocyanate-amine cyclisation of **4** and **5** to form the thiohydantoin core. Molecules **4** and **5** can be synthesised from the respective commercially available compounds, **8**, **9**, and **10**. The route is highly modular, which is preferable for efficiency and yield; it also allows for easy installation of alternative linkers and AR binders. The final steps in the synthetic route are simple esterification and amide coupling chemistry which are typically high yielding.

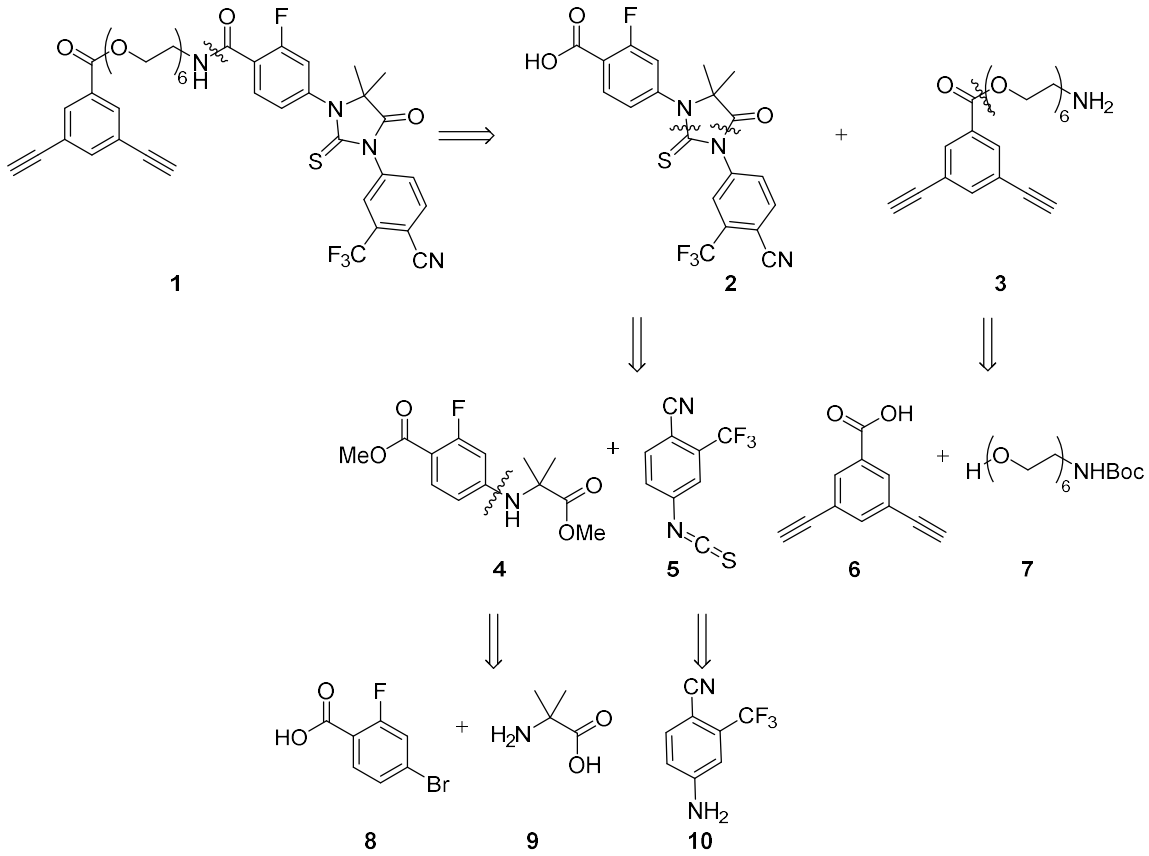

*Figure 39: Retrosynthesis of staple **1** to commercially available starting materials*

The general synthesis of enzalutamide is a patented procedure involving a key isothiocyanate-amine cyclisation to form the thiohydantoin core.[153] The synthesis proposed was a shorter, potentially more efficient route to reach the carboxylic acid rather than the *N*-methyl amide of enzalutamide.

Isothiocyanate **5** was initially synthesised from commercially available 4-amino-2-(trifluoromethyl)benzonitrile **10**. Literature procedures used thiophosgene,[153] however this is a particularly toxic, hazardous reagent and its use was undesirable. Alternative routes to this functional group were studied (scheme 1). Reacting the amine with carbon disulfide and triethylamine followed by *p*-toluenesulfonyl chloride is a standard route to isothiocyanates,[154] however, in this case no reaction was observed. A second attempt used carbon disulfide and triethylamine followed by Boc_2O and 4-(dimethylamino)pyridine (DMAP),[155] this was also unsuccessful and resulted in recovery of starting material. This was thought to be due to the electron deficiency of the arene due to strongly electron withdrawing nitrile and trifluoromethane groups, resulting in a less nucleophilic aniline.

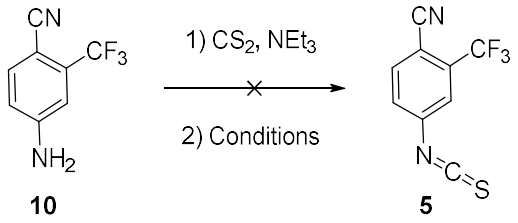

10 **5**

*Scheme 1: Initial attempted synthesis of isothiocyanate **5***

Next, the reaction was attempted using thiocarbonyl-diimidazole (TCI), and the desired product was observed (scheme 2). TCI is regarded as a non-hazardous alternative to thiophosgene, typically used to synthesise thioureas *via* isothiocyanates.[156] A quick solvent screen identified dichloromethane (DCM) as the optimal solvent for this reaction, which was likely to be due to the high solubility of both starting materials.

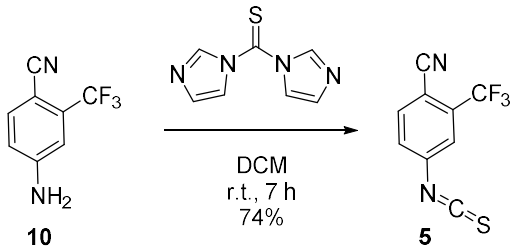

10 **5**

*Scheme 2: Synthesis of isothiocyanate **5** using TCI*

With the first building block in hand, work began towards the synthesis of the enzalutamide fragment (scheme 3). The first step involved an Ullman coupling between 2-fluoro-4-bromobenzoic acid **8** and 2-aminoisobutyric acid **9** to form diacid **11**. Purification of **11** was challenging due to its high polarity, resulting in poor yields. Diesterification of acid **11** using thionyl chloride gave **4** in 67% yield.

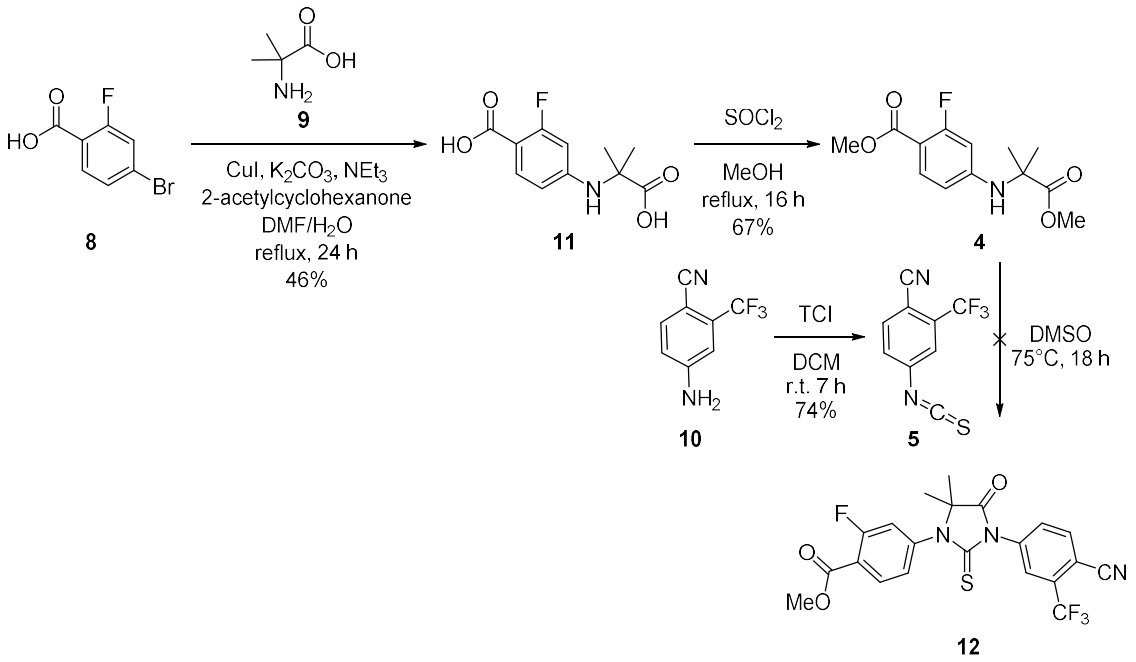

*Scheme 3: Attempted synthesis of **12***

This was followed by the cyclisation in DMSO. Unfortunately, no desired product was observed by LC-MS or TLC analysis of the reaction mixture, with substantial quantities of starting material **10** detected, indicating hydrolysis of **5** despite the anhydrous conditions. Attempts to optimise the reaction by varying solvents and equivalents of **5** resulted in complex mixtures of unidentified products. The mechanism for the cyclisation step is thought to begin with the nucleophilic attack of the amine onto the isothiocyanate, followed by intramolecular cyclisation through attack onto the adjacent ester. It was initially thought that the ring constraints meant that only the proximal ester would be subject to this intramolecular reaction, forming a favourable 5-membered ring (Baldwin's Rules). However, the intermolecular reaction with starting material **4** or a reaction intermediate would form a variety of products. This was not conclusively proven by LC-MS analysis of the reaction mixture nor ^{1}HNMR studies. It was thus decided to explore an alternative route to attain **2**.

The alternative approach to the synthesis of enzalutamide followed a patented procedure (scheme 4).[153] The initial step involves protecting **8** as an amide, prior to the Ullmann coupling. Product **14** was challenging to purify due to difficulties removing DMF and eluting the highly polar carboxylic acid. The carboxylic acid **14** was then converted to the methyl ester **15** using iodomethane. When purification of **14** was omitted, and the crude compound was directly methylated the yield was much improved and purification of ester **15** was simple.

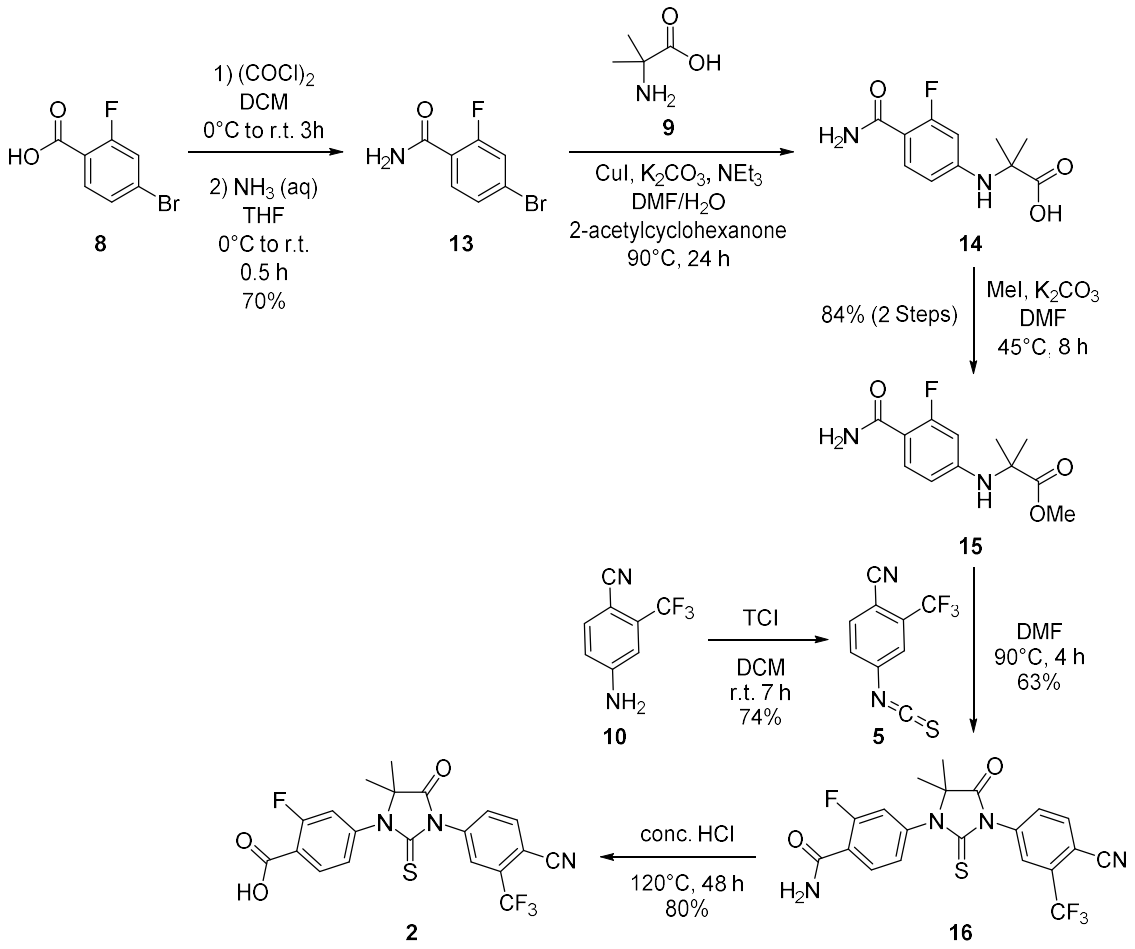

*Scheme 4: Alternative synthesis to carboxylic acid **2***

To form the thiohydratoin core, **15** was cyclised with isothiocyanate **5**. This reaction resulted in greater success than previous attempts. A solvent screen of DMSO and DMF both resulted in successful product formation, with DMF giving the higher yield. The yield was improved by increasing the quantity of isothiocyanate to 2 equivalents to give 63% yield. It is unknown exactly why this cyclisation procedure was successful with **15** but not with **4**, however was hypothesised to be a result of side reactivity of the aryl-ester present in **4**, masked as a less reactive amide in **15**.

Finally, amide **16** was hydrolysed by heating in concentrated hydrochloric acid (conc. HCl) in a sealed tube for two days, to successfully generate desired carboxylic acid **2**.

2.3.2. Initial synthesis of linker 3

Diyne-benzoic acid **6** was synthesised according to literature procedures,[157] through a three step route (scheme 5). Initial esterification of 3,5-dibromobenzoic acid gave **18**, followed by a Sonogashira coupling to form **19**. Hydrolysis of **19** formed **6** in an excellent 87% overall yield.

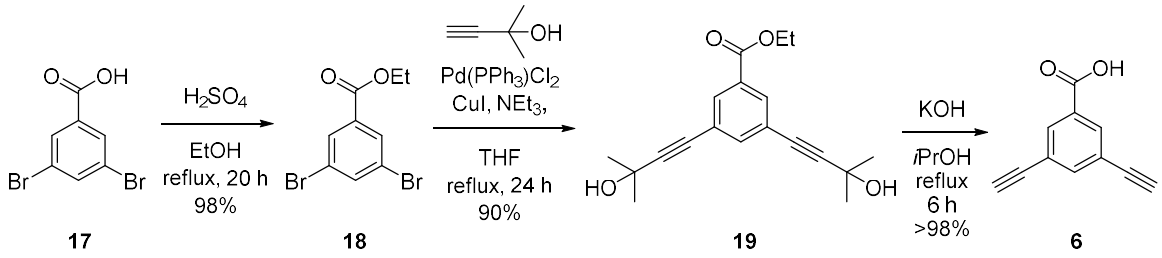

*Scheme 5: Synthesis of diyne benzoic acid **6** from commercially available **17***

Next, the mono-functionalised PEG chain was synthesised, according to a published route (scheme 6).[158] This involved mono-tosylation of six-unit PEG, using Ag_2O and KI to enhance selectivity for the monotosylated product **21**. This mono-tosylation is highly selective for symmetrical diols, proposed to be due to internal hydrogen bonding, which causes a difference in acidity between the two hydroxyl protons (figure 40).[159]

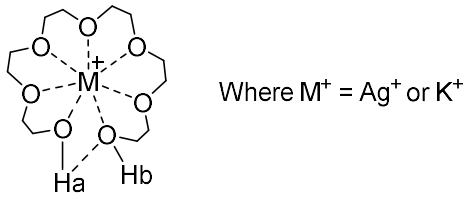

Figure 40: Internal hydrogen bonding of PEG chain chelate, where H_b is rendered more acidic

Nucleophilic substitution of **21** with sodium azide gave **22** in quantitative yield, which was followed by a reduction to produce amine **23**. Initial attempts subjected **22** to hydrogenation conditions, using palladium on carbon catalyst and H_2 gas at atmospheric pressure; however, after 24 h only starting material was isolated. This was likely to be due to H_2 pressure, since literature procedures employed 10 bars of H_2, instead of atmospheric pressure.[160] For ease of operation, alternative conditions were identified. The Staudinger reaction generated the desired amine **23** in quantitative yield,[158] which was then *N*-Boc-protected to give linker **7** in quantitative yield.

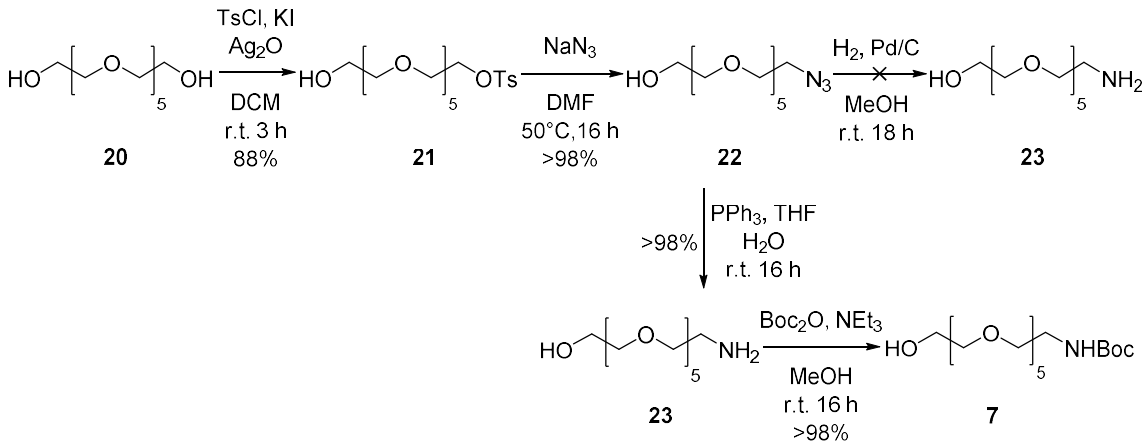

*Scheme 6: Mono-functionalisation of six-unit PEG chain to form **7***

It was decided to initially connect the linker to the diyne **6**, which was synthesised in fewer steps with a greater yield than AR-binder **2**. It was more efficient to introduce **2** in the penultimate step of the PROTAC synthesis. Diyne **6** was connected using an esterification reaction with *N*,*N'*-dicyclohexylcarbodiimide (DCC) and catalytic 4-dimethylaminopyridine (DMAP). This gave product **24** in relatively low yield of 48% due to difficulties purifying this highly polar compound through column chromatography (scheme 7). Initial attempts to remove the Boc group used 4 M HCl in dioxane, however this resulted in poor yields potentially due to stability issues. TFA was subsequently used to give amine **3** in quantitative yield.

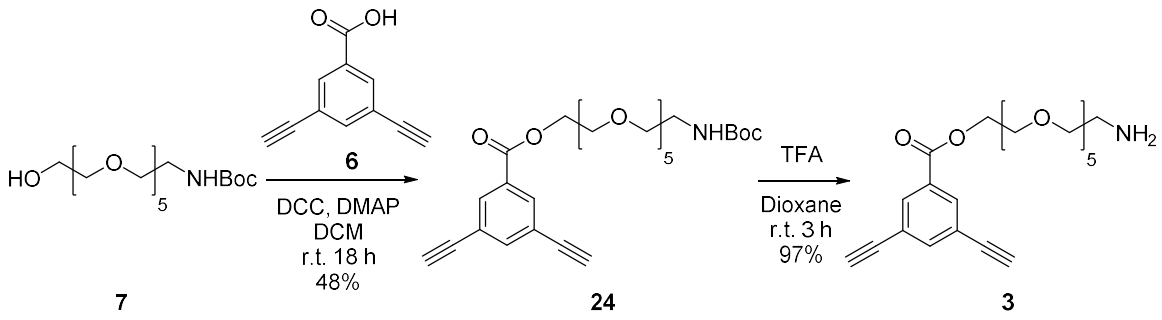

*Scheme 7: Synthesis of diyne PEG linker **3***

The next step was the amide coupling of linker **3** with carboxylic acid **2**. This proved to be challenging, requiring various conditions to be screened (table 2).

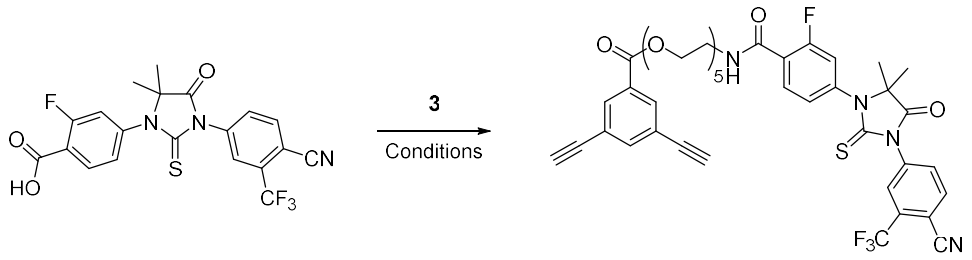

2 1

Entry	Conditions	Results
1	HATU (1.5 eq), DIPEA (3.0 eq)	Complex Mixture, by-product **25** observed
2	HATU (2.0 eq), DIPEA (2.0 eq)	Complex Mixture, trace product, unable to purify
3	DCC (1.2 eq), DMF	Complex Mixture
4	$(COCl)_2$ (3.0 eq), DMF, DCM	Complex Mixture

*Table 2: Conditions attempted for the amide coupling of **2** and **3***

The initial two attempts at this reaction used HATU/DIPEA conditions. Entry 1 gave significant levels of a by-product with 533 Da molecular weight observed through LCMS, proposed to be structure **25** (figure 41). The direct reaction of amine with HATU leading to compound **25** was thought to consume **3**, reducing the equivalents left to react with the activated ester. The order and timing of the reagent additions is known to be important for optimum reactivity.[161] For entry 2, equimolar quantities of HATU and DIPEA were used, and **2** was initially combined with HATU and DIPEA and stirred for *ca.* 30 mins to form the active ester prior to the addition of **3**. LCMS analysis of the reaction mixture showed a potential peak with the correct product mass; however, no product was isolated post-purification. Using DCC to form the active ester prior to reaction with **3** was also unsuccessful. The final conditions relied on forming the more reactive acyl chloride *in situ* using oxalyl chloride and catalytic DMF. This was also unsuccessful and gave complex mixtures of products by LC-MS analysis of the reaction mixture.

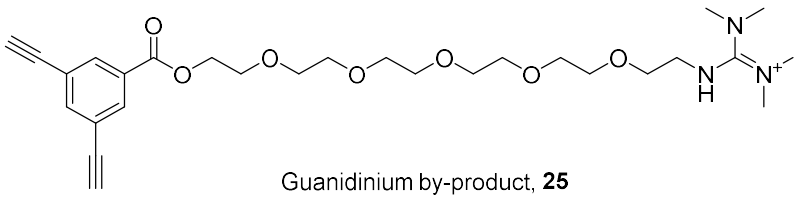

Guanidinium by-product, **25**

*Figure 41: Proposed guanidinium by-product **25** of HATU DIPEA based coupling*

Although there were a substantial amount of alternative coupling reagents which could be screened, after further consideration it was decided that the di-amide linker **26** (figure 42), would be synthesised rather than the ester alternative which was identified as unstable in these reactions.

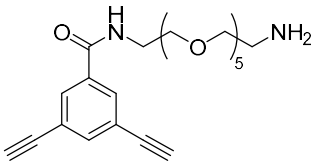

26

*Figure 42: Amide based linker **26***

Esters are generally not as robust to hydrolysis as amide bonds, due to their greater reactivity towards nucleophilic attack at the carbon centre. This biological instability may affect the PROTACs activity, hence avoiding esters where possible would be preferable for future PROTAC development.

2.3.3. Synthesis of linker 26

The initial route to mono-Boc protected diamine **30**, involved a four step procedure (scheme 8).[162] The initial di-tosylation and nucleophilic substitution to form di-azide **28** were successful in high yields. The Staudinger reaction, which was effective in the previous route, failed to yield any diamine **29** in this instance. Even though literature precedent for the transformation of this substrate exists,[163] competing inter- and intra-molecular processes at the iminophosphorane intermediate stage could be responsible for the observed lack of desired product formation.

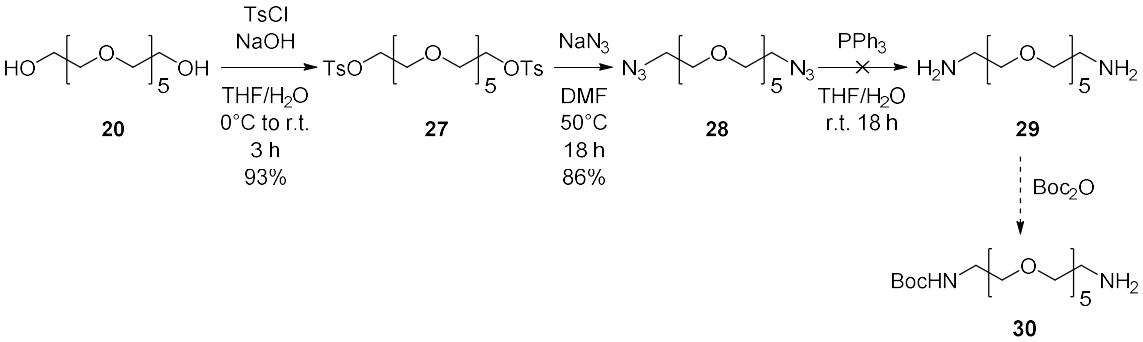

*Scheme 8: Attempted synthesis of mono-Boc protected diamine **30***

Known literature procedures to access **30** rely on a seven step synthesis, starting from **20** and installing the two amino groups separately (scheme 9).[158,164] Despite being fairly lengthy and inelegant, this route was found to be robust and reproducible, thus **30** was synthesised rapidly and in 73% yield over seven steps.

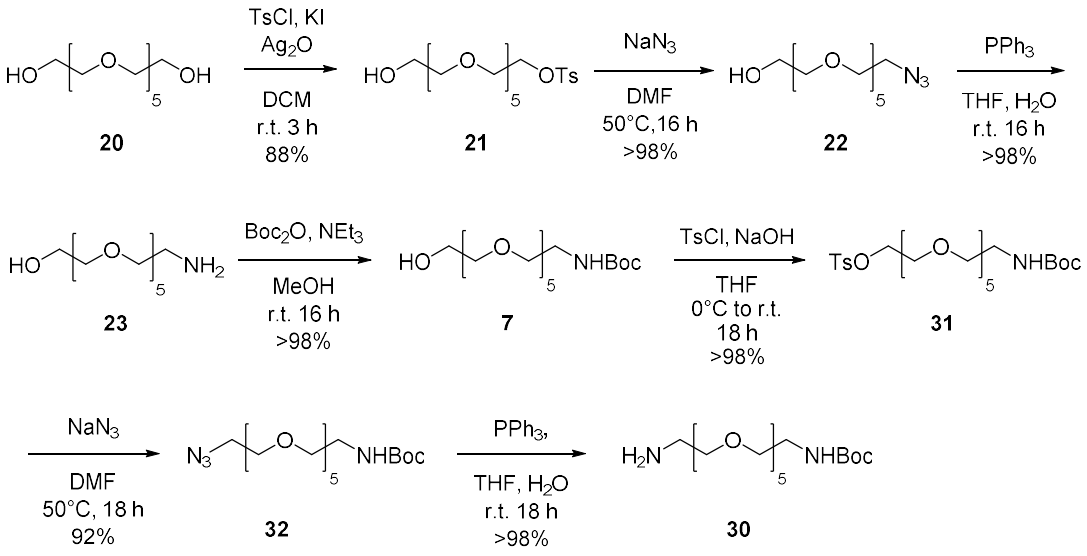

*Scheme 9: 7-step route to the mono-Boc protected diamine **30***

The subsequent coupling reaction between linker **30** and acid **6** using HATU and DIPEA was successful on a 10 mg scale to give **33**. Following this, **33** was deprotected using TFA before attempts were made to connect **2** to give staple **34** (scheme 10). However, the HATU/DIPEA coupling was unsuccessful, yielding a complex mixture of materials, including a guanidinium by-product analogous to **25**.

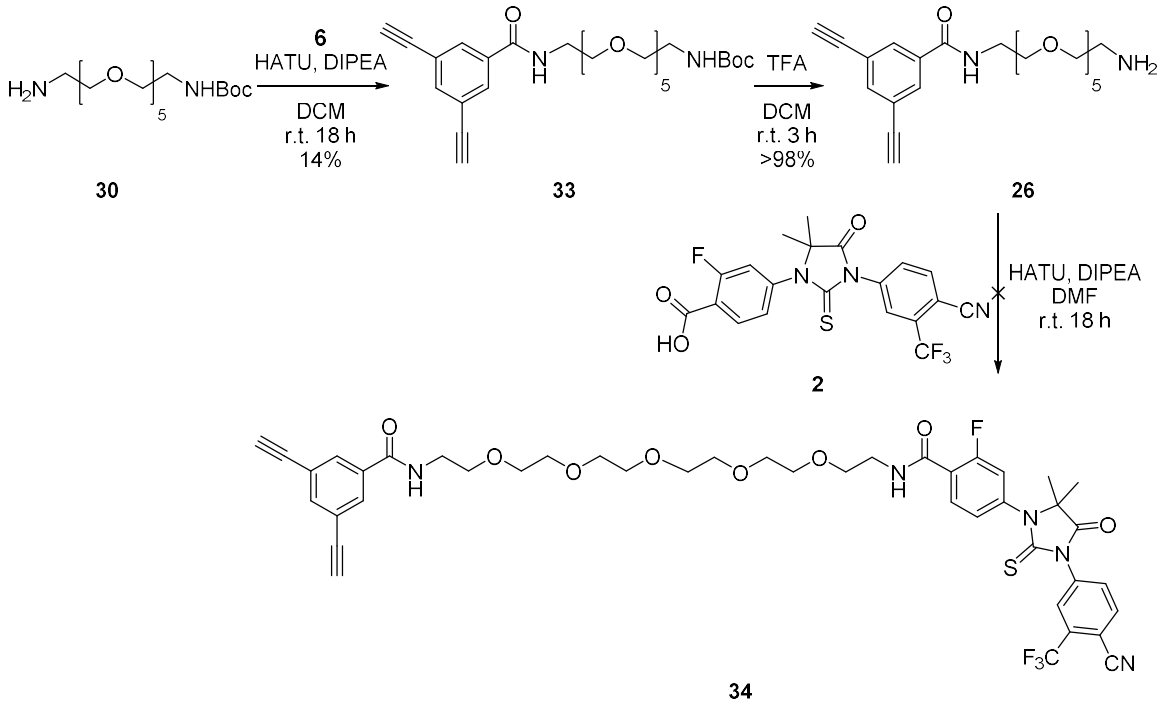

*Scheme 10: Attempted synthesis of staple motif **34***

To identify improved conditions for the amide coupling, a model system was developed. A shorter PEG chain was chosen, using commercially available 2,2'-(ethane-1,2-diylbis(oxy))bis(ethan-1-amine) **35**. The system would also serve as a shorter PEG linker for future PROTAC development.

The initial mono-Boc protection step was undertaken according to literature procedures (scheme 11).[165,166] Despite many attempts, varying the equivalents of Boc_2O used, concentration, temperature, and speed of addition, the optimal yield was only 27%. This was much lower than reported literature procedures and was thought to be due to purification difficulties commonly associated with amines due to column chromatography streaking. Due to the availability and low cost of the starting material, 27% yield was deemed acceptable for the purpose.

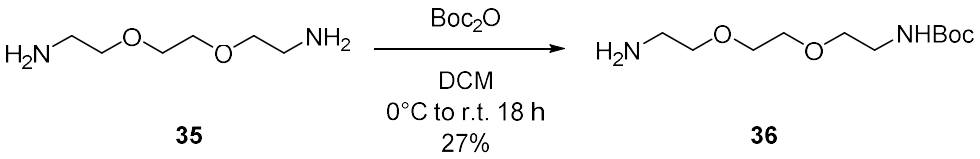

*Scheme 11: Synthesis of mono-Boc protected 3-PEG chain **36***

A screen of amide coupling conditions was then undertaken (table 3). Standard conditions using DCC/HOAt, PyAOP, HATU/DIPEA, and oxalyl chloride were attempted. Both DCC with HOAt additive and PyAOP were successful, giving **37** as the major product. Conditions using HATU/DIPEA and oxalyl chloride were unsuccessful and gave complex mixtures of products.

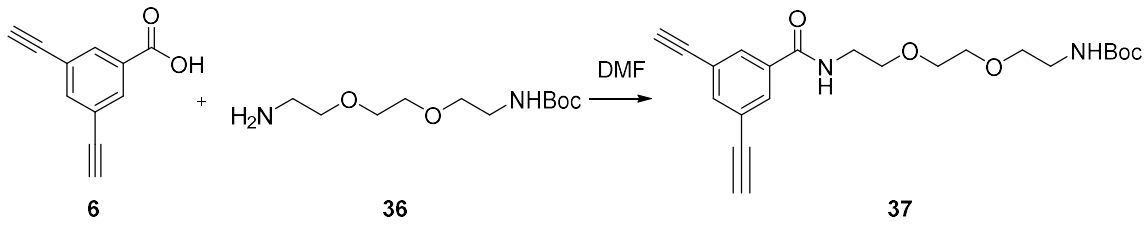

Entry	Conditions	Results
1	DCC, HOAt	Product observed
2	PyAOP	Product observed
3	HATU, DIPEA	Complex Mixture
4	$(COCl)_2$, DMF, DCM	Complex Mixture

*Table 3: Screen of amide coupling reagents for the synthesis of **37***

Following this, the *N*-Boc protecting group was removed using TFA to give **38** in good yield and purity (scheme 12).

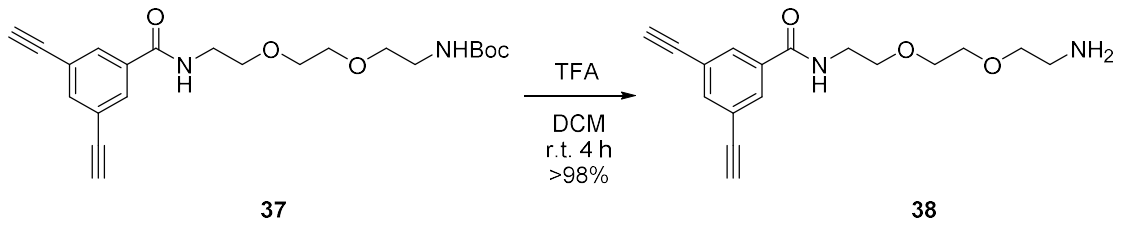

*Scheme 12: Deprotection of **37** to give amine **36***

To form staple **39**, the two sets of conditions found to be successful in the previous screen (table 3, entries 1 and 2), were attempted on milligram scales. Both reactions were successful, however DCC/HOAt conditions gave a higher yield of 36% (scheme 13).

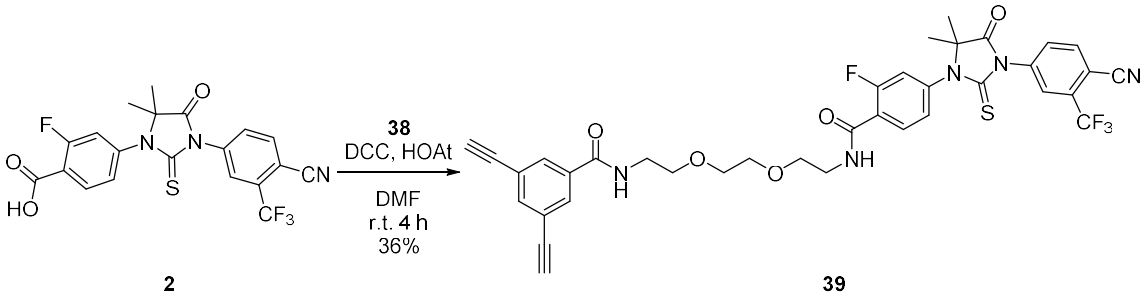

*Scheme 13: Synthesis of three-unit PEG staple **39***

After these more effective amide coupling conditions were found, they were applied to the desired six-unit PEG linker. Initially the amide coupling to give **33** was repeated using PyAOP, which gave an improved 65% yield compared to 14% for the HATU-mediated process. Following this, amide coupling of **26** with **2** was performed and staple **34** was isolated in 20% yield (scheme 14). The low yield was thought to be due to unoptimised conditions for the six-PEG linker, as well as the fact that **34** was found to be unstable to silica following 2D TLC analysis. The longer PEG chain results in a more polar compound, which elutes slower on silica compared to the three-PEG model system. Despite the low yield, additional optimisation of the reaction conditions and purification process was not attempted due to sufficient material for the subsequent stapling procedures.

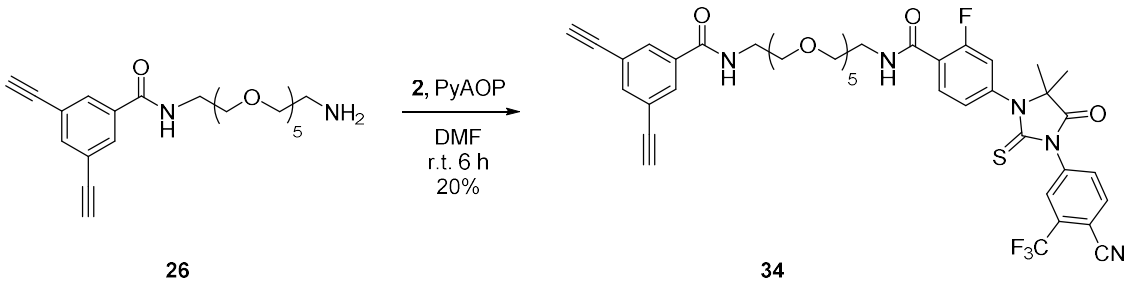

*Scheme 14: Synthesis of six-unit PEG based staple **34***

2.3.4. Synthesis of MDM2-binding peptide sequences

With the staple in hand, attention was turned to the synthesis of the peptidic part of the PROTAC. To synthesise the most cell permeable MDM2 binding peptide sequences, unnatural amino acid **43** was initially synthesised, containing the azide required for click stapling. The ornithine based azide was chosen as the three-carbon distance between the peptide backbone and the staple was found to be optimal in previous work.[167,168] Synthesis of the modified amino acid had already been reported by the Spring group,[168] and necessitates the synthesis of a diazo-transfer reagent. Reaction of sodium azide, sulfuryl chloride, and imidazole resulted in the isolation of **40** in 61% yield (scheme 15). The sulfuric acid salt was previously found to be safer and more stable than the HCl salt which can also be used.[169]

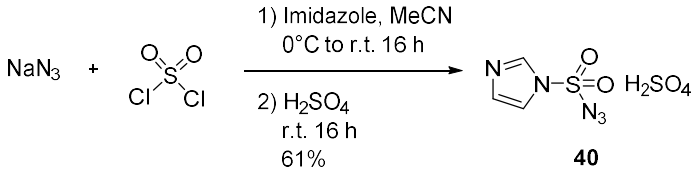

*Scheme 15: Synthesis of diazo-transfer reagent **40***

Boc-protected ornithine was then deprotected and acidified to give **42** in quantitative yield, which was then subjected to a copper-catalysed diazo-transfer reaction to give Fmoc-Orn(N_3)-OH **43** in 59% yield (scheme 16). This amino acid could then be directly coupled in solid phase peptide synthesis (SPPS).

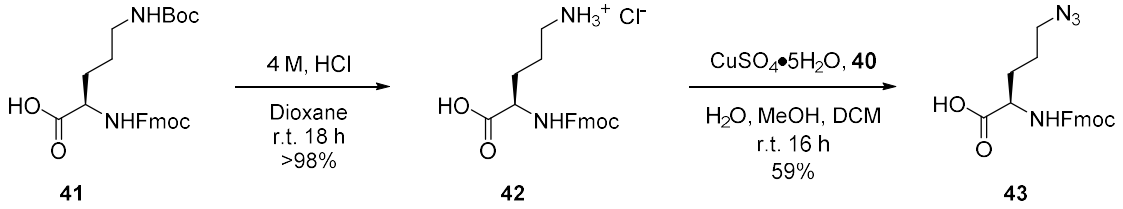

Scheme 16: Synthesis of Fmoc-Orn(N_3)-OH

Two peptide sequences were chosen for initial PROTAC formation, **P1**, and **P2** (table 4). These sequences gave high *in vitro* binding to MDM2, and both showed cell activity, although **P1** had greater cell penetration (section 2.2.3).[145]

Name	**Sequence**
P1	Ac-LTFXEYWAQLXS-NH_2
P2	Ac-TSFXEYWALLX-NH_2

Table 4: Chosen peptide sequences, where X = Orn(N_3) unnatural amino acid

Manual SPPS was used to synthesise peptide sequence **P1**, and automated SPPS was used to synthesise **P2** for the subsequent stapling experiments. Peptides were purified using semi-preparative HPLC prior to CuAAC click stapling reactions.

2.3.5. CuAAC peptide stapling

The peptide stapling reactions developed in the group use CuAAC click reactions to form 1,4-triazoles from azide and alkyne functional groups. A 1:1 ratio of *t*BuOH and water was found to be the best solvent system in previous studies. For optimal results, it was found that using $CuSO_4 \bullet 5H_2O$, THPTA ligand, and sodium ascorbate gave the most effective double click stapling.[167]

The CuAAC reaction of peptide sequence **P1** with **34** gave **PROTAC-1** (scheme 17), which was then purified using preparative HPLC. The isolated yield of **PROTAC-1** was just 27%, despite full conversion of **P1** to a single product by analytical HPLC analysis of the reaction mixture. This was thought to be due to the small scale and loss of product during HPLC purification.

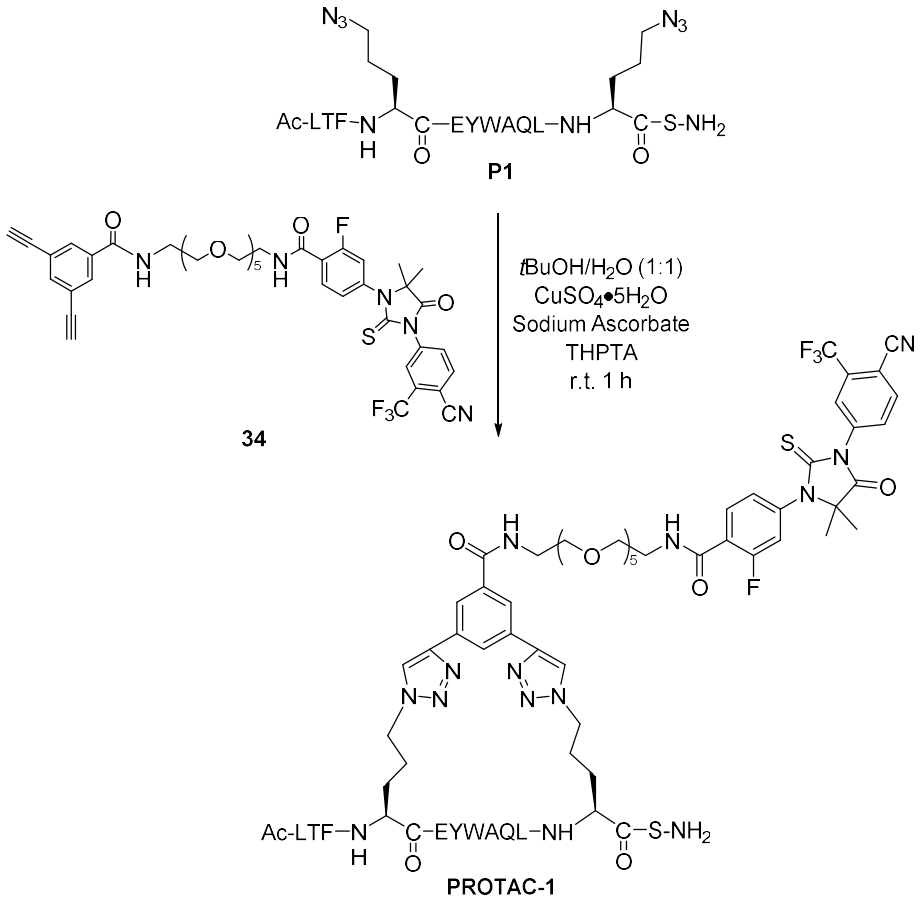

*Scheme 17: CuAAc stapling reaction to synthesise **PROTAC-1***

The stapling of **P2** with **34**, using synonymous reaction conditions, rapidly gave **PROTAC-2** in 30% yield (figure 43). Biological testing required under 1 mg of each PROTAC, hence the yields were deemed acceptable for purpose.

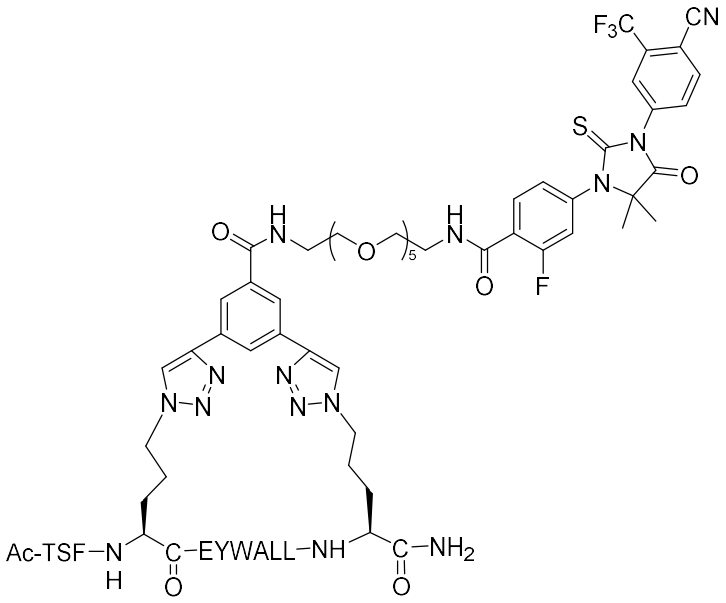

PROTAC-2

*Figure 43: Structure of **PROTAC-2***

2.3.6. Biological testing of PROTAC-1 and PROTAC-2

With the two PROTACs in hand, assessment of their biological activity commenced. Cell proliferation assays were run with Dr Daniel O'Neill (AstraZeneca). Androgen receptor positive cells, (LNCaP, lymph node carcinoma of the prostate) and AR negative cells (PC3, prostate cell line) were cultivated and treated with the two PROTACs at varying concentrations. The two cell lines were chosen to allow assessment of the activity of the compounds. The synthesised PROTACs should only degrade the AR, thus leading to reduced LNCaP cell proliferation, and should be inactive towards PC3. If PC3 cells were affected, then it would indicate cytotoxicity problems with the PROTACs. Cell confluency was measured over a five-day period (figure 44).

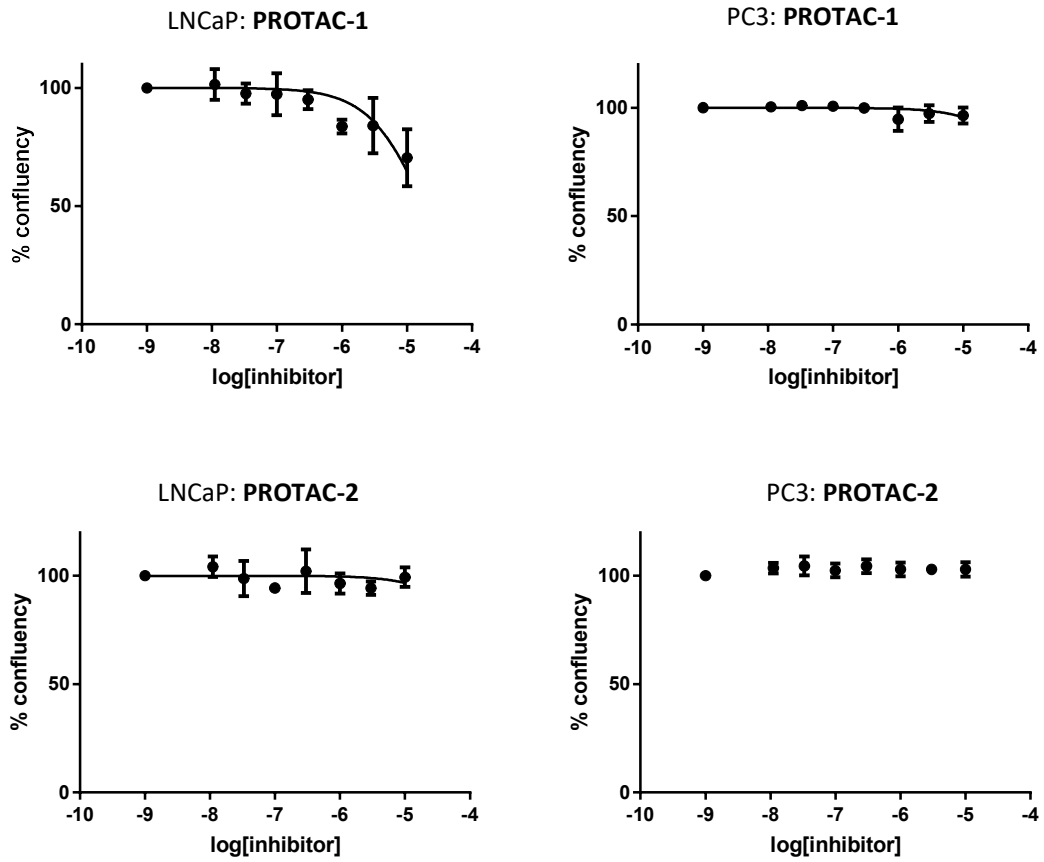

*Figure 44: Graphs showing the change in confluency of treated LNCaP and PC3 cell lines after 5 days at varying concentrations of **PROTAC-1** and **PROTAC-2**; assays performed by Dr Daniel O'Neill*

Results showed that for LNCaP cells, **PROTAC-1** had slight efficacy at the two highest concentrations: 30 µM and 10 µM. At the top concentration, **PROTAC-1** caused 30% reduction in cell proliferation. **PROTAC-2** showed no activity in either cell line. These results are in line with previous work carried out on the **P2** peptide,[145] which showed poorer cell activity, possibly due to reduced cell permeability. Importantly, these results showed that at these concentrations, no cell toxicity was observed, as AR-negative PC3 cells were not affected by either PROTAC.

2.3.7. Synthesis and biological testing of PROTAC-3

It has been shown in many previous PROTAC studies that the length and nature of the linker motif can have a significant effect on PROTAC activity (section 1.1). The first step in optimising the linker was to reduce the length, as this would result in a lower molecular weight and less polar PROTAC, potentially improving cell permeability. It was decided that the shorter, three-unit PEG linker synthesised previously **39**, would be used for the next PROTACs. The shorter length may also improve efficacy by

reducing the conformational flexibility and making the distance between the two protein complexes closer for optimal poly-ubiquitination.

It was decided that only the more active **P1** peptide sequence would be used for future PROTAC studies, as the **P2** sequence showed no activity in preliminary results. Using the three-unit PEG based staple, CuAAC click chemistry was carried out to form **PROTAC-3** (scheme 18).

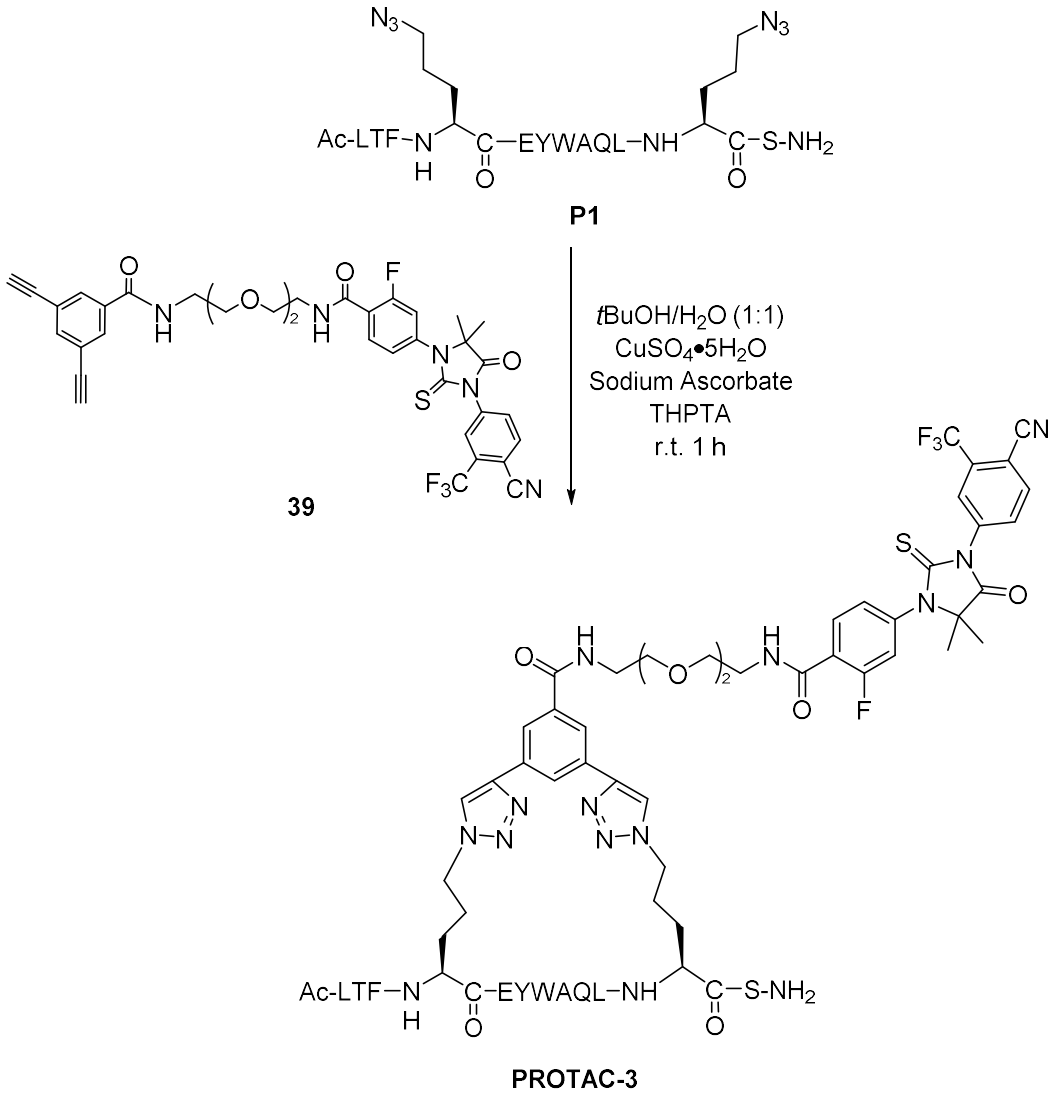

*Scheme 18: Synthesis of **PROTAC-3***

The LNCaP and PC3 cell assays used for the initial PROTAC studies were then used to assess the biological activity of **PROTAC-3** by Dr Daniel O'Neill (figure 45).

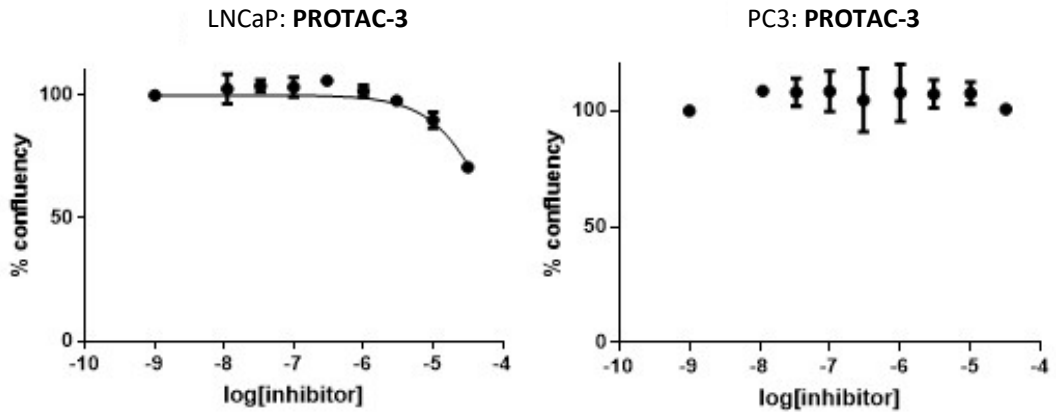

*Figure 45: Graphs showing the change in confluency of treated LNCaP and PC3 cell lines after 5 days at varying concentrations of **PROTAC-3**; assays performed by Dr Daniel O'Neill*

The graphs showed a limited effect on proliferation of the AR-positive cell line at the two highest concentrations. No effect on proliferation of PC3 cells was observed, showing the compounds do not have cytotoxicity issues. Unfortunately, the results showed no pronounced improvement on **PROTAC-1**.

PROTAC-3 was predicted to be an enhancement on **PROTAC-1**, as shortening the linker length could provide a more favourable distance between the E3 ligase and target protein. In addition, three PEG-units would ideally be more permeable than six, due to its reduced size and hydrophilicity. However, as proliferation was comparable to **PROTAC-1**, it was thought that the low activity could be related to the intrinsic properties of the PROTACs, most likely their limited cell permeability. Hence, the use of a PEG-chain linker was unlikely to be a viable option for developing highly efficacious PROTACs.

2.3.8. Synthesis of PROTAC-4 and PROTAC-5

For the 2nd generation PROTACs, it was decided that exploration of more permeable linkers would be attempted. One such linker was devised using six-carbon alkyl chains connected with amide bonds. The PEG-based linkers were thought to be too polar for optimal permeability. It was thought that this alkyl-based linker would be more effective at improving cell permeability due to its lipophilic nature. Short chain (eight linking atoms) and long chain (14 linking atoms) variants were synthesised for stapling with the **P1** peptide sequence, for a crude study of linker length effects.

The synthesis of the eight-atom linker **46** was performed using amide coupling and deprotection chemistry (scheme 19). Diyne **6** was reacted with *N*-Boc-1,6-hexanediamine to form **44** in 62% yield.

Deprotection using TFA/dichloromethane gave **45** in 87% yield. Finally, staple **46** was synthesised from the amide coupling of **45** with **2**, giving 60% yield.

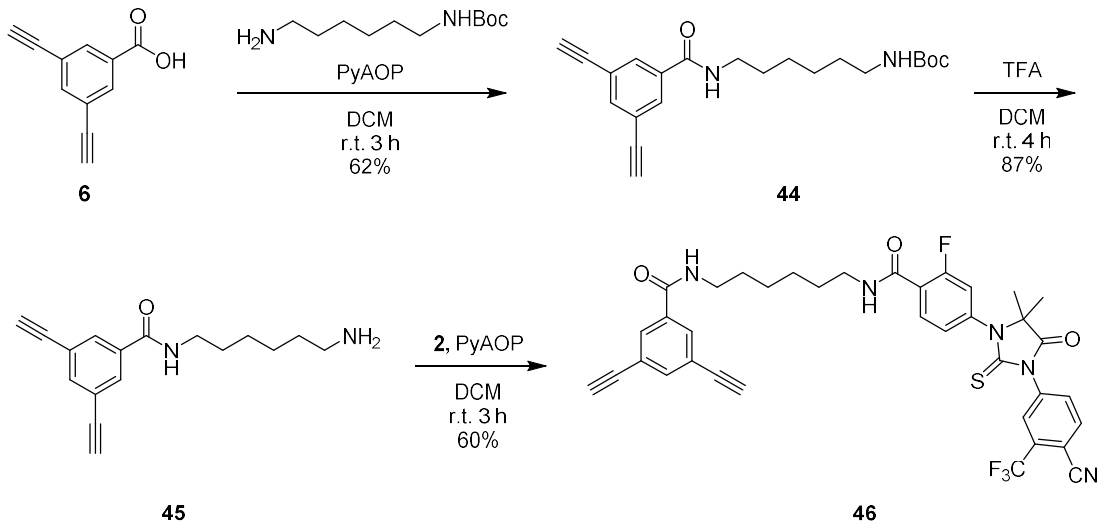

*Scheme 19: Synthesis of short alkyl linker staple **46***

To synthesise the longer linker staple **50**, amine **45** was coupled with **47**, which gave **48** in 74% yield (scheme 20). Deprotection using TFA formed **49**, which was coupled with **2**. The yield for this step was low, thought to be due to purification issues, as signs of enzalutamide decomposition were observed.

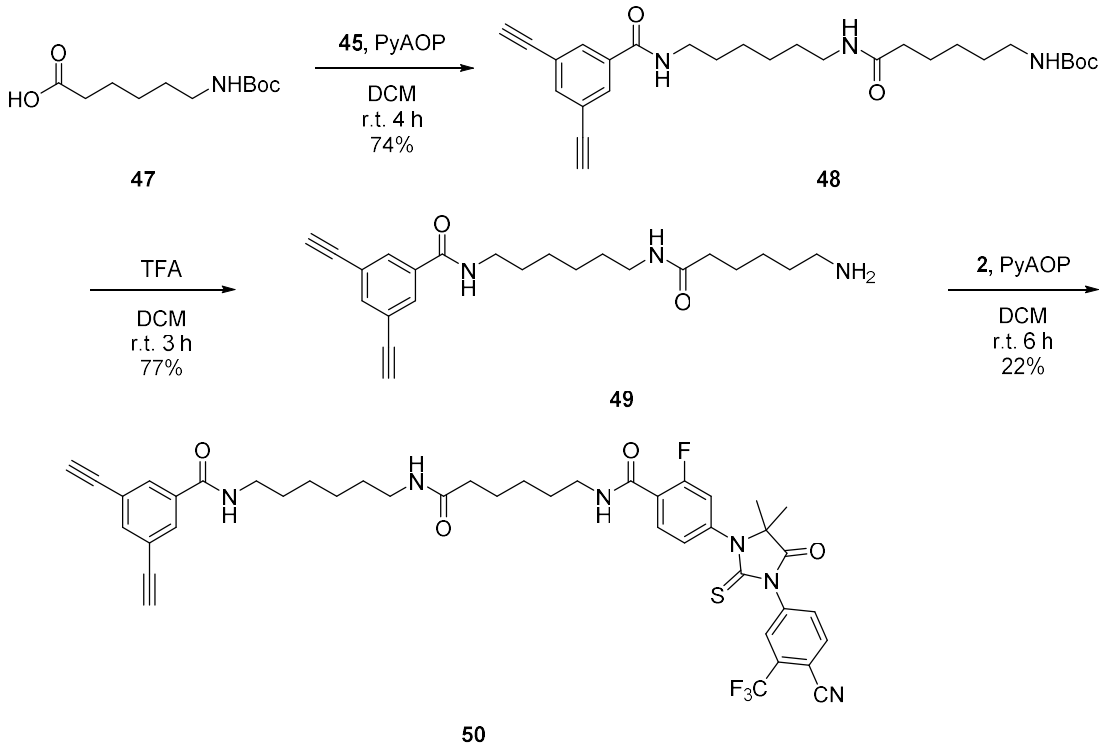

Scheme 20: Synthesis of longer alkyl linker staple

After synthesising the new alkyl-based staples, CuAAC click chemistry was utilised to form **PROTAC-4** (scheme 21).

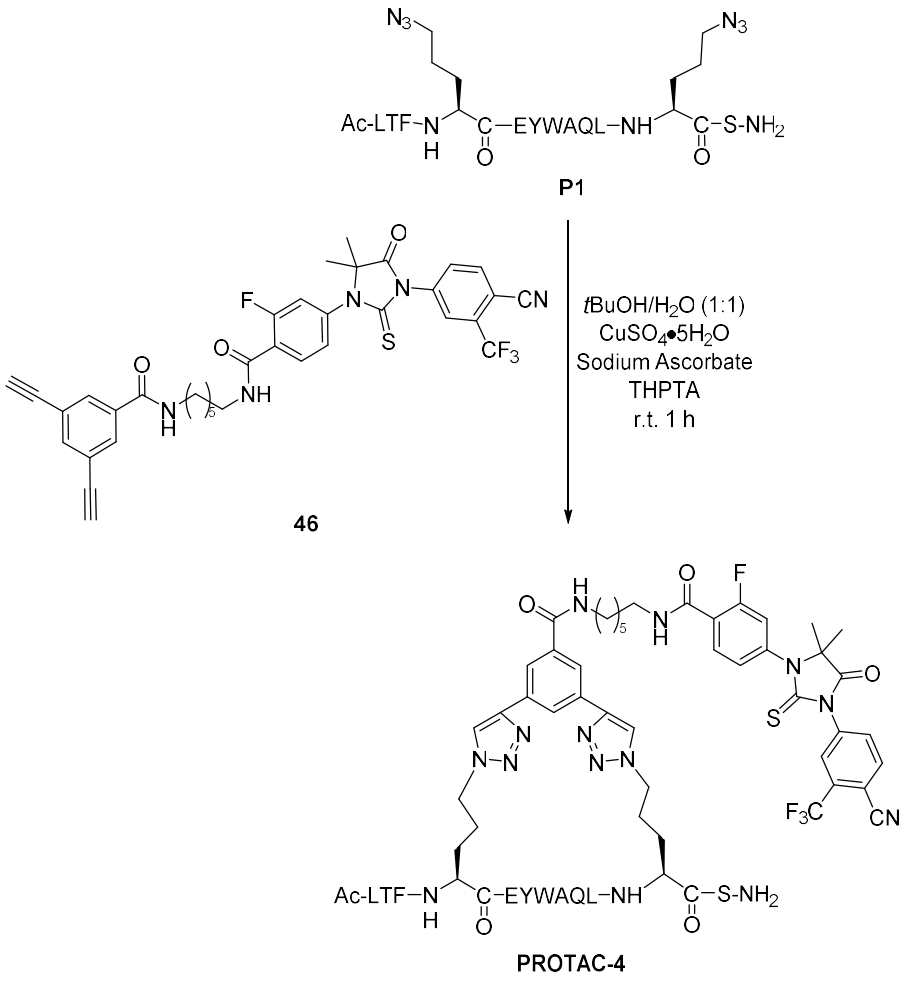

*Scheme 21: CuAAC stapling to form **PROTAC-4***

In an analogous reaction, **P1** reacted with staple **50** to form **PROTAC-5** (figure 46).

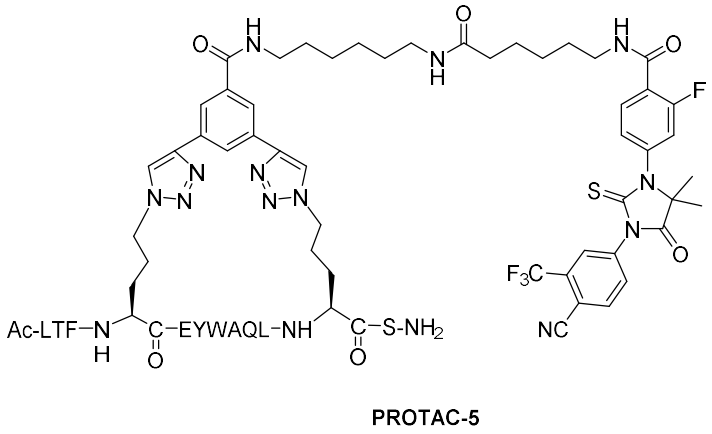

*Figure 46: Structure of **PROTAC-5***

2.3.9. Biological assessment: Cell proliferation assays of PROTAC-4 and PROTAC-5

The two 2nd generation PROTACs were then tested in AR-positive (LNCaP) and AR-negative (PC3) cells by Dr Daniel O'Neill, as previously (figure 47).

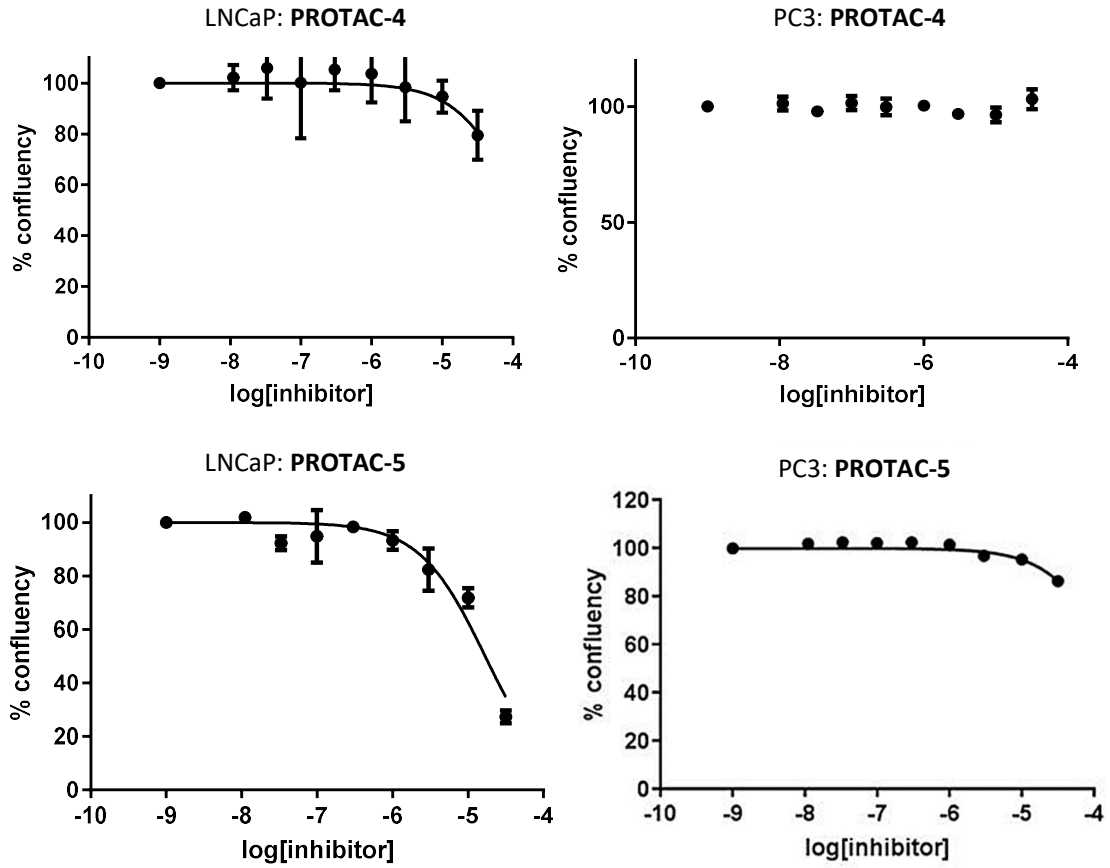

*Figure 47: Graphs showing the change in confluency of treated LNCaP and PC3 cell lines after 5 days at varying concentrations of **PROTAC-4** and **PROTAC-5** performed by Dr Daniel O'Neill*

Low levels of activity were observed with **PROTAC-4**, similarly to **PROTAC-1** there was slight reduction in proliferation at the highest concentration. Interestingly, **PROTAC-5** exhibited promising activity at the top concentration of 30 µM with a confluency reduction of *ca*. 70%, corresponding to a pIC_{50} of 4.8. This was in great contrast to **PROTAC-4** which showed minimal effects on cell proliferation, highlighting the importance of optimal linker length. The linker in **PROTAC-4** is very short compared to literature PROTACs (section 1.1.3). This may result in steric repulsion between the E3 ligase protein and AR, which limits formation of the active ternary complex, resulting in low activity. **PROTAC-5** appeared to have a slight effect on the control PC3 cells at the highest concentration. This low level of activity is classed as inactive hence does not flag cytotoxicity concerns.

Images of the control LNCaP cells and those treated with 30 µM of **PROTAC-5** showed a substantial reduction in confluency after 5 days (figure 48).

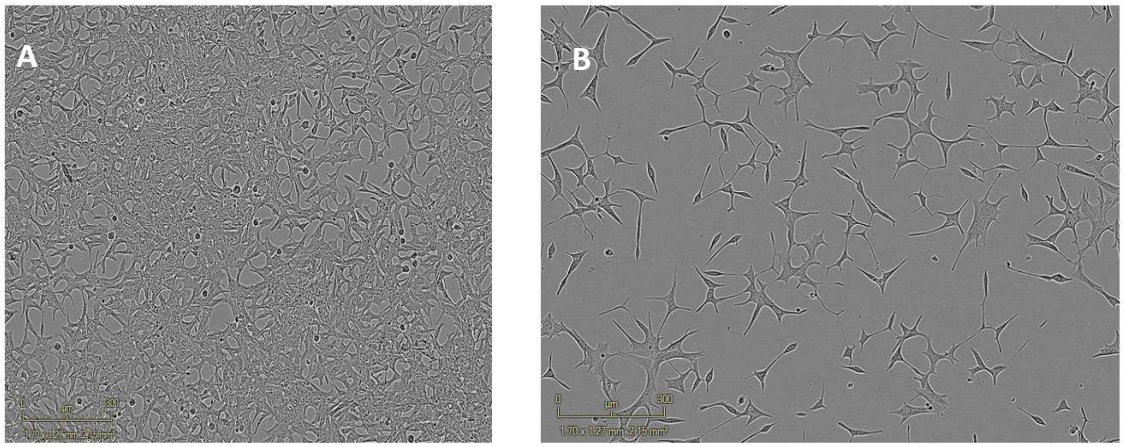

*Figure 48: A) Image of highly confluent control LNCaP cells after 5 days; B) Image of LNCaP cells dosed with 30 µM of **PROTAC-5** after 5 days; ; assays performed by Dr Daniel O'Neill*

A plot of confluence over five days showed a small reduction in cell confluency when treated with 10 µM of **PROTAC-5** compared to the DMSO control (figure 49). The maximum concentration of 30 µM gave a substantial reduction in confluency. It was noted that there were some solubility issues with **PROTAC-5**, with crystallisation occurring on addition to the assay. This was not unexpected, since the alkyl linker further reduces solubility of the already poorly soluble stapled peptide. It is possible that this crystallisation is causing the anti-proliferative effect, although if this was the case then the PC3 cells should also be affected. Results may be further improved if the solubility of the PROTAC could be increased without affecting the permeability.

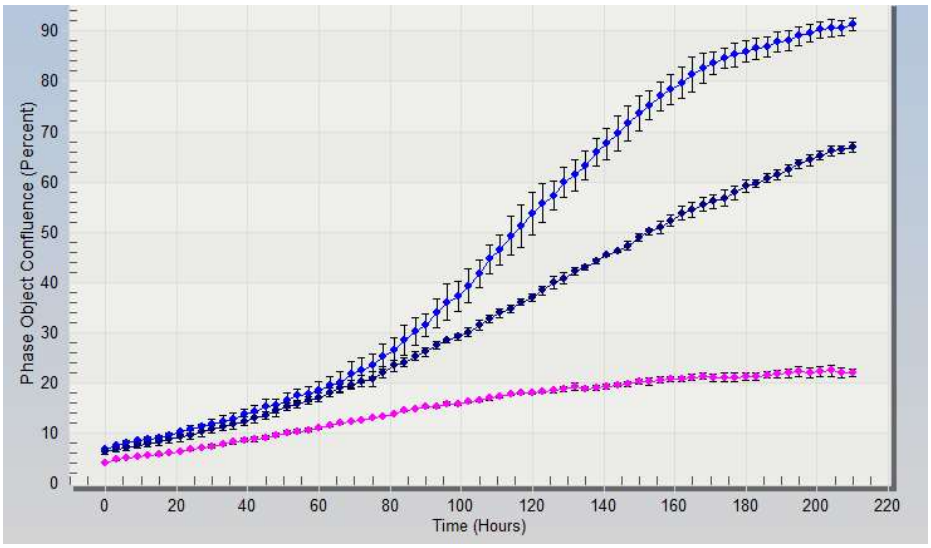

*Figure 49: LNCaP after 200 hours of growth (light blue trace: DMSO control; dark blue trace: 10 µM **PROTAC-5**; pink trace: 30 µM **PROTAC-5**); assays performed by Dr Daniel O'Neill*

Overall, the biological activity of **PROTAC-5** observed in the cell proliferation assays is a slight improvement on the cell permeable peptide-based PROTACs discussed previously (section 1.1.2). This data provides a vital indication of the viability of using stapled peptides to improve PROTAC properties.

2.3.10. Synthesis of dihydrotestosterone based PROTAC

The biological results obtained for **PROTAC-5** were very promising, however further work was required to increase the efficacy and produce a more active hit. The higher activity observed for the less polar alkyl linker compared to the PEG linker indicated that permeability may be a limiting factor. One way to improve the permeability of the PROTACs is to substitute the enzalutamide AR binder with the highly cell permeable, endogenous AR binder DHT, **51**.[170] DHT has been used in AR targeting PROTACs previously (section 1.1.2), and is known to have a very high binding affinity for AR. Due to the difference in functionality of DHT compared to enzalutamide, the previously synthesised diyne linkers were not suitable for directly attaching to DHT, hence a new synthesis was designed. Attachment of DHT to the linker *via* the hydroxyl was the most straightforward option, and unlikely to affect AR binding. The 14-atom linker was chosen due to its greater cellular activity.

DHT may be incorporated through esterification with *N*-Boc-protected aminocaproic acid, followed by a deprotection to give **53** (scheme 22). The ester **52** was attained in quantitative yield, however, following TFA deprotection, purification of **53** proved to be challenging. Although TLC analysis of **53** showed a single product, ^{1}H NMR showed impurities. It was decided that amine **53** would be used directly in the subsequent step without further purification.

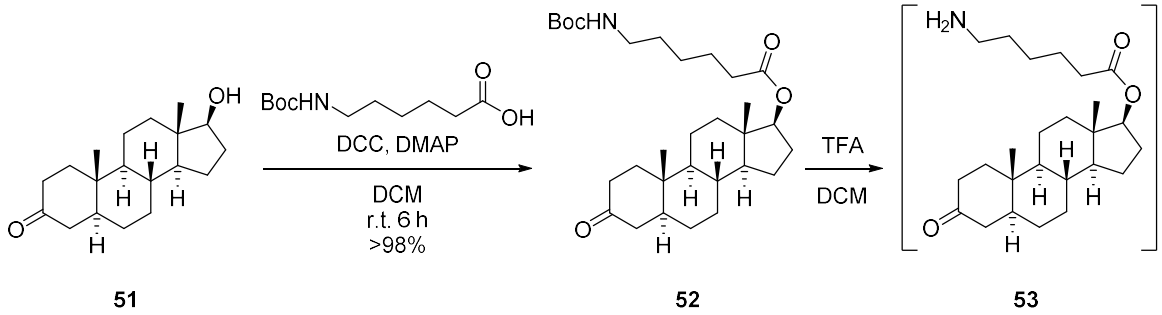

*Scheme 22: Synthesis of DHT linker **53** through esterification and deprotection*

To achieve a convergent synthesis, which would be more efficient for future elaboration of different linkers, it was envisaged that the second half of the linker could be synthesised independently through a selective intermolecular amide coupling (scheme 23). Unfortunately, no desired product was observed, likely due to intramolecular cyclisation of 6-aminocaproic acid to caprolactone. It had been thought that by activating **6** with DCC and DMAP to form the active ester, prior to the addition of the 6-aminocaproic acid, the intramolecular by-product could be avoided, however the reaction was unsuccessful.

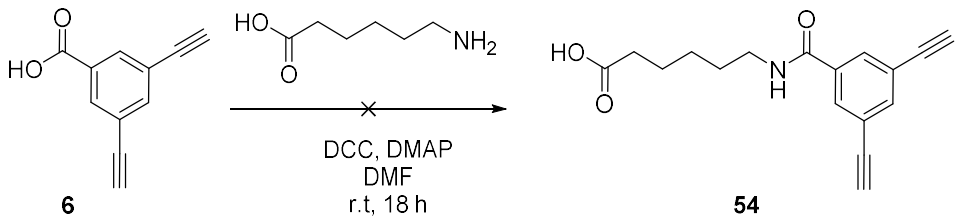

Scheme 23: Desired synthesis of second linker fragment

To overcome this problem, 6-aminocaproic acid was initially protected as *tert*-butyl ester **56** in 53% yield (scheme 24). Amine **56** was then treated with acid **6** with PyAOP to form **57** in high yield. The *tert*-butyl ester group was then removed using TFA to form acid **58** in quantitative yield.

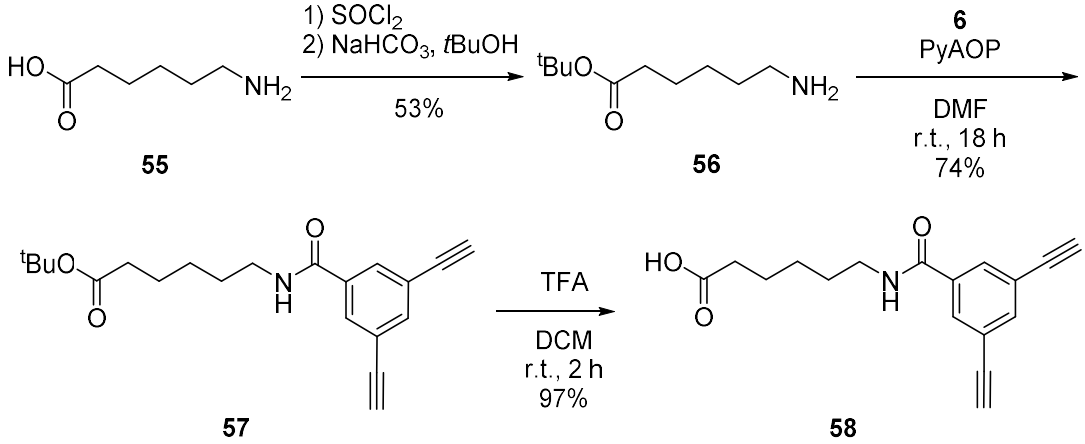

*Scheme 24: Synthesis of acid **58***

With **58** in hand, attempts were made to connect it to amine **53**, through an amide coupling to form staple **59** (scheme 25). This was found to be challenging and no product was detected by LC-MS or ^{1}H NMR despite numerous attempts. It was thought that the complication of potential imine formation between the free amine and ketone of the DHT fragment **53** was hindering the reaction, in addition to impurities associated with using crude and likely unstable amine **53**.

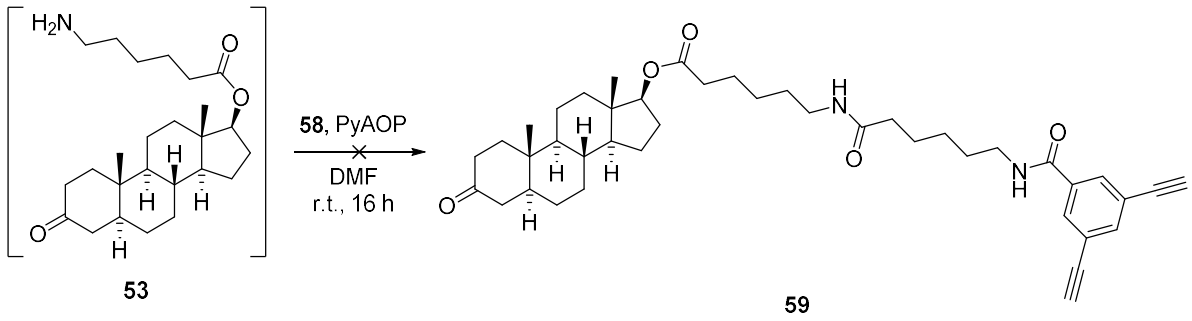

*Scheme 25: Attempted convergent synthesis of DHT staple **59***

An alternative stepwise approach from **58** was devised, where each intermediate could be purified (scheme 26). A simple procedure of amide coupling and deprotection gave acid **60** which could then be esterified using the DHT to give staple **59**. The final step in this sequence gave a fairly poor yield, thought to be due to the small scale of the reaction which resulted in more significant losses in the work up and purification procedure, in addition to steric issues resulting from the very hindered DHT alcohol. Adequate material was obtained for stapling purposes, hence the reaction was not optimised.

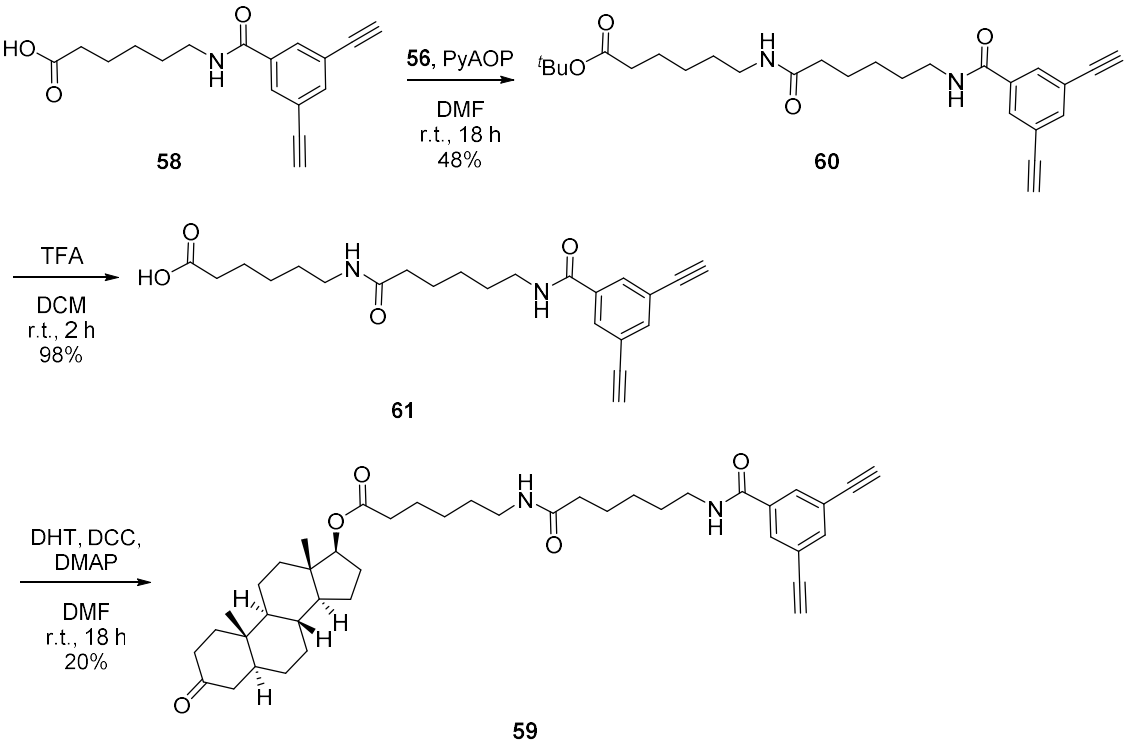

*Scheme 26: Successful synthesis of staple **59***

The final step to form **PROTAC-6** is the 'click' stapling to peptide **P1**, which was performed under the previous conditions and was successful in forming this PROTAC (scheme 27).

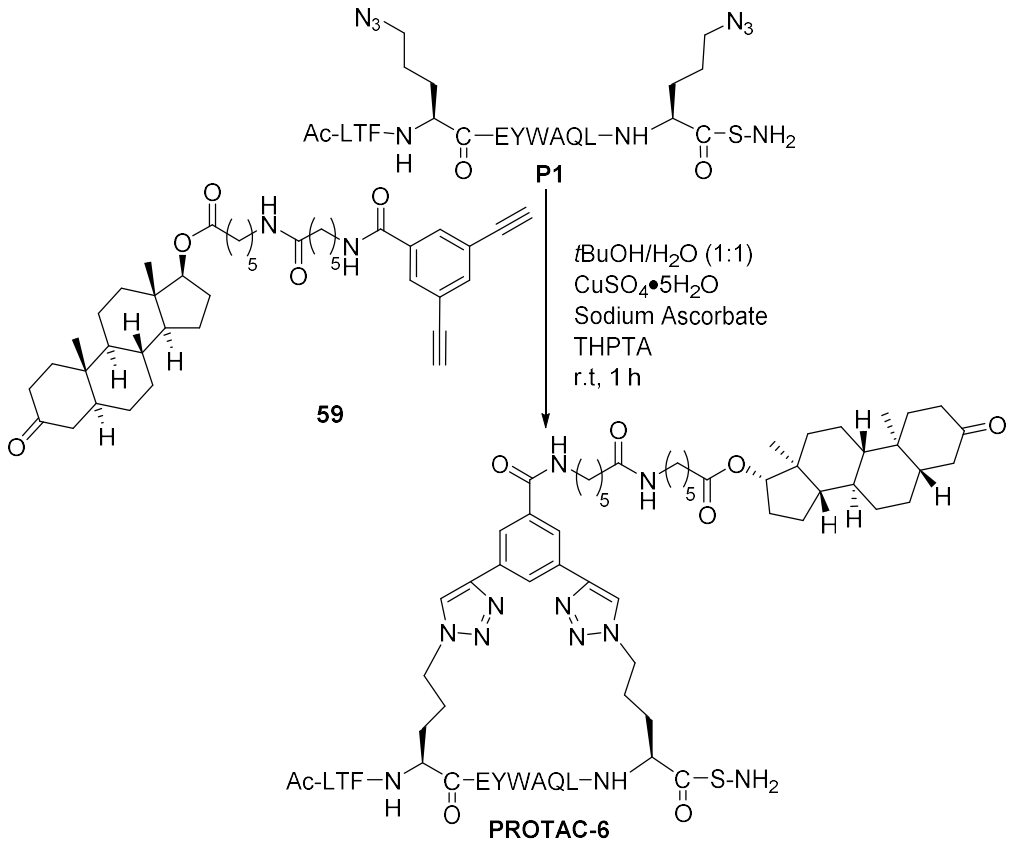

Scheme 27: Synthesis of PROTAC-6

2.3.11. Biological assessment: High Throughput CETSA Evaluation

PROTACs 1-**5** were previously analysed through cell proliferation assays to establish cellular activity, however these assays were unable to identify the cause for the antiproliferative effect, which could be complex in a cellular environment. Therefore, the most promising candidates **PROTAC-5** and **PROTAC-6** were tested in an assay which could specifically evaluate AR levels to confirm the PROTAC mechanism of action.

In recent years there has been greater focus on developing assays to establish target engagement in a cellular environment, which can provide a direct measurement of the cellular activity of different drugs. These assays provide more information than typical enzymatic assays as fundamental properties such as permeability and cellular stability will impact the results, making it more predictive of clinical efficacy. Cellular thermal shift assays (CETSA) have been developed for this purpose. CETSA provides an understanding of in-cell target engagement through the thermal stabilisation of a target protein when bound to a ligand.[171]

Protein thermal melting curves of purified proteins have been used to establish target binding through thermal shift assays (TSAs). A protein is treated with a compound and the melt curve is then measured, a positive shift in the melt temperature (ΔT_m) is indicative of a compound interacting with and stabilising the protein.[171,172]

CETSA takes the principles of TSA and applies it within a cellular environment. General cellular assays monitor drug efficacy through downstream responses rather than direct binding affinity, for example a cell proliferation assay, and this can lead to a poor understanding of a drugs action.[171] CETSA directly measures target engagement within a cell, which is necessary to conclusively validate the biological activity of a drug. Label-free and physiologically relevant methods of measuring target engagement are extremely useful for high throughput screening in early drug discovery. However, this technology has only been reported for a handful of cellular targets.[173]

A high-throughput CETSA protocol has recently been developed in a prostate cancer cell line endogenously expressing AR.[174] Differentiating between AR binders and AR co-regulator binders has been a significant challenge for the identification of new AR antagonists. This assay can differentiate between AR and related targets. The assay involves heat shocking the compound-treated cells over a range of temperatures causing AR to unfold and aggregate. Then the remaining levels of soluble AR is measured against the thermally denatured and precipitated proteins. The ΔT_m of AR depends on the protein's thermal stability and stabilisation occurs in the presence of a bound inhibitor. To increase the throughput of this assay, the soluble AR levels were quantified using AlphaScreen® FRET technology which measures an output fluorescence signal using an AR binding antibody pair. In the absence of a heat shock, this technology enables quantification of cellular AR levels in response to treatment with a PROTAC to determine whether AR degradation is occurring.

These CETSA assays were expected to indicate whether the antiproliferative effect of **PROTAC-5** observed previously in cell proliferation assays (section 2.8.2) was a direct result of AR degradation. This assay was conducted with the help of Dr Joseph Shaw (AstraZeneca), for **PROTAC**-**5** and **6** along with an assortment of controls (figure 50).

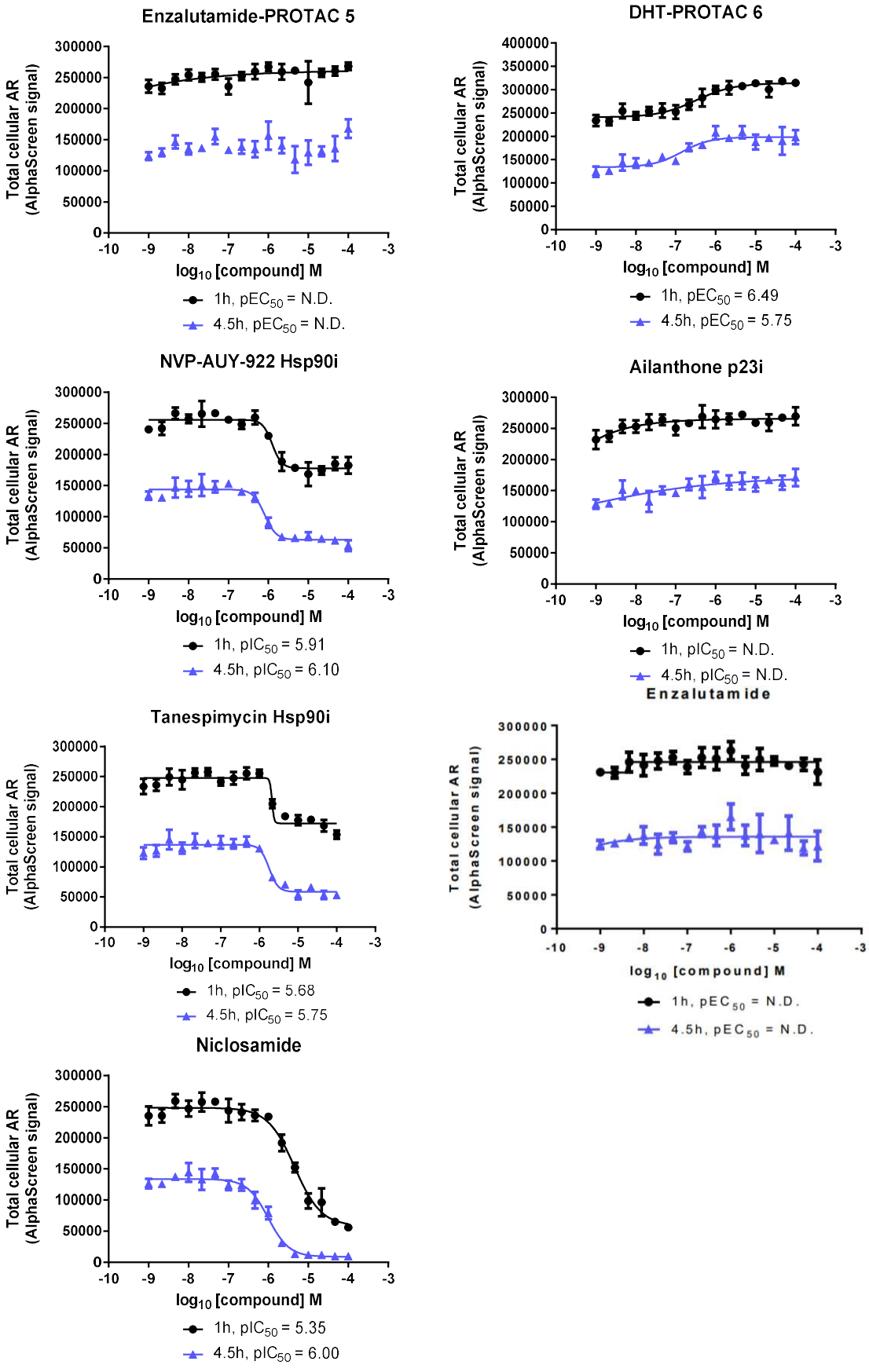

Figure 50: CETSA determined IC_{50} values for PROTACs and control compounds, performed with Dr Joseph Shaw

Unfortunately, no AR degradation was observed for **PROTAC-5**, and a slight increase in AR levels was observed for **PROTAC-6** indicating agonistic activity. Positive controls NVP-AUY-922, tanespimycin (both AR chaperone heat shock protein 90 inhibitors), and AR downregulator niclosamide all showed the expected lowering of AR levels. Negative controls ailanthone (p23 inhibitor) and enzalutamide showed no significant effect on AR levels, validating the assay. The assay was repeated over two timepoints 1 h and 4.5 h; AR degradation by the PROTAC mechanism is rapid and should be observed within this timeframe. The endpoint AR signal was lower after 4.5 h across all compounds due to the general instability of the cells observed over longer periods.

There were many potential reasons for the failure of these PROTACs to degrade AR. The PROTACs could have been unable to bind MDM2 or AR, unable to form the correct ternary structure conformation for efficient ubiquitination, suffer from instability or have poor cell permeability. The binding of the PROTACs to MDM2 and AR could be tested using either enzymatic or cellular assays with the respective proteins. The ternary structure conformation was much more difficult to understand without generating a crystal structure of the PROTAC bound to the two proteins, which is highly challenging. The permeability of stapled peptides was known to be a major challenge, due to their large size and polarity. Attaching the linker and enzalutamide staple to the peptide almost doubles its molecular weight, which may further reduce its cell permeability.

Further biological testing was required to understand why these PROTACs are inactive. However, the general complexity of PROTACs makes it very challenging to fully understand and resolve these issues. Testing the binding of the PROTACs to each protein partner was hypothesised to be a simple way to better understand these PROTACs.

2.3.12. Biological assessment: MDM2 expression, purification and competitive FP

In order to further investigate why the synthesised PROTACs were unable to degrade AR, the PROTACs binding affinity toward MDM2 was measured. Recruitment of MDM2 by the PROTAC is vital for the proteasomal mediated degradation of a target protein, thus if the peptide staple hindered its ability to bind MDM2, no AR degradation would be observed.

The MDM2 protein was expressed and purified with the assistance of Rohan Eapen in the lab of Dr Laura Itzhaki in the Department of Pharmacology. Firstly, the gene encoding for the region of MDM2 residues 6-125, which form the p53/MDM2 PPI interaction site, was cloned into a pRSETa vector from a plasmid provided by the Itzhaki group, which contained the gankyrin gene in addition to the MDM2 sequence (figure 51).

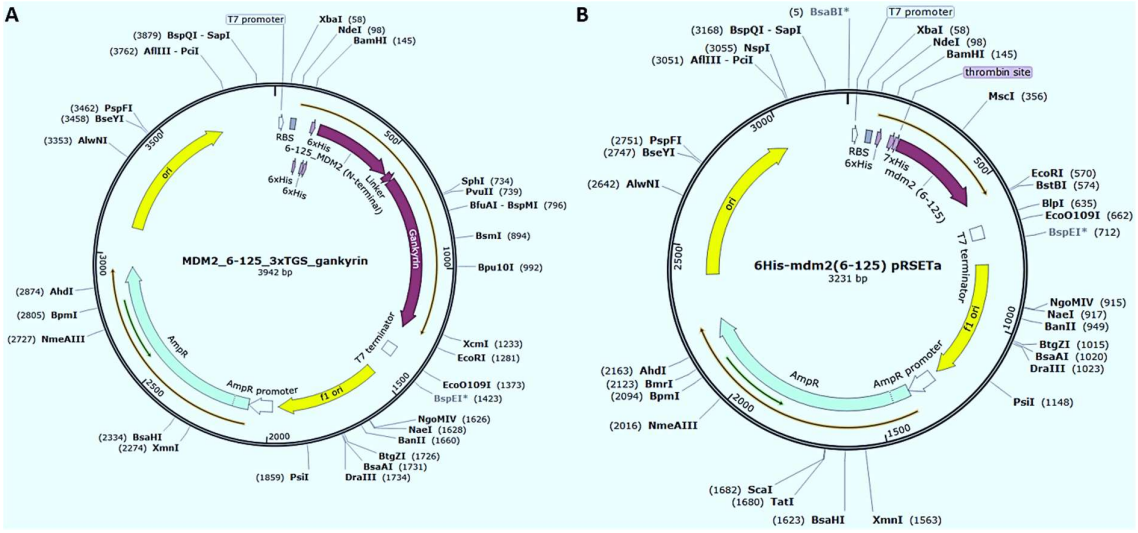

Figure 51: A: Composition of initial plasmid encoding gankyrin; B: Composition of generated plasmid encoding for MDM2

Next, the generated plasmid was amplified, the transformants sub-cultured and the DNA extracted prior to purification and analysis (figure 52A). The plasmid was then transformed in the *E. coli* expression cell line, C41(DE3), induced with IPTG, and the protein extracted. The protein was purified by His-tag trap, before treatment with thrombin to remove the tag. Finally, purification of the protein by high-performance ion exchange chromatography yielded MDM2 (6-125) protein, which was analysed by SDS-PAGE analysis (figure 52B). In this instance, it was found that the His-tag cleavage was unsuccessful, thus the protein generated was 6-His-tag MDM2 (6-125). This was not expected to affect the subsequent competitive FP experiments, as this tag was distal from the MDM2 binding site.

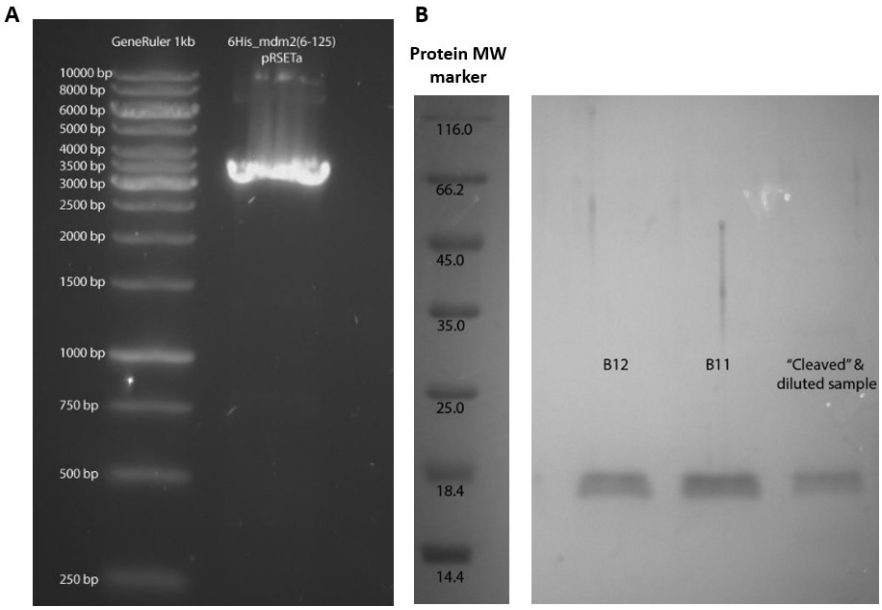

Figure 52: A: Amplified plasmid gel showing purity; B: SDS-PAGE of recombinant MDM2 protein following purification

With the recombinant MDM2 protein in hand, binding affinity of the stapled peptide PROTACs to MDM2 was assessed through competitive fluorescence polarisation (FP) as previously described.[147,175] Generally, in a competitive FP experiment a compound of interest is titrated against a fluorescently labelled protein binder of known binding affinity, known as the tracer, and the protein. This allows quantification of the strength of binding of a compound to the protein, assessed by the compound's ability to outcompete the tracer. The tracer used for these experiments was a 5-TAMRA-labelled peptide sequence (TAMRA-RFMDYWEGL-NH_2) based upon the native p53 MDM2 binding sequence and reported to bind MDM2 with a K_d value of 17.6 ± 1.7 nM.[175] Additionally, positive controls of **P1** and nutlin 3a were used to validate the generated six-His-tagged MDM2 protein.

PROTACs 3, **4**, and **5** were established to be potent MDM2 binders in this assay, with calculated K_d values of 68, 53, and 38 nM respectively (figure 53). Although the potencies calculated are slightly lower than the stapled peptides prepared in previous studies,[123] they are of the same order of magnitude indicating that the staple motif does not significantly hinder MDM2 binding.

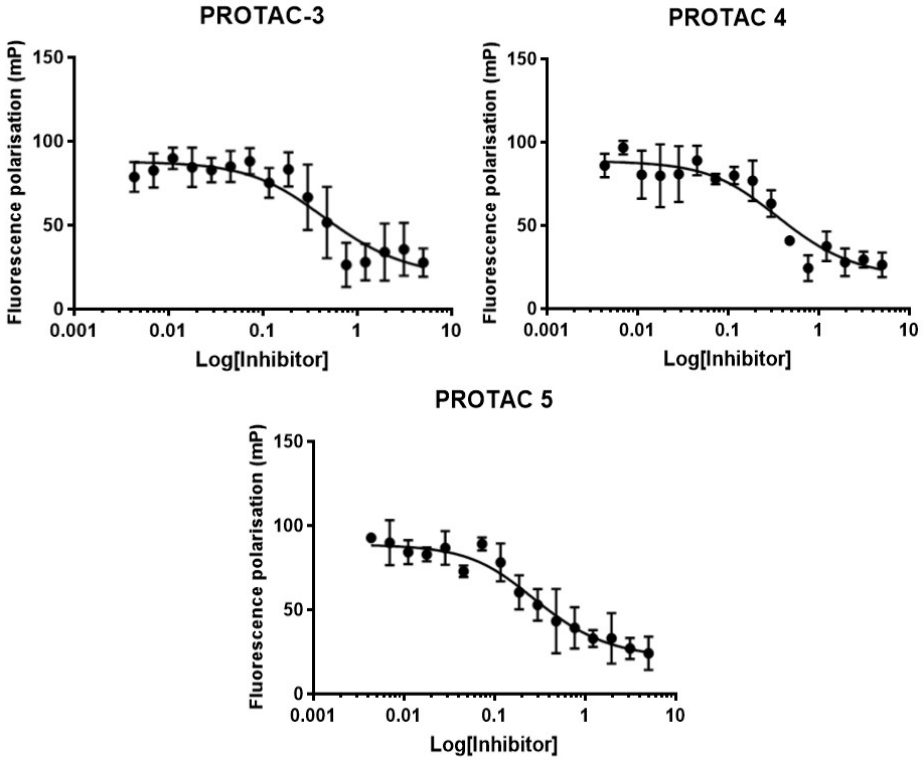

*Figure 53: Competitive FP curves for **PROTAC 3-5** establishing potency against MDM2*

Although **PROTAC-6** was not tested in this assay due to its limited supply, it was envisaged that the extent of MDM2 binding would be similar to **PROTACs 3**-**5** as a result of similarities between the PROTACs structure and size.

2.3.13. Biological Assessment: AR recruitment

With activity against MDM2 confirmed, AR recruitment was investigated. This was performed by Dr Joseph Shaw using the CETSA target engagement protocol to determine intracellular AR binding in LNCaP cells in both the antagonist (figure 54A) and agonist binding modes (figure 54B). For the antagonist mode, competition of 1 nM DHT added causes a reversal of DHT-induced thermal stabilisation after the 46 °C heat shock, which causes a decrease in AlphaScreen® signal. The agonist mode results in an increased AlphaScreen® signal after heat shock.

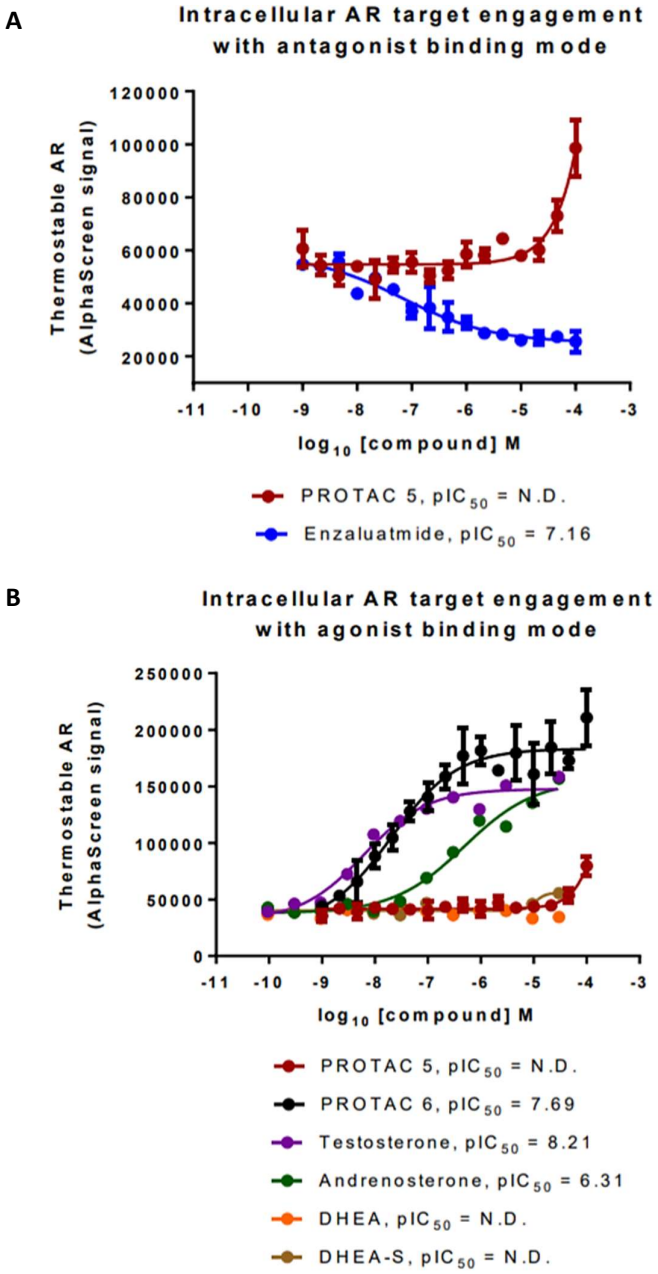

Figure 54: CETSA to show AR target engagement with both antagonist (A) and agonist (B) binding modes, performed by Dr Joseph Shaw

The ability of these enzalutamide derived PROTACs connected using the acid handle to bind AR is well-known in literature and patents,[64,74,176–178] hence this cellular assay was predominantly chosen to assess cell permeability and cellular stability.

PROTAC-5 was unable to bind AR in the antagonist binding mode cellular assay, compared to the positive control enzalutamide which bound with a pIC_{50} of 7.16. Although this implies that **PROTAC-5** is fundamentally unable to bind AR, the enzalutamide motif used is prominent in the literature and patents and AR binding is well-known. Hence, assuming this motif is capable of binding AR, the most likely reason for this negative result is the poor cellular permeability of **PROTAC-5**. It is likely that **PROTAC-5** is completely unable to cross the cell membrane to engage with AR.

PROTAC-5 and **PROTAC-6** were then examined in the agonist binding mode assay. As expected **PROTAC-5** showed insignificant levels of activity, as enzalutamide is an AR antagonist. **PROTAC-6** was found to bind AR with a pIC_{50} of 7.69, slightly lower than that of testosterone (pIC_{50} = 8.21). DHT is known to be a stronger AR binder than testosterone.[170] It is unknown from this assay whether **PROTAC-6** can cross the cell membrane or whether the cell stability of this PROTAC is low and the ester bond connecting the linker to DHT is hydrolysed to release the permeable and potent free DHT.

These results were extremely useful in answering some of the previously mentioned questions. Both PROTACs were unable to cause degradation of the AR. There may be several contributing factors causing this, however it is most likely to be the stapled peptides poor cellular permeability. Results for **PROTAC-6** have implied either a lack of intrinsic stability resulting in release of free DHT, which was anticipated due to the ester connection used, or again poor cellular permeability.

Despite the inconclusive nature of these results, further biological testing was not pursued. This was because regardless of the exact reason for their lack of activity, these issues with permeability or ternary complex formation would be extremely difficult to overcome. AR binding could be directly assessed using enzymatic assays, such as competitive FP and permeability assays such as PAMPA or Caco-2 could be used to quantify the exact level of cell permeability. However, there was no straight-forward access to these assays, hence this data was not pursued. In addition, the results would not be particularly useful for development of stapled peptide PROTACs, as imparting permeability to stapled peptides is not trivial.[179]

PROTACs recruiting MDM2 as an E3 ligase are not well known in literature compared to other E3 ligases such as VHL and cereblon. An alternative approach to developing MDM2-recruiting AR degrading PROTACs is to move to a small molecule approach. Small molecules are more inherently permeable than stapled peptides hence the resulting PROTACs are more likely to degrade AR.

2.4. Chapter 2: Conclusions

To conclude, novel stapled peptides have been synthesised aiming to degrade AR using MDM2 as an E3 ligase. The peptide sequence used is a p53 derived sequence previously shown to have a high affinity for MDM2. Through two-component peptide stapling it was possible to simultaneously stabilise the resulting stapled peptide and attach a linker and AR binding motif to generate the desired PROTAC. With this design, six stapled peptide PROTACs were generated, exploring different peptide sequences, linker lengths and types, and AR binding motifs.

Initially, the PROTACs were tested using AR cell proliferation assays of AR positive LNCaP cells and AR negative PC3 control cells. Little activity was observed for **PROTACs 1**-**4**; however, **PROTAC-5** showed a significant reduction in proliferation of the LNCaP cell-line at top concentration of 30 µM and limited activity at a lower concentration of 10 µM, with a pIC_{50} of 4.8. No antiproliferative effect was observed with AR negative PC3 cells indicating an AR dependent effect.

In addition, **PROTAC**-**6** was generated which used cell permeable endogenous steroid DHT to bind AR. However, when tested in direct AR degradation CETSA assays, no degradation was observed for **PROTAC**-**5** or **PROTAC**-**6**. **PROTAC**-**6** increased levels of AR, indicating that the DHT motif was working as an agonist. This was likely a result of the unstable ester linkage which was used to connect the DHT motif to the linker, which could be rapidly hydrolysed in a cellular setting to release agonist DHT. Ester bonds are well known to be fairly unstable in a cellular environment, a property often exploited for use in pro-drugs.[180]

Further studies of the stapled peptide PROTAC series showed that the PROTACs were able to bind MDM2 in competitive FP assays, with high potency. Unfortunately, **PROTAC-5** did not exhibit AR binding in a cellular assay indicating limited permeability which is known to be a problem for stapled peptides. **PROTAC-6** did show AR binding in the cellular agonist assay mode; however, this was thought to once again indicate the poor stability of this PROTAC.

Overall, after promising initial results, these PROTACs were found to be incapable of degrading AR in a cellular setting. Although the specific reasons behind this lack of activity were not conclusively shown, it was decided that the limitation of poor cellular permeability was too significant of an issue to overcome.

2.5. Chapter 2: Future Work

Synthesis of PROTACs with greater cell permeability is required to drive the cellular activity of stapled peptide PROTACs. One way to improve permeability is to append a cell penetrating tag to the PROTAC, which uses properties of known cell-penetrating peptides to promote cellular-uptake.[181] Examples include incorporation of a poly-arginine tail. It has been observed that polycationic peptides with chain lengths varying between 7 – 20 residues are able to enter cells more easily than neutral peptides.[182] The uptake of these peptides is commonly through endocytosis, however passive mechanisms have also been reported.[183] Poly-arginine chains could be incorporated into the PROTAC either as an alternative to the alkyl linker (figure 55A), or, if this additional bulk was found to disrupt poly-ubiquitination, it could be incorporated directly into the MDM2 peptide sequence, providing it doesn't affect intrinsic binding properties (figure 55B). A limitation of this approach is the potential for lysosomal entrapment, where the stapled peptide enters the cell through endosomes and is unable to escape.[184]

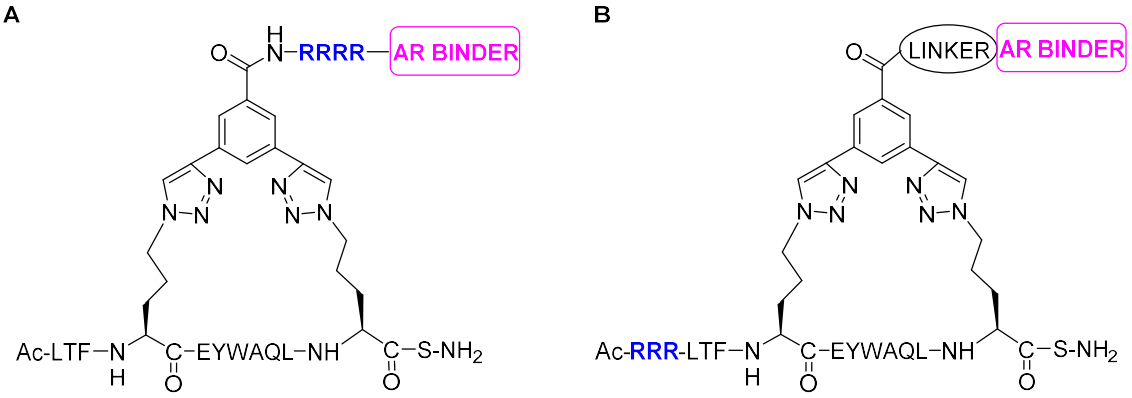

Figure 55: Methods of incorporating cell penetrating tag, A: as a PROTAC linker; B: directly into the peptide sequence

Another method of improving the permeability of stapled peptide PROTACs is through an *in situ* stapling strategy. This would require attachment of the AR binder and linker to a double SPAAC linker such as the Sondheimer diyne linker described previously (section 2.2.3). This means the peptide and linker could be introduced to cells separately to significantly reduce the molecular weight, increasing the likelihood of good permeability (figure 56A). Once in the cell, the components could react through a biorthogonal click to generate the full PROTAC structure. This strategy was previously shown to improve the cellular activity of these stapled peptides.[145] This approach was applied to PROTACs by Lebraud *et al.* and termed CLIPTACs.[185] CLIPTACs were prepared by splitting cereblon-recruiting small molecule PROTACs into two components and attaching a click precursor on each side. These CLIPTACs were shown to degrade two oncology target proteins BRD4 and ERK1/2 in a cellular environment. The challenge of using this method to generate stapled peptide PROTACs is the limitations in biorthogonal

double click reagents, which are typically challenging to synthetically modify.[186] An alternative approach would be to generate a stapled peptide with a click component attached and treat it with a click modified linker and AR binder in the cell (figure 56B). This approach would be synthetically simpler, however the permeability of this type of stapled peptide is unknown. PROTACs constructed using similar copper-catalysed click methodology to conjugate the two protein binders together have been shown to be highly effective and the modularity of the toolbox increases overall efficiency.[187]

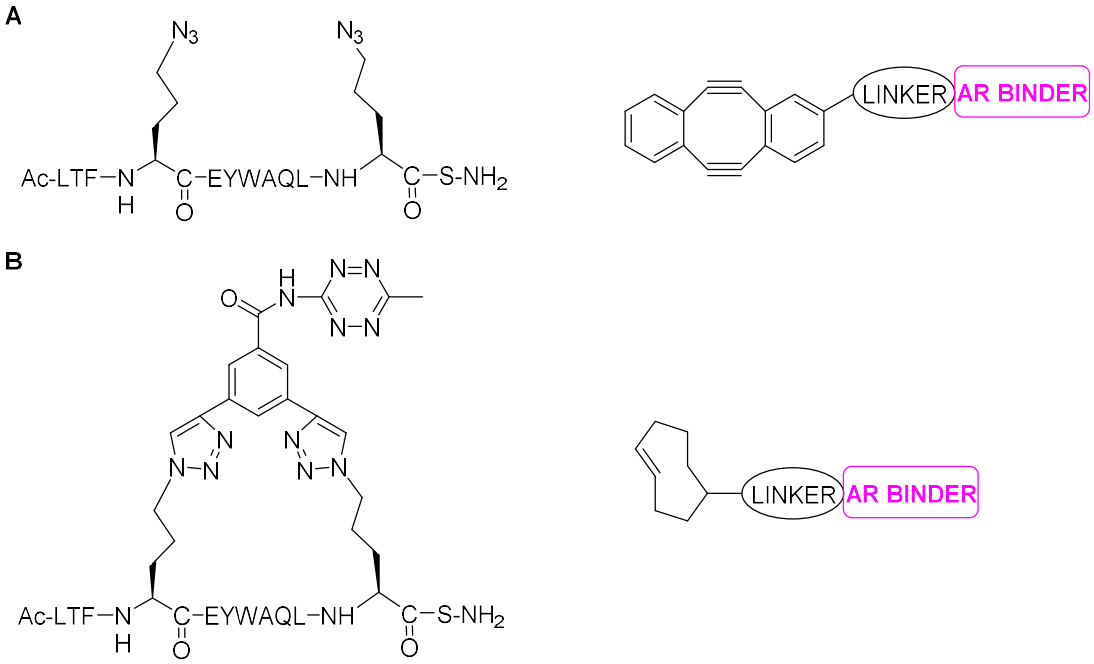

Figure 56: Approaches to in situ click to generate PROTAC, A: using double SPAAC for stapling and AR binder attachment; B: using single click reagents

Overall, strategies exist to generate stapled peptide PROTACs capable of overcoming the intrinsic permeability limitations. However, since the surge in activity of small molecule PROTACs, the use of peptide components has become considerably less popular. There is still some interest in this area, with a recent publication using stabilised peptides to degrade the ER α.[188] This paper reported the attachment of a peptide sequence targeting ERα *via* a short carbon linker to a peptide sequence targeting VHL. The ERα targeting peptide sequence was cyclised through one-component peptide stapling methods to stabilise the PROTACs. These PROTACs degraded ERα in a cellular environment with a DC_{50} < 20 µM, this is considerably less potent than small molecule alternatives. Further attempts to improve the activity of these PROTACs led to a slight improvement in potency IC_{50} ~ 9.7 µM.[189] These results highlight the significant challenges of achieving high potency with peptide based PROTACs, small molecule variants have greatly surpassed peptidic PROTACs and have achieved over 4 orders of magnitude greater activity.

3. Chapter 3

3.1. Chapter 3: Introduction

3.1.1. Overview of small molecule MDM2 inhibitors

As described within the previous chapter, many challenges were faced during the development of stapled peptide PROTACs, particularly the poor cell permeability and stability. As such, subsequent efforts focussed on identifying alternative strategies to construct potent PROTACs with more favourable properties. Aside from peptide-based warheads, small molecules offer many advantageous properties that could alleviate these issues. Indeed, within recent years several small molecule PROTACs featuring high potency and adequate bioavailability have been reported in the literature against a range of different proteins (section 1.1.4).[31,190]

The first reported small molecule PROTAC was published by Schneekloth *et al.* in 2008 (figure 57A) which used a nutlin derivative to recruit MDM2 for AR degradation.[18] This PROTAC was demonstrated to degrade AR through Western blotting at 10 µM concentration in HeLa cells (figure 57B). The nutlin derivative incorporated within this PROTAC is a racemic compound with a high molecular weight of 638 Da, resulting in a PROTAC with *ca.* 1200 Da molecular weight. This large size could be a contributing factor to the weak potency observed due to low cell permeability.[191]

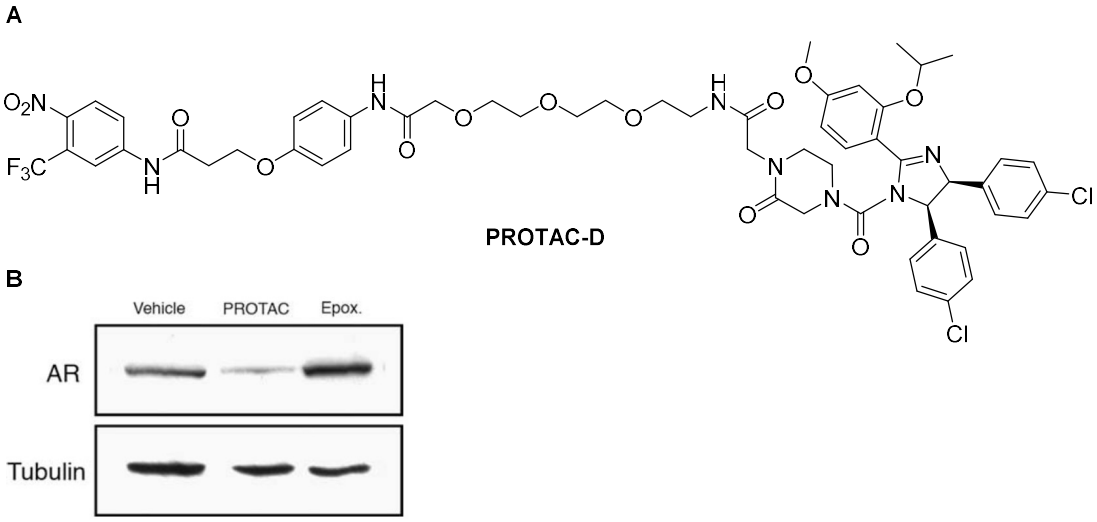

Figure 57: A: structure of small molecule PROTAC which used nutlin as an MDM2 binder for AR degradation; B: Western blotting analysis of PROTAC activity in HeLa cells,[18] reproduced with permission from Elsevier

Despite the promise of harnessing MDM2 as an E3 ligase for targeted protein degradation (section 2.2.4), no further examples of MDM2 recruiting PROTACs were present in the literature at the outset of this project. This highlighted the importance of identifying novel small molecule motifs capable of hijacking MDM2 for PROTAC mediated degradation.

There have been a large number of small molecule MDM2 inhibitors identified in the past decade, many of which are currently undergoing clinical trials with promising initial data (figure 58).[192]

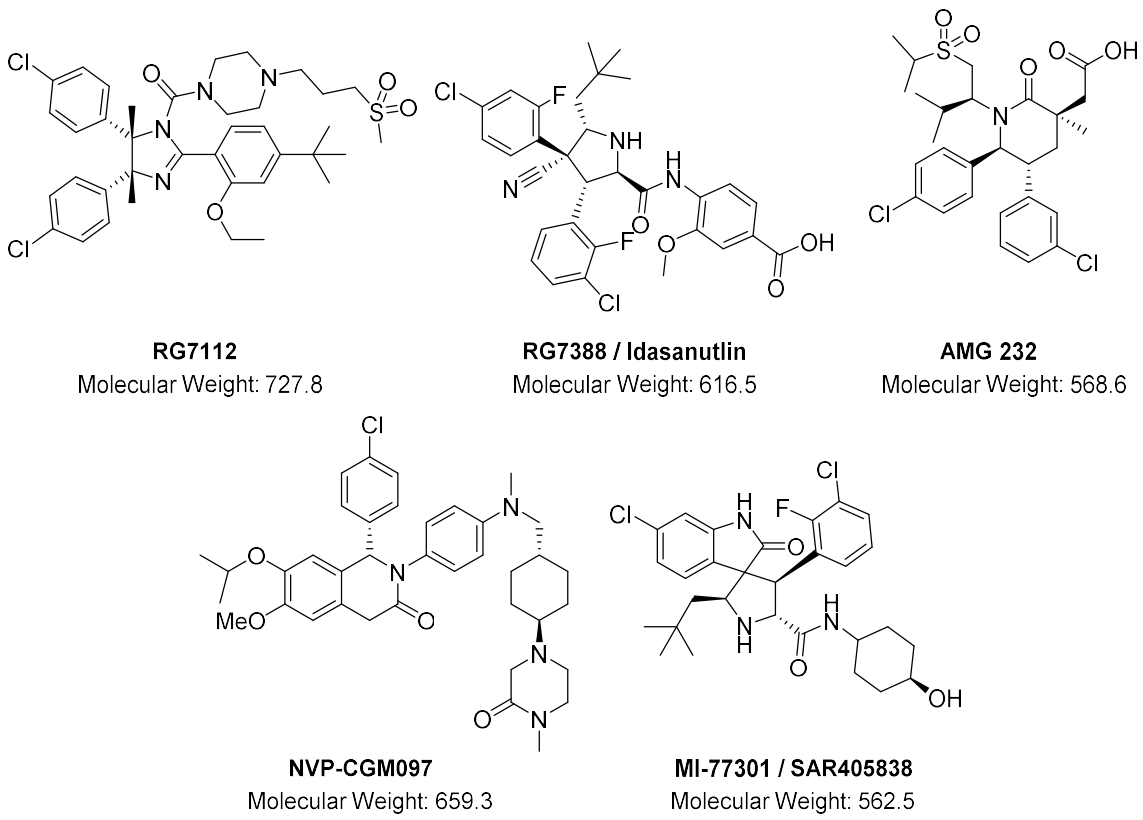

Figure 58: Structures and molecular weight of clinical candidates for the inhibition of MDM2

The nutlin series were the first reported small molecule MDM2 antagonists.[107] Further optimisation of this scaffold led to the discovery of RG7112,[193] the first clinical MDM2 inhibitor that was found to reactivate the p53 pathway and generate clinical responses in phase I trials.[109] The second generation clinical candidate RG7388 is based on a pyrrolidine core and was found to have higher potency and selectivity toward MDM2.[194] Another clinical candidate, AMG 232, was reported as a potent and selective piperidinone based MDM2 inhibitor with a binding affinity of 0.045 nM.[195,196] This drug proved efficacious and was well-tolerated in phase I studies.[197] Another MDM2 inhibitor to recently enter the clinic was NVP-CGM097,[198,199] a substituted 1,2-dihydroisoquinolinone derivative with an IC_{50} of 1.7 nM, which has been reported to demonstrate promising clinical activity.[200] SAR405838 has a binding affinity of 0.88 nM to MDM2, good pharmacokinetic properties, and has been shown to potently activate the p53 pathway *in vivo*.[201] Phase I studies of this inhibitor in patients with advanced solid tumours showed a good safety profile with limited activity.[202] Finally, SAR405838 is also being clinically evaluated as a combination therapy, where preliminary anti-tumour activity has been observed.[203]

Despite the potent nature of these clinical candidates, several factors limited their incorporation into PROTACs. Namely, this related to the fact all five candidates described had high molecular weights of >550 Da and required complex syntheses due to the presence of multiple stereocentres. In contrast, the features sought for this purpose were low molecular weight, simple chemical synthesis (or commercial availability), and an obvious and validated exit vector for PROTAC growth which would not significantly hamper MDM2 protein binding. E3 ligase recruiting motifs used in PROTACs do not need to have nanomolar binding affinities to generate extremely potent PROTACs,[76] hence, identification of less complex and more readily synthesisable MDM2 binders was investigated through *in silico* methods.

3.1.2. Computational methods to generate novel PPI inhibitors

Identification of novel small molecule inhibitor scaffolds for PPIs is highly challenging. A well-validated approach to rapidly and cost-effectively generate new hits against targets of interest is through computational methods.[204,205] One such strategy to identify novel hits is through *in silico* screening of virtual compound libraries against the target protein binding site.[206]

Two commonly adopted methods for computationally screening databases are *via* ligand-based and structure-based searching. Ligand-based screening methods harness structure-activity data from known binders. There are different methods for generating this data, whereby either the individual chemical functionalities responsible for binding towards specific residues for a given target are identified and matched or whole molecule shape similarity comparisons are drawn between known and new ligands. Often, this generated data is utilised to form a 3D pharmacophore describing the shape and functionality of a small molecule, which can then be compared to the known ligand to predict binding potential.[207,208] This approach has many advantageous features, such as the speed of hit identification and the rapid elimination of obvious non-binders. However, this methodology still suffers from a few limitations, such as its qualitative nature and often the production of very weakly binding hits due to difficulties in ranking quality.[209] In contrast, structure-based database searching uses docking techniques to assess the binding affinity of a virtual compound to the 3D protein structure. This has the advantage of providing docking scores which can roughly indicate hit binding affinity.[210] The limitations of this approach, however, are that the computing time required to generate the data is high and the accuracy of predictions correlates to the flexibility of compounds, with those featuring many conformations proving more challenging to accurately predict.[211] Nevertheless, there are significant advantages in efficiency associated with the use of virtual over physical compound collections for screening.

In a similar vein to high throughput screening approaches, hit generation through virtual screening methods relies on large databases of compounds that cover a broad area of chemical space.[212] There are many databases of compounds available for virtual screening with different properties and availabilities, such as the ZINC database that features over 120 million compounds.[213,214] The overall chemical space of small carbon-based molecules is predicted to encompass over 10^{60} compounds.[215] Similarly to the deficiencies of physical library coverage, it has been noted that only a minimal fraction of this space has also been explored using virtual methods.[216] Virtual libraries have many benefits associated with their use, including their ease of curation compared to physical collections; hence chemical space coverage is considerably easier to manipulate. It is now well known that the probability of identifying hits against a given target is highly dependent on the composition of a screening library.[217] Thus, it is vital to ensure a given virtual library is of sufficient diversity to increase this likelihood; this is even more essential when pursuing challenging targets such as PPIs.

The two computational approaches for hit identification have previously been applied in a synergistic fashion to identify small molecule binders at the MDM2-p53 interface.[218] These efforts resulted in the identification of nanomolar MDM2 inhibitor NSC 66811 through screening a virtual database (figure 59).[219] Lu *et al*. initially used pharmacophore screening to identify a series of hits from the National Cancer Institute (NCI) 3D database. These initial hits were then docked to the MDM2 surface and the predictive binding affinity of each compound ranked. Next, the compounds identified to be the most potent were obtained and biologically screened to confirm binding affinity to MDM2. These efforts proved successful, since NSC 66811 was identified to bind MDM2 with a K_i of 120 nM and was found to be active in a cell-based assay.

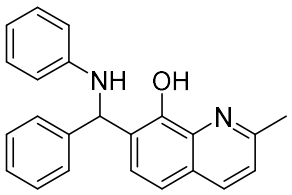

NSC 66811

Figure 59: Structure of racemic MDM2 binder NSC 66811, discovered through virtual screening of NCI's database

3.2. Chapter 3: Aims and Objectives

In order to identify novel MDM2 binding scaffolds, it was hypothesised that utilising the two previously described computational approaches in tandem could prove a powerful approach to identify potential small molecule binders that may be suitable for PROTAC construction. However, as noted within the previous section, the identification of a suitable virtual screening library is an essential factor that contributes to the viability of this process. Thus, it was envisaged that due to the challenging nature of PPI disruption, a structurally diverse and 3D library would be required for this strategy. Novel small molecule MDM2 binders identified through *in silico* screening methods could then be synthesised and validated before applying to the PROTAC field.

Over the past two decades, among others, the Spring group have pioneered the development of diversity-oriented synthesis (DOS).[220,221] DOS is a divergent approach for generating diverse compound libraries that cover large areas of chemical space in an efficient manner through common intermediates.[220,221] Importantly, DOS libraries have many advantages, including the low inherent bias towards a specific biological target since they are often constructed in a target-agnostic fashion. Inspired by these features, a virtual compound collection of novel, diverse and 3D structures had previously been generated using a DOS-inspired strategy. Importantly, due to the inherently modular approach of this chemistry, it would be assumed that resulting scaffolds would be readily synthetically tractable and thus, hits could be quickly validated. Moreover, the 50,000-member library had also been assessed in terms of biological space coverage and compound promiscuity, which highlighted the favourable properties of this library compared to other commercial collections. Following these studies, this DOS-derived compound collection was applied towards the identification of novel MDM2 binders.[222] The computational work described was performed by Dr Lewis H. Mervin.

The computational workflow involved initial mining of the library using ligand-based screening, comparing the library compounds with a set of known active and inactive small molecules to shortlist the 25,000 top compounds. These high scoring compounds were then docked against MDM2 protein using Glide[223] to generate docking scores which assess the degree of binding predicted. Four of these compounds, **62** - **65** were then chosen for further study because they featured within the top 30 ranked compounds and contained novel MDM2-binding scaffolds dissimilar from active compounds (figure 60).[222] It was important for the proposed MDM2 binders to encompass areas of chemical space which had not previously been explored. Similarity evaluation of these structures compared with known MDM2 binders found them to have little similarity with their nearest neighbours. Importantly, these identified compounds all contained a triazole core and could be easily prepared for testing using simple and robust chemistry. Compound **65** was prepared by Dr Sarah Kidd.

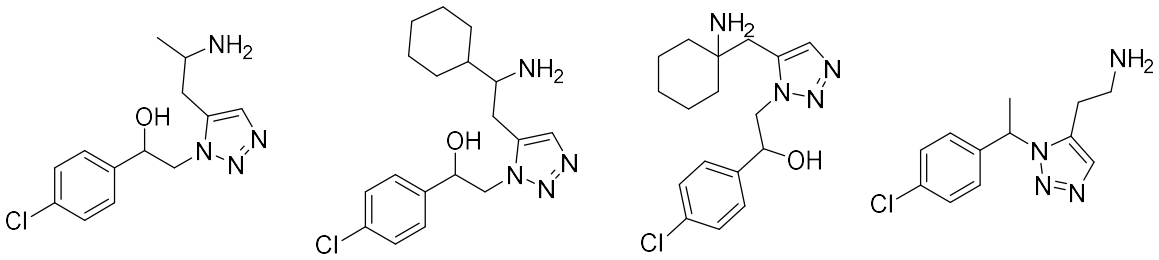

Figure 60: Structures of computationally predicted MDM2 inhibitors, relative docking scores are shown in blue[222]

The binding poses predicted for these compounds with MDM2 in the p53 protein binding interface are shown in figure 61A and B. Hydrogen bonding interactions were predicted between the amine functionality in all four compounds towards both GLN72 and TYR67 (figure 61C). Additionally, the triazole ring of each compound was predicted to bind in the same region of the interface with high overlap.

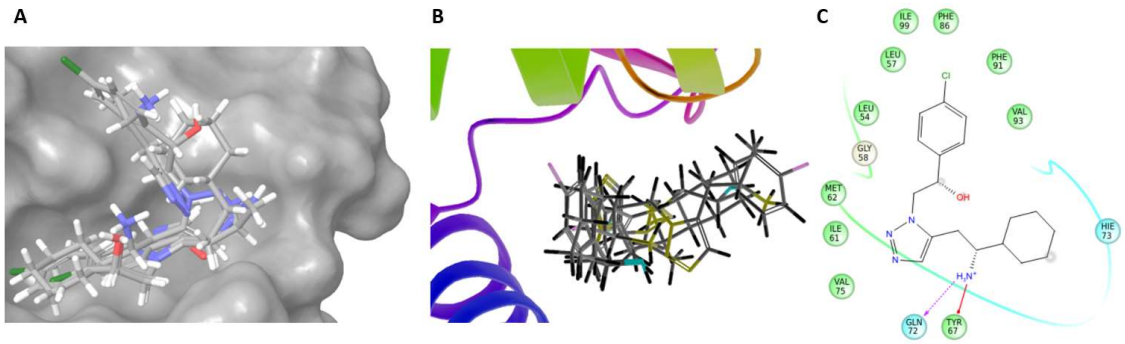

*Figure 61: A) Superposition of MDM2 ligands identified visualised with a solid molecular surface; B) a cartoon and stick representation; C) Structure of ligand **64** bound to MDM2 highlighting interactions made with surrounding amino acids*[222]

With these results in hand, the synthesis and biological evaluation of the potential MDM2 binders was proposed. In turn, if successful, it was hypothesised to incorporate these compounds into a series of novel PROTACs, which would recruit MDM2 as the E3 ligase for degradation of AR. In contrast to Chapter 2, where stapled peptides were used for this purpose these small molecule PROTACs were expected to have considerably improved permeability, which was anticipated to translate to improved activity and pharmacological properties.

3.3. Chapter 3: Results and Discussion

3.3.1. Synthesis of computationally derived small molecule MDM2 binders 62 - 64

A retrosynthetic analysis of the three proposed small molecule MDM2 binders highlighted a simple click chemistry-based route could be utilised to access the compounds (figure 62). Since the three compounds shared a central triazole ring, it was hypothesised this could be split into the respective alkyne and a common azide constituents. In the forward route, it was hoped these components could be reacted using a ruthenium catalysed azide-alkyne cycloaddition to give the 1,5-regioisomer. Moreover, the three proposed alkynes could all be synthesised using simple chemistry from commercially available building blocks **70** - **72**.

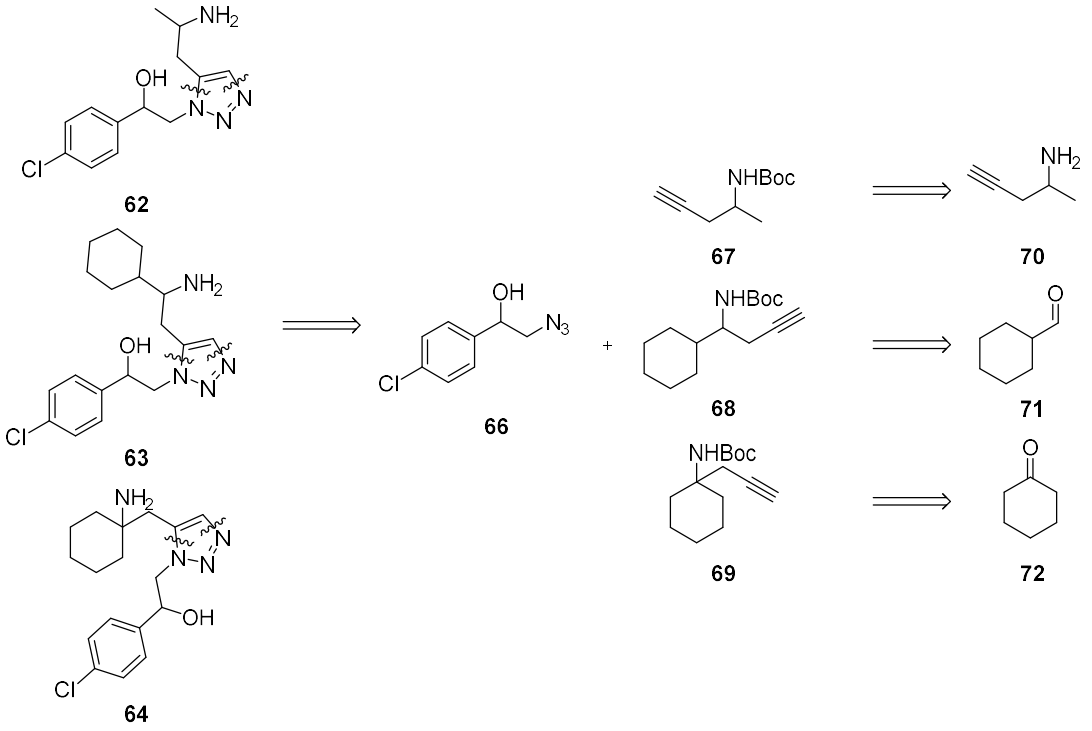

*Figure 62: Retrosynthetic analysis of the proposed MDM2 binders **62** – **64** from commercially available starting materials*

In line with this proposal, azide **66** was prepared from commercially available 4-chlorobenzoylmethyl bromide (scheme 28). This was achieved *via* a nucleophilic substitution with sodium azide, directly followed by ketone reduction using sodium borohydride to form the azido-alcohol **66** in good yield.

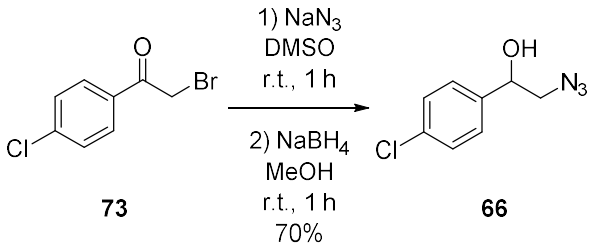

*Scheme 28: Synthesis of azide **66***

With the desired azide component in hand, next the synthesis of the three alkynes and related final products was pursued. Firstly, alkyne **67** was easily prepared through *N*-Boc protection of amine **70** (scheme 29). Here, the low yield of 42% was attributed to the compound's high volatility. Next, the core triazole ring of compound **74** was assembled through ruthenium-catalysed click chemistry of alkyne **67** and azide **66**, which proceeded in excellent 94% yield to generate a 1:1 mixture of diastereoisomers (calculated by ^{1}H NMR). Finally, *N*-Boc deprotection of **74** with TFA in dichloromethane gave final compound **62** in good yield.

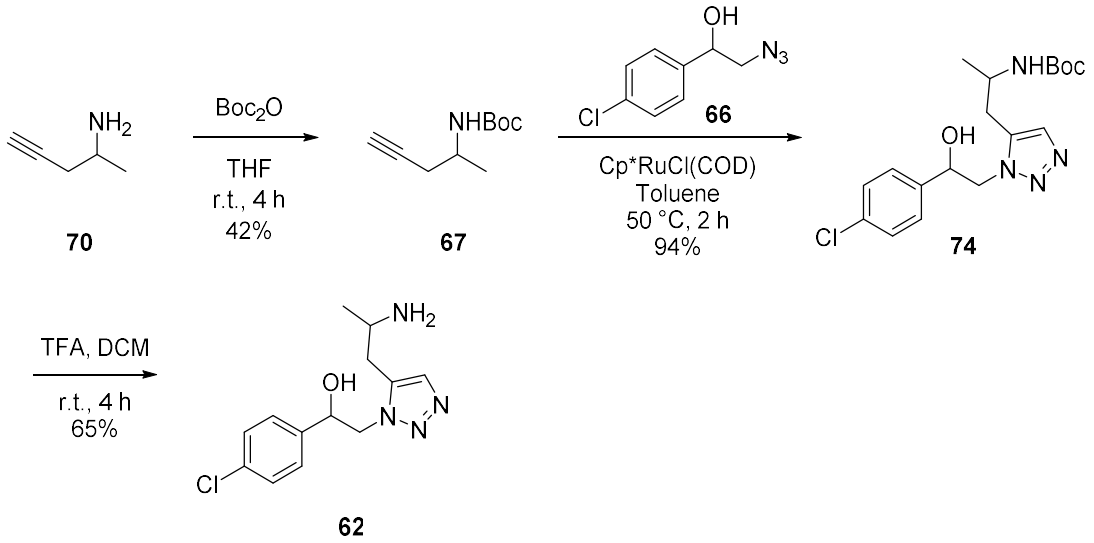

*Scheme 29: Synthesis of compound **62***

Following the success in the formation of **62**, the synthesis of the second potential binder **63** was investigated (scheme 30). Commercially available cyclohexanecarbaldehyde was treated with *p*-anisidine in the presence of dehydrating agent to form the PMP-imine, which was immediately reacted with propargyl bromide in a Barbier-type coupling in the presence of activated zinc (prepared through washing zinc metal with HCl) to produce a mixture of alkyne **75** and allene **76** products (*ca.* 1:0.56, determined by ^{1}H NMR). Purification of these two products by column chromatography proved to be extremely challenging, instead yielding an inseparable mixture of the two entities. Thus, the crude

mixture was telescoped into the next reaction since it was envisaged that the allene impurity would have no effect on the subsequent reaction. The PMP group was then removed with cerium (IV) ammonium nitrate (CAN) to yield the mixture of alkyne and allene amines **77** and **78**, which were then immediately re-protected with a Boc group to give **68** in 29% yield over two steps. The low yield is rationalised by the purging of allene impurity during the purification of **68**. Next, the triazole core was then constructed through a ruthenium-catalysed cycloaddition to give **79** as a 1:1 mixture of diastereoisomers, which was finally deprotected with TFA to afford **63** in high yield.

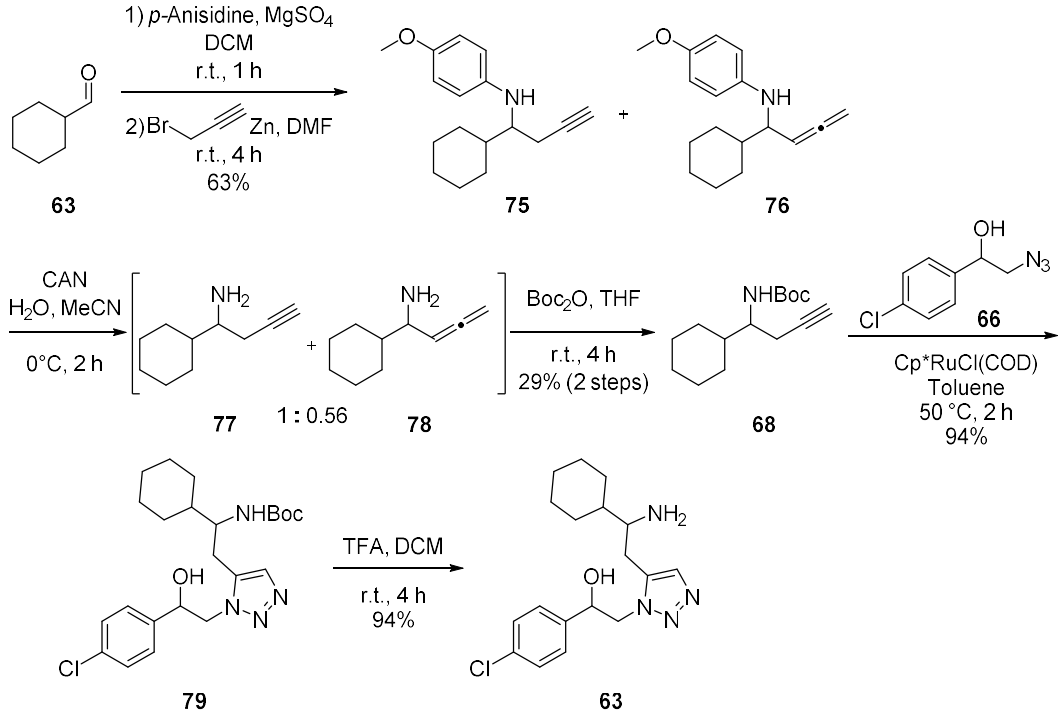

*Scheme 30: Synthesis of proposed binder **63***

The final molecule to be prepared was **64**. In this instance, commercially available cyclohexanone was reacted with 2-methyl-2-propanesulfinamide, in the presence of titanium (IV) ethoxide to give *N*-sulfinyl imine **80** in good 62% yield (scheme 31). Initially, the Barbier-type reaction previously used to generate **75** was attempted to form the quaternary carbon centre of **81**. Unfortunately, this was unsuccessful and only starting material was isolated upon purification. Next, a Grignard approach was proposed for the addition of a propargyl group to imine **80**. Propargylmagnesium bromide[224] has been prepared previously from propargyl bromide and magnesium turnings using mercury chloride,[225,226] however, due to the toxicity of $HgCl_2$ alternative approaches were sought. Initial attempts at forming this Grignard reagent using iodine as initiator were unsuccessful. After switching to a zinc bromide-catalysed procedure,[227] the Grignard reagent was successfully formed, however the molarity was considerably lower than expected (0.1 M, compared to literature 0.5 – 0.6 M[227]) after titrating against

menthol with 1,10-phenanthroline, indicating incomplete formation.[228] As a result, sulfinyl imine **80** was reacted with an excess of Grignard reagent to yield sulfinamide **81** in almost quantitative yield. The *tert*-butanesulfinyl auxiliary was subsequently removed under acidic conditions at 90 °C for 2 hours. Next, the nitrogen was re-protected with a Boc group, to avoid catalyst poisoning *via* coordination but enabling milder downstream deprotection. Pleasingly, this sequence afforded **69** in excellent yield over two steps. Finally, the central triazole ring was once more constructed using ruthenium catalysed click chemistry to give **82** in 84% yield, and the *N*-Boc group removed with TFA in dichloromethane to give compound **64** in high yield.

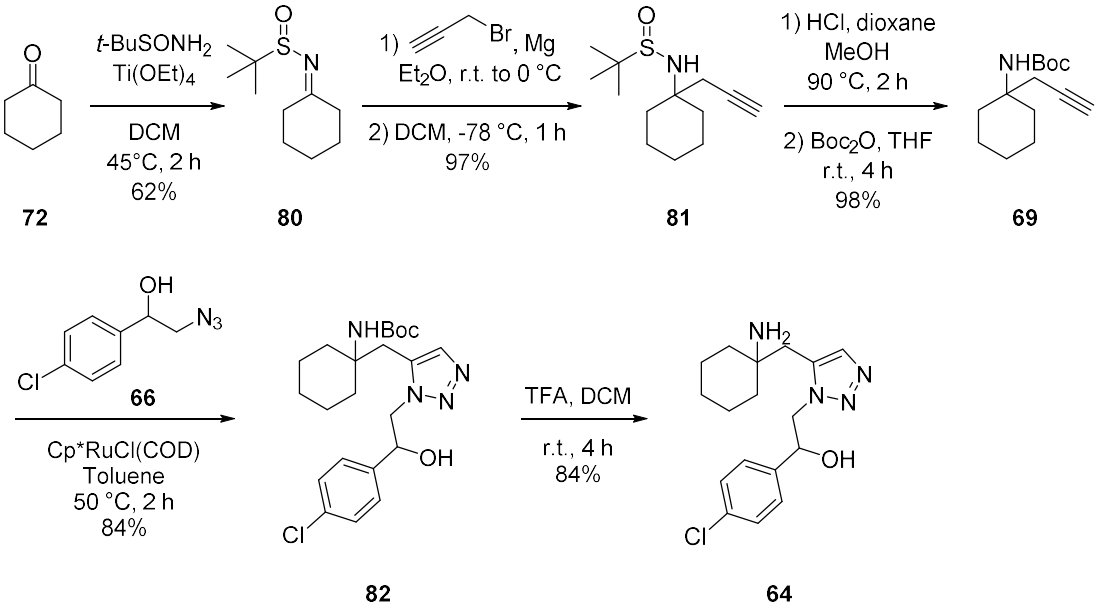

*Scheme 31: Synthesis of compound **64***

With these compounds and the fourth compound **65** (figure 63, synthesised and characterised by Dr Sarah Kidd) in hand, subsequent efforts focussed on assessing the biological activity of the four compounds.

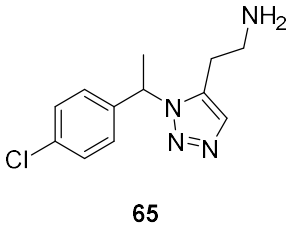

*Figure 63: Additional compound **65** synthesised by Dr Sarah Kidd*

3.3.2. Biological evaluation of MDM2 binders 62 - 65

Initially, the biological activity of the compounds towards MDM2 was assessed through competitive fluorescence polarisation (FP) with recombinant MDM2 protein as previously described in Chapter 2.[147,175] In this instance, the FP assay for compounds **62** - **65** was conducted in triplicate at a maximum concentration of 3 mM, which was found to be the highest concentration possible with respect to the solubility and upper limit of DMSO toleration within the assay.

In these experiments, the competitive FP showed no MDM2 activity of the small molecules at concentrations under 1 mM, with limited activity observed at > 1 mM concentrations. At these higher concentrations, the greatest inhibition of tracer binding was observed for **63** and **65**, whilst very little activity was observed for **62** (figure 64). No complete dose response curve was attained as the compounds were unable to saturate the protein, even at maximum concentration. Thus, without a complete curve the binding affinity of the molecules could not be established quantitively. As a result, only very weak binding could be identified.

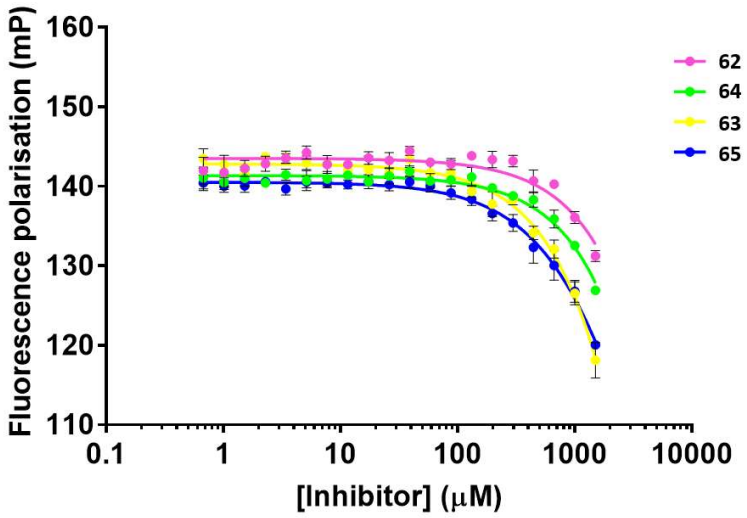

*Figure 64: Competitive FP curves attained for MDM2 ligands **62** - **65**[222]*

The lack of observed activity in this competitive FP assay could be attributed to the extremely high binding affinity of the tracer molecule to the protein (17.6 ± 1.7 nM[175]). As such, due to the small fragment-sized nature of the molecules in question, it was hypothesised that these molecules were unable to fully outcompete the tracer as a result of mismatched affinities. However, assay development was beyond the scope of this project, and as such an alternative strategy for compound evaluation was sought.

To better establish the biological activity for these fragment-sized molecules, differential scanning fluorimetry (DSF) was employed. DSF is a biophysical assay that can assess the binding of a compound to a protein through determination of the shift in protein melting temperature (T_m). This shift in melt temperature is proportional to the binding affinity of the compound due to protein stabilisation. Although it is more difficult to quantify the exact binding affinity of the compounds using this method, it was anticipated that the binding could be conclusively confirmed, and the binding potential of each compound could be compared.

DSF was conducted alongside the positive control nutlin, a known high affinity MDM2 binder and the negative control DMSO. The DSF data revealed all compounds shifted the melt temperature of MDM2 in a concentration dependent manner (figure 65). The most promising compound was **63**, which shifted the melt temperature by 2.4 °C at the maximum concentration of 2.5 mM. This result confirmed the ranking assigned by using FP data and provided additional confidence of MDM2 binding across the series.

Compound	Concentration (mM)	Average Melt (°C)	Average ΔT_m (°C)
None	-	58.9	-
62	0.1	59.1	0.2
	0.5	58.7	- 0.2
	2.5	59.4	0.5
64	0.1	59.2	0.3
	0.5	59.7	0.8
	2.5	60.5	1.6
63	0.1	59.1	0.2
	0.5	59.9	1.0
	2.5	61.3	2.4
65	0.1	59.3	0.4
	0.5	59.2	0.3
	2.5	61.1	2.2

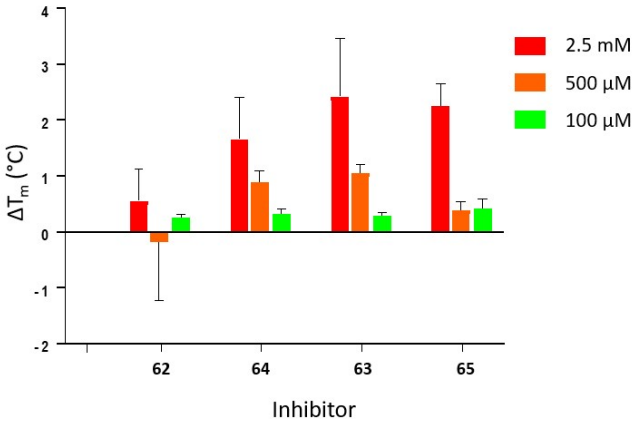

*Figure 65: DSF of MDM2 ligands **62** - **65** at 2.5 mM, 500 µM, and 100 µM concentrations*[222]

Whilst both the competitive FP and DSF were able to validate the binding of these fragment-like molecules toward MDM2, the binding affinity was concluded to be extremely low. This was highlighted when these compounds were compared to the known MDM2 binder nutlin 3a in both assays (figure 66). Nutlin 3a was shown to have *ca.* 90 nM binding affinity with a maximum shift in MDM2 melt temperature of over 20 °C.

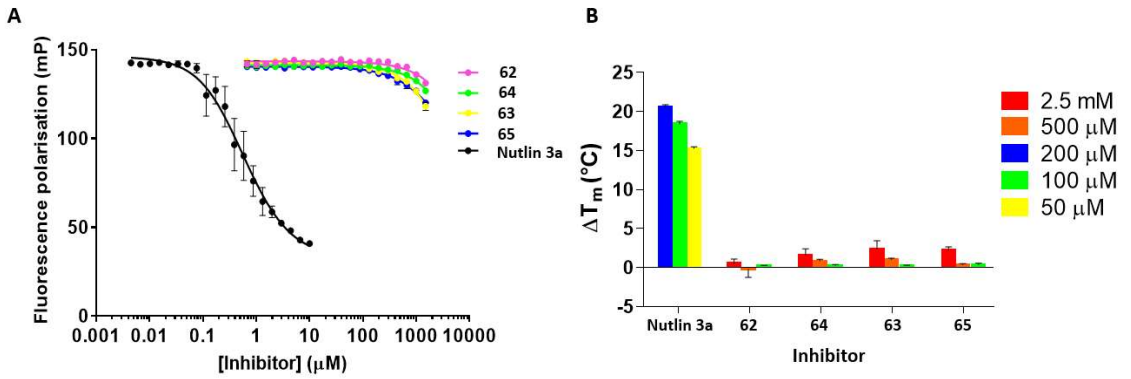

*Figure 66: Competitive FP graph and DSF melt temperature shifts of small molecules **62** - **65** compared to known MDM2 binder nutlin 3a*

Due to the hypothesised weak binding of these fragments and the challenges associated with establishing the binding affinities, it was decided that further compounds would not be synthesised. Although the binding affinity for each protein in a PROTAC can be considerably lower than for standard inhibition drugs due to their catalytic activity,[76] it was deemed that as a result of the extremely weak binding nature of these fragments that developing PROTACs would be challenging.

3.3.3. Overview of published MDM2 binder

Due to the lack of success in generating novel MDM2 binders for PROTAC generation using *in silico* methods, an alternative strategy to identify suitable small molecule components was sought. In this manner, it was envisaged that known literature MDM2 binders could be modified to enable incorporation into a novel PROTAC to validate this hypothesis.

Many clinical candidates which inhibit MDM2 are unsuitable for PROTAC incorporation due to their challenging syntheses, high molecular weights and lack of synthetically viable positions for PROTAC growth (growth vectors), as previously described (section 3.1.1). Therefore, known MDM2 binders were analysed against these criteria to identify more suitable PROTAC components.

SP-141 was developed by Wang *et al.*[229] and was shown to exhibit *in vitro* and *in vivo* activity against breast cancer cell-lines (figure 67). This compound was developed through a combination of HTS and computer-aided rational drug design and was hypothesised to occupy the p53 binding site of MDM2. It was also found to have an affinity of 28 ± 6 nM by FP and 43 nM in a Biacore assay, which was of a comparative magnitude to nutlin-3 (45 ± 4 nM and 90 nM, respectively). In addition, due to a molecular weight of just 324 Da, this molecule proved an ideal candidate for further PROTAC exploration. This feature was vital, since lower molecular weight and intrinsically linked properties such as rotatable bonds and number of hydrogen bond donors/acceptors could result in improved cell

permeability and pharmacokinetic properties of the overall PROTAC.[230] Significantly, to examine the specificity of the MDM2 binding, the researchers also conjugated a biotin tag to the indole nitrogen and conducted a pull-down assay to confirm MDM2 binding.[229] As such, this provided an ideal vector to attach the remainder of the PROTAC, since it had been previously demonstrated that conjugation of a linker and biotin molecule did not affect MDM2 recruitment. Moreover, the synthetic tractability was also a significant advantage of SP-141, since it was synthesised in just two steps from commercially available 5-methoxytryptamine and naphaldehyde.

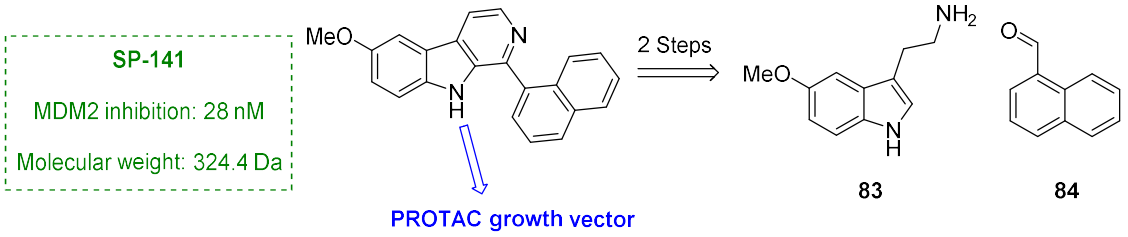

Figure 67: MDM2 inhibitor SP-141 prepared through two-step process from 5-methoxytryptamine and naphaldehyde

In addition to SP-141, the tyrosine-based compounds **85** and **86** had been reported by Giustiniano *et al.* as MDM2 inhibitors (figure 68).[231] Thus, it was hypothesised to also be a fruitful source for small molecules for PROTAC development. In these studies, **85** and **86** had been identified utilising computer-aided methods involving the virtual screening of compound libraries. In this case, the compounds were docked against the key hydrophobic hot spots between protein p53 and MDM2, Phe19, Trp23, and Leu26. The best ligands were assessed *in vitro* and found to bind MDM2 at low nanomolar potencies. Once more, this series of compounds proved attractive due to their relatively low molecular weights, rendering them appealing for PROTAC development. Importantly, this compound also offered two potential PROTAC growth vectors, which theoretically could be achieved using simple chemistry. An additional advantage was the ease of synthesis, whereby it was envisaged that the core could be constructed in one step from commercially available materials following the described procedure. In a similar fashion to SP-141, compound growth through the phenol exit vector had also been previously studied through connection of a propyl-aminopyridine group, with the resultant compound retaining activity and found to bind to MDM2 with 142 nM potency.[231] This further evidenced this position as a potentially viable region for PROTAC growth, without significantly hindering the MDM2 binding abilities.

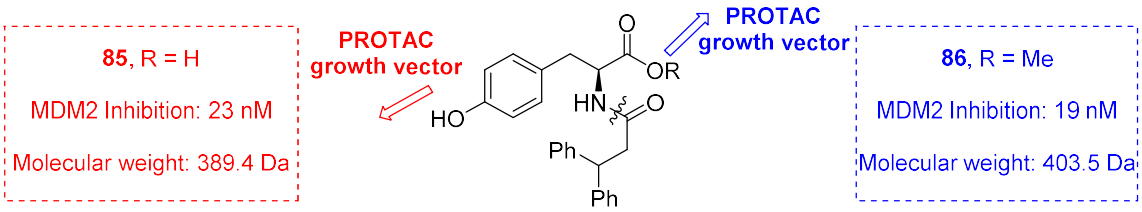

*Figure 68: Tyrosine based MDM2 binders **85** and **86** showing MDM2 inhibition*

The final MDM2 inhibitor chosen for PROTAC investigations was imidazole-based compound **87**, reported by Popowicz *et al.* (figure 69).[232] Initial studies by the researchers indicated that these compounds were low nanomolar binders of MDM2. This series of inhibitors contained a central imidazole scaffold and once again were designed to capitalise upon the key hydrophobic hot spots Phe19, Trp23, and Leu26 confirmed through crystal structure analysis. Further work from the same group expanded the study to optimise potency against MDM2 in cell-based assays.[233] This study found the optimised candidate had increased cytotoxicity in p53 positive cells and induced cell-cycle arrest. Importantly, within this paper a variety of analogues had been readily prepared, including an aliphatic chain attached through the carboxylate position, providing a well-scoped out potential exit vector. These analogues were also found to bind MDM2 with high affinity, validating this position as suitable for PROTAC growth without hindering MDM2 recruitment. In this instance, the higher molecular weight of this series was a concern, however, the higher potency towards MDM2 and ease of synthesis were deemed to be redeeming factors warranting their investigation.

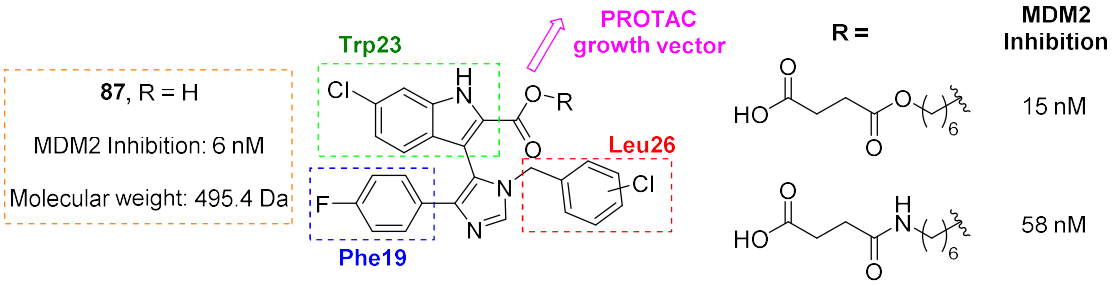

*Figure 69: Imidazole-based MDM2 binder **87** chosen for PROTAC development*

With the three MDM2 binders in mind, the synthesis of the corresponding PROTACs was next investigated. The strategy envisaged for PROTAC construction utilised installation of a linker moiety within the predefined exit vectors and connection to the AR binders previously used for the stapled peptide PROTAC development described in Chapter 2. Accordingly, these proposed small molecule PROTAC-variants combined elements of the previous stapled peptide PROTAC. In this case, it was decided that only enzalutamide would be used as the AR binding motif due its 'drug-like' properties and antagonistic binding mode. As such, efforts were first focussed on the optimisation of these components given the challenges described during the synthesis of these moieties in Chapter 2.

3.3.4. Synthetic procedure to access enzalutamide based AR binder

The route to the carboxylic acid **2** described in Chapter 2 involved a five step longest linear sequence, which proved to be time-consuming and inefficient. As such, a new one-step procedure from commercially available enzalutamide firstly was developed to provide faster access to this key PROTAC building block (table 5). Primary amide **16** was previously hydrolysed by heating with conc. HCl at 120 °C in a sealed tube. However, in an attempt to increase the safety of this reaction on larger scales, an alternative procedure was sought. Initially, hydrolysis of the *N*-methylamide was attempted through refluxing with concentrated HCl. This was found to be extremely ineffective giving 6% conversion by LCMS after 2 days and an overall isolated yield of 31% after 6 days.

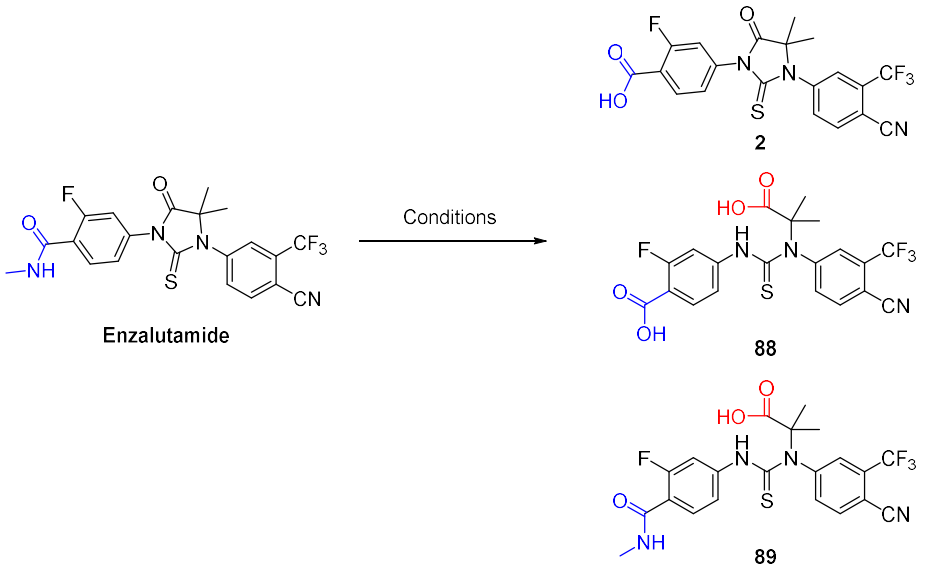

Entry	Scale (mg/mL)	Conditions	Time	LCMS Conversion
1	40	110 °C reflux	2 days	6% **2**, 94% SM
2	33	130 °C, 8-9 Bar, µwave	1.5 h	29% **2**, 29% SM, 26% **88**, 11% **89**
3	10	110 °C, 4-5 bar, µwave	1 h	14% **2**, 67% SM, 4% **88**, 6% **89**
4	10	100 °C, 3-4 bar, µwave	1 h	8% **2**, 92% SM
5	30	100 °C, 4-5 bar, µwave	12.5 h	22% **2**, 33% SM, 25% **88**, 12% **89**
6	10	100 °C, 4 bar, µwave	14 h	37% **2**, 4% SM, 27% **88**, 4% **89**
7	10	80 °C, 2-3 bar, µwave	3 h	7% **2**, 93% SM
8	10	80 °C, 2-3 bar, µwave	19 h	21% **2**, 79% SM

Table 5: Conditions screened for the hydrolysis of enzalutamide

In an attempt to increase the rate of hydrolysis, it was decided to investigate microwave conditions where additional pressure could be generated to improve the conversion. Initially, the reaction was heated to 130 °C, generating 8-9 bar pressure for 1.5 h. LCMS analysis of the crude mixture revealed 29% of both SM and **2**. However, this also resulted in the

identification of two prominent new impurities, hypothesised to be **88** and **89** where the central thiohydantoin ring amide had been hydrolysed. It was hoped that lowering the temperature and thus the pressure could achieve effective hydrolysis without disrupting the core ring. The following reaction at 110 °C, 4 – 5 bar for 1 h gave 14% **2**, 67% SM and cumulative 10% of impurities. Overall, it was found that high temperature and pressure led to greater conversion, however, considerable levels of impurities were also generated. At lower temperatures of 80 °C, conversion was reduced, however, the reaction was considerably cleaner. In addition, reaction concentration was found to be crucial despite the reaction being a heterogeneous slurry. More concentrated reactions led to lower conversion and greater overall impurity profiles.

The optimal temperature identified was 80 °C (2-3 bar), which led to 21% **2** after 19 h. Low conversion was observed; however, it was comparable to the reflux conditions, but enabled a significantly reduced reaction time. Moreover, due to the one-step nature, this enabled more efficient access to the key starting material.

3.3.5. Synthesis of SP-141-based MDM2 PROTACs

To incorporate SP-141 into a PROTAC, it was decided to functionalise at a carboxylic acid through *N*-alkylation with *tert*-butyl 2-bromoacetate (scheme 32). It was hypothesised that this would enable a facile amide coupling to generate the final PROTAC. Importantly, SP-141 was incorporated in the final step, owing to its limited supply from commercial sources, which is a result of the restricted nature of its starting materials. SP-141 was treated with a dilute solution of *tert*-butyl 2-bromoacetate in the presence of Cs_2CO_3 at ambient temperature, which yielded quantitative **90**. Administration of *tert*-butyl 2-bromoacetate as a dilute solution was discovered to be crucial to avoid over-alkylation. The final step to the SP-141-PROTAC precursor involved deprotection of the *tert*-butyl ester. This was achieved using a 1:1 mixture of TFA/DCM, which proceeded rapidly and gave full conversion to **91** without further purification.

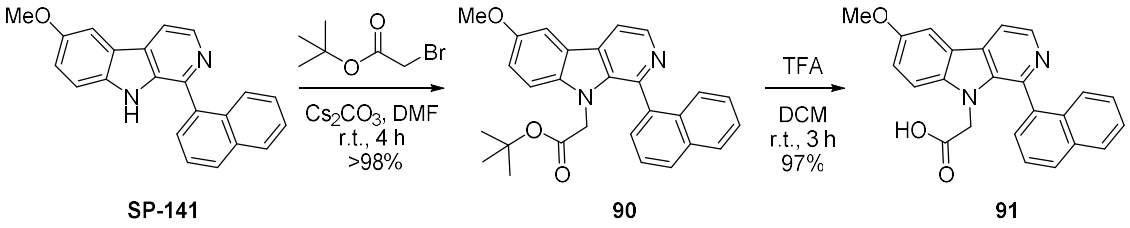

*Scheme 32: Synthesis of acid-tagged MDM2 binder **91** through N-alkylation and subsequent ester deprotection*

With **91** in hand, synthesis of the SP-141-based PROTAC could begin. For initial tests of the activity of this PROTAC, a linker length of four PEG units was chosen. This was designed to balance PROTAC solubility with spatial distribution between the two binding components.

The synthesis of the four-PEG linked SP-141 **PROTAC-7** first involved preparing the linker conjugated enzalutamide derivative **94** (scheme 33). Acid **2** was coupled with *N*-Boc protected amine **92** to yield **93** in good yield. The *N*-Boc-protecting group was then removed with TFA in DCM to form amine **94** in high yield.

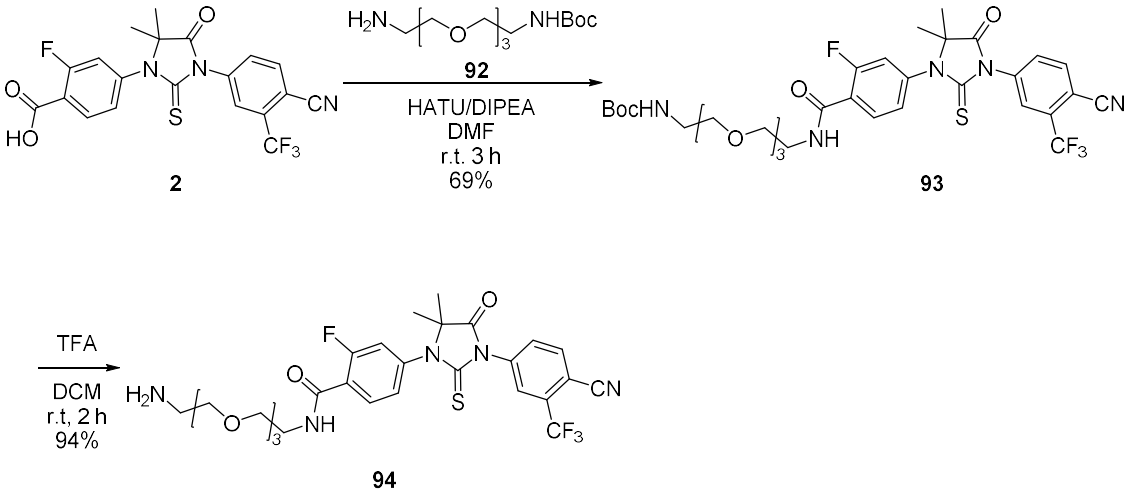

*Scheme 33: Preparation of linker-enzalutamide conjugate **94** through amide coupling and deprotection chemistry*

Next, the PEG-enzalutamide amine was reacted with the SP-141 derivative **91** in the presence of HATU and DIPEA to yield **PROTAC-7** in 34% yield (scheme 34).

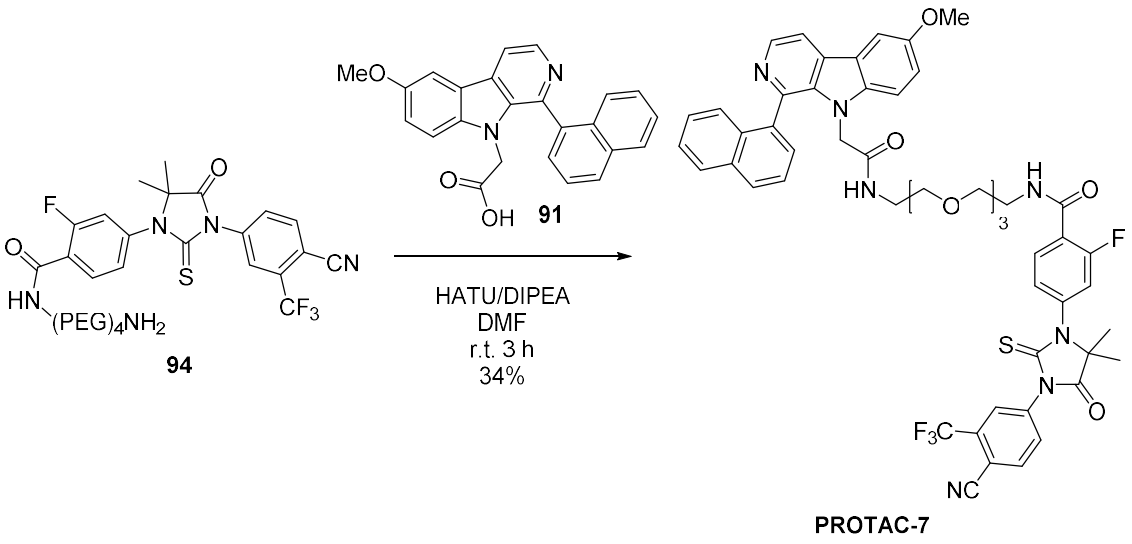

*Scheme 34: Synthesis of **PROTAC-7** through HATU-mediated amide coupling*

Due to the limited supply of SP-141, only the four-PEG linked **PROTAC-7** was prepared for initial testing to validate the feasibility of this MDM2 core before further optimisation. This linker length was expected to impart solubility whilst maintaining a reasonable distance between the two proteins in the PROTAC ternary complex.

3.3.6. Synthetic procedure for tyrosine based MDM2 PROTACs

The next MDM2 inhibitor to be synthesised was **86**.[231] This simple tyrosine derivative had two potential exit vectors which could be very easily harnessed for PROTAC growth (figure 70). Exit vector 1 grows from the ester group, which can be hydrolysed to the acid and coupled to the linker through amide couplings. In addition, exit vector 2 can be used, which would grow the PROTAC from the opposite end of the molecule through the phenol functionality. An *O*-alkylation strategy can be used to connect the linkers to this phenol in a simple fashion. As the exact binding conformation of this MDM2 series was unknown, it was hypothesised that exploring PROTAC incorporation through the two different exit vectors would maximise the possibility of generating an active PROTAC.

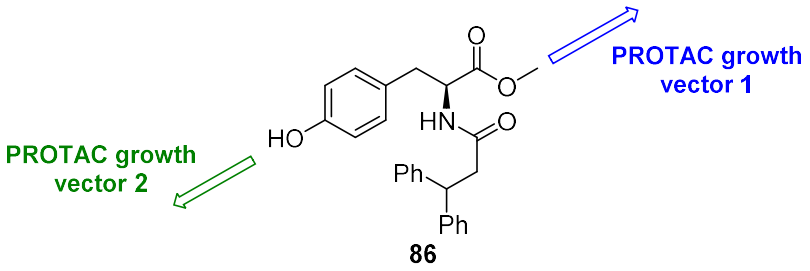

*Figure 70: MDM2 inhibitor **86** with exit vectors to be exploited*

MDM2 inhibitor **86** could be prepared in high yield *via* a simple amide coupling between commercially available tyrosine-methyl ester **95** and 3,3-diphenylpropionic acid **96** (scheme 35). It was decided that the PROTAC would be synthesised by attaching linkers to this central core, with the enzalutamide motif incorporated in the final step. This would be an efficient way to synthesise these PROTACs considering the lower availability of acid **2** compared to the easily synthesised MDM2 binder **86**.

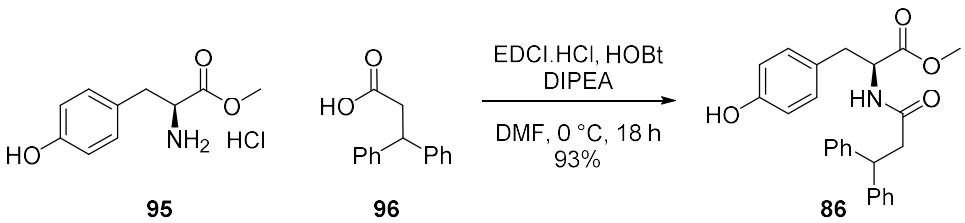

*Scheme 35: Synthesis of MDM2 inhibitor **86** through amide coupling chemistry*

The synthesis of PROTACs derivatised through growth vector 1 involved initial hydrolysis of the methyl ester with lithium hydroxide to produce acid **97** (scheme 36). Next, two commercially available *N*-Boc protected PEG amines containing three or four PEG units were coupled to **97** under EDCI.HCl, HOBt coupling conditions, proceeding with high yields. The *N*-Boc protecting groups were then removed with TFA to yield the free amines **100** and **101**, which were finally coupled with the enzalutamide acid **2** in the presence of HATU and DIPEA to form **PROTAC-8** and **9** in good respective yields.

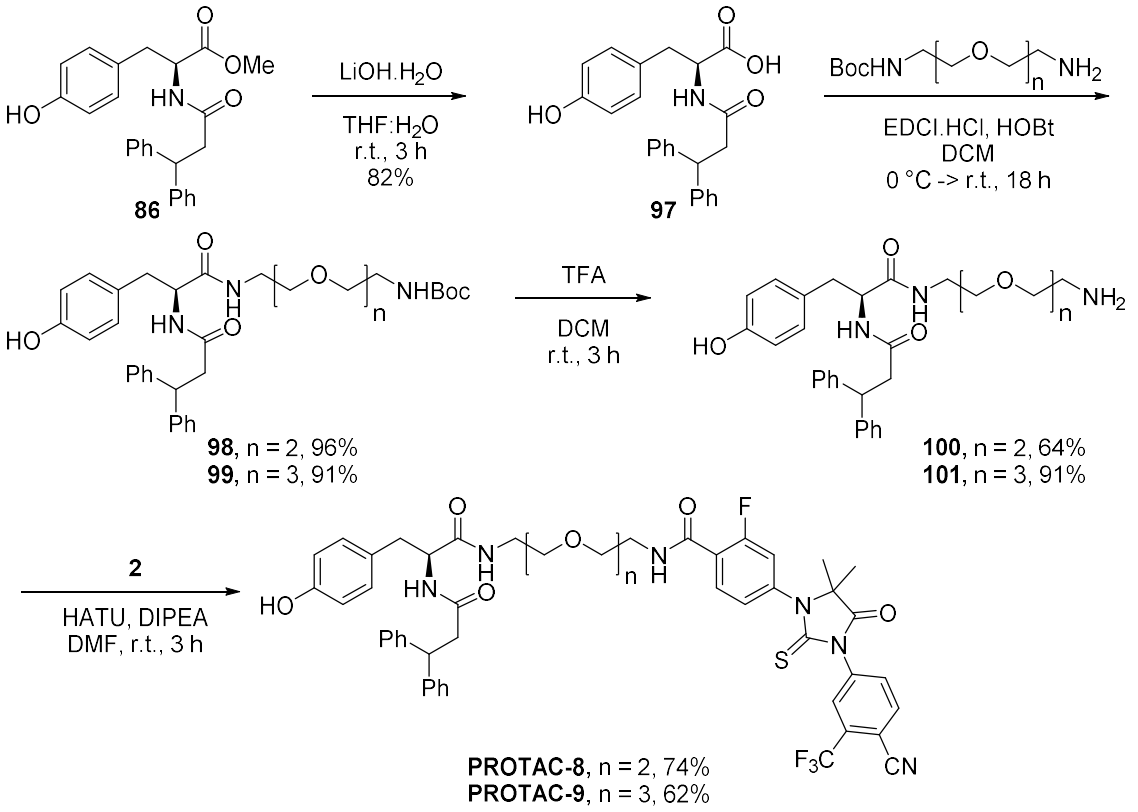

*Scheme 36: Preparation of **PROTACs 8-9** through exit vector 1 via deprotection and amide coupling chemistry*

Derivatisation through growth vector 2 was more complex as this required *O*-alkylation rather than simple amide coupling chemistry. Firstly, **86** was treated with alcohol **102** under Mitsunobu conditions (scheme 37). Unfortunately, this was unsuccessful, leading to a complex mixture of products.

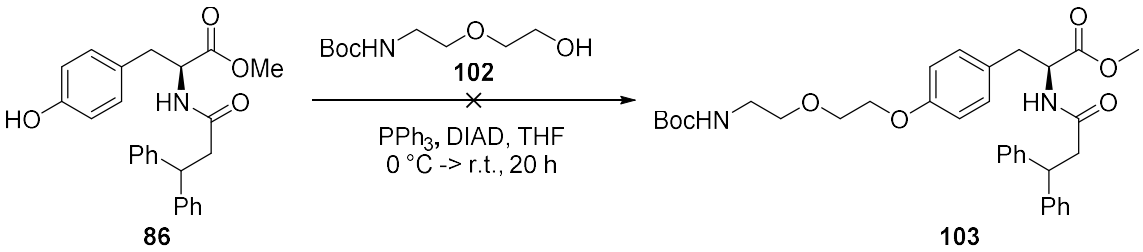

Scheme 37: Attempted Mitsunobu reaction to form linker conjugate 103

Preparation of reactive PEG linkers was next attempted to enable *O*-alkylation *via* direct nucleophilic substitution with the phenol. The mesylate and iodide derivatives of two- and three-unit PEG linkers were prepared for this purpose. Mesylation of *N*-Boc protected alcohol derivative **102** was achieved through treatment with methanesulfonyl chloride and triethylamine, providing **104** in high yield (scheme 38A). Additionally, *N*-Boc protected PEG alcohol **105** was iodinated using Appel conditions generating iodide **106** in a moderate 64% yield (scheme 38B).

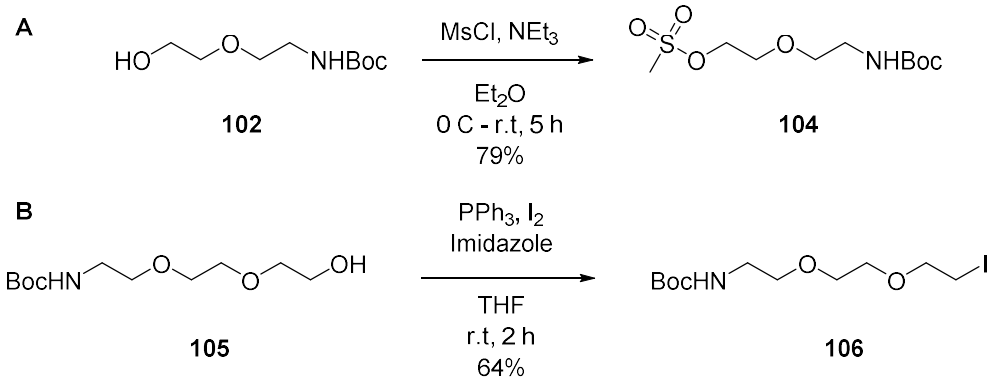

*Scheme 38: A: Mesylation strategy to prepare reactive linker **104**; B: Appel reaction used to prepare iodide derivative **106***

Next, *O*-alkylation of phenol **86** was carried out in the presence of K_2CO_3 at elevated temperature, generating **103** and **107** in good yields (scheme 39). Next, the *N*-Boc protecting groups were removed with TFA and resulting compounds **108** and **109** were coupled with **2** to yield **PROTAC-10** and -**11**.

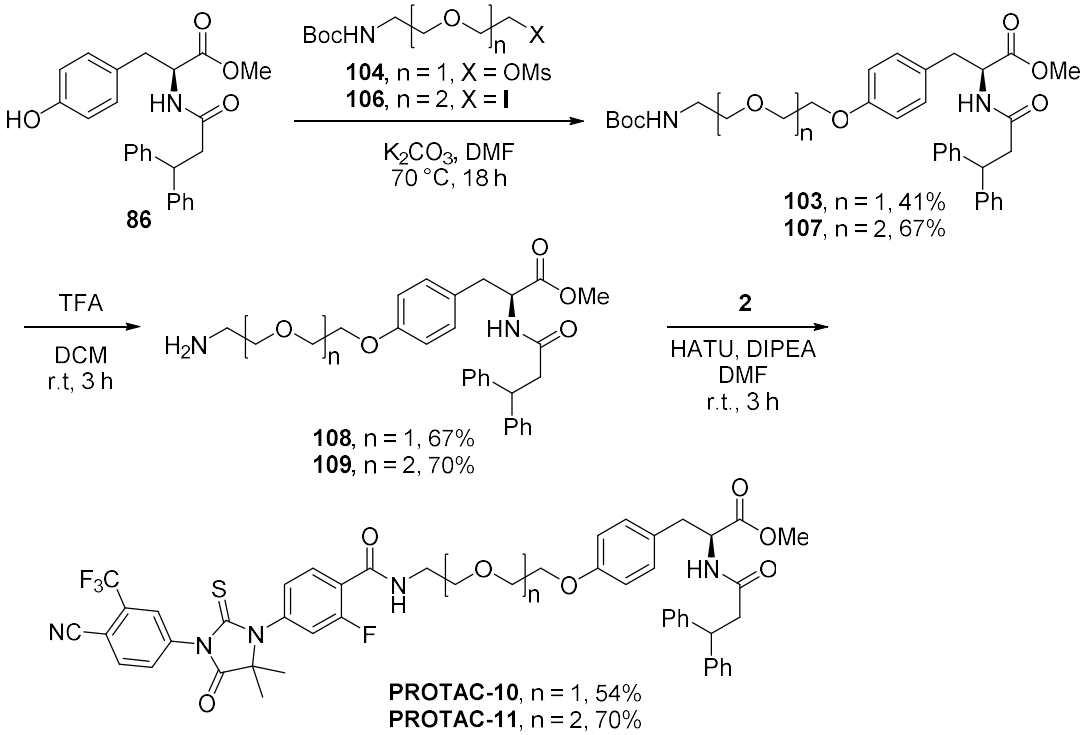

*Scheme 39: Synthesis of **PROTAC-10** and **11** through exit vector 2 via alkylation and subsequent amide coupling*

3.3.7. Synthetic procedure for imidazole based PROTACs

The final set of MDM2 binders to be incorporated into PROTACs were the imidazole scaffolds.[233] Two principle scaffolds were chosen for the PROTAC design, both of which contained useful carboxylic acid handles which could be harnessed as suitable PROTAC growth vectors (figure 71).

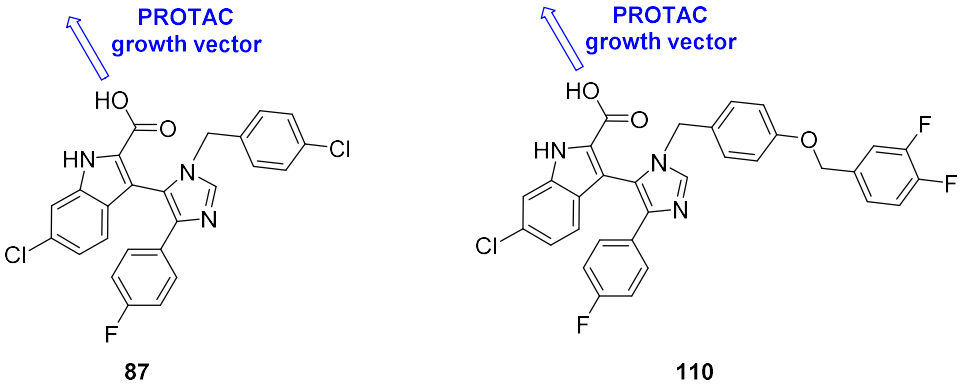

Figure 71: Structures of chosen MDM2 binding motifs with exit vector for PROTAC growth highlighted

These imidazole cores could be synthesised through a Van Leusen three-component reaction by combining an aldehyde, amine and tosyl-methyl isocyanate (TosMIC). This enabled construction of a significant level of complexity in a one-pot reaction (figure 72).

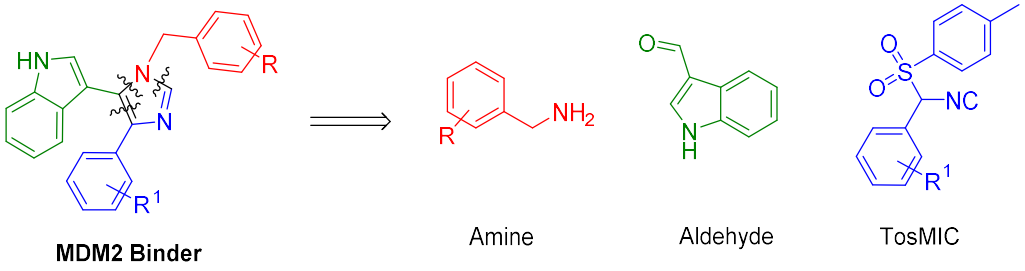

Figure 72: Retrosynthesis of the core imidazole scaffold to three components

The synthesis of these scaffolds involved reaction of common aldehydes and TosMICs with different amine derivatives. Aldehyde **112** was synthesised from commercially available substituted-indole **111** *via* a Vilsmeier-Haack formylation with $POCl_3$ and DMF (scheme 40).

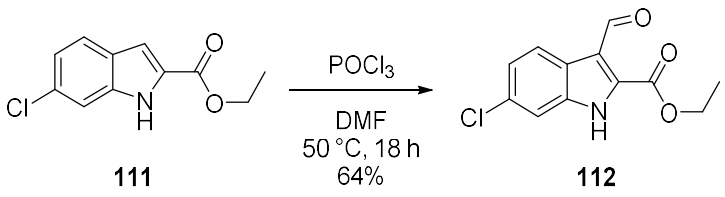

*Scheme 40: Vilsmeier-Haack formylation of indole **111** to prepare aldehyde **112***

Next, TosMIC **116** was prepared using a two-step literature process[234] from commercially available 4-fluorobenzaldehyde **113** (scheme 41). This procedure involved one-pot formation of formamide **115** *via* the intermediate bis-amide **114**. Next, formamide **115** was dehydrated using $POCl_3$ to generate TosMIC **116** in high yield.

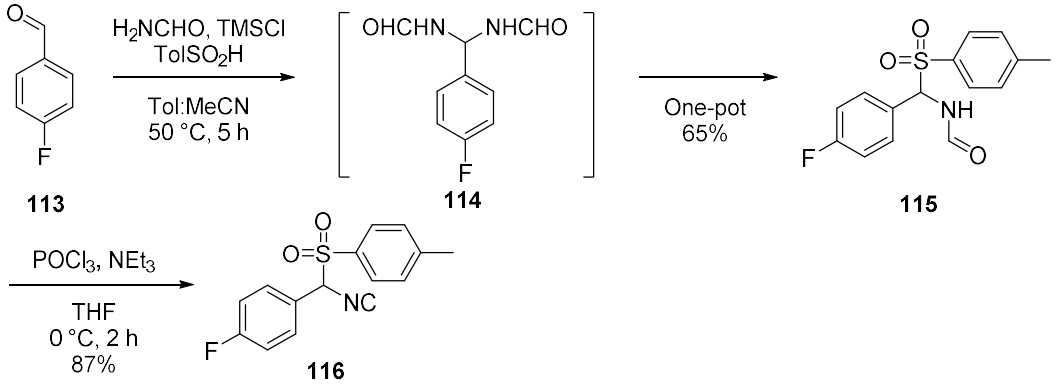

*Scheme 41: Synthesis of TosMIC **116** via two-step procedure from aldehyde **113***

With these components in hand, imidazole **118** was prepared *via* a Van Leusen imidazole formation with aldehyde **112**, TosMIC **116**, and commercially available amine **117** (scheme 42). Finally, **118** was hydrolysed under basic conditions which generated acid **87** in high yield.

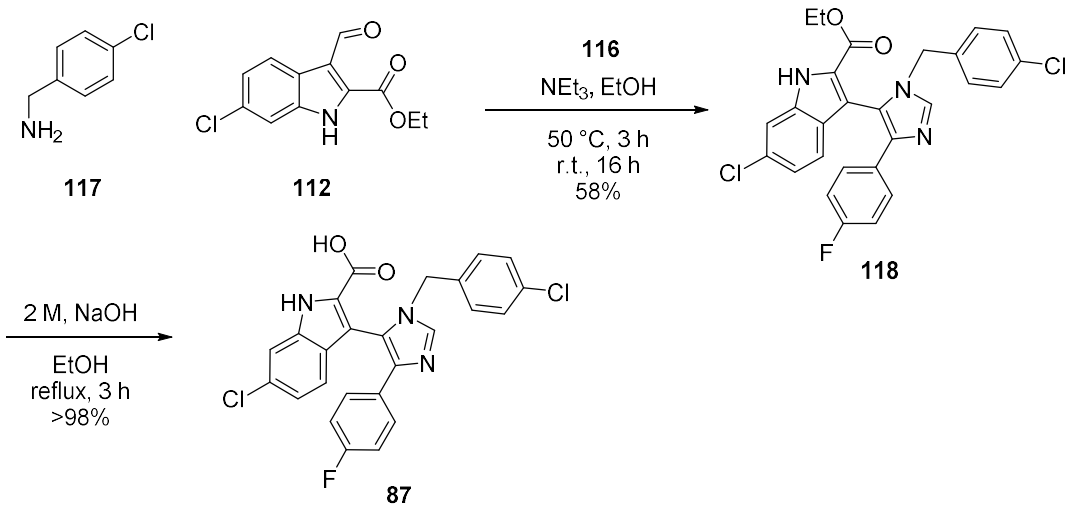

*Scheme 42: Three-component Van Leusen imidazole formation to produce inhibitor **87***

The final MDM2 binder required a more complex amine component, which was prepared through nucleophilic substitution between phenol **119** with bromide **120**, generating **121** in almost quantitative yield (scheme 43). Next, **121** was reduced to the desired amine **122** in high yield following treatment with $LiAlH_4$.

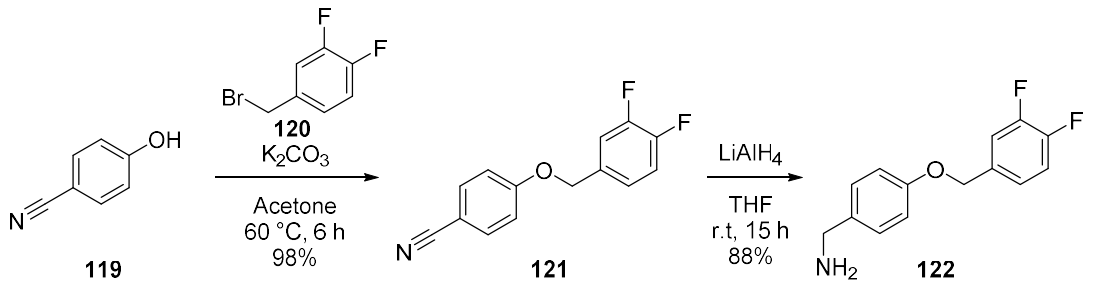

*Scheme 43: Synthesis of amine **122** through O-alkylation and subsequent reduction*

Finally, the three-component Van Leusen reaction enabled formation of the imidazole **123** in good yield (scheme 44). The ester was then hydrolysed to acid **110** in high yield.

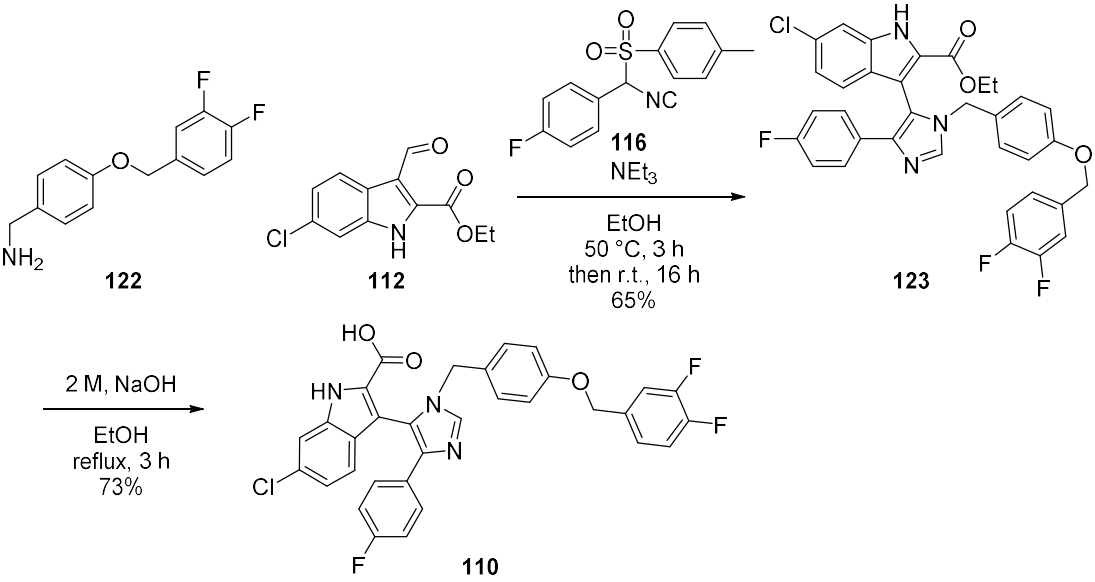

*Scheme 44: Three-component Van Leusen imidazole formation to form inhibitor **110***

With the MDM2 binders in hand, PROTAC formation was investigated through attachment of **87** and **110** to enzalutamide four-PEG linker **94**, and newly formed three-PEG derivative **125** (scheme 45).

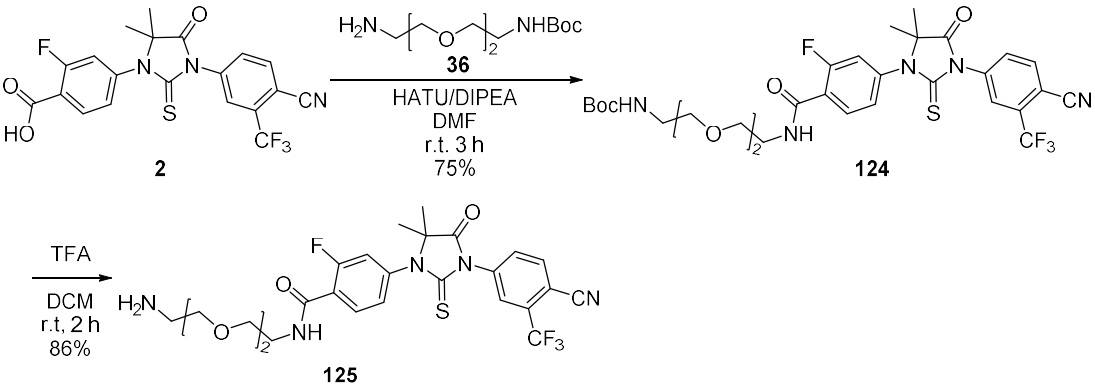

*Scheme 45: Synthesis of enzalutamide conjugated three-PEG linker **125** for direct MDM2 binder attachment*

Finally, the MDM2 recruiting **PROTACs 12-15** were generated through a series of amide coupling reactions between MDM2 binders **87** and **110** and enzalutamide PEG linkers **94** and **125** (scheme 46).

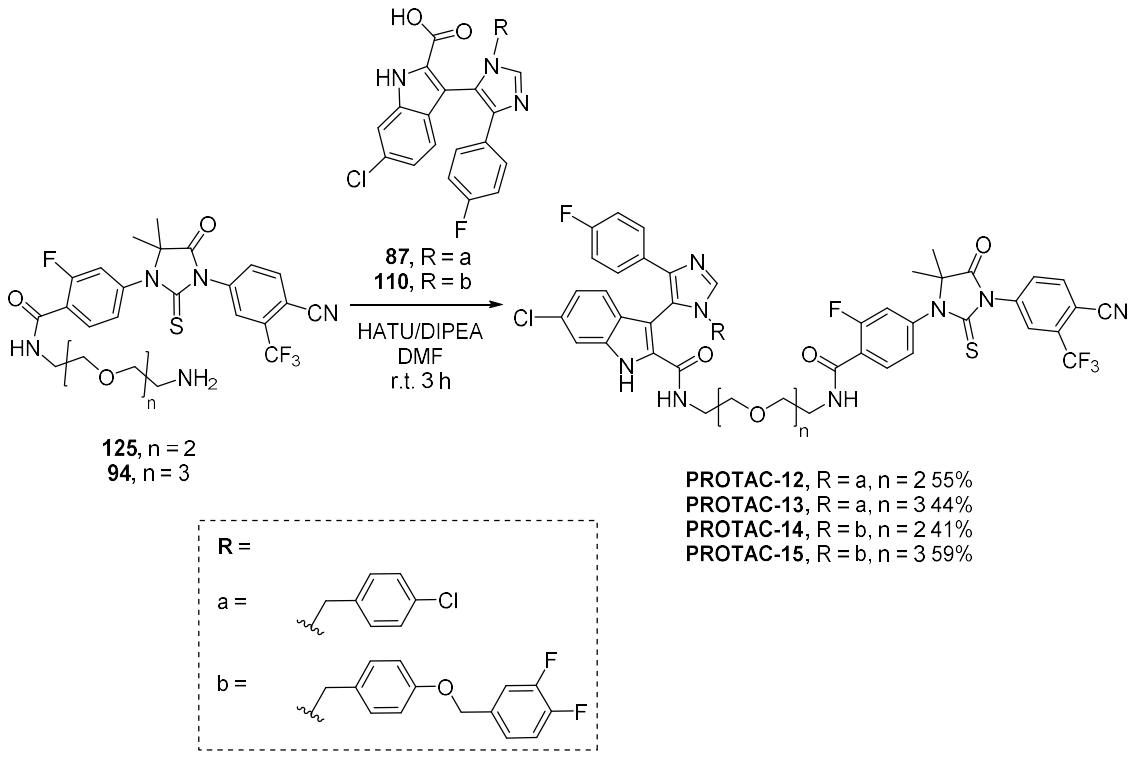

*Scheme 46: Synthesis of **PROTACs 12-15** through HATU-mediated amide coupling of MDM2 inhibitors with enzalutamide-linker derivatives **94** and **125***

3.3.8. Synthesis of small molecule VHL recruiting PROTAC

In order to enable comparison of the MDM2 PROTACs **7** – **15** in the downstream biological assessments, a VHL recruiting PROTAC targeting AR for degradation was also prepared. A VHL PROTAC would enable quantitative assessment of the activity of the MDM2 recruiting PROTACs compared to alternative E3 ligase recruiting PROTACs. Importantly, a VHL-recruiting PROTAC would be a positive control useful for future assay validation. In this case, a specific VHL binding motif was chosen based on literature examples that demonstrated high potency in the PROTAC form.[235]

The proposed **PROTAC-16** incorporated an alkyl-based linker (figure 73), in line with derivatives prepared in Chapter 2. It was hypothesised that this linker would generate a PROTAC with a comparable protein spacing to the MDM2 PROTACs, whilst avoiding the hydrophilic PEG linker, which could negatively impact the cell permeability when combined with the peptidic VHL binding moiety. The synthesis of this PROTAC was envisaged to proceed *via* simple amide coupling connections between the three PROTAC constituents VHL binder, linker and AR binder.

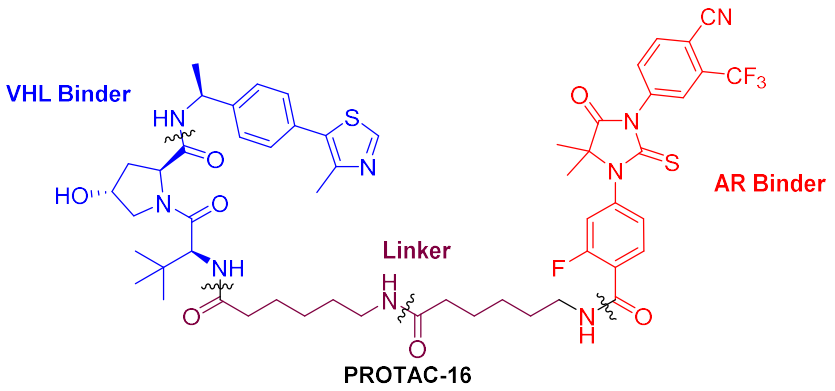

*Figure 73: Structure of VHL-recruiting **PROTAC-16** with key amide bond connections highlighted*

Synthesis of the VHL binder was carried out in line with literature procedures.[235] Firstly, commercially available amine **126** was *N*-Boc protected, followed by a palladium-catalysed C-H activation to connect 4-methyl thiazole affording **128**, which was deprotected to yield HCl salt **129** (scheme 47).

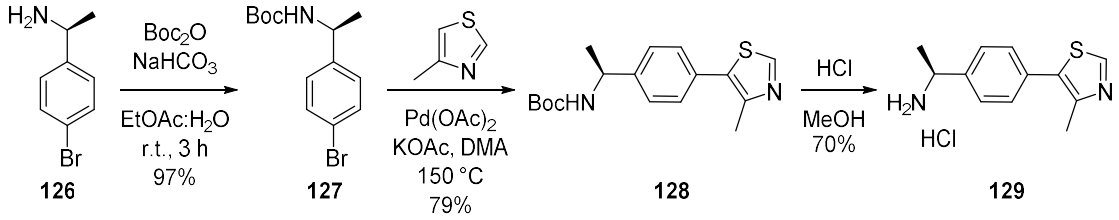

*Scheme 47: Synthesis of **129** as the HCl salt from commercially available amine **126***

Next, synthesis of the core dipeptide moiety began from commercially available amino acid **130**. This was initially protected as methyl ester **131** in good yield, then reacted with **132** to form **133**. Hydrolysis of **133** gave **134** in 70% yield. Subsequently, **134** was coupled with **129**, which afforded **135** in high yield, before a final TFA deprotection generated VHL binder **136**.

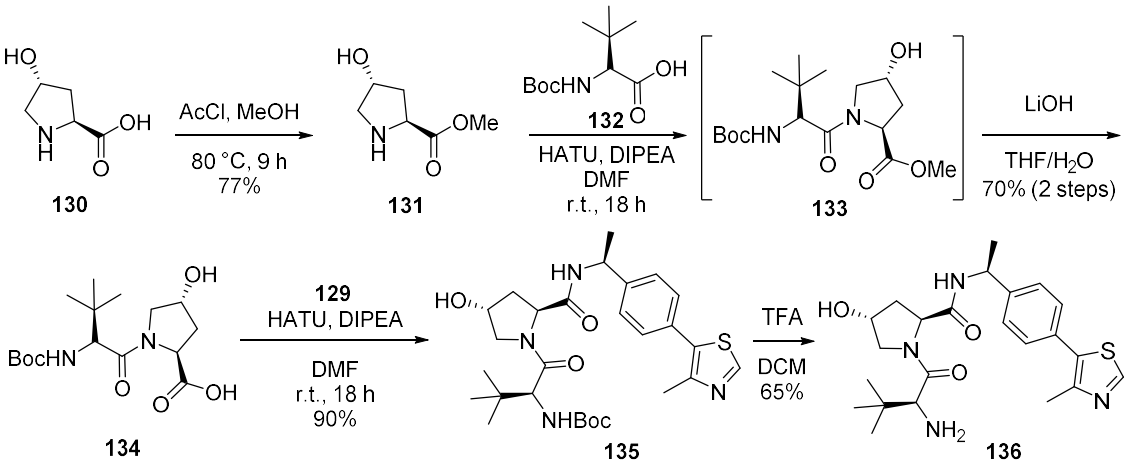

*Scheme 48: Synthesis of VHL binder **136** through a series of amide coupling and deprotection steps*

With the VHL binder in hand, the next step in the synthesis of **PROTAC-16** was to conjugate the linker. The alkyl-based linker was installed through sequential amide coupling reactions of six-carbon units **47**, followed by *N*-Boc deprotections to generate amines **138** and **140** in high respective yields (scheme 49). Finally, the AR binding derivative **2** was attached through an amide coupling, generating desired **PROTAC-16** in moderate yield.

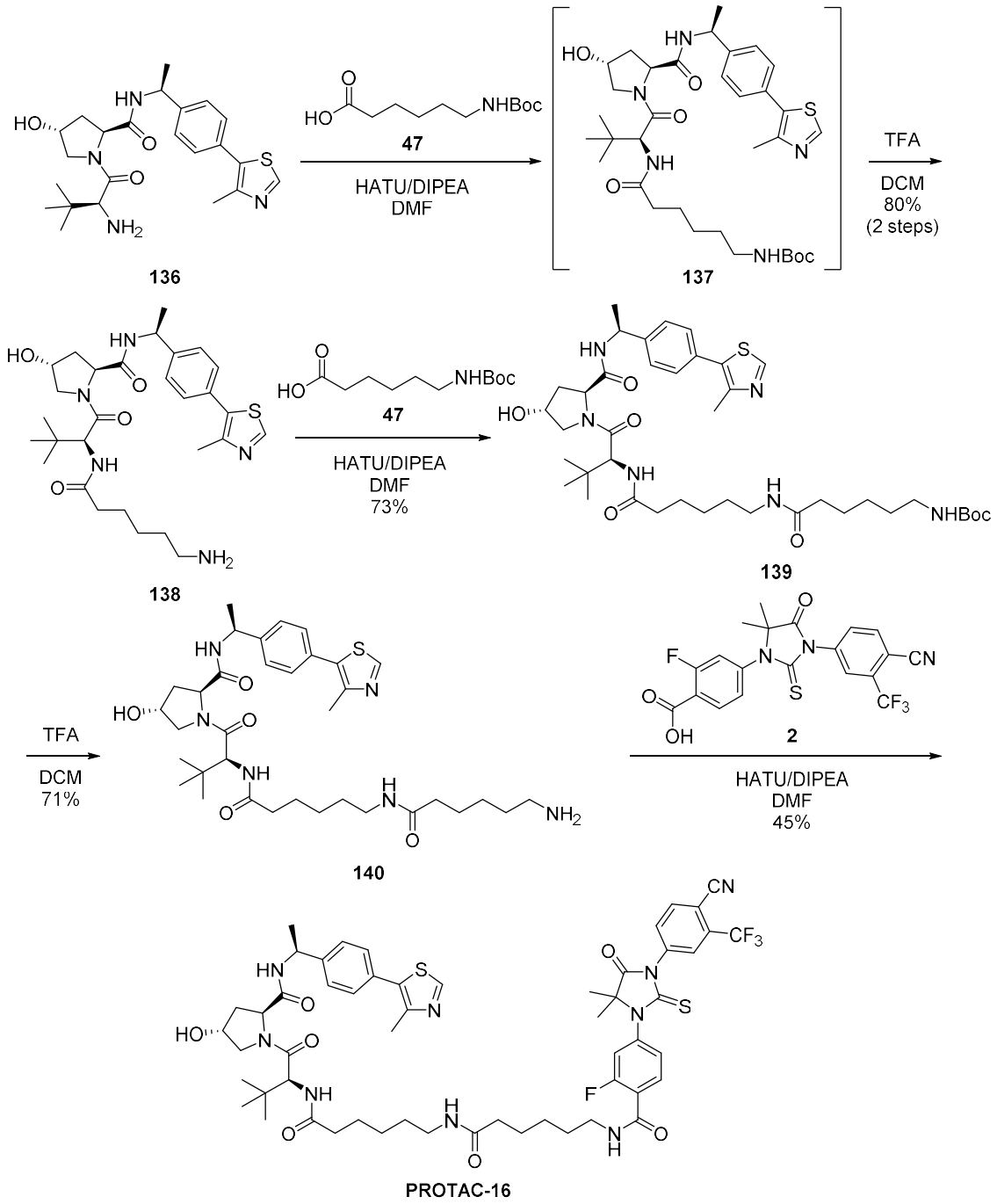

*Scheme 49: Synthesis of VHL-enzalutamide **PROTAC-16**, through amide coupling and deprotection chemistry*

Additionally, DHT-recruiting **PROTAC-17** was prepared *via* a similar route. Final conjugation of the DHT moiety was hypothesised through an esterification approach, following several unsuccessful attempts at alkylating DHT. Amine **138** was treated with succinic anhydride, which generated acid **141** in high yield. This compound was then reacted with DHT in the presence of DCC and catalytic DMAP to generate desired **PROTAC-17** (scheme 50). This final esterification proceeded in very low yield, likely due to the high steric hindrance of the DHT *neo*-pentyl alcohol. Additionally, **PROTAC-17** was discovered to be unstable with ester hydrolysis observed by NMR after one-week storage at room temperature. The instability of this PROTAC limited its utility in further biological studies, as the degradation product DHT behaves as an agonist, increasing AR levels and masking potential PROTAC degradation. Thus, incorporation of DHT into the AR degrading PROTACs was abandoned.

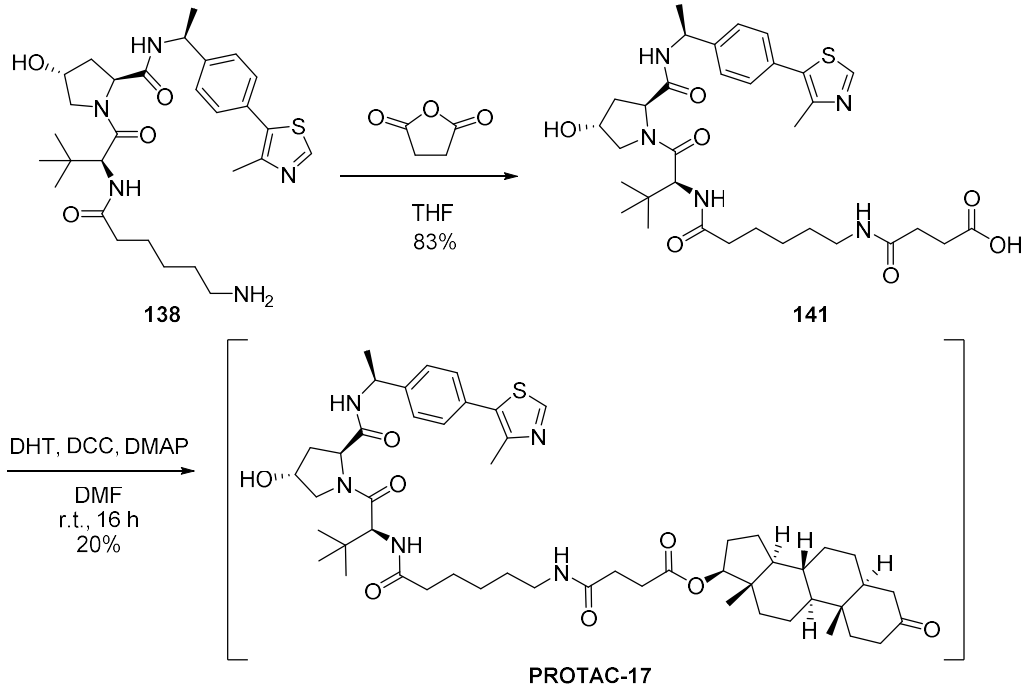

*Scheme 50: Synthesis of VHL-DHT **PROTAC-17** found to be unstable, DHT was connected through esterification*

With this series of PROTACs in hand, biological testing was conducted to establish activity of both the novel MDM2-recruiting PROTACs and the VHL-recruiting control **PROTAC-16**.

3.3.9. Biological analysis of small molecule MDM2 PROTACs

The synthesised MDM2-recruiting PROTACs were then biologically assessed using a high-throughput AlphaScreen® assay. This assay is based upon the CETSA AlphaScreen® AR degradation protocol used in Chapter 2 with slight modifications. Initially, each PROTAC was incubated for 16 h with AR-positive

LNCaP cells, followed by cell fixing, treatment with an AR antibody pair, and subsequent plate analysis. The endpoint of the assay is detection of endogenous AR by AlphaScreen®, hence cellular AR levels are measured following PROTAC treatment. This simple, high-throughput assay was used to narrow down the MDM2 inhibitors used for this series of PROTACs to the most promising ones. This efficient strategy allows for further synthetic efforts to be more focussed. The graphs were analysed and qAC50 values were reported corresponding to the concentration required to induce 50% activity. These assays were run by Dr Andreas Hock at AstraZeneca.

Firstly, a series of controls were analysed (figure 74). The positive control used for this assay was known degrader niclosamide. This gave a good dose-response curve correlating to 228 nM potency, within the accepted range expected for this AR degrader. The negative controls used were DMSO, which showed no response in this assay as well as enzalutamide. Enzalutamide is an AR antagonist, which is unable to degrade AR hence no obvious dose-response curve was observed. There was a slight downward correlation for the enzalutamide control which most likely corresponds to its anti-proliferative effect on AR-positive cell-lines, such as these LNCaPs, due to its strong antagonistic activity.

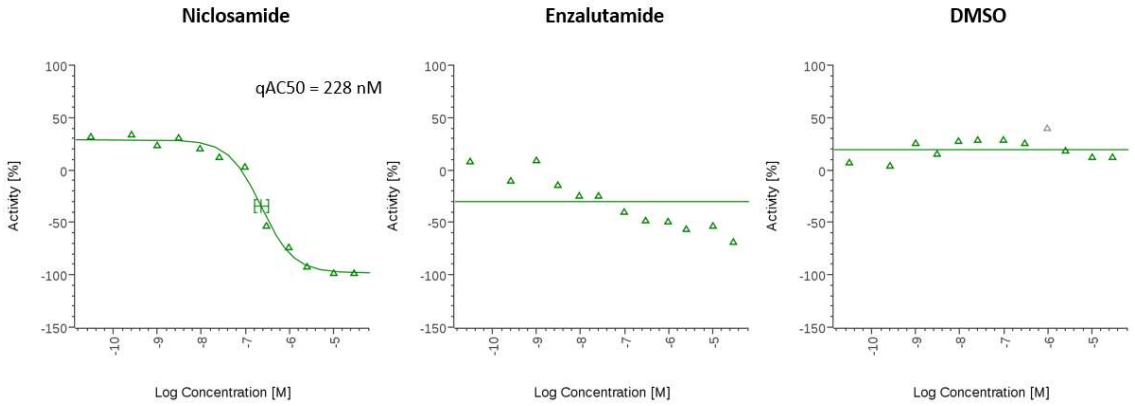

Figure 74: Dose-response curves for controls, positive control niclosamide and negative controls enzalutamide and DMSO, run by Dr Andreas Hock

The MDM2 binders were also run as controls, to understand whether they had any effect on AR levels independent to the PROTAC activity. Binders **85**, **86** and **110** were found to have no effect on AR levels in this assay (figure 75). However, the remaining two MDM2 binders had a positive concentration dependent effect on the cells, calculated to be around 6.0 µM for **87** and 1.2 µM for **SP-141**. There are a few different factors which may have caused this response. It could be a result of various limitations of the assay, which does not account for the toxicity or antiproliferative effects that these compounds may invoke. This is particularly relevant for known MDM2 inhibitors, which are able to invoke cell cycle arrest therefore limiting cell proliferation due to inhibition of the p53-MDM2 interaction.[236] This

effect has also been observed in LNCaP cells treated with MDM2 inhibitor nutlin 3a,[237] which further complicates the validation of these compounds. In addition, the assay also does not measure compound precipitation which can give false positives in the data. If the compound has poor solubility it will precipitate on addition to the cells on the plate, the precipitate may cause cell death which would be difficult to distinguish from a positive result. Solubility is unlikely to be an issue at these concentrations due to their low molecular weight and the presence of hydrophilic handles. However, solubility of the full PROTAC structures is expected to be lower due to the high molecular weight.

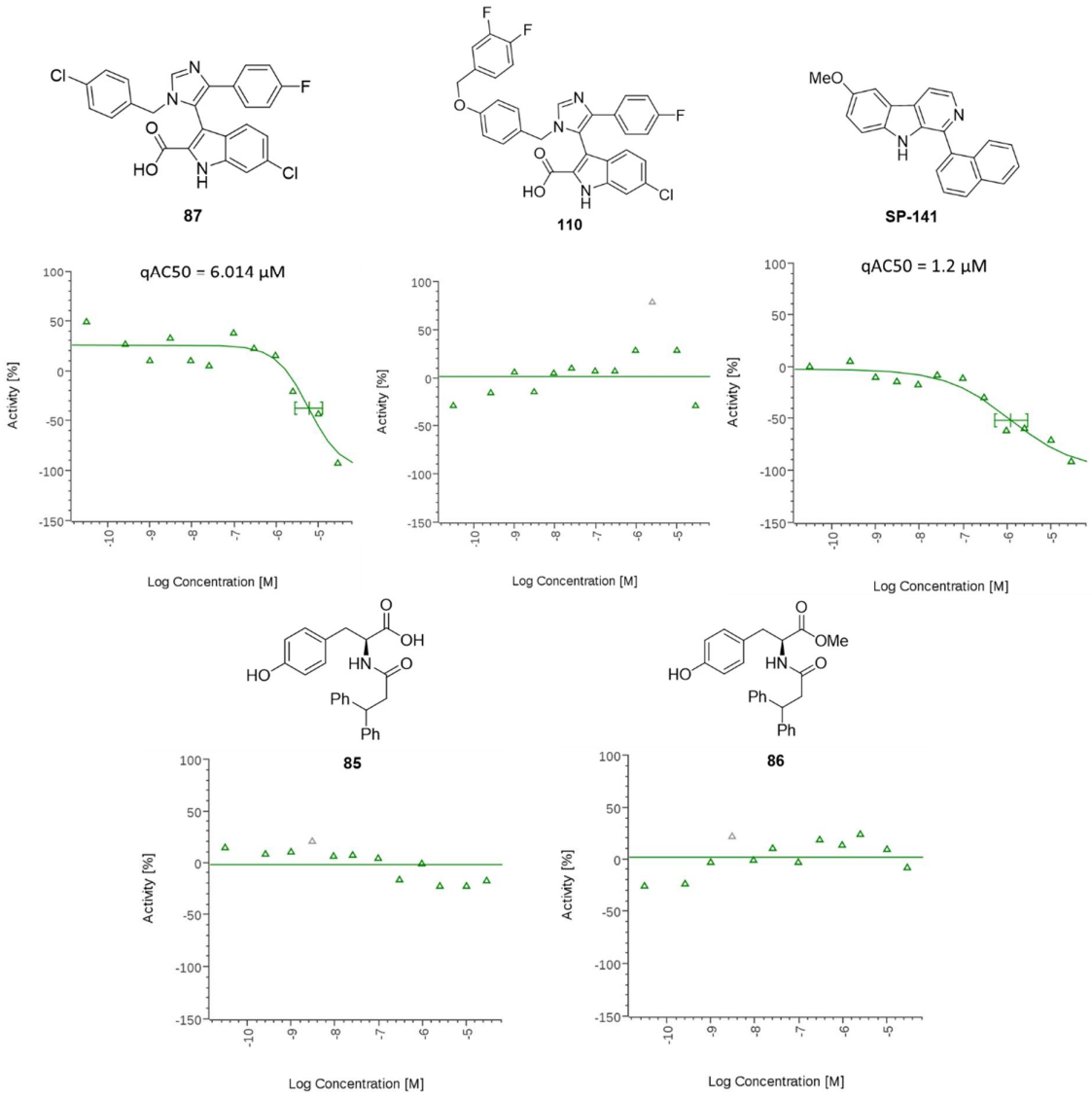

Figure 75: Dose-response curves for MDM2 inhibitor control compounds, run by Dr Andreas Hock

The SP-141-derived **PROTAC-7** also displayed reasonable activity in this assay (figure 76). However, the qAC_{50} calculated was 885 nM, which was of a similar magnitude to the inhibitor alone. This was not a promising result, as connecting the PROTAC had no obvious benefit.

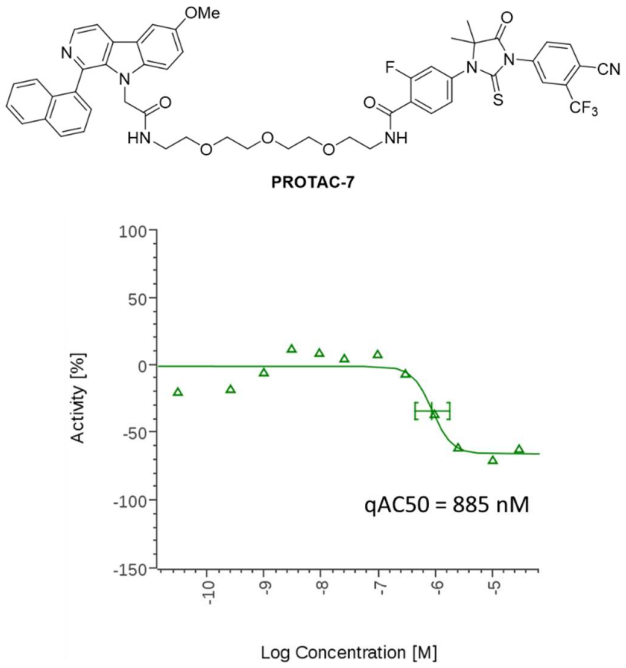

*Figure 76: Dose-response curve of SP-141-based **PROTAC-7**, run by Dr Andreas Hock*

Next, the tyrosine based PROTACs were investigated. Both MDM2 binders **85** and **86** exhibited no activity in the assay, thus any activity observed would be promising. PROTAC elaboration through exit vector 1 enabled degradation activity for **PROTAC-8** and **-9** with low µM qAC_{50} observed (figure 77).

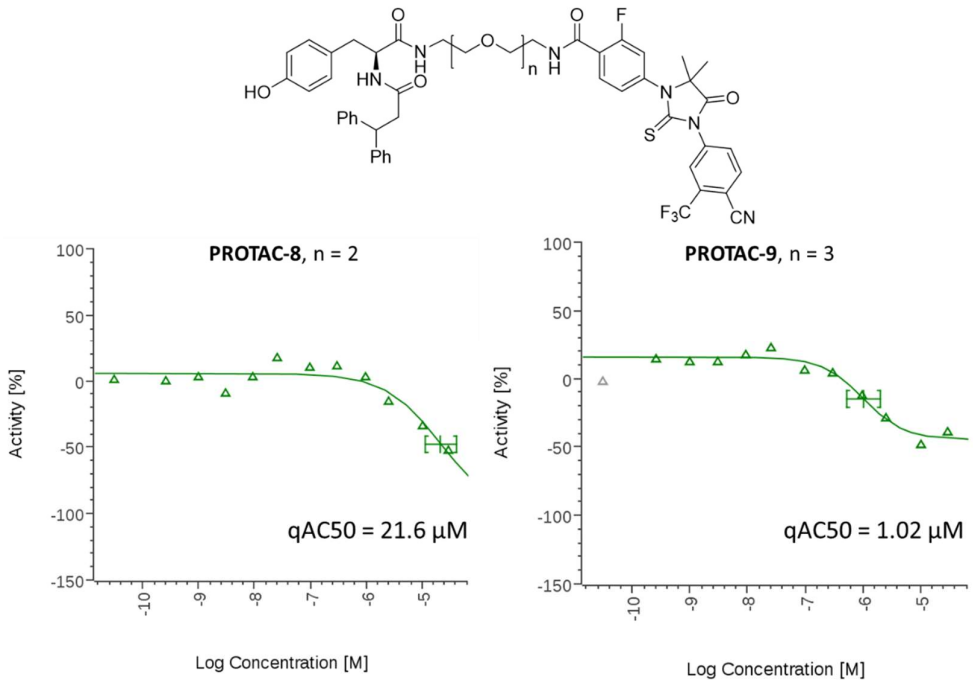

Figure 77: Dose-response curves for tyrosine-based PROTACs connected through exit vector 1, run by Dr Andreas Hock

Results attained from the phenol exit vector 2 looked generally more promising (figure 78). **PROTAC-10** and **-11** had reasonable activity in the low µM, with the longer PEG linker exhibiting higher potency and degrading AR to a greater extent compared to **PROTAC-8** and -**9**. Accordingly, this exit vector was hypothesised to be more promising for further PROTAC development.

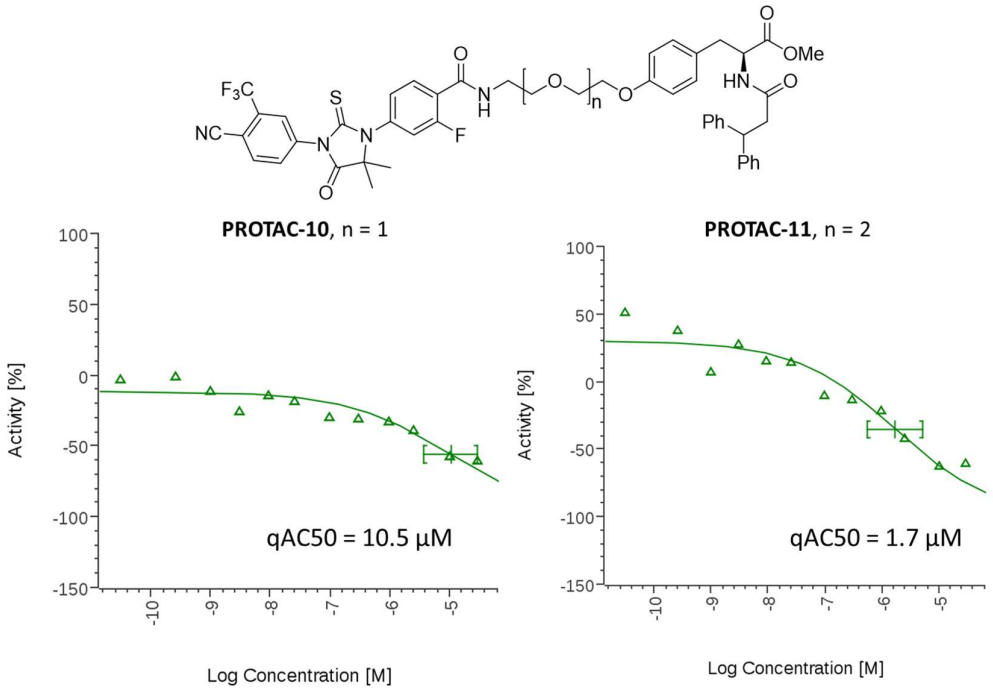

Figure 78: Dose-response curves for tyrosine-based PROTACs connected through exit vector 2, run by Dr Andreas Hock

Following these promising results, **PROTACs 12-15** which incorporated the imidazole based MDM2 binders **87** and **110** were examined (figure 79). The most potent compound was **PROTAC-13**, which gave a qAC_{50} of 348 nM. The shorter PEG chain length variant **PROTAC-12** showed no obvious activity. The potency of this compound was 20-fold higher than the control MDM2 inhibitor **87** alone, indicating potential PROTAC activity. The difluoroaryl substituted **PROTACs 14-15** gave slight activity at the highest concentrations, corresponding to qAC_{50} of 10.2 and 23.5 µM for the respective PEG chain lengths. Although the corresponding control inhibitor **110** exhibited no activity, these PROTACs had very weak effects in the assay. Overall, this indicated that **87** was the most promising of the two scaffolds, with good activity observed at the longer linker length.

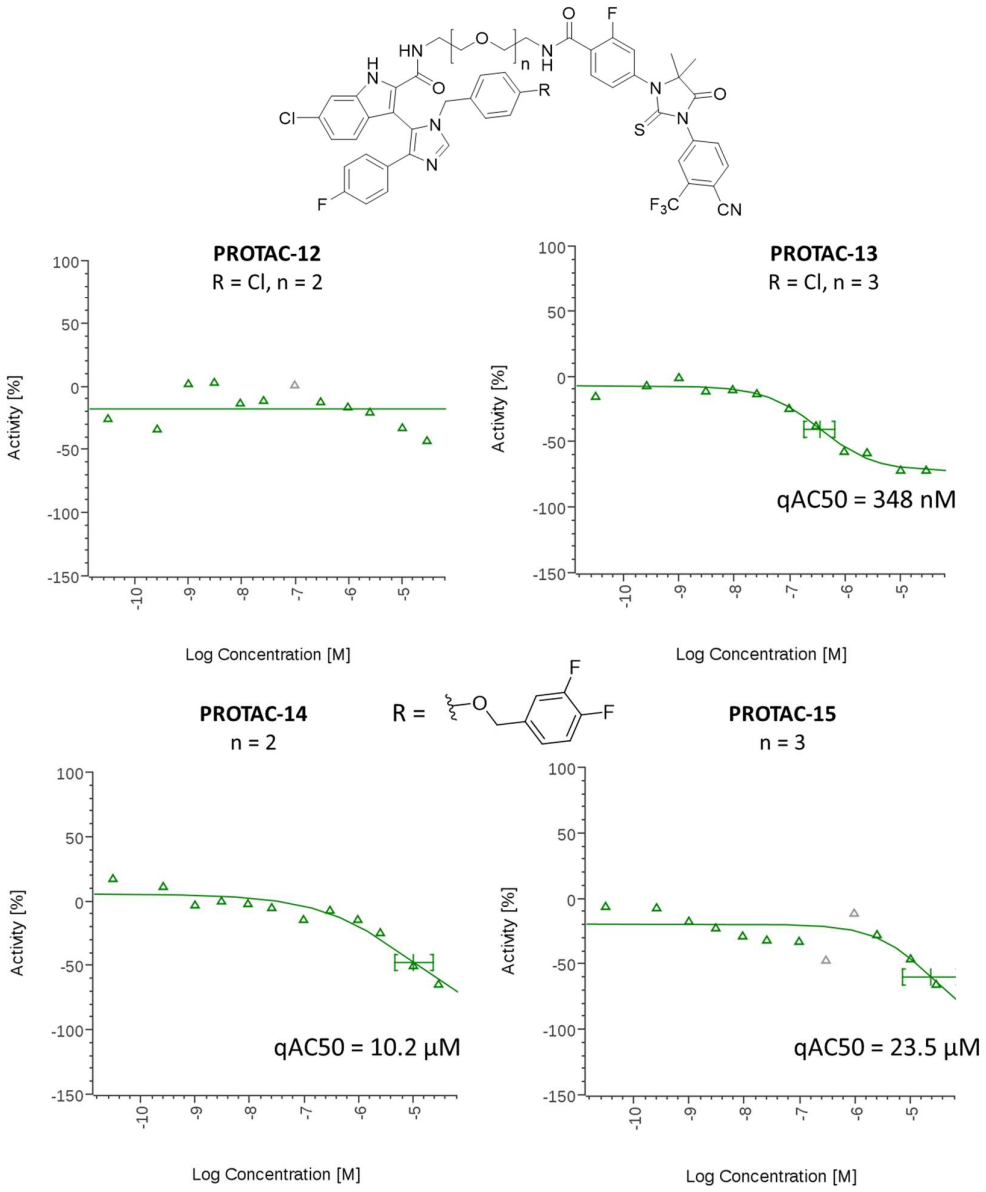

Figure 79: Dose-response curves for imidazole based MDM2 PROTACs, run by Dr Andreas Hock

Finally, the control VHL-recruiting **PROTAC-16** was screened (figure 80). Interestingly, **PROTAC-16** did not appear to be more active than the MDM2-recruiting PROTAC series despite recruiting VHL, a well-validated E3-ligase. This may result from the unoptimised linker, as many more variants would be required to optimise AR degradation levels and PROTAC potency.

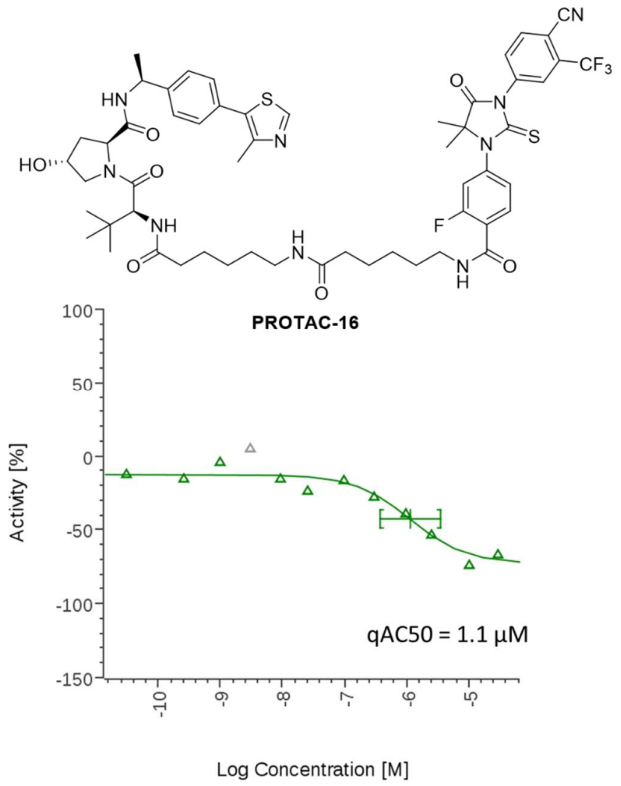

*Figure 80: Dose-response curves for VHL-recruiting **PROTAC-16** run by Dr Andreas Hock*

These initial findings were promising, as activity was observed for a large proportion of the synthesised PROTACs across almost all the MDM2 binding scaffolds. Notably, none of the tested PROTACs achieved 100% AR degradation, the reduction for all PROTACs was *ca.* 50% or under. This is not particularly unusual for unoptimized PROTACs, as it is well known that linker length and properties have a major effect on not only potency but extent of protein degradation. The activity observed in this assay for the MDM2 inhibitors alone additionally complicates PROTAC analysis, hence a more informative assay was required to elucidate this further. Ideally, future assays would be capable of differentiating between toxicity, precipitation and AR degradation activity.

3.3.10. Synthesis of additional PROTACs using alternative linkers

It was hypothesised that through additional linker variation the activity and extent of AR degradation could be optimised. Synthetic efforts were focussed on the scaffolds identified by the AlphaScreen® assay to be most promising, **87** and **86** connected through the phenol exit vector.

A longer linker was chosen for **PROTAC-17,** incorporating chloro-substituted MDM2 binder **87**. A PEG linker with a length of 19 atoms was hypothesised to be a good comparison to **PROTAC-12** and **-13**, containing 13 and 16 atoms respectively. Due to a low supply of enzalutamide acid **2**, the synthesis

was carried out in the direction of MDM2 binder **87** to AR binder **2** (scheme 51). Initially, acid **87** was coupled with amine **30** in the presence of HATU and DIPEA to form **142** in moderate yield. This was then *N*-Boc deprotected using TFA and the amine immediately coupled with enzalutamide acid **2** to generate **PROTAC-17** in 51% yield over two steps.

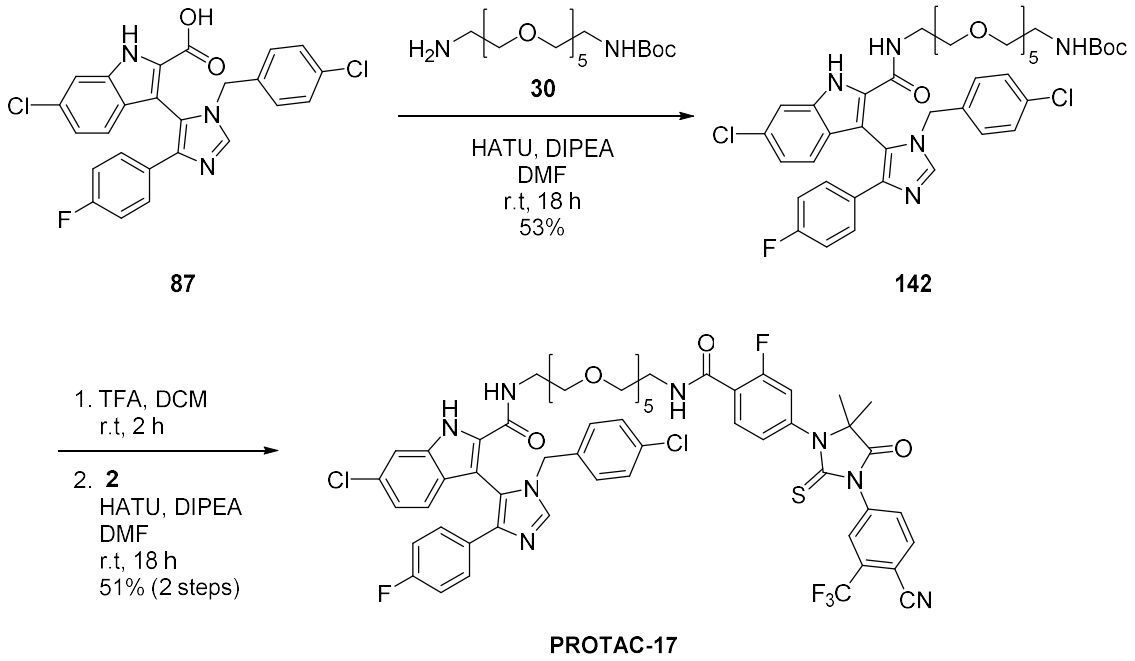

*Scheme 51: Synthesis of six-PEG linker imidazole based **PROTAC-17***

In addition, longer linkers were chosen for MDM2 binder **86**, a four-unit PEG linker gave an overall distance of 12 atoms. The required mesylate linker **144** was prepared through mesylation of commercially available alcohol **143** through the previously used procedure (scheme 52).

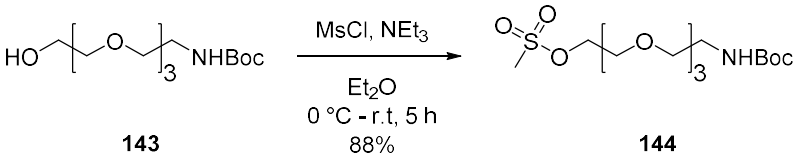

*Scheme 52: Mesylaton of alcohol **143** to form mesylate **144***

The mesylate **144** was then subjected to *O*-alkylation conditions with phenol **86** to form **145** (scheme 53). The *N*-Boc protecting group was then removed with TFA and the enzalutamide acid **2** was conjugated through an amide coupling reaction, generating **PROTAC-18** in good yield. Both the methyl ester **PROTAC-18** and the hydrolysed acid **PROTAC-19** were prepared for further biological testing. It was hypothesised that the acid moiety would improve the PROTACs overall solubility profile, whilst maintaining MDM2 binding affinity.

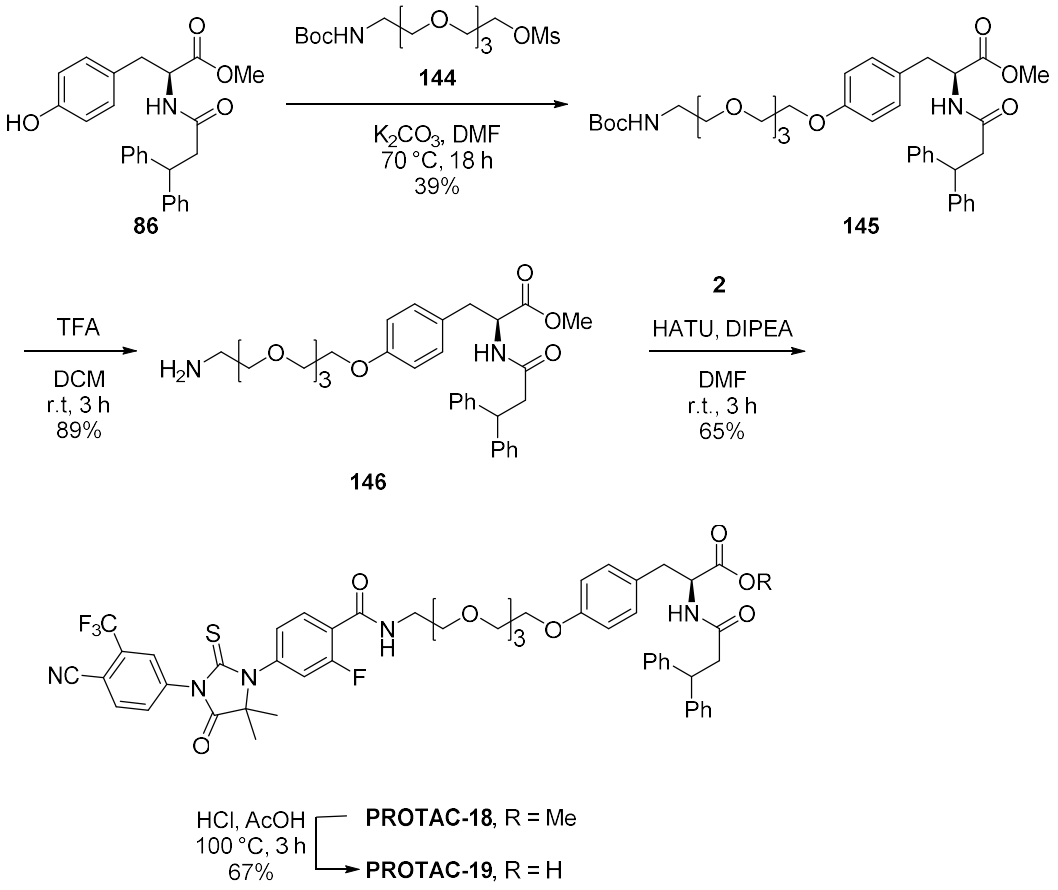

*Scheme 53: Synthesis of **PROTAC-18** and **-19** connected via a four-PEG linker*

Furthermore, an increased linker length was investigated to fully probe linker distance for this MDM2-recruiting PROTAC series. It was proposed that attachment of a two-carbon appendage to the phenol **86** could extend the linker length to 15 atoms (scheme 54). With this strategy in mind, phenol **86** was treated with *tert*-butyl bromoacetate in the presence of K_2CO_3 forming **147** in high yield. Next, the *tert*-butyl ester was deprotected using TFA to selectively hydrolyse this ester in the presence of the methyl ester giving acid **148** in almost quantitative yield. Acid **148** was then treated with four-PEG amine **92** to generate **149** in moderate yield. The *N*-Boc group was then removed in TFA in quantitative yield and the resulting amine **160** was subject to amide coupling conditions with enzalutamide acid **2** in the presence of HATU and DIPEA to generate desired **PROTAC-20**.

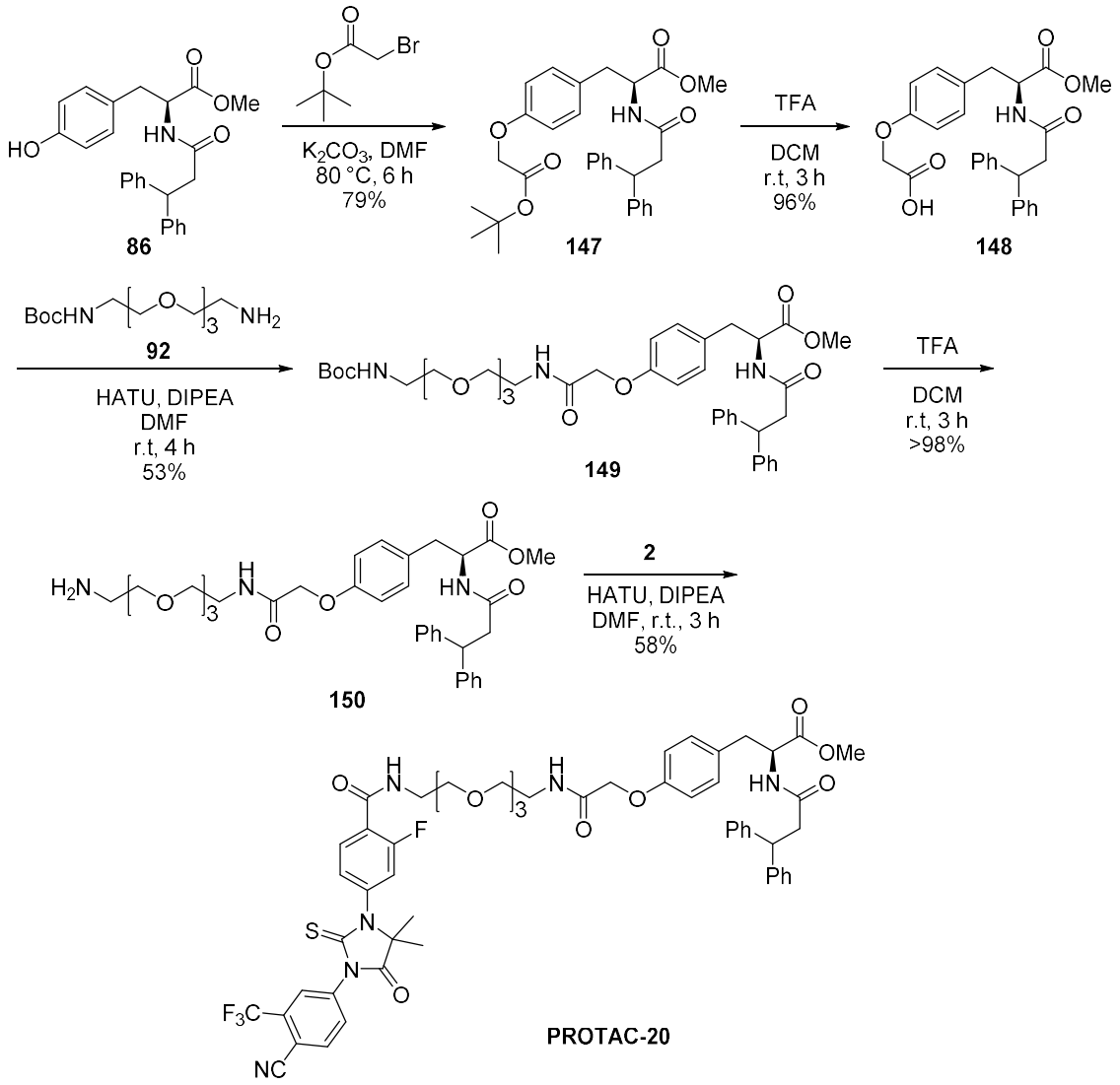

*Scheme 54: Synthesis of **PROTAC-20** with extended linker length*

3.3.11. Further biological testing considering AR levels

Due to the limitations with the high-throughput AlphaScreen® assay previously discussed, an alternative assay was investigated to further analyse this PROTAC series. An imaging assay developed by AstraZeneca was hypothesised to be a good alternative. This assay measured AR levels in addition to imaging the cells, which gave an indication of cell viability. Importantly, the assay was also able to calculate the number of live cells at the assay endpoint, hence could identify toxicity related effects. In addition, the assay could observe any compound solubility issues which could lead to unreliable results. This assay was performed by Dr Andreas Hock at AstraZeneca.

LNCaP cells were plated and compounds dosed in a 11-point, one in two dilution with a top concentration of 30 µM. The plates were incubated for 16 h before being fixed and stained for AR. The PROTACs were not run in replicate, as this enabled screening of all PROTACs on one plate to identify interesting hits. A subsequent assay run in the future would provide the duplicate data for validation.

Niclosamide and DMSO were used as the respective positive and negative controls in this assay (figure 81). Niclosamide exhibited a strong dose-response curve, comparable to previous runs. However, the reduction in nuclear count at top concentrations indicated some toxicity. DMSO treatment showed no overall trend in AR levels or reduction in nuclear count.

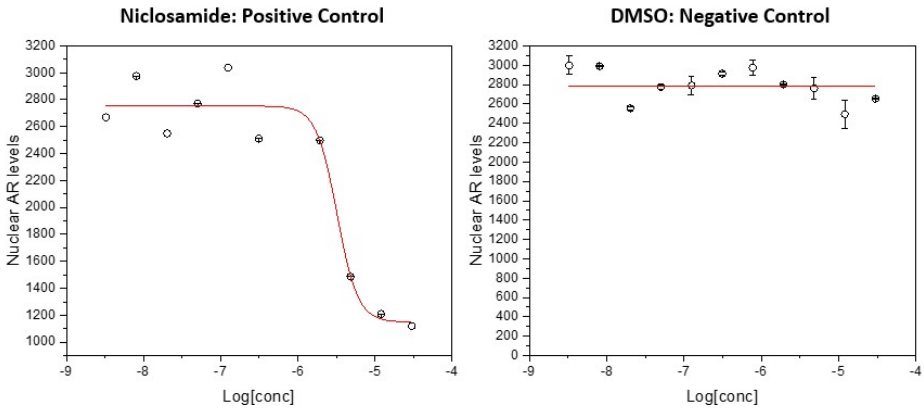

Figure 81: Dose response curves for positive control (niclosamide) and negative control (DMSO) run by Dr Andreas Hock

Next, the MDM2 inhibitor controls **85**, **86**, **87** and **110** were analysed. As three of the five MDM2 binders exhibited a positive dose response curve in the previously used AlphaScreen® assay, these results would enable further validation of this imaging assay. These MDM2 binders indicated no change in AR levels or toxicity (figure 82). Enzalutamide acid **2** also exhibited no degradation.

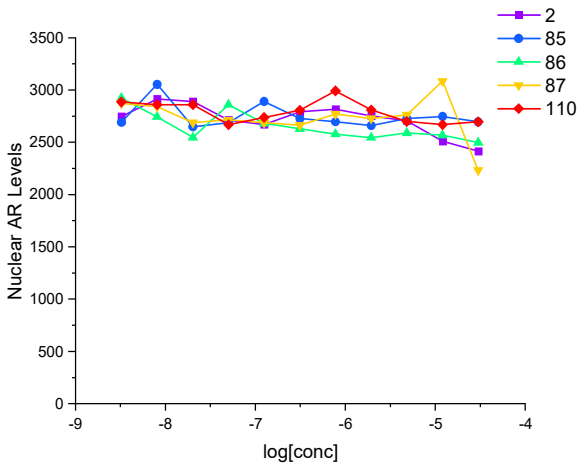

*Figure 82: MDM2 inhibitor controls **85**, **86**, **87** and **110** and enzalutamide acid **2**; performed by Dr Andreas Hock*

The final MDM2 binder considered, **SP-141**, conclusively indicated its high toxicity (figure 83). Considering only AR levels generates a strong dose response curve, indicating high potency. However, when nuclear count was considered, the toxicity of this compound was obvious, at high dose a substantial level of cell death was observed.

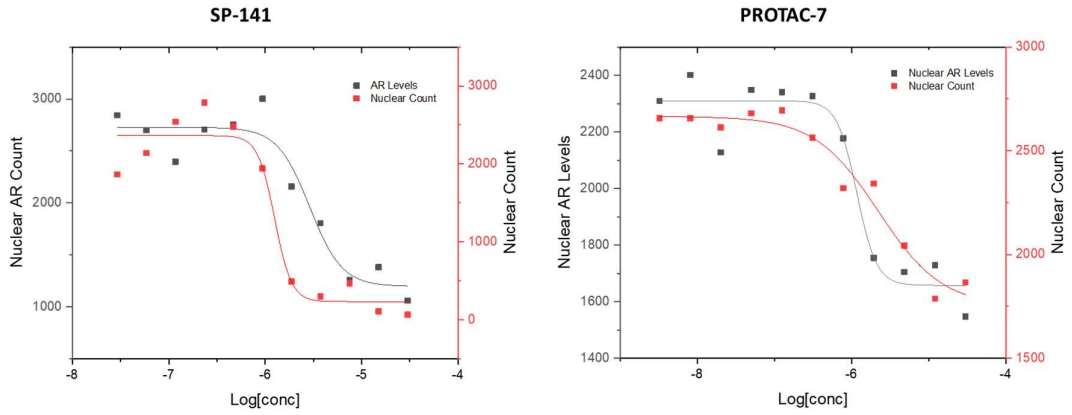

*Figure 83: SP-141 and **PROTAC-7** effects on LNCaP cells considering AR nuclear levels and cell count, performed by Dr Andreas Hock*

Next, the MDM2 PROTACs incorporating imidazole based binders were investigated. Independently, these MDM2 inhibitors exhibited no activity against the cells, with the nuclear count indicating no obvious toxicity effects. **PROTAC-14** and **-15**, based on MDM2 binder **110**, did not show clear dose-response curves (figure 84A). **PROTAC-14** showed a general downward trend in AR but with no plateauing at high or low concentration. **PROTAC-15** looked slightly more promising with stable AR levels until almost the top concentration (30 µM) where levels drop, however the potency of this PROTAC is far too weak to follow up. The PROTACs based on the chloro-substituted imidazole derivative looked more interesting (figure 84B). **PROTACs 12, 13** and **17** all showed more typical dose-response curves, **PROTACs 12** and **17** both did not plateau despite AR levels being reduced by *ca*. 33%. **PROTAC-13** displayed a good sigmoidal curve, indicating approximately low micromolar potency. However, the extent of AR degradation following incubation with this PROTAC was fairly low, *ca*. 20% AR reduction. Despite this incomplete AR degradation and low µM potency, **PROTAC-13,** which incorporated a four-PEG unit linker was the most promising of this imidazole PROTACs series. It was hypothesised that additional optimisation of linker length and characteristics would improve both activity indicators.

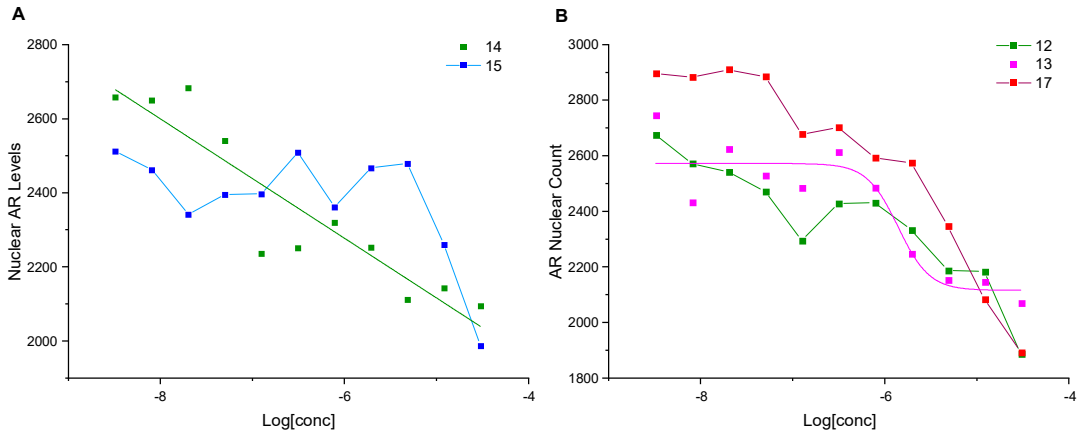

*Figure 84: Dose-response curves of imidazole-based MDM2 PROTACs A) **110** based MDM2 binder; B) **87** based MDM2 binder; performed by Dr Andreas Hock*

Additionally, the MDM2 PROTACs incorporating binders **85** and **86** also showed some promising results. **PROTAC-8** and **-9**, derived from the acid exit vector on the MDM2 inhibitor were less interesting (figure 85A). Despite a reasonable level of AR degradation observed, the curves did not plateau in the concentration ranges used, indicating extremely low potency. The phenol exit vector derived PROTACs had improved dose-response curves (figure 85B). **PROTAC-10** was the most potent with a DC_{50} of *ca.* 600 nM, and 33% AR degradation. **PROTAC-18**, which contained an additional PEG unit in the linker region, had a similar potency and degradation extent. **PROTAC-11** and **-20** exhibited AR degradation however the shape of their dose-response curves was less appealing as showed a downward trend rather than a typical sigmoidal shape. Finally, **PROTAC-19** looked even less promising for similar reasons.

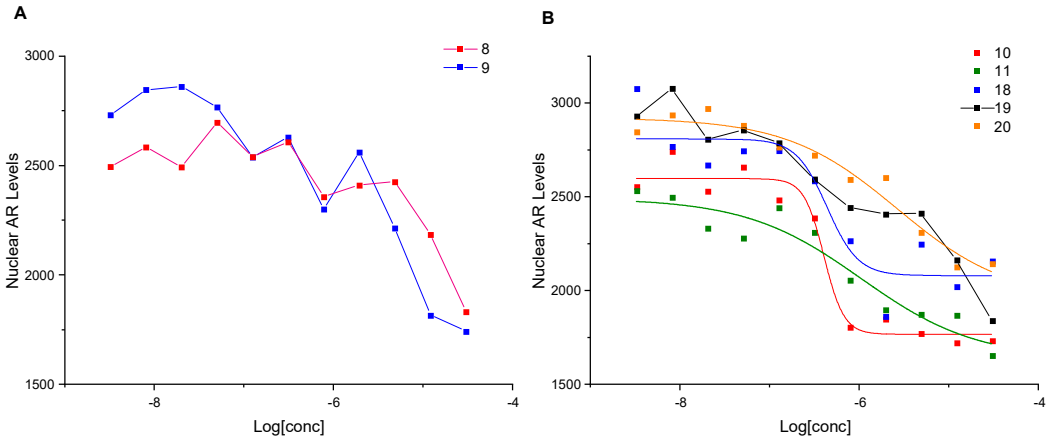

Figure 85: Dose-response curves of tyrosine based MDM2 PROTACs A) through acid exit vector; B) through phenol vector; performed by Dr Andreas Hock

Overall, some promising results were identified through this round of MDM2 PROTAC testing. Compared to the positive control niclosamide, **PROTAC-10** exhibited greater potency. Additionally, **PROTAC-13** generated a dose response curve with reasonable potency. Although AR degradation was displayed by most of these PROTACs, full AR degradation was not identified in any case. However, this is not unusual for a small set of unoptimized PROTACs, as considerable linker variation is a well-established strategy for improvement in potency and extent of degradation.

To gain further insight into the mode of action of these novel PROTACs, more biological testing was proposed. Firstly, the binding of the MDM2 PROTACs to MDM2 was investigated in enzymatic assays. This was an important control measure to ensure the degradation observed was *via* E3 ligase MDM2. It was theorised to be less important to validate AR binding, as these enzalutamide-based binders have been used commonly in literature and patents, hence their ability to bind and degrade AR was well-established as discussed in Chapter 2.

In addition, validation of the proteasome mediated AR degradation was postulated to be an important control. One way to investigate this would be to dose an excess of the E3 ligase binder with the PROTAC. This ligand would outcompete the PROTAC and prevent formation of the active ternary complex, thus eliminating AR degradation. This supports the theory that the PROTAC acts *via* recruitment of the E3 ligase and therefore the UPS. This control has been used predominantly for VHL and cereblon PROTACs, however, MDM2 PROTACs would be more difficult to investigate with this approach due to the biologically relevant MDM2-p53 PPI. MDM2 inhibitors are well-known to prevent cell proliferation and initiate cell death, hence dosing this inhibitor would not clearly show the correlation between AR degradation and MDM2 PROTAC, due to the convoluted data.

An alternative method of confirming the UPS degradation pathway, would be to block the proteasome using an inhibitor known as epoxomicin.[238] Dosing this inhibitor alongside the PROTAC is hypothesised to knockout degradation activity, as the proteasome would be unable to function. For MDM2 recruiting PROTACs, this could be the most conclusive strategy for UPS validation.

3.3.12. Assessment of MDM2 Binding through FP and DSF

In order to measure the binding of the PROTACs to MDM2, competitive FP was performed as described in Chapter 2. The assay was carried out in triplicate and the top concentration achieved was dictated by compound solubility, in most cases limited to 0.3 mM. A 23-point, two in three titration curve was obtained for each PROTAC following incubation with recombinant MDM2. Controls of nutlin 3a and the known MDM2 binding peptide sequence, **P1**, were used for assay validation.

SP-141 based **PROTAC-7** was first investigated, at top concentration of 0.3 mM (figure 86). **PROTAC-7** showed extremely limited activity against MDM2 under these conditions. Further studies were undertaken to measure the binding affinity of MDM2 binder **SP-141** to MDM2. Unfortunately, no obvious activity was observed even at top concentration of 50 µM. This was a surprising result as Wang *et al.* had reported the **SP-141** motif to bind to MDM2 with *ca*. 28 nM affinity.[229] In this publication, it was proposed that **SP-141** binds in the same pocket as p53, hence it would be expected to be active in this assay. In accordance with these results, further studies using DSF were proposed for validation.

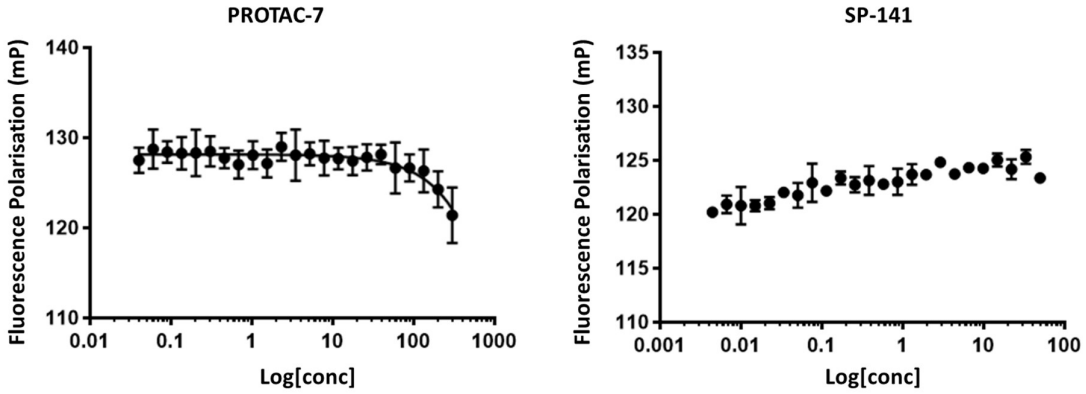

*Figure 86: FP curves for **PROTAC-7**, top concentration of 0.3 mM and **SP-141**, top concentration of 50 µM*

Following these disappointing results, the tyrosine based MDM2 PROTACs were analysed. **PROTAC-8** and **-9,** which incorporate the linker through the carboxylic acid exit vector, also showed extremely limited binding affinity even at top concentration of 0.3 mM (figure 87). These results indicated that PROTAC growth from this vector may have hindered inhibitor binding to MDM2.

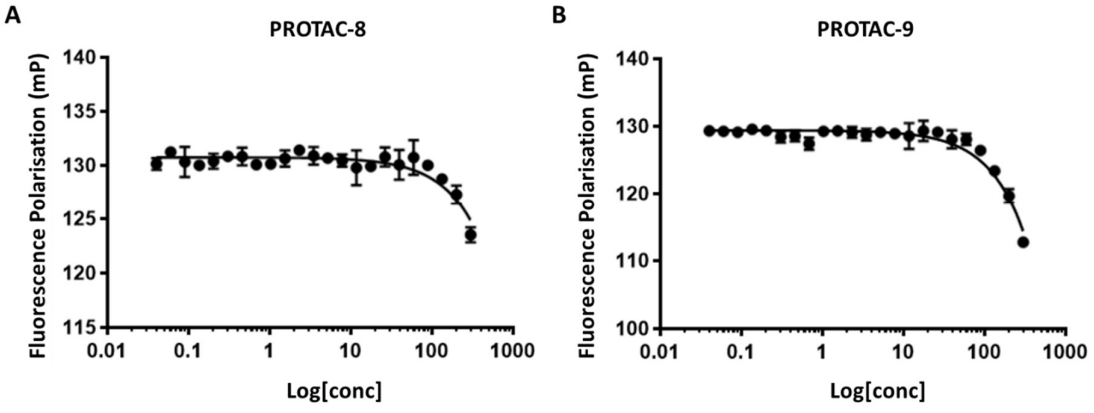

*Figure 87: FP curves for **PROTAC-8** and **-9**, top concentration of 0.3 mM*

Next, the tyrosine derived PROTACs which incorporated the linker through the phenol vector were studied (figure 88). Interestingly, **PROTAC-10**, **-11** and **-18** all showed very limited binding to MDM2, potentially due to steric hindrance from the linker.

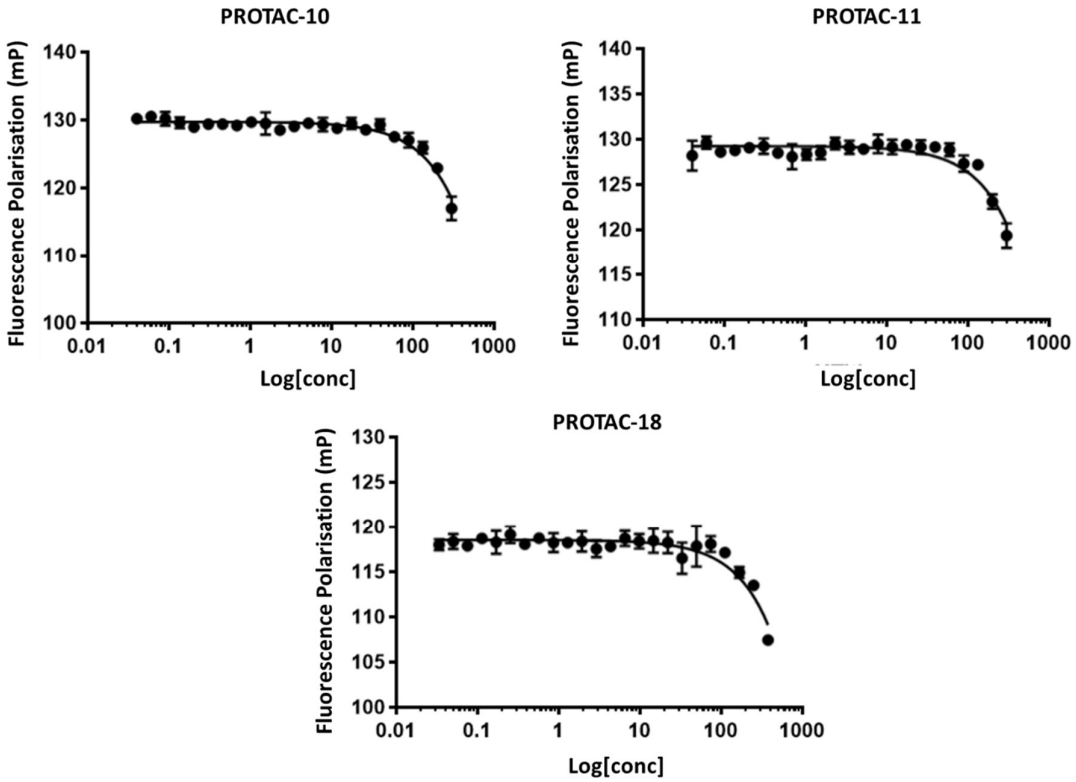

*Figure 88: FP curves for **PROTAC-10**, **-11**, and **-18**, top concentrations of 300, 300, and 376 µM respectively*

The tyrosine derived MDM2 inhibitors **85** and **86** were then screened to investigate whether the PROTAC appendage was preventing MDM2 binding or whether there was an intrinsic issue with the MDM2 binders (figure 89). Unfortunately, no binding was observed, indicating that these inhibitors may be unable to recruit MDM2. The literature reported MDM2 binding affinity of **86** was 19 nM, which was not observed in this assay. The compounds reported in the paper were also designed to bind the p53/MDM2 binding pocket using the three key hot spots commonly exploited.[231]

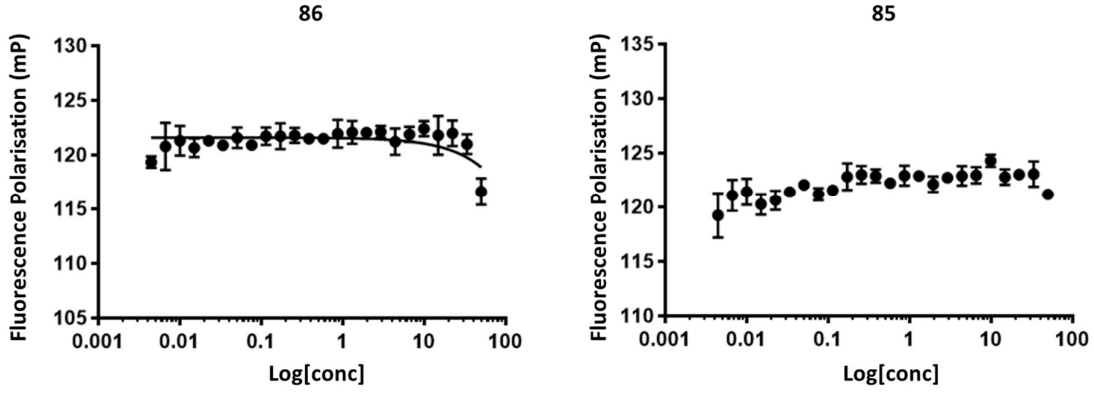

*Figure 89: FP curves for MDM2 inhibitors **85** and **86** at top concentration of 50 µM*

Finally, the imidazole based MDM2 PROTACs were studied. **PROTAC-14** and **-15** incorporated MDM2 inhibitor **110** and showed very low binding affinity at top concentrations of 300 µM (figure 90). Derivative **110** was a novel design; hence the binding affinity is unknown.

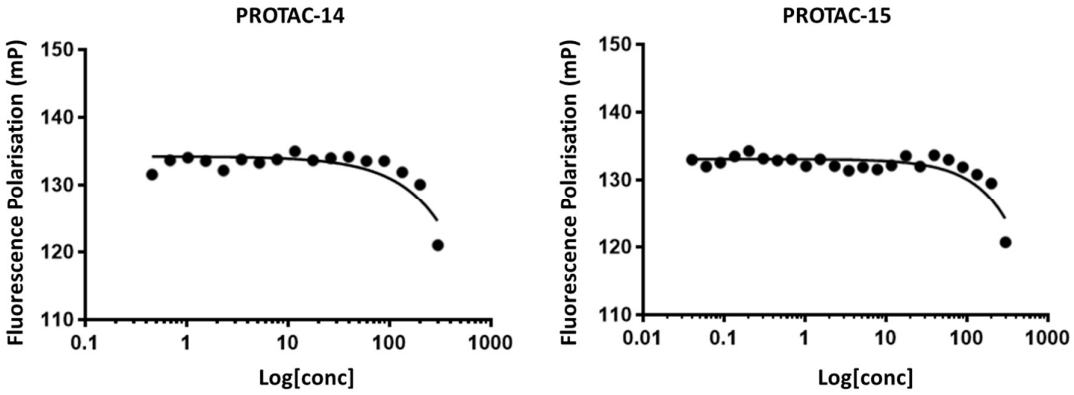

*Figure 90: FP curves for **PROTAC-14** and **-15**, top concentration of 0.3 mM*

Finally, the PROTAC that incorporated imidazole binder **87** looked considerably more promising. Two of the prepared PROTACs, **PROTAC-12** and **-17** were analysed through competitive FP (figure 91). The solubility of these PROTACs was considerably lower than the other PROTAC series previously reported, hence the top concentrations which could be screened were much lower. **PROTAC-12** exhibited inhibition at the top concentration of 10 µM, which was a substantial improvement on all previous results. **PROTAC-17** incorporated a six-PEG unit linker, which improved the overall solubility, enabling a top concentration of 75 µM. Almost complete inhibition was observed with this PROTAC at these concentrations, indicating binding affinity to be in the order of 50 µM. Despite the validation of the PROTACs binding to MDM2, this binding affinity is still lower than expected for this inhibitor.

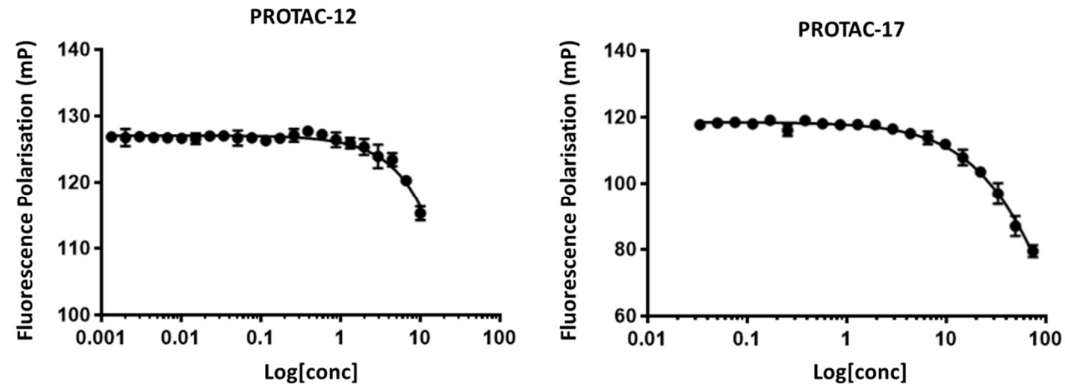

*Figure 91: FP curves for **PROTAC-12** and **-17**, top concentrations of 10 µM and 75 µM respectively*

Next, imidazole based MDM2 inhibitors, **87** and **110** were analysed for comparison with the literature reported value (figure 92). Inhibitor **87** bound MDM2 with a K_d of 110 ± 10 nM, and inhibitor **110** had

a K_d of 2.3 ± 0.3 µM. Compared to the literature value of 6 nM, binder **87** was almost 20 times less potent. This was hypothesised to be a considerable difference, potentially causing the low activity of this series of PROTACs.

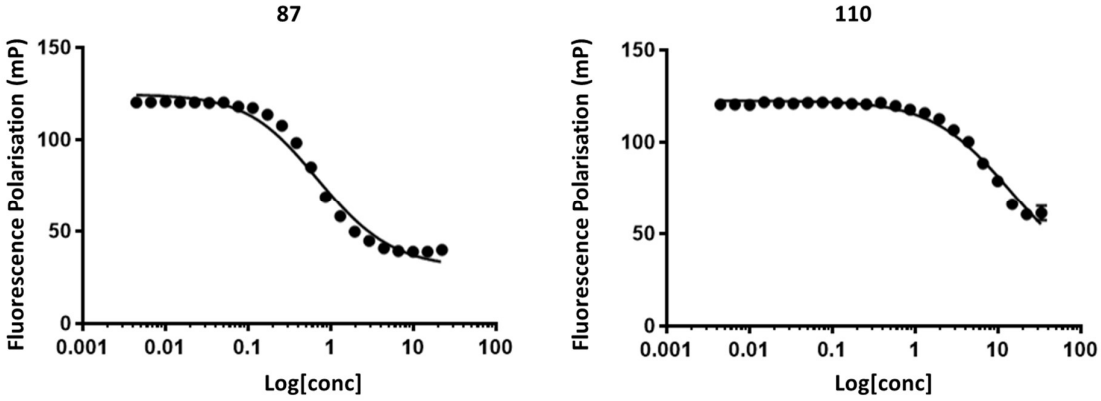

*Figure 92: FP curves for MDM2 inhibitors **87** and **110** at top concentration of 33 and 22 µM respectively*

Further validation of the binding of these published small molecule MDM2 inhibitors was acquired using DSF, as described in section 3.3.2. DSF can detect binding at a much weaker potency than the competitive FP assay, and theoretically could indicate whether weak MDM2 binding is occurring. DSF was performed with Rohan Eapen in the department of Pharmacology. MDM2 inhibitors were analysed in triplicate at three concentrations, 400, 200 and 100 µM. The melt temperature of MDM2 protein was determined in the presence of compound, enabling analysis of the protein stability.

The results of the DSF corresponded well with the competitive FP run previously (figure 93). **SP-141**, **85**, and **86** exhibited little effect on the melt temperature of MDM2, less than 1 °C difference at all concentrations. This validated that these three compounds were unable to bind MDM2. The imidazole based MDM2 binders, **87** and **110** exhibited a melting temperature shift across all concentrations. MDM2 binder **110** demonstrated a small temperature shift of *ca.* 2 °C at 400 µM. Analysis of **87** found the 400 µM top concentration to be insoluble, hence no data was collected. However, the remaining concentrations showed a significant temperature shift of *ca.* 14 °C.

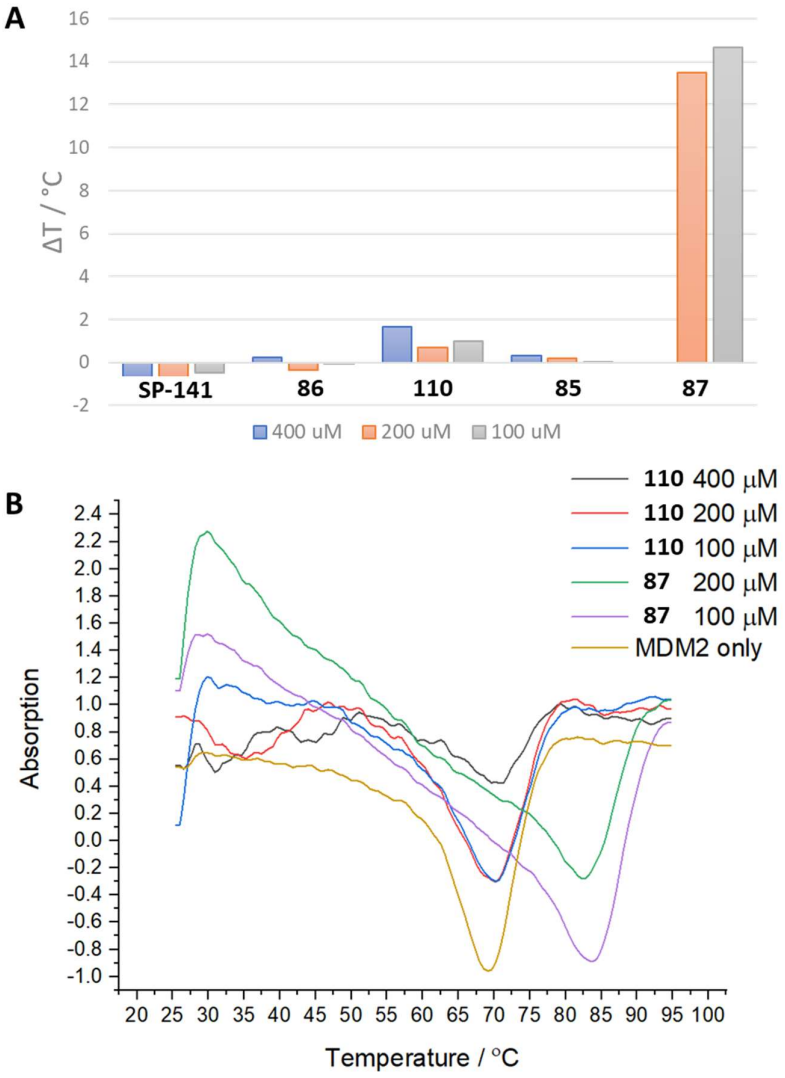

Figure 93: A: Plot of ΔT_m of MDM2 inhibitors at different concentrations; B: Observed shift in absorption minima at different concentrations of imidazole based inhibitors compared to MDM2 alone

The poor binding of MDM2 inhibitors **SP-141**, **85** and **86** to MDM2 was confirmed in two enzymatic assays, one of which was designed to detect very weak binding. The PROTACs developed based on these motifs are unable to recruit MDM2 for the degradation of AR, hence their development was subsequently abandoned. The remaining imidazole series of PROTACs were confirmed to bind MDM2 by competitive FP and DSF. Unfortunately, these PROTACs were less active compared to the tyrosine based series in the AR degradation assays. Although, **PROTAC-13** exhibited a promising dose-response curve despite relatively low potency, which warranted further study.

3.4. Chapter 3: Conclusions

Overall, a series of novel MDM2-recruiting small molecule PROTACs were prepared for degradation of AR. Following analysis of these PROTACs through a series of AR degradation assays, PROTAC binding to MDM2 was assessed. Unfortunately, two of the three MDM2 inhibitors incorporated into PROTAC designs showed no binding affinity to MDM2 in both competitive FP and DSF, making it challenging to understand the AR degradation observed in previous assays. It was postulated that the inhibitors could bind MDM2 in a region other than the p53 interface. If this was the case, then these enzymatic assays would be unable to detect this due to the MDM2 protein construct used. However, this was thought to be unlikely as the compounds were all reported to bind at the p53/MDM2 interface.

The degradation dose-response curve observed for **PROTAC-7** corresponded well with the general toxicity observed. Hence, the lack of MDM2 binding, although surprising, did not alter the assessment of this series, which was intrinsically limited by high toxicity.

The tyrosine based PROTACs were found to be incapable of binding MDM2 in competitive FP and DSF. However, promising dose response curves were observed through the AR degradation imaging assay for multiple compounds of the series. **PROTAC-10** had a DC_{50} of *ca.* 600 nM and exhibited *ca*. 33% AR degradation. It is hypothesised that these compounds could be acting as SARDs, where the compounds bind AR, inducing conformational changes, which ultimately cause proteasomal mediated AR degradation (figure 94). Further investigation is required to validate this mechanism of action.

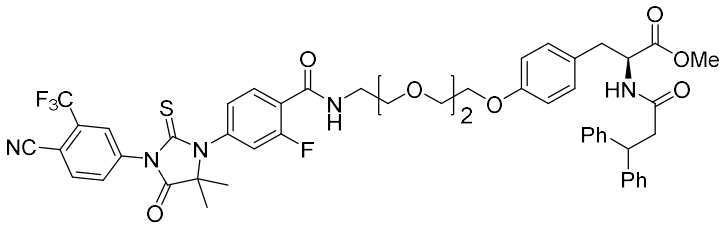

PROTAC-10

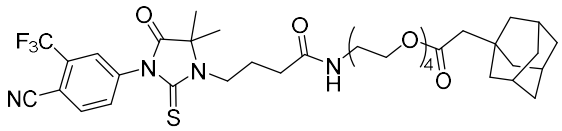

SARD279

*Figure 94: Structure of **PROTAC-10** compared to SARD279*

The imidazole based PROTACs were the most promising series. Both MDM2 binders **87** and **110** displayed affinity for MDM2 in enzymatic assays, although there was *ca*. 20-fold difference in the

reported K_d compared to the measured value for inhibitor **87**. It has been observed in the literature that weakly potent VHL binders can still achieve extremely potent degradation,[76] which indicated that these MDM2 binders would still be suitable for PROTAC use. Additionally, **PROTAC-13** exhibited a good dose response curve in the AR degradation assay, hence further validation of this activity is warranted.

Whilst the biological characteristics of these PROTACs was under investigation, an additional MDM2 recruiting PROTAC was reported by Hines *et al*.[239] The developed PROTAC comprised of a BRD4 binder connected to a nutlin derived MDM2 recruiter *via* a four-unit PEG linker. BRD4 was degraded by 98% with nanomolar potency. The additional p53 stabilisation induced by MDM2 inhibition caused a significant anti-proliferative effect on many cancer cell lines containing wild type p53, resulting in greater activity compared to VHL recruiting PROTAC alternatives. This study further highlights the utility of MDM2 as an E3 ligase, as the synergistic nature of p53 stabilisation and protein degradation led to enhanced biological activity. Although this study proved the hypothesis that MDM2 PROTACs have great potential, the MDM2 binders used were still of high molecular weight and synthetically complex. Development of PROTACs incorporating simple MDM2 binders would be a valuable addition to the PROTAC toolbox.

3.5. Chapter 3: Future Work

Further controls to validate the AR degradation study are required before additional synthetic work is initiated. The proteasomal mediated degradation of the imidazole series of PROTACs must be proven through inhibition of the proteasome. This is an important control which reduces the possibility of the observed dose-response curves being an artefact. It will also be important to run this control with potential SARD **PROTAC-10**.

Further validation of the SARD mechanism of action for **PROTAC-10** would be useful, as SARD degradation is also proteasome mediated. One method to validate the SARD mechanism would involve studying the effect of heat shock protein 90 (HSP90) on AR degradation in the presence of the compound.[64] HSPs play a key role by either stabilising misfolded proteins, or enabling UPS-mediated degradation.[240] A recent study found that incubation of cells with SARD and HSP90 inhibitor geldanamycin resulted in enhanced degradation activity. Inhibition of HSP90 causes upregulation of HSP70,[241] a key protein for targeting misfolded proteins for proteasomal degradation. Analysing the interactions of HSP inhibitors with **PROTAC-10** would provide a useful insight into the mechanism for degradation.

Additionally, the mechanism of action could also be probed by co-dosing **PROTAC-10** with a protein synthesis inhibitor.[66] This is hypothesised to significantly reduce protein levels to a greater extent than the molecule alone, due to prevention of protein synthesis, which would indicate that the compound is interacting with cellular AR protein rather than decreasing the rate of protein synthesis or mRNA levels.

Following the validation of the UPS-mediated mechanism of action of the imidazole PROTAC series, further linker design is necessary for optimisation of the extent of AR degradation and potency. Currently, only three different PEG linkers have been explored with three, four, and six PEG units, however, a comprehensive screen of linker lengths and properties would be required to fully optimise the biological response (figure 95). Insertion of methylene units into PEG linkers has been demonstrated to be effective for improving PROTAC activity, hence this would be incorporated into various linker lengths to compare activity.

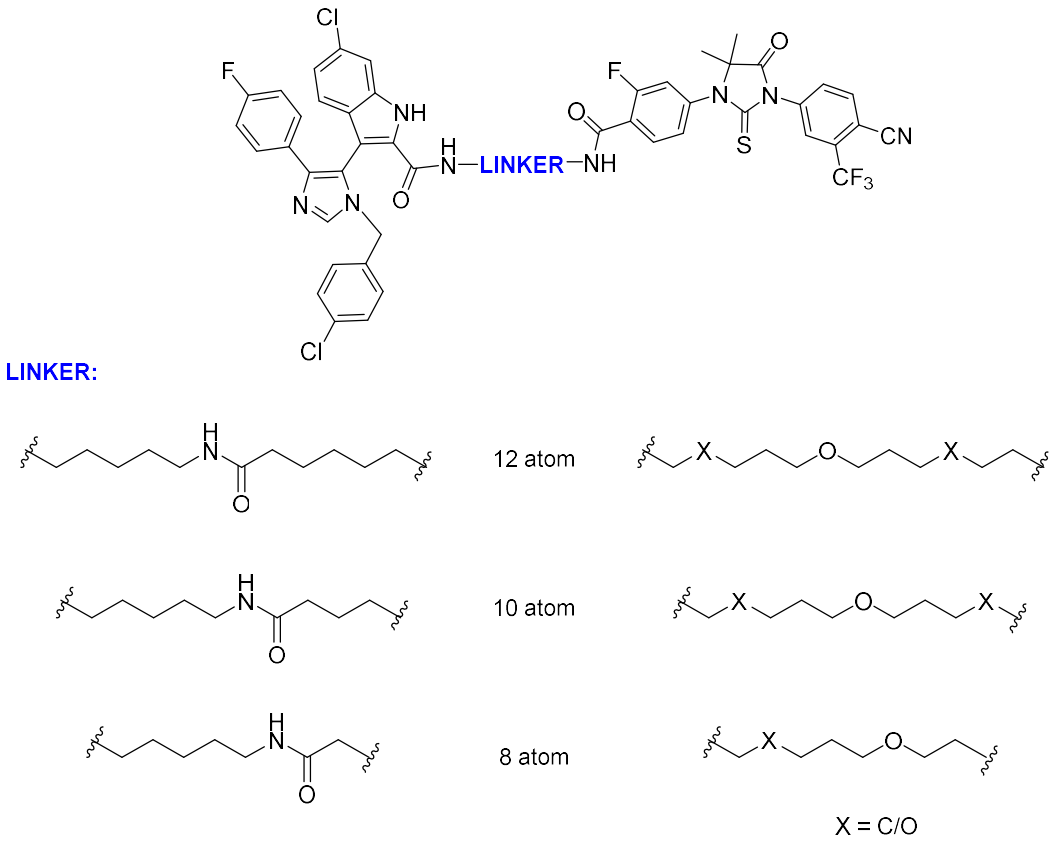

Figure 95: Potential linkers to be studied to optimise AR degradation and potency of imidazole based PROTAC series

Overall, there is promise in these novel small molecule MDM2 recruiting PROTACs, however, further biological validation in addition to optimisation studies would be required to maximise biological activity.

4. Chapter 4: Development of photoswitchable PROTACs

4.1. Chapter 4: Introduction

4.1.1. Introduction to photopharmacology

High attrition rates in the drug development process are a key problem which limits the approval of new medicines.[242] A recent study on causes of drug attrition noted that although failure due to pharmacokinetic limitations have reduced, overall attrition rates remain high due to an increase in efficacy and safety related failures.[243] Methods to predict safety problems in early development are lacking, despite recent developments in this area.[244] Toxicity is a major cause of drug attrition, which either stems from the drug's chemical structure, on-target effects or off-target effects.[245] On-target toxicity results from the drugs activity on the target of interest, which may be related to the general effects on both healthy and diseased cells. Off-target toxicity typically refers to a drug's affinity for multiple targets, which could be unrelated to the target of interest.[246] In addition, poor selectivity of a drug also lowers the toxicity threshold which narrows the therapeutic window, leading to suboptimal dosage. One approach to circumvent toxicity is through photopharmacology.[247]

Photopharmacology uses light to control biological systems. Light can influence the biological activity of a molecule by altering its pharmacokinetic or pharmacodynamic properties. There are many benefits of using light for this purpose, such as its non-invasive nature, speed of action and high spatial and temporal control.[248] Light's action on molecules can either be reversible or irreversible, and many successful therapeutic applications have been published.[248,249] Light-controlled drugs offer an opportunity to impart additional selectivity. Ideally, a safe and inactive drug can be dosed to a patient, and the drug can then be switched into its biologically active form at its site of action, limiting any toxicity and increasing the therapeutic index of a drug (figure 96).

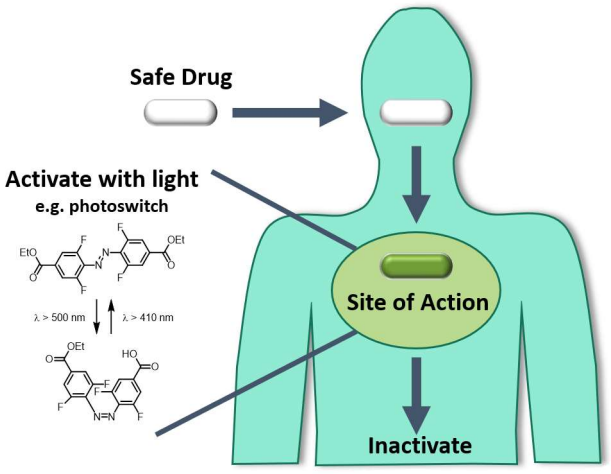

Figure 96: Photopharmacology summary

Photopharmacology has been successfully applied to a variety of targets both *in vitro* and *in vivo*, for example enzymes,[250] ion channels[251] and G protein coupled receptors (GPCRs).[252]

4.1.2. Chemical approaches to photopharmacology

There are many strategies which use light to control biological effects. Chemical methods include photodynamic therapy (PDT),[253] photocleavable protecting groups (photocages), photoaffinity labels (PAL), and photoswitchable moieties.

PDT uses light to activate a photosensitiser which then generates a highly reactive oxygen species which reacts with cellular biomolecules leading to cell death. PDT is well-established and has been applied to various cancers over the past two decades, highlighting the immense potential of light-controlled therapies.[254]

Another type of photopharmacology uses photocages to mask functionality, which can then be removed using light. Photocages can be used to eliminate biological activity in the caged form and then release the active drug following irradiation. There have been a variety of groups used as photoremovable protecting groups, classic examples include nitrobenzyl derivatives, arylcarbonyl methyls, and coumarin groups (figure 97).[255] A major limitation of many photocages is the requirement of high energy light sources to cleave the protecting group due to the high energy of standard organic bonds (350 – 400 kJ/mol). Cleavage of these strong bonds requires *ca*. 340 nm UV light which has poor tissue penetration and can be biologically damaging leading to toxic effects.[256] New photocleavable groups have been recently developed focusing on weaker bonds which can be cleaved using longer wavelengths, but these are still in early stages of development.[257,258] An additional limitation of this technology is its irreversibility. Once the photocage is removed the active drug is revealed and this can still be transferred around the body causing off-target toxicity.

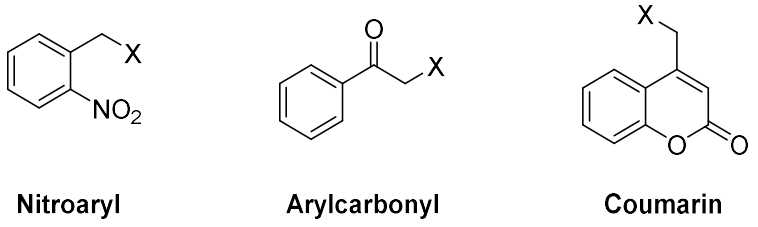

Figure 97: Examples of groups using for photocaging of drug molecules

PAL uses chemical probes to covalently bind a target molecule. These chemical probes bind to their cellular targets through competitive inhibition. Activation with light forms a reactive species which rapidly reacts with the nearest molecule, forming a covalently bound species. This technology has

been used to elucidate the cellular binding partners of numerous hit molecules and is a vital tool for chemical biology.[259] Many photoaffinity groups exist and commonly used groups include phenylazides, phenyldiazirines, and benzophenones which respectively form nitrenes, carbenes and diradicals as the reactive species (figure 98). PAL is typically used for molecular target identification rather than as a therapeutic strategy.

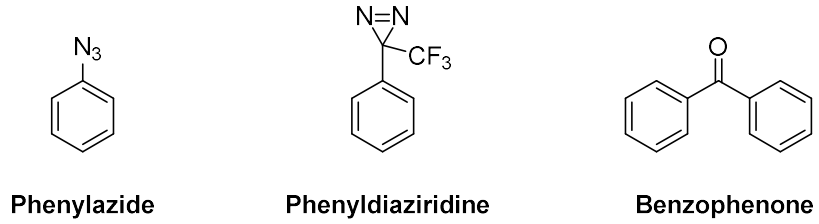

Figure 98: Examples of light-responsive functionalities for use in PAL

Photoswitches exist as different isomers which can be interconverted using light. The biological activity of a compound can be greatly changed by altering its structure due to the specific shape required to occupy distinct binding pockets or biological interfaces. Hence, a drug can either be inactive or active following incorporation of a photoswitch, depending on its environment. This is an ideal application of photopharmacology. The inactive, safe drug can be dosed, and light can then be used to switch the drug to the active conformation specifically at its site of action. This method greatly reduces toxicity by only exposing a localised area to the active drug. Photoswitches also benefit from their reversibility, which offers further advantages for their safety profiles.[248]

Photopharmacology is well-suited for diseases which are highly localised, particularly those located on skin and eyes where light can easily reach. One limitation of the light commonly used in photopharmacology is its short UV wavelengths, which poorly penetrates biological tissue.[260] This makes it highly challenging to apply these approaches to internal diseases non-invasively. Red or ideally near-IR wavelengths are much better suited for these biological applications due to its improved penetration, however most classes of photoswitches require higher energy light sources to induce isomerisation.

4.1.3. Introduction to photoswitches and their biological applications

There have been numerous examples of photoswitches designed for photopharmacology applications, the most prevalent of which are azobenzenes and diarylethenes (figure 99).

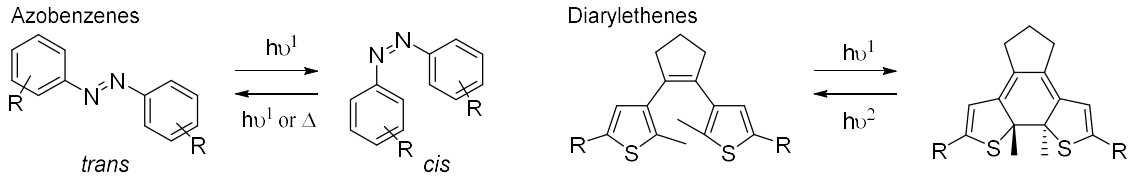

Figure 99: Prevalent photoswitches used in photopharmacology, azobenzenes and diarylethenes

Diarylethenes undergo a photochromic reaction which converts between the open-ring and closed-ring isomers. This reaction is thermally irreversible and typically requires UV light (280 – 400 nm) to form the closed-isomer and visible light (>400 nm) to re-open the ring. These photoswitches have been utilised for a broad range of applications, including fluorescence, electrical conductivity as well as biological applications such as photoswitchable DNA.[261,262]

Azobenzene converts into the *cis* isomer upon radiation with UV light.[263] The two isomers of azobenzene have distinctly different geometries and dipole moments. They are interconverted using 380 nm light to switch from the *trans* to the higher energy *cis* state and are switched back to the thermostable state using visible light or thermal energy. This photoisomerization is reversible and the resulting conformational change can affect a tethered protein's structure or a ligand's position within a protein's binding site.[264] Azobenzene has been used for biological modulation for over half a century, after first being applied to the photocontrol of chymotrypsin in 1968 by Erlanger *et al*. using its unique light sensitive nature to regulate the enzymes inactivation.[265]

Azobenzenes have also been applied to two-component peptide stapling to produce photoisomerisable stapled peptides (figure 100). These photoswitchable staples can change the helical nature of the peptide in response to light. They were initially used by Kumita *et al*.[266] and effectively increased helical content upon isomerisation from *trans* to *cis*. Substituted versions of these linkers were then applied to the BCL-x_L PPI, and substantial differences in binding were observed depending on light irradiation.[267] Azobenzene based stapled peptides have since been applied to numerous biological applications, highlighting their potential as optochemical tools and theraputics.[268]

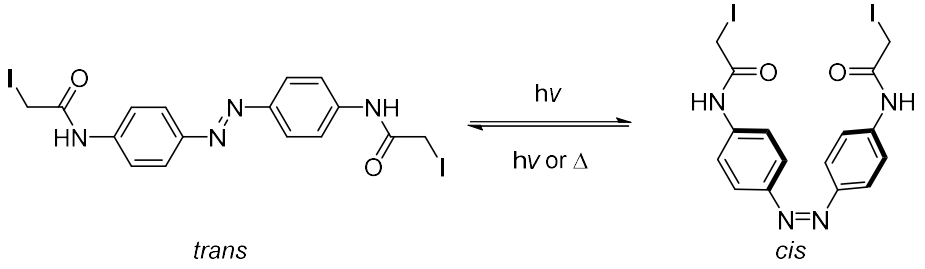

Figure 100: Photoswitchable linker for two-component peptide stapling used by Kumita et al.[266]

Ion channels are key for fast synaptic transmissions in the nervous system and are important therapeutic targets. There have been many examples of photoswitches designed to target these channels. One early example is the nicotinic acetylcholine receptors (nAChRs), a specific type of pentameric ligand-gated ion channel, targeted using azobenzene derived inhibitors AzoCharCh and Azo-PTA in 1969 (figure 101).[269] These azobenzenes were switched between the *cis* and *trans* isomers using 320 and 420 nm light. The more active *trans*-isomer inhibited this channel to a greater extent compared to the *cis* isomer, validating the concept that this channel could be regulated using light. More recently, further agonists of this channel have been developed to generate structure activity relationships leading to greater activity, including AzoCholine.[270] AzoCholine was photoswitched using 440 and 360 nm light and exhibited greater potency over earlier compounds.

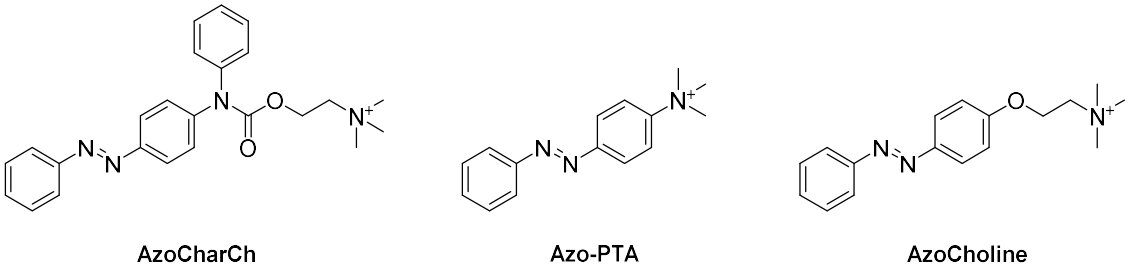

Figure 101: nAChR ion channel inhibitors developed based on azobenzene photoswitches

Another well-validated therapeutic target are GPCRs, which are transmembrane proteins vital for cellular signalling. One study combined the structure of known protein ligand VUO415374 with an azobenzene photoswitch to create the first photoswitchable allosteric modulator of a GPCR (figure 102).[271] This photoswitch was highly selective for one type of GPCR and found to have nanomolar potency, although a poor thermal half-life of 80 s. This photoswitch was then tested *in vivo* and light-dependent activity was exhibited. Further studies within the same group comprehensively optimised the structure of this scaffold, considering its photophysical characteristics in combination with biological effects and extended the *in vivo* studies to rodents.[272]

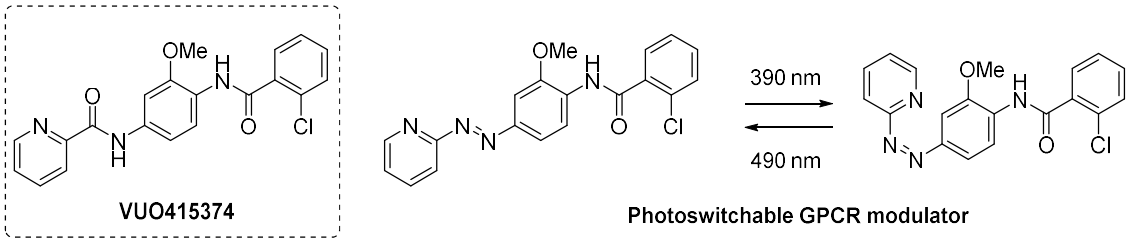

Figure 102: Structure of a novel photoswitchable allosteric modulator of a GPCR

An interesting recent study by Wegener *et al.* found that red light (630 – 700 nm) could be used to activate antibacterial agents for treatment of infections.[273] This photoresponsive antibacterial was

based on clinically approved antibiotic trimethoprim, which targets the biosynthesis of folate in a both Gram-positive and Gram-negative bacteria through inhibition of dihydrofolate reductase. Resistance to trimethoprim usage is a common occurrence, making it an important candidate for photopharmacology. The photoswitchable antibiotic developed showed an 8-fold difference in activity following its irradiation with red light (figure 103). This is an important application of photoswitches, as these photopharmacology strategies could limit the excessive exposure of active antibiotic to bacteria and therefore reduce the occurrence of resistance, a growing concern for global health.[274]

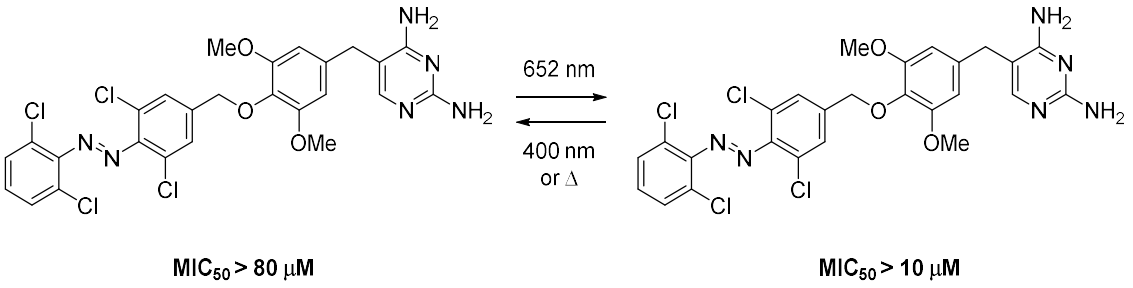

Figure 103: Azobenzene photoswitch antibacterial which becomes 8-fold more potent in response to red light

There are numerous further examples of photoswitch applications to biological targets, with new targets frequently reported. Multiple comprehensive reviews exist on new photoswitchable compounds developed for a range of biological applications.[248,250,275]

4.1.4. Recent developments in photoswitch design

The ideal photoswitch for use in biological systems would be non-toxic, undergo complete photoswitching to its active isomer with near-IR wavelengths of light and be completely stable to cellular molecules such as glutathione.

UV light is well-known to cause damage to biological tissue, either by direct biomolecule absorption of short genotoxic UV wavelengths (220 – 280 nm), or through the formation of reactive species following absorption of longer UV wavelengths (280 – 400 nm) which can damage biomolecules including DNA and cell membranes.[276] This damaging nature of UV light severely limits its utility in photopharmacology, in addition to its poor tissue penetration. Tissue penetration is affected by the extent of light scattering and biological chromophore absorption. Thus penetration is highly wavelength dependent, with UV wavelengths only penetrating up to 1 mm of tissue.[277] The optimal wavelength window is between 600 and 1200 nm, with penetration of *ca.* 2 cm achieved by 800 nm light. Despite this extent of penetration not being sufficient for many applications, light may be delivered deeper into the body through insertion of optical fibres.[249]

Azobenzenes have been shown to undergo reduction of the azo-core in the presence of glutathione and other thiols, inactivating the photoswitch.[278] This instability has great implications for the *in vivo* use of the azobenzene switching core. However, in a zebrafish study, switching was reliably observed over 2 days indicating this instability may not be a substantial problem, although the thermal relaxation of these compounds was rapid with a half-life of 7.5 mins.[279]

There have been many recent developments toward 'next-generation' photoswitches to address the wavelength limitations which hinder the clinical use of photoswitching drugs. Many new chemical systems have been developed alongside modifications made to known cores to improve the photoswitch properties, particularly stability and photoconversion.[280,281]

The highest wavelength transition of an unsubstituted azobenzene is *ca.* 400 nm, which is an overlap of n-π* and π-π* transitions. Through *ortho*-modification of the core azobenzene structure with either methoxy groups,[282] thiols,[283] chlorines,[284] or fluorines,[285] the n-π* transition is red-shifted with greater separation between the *cis* and *trans* forms (figure 104). This results in improved photostationary states (PSS, the steady state isomeric ratio generated following irradiation), higher stability, and more desirable red-shifted wavelengths for switching. Similar observations have been made with bridged azobenzenes known as diazocines,[286,287] as well as arylazo-heterocycles, which also have very promising switching wavelengths as well as good intrinsic properties.[288]

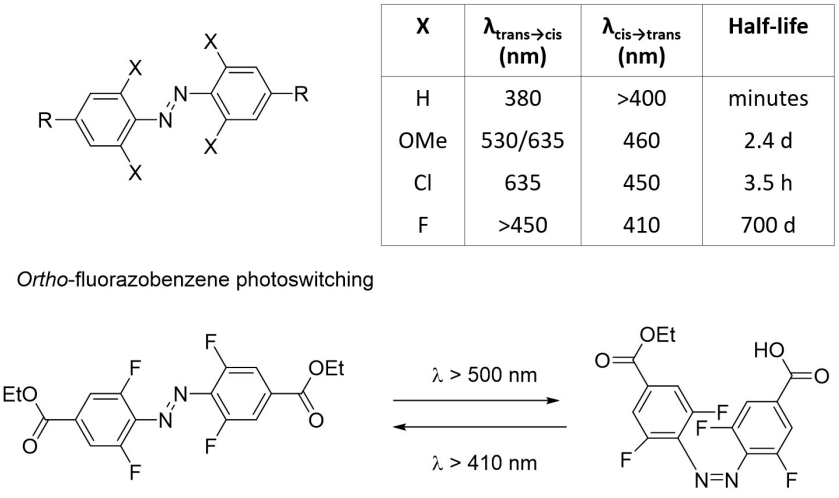

X	$\lambda_{trans \rightarrow cis}$ (nm)	$\lambda_{cis \rightarrow trans}$ (nm)	Half-life
H	380	>400	minutes
OMe	530/635	460	2.4 d
Cl	635	450	3.5 h
F	>450	410	700 d

Figure 104: Azobenzene photophysical characteristics, effect of ortho-substitutions on switching wavelengths and stability

Ortho-fluoroazobenzenes have greatly improved photophysical properties compared to the unsubstituted azobenzenes.[289] Through introduction of highly electron withdrawing fluorine atoms, the electron density in the N=N bond is reduced. This lowers the n-orbital energy and unusually renders the *cis* form more thermodynamically stable than the *trans*. This results in green light (520 – 560 nm) inducing *trans* to *cis,* and blue light (450 – 490 nm) inducing *cis* to *trans* isomerisation with

high photoconversions through n-π* excitation. This *ortho*-substitution does not cause significant distortion to the planar *trans* geometry of the azobenzene core due to the small size of the fluorine atoms. In addition, the half-life of the *cis*-isomers is remarkedly long, *ca.* 30 h at 60 °C.[290] Due to these highly desirable properties these photoswitches have been applied to a range of applications in addition to biological,[291,292] including liquid crystal polymers,[293,294] metal-organic frameworks,[295,296] molecular machines,[297] and crystal engineering.[298,299]

Another promising class of photoswitches are the indigoids (figure 105), which contains indigo, thioindigo and hemiindigo. These photoswitches switch in both directions using >400 nm light, and have been shown to be extremely stable, with high photoconversions.[300] In particular, the hemiindigos have been recently reported to be easily synthesised and have excellent photophysical characteristics.[301,302] Upon irradiation with 470 – 530 nm light, the *trans* isomer was formed with > 90% PSS, this could be switched back with 590 – 680 nm light yielding 99% of the *cis* isomer. In addition, the thermal stability was found to be extremely high, with a reported half-life of up to 83 years at 25 °C. Due to their favourable photophysical properties, these photoswitches are well-suited for photopharmacology applications demonstrated by their recent application to fluorescence switching in RNA binders. These derivatives were found to reversibly switch on or off using visible light without affecting their RNA association.[303]

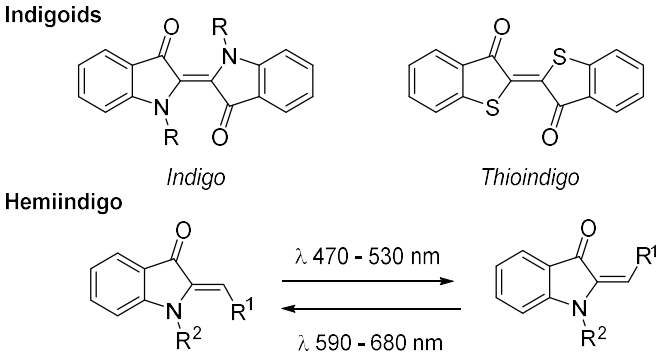

Figure 105: General structures of indigoid photoswitches and switching wavelengths of hemiindigo core

There are many alternative classes of recently developed photoswitch which switch using a variety of different conditions, including chiral imines,[304] acylhydrazones,[305] and donor-acceptor Stenhouse adducts.[306,307] These new photoswitches have a variety of uses and expand the photoswitch toolbox beyond therapeutic applications to a range of interdisciplinary fields.[280,281]

4.2. Chapter 4: Aims and Objectives

PROTACs are ideal candidates for application to photopharmacology. Firstly, the conformation of a PROTAC is key to its activity, hence the introduction of a photoswitch leads to two very different isomers hypothesised to have significantly distinct biological activity. In addition, a photoswitch can easily be incorporated into the structure due to the modularity of a PROTAC. PROTACs consist of two protein binders connected through a linker, this linker can be modified to contain a photoswitch with little synthetic effort.

Two photoswitches were chosen for incorporation into the novel photoswitchable PROTACs: *ortho*-fluoroazobenzene and hemiindigo. Initial designs for the two classes of photoswitchable PROTAC incorporated the VHL binding ligand and the enzalutamide-based AR binding ligand connected to the photoswitching units (figure 106).

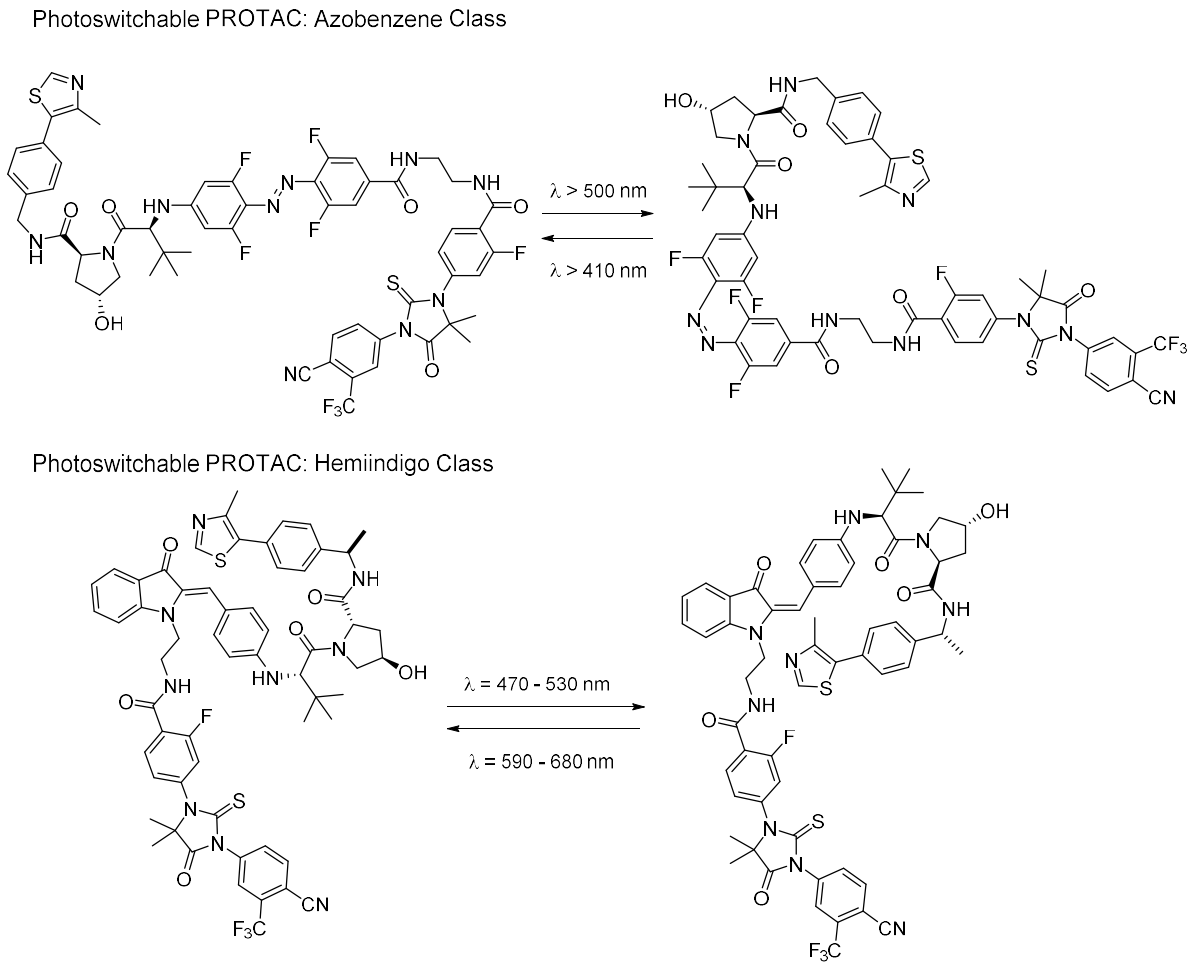

Figure 106: Structures of designed photoswitchable PROTACs based on azobenzene and hemiindigo core

These photoswitches were chosen due to their ease of synthesis, strong photophysical properties and high stability. The structural difference of the two azobenzene conformations is significantly larger than that of the hemiindigo conformers. This was hypothesised to optimise the likelihood of developing a successful AR degrading PROTAC with highly differentiated biological activity.

Following the preparation of the photoswitchable PROTACs, the photophysical characteristics were investigated to quantify switching wavelengths and efficiency. The biological activity of the PROTACs would then be studied and further optimisation of the structures would be carried out to improve the differential activity of the series. Finally, the technology was applied to alternative proteins of interest to provide a proof-of-concept study of the generality of photoswitchable PROTACs.

Whilst this PROTAC series was under biological analysis, alternative photoswitchable PROTACs have been reported providing validation of this photopharmacology strategy. Trauner *et al*. reported photoswitchable PROTACs which recruited cereblon for the degradation of both BET bromodomain proteins and FKBP12.[308] These PROTACs incorporated an azobenzene photoswitch unit into the linker and were demonstrated to switch with 390 nm light. Good differential biological activity was observed for the optimised linker lengths, and the more active PROTAC in this work was found to be the *cis* isomer. Unfortunately, the kinetic stability of the PROTACs necessitated continuous light pulsing throughout the experiment.

In addition, Pfaff *et al.* recently published *ortho*-fluoroazobenzene photoswitchable PROTACs also targeting the bromodomain proteins using E3 ligase VHL.[309] These PROTACs were found to be active in the *trans* form and offer further evidence of the utility of photoswitchable PROTACs.

Although these recent publications reduce the novelty of the photoswitchable PROTACs described in this chapter, they do validate the potential of this idea for achieving selective and potent degradation of a range of proteins. At the point of writing, no photoswitchable PROTAC targeting AR or ER have been reported, hence applying photoswitches to the light-enabled degradation of these clinically relevant proteins is a useful advance.

4.3. Chapter 4: Results and Discussion

4.3.1. Synthesis of Hemiindigo Core

Hemiindigo PROTAC **151** could be accessed through a convergent route which connected the three key components: VHL binder **154**, photoswitch **152** and bromo-enzalutamide derivative **153** (figure 107). The VHL binder was thought to be amenable for an *N*-arylation strategy to the aryl-bromide of the photoswitch *via* Buchwald or Ullmann coupling chemistry. The AR binding motif **153** was envisaged to connect through *N*-alkylation of the central hemiindigo nitrogen. This strategy was expected to provide a rapid and convergent route to the hemiindigo photoswitchable PROTACs, where the methodology could be extended to alternative protein binders at a late stage with few complications.

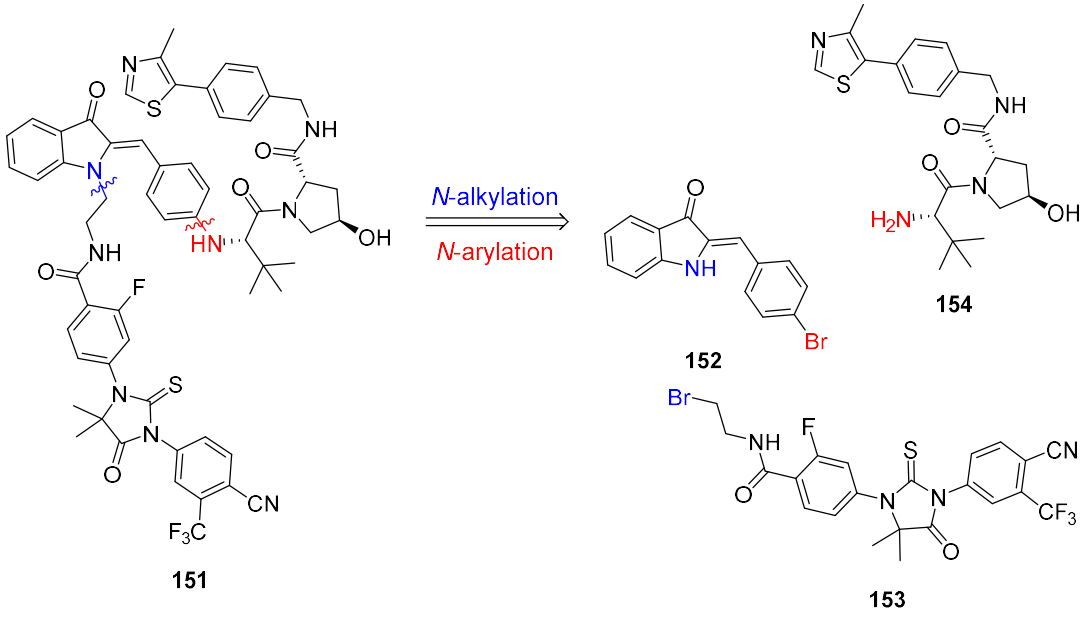

Figure 107: Retrosynthesis of hemiindigo photoswitchable PROTAC to three key components connectable by N-alkylation and N-arylation

Synthesis of the core hemiindigo scaffold was reported by Petermayer *et al.* from commercially available indoxyl acetate **156** and 4-bromobenzaldehyde.[301] Due to its high cost and low availability, a route to indoxyl acetate **156** was identified to provide a reliable and cost-effective source. A one-step procedure from indole was reported by Liu *et al*. which used mild conditions combining $PhI(OAc)_2$ with DBU to attain the desired product (scheme 55).[310] Although this procedure was reported to yield 76% product, after multiple attempts a maximum yield of 7% was isolated, which was not feasible to supply an early stage starting material. The reason for the great discrepancy between the published yield and this result was unknown, the product appeared to be quite unstable to the column conditions and it is possible that moving from the reported 0.3 mmol scale to the scale-up 4 mmol conditions could have resulted in discrepancies.

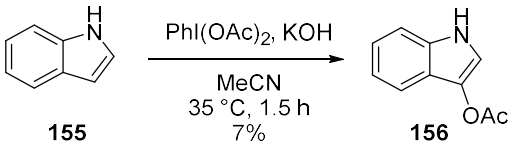

*Scheme 55: Synthesis of indoxyl acetate **156***

Next, a one-pot route to hemiindigo **159** through palladium-catalysed carbonylation of substituted alkynes and iodoanilines was attempted, reported by Li *et al.*[311] This route used formic acid as the CO source and acetic anhydride as the activator to give a variety of hemiindigos in good yields with high functional group tolerance. Initially, the procedure was attempted with 4-ethynylanisole as a readily available alkyne to test the feasibility of this reaction (scheme 56). The reaction was successful and generated 44% yield of methoxy-substituted hemiindigo **159**.

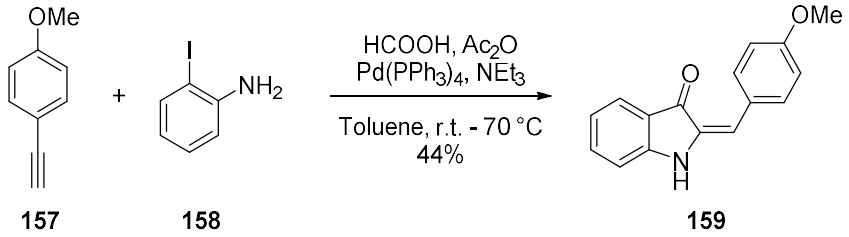

*Scheme 56: One-pot palladium-catalysed carbonylation to produce methoxy-substituted hemiindigo **159***

The one-pot route was then applied to the desired substrate, 1-bromo-4-ethynylbenzene **160** (scheme 57). This was found to be unsuccessful, giving multiple spots by TLC. The hypothesised direct Sonogashira product **161** was observed in a high quantity *via* LCMS. This was proposed to result from direct reaction between alkyne **160** and iodo-aniline **158**. The carbonylation product **152** was not observed. Despite the reported 58% yield of bromo-derivative **152** in the publication, no product was identified. It was hypothesised that complications arising from general cross-reactivity and the unsuccessful carbonylation gave a multitude of difficult to separate products. Hence, this route to the desired hemiindigo **152** was abandoned.

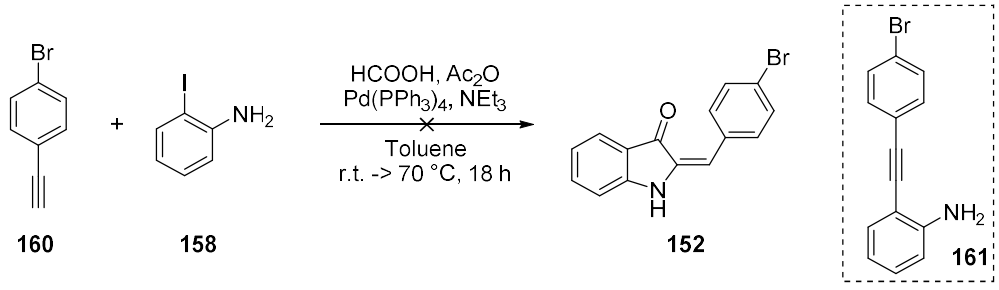

*Scheme 57: Attempted one-pot palladium-catalysed carbonylaion for the synthesis of bromo-substituted hemiindigo **152***

Due to the difficulties faced with the one-step protocols, an alternative approach to indoxyl acetate **156** was adapted from the Pitayatanakul *et* al. procedure.[312] This strategy attained hemiindigo **152** in a two-step procedure *via* the iodo-indole intermediate **162** which was immediately treated with AgOAc due to its low stability (scheme 58). This route was found to be more effective, with higher yields and shorter reaction times. Indoxyl acetate **156** was then hydrolysed with 1.5 M NaOH and treated with 4-bromobenzaldehyde to yield hemiindigo **152** in excellent yield.

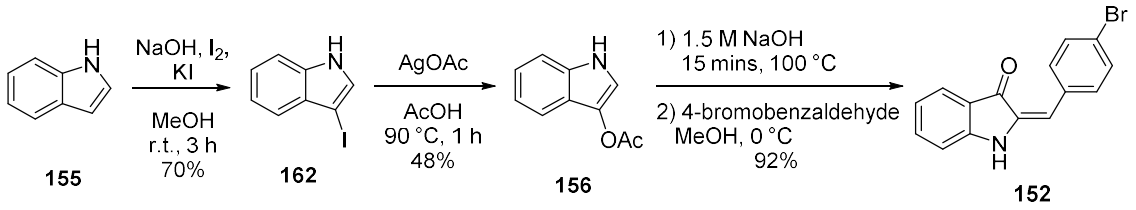

*Scheme 58: Synthesis of bromo-substituted hemiindigo **152***

4.3.2. *N*-Alkylation attempts of hemiindigo core

With a stock of the hemiindigo in hand, attempts were then made to alkylate the nitrogen with *N*-Boc-protected two-carbon linkers which would enable easy amide coupling connection of the AR binder.

N-Boc-ethanolamine was first activated using MsCl and DIPEA to form the mesylate **164**, which was then treated with hemiindigo **159** with NaH (scheme 59). Hemiindigo derivative **159** was used as a test substrate for the initial alkylation attempts, due to its ease of synthesis *via* a one-step reaction. This reaction was found to yield an inseparable 1:1 mixture of starting material and product **165** and despite increasing equivalents of alkylating agent **164** and NaH, greater conversion was not observed.

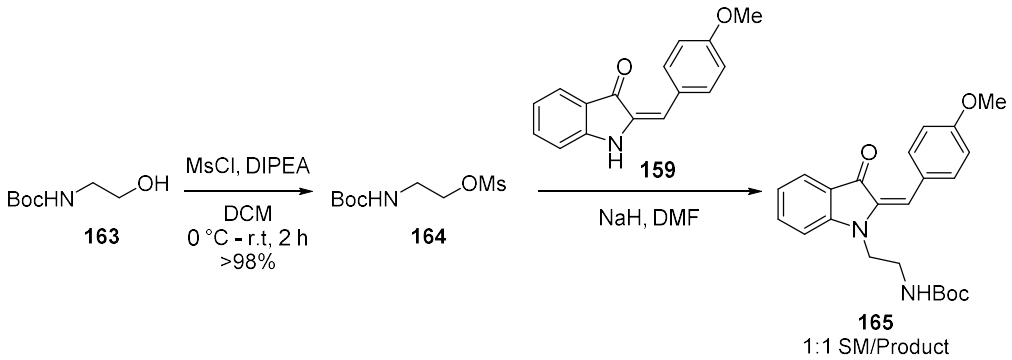

*Scheme 59: N-alkylation of hemiindigo with mesylate **164** to generate a mixture of 1:1 SM and product **165***

Alkylation of the desired bromo-substituted hemiindigo **152** was then attempted (scheme 60). Initial attempts with mesylate **164** did not yield any product, despite obvious deprotonation of the hemiindigo **152** observed through a distinct colour change from brown to turquoise. The equivalents

of NaH were lowered from 1.5 to 1 eq. however no change was observed. It was proposed that the mesylate **164** may not be reactive enough for this highly electron deficient aromatic system, hence the iodide derivative **167** was used in further attempts.

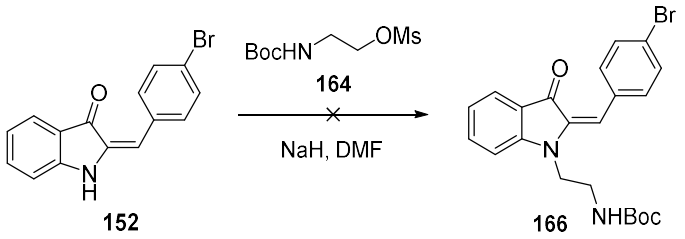

*Scheme 60: Attempted N-alkylation of bromo-substituted hemiindigo **152** with mesylate **164***

Alkylation of hemiindigo **152** with commercially available iodide **167** was attempted using NaH over 24 h, however only SM was recovered (scheme 61). Additionally, alkylation attempts using K_2CO_3 and 18-crown-6 ether at 120 °C for 24 h led to **152** decomposition.

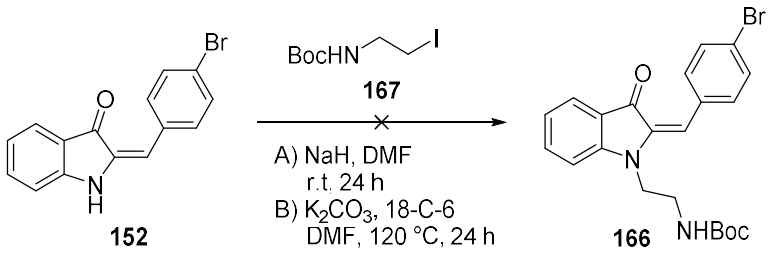

*Scheme 61: Conditions attempted for alkylation of bromo-substituted hemiindigo **152***

After little alkylation success using these two-carbon alkylating units, efforts were made to avoid the use of the *N*-Boc protecting group. Thus, the desired enzalutamide tagged substrate **168** was prepared in good yield from reaction of acid **2** with 2-bromoethylamine hydrobromide salt (scheme 62). This substrate was then immediately reacted with hemiindigo **152** in the presence of NaH. No product was detected, and the major LCMS product had a molecular weight corresponding to proposed structure **170**. This structure corresponds to an intramolecular reaction of the two-carbon tag with the neighbouring amide to form the five-membered ring cyclised product.

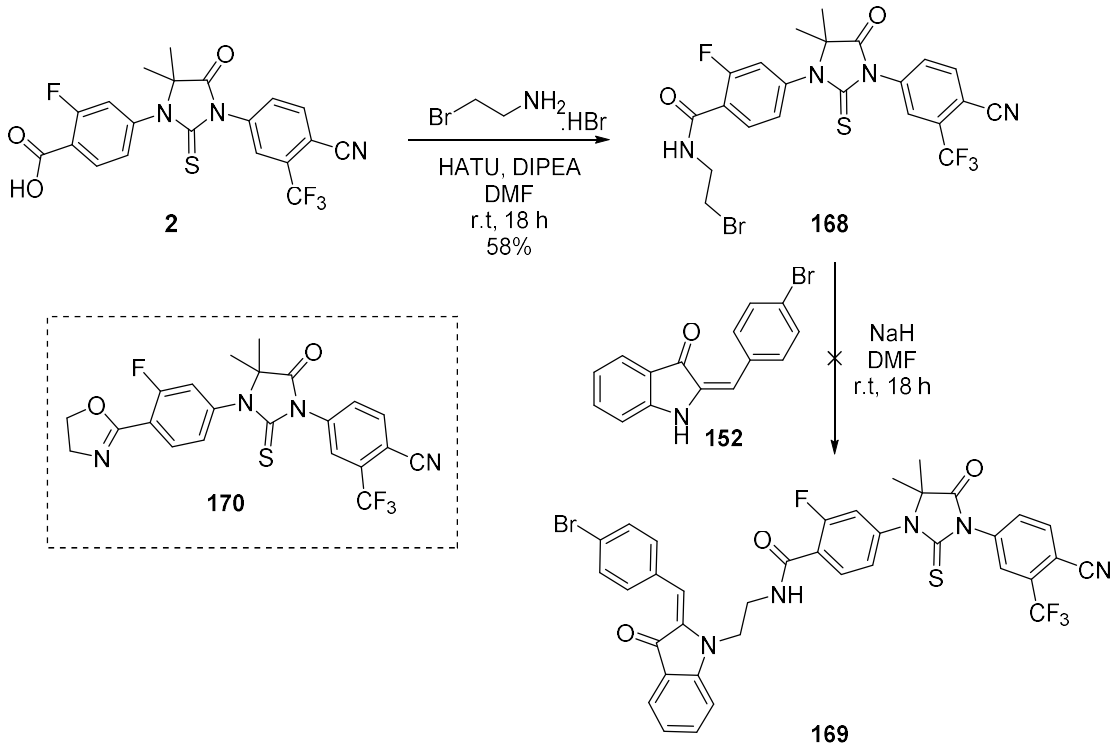

*Scheme 62: Attempted N-alkylation of bromo-substituted hemiindigo **152** with bromo-derived enzalutamide **168** and hypothesised cyclised enzalutamide derivative **170***

To circumvent the problem with the reactive amide nitrogen, a di-*N*-Boc derivative of the alkylating agent **172** was prepared by treating dibromoethane with $HN(Boc)_2$ in the presence of NaH (scheme 63). Unfortunately, attempts to attach this motif to hemiindigo core **152** were unsuccessful, with only starting material recovered.

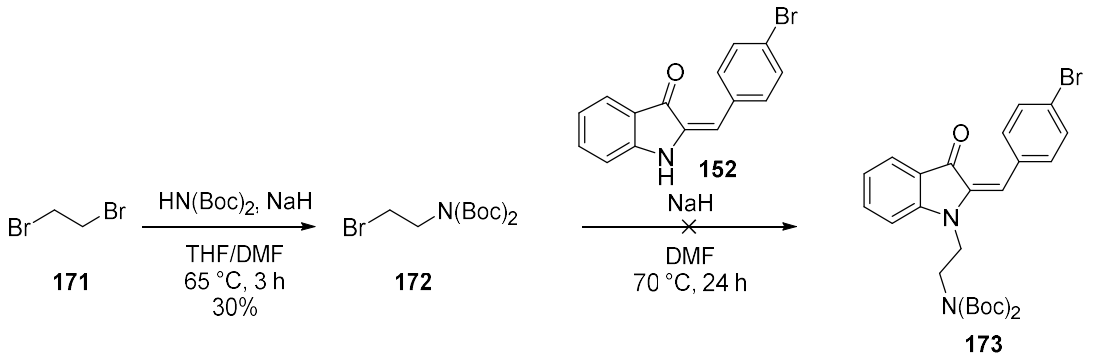

*Scheme 63: Synthesis of double N-Boc-protected bromo-substituent **172** for attempted N-alkylation of hemiindigo **152***

4.3.3. *N*-Alkylation attempts of indole

Due to the major difficulties encountered during alkylation attempts on the core hemiindigo scaffold, an alternative approach was sought where indole could be directly alkylated prior to formation of the hemiindigo core. Initial attempts at this alkylation used the mesylate **164** and NaH, however a low yield of 21% was isolated (table 6). When repeated with the iodide derivative **167**, the yield was improved to 27%. However, the conversion was still low with a significant quantity of starting material recovered. Further alkylation attempts were made using Cs_2CO_3 at reflux which also yielded little conversion, and upon increasing the equivalence of alkylating agent, no improvement was observed.

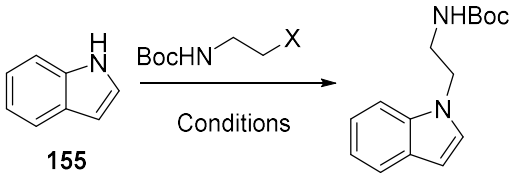

155 **174**

Run	X	Conditions	Results
1	OMs	1.25 eq. NaH, DMF, r.t.	21%
2	I	1.1 eq. NaH, DMF, r.t 18 h then 80 °C	27%
3	I	2 eq. Cs_2CO_3, MeCN, reflux 18 h	17%
4	I	1.5 eq. NaH, DMF, r.t. 24 h	Complex mix

*Table 6: Conditions attempted for the alkylation of indole **155** with N-Boc protected alkylating agents*

With the alkylated indole **174**, attempts were made to construct the hemiindigo core through a mild and direct palladium-catalysed oxidative acetoxylation of the indole, reported by Choy *et al.* (scheme 64).[313] This procedure was found to be relatively simple to conduct, however for this substrate system a low yield of 33% was obtained. Compound **175** was used immediately in the next step due to its poor stability. Unfortunately, attempts at the subsequent hemiindigo core formation using 4-bromobenzaldehyde were unsuccessful. Although product **166** was detected by LCMS and crude ^{1}H NMR, purification from significant levels of unknown by-products was challenging. Due to the low reaction scale, resulting from the previous poor yielding steps, isolation of **166** was unsuccessful.

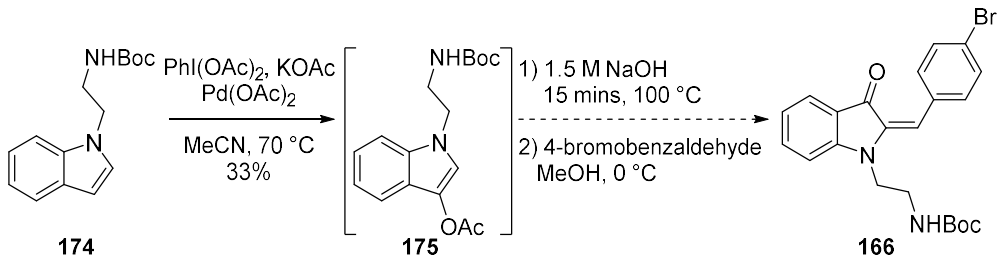

*Scheme 64: Attempted synthesis of N-alkylated hemiindigo **166** from substituted indole **174***

Due to the difficulties faced throughout the attempted alkylation of the highly unreactive hemiindigo nitrogen, it was decided to turn to an alternative photoswitch. Azobenzene scaffolds have many advantageous features, such as their high stability and distinctly different conformations. Hence, azobenzene-based photoswitchable PROTACs were developed for the proof of concept studies.

4.3.4. Synthesis of *ortho*-fluoroazobenzenes PROTAC series targeting AR

Retrosynthetic analysis of *ortho*-fluoroazobenzene based PROTAC **176** led to identification of four key fragments which can be combined in a convergent fashion (figure 108). It was proposed to build the azobenzene core through a Mills reaction between nitroso derivative **178** and aniline **179**. This core could then be combined with the VHL binder **154** through an *N*-arylation Buchwald/Ullman coupling approach and the AR binding motif **177** could be connected through an amide coupling. A two-carbon linker between the AR binder and the core photoswitch was introduced to increase the flexibility of the PROTAC, known to be important for ternary structure formation.[31] In addition, this enabled introduction of the amine functionality, important for connection to the core azobenzene.

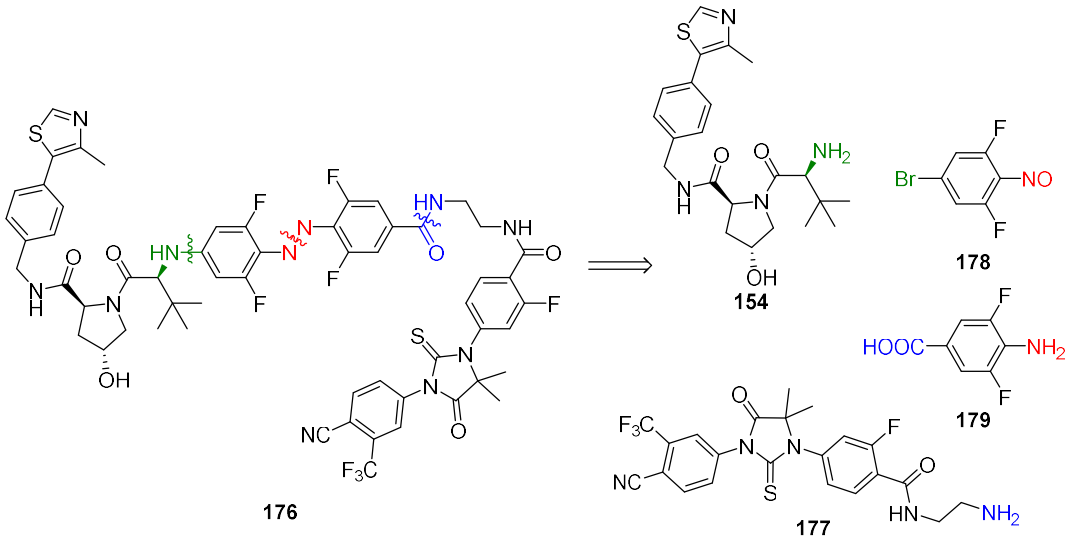

Figure 108: Retrosynthesis of azobenzene photoswitchable PROTACs into four simple components

To synthesise the azobenzene core **182**, firstly 2,6-dibromoaniline was treated with NBS to brominate the *para*-position to generate **181** in good yield (scheme 65). This compound was then oxidised using Oxone™ to the nitroso-derivative **178** in high yield, which was then reacted with commercially available aminobenzoic acid **179** in a mixture of toluene, acetic acid and TFA in the dark. After monitoring over 3 days, no product was observed, and only starting materials were isolated following purification. This was thought to be due to interference of the carboxylic acid in the reaction.

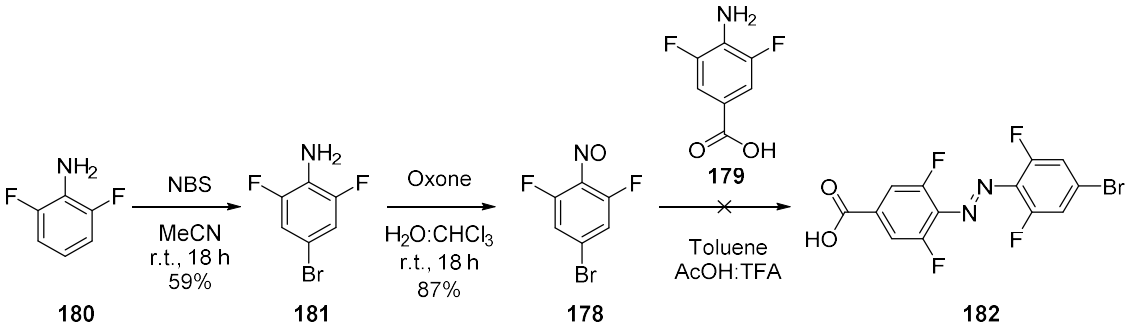

*Scheme 65: Attempted synthesis of bromo-carboxylic acid substituted azobenzene **182** through a Mills reaction from 2,6-dibromoaniline via NBS bromination and Oxone™ mediated oxidation to nitroso-substituent **178***

To circumvent this issue, aminobenzoic acid **179** was protected as ethyl ester **183** in high yield, prior to repeating the Mills reaction with **178** (scheme 66). After monitoring for 5 days, the reaction yielded a mixture of starting materials and product, upon purification, 27% **182** was isolated, alongside both starting materials, giving full mass balance. Despite the slow and low yielding nature of this reaction, it was acceptable due to easy recovery of the starting materials alongside product during purification.

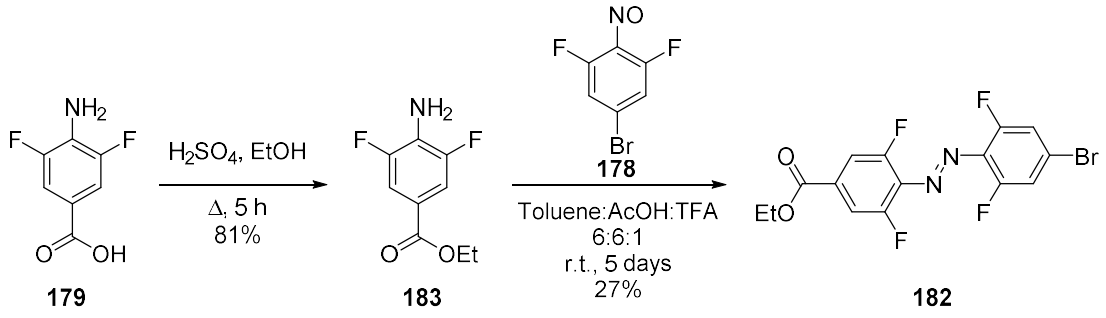

*Scheme 66: Alternative Mills reaction to synthesise bromo-carboxylic acid substituted azobenzene **182** from derivative **179***

With the core azobenzene building block **182** in hand, attempts were made to connect the VHL binder **154**. Initial attempts used Ullmann coupling conditions (scheme 67). After 4 h, all starting material was consumed, however LCMS analysis of the crude material showed very low amounts of product, and high levels of proposed S_NAr product **185** where the VHL amine **154** reacted directly with an *ortho*-fluoro substituent. It was hypothesised that due to the high temperatures required, the Ullman coupling conditions did not differentiate well between the bromo- and the fluoro- substituents in this

highly electron deficient aromatic system, leading to significant cross reactivity. To address this problem, palladium-catalysed *N*-arylation approaches were sought.

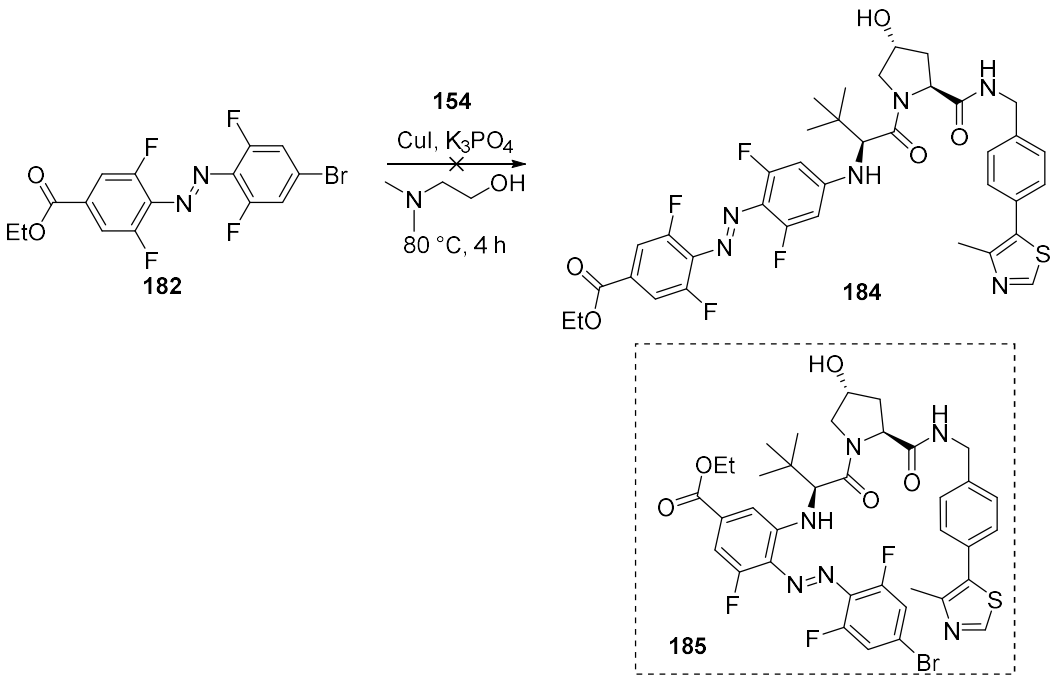

*Scheme 67: Attempted Ullmann coupling of **154** with bromoazobenzene **182,** S_NAr product **185** highlighted*

Buchwald Hartwig cross coupling conditions were attempted next, it was proposed that the oxidative addition into the bromo-aryl bond would be favourable compared to the aryl-fluoro substituents. Initial attempts used $Pd(PPh_3)_4$ and NaO^tBu at 100 °C for 22 h, which yielded a complex mixture of **185** and decomposed products (table 7). A change in the catalyst system to $Pd_2(dba)_3$ and BINAP at 110 °C for 18 h also gave a complex mixture with no desired product observed. It was thought that these temperatures were too high for this highly electron deficient system, hence a final attempt used XantPhos at 90 °C. This gave a mixture of S_NAr product **185** and desired product **184** in 1:1 ratio. Although product was identified by LCMS, the yield and poor conversion required high quantities of the VHL-binding ligand, the limiting reagent. Although there are a considerable number of different catalyst and ligand systems which could be attempted,[314,315] both starting materials for this reaction were too precious to undergo extensive screening. Hence, due to these inefficiencies, the direct conjugation of the VHL-binder strategy was abandoned, and alternative approaches were sought.

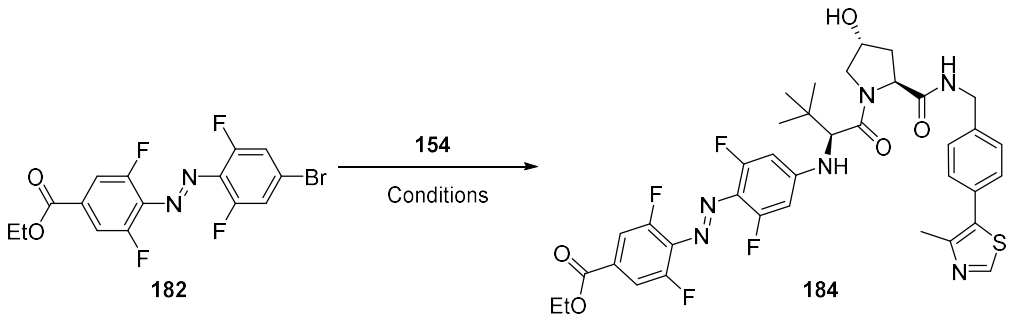

Run	Conditions	LCMS analysis
1	$Pd(PPh_3)_4$, NaO^tBu, K_2CO_3, Toluene, 100 °C, 22 h	Complex mix containing **185**
2	$Pd_2(dba)_3$, BINAP, NaO^tBu, Toluene, 110 °C, 18 h	Complex mix
3	$Pd_2(dba)_3$, XantPhos, Cs_2CO_3, Dioxane, 90 °C, 18 h	1:1 Mix **185**:**184**

*Table 7: Attempted conditions for the N-arylation of bromoazobenzene **182** using Buchwald-Hartwig conditions*

The high nucleophilicity of the aliphatic amine in **154** was identified to be a significant problem for its direct reaction with the electron deficient azobenzene **182**. One method to circumvent this, is through using a less nucleophilic amine source such as the benzophenone imine, which could then be unmasked in acidic conditions yielding aniline **187** (scheme 68). This strategy would form a core azobenzene substituted with both an acid and an amine on opposite sides of the core. The differential functionality could then be used for respective amide couplings with the two protein binding motifs. Unfortunately, this approach was also unsuccessful, and a complex mixture containing no identifiable product was obtained.

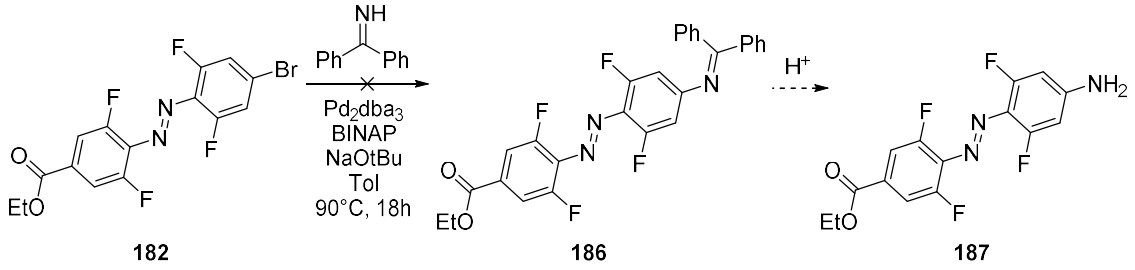

Scheme 68: Attempted Buchwald-Hartwig of benzophenone imine

A final attempt was made to directly attach a nitrogen to the aromatic azobenzene system through Buchwald-Hartwig reaction of less reactive acetamide with the aryl-bromide (scheme 69). The reaction proceeded extremely well, with quantitative yield of **188** attained after 1 h. Attempts were

then made to hydrolyse the amide (as well as the ester present) under acidic conditions. Although no starting material remained after 4 h at 100 °C, no product was identified through LCMS and the crude ^{1}H NMR showed a complex mixture of products. It was hypothesised that either the core azobenzene degraded in these extreme conditions, or the exposed acid and amine participated in side reactions after deprotection, which led to a complex mixture of polymeric species.

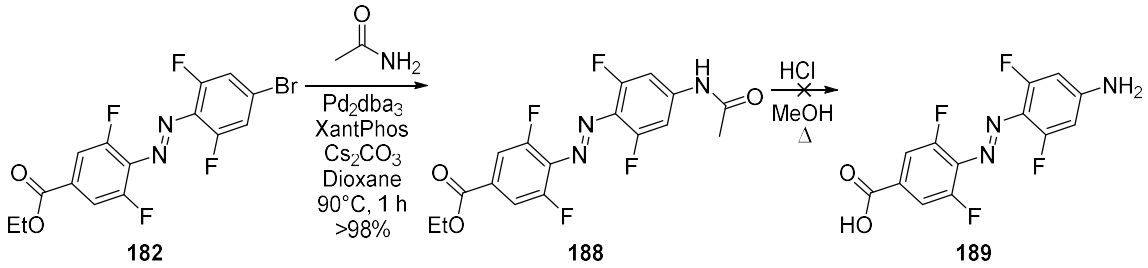

*Scheme 69: Buchwald-Hartwig conditions for acetamide reaction with **182** before attempted acidic amide hydrolysis*

Final attempts at this connection strategy proposed a Chan-Lam coupling between the VHL amine and a boronic acid derivative of the azobenzene core (scheme 70). Chan-Lam conditions are milder than Buchwald-Hartwig alternatives, which could discourage S_NAr reactivity. Unfortunately, formation of the boronic ester **190** from aryl bromide **182** proved unsuccessful, resulting in a complex mixture.

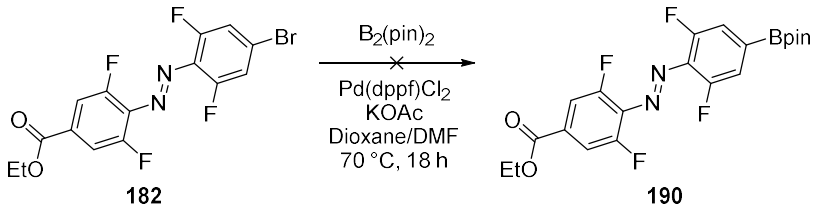

*Scheme 70: Attempted generation of boronic ester azobenzene derivative **190***

Due to the complications faced in this strategy, an alternative approach was identified using a simpler azobenzene core, which would theoretically yield a simpler and more robust route to this azobenzene series of photoswitchable PROTACs.

4.3.5. Alternative azobenzene conjugation strategy

To avoid the challenging *N*-arylation reaction, an alternative linkage was sought for connection of the VHL binder **154**. An amide coupling strategy was chosen due to its robust nature, high expected yields, and broad functional group tolerance (figure 109). Hence, azobenzene **191** was chosen as an ideal photoswitch for easy modulation and preparation. This photoswitch is functionalised with an ester on one end and an acid on the other, which enables a simple strategy of amide coupling one protein

binder, then ester deprotection to the acid, followed by amide couple of the second protein binder to form the full PROTAC structure.

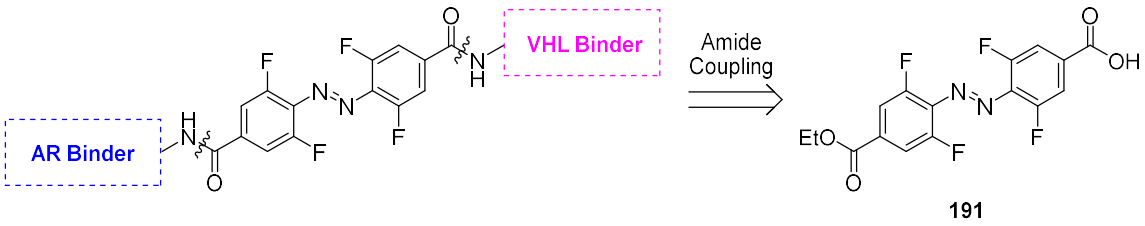

*Figure 109: Amide coupling strategy for conjugation of protein binders to core azobenzene **191***

The synthesis of azobenzene **191** followed the same oxidation then Mills reaction strategy of the previous azobenzene. Aniline **179** was oxidised *via* treatment with Oxone™ to form nitroso-intermediate **192**, which was then treated with aniline **183** through a Mills reaction to build the azo-core **191** (scheme 71). This final reaction was challenging, very low yields were consistently attained even with extended reaction times of over 7 days. Purification by column chromatography was also extremely challenging due to the polar nature of the product and starting materials which all were found to streak on the column, hindering pure product isolation. In addition, the nitroso-intermediate **192** was found to degrade on the column, introducing further impurities of a similar polarity to the desired product **191**. The best yield attained was 16% after 3 days, mainly due to the poor reaction conversion combined with purification difficulties. Despite these issues, enough product was isolated to continue the synthesis and due to the robust nature of the subsequent amide coupling reaction, some starting material impurities were tolerated.

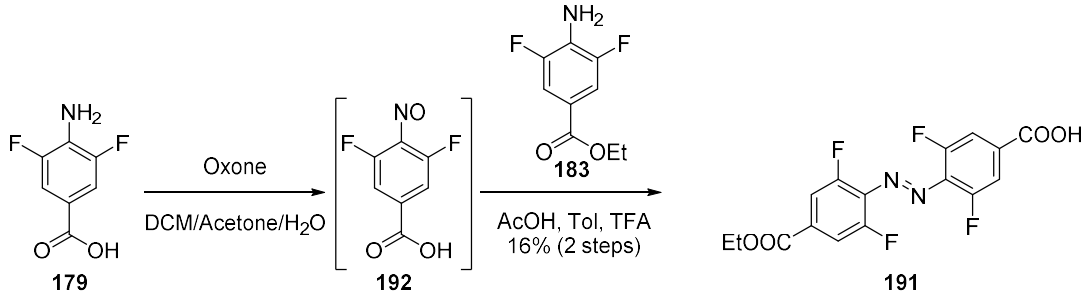

*Scheme 71: New route to alternative azobenzene core **191** via Mills reaction of nitroso-acid **192** and aniline **183***

Next, the AR-binding motif **177** was prepared (scheme 72). Enzalutamide acid **2** was reacted with two-carbon bis-amine **193**, obtaining **194** in high yield. The *N*-Boc protecting group was subsequently removed with TFA and desired the amine **177** was isolated in almost quantitative yield.

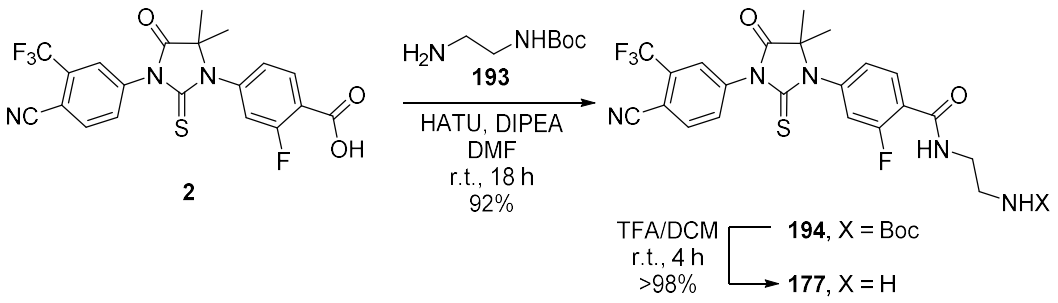

*Scheme 72: Preparation of amine-tagged enzalutamide derivative **177** via amide coupling and N-Boc deprotection*

With both AR-binder and VHL-binder amines in hand, **azoPROTAC1** could then be prepared through further simple amide couplings (scheme 73). Azobenzene **191** was treated with VHL binder **154** with HATU and DIPEA to form ester **195** in high yield, which was deprotected to unveil the acid **196** with LiOH. In order to avoid another challenging acid purification, this intermediate was immediately reacted with enzalutamide amine **177** to avoid unnecessary product loss through column chromatography. The final amide coupling also proceeded with high yield to generate the desired product, **azoPROTAC1**.

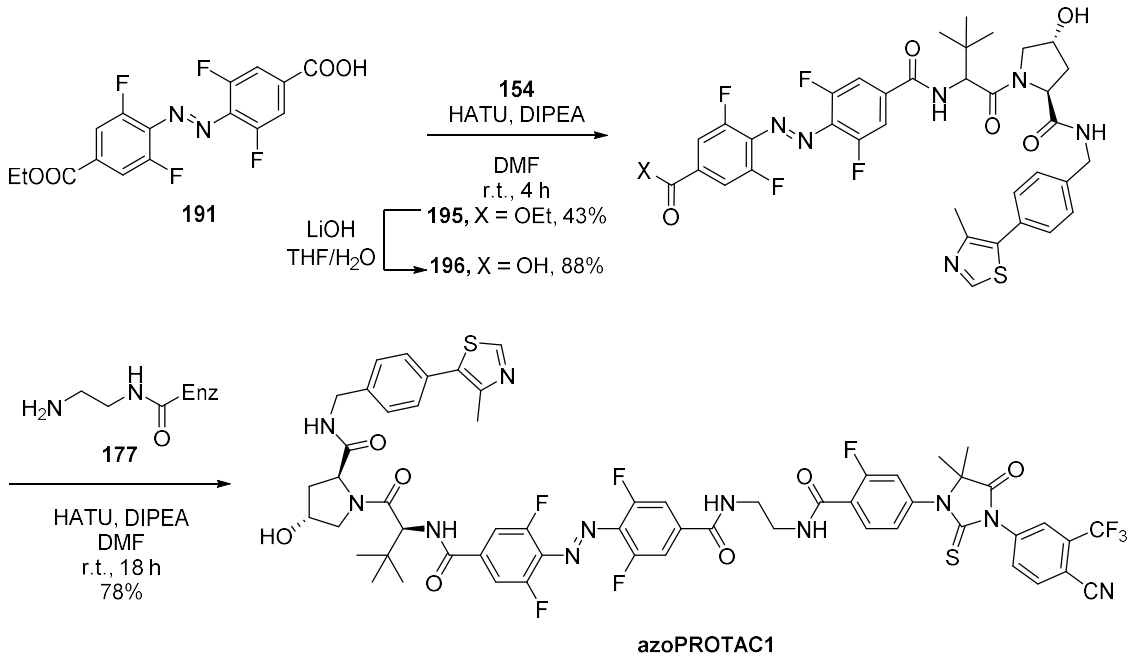

*Scheme 73: Preparation of **azoPROTAC1** through sequential amide couplings*

4.3.6. Photoswitching of azoPROTAC1

With **azoPROTAC1** in hand, the next challenge was to investigate the switching capabilities of the *ortho*-fluoroazobenzene core to ensure the large protein binding substituents on both ends of the

azobenzene did not hinder the efficiency and ease of switching. To analyse this, collaborators were sought in the Cavendish Laboratory in the Department of Physics. With the help of Jeffrey Gorman from the Optoelectronics group, switching of **azoPROTAC1** in both directions was demonstrated using a 405 nm and 520 nm continuous diode laser set-up.

It was important to consider solvent when assessing photophysical properties, as the solvent polarity can change the absorption spectra, known as solvatochromism.[316] The solvent absorption cutoff must also be accounted for, as below this the solvent absorbs all light. Ideally, the solvent used for the photoswitching study would be either aqueous or cell media, as this would be most applicable for biological applications, however, the solubility of the PROTACs was too poor to generate UV-vis spectra with a high signal-to-noise ratio. Therefore, acetonitrile was chosen to emulate the literature examples and provide a direct comparison to the reported photoswitches. In addition, the cutoff wavelength of acetonitrile is 190 nm, hence above this wavelength there would be no solvent effects interfering with the spectra. This enabled observation of the π-π* and n-π* characteristic absorptions.

Firstly, a UV-vis spectrum of **azoPROTAC1** was taken in its initial state, which was a mixture of the *cis* and *trans* isomers due to exposure to ambient light throughout the synthesis (figure 110). This UV-vis trace showed the two expected absorptions characteristic of these *ortho*-fluoroazobenzenes. At 250 - 350 nm in the UV region, a very strong π-π* absorption is observed, and a considerably weaker n-π* absorption was observed in the visible region between 375 - 500 nm.

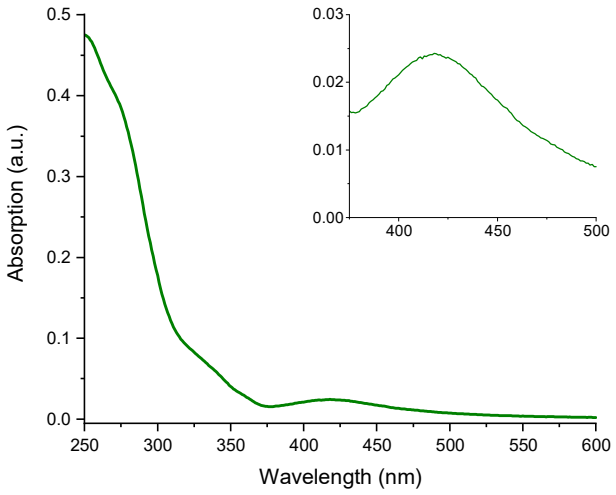

*Figure 110: UV-vis spectra of **azoPROTAC1**, inset displaying zoomed n-π* transition*

It is the presence of this red-shifted n-π* transition which is key for the visible light promoted switching of these azobenzenes, hence the sample was concentrated to magnify this region of interest, resulting

in complete saturation of the less interesting UV absorption. With improved absorption in this region, the switching was analysed through a cycle of cuvette irradiation and UV-vis spectroscopy, to observe a red-shift in the absorption over a series of timepoints (figure 111). The PSS for this *cis* to *trans* transition was observed after 17 minutes of irradiation with 405 nm light.

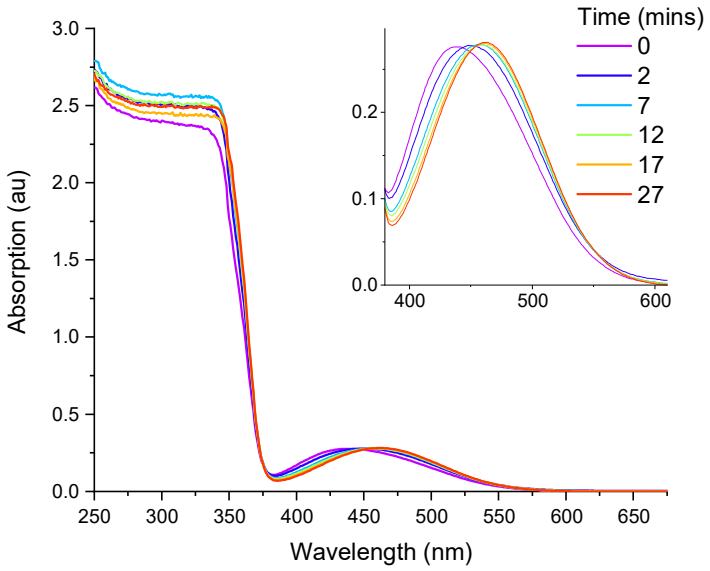

Figure 111: UV-vis spectra following irradiation with 405 nm light, inset displaying zoomed n-π transition*

The diluted, 405 nm irradiated **azoPROTAC1** was analysed by UV-vis spectroscopy to generate the full spectra without saturation (figure 112). The 300 – 350 nm region showed the characteristic red-shift in π-π* absorption expected for this azobenzene following irradiation.

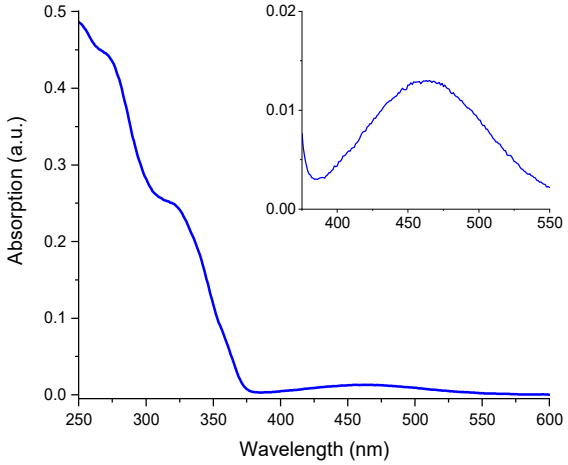

*Figure 112: UV-vis spectra for diluted 405 nm irradiated **azoPROTAC1.** inset displaying zoomed n-π* transition*

The next step was to test whether **azoPROTAC1** was able to switch back using a 520 nm light source. The same cuvette was then irradiated with 520 nm light for a series of timepoints and monitored by UV-vis spectroscopy (figure 113). The spectral shift was minimal after 32 minutes, however once the laser power was increased, the shift was rapid and substantial after 5 minutes of higher intensity irradiation. This highlights the importance of the light source intensity, as the absorption at this wavelength is considerably lower than at 405 nm, reflecting the longer switching time.

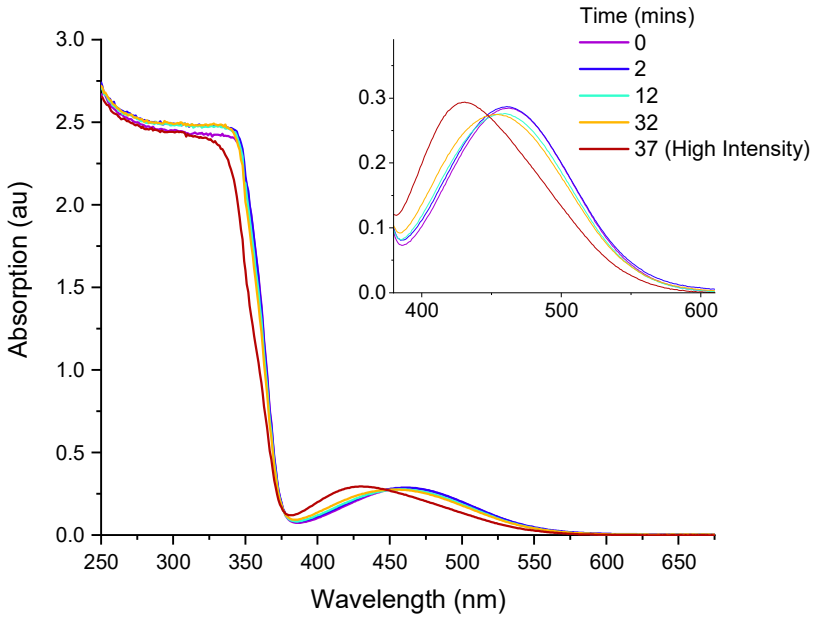

Figure 113: UV-vis spectra showing photoswitching following irradiation with 520 nm light for various times

Following these switching experiments, the UV-vis spectra of the PSS of switching in both directions were overlaid (figure 114). This enabled observation of the overlap in absorption between the two isomers, an indication of how effective the switching is. In addition, it was used to establish the wavelength where there was the greatest differential between the absorption of the two isomers. This preliminary data could then be used to identify the ideal wavelengths for further switching experimentation, 415 nm and 530 nm.

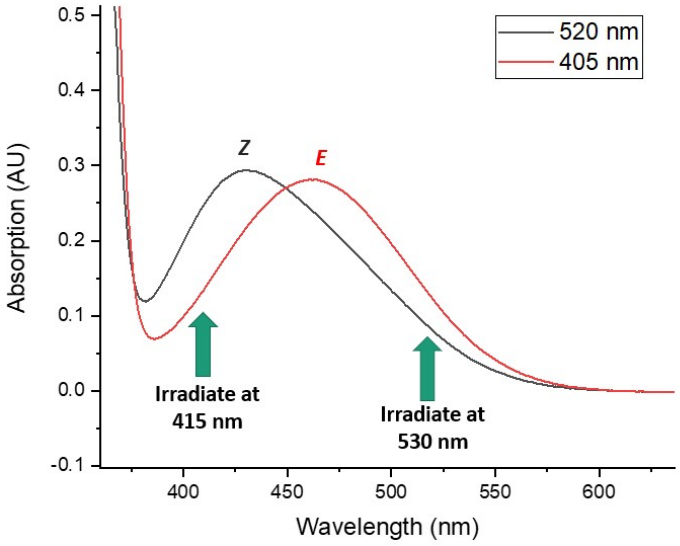

*Figure 114: Overlapped visible region of UV-vis spectra for both isomers of **azoPROTAC1** at their PSS with 405 and 520 nm*

Following the proof-of-concept switching experiments, a new set of LEDs were purchased from ThorLabs, at 415 nm and 530 nm wavelengths, which were used for all further experiments. These LEDs have a bandwidth of 14 nm for the 415 nm LED and 35 nm for the 530 nm LED. Although the switching observed at 405 nm was pleasing, moving to 415 nm was hypothesised to limit the level of < 400 nm light exposed to cells, which may be biologically harmful (section 4.1.4).

The switching experiments were then repeated with the 415 and 530 nm LEDs. The PSS overlay of the n-π* of the UV-vis spectra between the two isomers showed greatly improved differential overlap (figure 115). This highlighted the importance of wavelength in achieving optimal photoswitching.

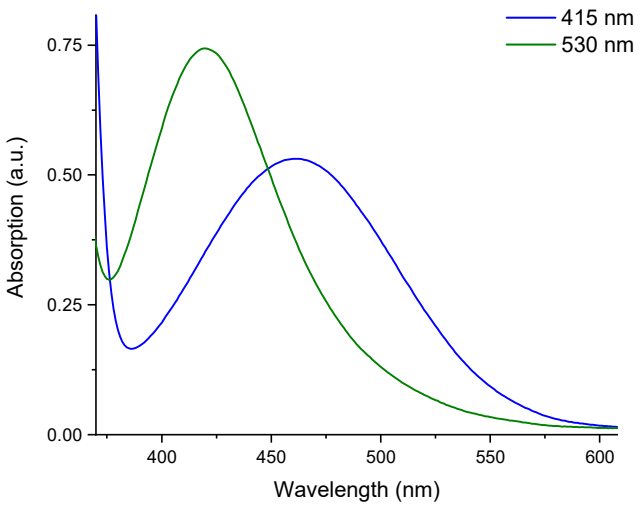

*Figure 115: Overlapped visible region of UV-vis spectra for both isomers of **azoPROTAC1** at the PSS with 415 and 530 nm*

4.3.7. Photophysical characterisation of azoPROTAC1

The next photophysical characterisation investigated was the switching PSS. This was measured using ^{1}H NMR, enabled by the distinctly different chemical shifts of selected functionalities within the two isomers leading to simple analysis of the isomer ratios. The most distinct shift was a doublet observed at 4.70 – 4.85 ppm which was used to measure the ratio between isomers (figure 116A). The sample was irradiated with 415 nm light and the ^{1}H NMR spectrum taken, complete shift of the doublet to 4.82 ppm was observed, indicating >98% *trans*-conversion after 10 minutes of irradiation. To establish whether the change in wavelength from 405 nm to 415 nm influenced this PSS, the experiment was repeated with 405 nm light. No difference was observed, both light wavelengths exhibited complete conversion. Pleasingly, this demonstrated that 415 nm LEDs were equally as effective as 405 nm, whilst importantly, being more red-shifted and further from the damaging UV region.

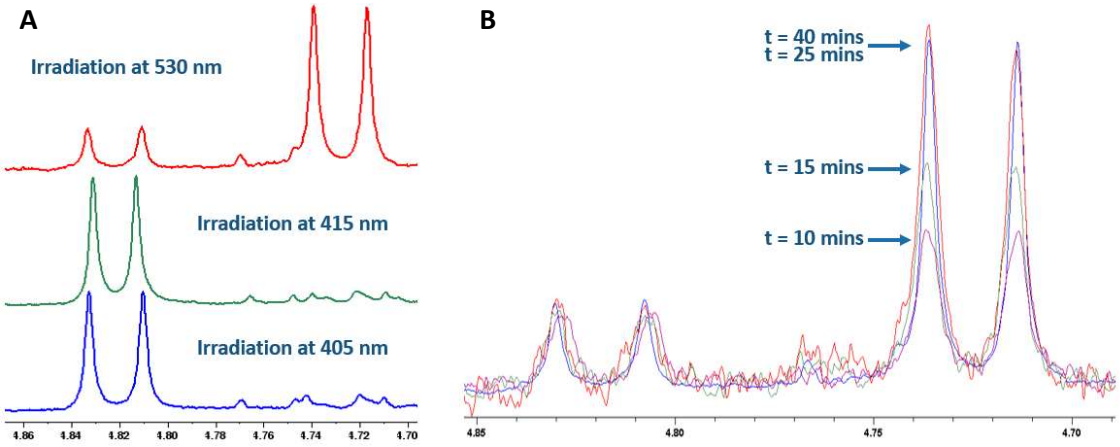

*Figure 116: A: ^{1}H NMR of **azoPROTAC1** following 530, 415 and 405 nm irradiation, B: overlaid ^{1}H NMR of 530 nm irradiation for 10, 15, 25 and 40 minute timepoints*

Next, the *cis*-conversion was tested using the 530 nm LEDs. This switch was found to be considerably slower than the *trans*-conversion which occurred within 10 minutes. After 25 minutes of 530 nm irradiation the PSS was reached, which was found to contain ~80% of the *cis*-isomer (figure 116B). Although this was less effective than the *trans*-conversion, this was still a highly *cis* enriched state which was expected to produce strong differential biological activity in the two isomers PSS. Additionally, the incomplete *cis*-conversion was in line with expected literature values.[285,290]

Next, the reversibility of the switching process and the photostability of **azoPROTAC1** were investigated. It was important to identify whether these azobenzene cores would be susceptible to photobleaching after extensive switching, as high stability is vital for therapeutic applications. This property was analysed by conducting eight isomerisation cycles. **AzoPROTAC1** was irradiated for 10 minutes with 415 nm light, followed by 25 minutes of 530 nm irradiation. The resultant UV-vis spectra

recorded following each radiation were overlaid (figure 117A), and the absorption at λ_{max} of the n-π* transition was then plotted (figure 117B). Fortunately, no instability was observed for **azoPROTAC1**. No drop-off in the UV-vis absorption was observed after eight cycles, with a cumulative irradiation time of 80 and 200 minutes for 415 and 530 nm respectively. Importantly, this highlighted the utility and robust nature of the *ortho*-fluoroazobenzene photoswitches.

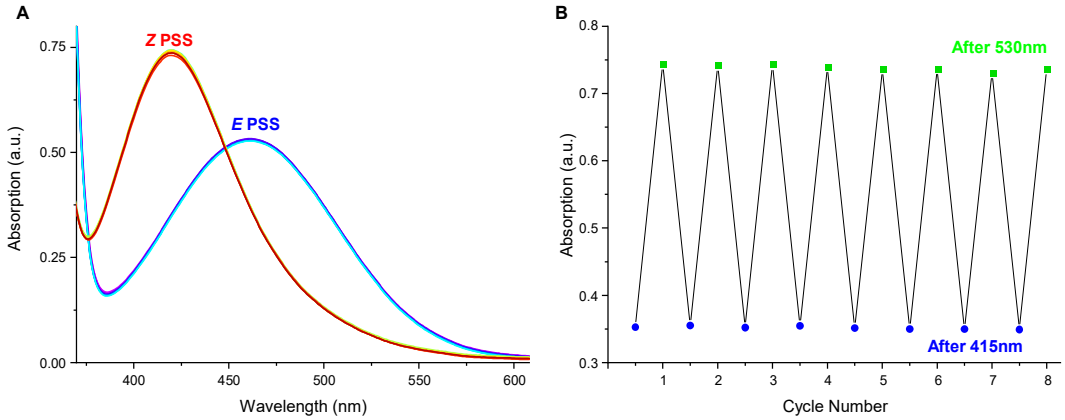

Figure 117: A: overlaid UV-vis spectra of eight switching cycles to observe change in intensity to indicate degradation, B: plot of absorption at maximum peak wavelength for eight switching cycles

Finally, the kinetic stability of **azoPROTAC1** was assessed at the biologically relevant temperature of 37 °C. **AzoPROTAC1** was irradiated to its excited *trans* PSS then incubated at 37 °C for 30 h, longer than the ideal 24 h biological assay timepoint, the UV-vis spectra were then overlaid to assess the extent of relaxation (figure 118A). After a 30 h incubation, no relaxation was observed, indicating high thermal stability in this PSS. To further study the kinetic stability of **azoPROTAC1**, an isomeric mixture was incubated for 1 h at 60 °C. UV-vis analysis demonstrated that there was no change in **azoPROTAC1**'s composition, indicating high kinetic stability of both isomers (figure 118B).

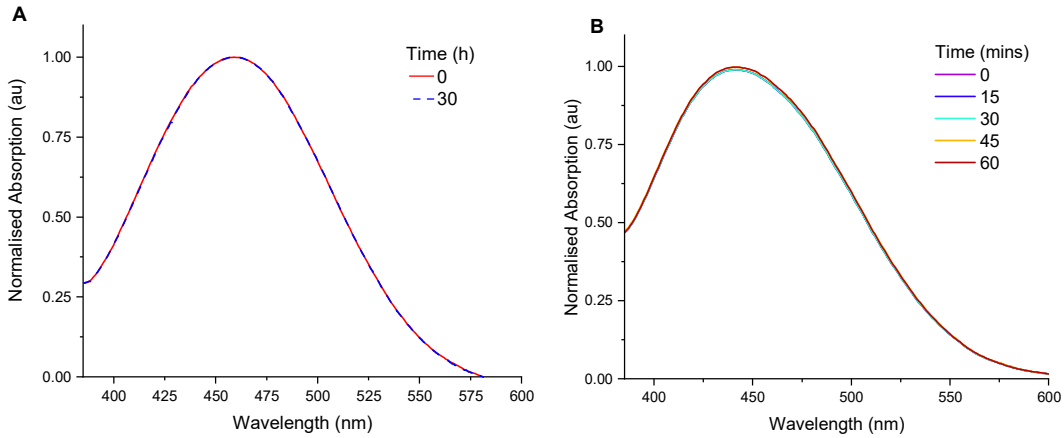

*Figure 118: A: Overlaid UV-vis spectra of t = 0 h trans **azoPROTAC1** isomer and t = 30 h incubation at 37 °C; B: Overlaid UV-vis spectra of **azoPROTAC1** isomeric mixture incubated at 60 °C*

This result further validated the use of this azobenzene core for biological application. With these results in hand, it was hypothesised that **azoPROTAC1** could be irradiated on the assay plate at the beginning of biological studies. The plate could then be incubated at 37 °C for the full time course without the composition of **azoPROTAC1** changing. Importantly, this prevented repeated irradiation throughout the assay, which could complicate the experimental set-up, in addition to introducing further variations which could affect the cells.

4.3.8. Biological evaluation of azoPROTAC1

Following the thorough assessment of **azoPROTAC1**'s photophysical properties, the effect of this PROTAC on AR-positive cell-lines was investigated. This was done in collaboration with Dr Andreas Hock at AstraZeneca, Cambridge. The imaging assay used for azoPROTAC analysis was described in Chapter 3. Initially, AR-positive LNCaP cells were treated with **azoPROTAC1** and then irradiated with either 415 nm or 530 nm LEDs on the assay plate (figure 119). The plate was then incubated in a dark incubator at 37 °C for 24 h before the cells were fixed. The cells were then stained with fluorescent antibodies to quantify AR levels within the cells following confocal microscopy. It was hypothesised that **azoPROTAC1** could be irradiated on the assay plate, rather than before dosing as this would be logistically simpler. If the compounds were irradiated prior to dosing, then the dosing procedure would require completely dark conditions to minimise the levels of ambient light, which could influence the results. Importantly, clear bottomed assay plates were used to ensure high light penetration.

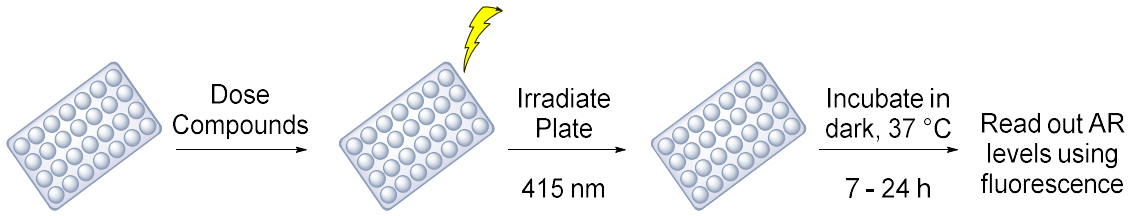

*Figure 119: Procedure for biological evaluation of **azoPROTAC1**, compound switching carried out on the assay plate*

The control compounds used to validate the experimental procedure were negative control DMSO, and positive control niclosamide. The assay was run in triplicate and the compound was dosed twice onto cells on the same plate. The plate was then irradiated for 10 minutes in two sections, with 415 and 530 nm LEDs to generate both isomers. The plate was then incubated for 24 h. Including the dosing of the compounds and irradiation, the cells were outside the incubator for *ca.* 1 h. After fixing, staining, and imaging, the fluorescence response was plotted for the two different irradiation wavelengths, essentially the two isomers (figure 120). This preliminary biological data showed some AR degradation, with the AR levels changing from *ca.* 200,000 units with no PROTAC to almost 120,000

units with PROTAC. Although only partial AR degradation was observed, there was differential activity between the wavelengths. Higher activity was observed following 415 nm irradiation. Interestingly, a hook effect was observed at high concentration, which is a common feature of PROTAC dose response curves. This is where activity is reduced at high concentrations due to greater formation of the binary protein complex between the PROTAC and one protein, over the active tertiary protein complex.

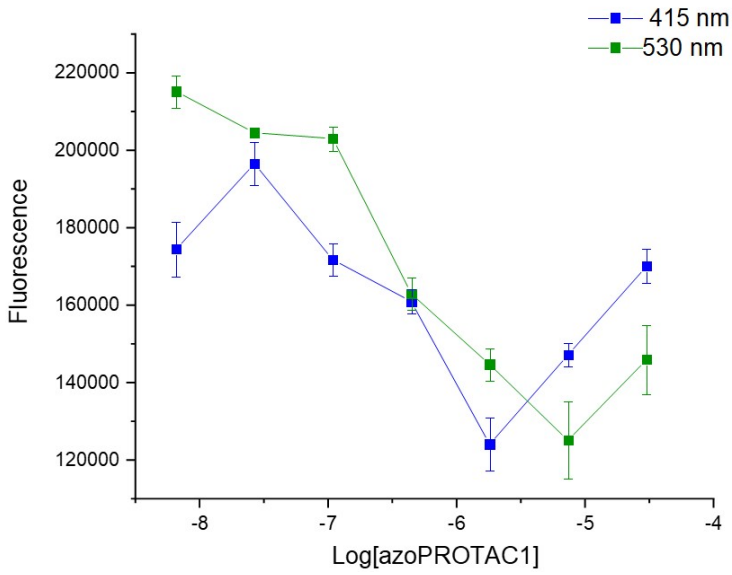

*Figure 120: Dose-response curve of **azoPROTAC1** following on-plate irradiation with 415 and 530 nm LEDs, 24 h incubation*

With these promising initial results in hand, further PROTACs were designed in an attempt at optimising the potency and extent of AR degradation. It was hypothesised that through linker length and property modification, improved efficacy and more complete AR degradation could be promoted.

4.3.9. Development of azoPROTAC2

One strategy hypothesised to improve the activity of this PROTAC, was reduction of the number of amide bond linkages, which could lead to instability and poor pharmacokinetic properties. An ether linkage was chosen between the enzalutamide AR binding motif and the azobenzene as this would alleviate the requirement for an amide linkage and was synthetically tractable.

Modification of the enzalutamide core through this strategy required an ether-linked aryl-fragment to build the diarylthiohydantoin core (scheme 74). Initially, commercially available 4-bromophenol **197** was alkylated using 2-(Boc-amino)ethyl bromide in the presence of K_2CO_3 to generate aryl-bromide **198** in almost quantitative yield. Next, the aryl-bromide **198** reacted *via* an Ullmann coupling with 2-aminoisobutyric acid to form acid **199** in 22% yield. The poor yield of this reaction was hypothesised

to be due to the challenging purification, in combination with the incomplete reaction. It was expected that optimisation of the reaction conditions could improve this yield, however, enough material was supplied for the synthesis of this series of azoPROTACs. With acid **199** in hand, methylation using iodomethane and K_2CO_3 formed ester **200** in 59% yield. This reaction gave complete conversion of starting material, however over-methylation of the aryl-amine group also occurred, which reduced the yield of the desired product. The diarylthiohydantoin core was then constructed *via* reaction of the amino-ester **200** with isothiocyanate **5**. Pleasingly, this reaction generated almost quantitative yield of desired enzalutamide derivative **201**. Finally, the *N*-Boc protecting group was removed using TFA to yield enzalutamide-amine **202**, ready for subsequent amide coupling to the azobenzene core.

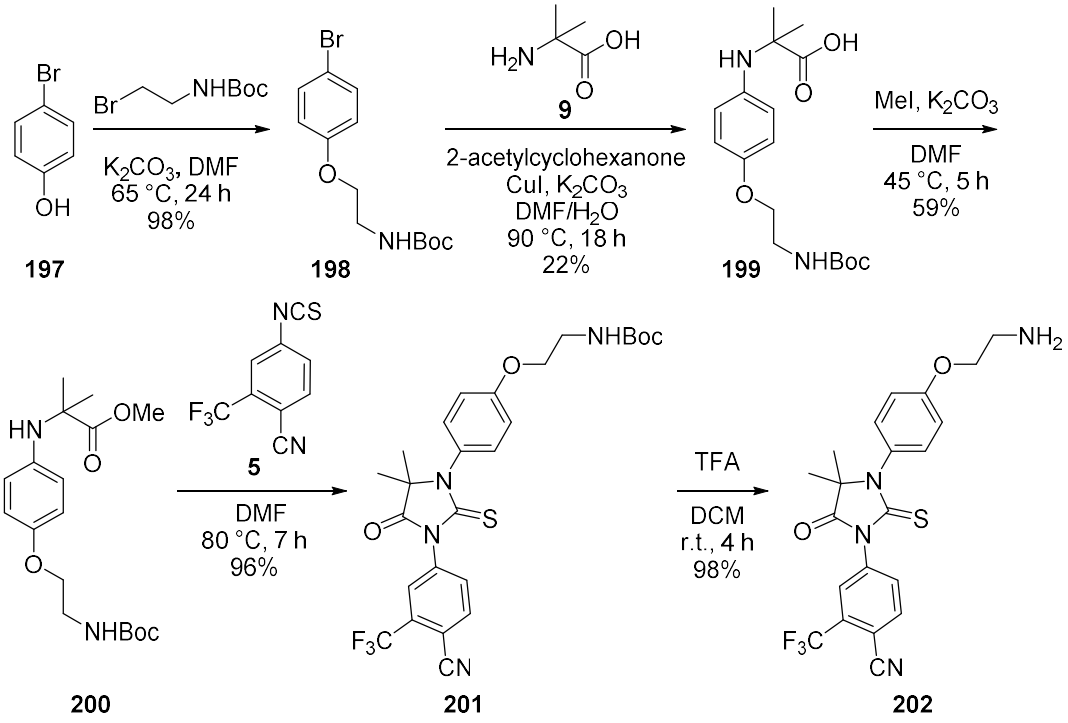

*Scheme 74: Synthesis of new ether enzalutamide derivative **202** through O-alkylation, Ullmann coupling, esterification and cyclisation of central diarylthiohydantoin core*

Next, the new enzalutamide fragment **202** was attached to **195** through amide coupling methodology to generate desired **azoPROTAC2** in moderate yield (scheme 75).

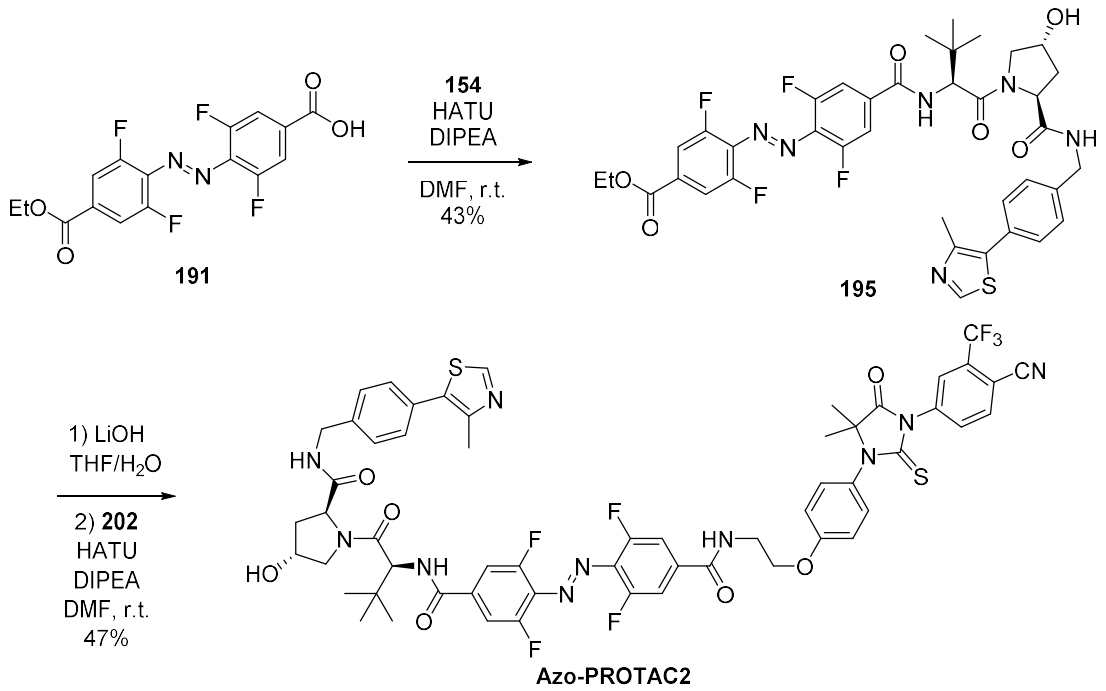

*Scheme 75: Synthesis of **azoPROTAC2** through sequential amide couplings*

4.3.10. Further biological assessment of azoPROTAC1 and azoPROTAC2

With the new PROTAC in hand, additional biological testing was conducted with Dr Andreas Hock at AstraZeneca for further validation of **azoPROTAC1**'s activity and for comparison to the newly developed **azoPROTAC2**.

A modified procedure was proposed where the cells would be fixed after 6 h rather than the full 24 h as previously conducted. AR-degrading PROTACs have been shown to completely eradicate AR in under 6 h,[290] hence reducing the assay length could give improved results if there was any instability of the azoPROTACs over 24 hours. In addition, the longer time course of the assay could result in greater background noise due to variability between cells over 24 h, this could lead to greater difficulty in analysing the data due to less pronounced differences in degradation.

An additional modification was also proposed. The compounds were dosed across two plates to reduce the potential for cross-contamination of the light sources when irradiating the plate in portions. Finally, following the full photophysical characterisation of **azoPROTAC1** it was established that 530 nm irradiation required greater time to reach the PSS compared to 415 nm irradiation. This was implemented for the subsequent biological studies; the cells would be irradiated for 30 minutes with 530 nm LEDs rather than the 10 minutes previously used.

The next run incorporated all of these modifications. The cells were plated across two assay plates and after PROTAC dosing were irradiated with each respective LED. The plates were then incubated for 6 h and the cells were examined. Unfortunately, on this occasion all cells were found to be dead, including both positive and negative controls across both plates. The specific reason for cell death was unknown and could have been completely independent of the assay procedure. However, it was hypothesised that potentially keeping the cells outside of the incubator for close to 1.5 h during dosing and the subsequent irradiation could have been a contributing factor to the cell death.

In the next assay, to reduce the length of time the cells were outside the incubator, it was proposed that the compounds would be irradiated with 530 nm LEDs for 30 minutes prior to dosing. This procedure enabled the 530 nm irradiated plate to be placed straight into the incubator after dosing, avoiding the lengthy plate irradiation procedure. Once again, the assay length was 6 h, and at this point, the cells across both plates were noted to be healthy. The plates were then fixed, stained, and imaged to assess the AR levels.

The results of this assay were not very promising, and the AR levels were found to fluctuate more significantly than previously observed (figure 121). **AzoPROTAC1** reduced AR levels by just 15%, considerably lower than the previously observed 40% AR reduction. The two wavelengths generated very similar profiles in the dose response curves, indicating little difference between isomers. In addition, the variability in AR levels between the plates was around 10%, which made it extremely difficult to analyse minor differences between the two plates. Despite variability in the data, a slight downward trend was observed in AR levels at increased concentration of PROTAC. Once again, a very slight hook effect was also observed at the maximum concentration.

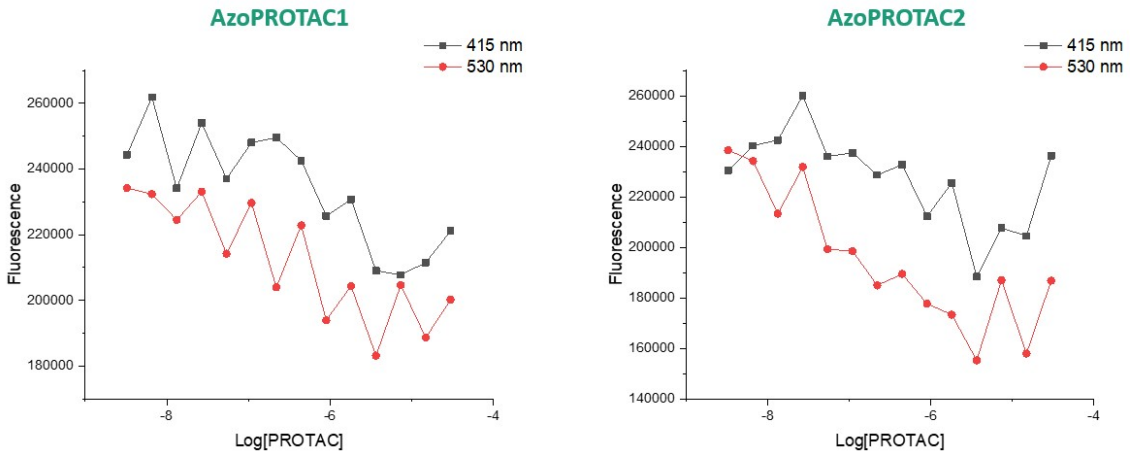

*Figure 121: Dose-response curves of **azoPROTAC1** and **azoPROTAC2** following initial compound irradiation with 530 nm then on-plate irradiation with 415 nm and incubation for 6 h*

It was thought that the irradiation process for this assay was not ideal. Following the 30 minute irradiation with 530 nm LEDs, the compounds needed to be kept completely in the dark, whilst being dosed to avoid any undesired photoswitching caused by ambient light. Unfortunately, this was very challenging to achieve in the laboratory used for this assay, particularly as the automated dosing machine used a blue LED to guide compound input. Hence, the compounds were exposed to light which may have been responsible for the extremely low difference in biological activity between the two irradiated forms of both PROTACs.

To overcome these issues and to verify the initial biological results observed for **azoPROTAC1**, it was proposed that the original assay conditions would be repeated with both PROTACs. This would enable confirmation of the reproducibility of the assay and facilitate comparison between the two PROTACs to establish whether the structural changes affect biological activity. These studies are ongoing.

4.3.11. Development of azoPROTAC3

The linker conjugation strategy is well-established to be vital for achieving active and highly potent PROTACs.[290] After the ether linkage approach was employed to attached the AR-binding motif to the azobenzene, it was hypothesised that a similar approach to the VHL binding motif could also enhance activity. In PROTAC literature there are few examples of the VHL ligand directly attached to an aryl amide, hence it is unknown whether this attachment type may hinder activity. One approach to alter this is to modify the *para*-linkages of the azobenzene core, from two carboxylic acids to one carboxylic acid and an aniline or phenol group (figure 122). This would also reduce the number of amide bonds required to form the PROTAC hence improving both the chemical stability and drug-like properties of the overall structure. Another fundamental advantage to these alternative azobenzenes is their ease of synthesis. The previous azobenzene cores were prepared through a Mills reaction of a nitroso-aryl combined with an aniline. This reaction was low yielding, difficult to purify and had very long reaction times which made it a poor choice for long-term supply.

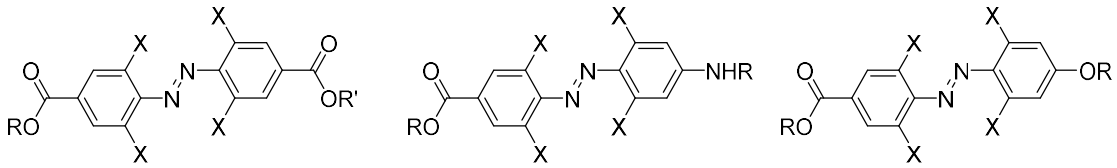

Figure 122: Structure of initial azobenzene core compared to new aniline and phenol-based azobenzene cores

Aniline azobenzene derivative **205** could be prepared through an azo-coupling reaction by reacting a diazonium salt with an aniline (scheme 76). Azo-coupling reactions are well-known to be high yielding and fast, which would be a substantial improvement on the Mills reaction. The azo-coupling was

initially attempted using 3-fluoroaniline derivative **204** as an available test substrate to scope out the viability of the reaction. Unfortunately, this reaction resulted in a complex mixture of products, and no desired azobenzene **205** was observed by LCMS or ^{1}H NMR. The reasons for this failure were unknown, however progression to the well-precedented phenol azo-coupling reaction was a sensible alternative to try, due to the subsequent *O*-alkylation conjugation strategy which would be beneficial in reducing the overall number of amide bonds.

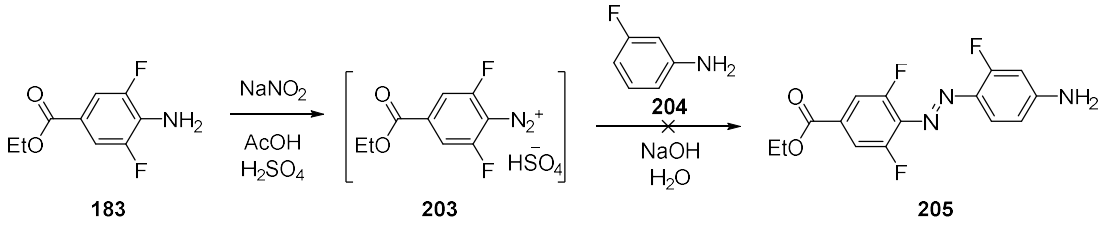

*Scheme 76: Attempted synthetic route to aniline azobenzene core **205** through azo-coupling chemistry*

Due to the higher cost of the *ortho*-fluoroester **183**, this phenol azo-coupling reaction was first attempted on commercially available ethyl-4-aminobenzoate **206**, which was treated with sodium nitrite in acid to form the diazonium sulfuric acid salt intermediate **207**. Intermediate **207** was immediately treated with 3,5-difluorophenol **208** in a one-pot reaction to yield desired azobenzene **209** in high yield (scheme 77). Due to the simplicity of this reaction, it was proposed that a PROTAC would be directly prepared from this di-fluorinated core. Additionally, this would enable comparison of the new core properties with the previously synthesised azoPROTACs.

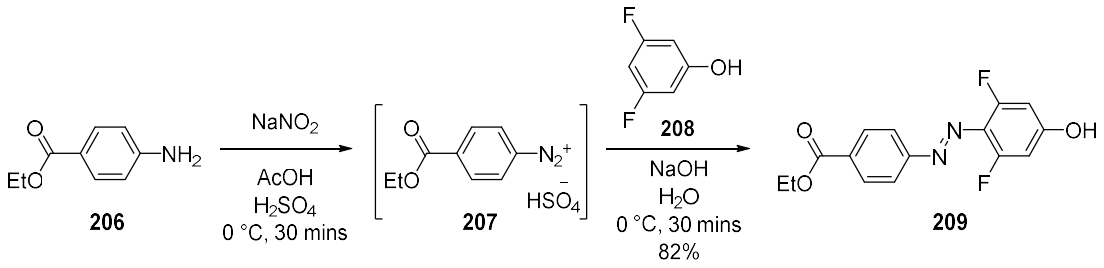

*Scheme 77: Azo-coupling route to new azobenzene core **209** via diazonium salt intermediate **207***

The new azobenzene core **209** was first alkylated with *tert*-butyl bromoacetate, in the presence of K_2CO_3 and catalytic potassium iodide to produce diester **210** in high yield (scheme 78). The difference in stability of the two esters made them orthogonal, hence the *tert*-butyl ester was selectively deprotected in TFA to yield acid **211** in reasonable yield. Next, the VHL binder **154** was then coupled to acid **211** using HATU and DIPEA, to produce ester **212** in high yield. Finally, the ethyl ester was deprotected using LiOH and the revealed acid reacted immediately in a final HATU mediated amide coupling with enzalutamide amine **202** to produce **azoPROTAC3** in high yield.

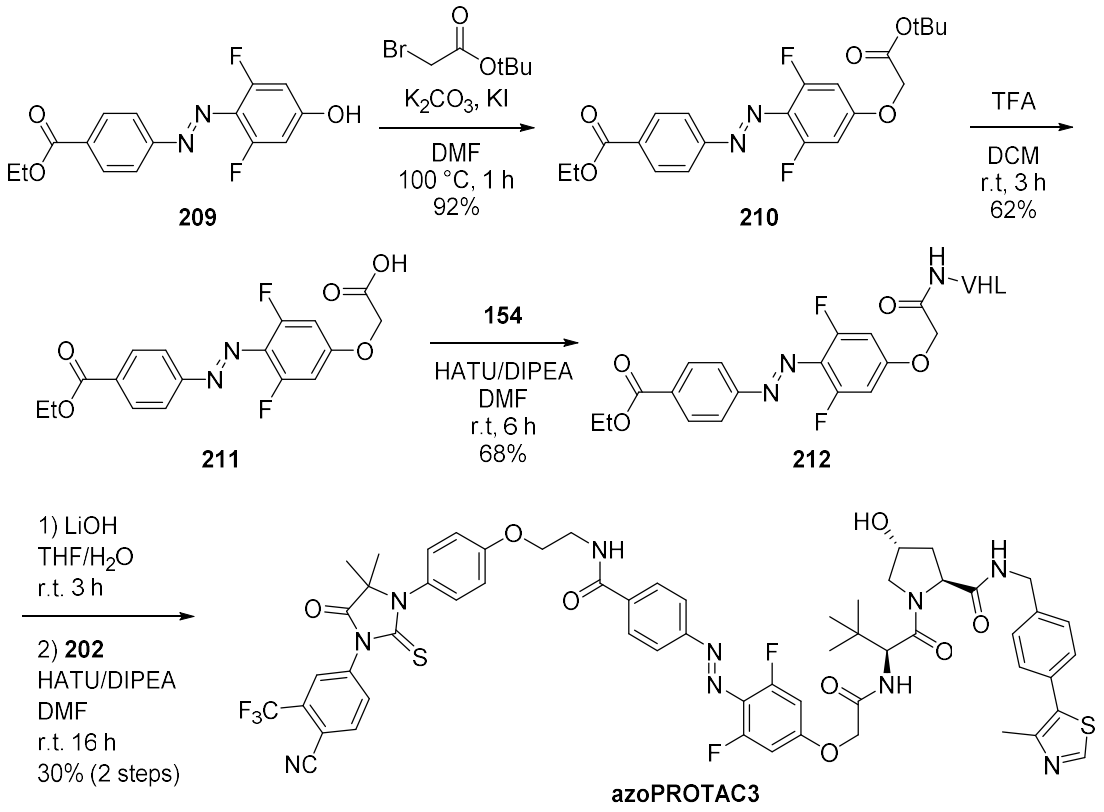

*Scheme 78: Synthesis of **azoPROTAC3** via O-alkylation of core **209** and subsequent deprotection and amide coupling*

With **azoPROTAC3** in hand, photophysical characterisation was repeated to compare the new azobenzene core to those previously used. The new azoPROTAC was irradiated with 415 nm LEDs for a series of timepoints and ^{1}H NMR spectra were recorded following each irradiation to establish the PSS. After complete switching was observed, the PROTAC was then irradiated with 530 nm LEDs to switch back (figure 123A). The *trans* PSS was reached after 10 minutes of 415 nm LED irradiation and was found to contain *ca*. 85% *trans* isomer. Photoswitching to the *cis* PSS using 530 nm with this azobenzene core took just 10 minutes, which was considerably faster compared to the previous azobenzene which took 25 minutes of irradiation to reach the PSS. The PSS following 530 nm irradiation was *ca*. 56%, lower than previously observed for **azoPROTAC1**. UV-vis spectroscopy was also used to study the overlap in absorption between the two species in the n-π* visible region (figure 123B). This showed a high degree of overlap in the absorption of the two species, considerably greater than observed for the earlier scaffolds. This overlap reflected the poorer PSS observed following 530 nm irradiation. However, there was greater differential between the two isomers at 415 nm, which corresponded well to the higher PSS reached.

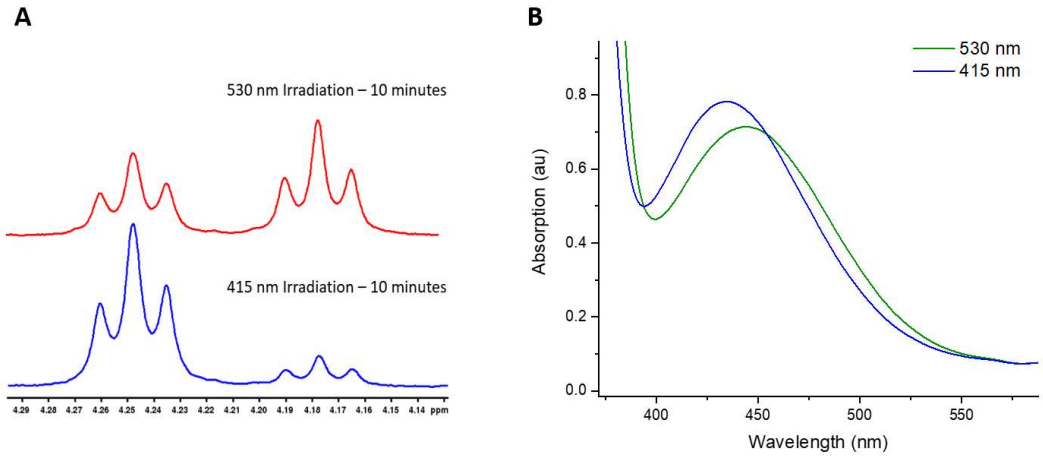

*Figure 123: PSS of **azoPROTAC3** following 415 and 530 nm irradiation for 10 minutes; A: ^{1}HNMR showing isomer composition at PSS; B: overlaid UV-vis spectra of visible region showing overlap of n-π* absorption*

Although these PSS were lower than those reached for the previously used scaffold, they were predicted to be satisfactory for further biological testing. Additionally, the UV-vis spectra of **azoPROTAC1** overlaid with **azoPROTAC3** showed a significant shift in λ_{max} (figure 124). Optimisation of either the core substitution or the wavelengths used for PROTAC excitation could be undertaken following the validation of biological activity.

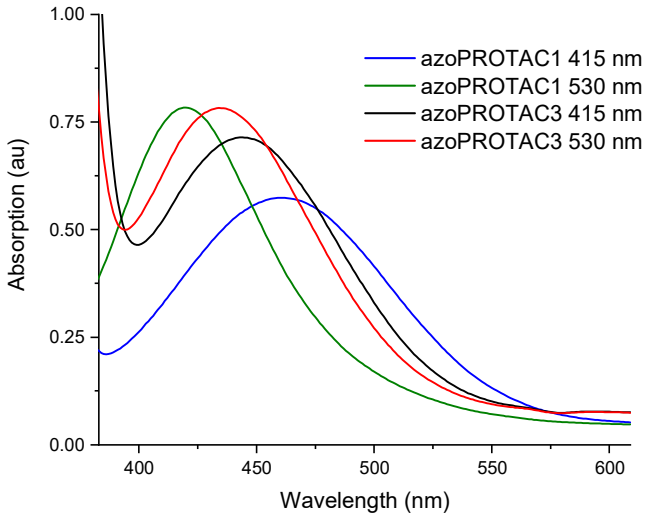

*Figure 124: Overlaid UV-vis spectra of **azoPROTAC1** and **azoPROTAC3** showing the difference in n-π* absorptions*

This new azoPROTAC along with all previously synthesised PROTACs are currently undergoing further biological testing with collaborators to validate the previously observed activity and establish activity of the new series.

4.3.12. Photoswitchable PROTACs targeting the estrogen receptor (ER)

Next, an additional protein of interest was chosen to validate the proof-of-concept photoswitchable linker technology and prove its generalisability. For this purpose, the estrogen receptor (ER) was chosen due to its importance in breast cancer and precedence in PROTAC literature.

A recent publication by Hu *et al.* reported a potent new ER degrading PROTAC, ERD-308 with a DC_{50} of 0.17 and 0.43 nM in two different ER+ cell-lines (figure 125).[317] Impressively, this PROTAC induced >95% degradation at just 5 nM and was found to be a more complete degrader than successful SERD fulvestrant (section 1.3.1). This optimised PROTAC incorporated selective estrogen receptor modulator (SERM) raloxifene to bind ER, and computational modelling was used to determine a suitable solvent exposed vector for the PROTAC linkage. Raloxifene is a clinically approved treatment for osteoporosis, which is also used to lower the risk of breast cancer.[318] Extensive optimisation of all three PROTAC components was carried out by the researchers to afford the most potent degrader. Alternative ER binders were also screened in addition to raloxifene, including tamoxifen and bazedoxifene and although all PROTACs were effective, the raloxifene binding motif was reported to be the most potent. Both VHL and cereblon recruiting PROTACs were also synthesised in the study, however only VHL was shown to degrade ER effectively. The cereblon recruiting PROTACs exhibited no degradation at concentrations up to 1 µM. The linker was also studied extensively, with different lengths, hydrophilicities and flexibilities considered. Overall, more flexible linkers were most effective with 6-9 atom linker lengths providing optimum degradation. However, the less flexible linkers also degraded ER, albeit at 10 nM concentrations compared to 1 nM for the flexible variants.

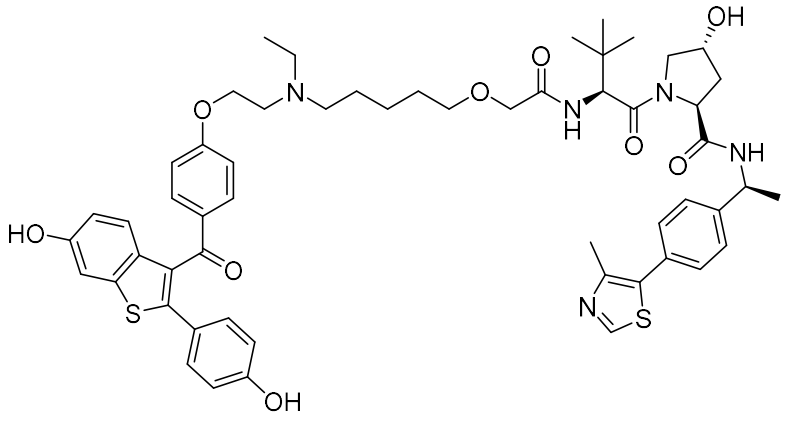

ERD-308

Figure 125: Structure of PROTAC ERD-308 discovered to eradicate ER at 1 nM dosing in two ER+ cell lines

Based on these findings, it was hypothesised that the ER protein system would be amenable to the photoswitching linker technology, due to the high potencies and extensive range of PROTAC structures

that were demonstrated to induce extensive ER degradation. Specifically, the raloxifene warhead was incorporated for ER binding, combined with the previously used VHL ligand (figure 126).

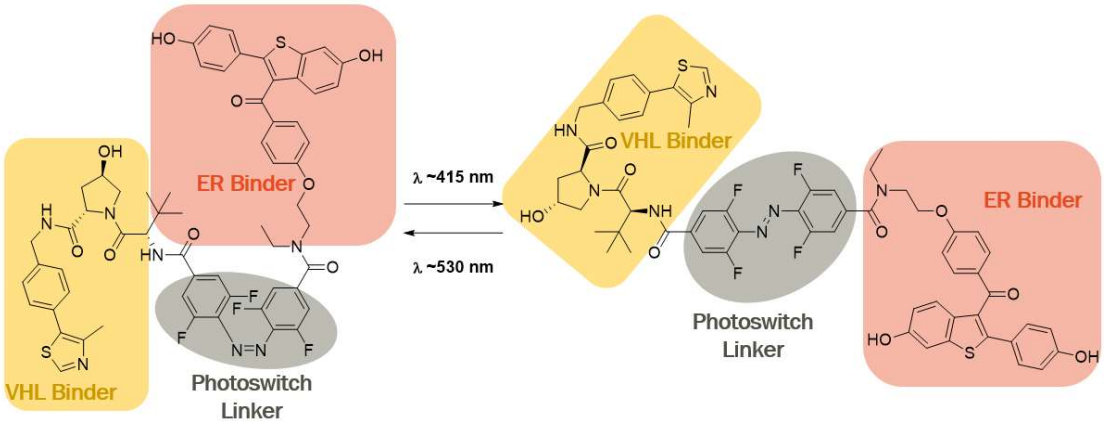

Figure 126: Design of ER degrading photoswitchable PROTAC recruiting VHL

Synthesis of ER warhead **219** was carried out according to the literature preparation in six steps (scheme 79).[317] Phenol **213** was first acylated to form **214** in almost quantitative yield. The acyl chloride was then generated *in situ* using oxalyl chloride, before directly undergoing a Friedel Crafts acylation with commercially available benzothiophene **215** to form **216** in 35% yield over two steps.

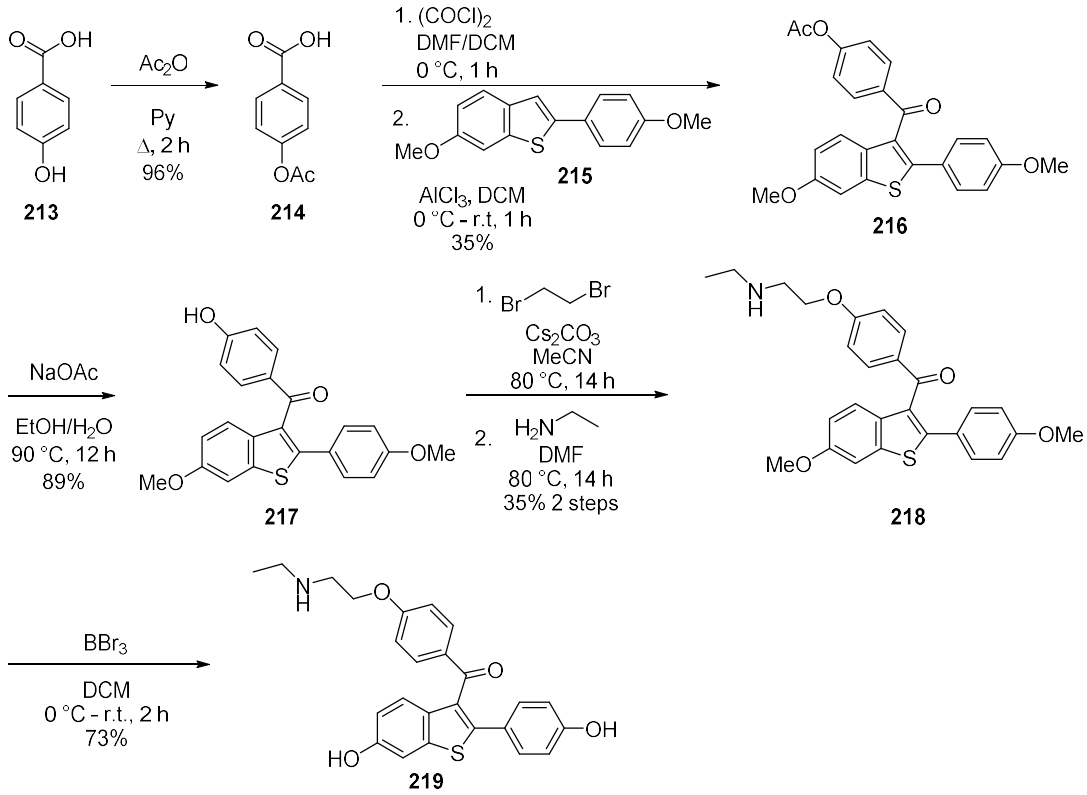

*Scheme 79: Synthesis of raloxifene-based SERM **219***

Next, the acyl-phenol **216** was deprotected with sodium acetate in high yield and the free phenol **217** was alkylated with 1,2-dibromoethane before being directly treated with ethylamine to form **218** in 35% yield over the two steps. This step was hypothesised to be low yielding due to the high potential side reactivity in both steps. Finally, the methyl groups were cleaved with boron tribromide to generate desired ER degrader **219** in good yield. Although the yields in this route were highly variable, enough ER degrader was attained for PROTAC generation, hence no reaction optimisation was undertaken.

With this SERM in hand, it could be combined with the previously generated PROTAC core to form photoswitchable ER-targeting **azoPROTAC4** (scheme 80). This was conjugated through the previously used protocol of *in situ* hydrolysis of ester **195** and subsequent amide coupling with SERM **219** forming desired **azoPROTAC4** in 35% yield.

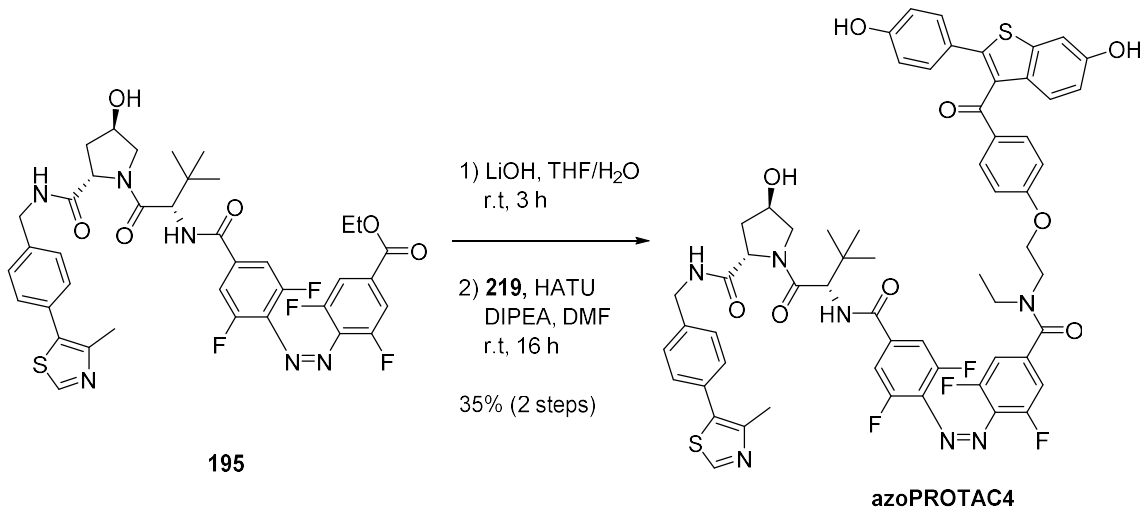

*Scheme 80: Synthesis of photoswitchable ER degrading **azoPROTAC4***

Next, photophysical characterisation of **azoPROTAC4** was carried out. Initially, UV-vis spectroscopy was considered for observing the switching. Unfortunately, due to the strongly absorbing chromophore present in the core structure of raloxifene this was extremely difficult to observe. The UV-vis spectrum of SERM **219** alone showed high absorption between 250 - 325 nm, saturating the detector and an additional absorption shoulder from 325 - 425 nm (figure 127). This absorption complicates analysis of the full PROTAC spectra, as without clear observation of the n-π* azobenzene absorption, switching efficiency cannot be easily assessed by UV-vis spectroscopy.

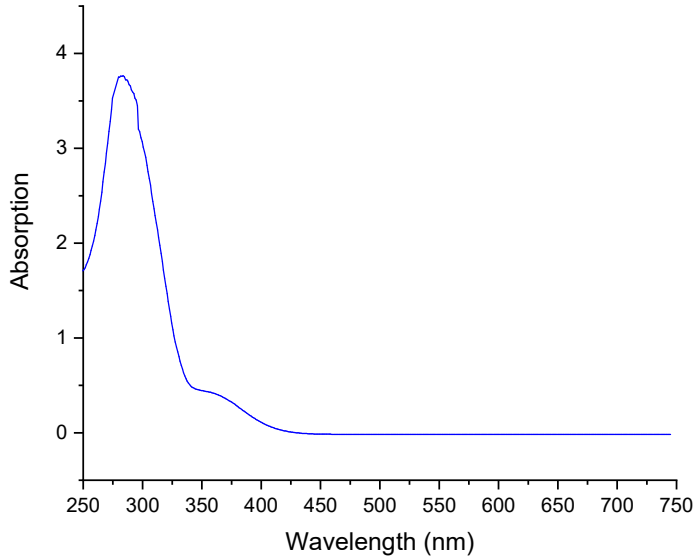

*Figure 127: UV-vis spectrum of SERM **219***

^{1}H NMR was therefore used to determine the PSS composition at the two wavelengths (figure 80). Irradiation of **azoPROTAC4** with 415 nm LEDs took 20 minutes to reach PSS, which was comprised of 92% *trans* isomer. This time was twice as long as previously observed for the AR PROTAC series, likely due to light absorption by raloxifene, lowering the intensity of radiation available to the azobenzene. Subsequent irradiation with 530 nm light required 40 minutes to reach PSS, also slightly longer than previously observed. The PSS reached after 530 nm radiation contained 81% of the *cis* isomer. The composition of both PSS was very similar to those attained previously for the AR PROTACs, validating the hypothesis that this photoswitching technology could be applicable to a range of protein targets.

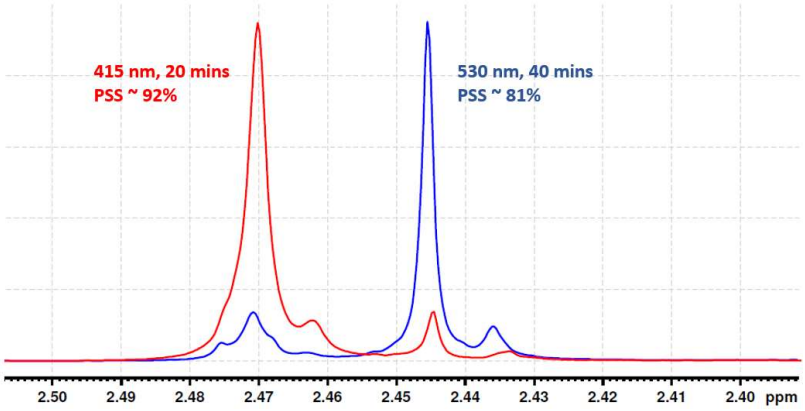

*Scheme 81: ^{1}HNMR used to determine PSS of ER targeting **azoPROTAC4** following irradiation with 415 nm (red trace) and 530 nm (blue trace) light*

Biological evaluation of this PROTAC is currently under investigation with collaborators at AZ.

4.3.13. Photoswitchable PROTACs recruiting E3 ligase cereblon

An additional important avenue to explore to increase the versatility of the photoswitchable PROTAC technology, was alternative E3 ligases which could be hijacked for protein degradation. VHL has been extensively validated in the literature as an effective mediator of protein degradation, however cereblon-recruiting PROTACs have also exhibited great success.[25,319,320] To maximise the possibility of identifying a successful light-induced degrader, it was proposed that both E3 ligases would be investigated. An additional benefit of using cereblon binders over VHL binders is the lower molecular weight and higher lipophilicity of the core thalidomide scaffold, which may lead to more permeable and 'drug-like' PROTACs.

A small toolbox of cereblon binding motifs was proposed to increase the efficiency of PROTAC formation and to enable rapid incorporation into both the AR and ER degrading PROTACs (figure 128). These cereblon binders all incorporated a small linking unit connected to a reactive amine handle to allow facile amide coupling to the azobenzene cores. The linkers were different lengths and rigidities to enable access to a variety of 3D structures, which are important for optimal protein ternary complex formation. The binder-linker pomalidomide conjugates could all be accessed from fluoro-thalidomide **223** through S_NAr reaction with the linker amine nucleophiles.

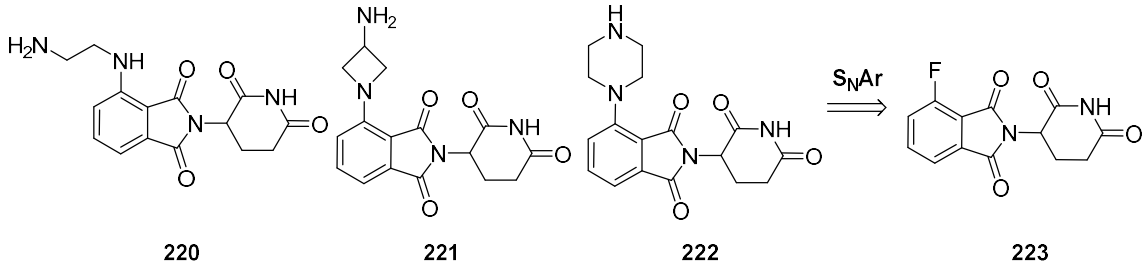

Figure 128: Design of cereblon binding motifs with functional synthetic handles

Synthesis of the cereblon binding ligand was simple (scheme 82). Commercially available 3-fluorophthalic acid **224** was refluxed in acetic anhydride to form anhydride **225**, which was treated with commercially available **226** to construct the thalidomide core of **223** in almost quantitative yield.

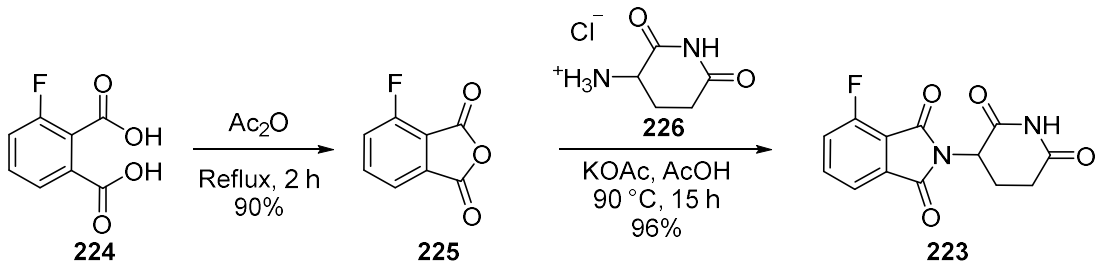

*Scheme 82: Synthesis of fluoro-thalidomide **223** in high yield over two steps*

From this fluoro-thalidomide common intermediate, S_NAr chemistry was used to displace the fluoride and form the desired pomalidomide scaffold. These reactions with the *N*-Boc diamine linkers gave the *N*-Boc products **227**, **228**, and **229** in high yields (scheme 83). Unfortunately, these yellow solids suffered from very poor solubility in all solvents except DMSO and DMF, making them challenging to work with due to the high volumes of solvent required for extractions and purifications.

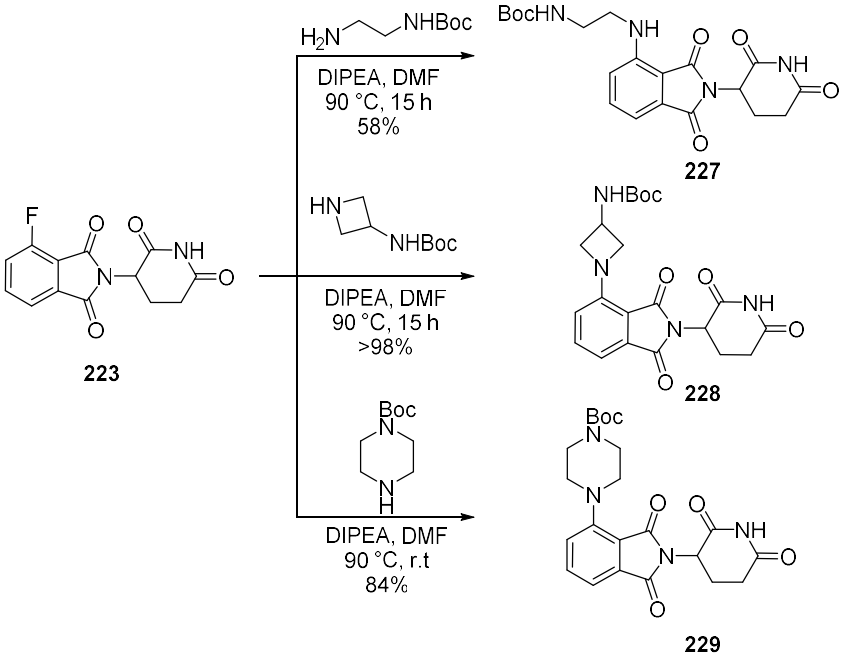

Scheme 83: Synthesis of N-Boc protected pomalidomide-linkers through S_NAr

It was thought that deprotecting the *N*-Boc amines could drastically improve the solubility of these compounds to make them easier to handle. With this in mind, the ethylene-linked amine **227** was deprotected with TFA yielding amine **220** in quantitative yield (scheme 84).

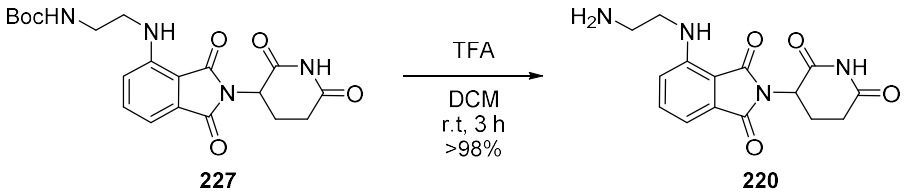

*Scheme 84: N-Boc deprotection of ethylene linked cereblon binder **220***

Unfortunately, the remaining *N*-Boc protected amines were considerably more challenging to deprotect. Following treatment of piperazine derivative **229** with TFA, a complex mixture of products was formed, none of which resembled amine product **222** by LCMS or ^{1}H NMR (scheme 85A). Deprotection of amino-azetidine derivative **228** also resulted in no observed amine product **221**, despite additional deprotection attempts trialling 4 M HCl in addition to TFA (scheme 85B). Although

these deprotections were reported in patent literature, unfortunately they were unsuccessful in yielding the respective amines.

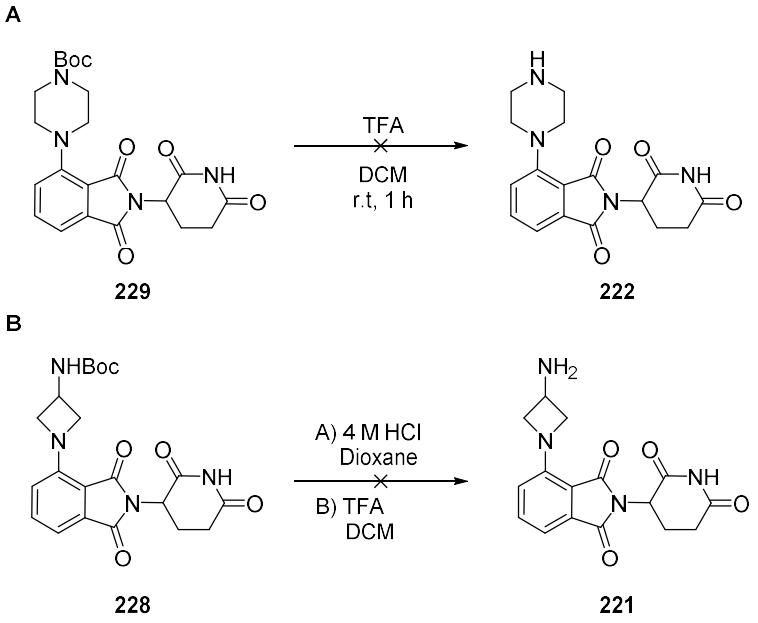

*Scheme 85: Attempts at acid-mediated N-Boc deprotection of pomalidomide units, A: piperazine derivative **229**; B: amino-azetidine derivative **228***

Incorporation of the cereblon recruiting moiety **220** into a photoswitchable PROTAC is currently ongoing (figure 129). The proposed synthetic route for this new azoPROTAC would involve attaching the cereblon binder to the azobenzene core *via* HATU-mediated amide coupling, followed by ester hydrolysis and final amide coupling to attach the enzalutamide binder.

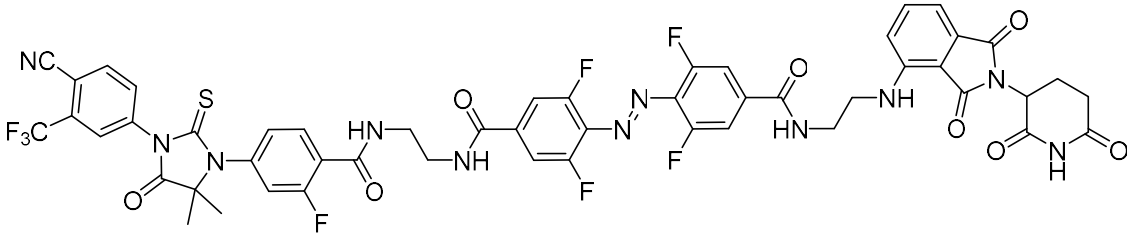

*Figure 129: Proposed structure of **azoPROTAC5** synthesised through amide coupling reactions*

4.4. Chapter 4: Conclusions

Overall, a series of photoswitchable PROTACs were designed and synthesised, primarily recruiting VHL for the degradation of AR. This approach was expected to greatly improve a PROTAC's selectivity by existing as two isomers with differential biological activity which can be interconverted using light. This means that the inactive PROTAC could be dosed and the active conformation generated at the site of action using visible light to reduce toxicity and widen the therapeutic index.

The photoswitchable PROTACs incorporated *ortho*-fluorosubstituted azobenzenes, which were found to switch using visible wavelengths of light with high efficiency. These PROTACs switched from the *cis* conformation to the *trans* with 415 nm light and were highly stable at physiological temperatures. In initial AR degradation assays of **azoPROTAC1**, some AR degradation was observed. Further optimisation of the linkage type and length between the protein binding motifs and the core azobenzene was hypothesised to improve potency and cellular stability.

Additionally, the generality of this technology was investigated through targeting an alternative protein of interest for degradation. In this case, potent ER binder raloxifene was incorporated, aiming to degrade ER, a key target for breast cancer treatment. This PROTAC is currently under biological investigation with collaborators at AZ. In addition, initial efforts were made to incorporate the cereblon binding warhead thalidomide instead of the commonly used VHL binder. Synthesis of this PROTAC is currently on-going.

The recent publication of additional photoswitchable PROTACs (section 4.2) targeting bromodomains with VHL and cereblon has reduced the impact of this research. However, the photoswitch strategy has been validated as a method to achieve light-enabled protein degradation. Despite their therapeutic potential, currently no photoswitchable PROTACs targeting either AR or ER have been reported. Therefore, applying this photoswitch technology to AR and ER degradation would be a useful advance.

4.5. Chapter 4: Future work

Further biological evaluation of this series of photoswitchable PROTACs is required to validate their potency and importantly, the differential activity between the two isomers. Currently, fundamental issues with assay reproducibility have limited the investigation of this PROTAC series, hence assay optimisation is required. In addition, important controls are necessary to validate the proteasomal mediated degradation. Competition experiments with the VHL binder would validate that the mechanism is *via* recruitment of E3 ligase VHL. Additionally, dosing a proteasomal inhibitor will further validate that AR degradation is through the UPS.

In addition, further photoswitch optimisation is required. It was hypothesised that one method of enhancing the differential biological activity of the two isomers would be through modification of the enzalutamide coupling strategy to a direct C-C conjugation (figure 130). This would further increase rigidity, which theoretically would lead to greater conformational differences between the *cis* and *trans* isomers, in addition to forming a highly stable C-C bond. To achieve this conjugation strategy, it was envisioned that a palladium-catalysed cross coupling reaction could combine an aryl-bromide or boronic ester enzalutamide derivative with the aryl bromide azobenzene core. This bi-phenyl enzalutamide motif has been reported in literature hence it is postulated that AR binding would not be affected by this attachment.[74]

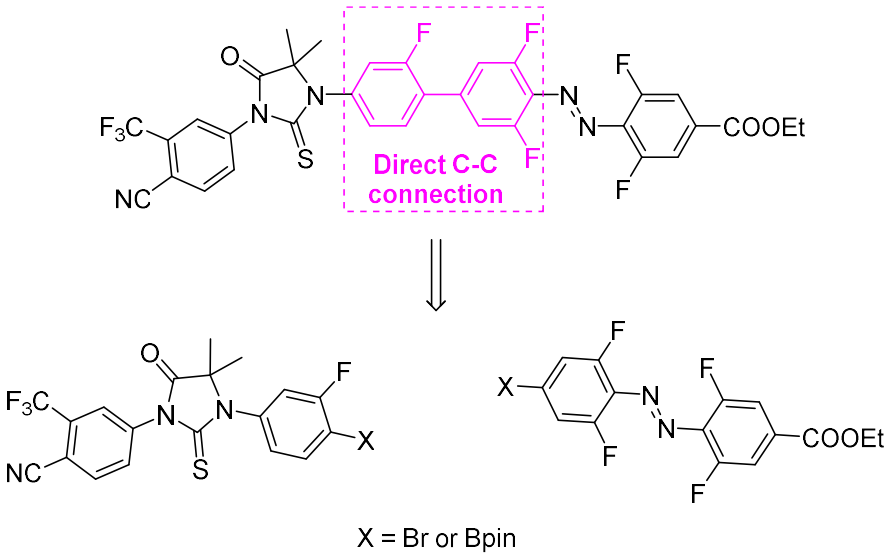

Figure 130: Palladium-catalysed cross coupling strategy to directly conjugate AR binder to photoswitchable linker

The application of photopharmacology to a wider range of diseases is intrinsically limited by the wavelengths of light required to induce a biological effect. Currently, most wavelengths used have very poor tissue penetration, which means that light is unable to reach vital organs without invasive

procedures. Shifting to red or near IR wavelengths would greatly improve tissue penetration, however this is challenging due to its low energy, which is generally unable to induce these chemical changes.

One way to shift photoswitching wavelengths further into the bio-optical window is through two-photon photoswitching. Azobenzene photoswitches can undergo two-photon absorption, however typically the cross-section and absorption intensity are poor. To improve these intrinsic characteristics, the push-pull character of the core must be optimised.[321,322] However, it is challenging to achieve high photostability and complete absorption using these approaches. An alternative method used to enhance near-IR absorption properties is the incorporation of a light-harvesting antenna into the photoswitch. This antenna then absorbs near-IR photons and switching occurs *via* resonant electronic energy transfer to the azobenzene core. This approach was applied to a light-gated glutamate receptor ion channel with photoswitch $MAGA_{2p}$ (figure 131).[323,324] This photoswitch was found to control the opening of the ion channel in response to near-IR light. The light sources required for these processes are typically specialised and high energy due to this slow and inefficient process, which limits their usage. In addition, incorporation of an antenna may hinder the biological activity of the photoswitch due to its large size and high lipophilicity, which promotes non-specific binding. These techniques could be applied to the photoswitchable PROTACs to enable their switching through two-photon absorption. Extensive core optimisation would be required, which may affect the biological activity. Attachment of an antenna would promote this process without requiring extensive optimisation, however it also may hinder ternary complex formation and prevent efficient protein degradation. One possibility of bypassing this problem would be to incorporate a protein binding ligand with good absorption properties, which may act as an antenna in addition to protein binding. However, assessing the absorption properties of common drug structures is not trivial and requires bespoke set-ups and high energy light sources.

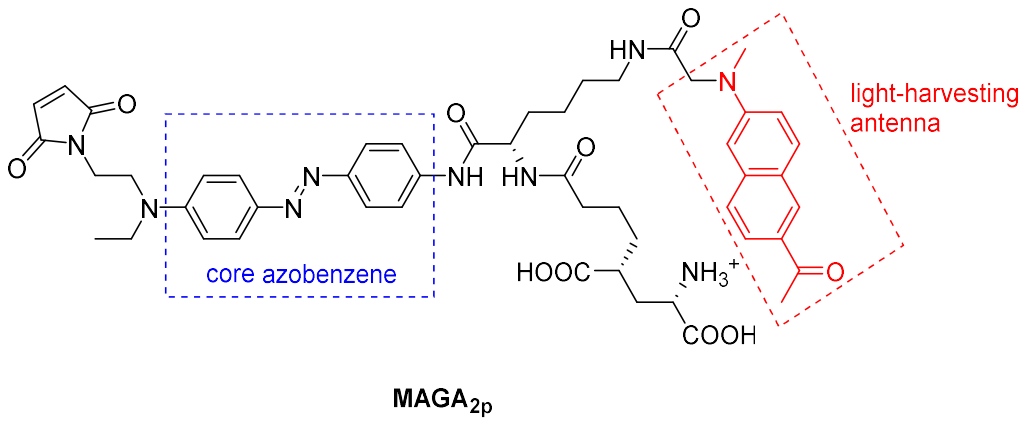

Figure 131: Structure of two-photon photoswitch targeting the glutamate receptor ion channel[323]

Alternatively, novel photoswitching scaffolds are in continuous development, many of which use alternative frameworks to lower the energy of the light required for switching. A recently published example of a substituted azobenzene that undergoes substantially red-shifted switching is DOM-azo (figure 132).[325] Wavelengths in the near-IR range (~ 720 nm) were demonstrated to switch this core, however, constant light pulsing was required to maintain the switch due to the poor thermal half-life in the order of seconds. Interestingly, this low stability could be desirable for long-term clinical applications as inactivation of the drug outside of the site of action is vital for reducing off-target toxicity.

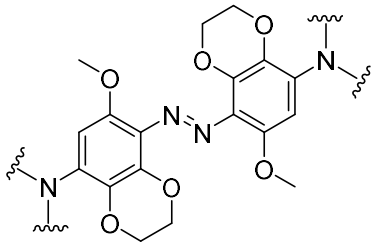

DOM-azo Photoswitch

Figure 132: Novel substituted azobenzene with near-IR absorption[325]

The hemiindigo photoswitches described in section 4.3.1. would also be a useful alternative to the azobenzene series, however conditions to promote the challenging *N*-alkylation must be identified. Incorporating these photoswitches into PROTACs would also require extensive optimisation of the conjugation methods and linker lengths, however the benefit of the more clinically relevant bio-optical window would be substantial.

A final approach to achieve red-shifted switching wavelengths is through up-conversion methods. This method has gained considerable traction over the past decade for a multitude of purposes, including therapeutics, imaging and photovoltaic applications.[326] Up-conversion is a nonlinear optical process where multiple low energy photons are absorbed and converted into a single higher energy photon which is emitted. This can be used to produce the high energy photons required to induce switching within a cellular environment, bypassing the penetration limitations of high energy light. For this process to occur, a sensitizer is needed to absorb the low energy photon and transfer this energy to an annihilator. This annihilator combines with another annihilator to yield a higher energy excited state annihilator, which can emit a high energy photon.[326]

Upconversion nanoparticles are commonly used for this purpose through doping of lanthanide ions, which can be varied in composition and size to achieve the required absorption and emission characteristics.[327] These types of nanoparticles have previously been applied to the two-way

photoswitching of azobenzene,[328] dithienylethene[329] and spiropyran[330] switches. In addition, toxicity studies have shown no obvious toxicity both *in vitro* and *in vivo*.[331] Despite many advancements in this field, the brightness and emission efficiencies of these nanoparticles must be improved for better clinical applications.[327] Once again, limitations of these materials also include the requirement of expensive custom light sources, poorly explored pharmacokinetic properties and the potential for water heating at particularly high wavelengths, which may be damaging to cells.[332]

Small molecule sensitizers and annihilators may also be used to achieve tuneable emission from low energy photons.[326] However, these approaches commonly require biologically incompatible conditions such as non-polar solvents and oxygen free conditions, limiting their use. Recent advances have been made to overcome these limitations through encapsulation of the sensitizer and annihilator in micelles.[333]

Upconversion methods may be combined with photoswitchable PROTACs to achieve red-shifted switching. Importantly, the wavelengths of the absorption and emission must be carefully chosen to optimise photoconversion.

Overall, there are many methods which could be used to improve the long-term applications of photoswitchable PROTACs, primarily by optimising the light wavelengths required and penetration levels, ultimately leading to more clinically viable photopharmacology applications.

5. Experimental details

5.1. General experimental procedures

All reagents were obtained from commercial sources with no further purification. Solvents were freshly distilled unless specified. THF was dried over sodium wire and distilled from calcium hydride and lithium aluminium hydride with indicator triphenylmethane. Diethyl ether was distilled from calcium hydride and lithium aluminium hydride. Acetonitrile, dichloromethane, hexane, MeOH, and toluene were all distilled from calcium hydride. Petroleum ether (PE 40–60) refers to the petroleum fraction with boiling point of 40–60 °C. Reactions were under a dry nitrogen atmosphere unless stated.

Yields refer to chromatographically and spectroscopically pure compounds. Flash column chromatography was carried out on silica gel (Merck Kieselgel 60 F254, 230-400 mesh) with distilled solvents under a positive pressure of nitrogen. Thin layer chromatography used silica-coated glass plates (Merck Kieselgel 60, F254), the plates were observed using potassium permanganate dip, or UV fluorescence (254 nm).

Melting points were measured using a Buchi B-545 melting point apparatus and are uncorrected. The term “did not melt” refers to gradual decomposition over temperature ramp up to 300 °C.

Infrared (IR) spectroscopy was recorded neat on a Perkin Elmer Spectrum One FT-IR Spectrometer fitted with an attenuated total reflectance (ATR) sampling accessory; maximum absorptions are quoted to the nearest 1 cm^{-1}, and classified using the following abbreviations: w, weak; m, medium; s, strong; br, broad; and combinations thereof.

Proton (^{1}H), carbon (^{13}C), and fluorine (^{19}F) nuclear magnetic resonance (NMR) spectra were recorded using Bruker Ultrashield 400 or 500 spectrometers. Assignments were supported by COSY, DEPT-135, HSQC, and HMBC spectra. Proton chemical shifts (δ) were measured in parts per million (ppm) relative to tetramethylsilane (δ =0 ppm), referenced to the appropriate solvent peak, and are quoted to the nearest 0.01 ppm, with coupling constants (*J*) reported to the nearest 0.1 Hz. Carbon chemical shifts (δ) were also measured in parts per million (ppm) relative to tetramethylsilane (δ =0), referenced to the appropriate solvent peak, and are quoted to the nearest 0.1 ppm with coupling constants quoted to 3 significant figures. Multiplicity is indicated using the following abbreviations: br, broad; s, singlet; d, doublet; t, triplet; q, quartet; quin, quintet; m, multiplet; and combinations thereof. The term ‘C_Q’ refers to a quaternary carbon.

High resolution mass spectrometry (HRMS) was carried out using a Waters LCT Premier Time of Flight mass spectrometer, Micromass Quadrupole Time of Flight mass spectrometer or Waters Vion IMS Qtof mass spectrometer.

LCMS chromatographs were recorded on an Agilent 1200 series LC with an ESCi Multi-Mode ionisation Waters ZQ spectrometer. The following conditions were used: solvent A: 10 mM ammonium acetate + 0.1% formic acid in water; solvent B: 95% acetonitrile + 5% H_2O + 0.05% formic acid; linear gradient: 0.0-0.7 mins: 0% B, 0.7-4.2 mins: 0-100% B, 4.2-7.7 mins: 100% B, 7.7-8.5 mins: 100-0% B; using a Supelcosil ABZ+PLUS column (33 mm × 4.6 mm,3 µm).

High-performance liquid chromatography (HPLC) analytical chromatographs were recorded on an Agilent 1260 Infinity using a Supelcosil ABZ+PLUS column (150 mm x 4.6 mm, 3 µm) eluting with a linear gradient system (solvent A: 0.05% (v/v) TFA in water, solvent B: 0.05% (v/v) TFA in acetonitrile) over 15 min at a flow rate of 1 mL/min. UV absorbance at 220 and 254 nm was recorded.

Semi-preparative HPLC was carried out on an Agilent 1260 Infinity using a Supelcosil ABZ+PLUS column (250 mm x 21.2 mm, 5 µm) eluting with a linear gradient system (solvent A: 0.1% (v/v) TFA in water, solvent B: 0.05% (v/v) TFA in acetonitrile) over 20 min at a flow rate of 20 mL/min.

UV-vis spectroscopy was carried out using a Perkin-Elmer Lambda 950 spectrophotometer, using a quartz cuvette with path length of 1 mm.

Initial photoswitching studies of **azoPROTAC1** were carried out using a 405 nm and 520 nm wavelength continuous wave lasers. All subsequent photoswitching was carried out using mounted LEDs at 415 nm and 530 nm wavelengths purchased from Thorlabs.

5.2. General Synthetic procedures

Manual Fmoc SPPS

Peptide sequence **P1** was prepared through SPPS on Wang resin (0.37 mmol/g) and *N*-terminal capped with acetic anhydride. The couplings were carried out using Fmoc-protected amino acids (4 eq) pre-activated with HATU (4 eq), and *N,N*-diisopropylethylamine (8 eq) in DMF for 10 min, and coupled for 1 h. The coupling of unnatural ornithine residue involved shaking for an additional 1 h to ensure complete coupling. The side-chain protecting groups used were: *t*-Bu for glutamic acid, serine, and threonine; Boc for tryptophan; and Trt for glutamine.

The coupling progression was monitored by acetaldehyde/chloranil test. A small amount of resin swelled in dichloromethane was taken and acetaldehyde (200 µL) was added followed by a saturated solution of chloranil in toluene (50 µL). After shaking at r.t. for *ca*. 5 mins no resin colour change signified complete coupling, whereas green colouration indicated incomplete coupling.

Fmoc deprotections were performed by shaking for *ca.* 10 mins with a solution of 20% piperidine in DMF. *N*-terminal capping was achieved by adding acetic anhydride (5 eq), and *N,N*-diisopropylethylamine (10 eq) to the resin in DMF and shaking for 3 h.

Peptide cleavage from the resin and side-chain deprotection were carried out by treatment with TFA/H_2O/dichloromethane/TIPS 92.5:2.5:2.5:2.5 over 3 h. Solvent was then removed under a stream of nitrogen, and the resulting residue triturated with diethyl ether (4 x 5 mL) and purified by semi-preparative HPLC.

Automated SPPS:

Peptide sequence **P2** was prepared through automated SPPS on Wang resin (0.37 mmol/g) using a CEM Liberty Automated Microwave Peptide Synthesiser. Peptide couplings used Fmoc-protected amino acids (5 eq) dissolved in DMF, HATU (5 eq) in DMF, and *N,N*-diisopropylethylamine (10 eq) in NMP. Amino acids were coupled with 25 W power at 75 °C for 15 min. Fmoc deprotection was carried out with 20% piperidine in DMF over 3 mins, using 45 W power at 75 °C.

The final deprotection, *N*-terminal acetyl capping and resin cleavage were all performed manually as previously stated.

General copper-catalysed double-click stapling:

Copper(II) sulfate pentahydrate (1 eq) and tris(3-hydroxypropyltriazolylmethyl)amine (1 eq) were dissolved in degassed water and stirred for 10 mins before sodium ascorbate (3 eq) was added. The solution was then added to the diazido-peptide (1 eq; 1 mL/mg) and dialkynyl linker (1.1 eq) which were dissolved in degassed *t*-butanol/water (1:1) at rt under nitrogen. The reaction mixture was stirred for 1 h, monitored by LC-MS analysis of the reaction mixture, and upon completion, dried under a stream of nitrogen. Purification by semi-preparative HPLC gave **PROTACs 1**-**6**.

5.3. Synthetic Characterisation

5.3.1. Peptide analysis

Peptide	Mass	m/z found	m/z calculated	Species
P1	1577.8	1579.1	1578.7	$[M+H]^+$
P2	1450.7	1451.3	1451.7	$[M+H]^+$
PROTAC-1	2444.6	1223.6	1223.3	$[M+2H]^{2+}$
PROTAC-2	2315.6	1159.5	1158.8	$[M+2H]^{2+}$
PROTAC-3	2312.4	1157.5	1157.2	$[M+2H]^{2+}$
PROTAC-4	2280.0	2281.3	2281.0	$[M+H]^+$
PROTAC-5	2393.0	2394.7	2394.1	$[M+H]^+$
PROTAC-6	2247.7	1125.3	1124.9	$[M+2H]^{2+}$

5.3.2. Synthetic protocols

4-Isothiocyanato-2-(trifluoromethyl)benzonitrile (5)

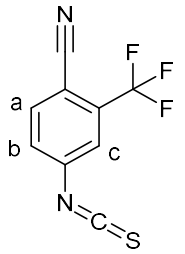

To a stirring solution of 4-amino-2-(trifluoromethyl)benzonitrile (0.60 g, 3.2 mmol) in DCM (12 mL) was added thiocarbonyldiimidazole (0.86 g, 4.8 mmol). After stirring for 7 h at r.t., H_2O (15 mL) was added, and the product extracted into dichloromethane (3 x 15 mL). The organic phase was washed with brine (15 mL), dried over $MgSO_4$, filtered, and concentrated *in vacuo*. The residue was purified through silica gel column chromatography (9:1, PE 40-60:EtOAc) to give the title compound as a white amorphous solid (0.546 g, 74%).

R_f: 0.18 (9:1, PE 40-60:EtOAc); **IR** (neat film, ν_{max}, cm^{-1}): 2075 (s, C≡N), 2039 (s br, NCS), 1608 (s), 1567 (w, C=C), 1496 (w, C=C), 1430 (m, C=C), 1321 (s), 1179 (s), 1140 (s), 1051 (m), 970 (w), 895 (m), 840 (m), 677 (w); **^{1}H NMR** (400 MHz, $CDCl_3$) δ: 7.84 (d, *J* = 8.3 Hz, 1H, Ha), 7.59 (d, *J* = 1.8 Hz, 1H, Hc), 7.48 (dd, *J* = 8.3, 1.8 Hz, 1H, Hb); **^{13}C NMR** (101 MHz, $CDCl_3$) δ: 142.1 (-N**C**S), 136.9 (-**C**-CN), 136.2 (Ca), 134.8

(q, *J* = 34 Hz, -**C**-CF_3), 129.0 (Cb), 124.1 (q, *J* = 4.7 Hz, Cc), 121.6 (q, *J* = 280 Hz, -CF_3), 114.7 (-C≡N), 107.9 (q, *J* = 2 Hz, -**C**-NCS); **^{19}F NMR** (376 MHz, $CDCl_3$) δ: -63.3 (CF_3).

Data are in accordance with those reported previously in literature.[334]

4-((2-carboxypropan-2-yl)amino)-2-fluorobenzoic acid (11)

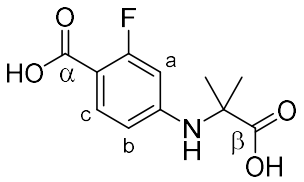

To a stirring solution of 4-bromo-2-fluorobenzoic acid (2.00 g, 9.1 mmol) in DMF (20 mL) were added 2-aminoisobutyric acid (1.13 g, 11.0 mmol), copper (I) iodide (0.26 g, 1.37 mmol), potassium carbonate (5.03 g, 36.4 mmol), 2-acetylcycohexanone (0.24 mL, 1.82 mmol), and water (6 mL). The mixture was heated to 90 °C for 24 h before concentrating *in vacuo* and washing with EtOAc (2 x 20 mL). The aqueous was acidified with citric acid to pH 3, before being extracted into EtOAc (3 x 20 mL), washed with brine (15 mL), dried over $MgSO_4$, filtered, and concentrated *in vacuo*. The residue was purified through silica gel column chromatography (1:1 PE 40-60:EtOAc to EtOAc) to give the title compound as a white amorphous solid (1.02 g, 46%).

R_f: 0.17 (EtOAc); **IR** (neat film, ν_{max}, cm^{-1}): 3440 (w, N-H), 3000 (w br, O-H), 1701 (m, C=O), 1670 (s, C=O), 1615 (s), 1582 (m, C=C), 1527 (m, C=C), 1415 (m, C=C), 1363 (m), 1311 (s), 1270 (s), 1252 (s), 1169 (s), 1098 (m), 925 (m), 827 (s), 770 (m), 761 (m), 685 (w); **^{1}H NMR** (400 MHz, DMSO-d6) δ: 12.51 (br s, 2H, 2 x COOH), 7.59 (t, *J* = 8.8 Hz, 1H, Hc), 6.94 (br s, 1H, N-H), 6.33 (dd, *J* = 2.1, 8.8 Hz, 1H, Hb), 6.15 (d, *J* = 2.1, 14.5 Hz, 1H, Ha), 1.45 (s, 6H, 2 x CH_3); **^{13}C NMR** (101 MHz, DMSO-d6) δ: 176.8 (βC=O), 165.4 (d, *J* = 3.5 Hz, αC=O), 163.5 (d, *J* = 250 Hz, C-F), 152.8 (d, *J* = 12 Hz, -**C**-COOH), 134.4 (d, *J* = 3.1 Hz, Cc), 109.5 (Cb), 105.4 (d, *J* = 9.5 Hz, Ar-**C**-NH), 99.7 (d, *J* = 27 Hz, Ca), 56.7 (**C**-$(CH_3)_3$), 26.0 (2 x CH_3); **^{19}F NMR** (376 MHz, $CDCl_3$) δ: -108.3 (C-F); **HRMS**: *m/z* $[M+H]^+$ calculated for $C_{11}H_{13}FNO_4$: 242.0823; Found: 242.0819.

Methyl-2-fluoro-4-((1-methoxy-2-methyl-1-oxopropan-2-yl)amino)benzoate (4)

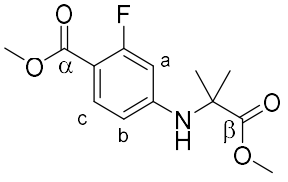

To a stirring solution of **11** (0.15 g, 0.62 mmol) in MeOH (2 mL) was added thionyl chloride (0.11 mL, 1.6 mmol). The solution was heated to reflux and stirred for 16 h, before being concentrated *in vacuo*. The residue was dissolved in water (5 mL) and EtOAc (5 mL) before sodium hydrogen carbonate (0.08 g) was added, and the organic layer separated, and concentrated *in vacuo*. The residue was purified through silica gel column chromatography (9:1 to 3:2 PE 40-60:EtOAc) to give the title compound as a white amorphous solid (0.11 g, 67%).

R_f: 0.52 (3:2 PE 40-60:EtOAc); **IR** (neat film, ν_{max}, cm^{-1}): 3381 (w, N-H), 2993 (w), 2952 (w), 1703 (m br, overlapped C=O), 1617 (s), 1523 (m, C=C), 1434 (m), 1273 (s), 1190 (m), 1140 (s), 1091 (m), 967 (w), 835 (w), 769 (m), 692 (w); **^{1}H NMR** (400 MHz, $CDCl_3$) δ: 7.72 (t, *J* = 8.6 Hz, 1H, Hc), 6.27 (dd, *J* = 8.8, 2.4 Hz, 1H, Hb), 6.16 (dd, *J* = 13.7, 2.3 Hz, 1H, Ha), 4.72 (br s, 1H, -NH), 3.84 (s, 3H, αCOO-CH_3), 3.72 (s, 3H, βCOO-CH_3), 1.58 (s, 6H, 2 x -CH_3); **^{13}C NMR** (101 MHz, $CDCl_3$) δ: 175.5 (βC=O), 165.0 (d, *J* = 1.4 Hz, αC=O), 163.7 (d, *J* = 260 Hz, C-F), 151.2 (d, *J* = 12 Hz, -**C**-αC), 133.4 (d, *J* = 2.9 Hz, Cc), 109.6 (d, *J* = 2.2 Hz, Cb), 106.9 (d, *J* = 10 Hz, Ar-**C**-NH-), 100.7 (d, *J* = 27 Hz, Ca), 57.3 (-**C**-$(CH_3)_3$), 52.8 (βCOO-**C**H_3), 51.7 (αCOO-**C**H_3), 25.9 (2 x CH_3); **^{19}F NMR** (376 MHz, $CDCl_3$) δ: -109.4 (C-F); **HRMS**: *m/z* $[M+H]^+$ calculated for $C_{13}H_{17}FNO_4$: 270.1136; Found: 270.1141.

4-Amino-2-fluorobenzamide (13)

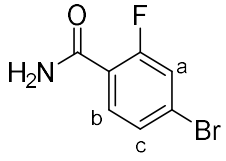

To a stirring solution of 4-bromo-2-fluorobenzoic acid (1.50 g, 6.7 mmol) in dichloromethane (25 mL) cooled to 0 °C was added oxalyl chloride (2.3 mL, 26.8 mmol). DMF (2 mL) was carefully added, and the mixture was stirred at r.t. for 3 h. The mixture was then concentrated *in vacuo*, dissolved in THF (25 mL), and cooled to 0 °C, before ammonia (2.3 mL, aq.) was slowly added. After stirring for 30 mins, the mixture was concentrated *in vacuo*, and azeotropic distillation with toluene gave the title compound as a white amorphous solid (1.03 g, 70%).

R_f: 0.68 (EtOAc); **IR** (neat film, ν_{max}, cm^{-1}): 3347 (m, N-H), 3176 (m, N-H), 1653 (s, C=O), 1625 (s, C=C), 1599 (s, C=C), 1565 (m, C=C), 1485 (m, C=C), 1390 (s), 1383 (s), 1213 (s), 1065 (m), 879 (s), 860 (s), 832 (m), 763 (m), 677 (w); **^{1}H NMR** (400 MHz, $CDCl_3$) δ: 8.04 (t, *J* = 8.5 Hz, 1H, Hb), 7.45 (dd, *J* = 8.5, 1.7 Hz, 1H, Hc), 7.37 (dd, *J* = 11.2, 1.7 Hz, 1H, Ha), 6.64 (br s, 1H, amide NH), 6.28 (br s, 1H, amide NH); **^{13}C NMR** (101 MHz, $CDCl_3$) δ: 164.0 (d, *J* = 2.9 Hz, C=O), 160.5 (d, *J* = 250 Hz, C-F), 133.5 (d, *J* = 2.6 Hz, Cb),

128.4 (d, *J* = 3.3 Hz, Cc), 127.2 (d, *J* = 10 Hz, -C-NH_2), 119.7 (d, *J* = 28 Hz, Ca), 119.2 (d, *J* = 12 Hz, -**C**-CON-); **^{19}F NMR** (376 MHz, $CDCl_3$) δ: -111.5 (C-F).

Data are in accordance with those reported previously in literature.[153]

Methyl-2-((4-carbamoyl-3-fluorophenyl)amino)-2-methylpropanoate (15)

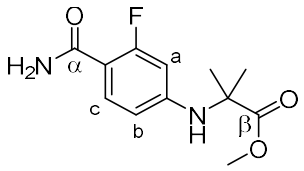

To a stirring solution of **13** (50 mg, 0.23 mmol) in DMF (1 mL) were added 2-aminoisobutyric acid (28 mg, 0.28 mmol), copper (I) iodide (7 mg, 0.04 mmol), potassium carbonate (0.127 g, 0.92 mmol), 2-acetylcycohexanone (6 µL, 0.05 mmol), and water (150 µL). The mixture was heated to 90 °C for 24 h, before concentrating *in vacuo* and washing with EtOAc (2 x 3 mL). The aqueous was acidified with citric acid to pH 3, before being extracted into EtOAc (3 x 3 mL), washed with brine (1 x 3 mL), dried over $MgSO_4$, filtered, and concentrated *in vacuo*. This residue was directly methylated by dissolving in DMF (1 mL) before the addition of potassium carbonate (48 mg, 0.35 mmol), and iodomethane (22 µL, 0.35 mmol). The solution was stirred at 45 °C for 2 h before an additional portion of iodomethane was added (22 µL, 0.35 mmol). The solution was stirred for a further 6 h, before being concentrated *in vacuo*. The residue was purified through silica gel column chromatography (1:1 to 4:1 EtOAc:PE 40-60) to give the title compound as a colourless oil (49 mg, 84% over two steps).

R_f: 0.33 (4:1 EtOAc:PE 40-60); **IR** (neat film, ν_{max}, cm^{-1}): 3507 (w, NH), 3332 (w, NH), 2291 (w), 1729 (m, C=O), 1649 (m, C=O), 1621 (s), 1597 (s, C=C), 1527 (m, C=C), 1431 (m, C=C), 1381 (m), 1219 (m), 1146 (s), 1094 (m), 833 (w), 771 (w); **^{1}H NMR** (400 MHz, $CDCl_3$) δ: 7.88 (t, *J* = 8.8 Hz, 1H, Hc), 6.50 (br s, 1H, NH), 6.36 (dd, *J* = 8.8, 2.3 Hz, 1H, Hb), 6.16 (dd, *J* = 2.3, 15.0 Hz, 1H, Ha), 5.78 (br s, 1H, NH), 4.72 (br s, 1H, NH), 3.72 (s, 3H, -O-CH_3), 1.59 (s, 6H, 2 x CH_3); **^{13}C NMR** (101 MHz, $CDCl_3$) δ: 175.6 (-β**C**=O), 165.2 (d, *J* = 3.4 Hz, αC=O) 162.4 (d, *J* = 250 Hz, C-F), 150.7 (d, *J* = 13 Hz, -**C**-αCO), 133.2 (d, *J* = 4.0 Hz, Cc), 110.6 (Cb), 108.7 (d, *J* = 12 Hz, Ar-**C**-N-), 99.7 (d, *J* = 30 Hz, Ca), 57.3 (-**C**-$(CH_3)_2$), 52.8 (O-CH_3), 25.9 (2 x CH_3); **^{19}F NMR** (376 MHz, $CDCl_3$) δ: -111.8 (C-F).

Data are in accordance with those reported previously in literature.[153]

4-(3-(4-Cyano-3-(trifluoromethyl)phenyl)-5,5-dimethyl-4-oxo-2-thioxoimidazolidin-1-yl)-2-fluorobenzamide (16)

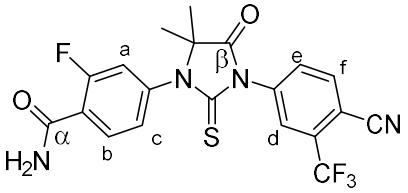

To a stirring solution of **15** (0.076 g, 0.3 mmol) in DMF (0.5 mL) was added **5** (0.13 g, 0.6 mmol). The mixture was stirred at 90 °C for 4 h before being cooled, diluted with H_2O (5 mL) and extracted into EtOAc (3 x 5 mL). The combined organic was washed with brine (10 mL), dried over $MgSO_4$, filtered, and concentrated *in vacuo*. The residue was purified through silica gel column chromatography (3:7 Acetone:Hexane) to give the title compound as a yellow oil (0.085 g, 63%).

R_f: 0.29 (50% Acetone:Hexane); **IR** (neat film, ν_{max}, cm^{-1}): 3344 (w, NH), 2922 (w), 2851 (w), 1755 (m, C=O), 1672 (m, C=O), 1619 (m), 1501 (m, C=C), 1415 (s, C=C), 1309 (s), 1216 (s), 1176 (s), 1135 (s), 1056 (m), 922 (w), 815 (m), 735 (m), 677 (w); **^{1}H NMR** (400 MHz, $CDCl_3$) δ: 8.29 (t, *J* = 8.4 Hz, 1H, Hb), 7.98 (d, *J* = 8.3 Hz, 1H, Hf), 7.95 (s, 1H, Hd), 7.82 (dd, *J* = 1.9, 8.3 Hz, 1H, He), 7.28 – 7.25 (m, 1H, Hc), 7.18 (dd, *J* = 1.8, 11.6 Hz, 1H, Ha), 6.67 (br d, *J* = 9.7 Hz, 1H, NH), 6.30 (br s, 1H, NH), 1.62 (s, 6H, 2 x CH_3); **^{13}C NMR** (101 MHz, $CDCl_3$) δ: 179.8 (C=S), 174.4 (βC=O), 165.3 (d, *J* = 2.9 Hz, αC=O), 160.7 (d, *J* = 250 Hz, Ar-C-F), 139.7 (d, *J* = 11 Hz, Ar**C**-$CONH_2$), 136.8 (-**C**-CN), 135.3 (Cf), 133.7 (q, *J* = 34 Hz, C-CF_3), 133.7 (d, *J* = 34 Hz, Cb), 132.2 (Ce), 127.1 (q, *J* = 4.8 Hz, Cd), 126.2 (d, *J* = 3.4 Hz, Cc), 121.8 (q, *J* = 280 Hz, -CF_3), 121.7 (d, *J* = 12 Hz, -**C**-N-$(CH_3)_2$-), 118.1 (d, *J* = 27 Hz, Ca), 114.7 (-**C**≡N), 110.4 (q, *J* = 2.0 Hz, -**C**-NCO-), 66.7 (-C-$(CH_3)_3$), 23.9 (2 x -CH_3); **^{19}F NMR** (376 MHz, $CDCl_3$) δ: -63.0 (CF_3), -111.8 (ArC-F).

Data are in accordance with those reported previously in literature.[153]

4-(3-(4-Cyano-3-(trifluoromethyl)phenyl)-5,5-dimethyl-4-oxo-2-thioxoimidazolidin-1-yl)-2-fluorobenzoic acid (2)

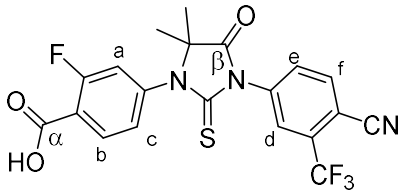

16 (50 mg, 0.11 mmol) was dissolved in conc. HCl (0.5 mL) and heated to 120 °C in a sealed tube for 48 h. After cooling to r.t., the residue was dissolved in EtOAc (2 mL) and the organic was separated and concentrated *in vacuo*. The residue was purified through silica gel column chromatography

(dichloromethane to 1:19 MeOH:dichloromethane) to give the title compound as a yellow oil (40 mg, 80%).

R_f: 0.11 (3:47 MeOH/dichloromethane); **IR** (neat film, ν_{max}, cm^{-1}): ~3000 (w br, OH), 2925 (w), 1758 (m, C=O), 1718 (m, C=O), 1618 (m), 1502 (m, C=C), 1414 (s, C=C), 1311 (s), 1222 (s), 1179 (s), 1135 (s), 1054 (m), 842 (w); **^{1}H NMR** (400 MHz, $CDCl_3$) δ: 8.20 (t, *J* = 8.0 Hz, 1H, Hb), 8.00 (d, *J* = 8.4 Hz, 1H, Hf), 7.95 (s, 1H, Hd), 7.82 (d, *J* = 8.4 Hz, 1H, He), 7.24 (d, *J* = 8.0 Hz, 1H, Hc), 7.19 (d, *J* = 11.1 Hz, 1H, Ha), 1.63 (s, 6H, 2 x CH_3); **^{13}C NMR** (101 MHz, $CDCl_3$) δ: 179.7 (C=S), 174.4 (βC=O), 167.8 (αC=O), 162.7 (d, *J* = 270 Hz, C-F), 141.3 (**C**-αCO), 136.8 (-**C**-CN), 135.4 (Cf), 133.9 (d, *J* = 6.2 Hz, Cb), 133.8 (q, *J* = 33 Hz, -**C**-CF_3) 132.1 (Ce), 127.1 (q, *J* = 4.5 Hz, Cd), 125.7 (Cc), 120.5 (-**C**-N-$(CH_3)_2$-), 119.1 (d, *J* = 24 Hz, Ca), 114.7 (-**C**≡N), 110.5 (-**C**-NCO-), 66.7 (-C-$(CH_3)_3$), 23.9 (2 x CH_3); **^{19}F NMR** (376 MHz, $CDCl_3$) δ: -63.0 (CF_3), -105.8 (ArC-F).

Data are in accordance with those reported previously in literature.[153]

Ethyl-3,5-dibromobenzoate (18)

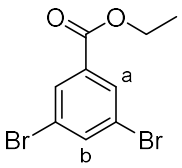

To a stirring solution of 3,5-dibromobenzoic acid (3.00 g, 10.7 mmol) in ethanol (30 mL) was added conc. sulfuric acid (0.57 mL, 10.7 mmol). The solution was heated to reflux and stirred for 20 h. The mixture was cooled and *ca*. half the solvent was removed *in vacuo* before being poured into iced water. The precipitate was filtered and washed with ethanol (2 x 5 mL), before drying *in vacuo* to give the title compound as an orange amorphous solid (3.24 g, 98%).

m.p.: 55 – 57 °C (ethanol, lit. 54 – 56 °C[335]); **R_f**: 0.59 (1:1 PE 40-60:EtOAc); **IR** (neat film, ν_{max}, cm^{-1}): 3084 (w), 2983 (w), 1725 (s, C=O), 1557 (m, C=C), 1425 (m, C=C), 1414 (m, C=C), 1364 (m), 1268 (s), 1140 (m), 1100 (m), 1020 (m), 871 (m), 762 (s), 746 (m), 658 (w); **^{1}H NMR** (400 MHz, $CDCl_3$) δ: 8.10 (d, *J* = 1.8 Hz, 2H, Ha), 7.84 (t, *J* = 1.8 Hz, 1H, Hb), 4.39 (q, *J* = 7.1 Hz, 2H, -CH_2), 1.40 (t, *J* = 7.1 Hz, 3H, -CH_3); **^{13}C NMR** (101 MHz, $CDCl_3$) δ: 164.0 (C=O), 138.1 (Cb), 133.7 (C-COO), 131.3 (Ca), 123.0 (C-Br), 61.9 (CH_2), 14.2 (CH_3).

Data are in accordance with those reported previously in literature.[157]

Ethyl 3,5-bis(3-hydroxy-3-methylbut-1-yn-1-yl)benzoate (19)

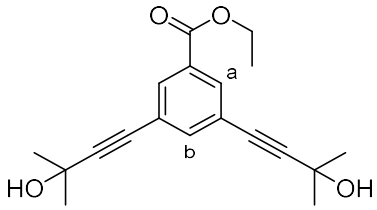

To a stirring solution of **18** (2.00 g, 6.5 mmol) in THF (20 mL) were added 2-methyl-3-butyn-2-ol (1.89 mL, 19.5 mmol) and triethylamine (3.6 mL, 26 mmol). The solution was stirred at r.t. for 30 mins before copper (I) iodide (0.124 g, 0.65 mmol) and bis(triphenylphosphine)palladium(II) dichloride (0.228 g, 0.33 mmol) were added. The mixture was heated to reflux and stirred for a further 24 h, before being cooled and concentrated *in vacuo*. The residue was purified through silica gel column chromatography (9:1 to 4:1, PE 40-60:EtOAc) to give the title compound as a yellow amorphous solid (1.85 g, 90%).

R_f: 0.45 (1:1 PE 40-60:EtOAc); **IR** (neat film, ν_{max}, cm^{-1}): 3362 (w br, OH), 2980 (m), 1723 (m, C=O), 1705 (m), 1593 (w, C=C), 1437 (m, C=C), 1369 (m), 1332 (s), 1242 (s), 1192 (s), 1111 (s), 1024 (m), 945 (s), 895 (m), 858 (w), 768 (m), 734 (w), 678 (w); **^{1}H NMR** (400 MHz, $CDCl_3$) δ: 7.98 (d, *J* = 1.5 Hz, 2H, Ha), 7.61 (d, *J* = 1.5 Hz, 1H, Hb), 4.37 (q, *J* = 7.1 Hz, 2H, -O-CH_2), 2.18 – 2.14 (br d, 2H, OH), 1.61 (s, 12H, 4 x CH_3), 1.39 (t, *J* = 7.1 Hz, 3H, CH_2-C**H**$_3$); **^{13}C NMR** (101 MHz, $CDCl_3$) δ: 165.3 (C=O), 138.4 (Cb), 132.2 (Ca), 130.9 (-**C**-COO-), 123.5 (Ar**C**-C≡C-), 95.3 (ArC-C≡**C**-), 80.5 (ArC-**C**≡C-), 65.6 (C-OH), 61.5 (-CH_2-), 31.4 (4 x -CH_3), 14.3 (-CH_2-**C**H_3).

Data are in accordance with those reported previously in literature.[157]

3,5-Diethynylbenzoic acid (6)

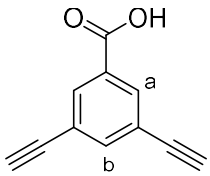

To a stirring solution of **19** (1.85 g, 5.9 mmol) in isopropanol (20 mL) was added potassium hydroxide (1.98 g, 35.3 mmol). The solution was heated to reflux and stirred for 6 h, before it was acidified to pH 1 with HCl (3 M, aq), and extracted into EtOAc (3 x 20 mL). The organic layer was then washed with brine (20 mL), dried over $MgSO_4$, filtered, and concentrated *in vacuo*. The residue was purified through silica gel column chromatography (250:50:1 dichloromethane:EtOAc:AcOH) to give the title compound as a cream amorphous solid (1.00 g, 99%).

R_f: 0.07 (1:24 MeOH:dichloromethane); **IR** (neat film, ν_{max}, cm^{-1}): 3287 (m), ~3000 (w br, OH), 1686 (s, C=O), 1626 (m), 1589 (m), 1444 (m), 1312 (m), 1241 (m), 900 (m), 828 (s), 773 (m), 723 (m), 670 (w); **^{1}H NMR** (400 MHz, DMSO-d6) δ: 13.46 (br s, 1H, -COOH), 7.93 (d, *J* = 1.6 Hz, 2H, Ha), 7.79 (t, *J* = 1.6 Hz, 1H, Hb), 4.38 (s, 2H, C≡C-H); **^{13}C NMR** (101 MHz, DMSO-d6) δ: 165.9 (-COOH), 138.6 (Cb), 132.9 (Ca), 132.5 (-**C**-COOH), 123.3 (-**C**-C≡CH), 83.2 (-C≡**C**-H), 81.9 (-**C**≡C-H).

Data are in accordance with those reported previously in literature.[157]

17-Hydroxy-3,6,9,12,15-pentaoxaheptadecyl 4-methylbenzenesulfonate (21)

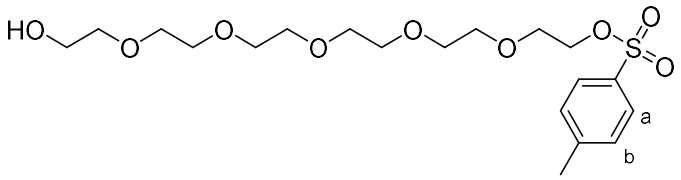

To a stirring solution of hexaethylene glycol (0.50 mL, 2.0 mmol) in dichloromethane (7 mL) cooled to 0 °C were added *p*-toluenesulfonyl chloride (0.42 g, 2.2 mmol), potassium iodide (0.07 g, 0.4 mmol), and silver (I) oxide (0.70 g, 3 mmol). After stirring at r.t. for 3 h, the mixture was filtered through silica and washed with EtOAc (4 x 10 mL) before concentrating *in vacuo*. The residue was purified through silica gel column chromatography (1:24 isopropanol:dichloromethane) to give the title compound as a colourless oil (0.77 g, 88%).

R_f: 0.29 (1:24 isopropanol/dichloromethane); **IR** (neat film, ν_{max}, cm^{-1}): 3444 (w br, OH), 2870 (m), 1597 (w), 1454 (w), 1351 (m), 1175 (s), 1095 (s), 1017 (m), 919 (m), 817 (m), 774 (m), 662 (m); **^{1}H NMR** (400 MHz, $CDCl_3$) δ: 7.79 (d, *J* = 8.2 Hz, 2H, Ha), 7.33 (d, *J* = 8.2 Hz, 2H, Hb), 4.15 (t, *J* = 4.1 Hz, 2H, -CH_2-OTs), 3.72 – 3.58 (m, 22H, 11 x CH_2), 2.70 (s, 1H, OH), 2.44 (s, 3H, CH_3); **^{13}C NMR** (101 MHz, $CDCl_3$) δ: 144.9 (-C-SO_3-), 133.1 (**C**-CH_3), 129.9 (Ca), 128.1 (Cb), 72.6, 70.8, 70.7, 70.7, 70.6, 70.6, 70.6, 70.4, 69.4 (-CH_2-OTs), 68.9, 61.8 (CH_2-OH), 21.7 (-CH_3).

Data are in accordance with those reported previously in literature.[162]

17-Azido-3,6,9,12,15-pentaoxaheptadecan-1-ol (22)

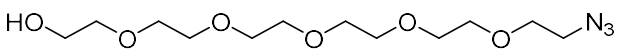

To a stirring solution of **21** (1.86 g, 4.3 mmol) in DMF (8 mL) was added sodium azide (0.42 g, 6.4 mmol). The solution was heated to 50 °C and stirred for 16 h, before the mixture was extracted with dichloromethane (6 x 10 mL), washed with brine (10 mL), dried over $MgSO_4$, filtered, and concentrated

in vacuo to give the title compound as a pale-yellow oil (1.22 g, 93%), with no need for further purification.

R_f: 0.17 (1:19 MeOH:dichloromethane); **IR** (neat film, ν_{max}, cm^{-1}): 3467 (w br, OH), 2867 (m), 2097 (m, N_3), 1451 (w), 1348 (w), 1285 (m), 1250 (m), 1097 (s), 940 (m), 847 (m); **^{1}H NMR** (400 MHz, $CDCl_3$) δ: 3.72 – 3.62 (m, 20H, 10 x CH_2), 3.59 (t, *J* = 4.9 Hz, 2H, -C**H**$_2$-CH_2-N_3), 3.37 (t, *J* = 4.9 Hz, 2H, CH_2-N_3), 2.68 (t, *J* = 6.2 Hz, 1H, OH); **^{13}C NMR** (101 MHz, $CDCl_3$) δ: 72.5, 70.7, 70.7, 70.6, 70.6, 70.5, 70.3, 70.0, 61.7 (CH_2-OH), 50.7 (-C-N_3).

Data are in accordance with those reported previously in literature.[162]

17-Amino-3,6,9,12,15-pentaoxaheptadecan-1-ol (23)

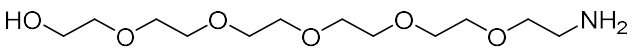

To a stirring solution of **22** (0.136 g, 0.33 mmol) in THF (5 mL) was added triphenylphosphine (0.132 g, 0.50 mmol). The solution was stirred at r.t. for 16 h, before water (1 mL) was added to induce precipitation. The organic phase was removed *in vacuo* before the residue was washed twice with toluene (2 x 10 mL). The aqueous was then concentrated *in vacuo* to give the title compound as a colourless oil (0.130 g, >98%), with no need for further purification.

R_f: 0.51 (1:9 MeOH:dichloromethane); **IR** (neat film, ν_{max}, cm^{-1}): 3362 (w br, OH), 2863 (m), 1455 (w), 1349 (m), 1296 (w), 1248 (w), 1094 (s), 944 (m), 884 (m), 838 (w); **^{1}H NMR** (400 MHz, $CDCl_3$) δ: 3.74 – 3.71 (m, 2H), 3.69 – 3.59 (m, 18H, 9 x CH_2), 3.53 (t, *J* = 5.2 Hz, 2H), 2.87 (t, *J* = 5.1 Hz, 2H, CH_2-N), 2.31 (s br, 3H, OH and NH_2); **^{13}C NMR** (101 MHz, $CDCl_3$) δ: 73.3, 72.9, 70.6, 70.6 – 70.5 (overlapping region), 70.3, 70.2, 61.5 (CH_2-OH), 41.7 (-C-NH_2).

Data are in accordance with those reported previously in literature.[162]

***tert*-Butyl(17-hydroxy-3,6,9,12,15-pentaoxaheptadecyl)carbamate (7)**

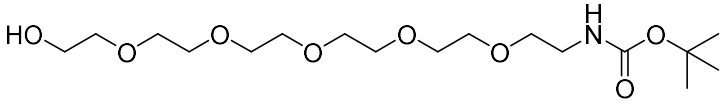

To a stirring solution of **23** (0.63 g, 2.2 mmol) in MeOH (7 mL) were added di-*tert*-butyl dicarbonate (0.56 mL, 2.5 mmol) and triethylamine (0.37 mL, 2.7 mmol). The solution was stirred at r.t. for 16 h before the mixture was concentrated *in vacuo* to give the title compound as a colourless oil (0.83 g, >98%), with no need for further purification.

R_f: 0.73 (1:9 MeOH:dichloromethane); **IR** (neat film, ν_{max}, cm^{-1}): 3452 (w br, OH), 2900 (m), 2868 (m), 1708 (m, C=O), 1520 (m), 1452 (w), 1365 (m), 1275 (m), 1249 (m), 1170 (m), 1098 (s), 944 (m), 864 (w); **^{1}H NMR** (400 MHz, $CDCl_3$) δ: 5.16 (br s, 1H, NH), 3.71 (t, *J* = 4.8 Hz, 2H, CH_2), 3.67 – 3.59 (18H, m), 3.52 (t, *J* = 5.1 Hz, 2H, -C**H**$_2$-CH_2-NHBoc), 3.29 (q, *J* = 5.1 Hz, 2H, -C**H**$_2$-NHBoc), 2.82 (br s, 1H, OH), 1.43 (s, 9H, 3 x CH_3); **^{13}C NMR** (101 MHz, $CDCl_3$) δ: 156.1 (C=O), 79.1 (-**C**-$(CH_3)_3$), 72.6, 70.6, 70.6, 70.6, 70.6, 70.6, 70.5, 70.3, 70.3, 70.2, 61.7, 40.4 (C-N), 28.4 (3 x CH_3).

Data are in accordance with those reported previously in literature.[162]

2,2-Dimethyl-4-oxo-3,8,11,14,17,20-hexaoxa-5-azadocosan-22-yl 3,5-diethynylbenzoate (24)

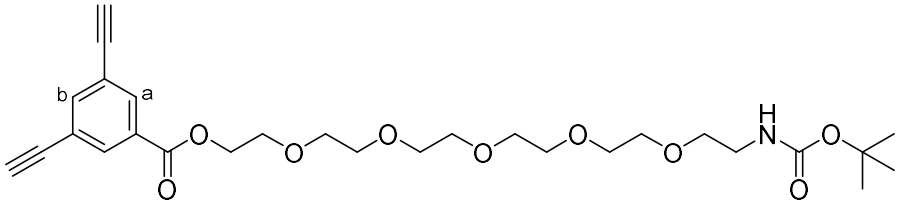

To a stirring solution of **6** (0.335 g, 2.0 mmol) in dichloromethane (10 mL) cooled to 0 °C were added DCC (0.488 g, 2.4 mmol) and DMAP (0.036 g, 0.3 mmol). The solution was stirred for 3 h at r.t., before a solution of **7** (0.825 g, 2.2 mmol) in dichloromethane (5 mL) was added. The mixture was stirred for a further 18 h, before being filtered, washed with dichloromethane (5 mL), and concentrated *in vacuo*. Et_2O (7 mL) was added, and the mixture was filtered, and concentrated *in vacuo*. The residue was purified through silica gel column chromatography (1:1 PE 40-60:EtOAc to EtOAc) to give the title compound as a colourless oil (0.450 g, 48%).

R_f: 0.37 (EtOAc); **IR** (neat film, ν_{max}, cm^{-1}): 3232 (w br, NH), 2929 (m), 2856 (m), 1710 (m, C=O), 1650 (m, C=O), 1512 (m, C=C), 1450 (m, C=C), 1364 (m), 1305 (m), 1213 (m), 1105 (s), 1042 (m), 897 (m), 769 (w); **^{1}H NMR** (400 MHz, $CDCl_3$) δ: 8.11 (d, *J* = 1.4 Hz, 2H, Ha), 7.75 (m, 1H, Hb), 5.03 (br s, 1H, NH), 4.47 (m, 2H, -CH_2-COO-), 3.82 (t, *J* = 4.7 Hz, 2H), 3.70 – 3.58 (m, 16H), 3.52 (m, 2H), 3.30 (m, 2H, CH_2-N), 3.15 (s, 2H, -C≡C-H), 1.43 (s, 9H, 3 x CH_3); **^{13}C NMR** (101 MHz, $CDCl_3$) δ: 164.9 (C=O), 156.0 (BocC=O), 139.4 (Cb), 133.3 (Ca), 130.8 (-**C**-COO-), 123.0 (**C**-C≡C-), 81.6 (**C**≡C-H), 79.1 (-**C**-$(CH_3)_3$), 79.0 (C≡**C**-H), 70.7, 70.7, 70.6, 70.5, 70.2, 69.0, 64.6 (**C**H_2-COO), 40.4 (CH_2-NH), 28.4 (3 x CH_3); **HRMS**: *m/z* $[M+H]^+$ calculated for $C_{28}H_{40}NO_9$: 534.2698; Found: 534.2690.

17-Amino-3,6,9,12,15-pentaoxaheptadecyl 3,5-diethynylbenzoate (3)

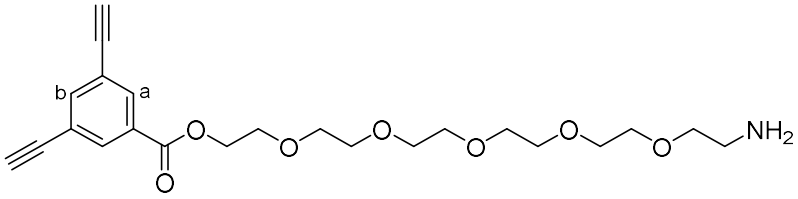

To a stirring solution of **24** (0.420 g, 0.79 mmol) in dichloromethane (3 mL) was added trifluoroacetic acid (3 mL). The solution was stirred for 3 h at r.t. before being concentrated *in vacuo*. The residue was purified through silica gel column chromatography (5:0.1:95 MeOH:NEt_3:dichloromethane) to give the title compound as a colourless oil (0.331 g, 97%).

R_f: 0.06 (1:19 MeOH:dichloromethane); **IR** (neat film, ν_{max}, cm^{-1}): 3226 (w, NH), 2916 (m), 2874 (m), 1722 (m, C=O), 1676 (m), 1436 (w, C=C), 1306 (m), 1200 (s), 1179 (s), 1111 (s), 1030 (m), 949 (m), 899 (m), 831 (m), 798 (m), 768 (m), 720 (m); **^{1}H NMR** (400 MHz, $CDCl_3$) δ: 8.09 (d, *J* = 1.5 Hz, 2H, Ha), 7.76 (t, *J* = 1.5 Hz, 1H, Hb), 4.49 (t, *J* = 4.8 Hz, 2H, -CH_2-COO-), 3.85 – 3.80 (m, 4H), 3.71 – 3.60 (m, 18H), 3.15 (br s, 4H, 2 x -C≡C-H and NH_2); **^{13}C NMR** (101 MHz, $CDCl_3$) δ: 164.8 (C=O), 139.4 (Hb), 133.2 (Ca), 130.7 (-**C**-COO-), 123.1 (**C**-C≡C-), 81.5 (**C**≡C-H), 79.1 (C≡**C**-H), 70.1, 70.1, 69.9, 69.9, 69.8, 68.9, 67.1, 64.2 (**C**H_2-COO-), 40.1 (-CH_2-NH_2); **HRMS**: *m/z* $[M+H]^+$ calculated for $C_{23}H_{32}NO_7$: 434.2173; Found: 434.2155.

3,6,9,12,15-Pentaoxaheptadecane-1,17-diyl bis(4-methylbenzenesulfonate) (27)

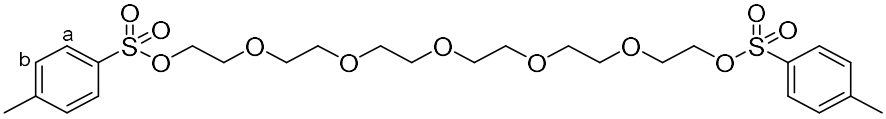

To a stirring solution of hexaethylene glycol (1.00 mL, 4.0 mmol) in THF (7 mL) cooled to 0 °C was added a solution of sodium hydroxide (0.64 g, 16 mmol) in water (5 mL). After stirring for *ca.* 15 mins a solution of *p*-toluenesulfonyl chloride (1.98 g, 10.4 mmol) in THF (7 mL) was added dropwise. The solution was warmed to r.t. before stirring for 3 h. At this point, further *p*-toluenesulfonyl chloride (1.00 g, 5.1 mmol) was added until complete conversion. The solution was concentrated *in vacuo* to *ca*. 5 mL then extracted into $CHCl_3$ (3 x 20 mL). The combined organic was washed with brine (20 mL), dried over $MgSO_4$, filtered, and concentrated *in vacuo*. The residue was purified through silica gel column chromatography (1:19 MeOH:dichloromethane) to give the title compound as a colourless oil (2.195 g, 93%).

R_f: 0.30 (1:19 MeOH:dichloromethane); **IR** (neat film, ν_{max}, cm^{-1}): 2870 (m), 1597 (w), 1451 (w), 1351 (s), 1292 (w), 1188 (m), 1175 (s), 1095 (s), 1011 (m), 917 (s), 815 (s), 774 (m), 662 (s); **^{1}H NMR** (400 MHz, $CDCl_3$) δ: 7.78 (d, *J* = 8.2 Hz, 4H, Ha), 7.33 (d, *J* = 8.2 Hz, 4H, Hb), 4.14 (t, *J* = 5.0 Hz, 4H, -C**H**$_2$-OTs),

3.67 (t, *J* = 5.0 Hz, 4H, -C**H**$_2$CH$_2$-OTs), 3.64 – 3.51 (m, 16H), 2.43 (s, 6H, 2 x -CH$_3$); **^{13}C NMR** (101 MHz, $CDCl_3$) δ: 144.8 (-**C**-SO$_3$), 133.0 (-**C**-CH$_3$), 129.8 (Cb), 128.0 (Ca), 70.7, 70.7, 70.6, 70.5, 70.5, 69.3 (-**C**H$_2$-OTs), 68.7 (-**C**H$_2$CH$_2$-OTs), 21.6 (2 x CH$_3$).

Data are in accordance with those reported previously in literature.[336]

1,17-Diazido-3,6,9,12,15-pentaoxaheptadecane (28)

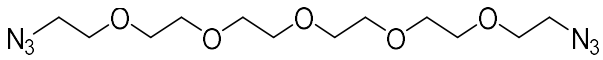

To a stirring solution of **27** (2.180 g, 3.7 mmol) in dry DMF (25 mL) was added sodium azide (0.959 g, 14.8 mmol). The solution was heated to 50 °C for 18 h. After cooling to r.t., water (50 mL) was added and the mixture was extracted into dichloromethane (6 x 15 mL). The combined organic was washed with brine (10 mL), dried over MgSO$_4$, filtered and concentrated *in vacuo* to give the title compound as a colourless oil (1.08 g, 86%), with no need for further purification.

R$_f$: 0.36 (1:19 MeOH:dichloromethane); **IR** (neat film, ν_{max}, cm^{-1}): 2867 (m), 2096 (m, N$_3$), 1451 (w), 1347 (w), 1284 (m), 1250 (m), 1098 (s br), 937 (m), 850 (m); **^{1}H NMR** (400 MHz, $CDCl_3$) δ: 3.68 – 3.65 (m, 20H), 3.38 (t, *J* = 5.2 Hz, 4H, C**H**$_2$-N$_3$); **^{13}C NMR** (101 MHz, $CDCl_3$) δ: 70.8, 70.8, 70.7, 70.7, 70.1 (-C**H**$_2$CH$_2$-N$_3$), 50.8 (-C**H**$_2$-N$_3$).

Data are in accordance with those reported previously in literature.[337]

2,2-Dimethyl-4-oxo-3,8,11,14,17,20-hexaoxa-5-azadocosan-22-yl 4-methylbenzenesulfonate (31)

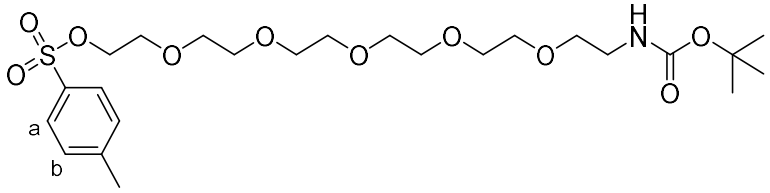

To a stirring solution of **7** (0.36 g, 0.9 mmol) in THF (3 mL) was added a solution of sodium hydroxide (0.075 g, 1.9 mmol) in H$_2$O (0.7 mL). After cooling to 0 °C, a solution of *p*-toluenesulfonyl chloride (0.22 g, 1.1 mmol) in THF (2.0 mL) was added dropwise. The mixture was stirred at r.t. for 18 h before concentrating *in vacuo*. H$_2$O (4 mL) was added before extracting into $CHCl_3$ (2 x 10 mL). The combined organic was washed with brine (10 mL), dried over MgSO$_4$, filtered, and concentrated *in vacuo*. The residue was purified through silica gel column chromatography (1:19 isopropanol/$CHCl_3$) to give the title compound as a colourless oil (0.505 g, >98%).

R_f: 0.23 (1:19 isopropanol/$CHCl_3$); **IR** (neat film, ν_{max}, cm^{-1}): 3356 (w, N-H), 2870 (m), 1708 (m, C=O), 1514 (m), 1454 (m), 1363 (m), 1249 (m), 1174 (s), 1095 (s), 1017 (m), 919 (m), 816 (m), 776 (m), 663 (m); **^{1}H NMR** (400 MHz, $CDCl_3$) δ: 7.79 (d, *J* = 8.2 Hz, 2H, Ha), 7.33 (d, *J* = 8.2 Hz, 2H, Hb), 5.03 (br s, 1H, NH), 4.15 (t, *J* = 4.7 Hz, 2H, -C**H**$_2$-OTs), 3.68 (t, *J* = 4.7 Hz, 2H, -C**H**$_2$-CH_2-OTs), 3.64 – 3.57 (m, 16H), 3.52 (t, *J* = 5.2 Hz, 2H, C**H**$_2$-CH_2-NHBoc), 3.30 (q, *J* = 5.2 Hz, 2H, -C**H**$_2$-NHBoc), 2.44 (s, 3H, tol-CH_3), 1.43 (s, 9H, 3 x -CH_3); **^{13}C NMR** (101 MHz, $CDCl_3$) δ: 156.0 (C=O), 144.8 (**C**-SO_3), 133.0 (-**C**-CH_3), 129.8 (Ca), 128.0 (Cb), 79.1 (-**C**-$(CH_3)_3$), 70.6, 70.6, 70.6, 70.5, 70.2, 69.2, 68.7, 40.4 (CH_2-N), 28.4 (3 x CH_3), 21.6 (tol-CH_3).

Data are in accordance with those reported previously in literature.[162]

***tert*-Butyl (17-azido-3,6,9,12,15-pentaoxaheptadecyl)carbamate (32)**

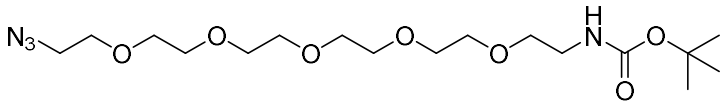

To a stirring solution of **31** (0.505 g, 0.9 mmol) in DMF (5 mL) was added sodium azide (0.092 g, 1.4 mmol). The solution was stirred at 50 °C for 18 h before H_2O (8 mL) was added and the mixture was extracted into dichloromethane (8 x 10 mL). The combined organic was washed with brine (15 mL), dried over $MgSO_4$, filtered, and concentrated *in vacuo* to give the title compound as a colourless oil (0.35 g, 92%), with no need for further purification.

R_f: 0.37 (1:19 MeOH:dichloromethane); **IR** (neat film, ν_{max}, cm^{-1}): 3347 (w, NH), 2869 (m), 2104 (m, N_3), 1709 (m, C=O), 1513 (m), 1365 (m), 1276 (m), 1249 (m), 1168 (m), 1101 (s), 1039 (m), 943 (m), 862 (m); **^{1}H NMR** (400 MHz, $CDCl_3$) δ: 5.03 (br s, 1H, NH), 3.68 – 3.59 (m, 18H), 3.53 (t, *J* = 5.1 Hz, 2H, -C**H**$_2$-CH_2-NHBoc), 3.38 (t, *J* = 5.0 Hz, 2H, -C**H**$_2$-N_3), 3.30 (q, *J* = 5.1 Hz, 2H, -C**H**$_2$-NHBoc), 1.43 (s, 9H, 3 x CH_3); **^{13}C NMR** (101 MHz, $CDCl_3$) δ: 156.0 (C=O), 79.1 (-**C**-$(CH_3)_3$), 70.7, 70.7, 70.6, 70.6, 70.5, 70.3, 70.2, 70.0, 50.7 (C-N_3), 40.4 (C-NHBoc), 28.4 (3 x CH_3).

Data are in accordance with those reported previously in literature.[162]

***tert*-Butyl (17-amino-3,6,9,12,15-pentaoxaheptadecyl)carbamate (30)**

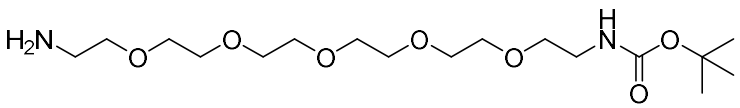

To a stirring solution of **32** (0.136 g, 0.33 mmol) in THF (5 mL) was added triphenylphosphine (0.132 g, 0.50 mmol). The solution was stirred for 18 h at r.t. before H_2O (2 mL) was added. The organic was

removed *in vacuo*, and the aqueous washed with toluene (2 x 5 mL), before being concentrated *in vacuo* to give the title compound as a colourless oil (0.130 g, >98%), with no need for further purification.

R_f: 0.16 (94:4:2 dichloromethane:MeOH:NEt_3); **IR** (neat film, ν_{max}, cm^{-1}): 3349 (w, NH), 2868 (m), 1707 (m, C=O), 1521 (m), 1365 (m), 1270 (m), 1250 (m), 1171 (m), 1103 (s); **^{1}H NMR** (400 MHz, $CDCl_3$) δ: 5.19 (br s, 1H, NH), 3.64 – 3.58 (m, 16H), 3.53 – 3.48 (m, 4H), 3.29 (q, *J* = 5.0 Hz, 2H, -C**H**$_2$-NHBoc), 2.84 (t, *J* = 5.2 Hz, 2H, -C**H**$_2$-NH_2), 1.71 (br s, 2H, NH_2), 1.42 (s, 9H, 3 x CH_3); **^{13}C NMR** (101 MHz, $CDCl_3$) δ: 156.1 (C=O), 79.1 (-**C**-$(CH_3)_3$), 73.2, 70.6, 70.6, 70.5, 70.5, 70.3, 70.2, 41.7 (-**C**H_2-NHBoc), 40.4 (**C**H_2-NH_2), 28.4 (3 x CH_3).

Data are in accordance with those reported previously in literature.[162]

tert-Butyl (1-(3,5-diethynylphenyl)-1-oxo-5,8,11,14,17-pentaoxa-2-azanonadecan-19-yl)carbamate (33)

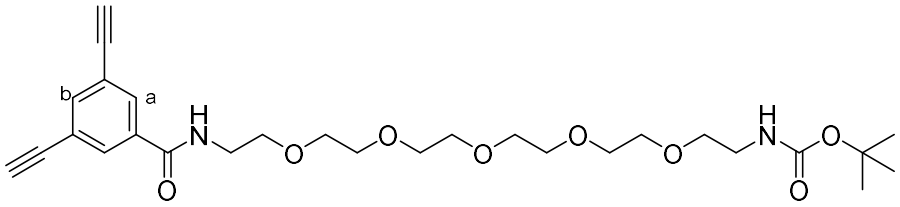

To a stirring solution of **6** (11 mg, 0.07 mmol) in dichloromethane (0.50 mL) were added PyAOP (47 mg, 0.09 mmol) and **30** (25 mg, 0.07 mmol). The mixture was stirred for 4 h at r.t., before being concentrated *in vacuo*. The residue was purified through silica gel column chromatography (EtOAc to 49:1 EtOAc:MeOH) to give the title compound as a colourless oil (24 mg, 65%).

R_f: 0.11 (EtOAc); **IR** (neat film, ν_{max}, cm^{-1}): cm^{-1}; 3283 (w, NH), 2916 (m), 2871 (m), 1697 (m, C=O), 1656 (m, C=O), 1586 (w, C=C), 1534 (m, C=C), 1454 (w, C=C), 1366 (m), 1248 (m), 1167 (m), 1101 (s), 844 (s); **^{1}H NMR** (400 MHz, $CDCl_3$) δ: 7.92 (d, *J* = 1.5 Hz, 2H, Ha), 7.69 (t, *J* = 1.5 Hz, 1H, Hb), 7.13 (br s, 1H, NH), 5.05 (br s, 1H, NH), 3.70 – 3.59 (m, 20H), 3.52 (t, *J* = 4.7 Hz, 2H, -C**H**$_2$-CH_2-NHBoc), 3.31 (q, *J* = 4.7 Hz, 2H, -C**H**$_2$-NHBoc), 3.14 (s, 2H, -C≡C-**H**), 1.43 (s, 9H, 3 x CH_3); **^{13}C NMR** (126 MHz, $CDCl_3$) δ: 166.0 (C=O amide), 156.5 (BocC=O), 137.9 (Cb), 135.2 (**C**-C=O), 131.0 (Ca), 122.9 (**C**-C≡C), 81.8 (**C**≡C-H), 79.3 (-**C**-$(CH_3)_3$), 78.9 (C≡**C**-H), 70.8, 70.3, 70.1, 70.0, 40.3 (CH_2-NHBoc), 39.9 (**C**H_2-NCOAr), 28.4 (3 x CH_3); **HRMS**: *m/z* $[M+H]^+$ calculated for $C_{28}H_{40}N_2O_8$: 533.2857; Found: 533.2836.

***N*-(17-Amino-3,6,9,12,15-pentaoxaheptadecyl)-3,5-diethynylbenzamide (26)**

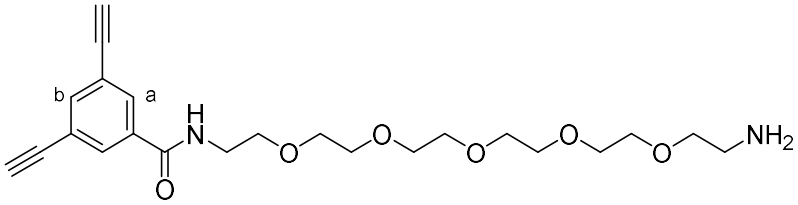

To a stirring solution of **33** (11 mg, 0.02 mmol) in dichloromethane (0.25 mL) was added trifluoroacetic acid (0.25 mL). The mixture was stirred for 3 h at r.t. before being concentrated *in vacuo*. The residue was purified through silica gel column chromatography (2:98 NEt_3:dichloromethane to 5:2:93 MeOH:NEt_3:dichloromethane) to give the title compound as a colourless oil (9 mg, >98%).

R_f: 0.29 (1:19 MeOH:dichloromethane); **IR** (neat film, ν_{max}, cm^{-1}): 3237 (w, NH), 2916 (m), 2875 (m), 1688 (m, C=O), 1676 (m), 1652 (m), 1585 (m, C=C), 1542 (m, C=C), 1300 (m), 1200 (m), 1126 (s), 829 (m), 799 (m), 719 (m); **^{1}H NMR** (400 MHz, $CDCl_3$) δ: 8.05 (d, *J* = 1.5 Hz, 2H, Ha), 8.00 (br s, 1H, HN-CO), 7.68 (t, *J* = 1.5 Hz, 1H, Hb), 3.74 (t, *J* = 5.2 Hz, 2H, -C**H**$_2$CH$_2$-NCO), 3.67 – 3.56 (m, 20H), 3.12 (s, 2H, -C≡C-H), 2.91 (t, *J* = 4.8 Hz, 2H, C**H**$_2$-NH$_2$); **^{13}C NMR** (101 MHz, $CDCl_3$) δ: 165.9 (C=O), 137.8 (Cb), 135.2 (**C**-C=O), 131.3 (Ca), 122.8 (**C**-C≡C), 81.9 (-**C**≡C-H), 78.6 (-C≡**C**-H), 70.5, 70.3, 70.3, 70.2, 70.2, 70.1, 69.6, 69.6, 41.3 (CH_2-NH_2), 39.9 (**C**H_2-NCO); **HRMS**: *m/z* $[M+H]^+$ calculated for $C_{23}H_{33}N_2O_6$: 433.2333; Found: 433.2323.

4-(3-(4-Cyano-3-(trifluoromethyl)phenyl)-5,5-dimethyl-4-oxo-2-thioxoimidazolidin-1-yl)-*N*-(1-(3,5-diethynylphenyl)-1-oxo-5,8,11,14,17-pentaoxa-2-azanonadecan-19-yl)-2-fluorobenzamide (34)

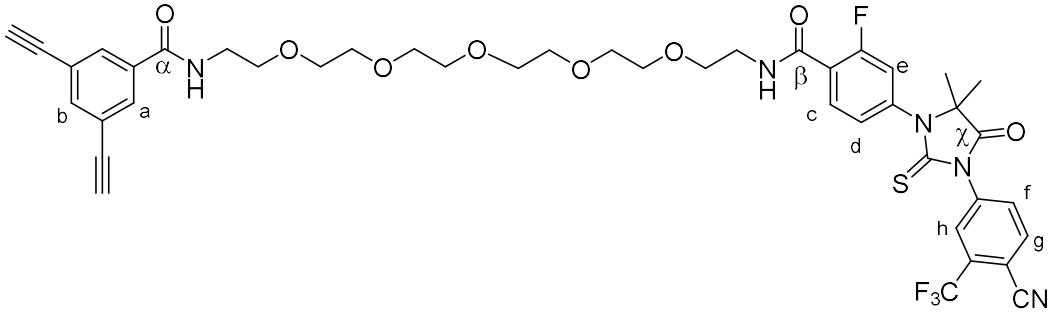

To a stirring solution of **2** (16 mg, 0.035 mmol) in DMF (100 µL) was added PyAOP (23 mg, 0.043 mmol). The mixture was stirred for *ca*. 10 mins at r.t. before a solution of **26** (15 mg, 0.035 mmol) in DMF (100 µL) was added. The mixture was stirred for a further 6 h at r.t. before being concentrated *in vacuo*. The residue was purified through silica gel column chromatography (dichloromethane to 1:19 MeOH:dichloromethane) to give the title compound as a colourless oil (6 mg, 20%).

R_f: 0.61 (1:9 MeOH:dichloromethane); **IR** (neat film, ν_{max}, cm^{-1}): 3388 (m, NH), 3200 (m), 1736 (m, C=O), 1714 (m, C=O), 1679 (s, C=O), 1647 (m), 1439 (m, C=C), 1373 (m), 1203 (s), 1137 (s); **^{1}H NMR** (500 MHz, $CDCl_3$) δ: 8.18 (t, *J* = 8.4 Hz, 1H, Hc), 8.00 (d, *J* = 8.2 Hz, 1H, Hg), 7.95 – 7.93 (m, 3H, Ha and Hh), 7.83 (dd, *J* = 8.1, 1.8 Hz, 1H, Hf), 7.69 (t, *J* = 1.5 Hz, 1H, Hb), 7.33 (br s, 1H, NH), 7.22 (dd, *J* = 8.2, 1.7 Hz, 1H, Hd), 7.13 (dd, *J* = 11.4, 1.8 Hz, 1H, He), 3.76 – 3.61 (m, 20H, 10 x CH_2), 3.18 – 3.13 (m, 6H, 2 x C**H**$_2$-NH and -C≡C-H), 1.61 (s, 6H, 2 x CH_3); **^{13}C NMR** (126 MHz, $CDCl_3$) δ: 179.7 (C=S), 174.5 (χC=O), 166.2 (αC=O), 162.8 (βC=O), 160.4 (d, *J* = 260 Hz, C-F), 139.0 (d, *J* = 8.0 Hz, -**C**-βC), 138.0 (Cb), 136.8 (-**C**-CN), 135.3 (Cg), 135.0 (-**C**-αC), 133.8 (q, *J* = 35 Hz, -**C**-CF_3), 133.1 (Cc), 132.1 (Cf), 131.1 (Ca), 127.1 (d, *J* = 6.3 Hz, Ch), 126.1 (Cd), 123.0 (-**C**-C≡C-), 122.9 (-**C**-N-C-$(CH_3)_2$-), 122.9 (Ch), 118.0 (d, *J* = 25 Hz, Ce), 114.7 (-C≡N), 110.5 (-**C**-NCO-), 81.8 (-**C**≡C-H), 78.9 (-C≡**C**-H), 70.3, 70.2, 70.1, 70.0, 69.9, 66.7 (-**C**-$(CH_3)_2$), 45.8 (-CH_2-NβCO), 39.8 (-CH_2-NαCO), 23.9 (2 x CH_3); **^{19}F NMR** (376 MHz, $CDCl_3$) δ: -63.0 (s, 3 F, CF_3), -111.2 (s, 1 F, ArC-F); **HRMS**: *m/z* $[M+H]^+$ calculated for $C_{43}H_{44}F_4N_5O_8S$: 866.2841; Found: 866.2811.

***tert*-Butyl (2-(2-(2-aminoethoxy)ethoxy)ethyl)carbamate (36)**

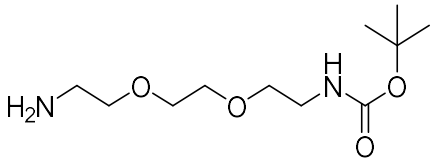

To a stirring solution of 2,2'-(ethylenedioxy)bis(ethylamine) (0.29 mL, 2.0 mmol) in dichloromethane (15 mL) cooled to 0 °C, was added a solution of Boc_2O (0.07 mL, 0.3 mmol) in dichloromethane (10 mL) over *ca*. 1 h. The solution was stirred for a further 3 h at 0 °C, before warming to r.t. and stirring for 18 h. The solution was washed with water (6 x 15 mL), and brine (15 mL), dried over $MgSO_4$, filtered, and concentrated *in vacuo* to give the title compound as a colourless oil (0.130 g, 27%), with no need for further purification.

R_f: 0.04 (1:24 MeOH:dichloromethane); **IR** (neat film, ν_{max}, cm^{-1}): 3341 (w, NH), 2968 (m), 2932 (m), 2873 (m), 1697 (s, C=O), 1517 (m), 1365 (m), 1272 (m), 1250 (m), 1170 (s), 1105 (s); **^{1}H NMR** (400 MHz, $CDCl_3$) δ: 5.16 (br s, 1H, NHBoc), 3.59 (s, 4H, -O-C**H**$_2$-C**H**$_2$-), 3.53 – 3.49 (m, 4H, 2 x -C**H**$_2$-CH_2-N-), 3.29 (q, *J* = 4.9 Hz, 2H, C**H**$_2$-NHBoc), 2.86 (t, *J* = 4.9 Hz, 2H, -C**H**$_2$-NH_2), 1.77 (br s, 2H, -NH_2), 1.41 (s, 9H, 3 x CH_3); **^{13}C NMR** (101 MHz, $CDCl_3$) δ: 156.0 (C=O), 79.1 (-**C**-$(CH_3)_3$), 73.2, 70.2, 70.2, 70.2, 41.6 (-CH_2-NH_2), 40.3 (CH_2-NHBoc), 28.4 (3 x CH_3).

Data are in accordance with those reported previously in literature.[338]

***tert*-Butyl (2-(2-(2-(3,5-diethynylbenzamido)ethoxy)ethoxy)ethyl)carbamate (37)**

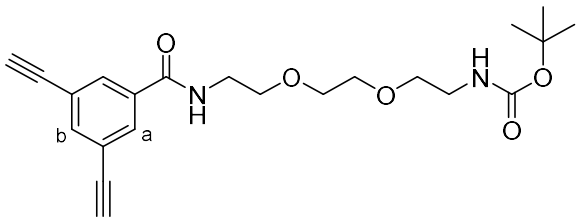

To a stirring solution of **6** (10 mg, 0.06 mmol) in DMF (100 µL) were added DCC (21 mg, 0.1 mmol) and HOAt (0.6 M in DMF, 42 µL, 0.07 mmol). The mixture was stirred at r.t. for 3 h, before a solution of **36** (15 mg, 0.06 mmol) in DMF (100 µL) was added. After stirring for a further 3 h, the mixture was filtered, washed with dichloromethane (2 mL), and concentrated *in vacuo*. Et_2O (2 mL) was added to the residue and the mixture was filtered and concentrated *in vacuo*. The residue was purified through silica gel column chromatography (1:3 to 3:1 EtOAc:PE 40-60) to give the title compound as a colourless oil (10 mg, 42%).

R_f: 0.46 (EtOAc); **IR** (neat film, ν_{max}, cm^{-1}): 3297 (m, NH), 2873 (m), 1699 (s, C=O), 1657 (s, C=O), 1586 (m, C=C), 1535 (s, C=C), 1249 (m), 1171 (s), 1103 (s); **^{1}H NMR** (400 MHz, $CDCl_3$) δ: 7.88 (s, 2H, Ha), 7.70 (s, 1H, Hb), 6.80 (br s, 1H, -NH-COAr), 4.97 (br s, 1H, -N**H**Boc), 3.67 – 3.64 (m, 8H, 4x CH_2), 3.58 – 3.54 (m, 2H, CH_2), 3.34 – 3.29 (m, 2H, -C**H**$_2$-NHBoc), 3.14 (br s, 2H, -C≡C-H), 1.42 (s, 9H, 3 x CH_3); **^{13}C NMR** (101 MHz, $CDCl_3$) δ: 165.7 (ArC=O), 156.0 (C=O Boc), 137.9 (Cb), 135.2 (-**C**-C=O-), 130.8 (Ca), 123.1 (-**C**-C≡C-), 81.7 (-**C**≡C-H), 79.4 (-**C**-$(CH_3)_3$), 79.0 (-C≡**C**-H), 70.3, 70.3, 70.1, 69.7 (4 x O-CH_2), 40.3 (-**C**H_2-NHBoc), 39.9 (-**C**H_2-NCOAr), 28.4 (3 x CH_3); **HRMS**: *m/z* $[M+Na]^+$ calculated for $C_{22}H_{28}N_2O_5Na$: 423.1890; Found: 423.1905.

***N*-(2-(2-(2-Aminoethoxy)ethoxy)ethyl)-3,5-diethynylbenzamide (38)**

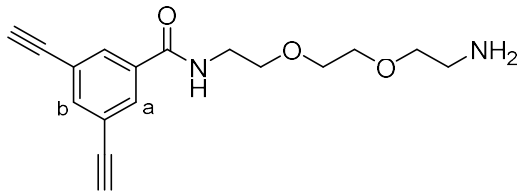

To a stirring solution of **37** (8 mg, 0.020 mmol) in dichloromethane (100 µL) was added trifluoroacetic acid (100 µL). The mixture was stirred at r.t. for 4 h, before being concentrated *in vacuo*. The residue was purified through silica gel column chromatography (6:0.1:94 MeOH:NEt_3:dichloromethane) to give the title compound as a yellow oil (6 mg, >98%).

R_f: 0.15 (3:47 MeOH:dichloromethane); **IR** (neat film, ν_{max}, cm^{-1}): 3286 (m, NH), 2920 (m), 2878 (m), 1642 (s, C=O), 1585 (s, C=C), 1540 (s, C=C), 1324 (m), 1201 (m), 1123 (s), 894 (m), 799 (w), 683 (w); **^{1}H**

NMR (400 MHz, $CDCl_3$) δ: 7.94 (d, *J* = 1.4 Hz, 2H, Ha), 7.66 (m, 1H, Hb), 7.56 (t, *J* = 5.2 Hz, 1H, NH), 3.68 – 3.61 (m, 12H, 5 x CH_2 and NH_2), 3.15 (s, 2H, -C≡C-H), 3.04 (t, *J* = 4.6 Hz, 2H, -C**H**$_2$-NH_2); **^{13}C NMR** (101 MHz, $CDCl_3$) δ: 166.0 (C=O), 137.9 (Cb), 135.0 (**C**-CON-), 131.1 (Ca), 122.9 (**C**-C≡C-), 81.8 (-**C**≡C-H), 79.0 (-C≡**C**-H), 70.2, 70.1, 69.8, 68.9 (4x O-CH_2), 40.3 (-**C**H_2-NH_2), 40.0 (-**C**H_2-NH-); **HRMS**: *m/z* $[M+H]^+$ calculated for $C_{17}H_{21}N_2O_3$: 301.1547; Found: 301.1528.

4-(3-(4-Cyano-3-(trifluoromethyl)phenyl)-5,5-dimethyl-4-oxo-2-thioxoimidazolidin-1-yl)-*N*-(2-(2-(2-(3,5-diethynylbenzamido)ethoxy)ethoxy)ethyl)-2-fluorobenzamide (39)

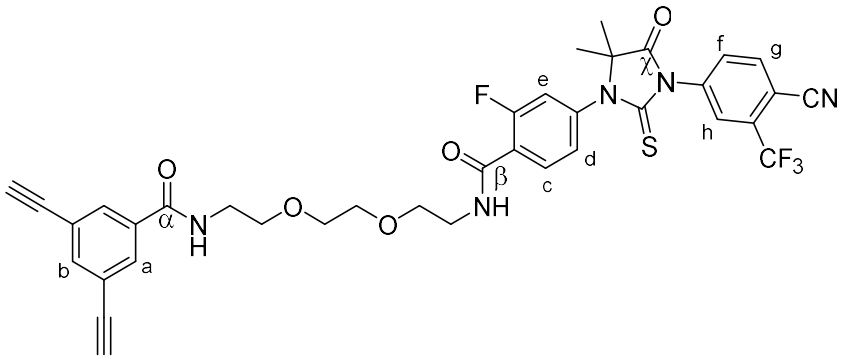

To a stirring solution of **2** (11 mg, 0.025 mmol) in DMF (100 µL) were added DCC (8 mg, 0.04 mmol) and HOAt (0.6 M in DMF, 63 µL, 0.04 mmol). The solution was stirred for 1 h at r.t. before a further portion of DCC (5 mg, 0.02 mmol) was added. After stirring for a further 30 mins, a solution of **38** (8 mg, 0.025 mmol) in DMF (180 µL) was added, and the mixture stirred for 4 h before being diluted with dichloromethane (2 mL), filtered, and concentrated *in vacuo*. Diethyl ether (3 mL) was then added and the mixture filtered and concentrated *in vacuo*. The residue was purified through silica gel column chromatography (1:1 EtOAc:PE 40-60 to EtOAc) to give the title compound as a colourless oil (6.5 mg, 36%).

R_f: 0.33 (EtOAc); **IR** (neat film, ν_{max}, cm^{-1}): 3286 (w br, NH), 2920 (w), 2869 (w), 1757 (m, C=O), 1710 (m, C=O), 1650 (m, C=O), 1620 (m), 1585 (w, C=C), 1537 (m, C=C), 1500 (m, C=C), 1440 (m), 1312 (s), 1220 (m), 1178 (m), 1136 (m), 1057 (w), 841 (s), 679 (w); **^{1}H NMR** (500 MHz, $CDCl_3$) δ: 8.22 (t, *J* = 8.5 Hz, 1H, Hc), 7.99 (d, *J* = 8.2 Hz, 1H, Hg), 7.94 (d, *J* = 2.0 Hz, 1H, Hh), 7.86 (d, *J* = 1.5 Hz, 2H, Ha), 7.82 (dd, *J* = 8.2, 2.0 Hz, 1H, Hf), 7.69 (t, *J* = 1.5 Hz, 1H, Hb), 7.22 (dd, *J* = 8.5, 1.9 Hz, 1H, Hd), 7.10 (dd, *J* = 11.7, 1.9 Hz, 1H, He), 6.70 (t, *J* = 4.8 Hz, 1H, NH), 3.71 – 3.65 (m, 10H, 5 x CH_2), 3.13 (s, 2H, -C≡C-H), 1.63 – 1.55 (m, 8H, CH_2 and 2 x CH_3); **^{13}C NMR** (126 MHz, $CDCl_3$) δ: 179.9 (C=S), 174.6 (χC=O), 165.8 (αC=O), 162.3 (βC=O), 160.6 (d, *J* = 250 Hz, C-F), 139.2 (d, *J* = 11 Hz, -**C**-Cβ), 138.2 (Cb), 136.9 (-**C**-CN), 135.5 (**C**-Cα), 135.3 (Cg), 133.9 (d, *J* = 33 Hz, **C**-CF_3), 133.5 (Cc), 132.3 (Cf), 130.9 (Ca), 127.2 (d, *J* = 5.2 Hz, Ch), 126.3 (Cd), 123.2 (-**C**-C≡C), 122.7 (d, *J* = 16 Hz, -**C**-N-C-$(CH_3)_2$-), 122.0 (q, *J* = 280 Hz, CF_3), 118.1

(d, *J* = 27 Hz, Ce), 114.9 (-C≡N), 110.6 (-**C**-NχCO-), 81.8 (-**C**≡C-H), 79.2 (-C≡**C**-H), 70.5, 70.4, 69.8, 69.7 (4x O-CH_2), 66.8 (-**C**-$(CH_3)_2$), 40.0 (2C, 2 x CH_2-NH), 24.0 (2 x CH_3); **^{19}F NMR** (376 MHz, $CDCl_3$) δ: -63.0 (CF_3), -111.4 (ArC-F); **HRMS**: *m/z* $[M+H]^+$ calculated for $C_{37}H_{32}F_4N_5O_5S$: 734.2055; Found: 734.2031.

3-Azidosulfonyl-3*H*-imidazol-1-ium hydrogen sulfate (40)

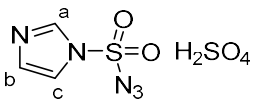

To a stirring solution of sodium azide (0.65 g, 10 mmol) in acetonitrile (15 mL) cooled to 0 °C, was added sulfuryl chloride (0.81 mL, 10 mmol) dropwise. The mixture was stirred at r.t. for 16 h before cooling to 0 °C. Imidazole (1.29 g, 19 mmol) was added and the mixture stirred for a further 5 h at r.t. before the mixture was diluted with EtOAc (20 mL) and H_2O (20 mL). The organic layer was separated, washed twice with $NaHCO_3$ (2 x 20 mL), dried over $MgSO_4$, and filtered. The volume was reduced to *ca*. 10 mL *in vacuo* and the mixture was cooled to 0 °C, before conc. sulfuric acid (0.53 mL, 10 mmol) was added dropwise. The mixture was stirred for 16 h at r.t. The precipitate was then filtered, washed with EtOAc (3 x 3 mL), and dried *in vacuo* to give the title compound as a white amorphous solid (1.64 g, 61%), with no need for further purification.

R_f: 0.80 (1:24 MeOH:dichloromethane); **IR** (neat film, ν_{max}, cm^{-1}): 3110 (w), 3082 (w), 2982 (w), 2751 (w), 2433 (w), 2177 (m, N_3), 1586 (m, C=C), 1516 (m), 1430 (m), 1302 (m, S=O), 1233 (s), 1190 (m), 1151 (s), 1127 (s, S=O), 1099 (s), 1067 (m), 1018 (m), 983 (m), 883 (m), 872 (m), 834 (m), 773 (s), 739 (s); **^{1}H NMR** (400 MHz, DMSO-d6) δ: 14.27 (br s, 1H, NH^+), 12.71 (br s, 3H, H_2SO_4 expected 1H), 9.09* (t, *J* = 1.2 Hz, 1H, C-H), 8.63 (m, 1H, Hc), 7.99 (t, *J* = 1.6 Hz, 1 H, Ha), 7.69* (d, *J* = 1.2 Hz, 2H), 7.36 (dd, *J* = 1.6, 0.8 Hz, Hb); **^{13}C NMR** (100 MHz, DMSO-d6) δ: 138.2 (Cc), 134.9*, 131.0 (Ca), 119.8*, 119.4 (Cb).

Product partially decomposes in DMSO-d6 to form 1,3*H*-imidazol-1-ium salts, these are marked with an asterisk (*).

Data are in accordance with those reported previously in literature.[169]

Fmoc-Orn-OH.HCl (42)

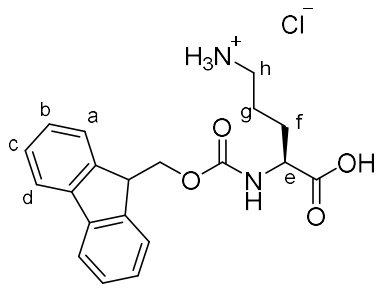

To a stirring solution of Fmoc-Orn(Boc)-OH (1.75 g, 3.8 mmol) in 1,4-dioxane (13 mL) was added HCl solution (13 mL, 4 M in dioxane) in a single portion. The mixture was stirred at r.t. for 18 h before Et_2O (60 mL) was added. The white precipitate was filtered, washed with Et_2O (4 x 10 mL), and dried *in vacuo* to give the title compound as a white amorphous powder (1.74 g, >98%), with no need for further purification.

R_f: 0.0 (1:24 MeOH:dichloromethane); **IR** (neat film, ν_{max}, cm^{-1}): 3330 (w, NH), 2993 (m br, OH), 1725 (m, C=O), 1689 (s, C=O), 1530 (s, C=C), 1477 (m, C=C), 1450 (m, C=C), 1286 (m), 1260 (m), 1221 (m), 1120 (m), 1036 (m), 984 (m), 870 (m), 759 (m), 734 (s); **^{1}H NMR** (400 MHz, DMSO-d6) δ: 12.71 (br s, 1H, COOH), 8.02 (br s, 3H, NH^{3+}), 7.90 (d, *J* = 7.5 Hz, 2H, Hd), 7.73 (t, *J* = 8.0 Hz, 2H, Ha), 7.42 (t, *J* = 7.4 Hz, 2H, Hc), 7.34 (t, *J* = 7.4 Hz, 2H, Hb), 4.32 – 4.22 (m, 3H, Fmoc CH and CH2), 3.99 – 3.94 (m, 1H, Ce), 2.77 (br s, 2H, Hh), 1.84 – 1.60 (m, 4H, Hf and Hg); **^{13}C NMR** (101 MHz, DMSO-d6) δ: 174.0 (COOH), 156.6 (CONH), 144.3 (2 x C_QAr), 141.2 (2 x C_QAr), 128.1 (2 x CHAr), 127.6 (2 x CHAr), 125.7 (2 x CHAr), 120.6 (2 x CHAr), 66.1 (Fmoc-CH_2), 53.9 (Ce), 47.1 (Fmoc-CH), 38.8 (CH), 28.2 (Cf), 24.4 (Cg); **$[\alpha]_D^{20}$:** -2.9 (c = 1.0, MeOH, lit. $[\alpha]_D^{27}$ - 3.0[168]).

Data are in accordance with those reported previously in literature.[168]

Fmoc-Orn(N_3)-OH (43)

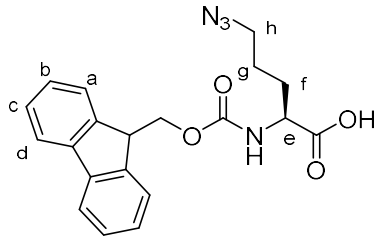

To a stirring, biphasic mixture of H_2O (40 mL), MeOH (80 mL), and dichloromethane (68 mL) were added Fmoc-Orn-OH.HCl (2.80 g, 7.2 mmol), copper(II) sulfate pentahydrate (14 mg, 0.058 mmol), and 3-azidosulfonyl-3*H*-imidazol-1-ium hydrogen sulfate (7.16 g, 26.5 mmol). Aqueous potassium carbonate solution was added to pH 9, and the mixture was stirred for 16 h. Dichloromethane (90 mL)

was added and the two phases separated, before the organic was further extracted with saturated $NaHCO_3$ (2 x 120 mL). The combined aqueous was then washed with Et_2O (2 x 120 mL), acidified to pH 2 using conc. HCl, and extracted into Et_2O (3 x 140 mL). The organic layer was dried over $MgSO_4$, filtered, and concentrated *in vacuo* to give the title compound as a cream amorphous solid (1.62 g, 59%), with no need for further purification.

R_f: 0.10 (1:24 MeOH:dichloromethane); **m.p.**: 130 – 132 °C (Et_2O, lit. 127 – 128 °C[339]); **IR** (neat film, ν_{max}, cm^{-1}): 3283 (m, NH), 3070 (br m, OH), 2098 (s, N_3), 1715 (s br, C=O), 1522 (m, C=C), 1450 (m, C=C), 1231 (s), 1183 (m), 1041 (s), 760 (m), 741 (s); **^{1}H NMR** (400 MHz, DMSO-d6) δ: 12.63 (br s, 1H, COOH), 7.89 (d, *J* = 7.6 Hz, 2H, Hd), 7.73 – 7.68 (m, 2H, Ha), 7.42 (t, *J* = 7.5 Hz, 2H, Hc), 7.33 (t, *J* = 7.4 Hz, 2H, Hb), 4.34 – 4.21 (m, 3H, Fmoc CH and CH_2), 4.00 – 3.94 (m, 1H, He), 3.39 – 3.29 (m, 2H, Hh), 1.83 – 1.55 (m, 4H, Hf and Hg); **^{13}C NMR** (101 MHz, DMSO-d6) δ: 174.1 (COOH), 156.6 (CONH), 144.3 (C_QAr), 144.2 (C_QAr), 141.2 (C_QAr), 141.2 (C_QAr), 128.1 (Cc), 127.5 (Cb), 125.7 (Ca), 125.7 (Ca), 120.6 (2 x Cd), 66.1 (Fmoc-CH_2), 53.8 (Ce), 50.7 (Ch), 47.1 (Fmoc-CH), 28.5 (Cf), 25.6 (Cg); **$[\alpha]_D^{20}$:** - 3.8 (c = 1.0, MeOH, lit**. $[\alpha]_D^{27}$** – 2 .3[340]).

Data are in accordance with those reported previously in literature.[339]

***tert*-Butyl (6-(3,5-diethynylbenzamido)hexyl)carbamate (44)**

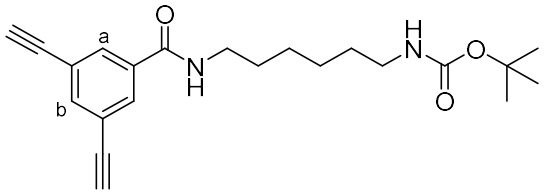

To a stirring solution of **6** (0.144 g, 0.85 mmol) in dichloromethane (2 mL) were added PyAOP (0.574 g, 1.1 mmol) and *N*-Boc-1,6-hexanediamine (0.19 mL, 0.85 mmol). The mixture was stirred at r.t. for 3 h before H_2O (2 mL) was added. The organic was separated, and the aqueous further extracted with dichloromethane (3 x 2 mL), before the combined organics were washed with brine (3 mL), dried over $MgSO_4$, filtered, and concentrated *in vacuo*. The residue was purified through silica gel column chromatography (1:1 EtOAc:Hexane) to give the title compound as a white amorphous solid (0.193 g, 62%).

R_f: 0.40 (1:1 EtOAc:Hexane); **IR** (neat film, ν_{max}, cm^{-1}): 3360 (m, NH), 3294 (m, NH), 2936 (m), 1679 (s, C=O), 1634 (s, C=O), 1585 (m, C=C), 1519 (s, C=C), 1480 (m, C=C), 1344 (m), 1283 (m), 1249 (m), 1167 (s), 1042 (w), 888 (m), 759 (w), 657 (w); **^{1}H NMR** (500 MHz, $CDCl_3$) δ: 7.88 (s, 2H, Ha), 7.69 (t, *J* = 1.4 Hz, 1H, Hb), 6.49 (br s, 1H, ArCON**H**), 4.56 (br s, 1H, -N**H**Boc), 3.43 (dd, *J* = 6.8, 6.2 Hz, 2H, -C**H**$_2$-

NHCOAr), 3.13 (br m, 4H, -C≡C-H and -C**H**$_2$-NHBoc), 1.61 (quin, *J* = 7.0 Hz, 2H, -C**H**$_2$-CH$_2$-NHBoc), 1.51 – 1.33 (m, 15H, 3 x CH_3 and 3 x CH_2); **^{13}C NMR** (126 MHz, $CDCl_3$) δ: 165.7 (Ar-C=O), 156.2 (C=O-Boc), 137.8 (Cb), 135.4 (-**C**-CON-), 130.8 (Ca), 123.0 (-**C**-C≡C-H), 81.8 (-**C**≡C-H), 79.2 (-**C**-$(CH_3)_3$), 78.9 (-C≡**C**-H), 39.9 (-**C**H_2-NHBoc), 39.6 (-**C**H_2-NHCOAr), 30.1, 29.3, 28.4 (3 x CH_3), 25.9, 25.7; **HRMS**: *m/z* $[M+H]^+$ calculated for $C_{22}H_{29}N_2O_3$: 369.2173; Found: 369.2185.

***N*-(6-Aminohexyl)-3,5-diethynylbenzamide (45)**

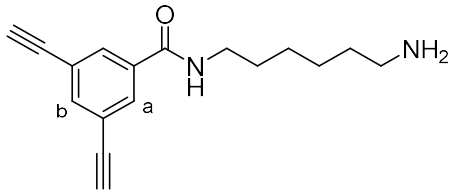

To a stirring solution of **44** (0.193 g, 0.52 mmol) in dichloromethane (1 mL) was added trifluoroacetic acid (1 mL). After stirring at r.t. for 4 h, the mixture was concentrated *in vacuo* before H_2O (2 mL) was added. The aqueous was extracted into $CHCl_3$ (8 x 5 mL), and the combined organics were dried over $MgSO_4$, filtered, and concentrated *in vacuo*. The residue was purified through silica gel column chromatography (10:0.1:90 MeOH:NEt_3:dichloromethane) to give the title compound as a colourless oil (0.122 g, 87%).

R_f: 0.06 (10:2:88 MeOH:NEt_3:dichloromethane); **IR** (neat film, ν_{max}, cm^{-1}): 3289 (m, NH), 2929 (m), 2857 (m), 1637 (s, C=O), 1584 (s, C=C), 1542 (s, C=C), 1436 (m, C=C), 1324 (m), 1245 (m), 932 (w), 893 (m), 737 (w), 683 (w); **^{1}H NMR** (400 MHz, DMSO-d6) δ: 8.64 (t, *J* = 5.3 Hz, 1H, N**H**), 7.95 (d, *J* = 1.4 Hz, 2H, Ha), 7.70 (t, *J* = 1.3 Hz, 1H, Hb), 4.37 (s, 2H, -C≡C-**H**), 3.24 (dd, *J* = 6.8, 6.0 Hz, 2H, -C**H**$_2$-NCOAr), 2.60 – 2.50 (m, 4H, -C**H$_2$**N**H**$_2$), 1.51 (quin, *J* = 6.5 Hz, 2H, -C**H**$_2$-NCOAr), 1.36- 1.29 (m, 6H, 3x CH_2); **^{13}C NMR** (101 MHz DMSO-d6) δ: 164 (C=O), 137.0 (Cb), 136.0 (-**C**-CON-), 131.1 (Ca), 122.9 (-**C**-C≡C-H), 82.8 (-C≡**C**-H), 82.3 (-**C**≡C-H), 42.0 (-**C**H_2-NH_2), 39.8 (-**C**H_2-NCOAr), 33.5, 29.4, 26.9, 26.6 (4x CH_2); **HRMS**: ESI *m/z*: mass not found.

4-(3-(4-Cyano-3-(trifluoromethyl)phenyl)-5,5-dimethyl-4-oxo-2-thioxoimidazolidin-1-yl)-*N*-(6-(3,5-diethynylbenzamido)hexyl)-2-fluorobenzamide (46)

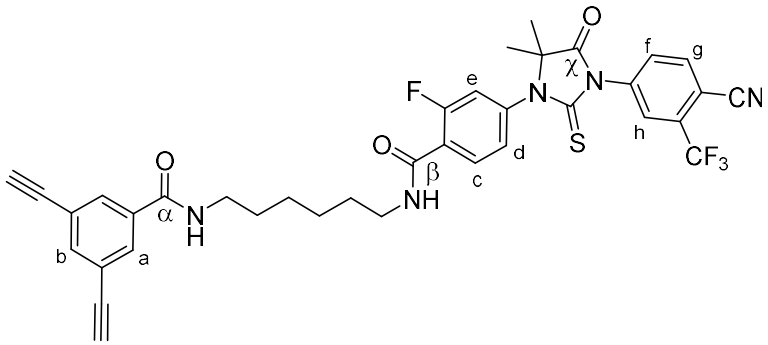

To a stirring solution of **2** (8 mg, 0.022 mmol) in dichloromethane (200 µL) were added PyAOP (16 mg, 0.031 mmol) and **45** (4.7 mg, 0.022 mmol). The mixture was stirred at r.t. for 3 h before being concentrated *in vacuo*. The residue was purified through silica gel column chromatography (3:2 EtOAc:Hexane) to give the title compound as a yellow oil (9 mg, 60%).

R_f: 0.35 (3:2 EtOAc:Hexane); **IR** (neat film, ν_{max}, cm^{-1}): 3292 (w br, NH), 2926 (w), 2856 (w), 1756 (m, C=O), 1649 (m, C=O), 1620 (m, C=O), 1585 (w, C=C), 1535 (m, C=C), 1498 (m, C=C), 1437 (m, C=C), 1412 (m, C=C), 1310 (s), 1218 (m), 1177 (m), 1137 (s), 1056 (m), 923 (w), 893 (w), 813 (w), 736 (w); **^{1}H NMR** (500 MHz, $CDCl_3$) δ: 8.24 (t, *J* = 8.4 Hz, 1H, Hc), 7.98 (d, *J* = 8.2 Hz, 1H, Hg), 7.94 (d, *J* = 1.8 Hz, 1H, Hh), 7.87 (d, *J* = 1.6 Hz, 2H, Ha), 7.82 (dd, *J* = 8.2, 1.8 Hz, 1H, Hf), 7.69 (t, *J* = 1.6 Hz, 1H, Hb), 7.23 (dd, *J* = 8.4, 2.0 Hz, 1H, Hd), 7.14 (dd, *J* = 11.7, 2.0 Hz, 1H, He), 6.73 (dt, *J* = 11.5, 5.9 Hz, 1H, βCON**H**), 6.32 (t, *J* = 5.4 Hz, 1H, αCON**H**), 3.52 (dd, *J* = 12.8, 6.3 Hz, 2H, C**H**$_2$-NHβC-), 3.45 (dd, *J* = 13.1, 6.9 Hz, 2H, C**H**$_2$-NHαC-), 3.12 (s, 2H, -C≡C-H), 1.68 – 1.60 (m, 10H, 2 x CH_2 and 2 x CH_3), 1.46 – 1.44 (m, 2H, CH_2), 1.27 – 1.23 (m, 2H, CH_2); **^{13}C NMR** (126 MHz, $CDCl_3$) δ: 179.8 (C=S), 174.4 (χC=O), 165.7 (αC=O), 162.1 (d, *J* = 3.3 Hz, βC=O), 160.3 (d, *J* = 250 Hz, C-F), 139.0 (d, *J* = 11 Hz, -**C**-Cβ), 137.9 (Cb), 136.8 (-**C**-CN), 135.4 (**C**-Cα), 135.3 (Cg), 133.7 (q, *J* = 34 Hz, -**C**-CF_3), 133.4 (d, *J* = 3.3 Hz, Cc), 132.1 (Cf), 130.7 (Ca), 127.1 (q, *J* = 4.6 Hz, Ch), 126.2 (d, *J* = 3.2 Hz, Cd), 123.1 (-**C**-C≡C-H), 122.9 (-**C**-N-C-$(CH_3)_2$-), 121.8 (q, *J* = 270 Hz, -CF_3), 117.9 (d, *J* = 26 Hz, Ce), 114.7 (-C≡N), 110.5 (q, *J* = 2.0 Hz, -**C**-NχC-), 81.7 (-**C**≡C-H), 78.9 (-C≡**C**-H), 66.6 (-**C**-$(CH_3)_2$), 39.7 (2 x -CH_2-NH-), 29.7, 29.4, 29.4, 26.1, 23.9 (2 x CH_3); **^{19}F NMR** (376 MHz, $CDCl_3$) δ: -63.0 (s, 3 F, CF_3), -111.6 (s, 1 F, ArC-F); **HRMS**: *m/z* $[M+H]^+$ calculated for $C_{37}H_{32}F_4N_5O_3S$: 702.2156; Found: 702.2164.

6-((*tert*-Butoxycarbonyl)amino)hexanoic acid (47)

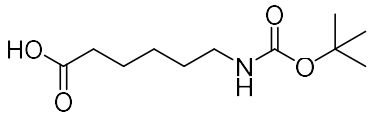

To a stirring solution of 6-aminocaproic acid (2.62 g, 20.0 mmol) in 1,4-dioxane (17 mL) and H_2O (8 mL) cooled to 0 °C, were added NaOH (1 M, 20 mL) and Boc_2O (5.05 mL, 22.0 mL). The mixture was stirred at r.t. for 3 h, before being concentrated *in vacuo*, washed with EtOAc (25 mL), and acidified with HCl (1 M) to pH 1. The aqueous layer was then extracted into EtOAc (3 x 25 mL), and the combined organic was dried over $MgSO_4$, filtered, and concentrated *in vacuo* to give the title compound as a white crystalline solid (3.50 g, 76%), with no need for further purification.

m.p.: 35 – 37 °C (EtOAc, lit. 35 - 37 °C[341]); **R_f**: 0.70 (EtOAc); **IR** (neat film, ν_{max}, cm^{-1}): 3342 (w br, NH), ~3000 (w br, OH), 2976 (m), 2861 (m), 1705 (s br, C=O), 1519 (m), 1454 (m), 1366 (m), 1249 (m), 1163 (s), 864 (w), 779 (w); **^{1}H NMR** (400 MHz, $CDCl_3$) δ: 4.57 (br s, 1H, -NH), 3.13 – 3.05 (m, 2H, C**H_2**-NHBoc), 2.34 (t, *J* = 7.4 Hz, 2H, C**H_2**-COOH), 1.64 (quin, *J* = 7.4 Hz, 2H, -C**H_2**-CH_2-COOH), 1.52 – 1.32 (m, 13H); **^{13}C NMR** (101 MHz, $CDCl_3$) δ: 179.0 (HO-C=O), 156.0 (-N-C=O), 79.2 (-**C**-$(CH_3)_3$), 40.4 (**C**H_2-NH-), 33.9 (**C**H_2-COOH), 29.7 (-CH_2), 28.4 (3x -CH_3), 26.2 (-CH_2), 24.3 (CH_2).

Data are in accordance with those reported previously in literature.[342]

***tert*-Butyl (6-((6-(3,5-diethynylbenzamido)hexyl)amino)-6-oxohexyl)carbamate (48)**

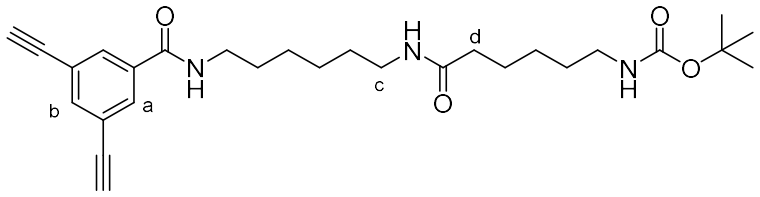

To a stirring solution of **47** (43 mg, 0.19 mmol) in dichloromethane (0.5 mL) were added PyAOP (0.149 g, 0.29 mmol) and **45** (50 mg, 0.19 mmol). The mixture was stirred at r.t. for 4 h before being concentrated *in vacuo*. The residue was purified through silica gel column chromatography (EtOAc) to give the title compound as a yellow amorphous solid (0.067 g, 74%).

R_f: 0.35 (EtOAc); **IR** (neat film, ν_{max}, cm^{-1}): 3288 (m, NH), 2932 (m), 2858 (m), 1683 (m, C=O), 1631 (s, C=O), 1586 (m, C=C), 1534 (s, C=C), 1463 (m, C=C), 1364 (m), 1248 (m), 1168 (s), 893 (m), 762 (w); **^{1}H NMR** (400 MHz, $CDCl_3$) δ: 7.89 (d, *J* = 1.4 Hz, 2H, Ha), 7.69 (t, *J* = 1.4 Hz, 1H, Hb), 6.65 (t, *J* = 5.0 Hz, 1H, Ar-CO-NH), 5.68 (br s, 1H, NH), 4.58 (br s, 1H, -NHBoc), 3.43 (dd, *J* = 6.7, 6.2 Hz, 2H, -C**H_2**-NHBoc), 3.24 (dd, *J* = 6.7, 6.2 Hz, 2H, Hc), 3.13 (s, 2H, -C≡C-H), 3.08 (dd, *J* = 6.5, 6.7 Hz, 2H, -C**H_2**-NCOAr), 2.17 (t, *J* =

7.4 Hz, 2H, Hd), 1.80 – 1.57 (m, 6H, 2 x CH_2 and NH_2), 1.54 – 1.25 (m, 17H, 4 x CH_2 and 3 x CH_3); **^{13}C NMR** (101 MHz, $CDCl_3$) δ: 173.0 (CH_2C=O), 165.8 (Ar-C=O), 156.1 (C=OBoc), 137.8 (Cb), 135.4 (Ar**C**-CON-), 130.8 (Ca), 123.0 (-**C**-C≡C-H), 81.8 (-**C**≡C-H), 79.1 (-**C**-(CH_3)$_3$), 78.9 (-C≡**C**-H), 40.4 (-**C**H_2-NCOAr), 39.6 (CH_2-NHBoc), 38.8 (Cc), 36.6 (Cd), 29.8, 29.5, 29.3, 28.3 (3 x CH_3), 26.4, 25.9, 25.8, 25.4; **HRMS**: *m/z* $[M+H]^+$ calculated for $C_{28}H_{40}N_3O_4$: 482.3013; Found: 482.3026.

***N*-(6-(6-aminohexanamido)hexyl)-3,5-diethynylbenzamide (49)**

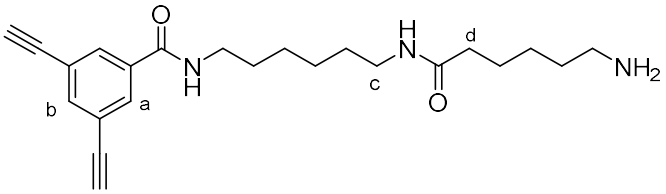

To a stirring solution of **48** (0.056 g, 0.12 mmol) in dichloromethane (1 mL) was added trifluoroacetic acid (1 mL). The mixture was stirred at r.t. for 3 h, before being concentrated *in vacuo*. The residue was purified through silica gel column chromatography (dichloromethane to 10:0.1:90 MeOH:NEt_3:dichloromethane) to give the title compound as a yellow oil (34 mg, 77%).

R_f: 0.10 (10:0.1:90 MeOH:NEt_3); **IR** (neat film, ν_{max}, cm^{-1}): 3291 (m, NH), 2935 (m), 1638 (s, C=O), 1583 (m, C=C), 1547 (s, C=C), 1462 (w, C=C), 1327 (w), 1201 (w), 1175 (w), 1024 (w); **^{1}H NMR** (400 MHz, DMSO-d6) δ: 8.65 – 8.63 (br m, 1H, NH), 7.94 (m, 2H, Ha), 7.78 – 7.73 (br m, 1H, NH), 7.69 (m, 1H, Hb), 4.38 – 4.36 (m, 2H, -C≡C-H), 3.26 – 3.20 (m, 2H, -C**H**$_2$-NCOAr), 3.03 – 2.95 (m, 2H, Hc), 2.65 (t, *J* = 7.3 Hz, 2H, -C**H**$_2$-NH_2), 2.07 – 2.00 (m, 2H, Hd), 1.49 – 1.21 (m, 16H, 7 x -CH_2 and -NH_2); **^{13}C NMR** (101 MHz, DMSO-d6) δ: 171.8 (-CH_2-**C**=O), 164.2 (Ar-C=O), 136.6 (Cb), 135.6 (Ar**C**-CON-), 130.8 (Ca), 122.6 (-**C**-C≡C-H), 82.5 (-C≡**C**-H), 81.9 (-**C**≡C-H), 39.8 (-**C**H_2-NH_2), 39.4 (-**C**H_2-NCOAr), 38.4 (C_c), 35.3 (Cd), 29.2, 29.1, 29.0, 26.2, 26.2, 25.8, 25.0; **HRMS**: *m/z* $[M+H]^+$ calculated for $C_{23}H_{32}N_3O_2$: 382.2489; Found: 382.2539.

4-(3-(4-cyano-3-(trifluoromethyl)phenyl)-5,5-dimethyl-4-oxo-2-thioxoimidazolidin-1-yl)-*N*-(6-((6-(3,5-diethynylbenzamido)hexyl)amino)-6-oxohexyl)-2-fluorobenzamide (50)

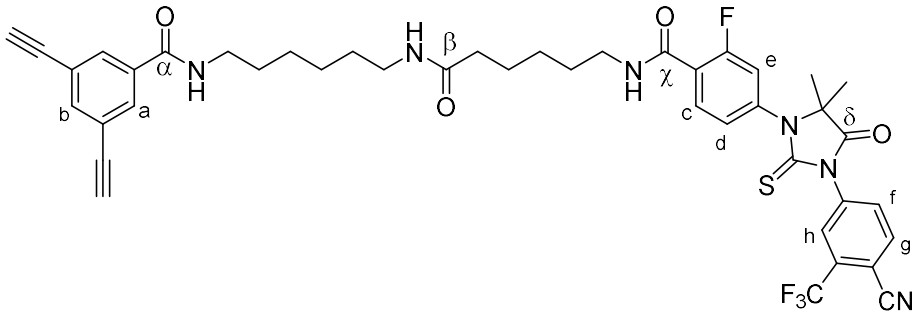

To a stirring solution of **2** (15 mg, 0.03 mmol) in dichloromethane (100 µL) was added PyAOP (26 mg, 0.05 mmol). The mixture was stirred at r.t. for 10 mins before a solution of **49** (13 mg, 0.03 mmol) in dichloromethane (100 µL) was added. The solution was stirred for a further 6 h at r.t. before being concentrated *in vacuo*. The residue was purified through silica gel column chromatography (dichloromethane to 10:0.1:90 MeOH:NEt_3:dichloromethane) to give the title compound as a yellow oil (6 mg, 22%).

R_f: 0.28 (EtOAc); **IR** (neat film, ν_{max}, cm^{-1}): 3293 (w, NH), 2930 (w), 2857 (w), 1756 (m, C=O), 1709 (m, C=O), 1642 (s, C=O), 1617 (m, C=O), 1585 (m, C=C), 1537 (m, C=C), 1499 (m, C=C), 1412 (s, C=C), 1310 (s), 1219 (s), 1176 (s), 1137 (s), 1056 (m), 923 (w), 893 (w), 840 (w), 813 (w), 678 (w); **^{1}H NMR** (500 MHz, $CDCl_3$) δ: 8.22 (t, *J* = 8.5 Hz, 1H, Hc), 7.99 (d, *J* = 8.0 Hz, 1H, Hg), 7.95 (d, *J* = 1.9 Hz, 1H, Hh), 7.88 (d, *J* = 1.5 Hz, 2H, Ha), 7.82 (dd, *J* = 8.0, 1.9 Hz, 1H, Hf), 7.69 (t, *J* = 1.5 Hz, 1H, Hb), 7.23 (dd, *J* = 8.5, 2.0 Hz, 1H, Hd), 7.14 (dd, *J* = 11.6, 2.0 Hz, 1H, He), 6.75 (dt, *J* = 11.3, 5.5 Hz, 1H, NH), 6.52 (t, *J* = 5.6 Hz, 1H, NH), 5.60 (t, *J* = 5.7 Hz, 1H, NH), 3.51 (dd, *J* = 13.0, 6.7 Hz, 2H, C**H**$_2$-NHαC=O), 3.44 (dd, *J* = 13.0, 7.0 Hz, 2H, C**H**$_2$-NH-δC=O), 3.27 (dd, *J* = 13.0, 6.7 Hz, 2H, C**H**$_2$-NH-Cβ), 3.13 (s, 2H, 2 x -C≡C-H), 2.21 (t, *J* = 6.9 Hz, 2H, -C**H**$_2$-Cβ-), 1.74 – 1.61 (m, 10H, 2 x CH_2 and 2 x CH_3), 1.53 – 1.36 (m, 8H, 4 x CH_2), 1.28 – 1.22 (m, 2H, CH_2); **^{13}C NMR** (126 MHz, $CDCl_3$) δ: 179.8 (C=S), 174.4 (βC=O), 172.9 (δC=O), 165.8 (αC=O), 162.1 (χC=O), 160.3 (d, *J* = 250 Hz, C-F), 138.9 (d, *J* = 9.7 Hz, **C**-Cχ), 137.9 (Cb), 136.8 (-**C**-CN), 135.4 (**C**-Cα), 135.3 (Cg), 133.7 (q, *J* = 34 Hz, -**C**-CF_3), 133.4 (Cc), 132.1 (Cf), 130.8 (Ca), 127.1 (q, *J* = 4.5 Hz, Ch), 126.2 (d, *J* = 2.1 Hz, Cd), 123.0 (-**C**-C≡C), 122.9 (d, *J* = 6.0 Hz, -**C**-N-C-$(CH_3)_2$),121.8 (q, *J* = 280 Hz, CF_3), 118.0 (d, *J* = 28 Hz, Ce), 114.7 (-C≡N), 110.5 (-**C**-NαCO-), 81.8 (-**C**≡C-H), 78.9 (-C≡**C**-H), 66.6 (-**C**-$(CH_3)_2$), 40.0 (C**H**$_2$-NHαC=O), 39.6 (C**H**$_2$-NH-δC=O), 38.8 (C**H**$_2$-NH-Cβ), 36.6 (C**H**$_2$-Cβ), 29.7, 29.5, 29.4, 29.2, 26.4, 25.8, 25.2, 23.9 (2 x CH_3); **^{19}F NMR** (376 MHz, $CDCl_3$) δ: -63.0 (CF_3), -111.5 (ArC-F); **HRMS**: *m/z* $[M+H]^+$ calculated for $C_{43}H_{43}F_4N_6O_4F$: 815.2997; Found: 815.2928.

(5S,8R,9S,10S,13S,14S,17S)-10,13-Dimethyl-3-oxohexadecahydro-1*H*-cyclopenta[*a*]phenanthren-17-yl 6-((*tert*-butoxycarbonyl)amino)hexanoate (52)

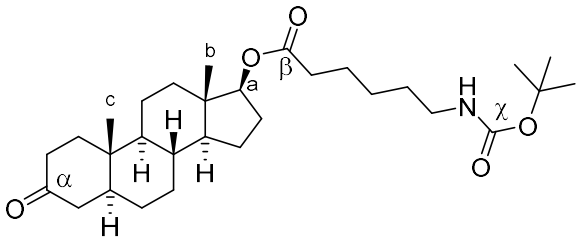

To a stirring solution of 5α-dihydrotestosterone (0.079 g, 0.34 mmol) in dichloromethane (1 mL) were added DCC (0.091 g, 0.44 mmol) and DMAP (0.006 g, 0.05 mmol). The mixture was stirred at r.t. for 3 h before DHT (0.100 g, 0.34 mmol) was added, and the solution was stirred for a further 6 h. The mixture was then filtered and concentrated *in vacuo*. The residue was purified through silica gel column chromatography (1:3 EtOAc:Hexane) to give the title compound as a colourless oil (0.170 g, 99%).

R_f: 0.67 (1:1 EtOAc:Hexane); **IR** (neat film, ν_{max}, cm^{-1}): 3373 (w, NH), 2937 (m), 1731 (m, C=O), 1718 (s, C=O), 1691 (m, C=O), 1520 (w), 1442 (w), 1365 (m), 1234 (m), 1218 (m), 1174 (m); **^{1}H NMR** (500 MHz, $CDCl_3$) δ: 4.60 (dd, *J* = 8.9, 8.1 Hz, 1H, Ha), 4.51 (br s, 1H, NH), 3.10 (dd, *J* = 12.6, 6.3 Hz, 2H, -C**H**$_2$-NH), 2.41 – 2.23 (m, 4H, CH_2-Cα and CH_2-Cβ), 2.18 – 1.99 (m, 4H, CH_2-Cα and 2 x DHT CH), 1.69 – 1.24 (m, 27H, including 3 x BocCH_3), 1.17 (dt, *J* = 12.8, 4.2 Hz, 1H, DHT-CH), 1.08 – 1.04 (m, 1H, DHT-CH), 1.01 (s, 3H, CcH_3), 0.96 – 0.88 (m, 1H, DHT-CH), 0.80 (s, 3H, CbH_3), 0.78 – 0.72 (m, 1H, DHT-CH); **^{13}C NMR** (126 MHz, $CDCl_3$) δ: 211.9 (αC=O), 173.6 (βC=O), 156.0 (χC=O), 82.5 (Ca), 79.1 (-**C**-$(CH_3)_3$), 53.7, 50.6, 46.6, 44.7 (**C**-Cα), 42.7, 40.4 (**C**H_2-NH), 38.5, 38.1 (**C**-Cα), 36.9, 35.7, 35.2, 34.4, 31.2, 29.8, 28.8, 28.4 (Boc 3 x CH_3), 27.6, 26.3, 24.7, 23.6, 20.9, 12.2 (**C**bH_3), 11.5 (**C**cH_3); **HRMS**: *m/z* $[M+H]^+$ calculated for $C_{30}H_{50}NO_5$: 504.3684; Found: 504.3688; **$[\alpha]_D^{20}$** 20.3 (c = 0.4, MeOH).

***tert*-Butyl 6-aminohexanoate (56)**

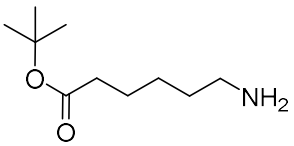

6-Aminohexanoic acid (1.00 g, 7.5 mmol) was dissolved in thionyl chloride (2.50 mL, 35 mmol) and stirred for 3 h at r.t. before being concentrated *in vacuo*. A slurry of $NaHCO_3$ (1.30 g, 15 mmol) in *tert*-butanol (2.5 mL) was then added and the reaction was stirred for a further 3 h at r.t. The reaction was then concentrated *in vacuo*, and dissolved in EtOAc (30 mL), before being washed with 1 M NaOH (4

x 25 mL), H_2O (3 x 25 mL), brine (25 mL), dried over $MgSO_4$, filtered, and concentrated *in vacuo* to give the title compound as a colourless oil (0.744 g, 53%) which was used directly with no further purification.

Rf: 0.18 (6% MeOH/DCM); **IR** (neat film, ν_{max}, cm^{-1}): 3267 (w, NH), 2980 (m, CH), 2933 (m, CH), 2865 (m, CH), 1726 (s, C=O), 1649 (m), 1554 (w), 1457 (w), 1391 (w), 1366 (s), 1254 (m), 1149 (s, C-O), 1107 (m); **^{1}H NMR** (400 MHz, CDCl3) δ: 2.71 (t, *J* = 7.1 Hz, 2 H, CH_2-N), 2.21 (t, *J* = 7.1 Hz, 2 H, CH_2-CO), 2.08 (br s, 2 H, NH_2), 1.59 (quin., *J* = 7.7 Hz, 2 H, CH_2), 1.51 – 1.43 (m, 11 H, 3 x CH_3 and CH_2), 1.38 – 1.30 (m, 2 H, CH_2); **^{13}C NMR** (101 MHz, CDCl3) δ: 173.3 (C=O), 80.2, 41.9, 35.6, 33.0, 28.2, 26.4, 25.0.

Data are in accordance with those reported previously in literature.[343]

tert-Butyl 6-(3,5-diethynylbenzamido)hexanoate (57)

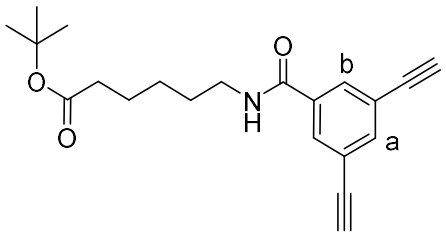

To a stirring solution of **6** (0.150 g, 0.88 mmol) in *N*,*N*-dimethylformamide (1.5 mL) were added PyAOP (0.573 g, 1.1 mmol) and **56** (0.181 g, 0.97 mmol). The mixture was stirred at r.t. for 18 h before concentrating *in vacuo*. The residue was purified through silica gel column chromatography (3:1 Hexane:EtOAc) to give the title compound as a colourless oil (0.220 g, 74%).

Rf: 0.50 (1% MeOH/DCM); **IR** (neat film, ν_{max}, cm^{-1}): 3294 (w, NH), 2980 (w, CH), 2934 (w, CH), 2865 (w, CH), 1722 (m, C=O), 1639 (m), 1585 (m), 1540 (m), 1455 (w), 1366 (m), 1320 (m), 1244 (m), 1148 (s), 1102 (w); **^{1}H NMR** (400 MHz, CDCl3) δ: 7.85 (d, *J* = 1.2 Hz, 2 H, Hb), 7.69 (s, 1 H, Ha), 6.36 (br s, 1 H, NH), 3.46 (q, *J* = 6.6 Hz, 2 H, CH_2-N), 3.13 (s, 2 H, C≡C-H), 2.24 (t, *J* = 7.2 Hz, 2 H, CH_2-CO), 1.66 – 1.58 (m, 4 H, 2 x CH_2), 1.43 – 1.36 (m, 11 H, 3 x CH_3 and CH_2); **^{13}C NMR** (101 MHz, CDCl3) δ: 173.3 (C=O), 165.8 (C=O), 138.0 (Cb), 135.5 (**C**-CON), 130.9 (Ca), 123.2 (**C**-C≡C-H), 81.9 (**C**≡C-H), 80.4 (C≡**C**-H), 39.9 (CH_2-N), 35.3 (CH_2-CO), 29.1, 28.3 (3 x CH_3), 26.3, 24.4; **HRMS** *m/z* $[M+Na]^+$ calculated for $C_{21}H_{25}NO_3Na$: 362.1726; Found: 362.1725

6-(3,5-Diethynylbenzamido)hexanoic acid (58)

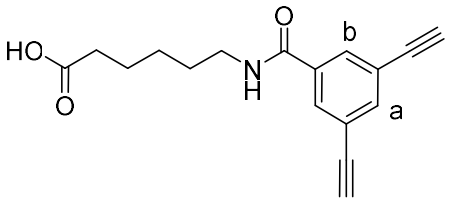

To a stirring solution of **57** (38 mg, 0.112 mmol) in dichloromethane (0.25 mL) was added trifluoroacetic acid (0.25 mL). The reaction was stirred for 2 h before being concentrated *in vacuo* to give the title compound as a white amorphous solid (31 mg, 97%) which was used directly with no further purification.

Rf: 0.25 (1% MeOH/DCM); **IR** (neat film, ν_{max}, cm^{-1}): 3233 (m, NH), ~3000 (br w, OH), 2943 (w, CH), 1712 (s, C=O), 1652 (s), 1628 (s), 1583 (m), 1551 (m), 1521 (s), 1406 (w), 1372 (w), 1252 (w), 1185 (s), 1102 (m); **^{1}H NMR** (400 MHz, MeOD) δ: 7.89 (d, *J* = 1.3 Hz, 2 H, Hb), 7.66 (s, 1 H, Ha), 3.66 (s, 2 H, C≡C-H), 3.36 (t, *J* = 7.0 Hz, 2 H, CH_2-N), 2.31 (t, *J* = 7.3 Hz, 2 H, CH_2-COOH), 1.69 – 1.59 (m, 4 H, 2x CH_2), 1.45 – 1.38 (m, 2 H, CH_2); **^{13}C NMR** (101 MHz, MeOD) δ: 176.1 (C=O), 166.6 (C=O), 137.1 (Cb), 135.3 (C-CON), 130.4 (Ca), 123.2 (**C**-C≡C-H), 81.1 (**C**≡C-H), 79.2 (**C**≡C-H), 39.5 (CH_2-N), 33.3 (CH_2-COOH), 28.6, 26.2, 24.3 (3x CH_2); **HRMS:** *m/z* $[M-H]^-$ calculated for $C_{17}H_{16}NO_3$: 282.1135; Found: 282.1135

***tert*-butyl 6-(6-(3,5-diethynylbenzamido)hexanamido)hexanoate (60)**

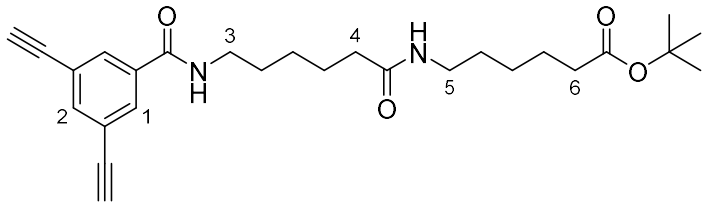

To a stirring solution of **58** (50 mg, 0.176 mmol) in *N*,*N*-dimethylformamide (0.1 mL) were added PyAOP (0.110 g, 0.21 mmol) and **56** (35 mg, 0.185 mmol). The mixture was stirred at r.t. for 18 h before concentrating *in vacuo*. The residue was purified through silica gel column chromatography (1:1 Hexane:EtOAc) to give the title compound as a colourless oil (38 mg, 48%).

Rf: 0.29 (2% MeOH/DCM); **IR** (neat film, ν_{max}, cm^{-1}): 3290 (m, NH), 2934 (m, CH), 2864 (w, CH), 1717 (m, C=O), 1638 (s), 1585 (m), 1539 (s), 1455 (m), 1366 (m), 1322 (m), 1245 (m), 1149 (s); **^{1}H NMR** (400 MHz, CDCl3) δ: 7.91 (d, *J* = 1.5 Hz, 2 H, H1), 7.69 (t, *J* = 1.5 Hz, 1 H, H2), 6.65 (br s, 1 H, NH), 5.58 (br s, 1 H, NH), 3.48 (q, *J* = 6.9 Hz, 2 H, H3), 3.25 (q, *J* = 6.6 Hz, 2 H, H5), 3.13 (s, 2 H, C≡C-H), 2.22 – 2.18 (m,

4 H, C4 and C6), 1.71 – 1.63 (m, 4 H, 2x CH_2), 1.61 – 1.37 (m, 15 H, 3x CH_3 and 3x CH_2), 1.35 – 1.30 (m, 2 H, CH_2); **^{13}C NMR** (101 MHz, CDCl3) δ: 173.1 (C6-**C**=O), 172.8 (C4-**C**=O), 165.7 (Ar-C=O), 137.8 (C2), 135.4 (Ar**C**-CON), 130.9 (C1), 123.0 (-**C**-C≡), 81.8 (**C**≡C-H), 80.2 (**C**-$(CH_3)_3$), 78.8 (C≡**C**-H), 39.5 (C3), 39.2 (C5), 36.1, 35.3 (C4 and C6), 29.2, 28.7, 28.1 (3 x CH_3), 26.3, 26.0, 24.5, 24.4; **HRMS**: *m/z* $[M+K]^+$ calculated for $C_{27}H_{36}N_2O_4K$: 491.2307; Found: 491.2299

6-(6-(3,5-Diethynylbenzamido)hexanamido)hexanoic acid (61)

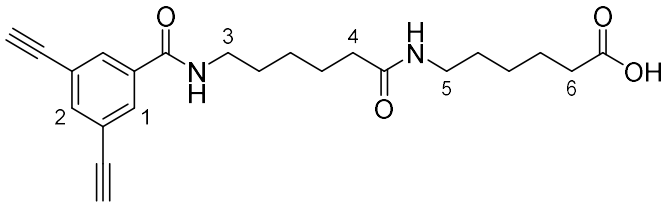

To a stirring solution of **60** (42 mg, 0.093 mmol) in dichloromethane (0.25 mL) was added trifluoroacetic acid (0.25 mL). The reaction was stirred for 2 h before being concentrated *in vacuo* to give the title compound as a white amorphous solid (36 mg, 98%) which was used directly with no further purification.

Rf: 0.09 (1:1 EtOAc/Hex + 2% AcOH); **IR** (neat film, ν_{max}, cm^{-1}): 3283 (m, NH), 3194 (w, CH), 2946 (w, CH), 2867 (w, CH), 1734 (m, C=O), 1638 (s), 1582 (m), 1533 (s), 1458 (m), 1412 (m), 1390 (m), 1328 (m), 1299 (m), 1257 (m), 1205 (m), 1186 (m), 1169 (m); **^{1}H NMR** (400 MHz, MeOD) δ: 7.90 (d, *J* = 1.5 Hz, 2 H, H1), 7.66 (t, *J* = 1.5 Hz, 1 H, H2), 3.66 (s, 2H, ≡C-H), 3.36 (t, *J* = 7.0 Hz, 2 H, H3), 3.15 (t, *J* = 7.0 Hz, 2 H, H5), 2.26 – 2.17 (m, 4 H, H4 and H6), 1.67 – 1.58 (m, 6 H, 3x CH_2), 1.51 – 1.48 (m, 2 H, CH_2), 1.41 – 1.32 (m, 4 H, 2x CH_2); **^{13}C NMR** (101 MHz, MeOD) δ: 178.1 (acid C=O), 174.6 (C4-**C**=O), 166.6 (Ar-C=O), 137.1 (C2), 135.3 (Ar**C**-CON), 130.4 (C1), 123.2 (-**C**-C≡), 81.1 (**C**≡C-H), 79.2 (C≡**C**-H), 39.5 (C3), 38.8 (C5), 35.6, 34.9 (C4 and C6), 28.7, 28.6, 26.3, 26.1, 25.3, 24.9 (6x CH_2); **HRMS**: *m/z* $[M-H]^-$ calculated for $C_{23}H_{27}N_2O_4$: 395.1976; Found: 395.1970

(5*S*,8*R*,9*S*,10*S*,13*S*,14*S*,17*S*)-10,13-dimethyl-3-oxohexadecahydro-1*H*-cyclopenta[*a*]phenanthren-17-yl 6-(6-(3,5-diethynylbenzamido)hexanamido)hexanoate (59)

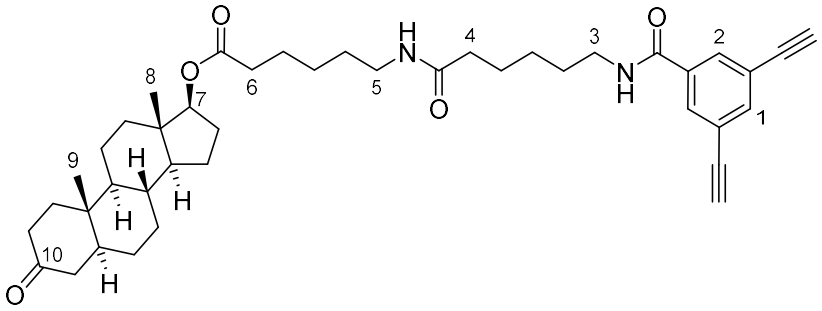

To a stirring solution of **61** (12 mg, 0.0303 mmol) in DMF (0.1 mL) were added *N*,*N*'-dicyclohexylcarbodiimide (8 mg, 0.039 mmol), and 4-dimethylaminopyridine (0.6 mg, 0.0045 mmol). The mixture was stirred at r.t. for 3 h before dihydrotestosterone (10 mg, 0.033 mmol) was added and the reaction was stirred for a further 18 h. The mixture was then concentrated and triturated in dichloromethane. The residue was purified through silica gel column chromatography (9:1 Hexane:EtOAc to EtOAc) to give the title compound as a colourless oil (4 mg, 20%).

Rf: 0.50 (EtOAc); **IR** (neat film, ν_{max}, cm^{-1}): 3301 (w, NH), 2926 (m, CH), 2854 (m, CH), 1709 (m, C=O), 1640 (s), 1583 (m), 1541 (s), 1447 (m), 1379 (w), 1318 (m), 1250 (m), 1171 (m), 1088 (w), 1026 (w); **^{1}H NMR** (500 MHz, CDCl3) δ: 7.91 (d, *J* = 1.5 Hz, 2 H, H2), 7.70 (s, 1 H, H1), 6.59 (br s, 1 H, NH), 5.52 (br s, 1 H, NH), 4.59 (t, *J* = 8.5 Hz, 1 H, H7), 3.48 (q, *J* = 6.6 Hz, 2 H, H3), 3.26 (q, *J* = 6.8 Hz, 2 H, H5), 3.13 (s, 2 H, ≡C-H), 2.42 – 1.93 (m, 10 H), 1.75 – 1.60 (m, 8 H), 1.54 – 1.27 (m, 15 H), 1.18 – 0.99 (m, 5 H), 0.93 – 0.71 (m, 6 H); **^{13}C NMR** (126 MHz, CDCl3) δ: 211.9 (C10), 173.7 (C=O ester), 172.8 (C=O amide), 165.6 (Ar-C=O), 137.8 (C1), 135.3 (Ar**C**-CON), 130.8 (C2), 123.0 (-**C**-C≡), 82.6 (C7), 81.8 (**C**≡C-H), 78.8 (C≡**C**-H), 53.7, 50.6, 46.6, 44.6, 42.7, 39.5 (C3), 39.2 (C5), 38.5, 38.1, 36.9, 36.1, 35.7, 35.2, 34.3, 31.2, 29.7, 29.3, 28.8, 28.7, 27.6, 26.3, 26.0, 24.6, 23.5, 20.9, 12.2 (C8), 11.5 (C9); **HRMS**: *m/z* $[M+H]^+$ calculated for $C_{42}H_{57}N_2O_5$: 669.4262; Found: 669.4258; **$[\alpha]_D^{25}$:** +154.2 (c = 0.048, MeOH)

2-azido-1-(4-chlorophenyl)ethan-1-ol (66)

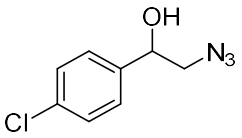

Following a modified version of a reported procedure,[344] to a stirring solution of 2-bromo-4'-chloroacetophenone (1.17 g, 5.0 mmol) in dimethylsulfoxide (20 mL) was added sodium azide (0.65 g, 10.0 mmol). The mixture was stirred at r.t. for 30 mins before being extracted with Et_2O (3 x 20 mL), washed with H_2O (40 mL), and brine (40 mL), dried over Na_2SO_4, filtered, and concentrated *in vacuo*. The crude oil was immediately dissolved in methanol (20 mL), and sodium borohydride (0.378 g, 10.0 mmol) was added and the reaction was stirred at r.t. for 1 h. The mixture was then extracted with DCM (3 x 20 mL), washed with H_2O (40 mL), and brine (40 mL), dried over Na_2SO_4, filtered, and concentrated *in vacuo* to give the title compound as an orange oil (0.692 g, 70%).

Rf: 0.79 (1:1 EtOAc:Hex); **IR** (neat film, ν_{max}, cm^{-1}): 3384 (br w, OH), 2917 (w, CH), 2099 (s, N_3), 1597 (w, C=C), 1491 (m), 1254 (m), 1088 (s), 1013 (s); **^{1}H NMR** (400 MHz, $CDCl_3$) δ: 7.35 (d, *J* = 8.5 Hz, 2H), 7.30 (d, *J* = 8.5 Hz, 2H), 4.84 (dd, *J* = 5.4, 6.7 Hz, 1H), 3.47 – 3.40 (m, 2H), 2.54 (br s, 1H); **^{13}C NMR** (101 MHz, $CDCl_3$) δ: 139.1, 134.2, 129.0, 127.4, 72.8, 58.1;

The spectroscopic data are in agreement with those previously reported in the literature.[345]

tert-Butyl pent-4-yn-2-ylcarbamate (67)

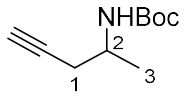

To a stirring solution of pent-4-yn-2-amine (190 mg, 2.3 mmol) in THF (5 mL) was added di-*tert*-butyl dicarbonate (0.523 mL, 2.3 mmol). The mixture was stirred at r.t. for 3 h before concentrating *in* vacuo. The residue was purified through silica gel column chromatography (1:19 to 1:9 EtOAc:Hexane) to give the title compound as a colourless oil (175 mg, 42%)

Rf: 0.41 (1:9 EtOAc:Hexane); **IR** (neat film, ν_{max}, cm^{-1}): 3305 (w, NH), 2977 (w, CH), 2931 (w), 1686 (s, C=O), 1504 (s), 1454 (m), 1391 (m), 1365 (s), 1247 (s), 1159 (s), 1053 (s); **^{1}H NMR** (400 MHz, $CDCl_3$) δ: 4.64 (br s, 1H, NH), 3.83 (br s, 1H, H2), 2.44 – 2.30 (m, 2H, H1), 1.99 (t, *J* = 2.7 Hz, 1H, C≡C-H), 1.42 (s, 9H, Boc-3x CH_3), 1.21 (d, *J* = 6.5 Hz, 3H, H3); **^{13}C NMR** (101 MHz, $CDCl_3$) δ: 155.2 (C=O), 80.6 (**C**≡C-H), 79.4 (C≡**C**-H), 70.8 (qC), 44.7 (C2), 28.5 (Boc-CH_3), 26.3 (C1), 19.9 (C3); **HRMS** (ESI): m/z calcd for $C_{10}H_{17}NO_2Na$ $[M+Na]^+$: 206.1152; found: 206.1149

***tert*-butyl (1-(1-(2-(4-chlorophenyl)-2-hydroxyethyl)-1*H*-1,2,3-triazol-5-yl)propan-2-yl)carbamate (74)**

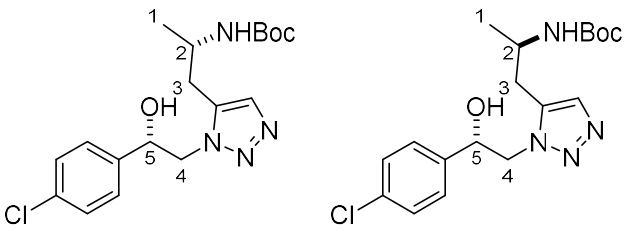

To a stirring solution of chloro(pentamethylcyclopentadienyl)(cyclooctadiene)ruthenium(II) (0.6 mg, 0.0016 mmol) in degassed toluene (0.2 mL) were added **67** (15 mg, 0.08 mmol) and **66** (16.2 mg, 0.08 mmol). The mixture was heated to 75 °C for 2 h before being cooled and concentrated *in vacuo*. The residue was purified through silica gel column chromatography (8:2 EtOAc:Hexane) to give the title compounds, an inseparable mixture of diastereoisomers (d.r. 1:1 determined by ^{1}H NMR) as a colourless oil (29 mg, 94%).

Rf: 0.29 (8:2 EtOAc/PE 40-60); **IR** (neat film, ν_{max}, cm^{-1}): 3306 (br m, NH), 2975 (m, CH), 1688 (s, C=O), 1518 (m, C=C), 1494 (m, C=C), 1454 (m, C=C), 1366 (m), 1248 (m), 1167 (s), 1089 (m); Data reported for mixture of isomers; **^{1}H NMR** (400 MHz, $CDCl_3$) δ: 7.45 – 7.32 (m, 10H, Ar-H), 5.32 (dd, *J* = 8.7, 2.4 Hz, 1H, H5), 5.25 (dd, *J* = 8.7, 2.4 Hz, 1H, H5), 4.69 – 4.21 (m, 8H, H2, H3, NH), 3.91 – 3.77 (m, 2H, OH), 2.88 – 2.75 (m, 2H, H4), 2.70 – 2.64 (m, 2H, H4), 1.41 – 1.37 (2 x s, 18H, Boc-CH_3), 1.19 – 1.13 (2 x d, *J* = 6.7 Hz, 6H, H1); **^{13}C NMR** (101 MHz, $CDCl_3$) δ: 155.5, 155.5 (C=O), 139.1, 138.9 (qC), 134.0, 133.9 (Ar-H), 128.9, 128.8 (Ar-H), 128.8, 128.7 (qC), 127.5, 127.4 (Ar-H), 80.2, 80.1 (qC), 72.7, 72.6 (C5), 55.3, 54.7 (C3), 45.8, 45.8 (C2), 31.0, 30.5 (C4), 28.3, 28.3 (Boc-CH_3), 20.3, 19.7 (C1); **HRMS** (ESI): m/z calcd for $C_{18}H_{26}ClN_4O_3$ $[M+H]^+$: 381.1688; found: 381.1692

2-(5-(2-aminopropyl)-1*H*-1,2,3-triazol-1-yl)-1-(4-chlorophenyl)ethan-1-ol (62)

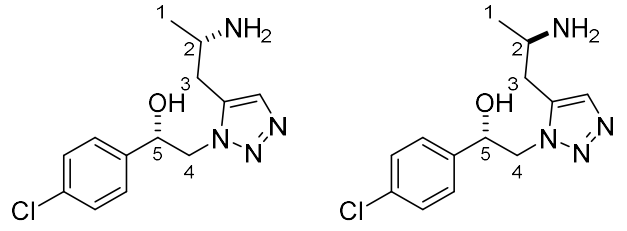

To a stirring solution of **74** (24 mg, 0.06 mmol) in dichloromethane (0.4 mL) was added trifluoroacetic acid (0.1 mL). The mixture was stirred at r.t. for 4 h before diluting in sat. aq. $NaHCO_3$ (4 mL) and extracting into dichloromethane (3 x 10 mL). The combined organics were dried over Na_2SO_4, filtered

and concentrated *in vacuo* to give the title compounds as an inseparable mixture of diastereoisomers (d.r. 1:1 determined by ^{1}H NMR) as a colourless oil (11.5 mg, 65%) which required no further purification.

IR (neat film, ν_{max}, cm^{-1}): 3083 (br m, OH), 2925 (CH), 1676 (m), 1597, 1547 (m), 1491 (m), 1456 (m), 1394 (m), 1242 (m), 1202 (m), 1089 (s), 1014 (m); Data reported for mixture of isomers; **^{1}H NMR** (500 MHz, $CDCl_3$) δ: 7.51 (d, *J* = 11.6 Hz, 2H, Ar-H), 7.41 (d, *J* = 8.4 Hz, 2H, Ar-H), 7.36 – 7.32 (m, 6H, Ar-H), 5.23 (dd, *J* = 8.7, 2.6 Hz, 1H, H5), 5.14 – 5.13 (m, 1H, H5), 4.62 (dd, *J* = 14.6, 1.9 Hz, 1H, H3), 4.51 (dd, *J* = 14.6, 2.3 Hz, 1H, H3), 4.32 – 4.23 (m, 2H, H2), 3.38 – 3.31 (m, 2H, OH), 3.31 – 3.16 (m, 4H, NH_2), 2.82 – 2.75 (m, 3H, H4), 2.71 – 2.67 (m, 1H, H4), 1.27 (d, *J* = 6.4 Hz, 3H, H1), 1.21 (d, *J* = 6.4 Hz, 3H, H1); **^{13}C NMR** (126 MHz, $CDCl_3$) δ: 139.5, 139.3 (qC), 136.0, 134.9 (qC), 134.0, 133.9 (qC), 133.2, 132.6 (Ar-H), 129.0 (Ar-H), 127.5, 127.4 (Ar-H), 72.8, 72.4 (C5), 56.7, 55.6 (C3), 47.3, 46.1 (C2), 32.0, 31.6 (C4), 23.3 (C1); **HRMS** (ESI): m/z calcd for $C_{13}H_{18}ClN_4O$ $[M+H]^+$: 281.1164; found: 281.1166

(*E*)-1-cyclohexyl-*N*-(4-methoxyphenyl)methanimine (75) and *N*-(1-cyclohexylbuta-2,3-dien-1-yl)-4-methoxyaniline (76)

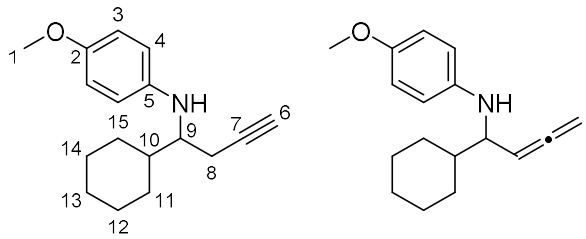

To a stirring solution of *p*-anisidine (0.246 g, 2.0 mmol) in dichloromethane (10 mL) were added magnesium sulfate (2.0 g) and **63** (0.24 mL, 2.0 mmol). The mixture was stirred at r.t. for 1 h before being filtered through Celite®, washed with dichloromethane (10 mL), and concentrated *in vacuo*. The crude residue was dissolved in DMF (18 mL) and cooled to 0 °C, before propargyl bromide (80% in toluene 0.30 mL, 2.7 mmol) and activated zinc (0.241 g, 3.7 mmol) were added. After stirring at r.t. for 1 h the mixture was cooled to 0 °C and quenched with sat. aq. NH_4Cl (25 mL). The mixture was then extracted into EtOAc (3 x 25 mL), washed with brine (25 mL), dried over Na_2SO_4, filtered and concentrated *in vacuo* to give the title compounds as an inconsequential mixture of allene:alkyne (ratio of 0.56:1 determined by ^{1}H NMR), isolated as a yellow oil (0.323 g, 63%).

Rf: 0.24 (1:19 EtOAC:PE 40-60); **IR** (neat film, ν_{max}, cm^{-1}): 3292 (w, NH), 2925 (m, CH), 2852 (m), 1510 (s), 1449 (w), 1234 (m), 1179 (w), 1038 (w); Reported as 0.56:1 allene:alkyne mixture; **^{1}H NMR** (400 MHz, $CDCl_3$) δ: 6.79 – 6.76 (m, 3H, H3/4), 6.61 (m, 3H, H3/4), 5.05 (dd, *J* = 6.7, 13.5 Hz, 0.56 H, allene-

H), 4.81 – 4.72 (m, 1.2 H, 2 x allene-H), 3.75 (s, 4.5H, H1) 3.68 – 3.48 (m, 2H), 3.23 – 3.19 (m, 1H), 2.51 – 2.39 (m, 2H, alkyne-CH_2), 1.98 (t, *J* = 2.6 Hz, 1H, alkyne-H), 1.90 – 1.52 (m, 8.5H), 1.34 – 0.98 (m, 7.9H); **^{13}C NMR** (101 MHz, $CDCl_3$) δ: 208.3 (allene =C=), 152.2 (C2), 142.0 (C5), 115.2, 115.1, 114.9 (C3/C4), 91.9 (allene), 81.5 (alkyne), 76.5 (allene), 70.3 (alkyne), 58.8, 57.7 (C9), 55.9 (C1), 43.2, 40.9 (C10), 30.1 (C8), 29.7, 29.4, 29.3, 26.7, 26.6, 26.4, 26.4, 26.3, 21.2 (C11-15); **HRMS** (ESI): m/z calcd for $C_{17}H_{24}NO$ $[M+H]^+$: 258.1858; found: 258.1866

***tert*-Butyl (1-cyclohexylbut-3-yn-1-yl)carbamate (68)**

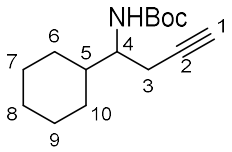

To a stirring solution of **75** (0.296 g, 1.15 mmol) in acetonitrile (8 mL) cooled to 0 °C, was dropwise added a solution of ammonium cerium(IV) nitrate (1.26 g, 2.3 mmol) in water (8 mL). The reaction was stirred for 2 h at r.t. before being treated with 2 M HCl to pH 1. The aqueous phase was then washed with EtOAc (3 x 10 mL), and then taken to basic by addition of Na_2CO_3. The suspension was then extracted with dichloromethane (3 x 30 mL), dried over Na_2SO_4, filtered, and concentrated *in vacuo*. The crude residue was then dissolved in THF (2 mL) and di-*tert*-butyl decarbonate (0.26 mL, 1.15 mmol) was added. The mixture was stirred at r.t. for 3 h before concentrating *in vacuo*. The residue was purified through silica gel column chromatography (1% EtOAc/PE 40-60) to give the title compound as a colourless oil (85 mg, 29%).

Rf: 0.15 (1% EtOAc/PE 40-60); **IR** (neat film, ν_{max}, cm^{-1}): 2984 (w, CH), 2937 (w), 1799 (m), 1755 (m), 1460 (w), 1396 (w), 1371 (m), 1306 (w), 1262 (w), 1210 (m), 1111 (s), 1056 (s); **^{1}H NMR** (400 MHz, $CDCl_3$) δ: 4.62 (d, *J* = 8.7 Hz, 1H, NH), 3.53 – 3.49 (m, 1H, H4), 2.43 – 2.41 (m, 2H, H3), 1.96 (t, *J* = 2.6 Hz, 1H, H1), 1.82 – 1.62 (m, 6H), 1.43 (s, 9H, 3x CH_3), 1.28 – 1.08 (m, 3H), 1.03 – 0.92 (m, 2H); **^{13}C NMR** (101 MHz, $CDCl_3$) δ: 155.8 (C=O), 80.9 (Boc-qC), 79.3 (**C**≡C-H), 70.5 (C≡**C**-H), 53.3 (C4), 40.5 (C5), 30.0 (C3), 29.0, 28.5 (Boc-CH_3), 26.4, 26.2, 26.1, 22.4; **HRMS** (ESI): mass not found.

***tert*-butyl (2-(1-(2-(4-chlorophenyl)-2-hydroxyethyl)-1*H*-1,2,3-triazol-5-yl)-1-cyclohexylethyl) carbamate (79)**

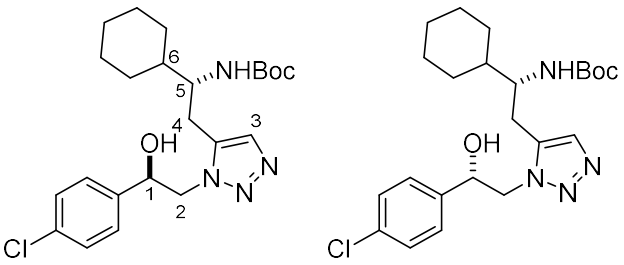

To a stirring solution of chloro(pentamethylcyclopentadienyl)(cyclooctadiene)ruthenium(II) (1.0 mg, 0.002 mmol) in degassed toluene (0.5 mL) were added **68** (25 mg, 0.1 mmol) and **66** (20 mg, 0.1 mmol). The mixture was heated to 70°C for 2 h before being cooled and concentrated *in vacuo*. The residue was purified through silica gel column chromatography (1:1 EtOAc:Hexane) to give the title compound as an inseparable mixture of diastereoisomers (d.r. 1:1 determined by ^{1}H NMR) as a colourless oil (42 mg, 94%).

Rf: 0.10 (1:1 EtOAc:Hexane); **IR** (neat film, ν_{max}, cm^{-1}): 3307 (w, NH), 2925 (s, CH), 2853 (m, CH), 1685 (s, C=O), 1520 (m), 1493 (m), 1450 (m), 1391 (m), 1366 (m), 1249 (m), 1169 (s), 1089 (m), 1014 (m); Data reported for the mixture of isomers; **^{1}H NMR** (400 MHz, $CDCl_3$) δ: 7.45 – 7.40 (m, 4H), 7.36 – 7.32 (m, 6H), 5.36 – 5.26 (m, 2H, H1), 4.87 (d, *J* = 3.2 Hz, 1H), 4.52 – 4.44 (m, 4H, H4), 4.38 – 4.33 (m, 1H, H5), 4.27 – 4.22 (m, 1H, H5), 4.01 (d, *J* = 4.1 Hz, 1H), 3.78 – 3.73 (m, 1H), 3.69 – 3.62 (m, 1H), 2.79 – 2.73 (m, 2H, H2), 2.65 – 2.56 (m, 2H, H2), 1.81 – 1.68 (m, 12H, 6x CH_2), 1.36 – 1.33 (2 x s, 18H, Boc-CH_3), 1.25 – 0.97 (m, 10H, 5x CH_2); **^{13}C NMR** (101 MHz, $CDCl_3$) δ: 156.1, 155.8 (C=O), 139.0 (qC), 135.2, 135.1 (qC), 134.0, 133.8 (Ar-H), 133.5, 133.4 (qC), 128.9, 128.8 (Ar-H), 127.4 (Ar-H), 80.2, 79.9 (Boc-qC), 72.58, 72.5 (C1), 55.7, 54.8 (C4), 54.2, 53.9 (C5), 41.4, 40.9 (C6), 30.0, 29.9 (C2), 28.4, 28.3, 28.3 (Boc-CH_3), 27.9, 26.7, 26.2, 26.0, 26.0; **HRMS** (ESI): m/z calcd for $C_{23}H_{34}ClN_4O_3$ $[M+H]^+$: 449.2314; found: 449.2298

2-(5-(2-amino-2-cyclohexylethyl)-1*H*-1,2,3-triazol-1-yl)-1-(4-chlorophenyl)ethan-1-ol (63)

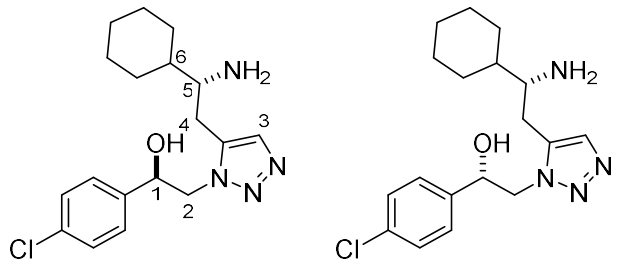

To a stirring solution of **79** (18 mg, 0.06 mmol) in dichloromethane (0.2 mL) was added trifluoroacetic acid (0.05 mL). The mixture was stirred at r.t. for 4 h before diluting in sat. aq. $NaHCO_3$ (4 mL) and extracting into dichloromethane (3 x 10 mL). The combined organics were dried over Na_2SO_4, filtered and concentrated *in vacuo* to give the title compound as an inseparable mixture of diastereoisomers (d.r. 1:1 determined by ^1H NMR) as a colourless oil (13.1 mg, 94%) which required no further purification.

IR (neat film, ν_{max}, cm^{-1}): 3219 (br, w, OH), 2925 (s, CH), 2852 (m, CH), 1664 (w), 1593 (w), 1548 (w), 1491 (m), 1449 (m), 1406 (w), 1240 (w), 1089 (m), 1014 (m); Data reported for the mixture of isomers; **^{1}H NMR** (400 MHz, $CDCl_3$) δ: 7.52 – 7.32 (m, 10H, Ar-H), 5.22 (dd, *J* = 8.2, 2.8 Hz, 1H, H1), 5.12 (dd, *J* = 9.0, 1.5 Hz, 1H, H1), 4.65 (dd, *J* = 14.4, 2.0 Hz, 1H), 4.53 (dd, *J* = 14.4, 2.8 Hz, 1H), 4.38 – 4.32 (m, 1H), 4.25 – 4.19 (m, 1H), 2.91 – 2.62 (m, 10H), 1.79 – 1.70 (m, 10H), 1.43 – 1.41 (m, 1H), 1.34 – 0.95 (m, 13H); **^{13}C NMR** (101 MHz, $CDCl_3$) δ: 139.6, 139.3 (qC), 136.6, 135.7 (qC), 133.8, 133.7 (Ar-H), 132.7, 132.3 (qC), 128.8 (Ar-H), 127.3, 127.3 (Ar-H), 72.8, 72.3 (C1), 56.9, 56.4 (C4), 55.6, 55.2 (C5), 43.5, 43.3 (C6), 29.7, 29.6 (C2), 29.3, 28.7, 28.6, 27.6, 27.4, 26.3, 26.3, 26.2, 26.1, 26.1; **HRMS** (ESI): m/z calcd for $C_{18}H_{26}ClN_4O$ $[M+H]^+$: 349.1790; found: 349.1793

***N*-cyclohexylidene-2-methylpropane-2-sulfinamide (80)**

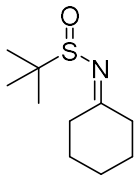

Following a modified version of a reported procedure[346], To a stirring solution of cyclohexanone (0.912 mL, 8.8 mmol) in DCM (22 mL) were added 2-methyl-2-propanesulfinamide (0.968 g, 8.0 mmol) and titanium (IV) ethoxide (3.32 mL, 16 mmol). The mixture was heated to 45 °C for 2 h before methanol (5 mL) was added, followed by $NaHCO_3$ added dropwise until precipitation of titanium salts. The mixture was then filtered through Na_2SO_4, washed with EtOAc, and concentrated *in vacuo*. The residue was purified through silica gel column chromatography (7:13 EtOAc:Hexane) to give the title compound as a yellow oil (1.095 g, 62%).

Rf: 0.75 (1:1 EtOAc:Hex); **IR** (neat film, ν_{max}, cm^{-1}): 2962 (w), 2924 (w), 2869 (w), 1673 (w), 1472 (w), 1456 (w), 1363 (m), 1297 (s), 1218 (w), 1181 (w), 1124 (s); **^{1}H NMR** (400 MHz, $CDCl_3$) δ: 2.92 – 2.85 (m, 1H), 2.75 – 2.68 (m, 1H), 2.42 (t, *J* = 6.4 Hz, 2H), 1.84 – 1.61 (m, 6H), 1.22 (s, 9H); **^{13}C NMR** (101 MHz, $CDCl_3$) δ: 188.8, 56.1, 40.8, 34.5, 28.0, 27.5, 25.5, 22.2

The spectroscopic data are in agreement with those previously reported in the literature.[347]

2-methyl-*N*-(1-(prop-2-yn-1-yl)cyclohexyl)propane-2-sulfinamide (81)

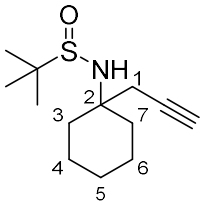

To a stirring solution of magnesium turnings (10.3 g, 424 mmol) and zinc bromide (1.90 g, 8.44 mmol) in Et_2O (120 mL) was carefully added 3-bromopropyne (80% wt. in tol, 15.9 mL, 184 mmol). The mixture was then stirred at r.t. for 1 h, and then titrated using (-)-menthol and 1,10-phenanthroline in THF to give a concentration of 0.10 M. **80** (0.550 g, 2.7 mmol) was dissolved in DCM (19 mL) and cooled to -78 °C before the Grignard solution (30 mL) was added slowly. After stirring for 1 h, the solution was quenched with sat. aq. NH_4Cl (10 mL) and warmed to r.t. The mixture was then extracted with EtOAc (3 x 20 mL), dried over Na_2SO_4, filtered, and concentrated *in vacuo* to give the title compound as a yellow oil (0.639 g, 97%) which required no further purification.

Rf: 0.35 (1:1 EtOAc:Hex); **IR** (neat film, ν_{max}, cm^{-1}): 3308 (w, NH), 3225 (w, NH), 2929 (m, CH), 2859 (m, CH), 1473 (w), 1453 (w), 1362 (w) 1184 (w), 1154 (w), 1052 (s); **^{1}H NMR** (400 MHz, $CDCl_3$) δ: 3.49 (s, 1H, NH), 2.62 (dd, *J* = 16.5, 2.6 Hz, 1H, H1), 2.40 (dd, *J* = 16.5, 2.6 Hz, 1H, H1), 2.06 (t, *J* = 2.6 Hz, 1H, C≡C-H), 1.95 – 1.92 (m, 1H, H3), 1.78 – 1.32 (m, 9H, H3 – H7), 1.23 (s, 9H); **^{13}C NMR** (101 MHz, $CDCl_3$) δ: 80.7 (**C**≡C-H), 71.8 (C≡**C**-H), 56.4 (C2), 56.0 (qC), 37.2, 34.7 (C3/C7), 32.7 (C1), 25.6 (C5), 22.9 (CH_3), 21.8, 21.7 (C4/C6); **HRMS** (ESI): m/z calcd for $C_{13}H_{23}NOSNa$ $[M+Na]^+$: 264.1392; found: 264.1381

***tert*-butyl (1-(prop-2-yn-1-yl)cyclohexyl)carbamate (69)**

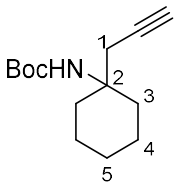

To a stirring solution of **81** (0.611 g, 2.5 mmol) in methanol (25 mL) was carefully added hydrochloric acid (4 M in dioxane, 6.33 mL). The mixture was then heated to 90 °C for 2 h before being cooled to r.t. and concentrated *in vacuo*. $NaHCO_3$ (sat. aq. 5 mL) was added and the mixture was extracted with

DCM (3 x 15 mL), dried over Na_2SO_4, filtered and concentrated *in vacuo*. The crude amine was then dissolved in THF (10 mL) and di-*tert*-butyl decarbonate (0.58 mL, 2.5 mmol) was added. The solution was stirred at r.t. for 4 h before concentrating *in vacuo*. The residue was purified through silica gel column chromatography (1:19 EtOAc:Hexane) to give the title compound as a colourless oil (0.589 g, 98%).

Rf: 0.23 (1:19 EtOAc:Hexane); **IR** (neat film, ν_{max}, cm^{-1}): 3305 (w, NH), 2982 (w, CH), 2936 (w, CH), 1804 (m), 1756 (m, C=O), 1716 (m), 1497 (w), 1371 (m), 1211 (m), 1167 (m), 1112 (s), 1060 (s); **^{1}H NMR** (400 MHz, $CDCl_3$) δ: 4.42 (br s, 1H, NH), 2.00 (br s, 2H, H1), 1.96 (t, *J* = 2.6 Hz, 1H, C≡C-H), 1.62 – 1.43 (m, 17H), 1.27 – 1.25 (m, 1H); **^{13}C NMR** (101 MHz, $CDCl_3$) δ: 146.8 (C=O), 85.3 (Boc-qC), 81.2 (**C**≡C-H), 70.2 (C≡**C**-H), 53.8 (C2), 34.4 (C1), 28.5 (CH_3), 27.5, 25.6, 21.7 (C3-5); **HRMS** (ESI): mass not found.

tert-butyl (1-((1-(2-(4-chlorophenyl)-2-hydroxyethyl)-1_H_-1,2,3-triazol-5-yl)methyl)cyclohexyl) carbamate (82)

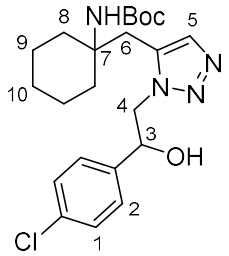

To a stirring solution of chloro(pentamethylcyclopentadienyl)(cyclooctadiene)ruthenium(II) (0.99 mg, 0.0026 mmol) in degassed toluene (0.3 mL) were added **69** (27 mg, 0.11 mmol) and **66** (22.5 mg, 0.11 mmol). The mixture was heated to 50 °C for 2 h before being cooled and concentrated *in vacuo*. The residue was purified through silica gel column chromatography (1:1 EtOAc:Hexane) to give the title compound as a colourless oil (32 mg, 84%)

Rf: 0.16 (1:1 EtOAc:Hexane); **IR** (neat film, ν_{max}, cm^{-1}): 3306 (br, m, OH), 2931 (m, CH), 2857 (w, CH), 1704 (m, C=O), 1493 (m), 1451 (m), 1391 (w), 1366 (m), 1245 (m), 1162 (s), 1088 (s), 1014 (w); **^{1}H NMR** (400 MHz, $CDCl_3$) δ: 7.39 (s, 1H, H5), 7.31 (s, 4H, H1, H2), 5.21 (m, 1H, H3), 4.47 – 4.37 (m, 2H, H4), 4.23 (s, 1H, NH), 4.07 (s, 1H, OH), 3.03 – 2.90 (m, 2H, CH_2), 1.90 (m, 2H, H6), 1.62 – 1.50 (m, 3H), 1.38 – 1.20 (m, 14H, 3x CH_3); **^{13}C NMR** (101 MHz, $CDCl_3$) δ: 154.6 (C=O), 139.0 (qC), 134.5 (qC), 134.1 (qC), 133.8 (C5), 128.9 (Ar-H), 127.5 (Ar-H), 79.6 (Boc-qC), 72.5 (C3), 54.7 (C4), 54.3 (C7), 34.9 (C6), 32.0, 28.4 (Boc CH_3), 25.4, 21.4; **HRMS** (ESI): m/z calcd for $C_{22}H_{32}ClN_4O_3$ $[M+H]^+$: 435.2158; found: 435.2178.

2-(5-((1-aminocyclohexyl)methyl)-1*H*-1,2,3-triazol-1-yl)-1-(4-chlorophenyl)ethan-1-ol (64)

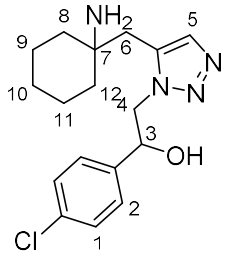

To a stirring solution of **82** (31 mg, 0.07 mmol) in dichloromethane (0.4 mL) was added trifluoroacetic acid (0.1 mL). The mixture was stirred at r.t. for 4 h before diluting in sat. aq. $NaHCO_3$ (4 mL) and extracting into dichloromethane (3 x 10 mL). The combined organics were dried over Na_2SO_4, filtered and concentrated *in vacuo* to give the title compound as a colourless oil (20 mg, 84%), which required no further purification.

IR (neat film, ν_{max}, cm^{-1}): 3079 (w, NH), 2929 (m, CH), 2850 (w, CH), 1582 (m, C=C), 1540 (w), 1489 (m), 1450 (m), 1291 (w), 1230 (w), 1135 (w), 1074 (m); **^{1}H NMR** (400 MHz, $CDCl_3$) δ: 7.51 (s, 1H, H5), 7.44 – 7.41 (m, 2H), 7.40 – 7.33 (m, 2H), 5.15 (dd, *J* = 1.7, 8.9 Hz, 1H, H3), 4.67 (dd, *J* = 2.0, 14.4 Hz, 1H, H4), 4.28 (dd, *J* = 8.9, 14.4 Hz, 1H, H4), 3.19 (br s, 2H, NH_2), 2.83 (s, 2H, H6), 1.59 – 1.24 (m, 11H); **^{13}C NMR** (101 MHz, $CDCl_3$) δ: 139.8 (qC), 134.0 (qC), 133.7 (qC), 133.3 (C5), 128.9, 127.5 (C1/C2), 72.7 (C3), 57.1 (C4), 51.6 (C7), 39.0, 38.5, 34.9 (C6), 25.5, 22.1, 21.9 (C7-12); **HRMS** (ESI): m/z calcd for $C_{17}H_{24}ClN_4O$ $[M+H]^+$: 335.1633; found: 335.1621.

***tert*-Butyl 2-(6-methoxy-1-(naphthalen-1-yl)-9*H*-pyrido[3,4-*b*]indol-9-yl)acetate (90)**

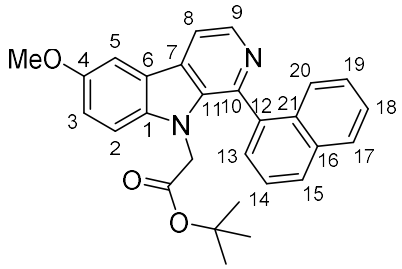

To a stirring solution of **SP-141** (9 mg, 0.03 mmol) in DMF (133 µl) was added caesium carbonate (12.66 mg, 0.04 mmol). The reaction was stirred for *ca*. 15 mins before a solution of *tert*-butyl 2-bromoacetate (5.74 µl, 0.04 mmol) in DMF (133 µl) was slowly added. The reaction was stirred for a further 4 h before being dissolved in DCM (5 mL) and water (5 mL), extracted thrice into DCM (3 x 10

mL), dried over $MgSO_4$, filtered and concentrated *in vacuo* to give the title compound (12.00 mg, >98%) as a yellow oil used without further purification.

IR (neat film, ν_{max}, cm^{-1}): 2976 (w, CH), 1743 (s, C=O), 1586 (w), 1561 (m), 1489 (s), 1454 (m), 1437 (m), 1394 (w), 1368 (m), 1296 (m), 1280 (m), 1229 (s), 1196 (s), 1155 (s), 1046 (w); **^{1}H NMR** (500 MHz, $CDCl_3$) δ: 8.59 (d, *J* = 5.2 Hz, 1 H, H9), 8.03 (d, *J* = 5.2 Hz, 1 H, H8), 7.99 (dd, *J* = 7.2, 2.3 Hz, 1 H, H15), 7.94 (d, *J* = 8.2 Hz, 1 H, H20), 7.67 (d, *J* = 2.4 Hz, 1 H, H5), 7.54 – 7.61 (m, 2 H, H13, H14), 7.49 (ddd, *J* = 8.2, 6.7, 1.2 Hz, 1 H, H18/H19), 7.42 (d, *J* = 8.2 Hz, 1 H, H17), 7.34 (ddd, *J* = 8.2, 6.7, 1.2 Hz, 1 H, H18/H19), 7.21 (dd, *J* = 8.9, 2.5 Hz, 1 H, H3), 7.12 (d, *J* = 8.9 Hz, 1 H, H2), 4.28 (d, *J* = 18.2 Hz, 1 H, -CH_2), 4.05 (d, *J* = 18.2 Hz, 1 H, -CH_2), 3.96 (s, 3 H, -OMe), 1.15 (s, 9 H, *t*Bu-CH_3); **^{13}C NMR** (126 MHz, $CDCl_3$) δ: 167.1 (C=O), 154.6 (C4), 142.7 (C10), 138.6 (C9), 137.5 (C1), 136.5 (C16), 136.2 (C11), 133.7 (C21), 132.4 (C12), 130.1 (C7), 129.1 (C15), 128.3 (C20), 127.4 (C13/C14), 126.9 (C18/C19), 126.3 (C18/C19), 126.0 (C17), 125.4 (C13/C14), 122.0 (C6), 118.6 (C3), 114.0 (C8), 110.4 (C2), 103.8 (C5), 82.0 (q-ali-C), 56.2 (OMe), 46.4 (CH_2), 27.7 (CH_3); **HRMS**: *m/z* $[M+H]^+$ calculated for $C_{28}H_{27}N_2O_3$: 439.2016; Found: 439.2013.

2-(6-methoxy-1-(naphthalen-1-yl)-9*H*-pyrido[3,4-*b*]indol-9-yl)acetic acid (91)

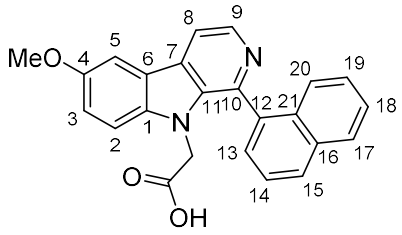

To a stirring solution of **90** (20 mg, 0.05 mmol) in DCM (228 µl) was added 2,2,2-trifluoroacetic acid (520 mg, 4.56 mmol). The reaction was stirred at r.t for 2 h before concentrating. The residue was then twice dissolved in toluene (2 x 5 mL) and concentrated *in vacuo* to give the title compound (17.00 mg, 97%) as a yellow oil used without further purification.

IR (neat film, ν_{max}, cm^{-1}): 2926 (w, CH), 2853 (w, CH), 1708 (s, C=O), 1666 (m), 1602 (m), 1496 (m), 1478 (m), 1361 (m), 1296 (m), 1224 (m), 1178 (s), 1131 (s), 1090 (m), 1046 (m); **^{1}H NMR** (500 MHz, Acetone) δ: 8.75 (s, 2 H), 8.23 (d, *J* = 8.2 Hz, 1 H), 8.12 – 8.08 (m, 2 H), 7.74 (dd, *J* = 7.0, 1.1 Hz, 1 H), 7.71 – 7.59 (m, 3 H), 7.48 – 7.39 (m, 2 H), 7.35 (d, *J* = 8.4 Hz, 1 H), 4.74 (d, *J* = 18.6 Hz, 1 H, CH_2), 4.22 (d, *J* = 18.6 Hz, 1 H, CH_2), 3.99 (s, 3 H, OMe); **^{13}C NMR** (126 MHz, Acetone) δ: 168.9 (C=O), 156.8 (C4), 141.4, 138.2, 136.0, 135.4, 134.2, 132.9, 132.4 (Ar-H), 132.0 (Ar-H), 130.4 (Ar-H), 129.7 (Ar-H), 128.8 (Ar-H), 128.5,

127.9 (Ar-H), 126.1 (Ar-H), 125.6 (Ar-H), 123.5 (Ar-H), 121.6, 117.4 (Ar-H), 113.0 (Ar-H), 104.7 (Ar-H), 56.4 (OMe), 46.3 (CH_2); **HRMS**: *m/z* $[M+H]^+$ calculated for $C_{24}H_{19}N_2O_3$: 383.1390; Found: 383.1394.

***tert*-Butyl (1-(4-(3-(4-cyano-3-(trifluoromethyl)phenyl)-5,5-dimethyl-4-oxo-2-thioxoimidazolidin-1-yl)-2-fluorophenyl)-1-oxo-5,8,11-trioxa-2-azatridecan-13-yl)carbamate (93)**

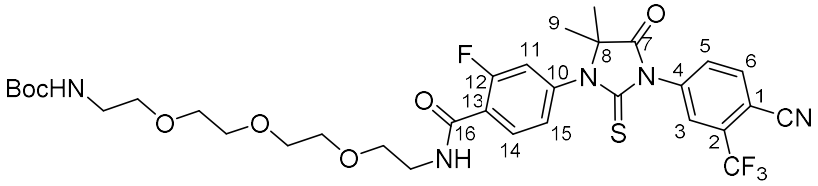

To a stirring solution of **2** (27 mg, 0.06 mmol) in DMF (267 µl) were added HATU (27.3 mg, 0.07 mmol) and DIPEA (12.50 µl, 0.07 mmol). After stirring at r.t. for *ca*. 15 mins **92** (19.99 µl, 0.07 mmol) was added and the reaction stirred for a further 3 h. The mixture was then dissolved in EtOAc (10 mL) and H_2O (5 mL) and extracted into EtOAc (3 x 10 mL), dried over $MgSO_4$, filtered and concentrated *in vacuo*. The residue was then purified by silica gel chromatography (50 to 100% EtOAc/Heptane) to give the title compound (30.0 mg, 69%) as a yellow oil.

IR (neat film, ν_{max}, cm^{-1}): 3365 (br w, NH), 2932 (w, CH), 1758 (m, C=O), 1702 (m, C=O), 1659 (m, C=O), 1620 (m), 1532 (m), 1499 (m), 1438 (s), 1411 (s), 1366 (m), 1311 (s), 1286 (s), 1220 (s), 1176 (s), 1134 (s), 1056 (w); ^{1}H NMR (400 MHz, $CDCl_3$) δ: 8.23 (t, *J* = 8.3 Hz, 1 H, H14), 7.99 (d, *J* = 8.3 Hz, 1 H, H6), 7.95 (d, *J* = 2.0 Hz, 1 H, H3), 7.83 (dd, *J* = 8.3, 1.9 Hz, 1 H, H5), 7.24 (dd, *J* = 8.3, 1.8 Hz, 1 H, H15), 7.16 (dd, *J* = 11.4, 1.9 Hz, 2 H, H11, NH), 5.00 (br s, 1 H, NH), 3.73 – 3.58 (m, 12 H, 6x CH_2), 3.52 (t, *J* = 5.2 Hz, 2 H, CH_2), 3.32 – 3.22 (m, 2 H, CH_2), 1.61 (s, 6 H), 1.43 (s, 9 H); 8.14 (t, *J* = 8.2 Hz, 1 H, H14), 7.98 (d, *J* = 8.3 Hz, 1 H, H6), 7.95 (d, *J* = 1.8 Hz, 1 H, H3), 7.82 (dd, *J* = 8.3, 1.9 Hz, 1 H, H5), 7.56 (s, 1 H, NH), 7.21 (dd, *J* = 8.3, 1.8 Hz, 1 H, H15), 7.15 (dd, *J* = 11.2, 1.7 Hz, 1 H, H11), 4.35 (br s, 2 H, NH_2), 3.82 – 3.50 (m, 14 H, 7x CH_2), 3.07 – 2.90 (m, 2 H, N-CH_2), 1.60 (s, 6 H, H9); **^{13}C NMR** (126 MHz, $CDCl_3$) δ: 179.8 (C=S), 174.5 (C=O), 162.3 (C=O), 160.4 (d, *J* = 250 Hz, C12), 156.0 (Boc C=O), 139.0 (d, *J* = 10 Hz, C13), 136.9 (C1), 135.3 (C6), 133.7 (q, *J* = 34 Hz, C2), 133.2 (C14), 132.2 (C5),127.1 (q, *J* = 5.2 Hz, C3), 126.1 (C15), 123.0 (d, *J* = 11.6 Hz, C10), 121.8 (q, *J* = 275 Hz, CF_3), 118.0 (d, *J* = 28 Hz, C11), 114.7 (-C≡N), 110.4 (C4), 79.3 (Boc qC), 70.5, 70.4, 70.3, 70.2 (2C), 69.6 (overlapping 6x O-CH_2), 66.6 (C8), 40.4, 39.9 (2x N-CH_2), 28.4 (Boc-CH_3), 23.8 (C9); **^{19}F NMR** (471 MHz, $CDCl_3$) δ: -61.98, -110.36; **HRMS (ESI):** m/z calcd for $C_{33}H_{39}F_4N_5O_7SNa$ $[M+Na]^+$: 748.2399; found: 748.2407.

***N*-(2-(2-(2-(2-aminoethoxy)ethoxy)ethoxy)ethyl)-4-(3-(4-cyano-3-(trifluoromethyl)phenyl)-5,5-dimethyl-4-oxo-2-thioxoimidazolidin-1-yl)-2-fluorobenzamide (94)**

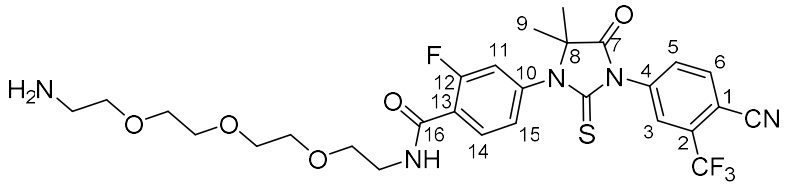

To a stirring solution of **93** (21 mg, 0.03 mmol) in DCM (0.2 mL) was added 2,2,2-trifluoroacetic acid (0.2 mL, 2.61 mmol). The reaction was stirred at 25 °C for 2 h before concentrating and dissolving in sat. aq. $NaHCO_3$ (5 mL) and extracting into EtOAc (3 x 10 mL), drying over $MgSO_4$, filtering and concentrating *in vacuo* to give the title compound (17.00 mg, 94%) as a yellow oil used without further purification.

IR (neat film, ν_{max}, cm^{-1}): 3397 (br w, NH), 2921 (w, CH), 1757 (m, C=O), 1706 (m, C=O), 1656 (m), 1620 (m), 1540 (m), 1500 (m), 1438 (m), 1415 (m), 1363 (m), 1311 (s), 1221 (s), 1202 (m), 1177 (s), 1129 (s), 1090 (s), 1056 (m); **^{1}H NMR** (500 MHz, $CDCl_3$) δ: 8.14 (t, *J* = 8.2 Hz, 1 H, H14), 7.98 (d, *J* = 8.3 Hz, 1 H, H6), 7.95 (d, *J* = 1.8 Hz, 1 H, H3), 7.82 (dd, *J* = 8.3, 1.9 Hz, 1 H, H5), 7.56 (s, 1 H, NH), 7.21 (dd, *J* = 8.3, 1.8 Hz, 1 H, H15), 7.15 (dd, *J* = 11.2, 1.7 Hz, 1 H, H11), 4.35 (br s, 2 H, NH_2), 3.82 – 3.50 (m, 14 H, 7x CH_2), 3.07 – 2.90 (m, 2 H, N-CH_2), 1.60 (s, 6 H, H9); **^{13}C NMR** (126 MHz, $CDCl_3$) δ: 179.8 (C=S), 174.5 (C=O), 162.9 (C=O), 160.3 (d, *J* = 250 Hz, C12), 138.9 (d, *J* = 10 Hz, C13), 136.9 (C1), 135.3 (C6), 133.7 (q, *J* = 34 Hz, C2), 133.0 (C14), 132.2 (C5), 127.1 (q, *J* = 5.2 Hz, C3), 126.0 (C15), 123.4 (d, *J* = 11.6 Hz, C10), 121.8 (q, *J* = 275 Hz, CF_3), 118.0 (d, *J* = 28 Hz, C11), 114.7 (-C≡N), 110.4 (C4), 70.5, 70.3, 70.1, 70.0, 69.8, 69.6 (6x O-CH_2), 66.7 (C8), 40.4, 39.9 (2x N-CH_2), 23.8 (C9); **^{19}F NMR** (471 MHz, $CDCl_3$) δ: -62.0, -110.4; **HRMS (ESI):** m/z calcd for $C_{28}H_{32}F_4N_5O_5S$ $[M+H]^+$: 626.2055; found: 626.2055.

4-(3-(4-cyano-3-(trifluoromethyl)phenyl)-5,5-dimethyl-4-oxo-2-thioxoimidazolidin-1-yl)-2-fluoro-N-(1-(6-methoxy-1-(naphthalen-1-yl)-9H-pyrido[3,4-b]indol-9-yl)-2-oxo-6,9,12-trioxa-3-azatetradecan-14-yl)benzamide (PROTAC-7)

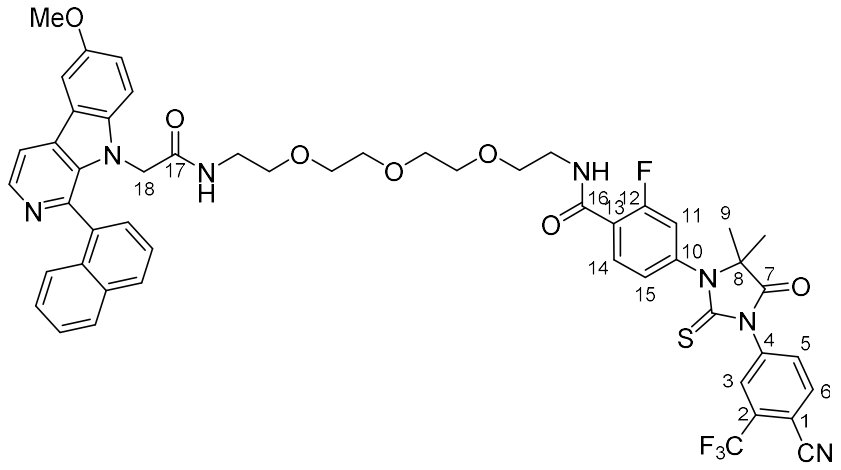

To a stirring solution of **91** (3 mg, 7.84 µmol) in DMF (77 µl) were added HATU (4.18 mg, 10.98 µmol) and DIPEA (1.913 µl, 10.98 µmol). After stirring at r.t. for *ca*. 15 mins **94** (5.15 mg, 8.24 µmol) was added and the reaction stirred for a further 3 h. The mixture was then dissolved in EtOAc (10 mL) and H_2O (5 mL) and extracted into EtOAc (3 x 10 mL), dried over MgSO4, filtered and concentrated *in vacuo*. The residue was then purified by silica gel chromatography (0 to 5% MeOH/DCM) to give the title compound (2.60 mg, 34%) as a yellow oil.

R_f: 0.30 (5% MeOH/DCM); **IR** (neat film, ν_{max}, cm^{-1}): 3322 (w, NH), 2929 (w, CH), 1758 (m, C=O), 1658 (m, C=O), 1620 (m, C=O), 1535 (w), 1489 (m), 1438 (m), 1409 (m), 1311 (m), 1261 (m), 1221 (m), 1198 (m), 1178 (m), 1132 (m), 1105 (m), 1057 (m), 1023 (w), 837 (s), 728 (s); **^{1}H NMR** (500 MHz, $CDCl_3$) δ: 8.51 (d, *J* = 5.2 Hz, 1 H), 8.14 (t, *J* = 8.3 Hz, 1 H, H14), 8.05 (d, *J* = 5.2 Hz, 1 H,), 8.01 - 7.89 (m, 4H), 7.82 (dd, *J* = 8.3, 1.8 Hz, 1 H, H5), 7.66 (d, *J* = 2.2 Hz, 1H), 7.60 – 7.54 (m, 2H), 7.48 (t, *J* = 7.3 Hz, 1H), 7.37 – 7.30 (m, 2H), 7.23 – 7.10 (m, 5H), 5.65 (t, *J* = 5.7 Hz, 1 H, NH), 4.24 (d, *J* = 17.8 Hz, 1 H, H18), 4.05 (d, *J* = 17.8 Hz, 1 H, H18), 3.95 (s, 3 H, OMe), 3.68 (p, *J* = 6.7 Hz, 3 H), 3.59 (d, *J* = 3.2 Hz, 2 H), 3.53 (dd, *J* = 5.6, 3.0 Hz, 2 H), 3.48 (dd, *J* = 5.5, 3.2 Hz, 2 H), 3.41 (s, 2 H), 3.30 (qt, *J* = 9.7, 5.0 Hz, 2 H), 3.15 (q, *J* = 7.4 Hz, 3 H), 1.57 (s, 6 H, H9); **^{13}C NMR** (126 MHz, $CDCl_3$) δ: 179.8 (C=S), 174.4 (C=O), 167.3 (C=O), 162.3 (C=O), 160.3 (d, *J* = 250 Hz, C12), 155.0 (C-OMe), 142.6, 139.0, 138.4, 137.3, 136.8, 135.7, 135.3 (C6), 135.1 (C1), 133.7 (d, *J* = 34 Hz, C2), 133.5, 133.1, 132.2 (2C), 130.5, 129.6, 128.6, 127.4, 127.1 (d, *J* = 5 Hz, C3), 126.9, 126.4, 126.1 (C15), 125.5, 125.2, 123.0 (d, *J* = 11 Hz, C10), 121.9, 121.8 (q, *J* = 275 Hz, CF_3), 119.2, 118.0 (d, *J* = 27 Hz, C11), 114.7 (-C≡N), 114.2, 110.9, 110.4 (d, *J* = 2.2 Hz, C4), 103.7, 70.3 (2C), 70.2, 70.1, 69.5, 69.3 (6x O-CH_2), 66.6 (C8), 55.8 (OMe), 43.7 (C18), 39.8, 39.0 (2x N-CH_2), 23.8

(C9); **^{19}F NMR** (471 MHz, $CDCl_3$) δ: -62.0, -110.5; **HRMS (ESI):** m/z calcd for $C_{52}H_{48}F_4N_7O_7S$ $[M+H]^+$: 990.3267; found: 990.3251.

Methyl (3,3-diphenylpropanoyl)-*L*-tyrosinate (86)

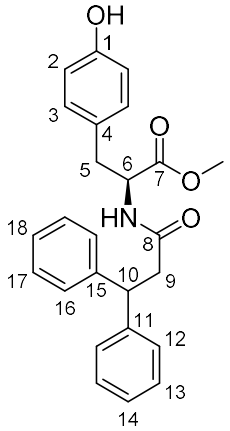

To a stirring solution of **96** (2.00 g, 8.6 mmol) in chloroform (30 mL) cooled to 0 °C, were added EDCI.HCl (1.81 g, 9.46 mmol) and HOBt (80%, 1.74 g, 10.3 mmol). After stirring for *ca*. 20 mins 3,3-diphenylpropionic acid (1.946 g, 8.6 mmol) was added and the reaction was stirred at r.t for a further 18 h. The reaction was then diluted with dichloromethane (30 mL), washed with 1 M HCl (2 x 20 mL), sat. aq. $NaHCO_3$ (2 x 20 mL), brine (20 mL), dried over Na_2SO_4, filtered, and concentrated *in vacuo* to give the title compound as a yellow oil (3.24 g, 93%) used without further purification.

R_f: 0.56 (1:1 EtOAc:PE 40-60); **IR** (neat film, ν_{max}, cm^{-1}): 3304 (m), 3027 (m), 2948 (m), 1742 (m), 1647 (s), 1613 (m), 1597 (m), 1515 (s), 1492 (m), 1448 (m), 1374 (w), 1260 (m), 1221 (m), 1171 (m); **^{1}H NMR** (400 MHz, $CDCl_3$) δ: 7.35 – 7.18 (m, 11 H, Ar-H), 6.69 – 6.61 (m, 4 H, H2 and H3), 5.96 (d, *J* = 7.5 Hz, 1 H, NH), 4.82 – 4.77 (m, 1 H, H6), 4.60 (t, *J* = 8.0 Hz, 1 H, H10), 3.67 (s, 3 H, CH_3), 3.00 – 2.80 (m, 4 H, H5 and H9); **^{13}C NMR** (101 MHz, $CDCl_3$) δ: 172.0 (C7), 170.9 (C8), 155.4 (C1), 143.6, 143.4, 130.3 (C3), 128.7 (Ar-CH), 128.6 (Ar-CH), 127.9, 127.6, 126.9 (C4), 126.7, 126.6 (Ar-CH), 115.5 (C2), 53.2 (C6), 52.3 (CH_3), 47.2 (C10), 43.0 (C9), 37.1 (C5); **$[\alpha]_D^{25}$** 0.364 (c = 1.1, MeOH).

Data are in accordance with those reported previously in literature[231].

(3,3-diphenylpropanoyl)-*L*-tyrosine (97)

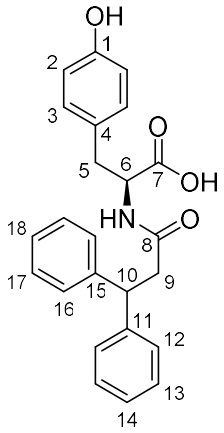

To a stirring solution of **86** (0.631 g, 1.56 mmol) in a mixture of THF (9 mL) and H_2O (3 mL), was added lithium hydroxide (0.131 g, 3.13 mmol). The reaction was stirred at r.t. for 3 h before concentrating *in vacuo.* The residue was then dissolved in H_2O (10 mL) and washed with EtOAc (3 x 8 mL), before being acidified with 1 M HCl and extracted into EtOAc (3 x 10 mL), dried over Na_2SO_4, filtered, and concentrated *in vacuo* to give the title compound as a white amorphous solid (0.498 g, 82%) used without further purification.

IR (neat film, ν_{max}, cm^{-1}): 3341 (w), 3030 (w), 1722 (m), 1696 (m), 1641 (m), 1611 (m), 1513 (s), 1494 (m), 1448 (m), 1417 (w), 1217 (m), 1197 (m), 1173 (m), 1106 (w); **^{1}H NMR** (400 MHz, DMSO) δ: 12.56 (br s, 1 H, COOH), 9.19 (s, 1 H, Ar-OH), 8.14 (d, *J* = 8.1 Hz, 1 H, NH), 7.26 – 7.13 (m, 10 H, Ar-H), 6.86 (d, *J* = 8.4 Hz, 2 H, H3), 6.62 (d, *J* = 8.4 Hz, 2 H, H2), 4.43 (t, *J* = 7.9 Hz, 1 H, H6), 4.29 – 4.24 (m, 1 H, H10), 2.96 – 2.91 (m, 1 H, H9), 2.84 – 2.79 (m, 2 H, H5 and H9), 2.70 – 2.64 (m, 1 H, H5); **^{13}C NMR** (101 MHz, DMSO) δ: 173.5 (C7), 170.5 (C8), 156.3 (C1), 145.0, 144.7, 130.4 (C3), 128.7 (2C), 128.0 (2C), 127.9, 126.5 (C4), 115.4 (C2), 54.1 (C6), 47.0 (C10), 41.3 (C9), 36.6 (C5); **$[\alpha]_D^{25}$** 2.17 (c = 1.2, MeOH).

Data are in accordance with those reported previously in literature[231].

***tert*-Butyl (*S*)-(11-(4-hydroxybenzyl)-10,13-dioxo-15,15-diphenyl-3,6-dioxa-9,12-diazapentadecyl)carbamate (98)**

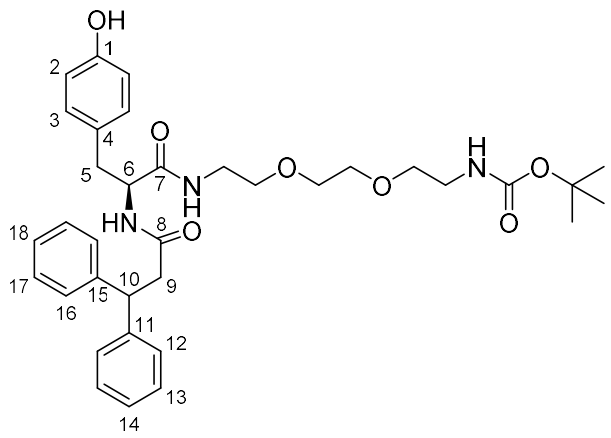

To a stirring solution of **97** (30 mg, 0.077 mmol) in dichloromethane (1 mL), were added EDCI.HCl (18 mg, 0.092 mmol), HOBt (80%, 16 mg, 0.092 mmol) and **36** (20 µL, 0.085 mmol). The reaction was stirred at r.t. for 18 h before being diluted with dichloromethane (10 mL), washed with sat. aq. $NaHCO_3$ (5 mL), brine (5 mL), dried over Na_2SO_4, filtered, and concentrated *in vacuo.* The residue was then purified by silica gel chromatography (1 to 5 % MeOH/DCM) to give the title compound as a yellow oil (46 mg, 96%).

R_f: 0.11 (2% MeOH/DCM); **IR** (neat film, ν_{max}, cm^{-1}): 3296 (m), 2976 (m), 2927 (m), 1641 (s), 1613 (m), 1597 (m), 1520 (s), 1494 (m), 1451 (m), 1366 (m), 1264 (m), 1248 (m), 1170 (m), 1101 (m); **^{1}H NMR** (400 MHz, $CDCl_3$) δ: 7.71 (br s, 1 H, OH), 7.30 – 7.16 (m, 10 H, Ar-H), 6.89 (d, *J* = 8.2 Hz, 2 H, H3), 6.72 (d, *J* = 8.2 Hz, 2 H, H2), 6.42 (d, *J* = 7.9 Hz, 1 H, NH), 6.04 (br s, 1 H, NH), 5.17 (br s, 1 H, NH), 4.58 (t, *J* = 8.0 Hz, 1 H, H6), 4.52 – 4.46 (m, 1 H, H10), 3.67 – 3.29 (m, 12 H, 6x CH_2), 3.00 – 2.89 (m, 2 H, H5), 2.82 – 2.77 (m, 1 H, H9), 2.66 – 2.64 (m, 1 H, H9), 1.46 (s, 9 H, 3x CH_3); **^{13}C NMR** (101 MHz, $CDCl_3$) δ: 171.0 (C7), 170.7 (C8), 156.4 (Boc-C=O), 155.6 (C1), 143.5, 143.4, 130.3 (C3), 128.6 (2C), 127.8, 127.7, 126.6, 126.5 (C4), 115.6 (C2), 79.7 (qC), 70.3, 70.1, 69.9, 69.4 (4x O-CH_2), 54.8 (C6), 47.4 (C10), 42.9 (C9), 40.3, 39.2 (2x N-CH_2), 37.9 (C5), 28.4 (CH_3); **HRMS (ESI):** m/z calcd for $C_{35}H_{45}N_3O_7Na$ $[M+Na]^+$: 642.3150; found: 642.3128; **$[\alpha]_D^{25}$** -4.31 (c = 0.116, MeOH).

(*S*)-*N*-(2-(2-(2-aminoethoxy)ethoxy)ethyl)-2-(3,3-diphenylpropanamido)-3-(4-hydroxyphenyl) propenamide (100)

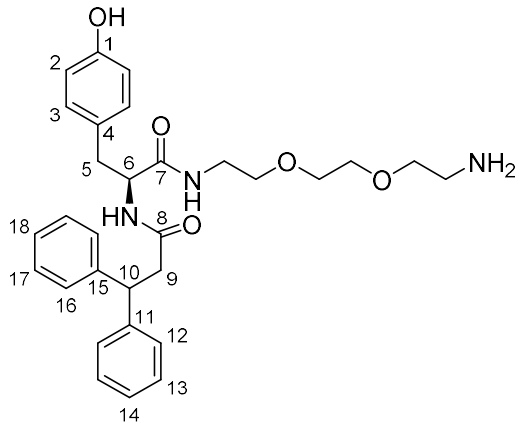

To a stirring solution of **98** (45 mg, 0.07 mmol) in dichloromethane (0.3 mL) was added trifluoroacetic acid (0.3 mL). The reaction was stirred for 3 h at r.t. before being concentrated, diluted with sat. aq. $NaHCO_3$ (2 mL), extracted into dichloromethane (3 x 10 mL), dried over Na_2SO_4, filtered, and concentrated *in vacuo* to give the title compound as a yellow oil (24 mg, 64%) used without further purification.

IR (neat film, ν_{max}, cm^{-1}): 3286 (m, NH), 2920 (m, CH), 2849 (m, CH), 1641 (s, C=O), 1613 (m), 1597 (m), 1542 (m), 1515 (s), 1450 (m), 1376 (w), 1264 (m), 1201 (m), 1177 (m), 1132 (m); **^{1}H NMR** (400 MHz, MeOD) δ: 7.26 – 7.13 (m, 10 H, ArH), 6.92 (d, *J* = 8.4 Hz, 2 H, H3), 6.66 (d, *J* = 8.4 Hz, 2 H, H2), 4.46 (t, *J* = 7.9 Hz, 1 H, H6), 4.34 (t, *J* = 7.3 Hz, 1 H, H10), 3.64 – 3.52 (m, 6 H, 3x CH_2), 3.40 – 3.33 (m, 2H, CH_2), 3.29 – 3.15 (m, 2 H, CH_2), 3.03 – 2.81 (5 H, CH_2, H5 and H9), 2.68 – 2.63 (m, 1 H, H9); **^{13}C NMR** (101 MHz, MeOD) δ:172.4 (C7), 172.1 (C8), 155.9 (C1), 143.8, 143.6, 129.8 (C3), 128.1 (2C), 127.5, 127.4 (2C), 126.1, 126.0 (C4), 114.8 (C2), 69.9 (2C), 69.0, 67.4 (4x O-CH_2), 55.0 (C6), 47.3 (C10), 41.5 (C9), 39.5, 38.8 (2x N-CH_2), 36.7 (C5); **HRMS (ESI):** m/z calcd for $C_{30}H_{37}N_3O_5Na$ $[M+Na]^+$: 542.2625; found: 542.2639; **$[\alpha]_D^{25}$** -3.03 (c = 0.132, MeOH).

(*S*)-4-(3-(4-cyano-3-(trifluoromethyl)phenyl)-5,5-dimethyl-4-oxo-2-thioxoimidazolidin-1-yl)-2-fluoro-*N*-(11-(4-hydroxybenzyl)-10,13-dioxo-15,15-diphenyl-3,6-dioxa-9,12-diazapentadecyl)benzamide (PROTAC-8)

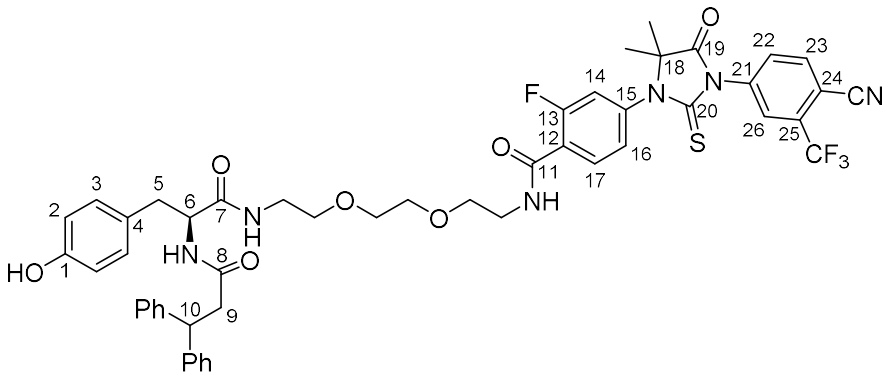

To a stirring solution of **2** (7 mg, 0.016 mmol) in DMF (0.1 mL), were added HATU (7 mg, 0.019 mmol) and DIPEA (6.6 µL, 0.0341 mmol). The reaction was stirred at r.t. for *ca*. 15 mins before **100** (8.9 mg, 0.017 mmol) in DMF (0.1 mL) was added. The reaction was stirred for a further 18 h before being diluted with EtOAc (5 mL) and H_2O (3 mL), extracted into EtOAc (2 x 5 mL), washed with brine (5 mL), dried over Na_2SO_4, filtered, and concentrated *in vacuo.* The residue was then purified by silica gel chromatography (1 to 5% MeOH/DCM) to give the title compound as a yellow oil (11 mg, 74%).

R_f: 0.09 (3% MeOH/DCM); **IR** (neat film, ν_{max}, cm^{-1}): 3304 (w), 2921 (w), 1758 (m), 1730 (w), 1646 (s), 1618 (m), 1536 (m), 1515 (s), 1497 (s), 1440 (s), 1415 (s), 1311 (s), 1219 (m), 1177 (m), 1140 (s), 1056 (m); **^{1}H NMR** (400 MHz, $CDCl_3$) δ: 8.21 (t, *J* = 8.2 Hz, 1 H, H17), 7.96 – 7.94 (m, 2 H, H23 and H26), 7.80 (dd, *J* = 8.1, 1.5 Hz, 1 H, H22), 7.27 – 7.16 (m, 12 H, 10x Ar-H, H14 and H16), 6.87 (d, *J* = 8.2 Hz, 2 H, H3), 6.74 (br s, 1 H, NH), 6.68 (d, *J* = 8.2 Hz, 2 H, H2), 6.20 (d, *J* = 8.0 Hz, 1 H, NH), 5.84 (t, *J* = 6.1 Hz, 1 H, NH), 4.52 (t, *J* = 7.9 Hz, 1 H, H6), 4.43 – 4.38 (m, 1 H, H10), 3.69 – 3.63 (m, 4 H, 2x CH_2), 3.58 – 3.56 (m, 2 H, CH_2), 3.51 – 3.46 (m, 2 H, CH_2), 3.39 – 3.22 (m, 4 H, 2x CH_2), 2.94 – 2.84 (m, 2 H, H5), 2.76 (dd, *J* = 13.6, 5.1 Hz, 1 H, H9), 2.57 (dd, *J* = 13.6, 8.8 Hz, H9), 1.68 (s, 6 H, 2x CH_3); **^{13}C NMR** (101 MHz, $CDCl_3$) δ: 179.8 (C=S), 174.4 (C19), 170.8 (C7), 170.5 (C8), 162.7 (C11), 160.4 (d, *J* = 250 Hz, C13), 155.3 (C1), 143.4 (2C), 139.3 (d, *J* = 10.6 Hz, C12), 136.8 (C24), 135.3 (C23), 133.5 (C25), 133.3 (d, *J* = 3.2 Hz, C17), 132.1 (C22), 130.4, 128.6 (2C), 128.0, 127.8, 127.6, 127.1 (q, *J* = 4.6 Hz, C26), 126.7, 126.6, 126.2 (d, *J* = 2.8 Hz, C16), 122.6 (d, *J* = 12 Hz, C15), 121.8 (q, *J* = 275 Hz, CF_3), 118.1 (d, *J* = 26 Hz, C14), 115.6 (C2), 114.7 (-C≡N), 110.5 (C21), 70.4, 70.3, 69.5, 69.5 (4x O-CH_2), 66.7 (C20), 54.8 (C6), 47.3 (C10), 43.0 (C9), 40.0, 39.1 (2x N-CH_2), 38.0 (C5), 23.8 (2x CH_3); **^{19}F NMR** (376 MHz, $CDCl_3$) δ: -62.0, -110.2; **HRMS (ESI):** m/z calcd for $C_{50}H_{48}F_4N_6O_7SNa$ $[M+Na]^+$: 975.3133; found: 975.3125; **$[\alpha]_D^{25}$** 3.29 (c = 0.4, MeOH).

***tert*-Butyl (*S*)-(14-(4-hydroxybenzyl)-13,16-dioxo-18,18-diphenyl-3,6,9-trioxa-12,15-diazaoctadecyl) carbamate (99)**

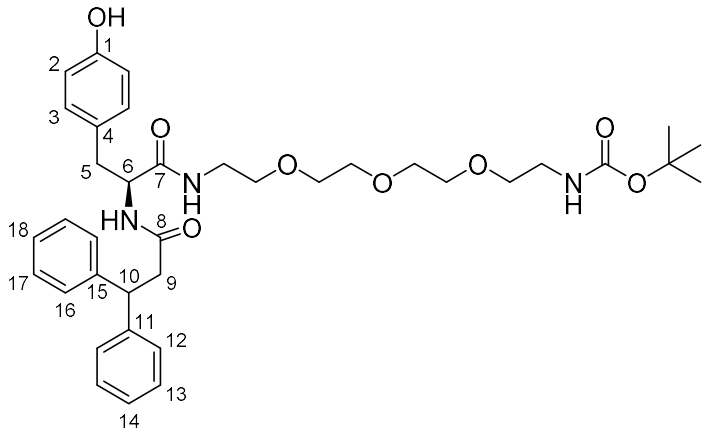

To a stirring solution of **97** (20 mg, 0.05 mmol) in dichloromethane (2 mL), were added EDCI.HCl (11.5 mg, 0.06 mmol), HOBt (80%, 10 mg, 0.06 mmol) and 1-Boc-amine-11-amino-3,6,9-trioxaundecane (15 mg, 0.05 mmol). The reaction was stirred at r.t. for 18 h before being diluted with dichloromethane (10 mL), washed with sat. aq. $NaHCO_3$ (5 mL), brine (5 mL), dried over Na_2SO_4, filtered, and concentrated *in vacuo.* The residue was then purified by silica gel chromatography (4% MeOH/DCM) to give the title compound as a yellow oil (30 mg, 91%).

R_f: 0.40 (6% MeOH/DCM); **IR** (neat film, ν_{max}, cm^{-1}): 3286 (m), 2964 (w), 2876 (w), 1686 (m), 1641 (s), 1615 (m), 1515 (s), 1451 (m), 1366 (m), 1268 (m), 1248 (m), 1170 (m), 1099 (m); **^{1}H NMR** (400 MHz, $CDCl_3$) δ: 7.28 – 7.17 (m, 10 H, Ar-H), 6.91 (d, *J* = 8.4 Hz, 2 H, H3), 6.73 (d, *J* = 8.4 Hz, 2 H, H2), 6.33 (d, *J* = 6.4 Hz, 1 H, NH), 5.85 (br s, 1 H, NH), 5.21 (br s, 1 H, NH), 4.59 (t, *J* = 8.1 Hz, 1 H, H6), 4.47 – 4.42 (m, 1 H, H10), 3.65 – 3.54 (m, 8 H, 4x CH_2), 3.47 – 3.44 (m, 2 H, CH_2), 3.39 – 3.17 (m, 6 H, 3x CH_2), 3.00 – 2.82 (m, 3 H, H5 and H9), 2.54 (dd, *J* = 13, 9.0 Hz, H9), 1.45 (s, 9 H, 3x CH_3); **^{13}C NMR** (101 MHz, $CDCl_3$) δ: 170.6 (C7), 170.5 (C8), 156.3 (Boc-C=O), 155.5 (C1), 143.5 (2C), 130.3 (C3), 128.6 (2C), 127.9, 127.7, 126.6, 126.5 (C4), 115.8 (C2), 79.5 (qC), 70.5, 70.4, 70.3, 70.2, 70.1, 69.6 (6x O-CH_2), 54.8 (C6), 47.4 (C10), 43.0 (C9), 40.3, 39.1 (2x N-CH_2), 38.2 (C5), 28.4 (CH_3); **HRMS (ESI):** m/z calcd for $C_{37}H_{49}N_3O_8Na$ $[M+Na]^+$: 686.3412; found: 686.3417; **$[\alpha]_D^{25}$** -5.00 (c = 0.08, MeOH).

(*S*)-*N*-(1-amino-15-(4-hydroxyphenyl)-13-oxo-3,6,9-trioxa-12-azapentadecan-14-yl)-3,3-diphenylpropanamide (101)

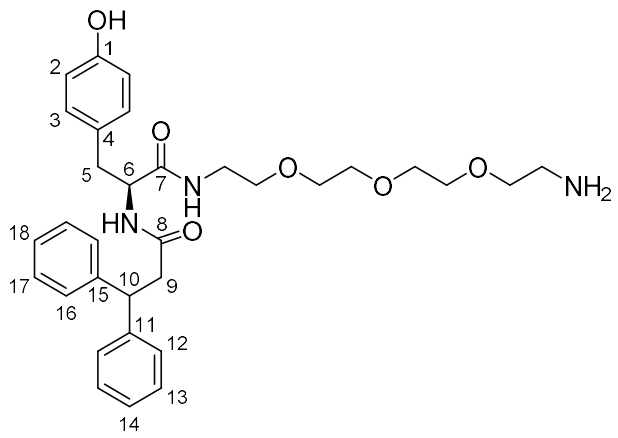

To a stirring solution of **99** (27 mg, 0.041 mmol) in dichloromethane (0.4 mL) was added trifluoroacetic acid (0.2 mL). The reaction was stirred for 3 h at r.t. before being concentrated, diluted with sat. aq. $NaHCO_3$ (2 mL), extracted into dichloromethane (3 x 10 mL), dried over Na_2SO_4, filtered, and concentrated *in vacuo* to give the title compound as a yellow oil (21 mg, 91%) used without further purification.

IR (neat film, ν_{max}, cm^{-1}): 3284 (w), 3054 (w), 2919 (w), 2865 (w), 1639 (s), 1596 (m), 1544 (m), 1515 (s), 1494 (m), 1450 (m), 1348 (w), 1263 (m), 1248 (m), 1098 (s), 1030 (w); **^{1}H NMR** (400 MHz, $CDCl_3$) δ: 7.31 – 7.16 (m, 10 H, Ar-H), 6.91 (d, *J* = 8.5 Hz, 2 H, H3), 6.71 (d, *J* = 8.5 Hz, 2 H, H2), 6.47 (d, *J* = 7.9 Hz, 1 H, NH), 6.29 (br s, 1 H, NH), 4.60 – 4.42 (m, 4 H, H6, H10 and NH_2), 3.63 – 3.55 (m, 8 H, 4x CH_2), 3.48 – 3.46 (m, 2 H, CH_2), 3.41 – 3.21 (m, 4 H, 2x CH_2), 3.00 – 2.82 (m, 5 H, CH_2, H5 and H9), 2.56 (dd, *J* = 13.5, 8.9 Hz, 1 H, H9); **^{13}C NMR** (101 MHz, $CDCl_3$) δ: 170.7 (2C, C7, C8), 156.3 (C1), 143.5, 130.4, 128.6 (2C), 127.8, 127.7, 127.2, 126.6, 126.5 (C4), 115.8 (C2), 71.6, 70.5, 70.4, 70.2, 70.1, 69.6 (6x O-CH_2), 54.8 (C6), 47.4 (C10), 43.0 (C9), 41.0, 39.2 (2x N-CH_2), 38.2 (C5); **HRMS (ESI):** m/z calcd for $C_{32}H_{42}N_3O_6$ $[M+H]^+$: 564.3068; found: 564.3067; **$[\alpha]_D^{25}$** 2.632 (c = 0.228, MeOH).

(*S*)-4-(3-(4-cyano-3-(trifluoromethyl)phenyl)-5,5-dimethyl-4-oxo-2-thioxoimidazolidin-1-yl)-2-fluoro-*N*-(14-(4-hydroxybenzyl)-13,16-dioxo-18,18-diphenyl-3,6,9-trioxa-12,15-diazaoctadecyl)benzamide (PROTAC-9)

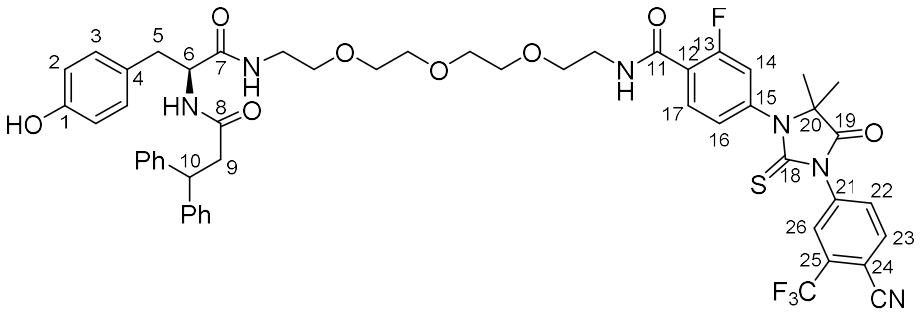

To a stirring solution of **2** (5 mg, 0.011 mmol) in DMF (0.1 mL), were added HATU (4.6 mg, 0.012 mmol) and DIPEA (2.3 µL, 0.012 mmol). The reaction was stirred at r.t. for *ca*. 15 mins before **101** (6.6 mg, 0.012 mmol) in DMF (0.1 mL) was added. The reaction was stirred for a further 18 h before being diluted with EtOAc (5 mL) and H_2O (3 mL), extracted into EtOAc (2 x 5 mL), washed with brine (5 mL), dried over Na_2SO_4, filtered, and concentrated *in vacuo.* The residue was then purified by silica gel chromatography (3% MeOH/DCM) to give the title compound as a yellow oil (6.8 mg, 62%).

R_f: 0.18 (3% MeOH/DCM); **IR** (neat film, ν_{max}, cm^{-1}): 3284 (w), 2956 (w), 2921 (m), 2849 (w), 1758 (m), 1647 (s), 1619 (m), 1515 (m), 1497 (s), 1438 (s), 1411 (s), 1311 (s), 1262 (m), 1219 (s), 1177 (m), 1135 (s), 1105 (s), 1056 (m); **^{1}H NMR** (400 MHz, $CDCl_3$) δ: 8.17 (t, *J* = 8.5 Hz, 1 H, H17), 8.01 – 7.94 (m, 2 H, H23 and H26), 7.82 (dd, *J* = 8.3, 1.7 Hz, 1 H, H22), 7.33 – 7.15 (m, 11 H, 10x Ar-H and H16), 7.11 (dd, *J* = 11.4, 1.7 Hz, 1 H, H14), 6.89 (d, *J* = 8.1 Hz, 2 H, H3), 6.82 (br s, 1 H, NH), 6.70 (d, *J* = 8.1 Hz, 2 H, H2), 6.22 (d, *J* = 7.9 Hz, 1 H, NH), 5.64 (br s, 1 H, NH), 4.55 (t, *J* = 8.0 Hz, 1 H, H6), 4.40 – 4.35 (m, 1 H, H10), 3.72 – 3.60 (m, 6 H, 3x CH_2), 3.51 (t, *J* = 4.3 Hz, 2 H, O-CH_2), 3.39 – 3.37 (m, 2 H, O-CH_2), 3.34 – 3.26 (m, 2 H, O-CH_2), 3.16 – 3.08 (m, 2 H, N-CH_2), 2.96 – 2.79 (m, 5 H, N-CH_2, H5 and H9), 2.45 (dd, *J* = 13.5, 9.7 Hz, 1 H, H9), 1.59 (s, 6 H, 2x CH_3); **^{13}C NMR** (101 MHz, $CDCl_3$) δ: 179.8 (C=S), 174.5 (C19), 170.5 (C7), 170.3 (C8), 162.6 (C11), 160.4 (d, *J* = 250 Hz, C13), 155.2 (C1), 143.5, 143.4, 139.0 (d, *J* = 10.4 Hz, C12), 136.8 (C24), 135.3 (C23), 133.6 (C25), 133.1 (d, *J* = 3.3 Hz, C17), 132.2 (C22), 130.2, 128.6 (2C), 128.1, 127.8, 127.6, 127.1 (d, *J* = 5.5 Hz, C26), 126.6 (2C), 126.1 (d, *J* = 3.5 Hz, C16), 123.0 (d, *J* = 13.5 Hz, C15), 118.0 (d, *J* = 25.7 Hz, C14), 115.9 (C2), 114.7 (-C≡N), 110.4 (d, *J* = 2.2 Hz, C21), 70.5, 70.4, 70.3, 70.0, 69.9, 69.6 (6x O-CH_2), 66.6 (C20), 54.9 (C6), 47.4 (C10), 43.1 (C9), 40.0, 39.0 (2x N-CH_2), 38.3 (C5), 23.8 (2x CH_3); **^{19}F NMR** (376 MHz, $CDCl_3$) δ: -62.0, -110.0; **HRMS (ESI):** m/z calcd for $C_{52}H_{52}F_4N_6O_8S$ $[M+Na]^+$: 1019.3395; found: 1019.3385; **$[\alpha]_D^{25}$** 1.25 (c = 0.4, MeOH).

2-(2-((*tert*-Butoxycarbonyl)amino)ethoxy)ethyl methanesulfonate (104)

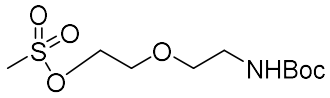

To a stirring solution of **102** (0.200 g, 1.0 mmol) in Et_2O (2 mL) cooled to 0 °C, were added triethylamine (163 µL, 1.17 mmol) and methanesulfonyl chloride (90 µL, 1.17 mmol). The reaction was stirred at r.t. for 6 h before being poured over brine (5 mL), extracted into Et_2O (3 x 10 mL), dried over Na_2SO_4, filtered and concentrated *in vacuo* to give the title compound as a colourless oil (0.219 g, 79%) used without further purification.

R_f: 0.25 (1:1 Hex:EtOAc); **IR** (neat film, ν_{max}, cm^{-1}): 3398 (w), 2978 (w), 2933 (w), 2876 (w), 1695 (m), 1515 (m), 1455 (w), 1392 (w), 1348 (s), 1273 (m), 1249 (m), 1169 (s), 1127 (s), 1016 (m); **^{1}H NMR** (400 MHz, $CDCl_3$) 1.44 (s, 9 H, 3 x CH_3), 3.05 (s, 3 H, CH_3), 3.32 (q, *J* = 5.2 Hz, CH_2-NHBoc), 3.55 (t, *J* = 5.2 Hz, -CH_2), 3.71 – 3.73 (m, 2 H, -**C**H_2-CH_2-OMs), 4.35 – 4.37 (m, 2 H, -CH_2-OMs), 4.89 (br s, 1 H, -NH); **^{13}C NMR** (101 MHz, $CDCl_3$) 28.5 (3 x CH_3), 37.8 (CH_3), 40.4 (CH_2-NHBoc), 68.8 (CH_2-O), 68.9 (CH_2-O), 70.9 (CH_2-OMs), 79.6 (**C**-$(CH_3)_3$), 156.0 (C=O).

Data are in accordance with those reported previously in literature.[348]

***tert*-Butyl (2-(2-(2-iodoethoxy)ethoxy)ethyl)carbamate (106)**

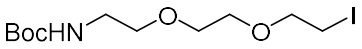

To a stirring solution of 1*H*-imidazole (61.4 mg, 0.90 mmol) and triphenylphosphane (237 mg, 0.90 mmol) in THF (2.7 ml) cooled to 0 °C, was added iodine (229 mg, 0.90 mmol). The mixture was then vigorously stirred at r.t. for 15 mins before a solution of *tert*-butyl (2-(2-(2-hydroxyethoxy)ethoxy)ethyl)carbamate (150 mg, 0.60 mmol) in THF (2.7 ml) was added. The mixture was stirred at r.t. for 2 h then filtered and washed with EtOAc before concentrating *in vacuo*. The residue was then purified through flash silica gel chromatography (0 to 50% EtOAc in Heptane) to give the title compound (138 mg, 64%) as a pale yellow oil.

R_f: 0.62 (1:1 Hex:EtOAc); **IR** (neat film, ν_{max}, cm^{-1}): 3374 (w, NH), 2975 (w, CH), 2866 (w, CH), 1707 (s, C=O), 1505 (m), 1454 (w), 1390 (w), 1364 (m), 1270 (m), 1249 (s), 1167 (s), 1094 (s), 1037 (m); **^{1}H NMR** (500 MHz, $CDCl_3$) 5.00 (s, 1H), 3.76 – 3.70 (m, 2H), 3.61 (dddd, *J* = 9.8, 6.0, 3.3, 1.9 Hz, 4H), 3.53 (t, *J* = 5.2 Hz, 2H), 3.30 (d, *J* = 5.0 Hz, 2H), 3.22 – 3.27 (m, 2H), 1.42 (s, 9H). **^{13}C NMR** (126 MHz, $CDCl_3$) 156.0, 79.2, 71.9, 70.3, 70.2, 70.1, 40.3, 28.4, 2.8.

Data are in accordance with those reported previously in literature.[349]

Methyl (*S*)-3-(4-(2-(2-((*tert*-butoxycarbonyl)amino)ethoxy)ethoxy)phenyl)-2-(3,3-diphenylpropanamido)propanoate (103)

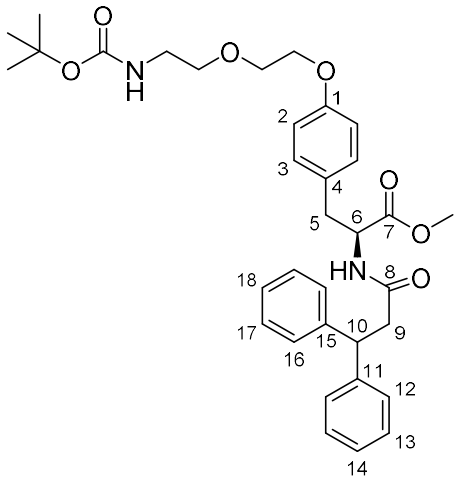

To a stirring solution of **86** (40 mg, 0.1 mmol) in DMF (0.5 mL), were added potassium carbonate (28 mg, 0.2 mmol), and **104** (56 mg, 0.2 mmol). The reaction was heated to 70 °C for 18 h before being cooled, diluted with H_2O (2 mL), extracted into EtOAc (3 x 10 mL), washed with brine (5 mL), dried over Na_2SO_4, filtered, and concentrated *in vacuo*. The residue was then purified by silica gel chromatography (1:1 Hex:EtOAc) to give the title compound as a yellow oil (24 mg, 41%).

R_f: 0.37 (1:1 Hex:EtOAc); **IR** (neat film, ν_{max}, cm^{-1}): 3335 (w), 2928 (w), 2865 (w), 1742 (m), 1710 (m), 1651 (m), 1511 (s), 1451 (m), 1366 (m), 1247 (s), 1173 (s), 1124 (m), 1065 (m); **^{1}H NMR** (400 MHz, $CDCl_3$) δ: 7.34 – 7.20 (m, 10 H, Ar-H $CDCl_3$ overlapped), 6.76 (d, *J* = 8.6 Hz, 2 H, H3), 6.67 (d, *J* = 8.6 Hz, 2 H, H2), 5.91 – 5.83 (br m, 1 H, NH), 4.99 (br s, 1 H, NH), 4.80 – 4.78 (m, 1 H, H6), 4.62 (t, *J* = 7.9 Hz, 1 H, H10), 4.10 (t, *J* = 4.5 Hz, 2H, O-CH_2), 3.83 (t, *J* = 4.9 Hz, 2 H, O-CH_2), 3.67 (s, 3 H, OMe), 3.63 (t, *J* = 4.9 Hz, 2 H, O-CH_2), 3.37 – 3.36 (m, 2 H, N-CH_2), 2.99 – 2.92 (m, 3 H, H5 and H9), 2.84 (dd, *J* = 13.9, 5.7 Hz, 1 H, H9), 1.47 (s, 9 H, 3x CH_3); **^{13}C NMR** (101 MHz, $CDCl_3$) δ: 171.8 (C7), 170.3 (C8), 157.7 (C1), 156.0 (Boc-C=O), 143.8, 143.6, 130.2, 128.6 (2C), 128.0, 127.6, 126.6, 126.5 (C4), 121.9, 114.6 (C2), 79.3 (qC), 70.4, 69.5, 67.3 (3x O-CH_2), 53.1 (C6), 52.2 (OMe), 47.1 (C10), 43.0 (C9), 40.4 (N-CH_2), 37.0 (C5), 28.4 (3x CH_3); **HRMS (ESI):** m/z calcd for $C_{34}H_{42}N_2O_7Na$ $[M+Na]^+$: 613.2884; found: 613.2893; **$[\alpha]_D^{25}$** 8.00 (c = 0.1, MeOH).

Methyl (*S*)-3-(4-(2-(2-aminoethoxy)ethoxy)phenyl)-2-(3,3-diphenylpropanamido) propanoate (108)

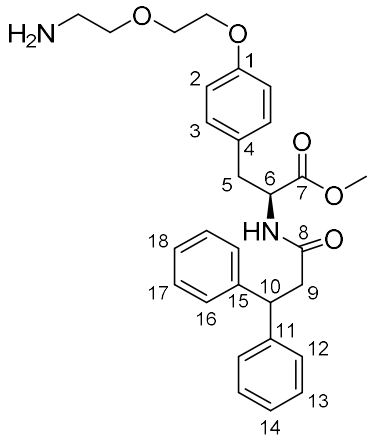

To a stirring solution of **103** (15 mg, 0.025 mmol) in dichloromethane (0.4 mL) was added trifluoroacetic acid (0.1 mL). The reaction was stirred for 3 h at r.t. before being concentrated, diluted with sat. aq. $NaHCO_3$ (2 mL), extracted into dichloromethane (3 x 10 mL), dried over Na_2SO_4, filtered, and concentrated *in vacuo* to give the title compound as a yellow oil (8 mg, 67%) used without further purification.

IR (neat film, ν_{max}, cm^{-1}): 3311 (m), 2927 (m), 1740 (m), 1646 (s), 1536 (m), 1510 (s), 1492 (m), 1450 (m), 1367 (m), 1245 (s), 1218 (s), 1176 (m), 1122 (m), 1065 (m), 1030 (m); **^{1}H NMR** (400 MHz, $CDCl_3$) δ: 7.34 – 7.20 (m, 10 H, Ar-H $CDCl_3$ overlapped), 6.76 (d, *J* = 8.9 Hz, 2 H, H3), 6.65 (d, *J* = 8.9 Hz, 2 H, H2), 5.94 (d, *J* = 7.9 Hz, 1 H, NH), 4.82 – 4.77 (m, 1 H, H6), 4.64 – 4.61 (m, 1 H, H10), 4.14 – 4.11 (m, 2 H, O-CH_2), 3.84 (t, *J* = 4.9 Hz, 2 H, O-CH_2), 3.68 (s, 3 H, OMe), 3.59 (t, *J* = 4.9 Hz, O-CH_2), 3.02 – 2.81 (m, 6 H, N-CH_2, H5 and H9); **^{13}C NMR** (101 MHz, $CDCl_3$) δ: 171.8 (C7), 170.3 (C8), 157.8 (C1), 143.8, 143.6, 130.2, 128.6 (2C), 128.0, 127.7, 126.6, 126.5 (C4), 121.9, 114.7 (C2), 73.6, 69.6, 67.3 (3x O-CH_2), 53.1 (C6), 52.2 (OMe), 47.1 (C10), 43.0 (C9), 41.8 (N-CH_2), 37.0 (C5); **HRMS (ESI):** m/z calcd for $C_{29}H_{35}N_2O_5$ $[M+H]^+$: 491.2541; found: 491.2531; **$[\alpha]_D^{25}$** 35.0 (c = 0.1, MeOH).

Methyl (*S*)-3-(4-(2-(2-(4-(3-(4-cyano-3-(trifluoromethyl)phenyl)-5,5-dimethyl-4-oxo-2-thioxoimidazolidin-1-yl)-2-fluorobenzamido)ethoxy)ethoxy)phenyl)-2-(3,3-diphenylpropanamido)propanoate (PROTAC-10)

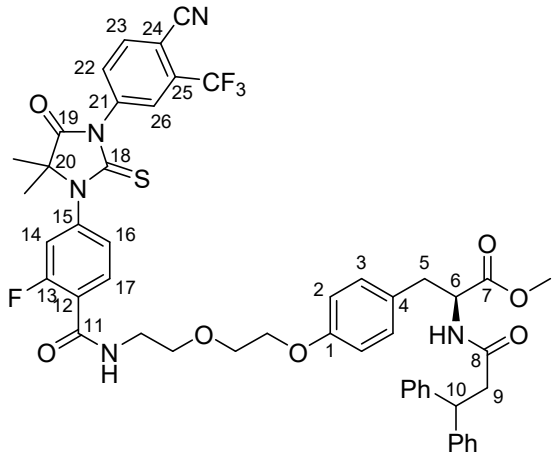

To a stirring solution of **2** (5 mg, 0.011 mmol) in DMF (0.1 mL), were added HATU (4.6 mg, 0.012 mmol) and DIPEA (2.3 µL, 0.012 mmol). The reaction was stirred at r.t. for *ca*. 15 mins before **108** (5.7 mg, 0.012 mmol) in DMF (0.1 mL) was added. The reaction was stirred for a further 18 h before being diluted with EtOAc (5 mL) and H_2O (3 mL), extracted into EtOAc (2 x 5 mL), washed with brine (5 mL), dried over Na_2SO_4, filtered, and concentrated *in vacuo.* The residue was then purified by silica gel chromatography (1% MeOH/DCM) to give the title compound as a yellow oil (5.5 mg, 54%).

R_f: 0.44 (3% MeOH/DCM); **IR** (neat film, ν_{max}, cm^{-1}): 3330 (w), 2928 (m), 2853 (w), 1752 (m), 1655 (s), 1620 (m), 1530 (m), 1510 (s), 1499 (s), 1439 (s), 1413 (s), 1367 (m), 1312 (s), 1286 (m), 1246 (m), 1219 (s), 1177 (s), 1139 (s), 1057 (m); **^{1}H NMR** (400 MHz, $CDCl_3$) δ: 8.25 (t, *J* = 8.4 Hz, 1 H, H17), 7.98 – 7.94 (m, 2 H, H23 and H26), 7.82 (dd, *J* = 8.4, 1.9 Hz, 1 H, H22), 7.30 – 7.07 (m, 13 H, 10x Ar-H, H14, H16, NH, overlapped $CHCl_3$), 6.73 (d, *J* = 8.4 Hz, 2 H, H3), 6.65 (d, *J* = 8.4 Hz, 2 H, H2), 5.80 (d, *J* = 8.2 Hz, 1 H, NH), 4.77 – 4.74 (m, 1 H, H6), 4.60 – 4.57 (m, 1 H, H10), 4.11 – 4.09 (m, 2 H, O-CH_2), 3.87 – 3.85 (m, 2 H, O-CH_2), 3.76 (s, 3 H, OMe), 3.67 – 3.64 (m, 2 H, O-CH_2), 2.97 – 2.83 (m, 6 H, N-CH_2, H5 and H9), 1.60 (s, 6 H, 2x CH_3); **^{13}C NMR** (101 MHz, $CDCl_3$) δ 179.8 (C=S), 174.4 (C19), 171.8 (C7), 170.3 (C8), 162.1 (d, *J* = 3.2 Hz, C11), 160.4 (d, *J* = 250 Hz, C13), 157.7 (C1), 143.8, 143.5, 139.1 (d, *J* = 11.6 Hz, C12), 136.8 (C24), 135.3 (C23), 133.6 (C25), 133.3 (d, *J* = 3.2 Hz, C17), 132.1 (C22), 130.3, 128.6 (2C), 128.0 (2C), 127.6, 127.1 (q, *J* = 4.6 Hz, C26), 126.6, 126.5, 126.1 (d, *J* = 3.2 Hz, C16), 122.9 (d, *J* = 7 Hz, C15), 121.8 (q, *J* = 273 Hz, CF_3), 118.0 (d, *J* = 25.6 Hz, C14), 114.7 (C2), 114.5 (-C≡N), 110.5 (d, *J* = 2.2 Hz, C21), 69.7, 69.6, 67.3 (3x O-CH_2), 66.6 (C20), 53.1 (C6), 52.2 (OMe), 47.1 (C10), 43.0 (C9), 39.9 (N-CH_2), 38.6 (C5), 23.9 (2x CH_3); **^{19}F NMR** (376 MHz, $CDCl_3$) δ: -62.0, -110.1; **HRMS (ESI):** m/z calcd for $C_{49}H_{45}F_4N_5O_7SNa$ $[M+Na]^+$: 946.2868; found: 946.2841; **$[\alpha]_D^{25}$** 0.143 (c = 0.7, MeOH).

Methyl (*S*)-3-(4-((2,2-dimethyl-4-oxo-3,8,11-trioxa-5-azatridecan-13-yl)oxy)phenyl)-2-(3,3-diphenylpropanamido)propanoate (107)

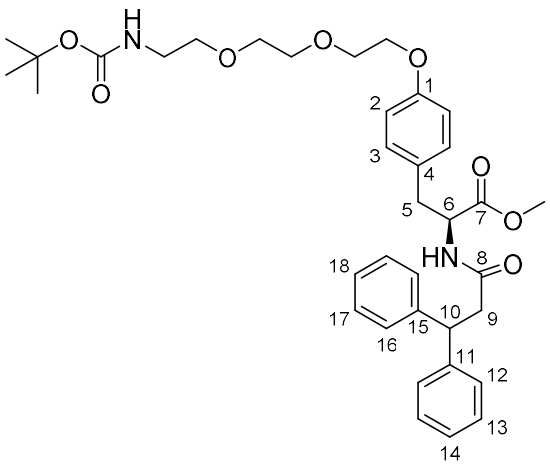

To a stirring solution of **86** (51 mg, 0.13 mmol) in DMF (1 mL), were added potassium carbonate (19 mg, 0.14 mmol), and **106** (50 mg, 0.14 mmol). The reaction was heated to 70 °C for 18 h before being cooled, diluted with H_2O (2 mL), extracted into EtOAc (3 x 10 mL), washed with brine (5 mL), dried over Na_2SO_4, filtered, and concentrated *in vacuo*. The residue was then purified by silica gel chromatography (1:1 Hex:EtOAc) to give the title compound as a yellow oil (53 mg, 67%).

R_f: 0.22 (1:1 Hex:EtOAc); **IR** (neat film, ν_{max}, cm^{-1}): 3310 (w), 2931 (w), 1742 (m), 1707 (m), 1652 (m), 1612 (w), 1510 (s), 1451 (m), 1365 (m), 1245 (s), 1171 (s), 1119 (s), 1108 (s), 1064 (m); **^{1}H NMR** (400 MHz, $CDCl_3$) δ: 7.34 – 7.20 (m, 10 H, Ar-H $CDCl_3$ overlapped), 6.75 (d, *J* = 8.6 Hz, 2 H, H3), 6.66 (d, *J* = 8.6 Hz, 2 H, H2), 5.85 (br s, 1 H, NH), 5.02 (br s, 1 H, NH), 4.81 – 4.76 (m, 1 H, H6), 4.64 – 4.60 (m, 1 H, H10), 4.12 (t, *J* = 4.5 Hz, 2 H, O-CH_2), 3.87 (t, *J* = 5.1 Hz, 2 H, O-CH_2), 3.75 – 3.72 (m, 2 H, O-CH_2), 3.68 – 3.65 (m, 5 H, O-CH_2 and OMe), 3.57 (t, *J* = 5.1 Hz, 2 H, O-CH_2), 3.34 – 3.33 (m, 2 H, N-CH_2), 3.00 – 2.90 (m, 3 H, H5 and H9), 2.83 (dd, *J* = 14.0, 5.7 Hz, 1 H, H9), 1.46 (s, 9 H, 3x CH_3); **^{13}C NMR** (101 MHz, $CDCl_3$) δ: 171.8 (C7), 170.3 (C8), 157.8 (C1), 156.0 (Boc-C=O), 143.8, 143.6, 130.2, 128.6 (2C), 128.0, 127.8, 127.6, 126.6, 126.5 (C5), 114.6 (C2), 79.2 (qC), 70.8, 70.3 (2C), 69.8, 67.3 (5x O-CH_2), 53.1 (C6), 52.2 (OMe), 47.1 (C10), 43.0 (C9), 40.4 (N-CH_2), 37.0 (C5), 28.4 (3x CH_3); **HRMS (ESI):** m/z calcd for $C_{36}H_{46}N_2O_8Na$ $[M+Na]^+$: 657.3146; found: 657.3156; **$[\alpha]_D^{25}$** 4.167 (c = 0.24, MeOH).

Methyl (*S*)-3-(4-(2-(2-(2-aminoethoxy)ethoxy)ethoxy)phenyl)-2-(3,3-diphenylpropanamido)propanoate (109)

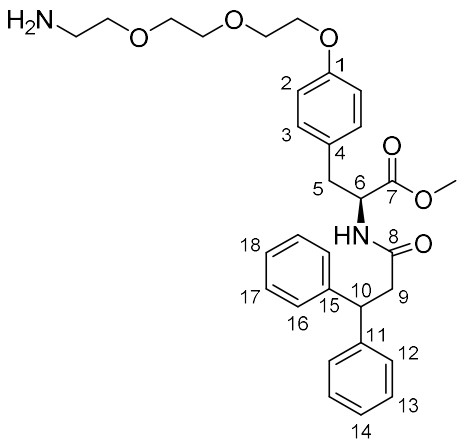

To a stirring solution of **107** (47 mg, 0.0472mmol) in dichloromethane (0.8 mL) was added trifluoroacetic acid (0.2 mL). The reaction was stirred for 3 h at r.t. before being concentrated, diluted with sat. aq. $NaHCO_3$ (2 mL), extracted into dichloromethane (3 x 10 mL), dried over Na_2SO_4, filtered, and concentrated *in vacuo* to give the title compound as a yellow oil (27 mg, 70%) used without further purification.

IR (neat film, ν_{max}, cm^{-1}): 3397 (w), 2988 (m), 2925 (m), 1741 (m), 1706 (s), 1648 (s), 1612 (m), 1536 (m), 1511 (s), 1451 (m), 1361 (m), 1246 (s), 1222 (s), 1179 (m), 1111 (s), 1065 (s); **^{1}H NMR** (400 MHz, $CDCl_3$) δ: 7.34 – 7.18 (m, 10 H, Ar-H $CDCl_3$ overlapped), 6.75 (d, *J* = 8.6 Hz, 2 H, H3), 6.64 (d, *J* = 8.6 Hz, 2 H, H2), 6.14 (d, *J* = 7.4 Hz, 1 H, NH), 4.82 – 4.78 (m, 1 H, H6), 4.65 – 4.61 (m, 1 H, H10), 4.12 (t, *J* = 4.6 Hz, 2 H, O-CH_2), 3.88 – 3.86 (m, 2 H, O-CH_2), 3.76 – 3.74 (m, 2 H, O-CH_2), 3.68 – 3.66 (m, 5 H, O-CH_2 and OMe), 3.52 (t, *J* = 4.9 Hz, 2 H, N-CH_2), 2.98 – 2.87 (m, 3 H, H5 and H9), 2.82 (dd, *J* = 13.8, 5.7 Hz, 1 H, H9); **^{13}C NMR** (101 MHz, $CDCl_3$) δ: 171.8 (C7), 170.3 (C8), 157.8 (C1), 143.8, 143.6, 130.3, 128.6 (2C), 128.0, 127.9, 127.7, 126.6, 126.5 (C5), 114.5 (C2), 73.6, 70.8, 70.4, 69.8, 67.4 (5x O-CH_2), 53.1 (C6), 52.2 (OMe), 47.1 (C10), 42.9 (C9), 41.7 (N-CH_2), 37.0 (C5); **HRMS (ESI):** m/z calcd for $C_{31}H_{39}N_2O_6$ $[M+H]^+$: 535.2803; found: 535.2814; **$[\alpha]_D^{25}$** 11.058 (c = 0.208, MeOH).

Methyl (*S*)-3-(4-(2-(2-(2-(4-(3-(4-cyano-3-(trifluoromethyl)phenyl)-5,5-dimethyl-4-oxo-2-thioxoimidazolidin-1-yl)-2-fluorobenzamido)ethoxy)ethoxy)ethoxy)phenyl)-2-(3,3-diphenylpropanamido)propanoate (PROTAC-11)

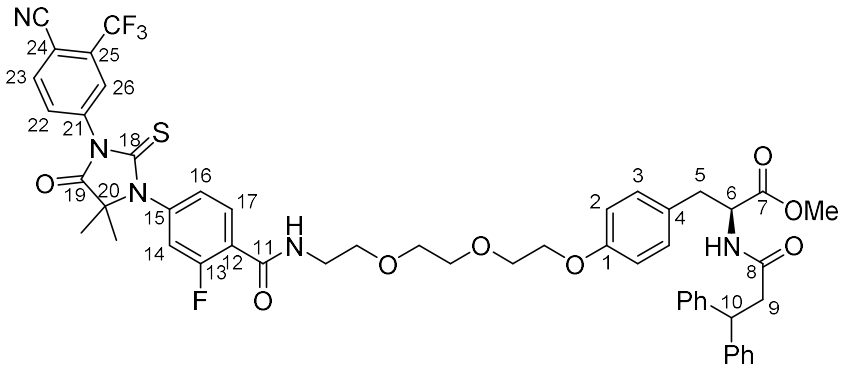

To a stirring solution of **2** (10 mg, 0.022 mmol) in DMF (0.1 mL), were added HATU (10.1 mg, 0.027 mmol) and DIPEA (5.2 µL, 0.027 mmol). The reaction was stirred at r.t. for *ca*. 15 mins before **109** (13 mg, 0.024 mmol) in DMF (0.1 mL) was added. The reaction was stirred for a further 18 h before being diluted with EtOAc (5 mL) and H_2O (3 mL), extracted into EtOAc (2 x 5 mL), washed with brine (5 mL), dried over Na_2SO_4, filtered, and concentrated *in vacuo.* The residue was then purified by silica gel chromatography (1% MeOH/DCM) to give the title compound as a yellow oil (15 mg, 70%).

R_f: 0.36 (3% MeOH/DCM); **IR** (neat film, ν_{max}, cm^{-1}): 3304 (w), 2916 (w), 1751 (m), 1654 (m), 1620 (m), 1532 (m), 1497 (m), 1437 (m), 1411 (m), 1310 (s), 1246 (m), 1217 (s), 1176 (s), 1134 (s), 1055 (m); **^{1}H NMR** (400 MHz, $CDCl_3$) δ: 8.22 (t, *J* = 8.2 Hz, 1 H, H17), 7.98 – 7.95 (m, 2 H, H23 and H26), 7.83 – 7.81 (m, 1 H, H22), 7.30 – 7.09 (m, 13 H, 10x Ar-H, H14, H16, NH), 6.71 (d, *J* = 8.5 Hz, 2 H, H3), 6.63 (d, *J* = 8.5 Hz, 2 H, H2), 5.84 (d, *J* = 7.7 Hz, 1 H, NH), 4.77 – 4.72 (m, 1 H, H6), 4.58 (t, *J* = 7.9 Hz, 1 H, H10), 4.07 (t, *J* = 4.2 Hz, 2 H, O-CH_2), 3.85 (t, *J* = 5.0 Hz, 2 H, O-CH_2), 3.76 – 3.73 (m, 2 H, O-CH_2), 3.71 – 3.67 (m, 4 H, 2x O-CH_2), 3.64 (s, 3 H, OMe), 2.97 – 2.78 (m, 6 H, N-CH_2, H5 and H9), 1.58 (s, 6 H, 2x CH_3); **^{13}C NMR** (101 MHz, $CDCl_3$) δ: 179.7 (C=S), 174.4 (C19), 171.8 (C7), 170.3 (C8), 162.1 (d, *J* = 3.0 Hz, C11), 160.4 (d, *J* = 250 Hz, C13), 157.7 (C1), 143.8, 143.5, 138.9 (d, *J* = 10.9 Hz, C12), 136.8 (C24), 135.3 (C23), 133.9 (C25), 133.3 (d, *J* = 3.3 Hz, C17), 132.1 (C22), 130.2, 128.6 (2C), 127.9 (2C), 127.6, 127.1 (d, *J* = 4.8 Hz, C26), 126.6, 126.5, 126.1 (d, *J* = 3.3 Hz, C16), 123.0 (d, *J* = 12.0 Hz, C15), 121.8 (q, *J* = 275 Hz, CF_3), 117.9 (d, *J* = 27 Hz, C14), 114.7 (C2), 114.5 (-C≡N), 110.4 (d, *J* = 2.1 Hz, C21), 70.8, 70.4, 69.8, 69.6, 67.3 (5x O-CH_2), 66.6 (C20), 53.1 (C6), 52.2 (OMe), 47.1 (C10), 42.9 (C9), 39.9 (N-CH_2), 37.0 (C5), 23.8 (2x CH_3); **^{19}F NMR** (376 MHz, $CDCl_3$) δ: -62.0, -110.3; **HRMS (ESI):** m/z calcd for $C_{51}H_{49}F_4N_5O_8SNa$ $[M+Na]^+$: 990.3130; found: 990.3131; **$[\alpha]_D^{25}$** 0.286 (c = 0.7, MeOH).

Ethyl 6-chloro-3-formyl-1*H*-indole-2-carboxylate (112)

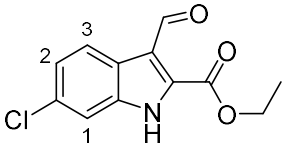

Following a modified literature procedure,[350] to a stirring solution of ethyl 6-chloroindole-2-carboxylate (0.336 g, 1.5 mmol) in DMF (1.5 mL), was dropwise added $POCl_3$ (0.17 mL, 1.8 mmol). The reaction was heated to 50 °C for 18 h before cooling and quenching with sat. aq. $NaHCO_3$ (10 mL). The reaction was then extracted into EtOAc (3 x 20 mL), washed with H_2O (10 mL) and brine (10 mL), dried over Na_2SO_4, filtered, and concentrated *in vacuo*. The residue was then triturated in Et_2O and filtered to give the title compound as a beige amorphous solid (0.240 g, 64%).

R_f: 0.71 (1:1 Hex:EtOAc); **IR** (neat film, ν_{max}, cm^{-1}): 3140 (m), 2985 (w), 1725 (s, C=O), 1638 (s, C=O), 1570 (m), 1531 (m), 1430 (s), 1391 (m), 1373 (m), 1299 (m), 1219 (s), 1192 (s), 1145 (m), 1099 (m), 1063 (m), 1028 (m); **^{1}H NMR** (400 MHz, d6-DMSO) δ: 12.88 (s, 1 H, NH) , 10.57 (s, 1 H, -CHO), 8.21 (d, *J* = 8.6 Hz, 1 H, H3), 7.55 (d, *J* = 1.8 Hz, 1 H, H1), 7.31 (dd, *J* = 8.6, 1.8 Hz, 1H, H2), 4.46 (q, *J* = 7.1 Hz, 2 H, CH_2), 1.40 (t, *J* = 7.1 Hz, 3 H, CH_3); **^{13}C NMR** (101 MHz, d6-DMSO) δ: 187.4 (CHO), 159.9 (COO), 136.1, 133.5, 130.4, 124.0, 123.9 (ArCH), 123.4 (ArCH), 118.2, 112.6 (ArCH), 62.0 (CH_2), 14.0 (CH_3).

Data are in accordance with those reported previously in literature[350].

***N*-((4-fluorophenyl)(tosyl)methyl)formamide (115)**

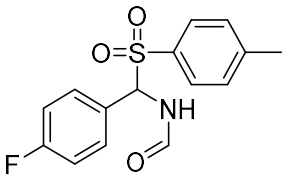

Following a literature procedure,[234] to a stirring solution of sodium *p*-toluenesulfinate (3.56 g, 20 mmol) in a 1:1 mixture of Et_2O and H_2O (50 mL) cooled to 0 °C, was dropwise added conc. HCl (1.8 mL). The mixture was stirred for 1 h at r.t. before being separated, extracted into Et_2O (3 x 20 mL), dried over Na_2SO_4, filtered, and the volume reduced by 2/3 *in vacuo*. PE 40-60 (20 mL) was then added and the solid was filtered, washed with petroleum ether (5 mL) and dried *in vacuo* to give *p*-toluenesulfinic acid as a white solid (2.79 g, 89%), which was then combined with 4-fluorobenzaldehyde (1.28 mL, 12 mmol), formamide (1.19 mL, 30 mmol), chlorotrimethylsilane (1.68 mL, 13.2 mmol) in a 1:1 mixture of toluene and acetonitrile (14 mL). The reaction was heated to 50 °C for 5 h before being cooled to 0 °C and H_2O (20 mL) and MTBE (5 mL) were added. The mixture was stirred for a further 30 mins before

being filtered and dried *in vacuo* to give the title compound as an amorphous white powder (2.39 g, 65%).

R_f: 0.76 (6:4 Hex:EtOAc); **IR** (neat film, ν_{max}, cm^{-1}): 3174 (m), 3064 (m), 2896 (m), 1699 (w), 1599 (w), 1456 (m), 1426 (m), 1155 (s), 1125 (s); **^{1}H NMR** (400 MHz, $CDCl_3$) δ: 8.16 (s, 1 H, CHO), 7.73 (d, *J* = 7.8 Hz, 2 H,), 7.45 – 7.42 (m, 2 H), 7.16 – 7.08 (m, 3 H), 6.33 (d, *J* = 10.3 Hz, 1 H), 2.47 (s, 3 H); **^{13}C NMR** (101 MHz, $CDCl_3$) δ: 163.7 (d, *J* = 250 Hz, C-F), 159.6 (C=O), 145.8, 132.8, 130.8 (d, *J* = 8.6 Hz), 129.9, 129.4, 116.2, 115.9, 69.8, 21.8; **^{19}F NMR** (376 MHz, $CDCl_3$) δ: -111.3.

Data are in accordance with the literature.[351]

1-Fluoro-4-(isocyano(tosyl)methyl)benzene (116)

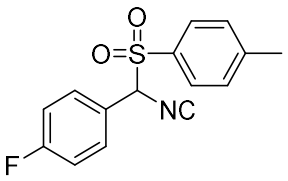

Following a literature procedure,[234] to a stirring solution of **115** (1.20 g, 4.0 mmol) in tetrahydrofuran (20 mL) cooled to 0 °C, were dropwise added $POCl_3$ (1.12 mL, 12 mmol) and triethylamine (2.81 mL, 20 mmol) in tetrahydrofuran (2 mL). The reaction was stirred at 0 °C for 2 h before being poured into H_2O (35 mL). The mixture was then extracted into EtOAc (3 x 20 mL), washed with sat. aq. $NaHCO_3$ (10 mL), dried over Na_2SO_4, filtered, and concentrated *in vacuo*. The residue was then triturated in hexane to give the title compound as a brown amorphous powder (1.00 g, 87%).

R_f: 0.70 (6:4 Hex:EtOAc); **IR** (neat film, ν_{max}, cm^{-1}): 3079 (w), 2937 (w), 2137 (m), 1689 (m), 1596 (m), 1508 (m), 1330 (m), 1304 (m), 1289 (m), 1232 (m), 1145 (s), 1083 (m); **^{1}H NMR** (400 MHz, $CDCl_3$) δ: 7.65 (d, *J* = 8.5 Hz, 2 H), 7.38 – 7.35 (m, 4 H), 7.12 (t, *J* = 8.5 Hz, 2 H), 5.62 (s, 1 H), 2.50 (s, 3 H); **^{13}C NMR** (101 MHz, $CDCl_3$) δ: 165.9 (d, *J* = 250 Hz, CF), 162.9 (NC), 146.8, 130.5 (overlapping signals), 129.9, 122.5 (d, *J* = 4 Hz), 116.2, 115.9, 75.7, 21.8; **^{19}F NMR** (376 MHz, $CDCl_3$) δ: -109.0.

Data are in accordance with the literature.[351]

Ethyl 6-chloro-3-(1-(4-chlorobenzyl)-4-(4-fluorophenyl)-1*H*-imidazol-5-yl)-1*H*-indole-2-carboxylate (118)

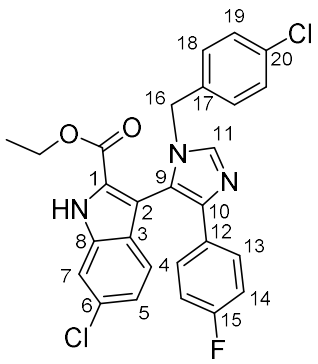

To a stirring solution of **112** (100 mg, 0.4 mmol) in ethanol (2 mL) was added 4-chlorobenzylamine (48.7 µL, 0.4 mmol). The reaction was stirred at r.t. for 30 mins before **116** (115.7 mg, 0.4 mmol) and triethylamine (56 µL, 0.4 mmol) were added. The reaction was then heated to 50 °C for 3 h before cooling to r.t., stirring for a further 16 h, and concentrating *in vacuo*. The residue was then purified by silica gel chromatography (7:3 to 1:1 Hex/EtOAc) to give the title compound as a yellow oil (118 mg, 58%).

R_f: 0.35 (1:1 Hex:EtOAc); **IR** (neat film, ν_{max}, cm^{-1}): 2983 (w), 1704 (s), 1601 (w), 1568 (w), 1527 (m), 1493 (m), 1439 (m), 1410 (m), 1365 (m), 1312 (m), 1218 (s), 1194 (m), 1155 (m), 1121 (m), 1090 (m), 1060 (m), 1015 (m); **^{1}H NMR** (400 MHz, $CDCl_3$) δ: 9.89 (s, 1H, NH), 7.81 (s, 1 H, H11), 7.46 – 7.42 (m, 3 H, H7 and H13), 7.13 – 7.05 (m, 4 H, H4, H5 and H19), 6.86 – 6.80 (m, 2 H, H14), 6.76 (d, *J* = 8.3 Hz, 2 H, H18), 4.91 – 4.82 (m, 2 H, H16), 4.19 – 4.10 (m, 2 H, O-CH_2), 1.12 (t, *J* = 7.2 Hz, CH_3); **^{13}C NMR** (101 MHz, $CDCl_3$) δ: 161.7 (d, *J* = 246 Hz, C15), 160.8 (C=O), 139.9 (C10), 137.6 (C11), 136.2 (C8), 134.5 (C17), 133.9 (C20), 132.3 (C6), 130.6 (d, *J* = 2.9 Hz, C12), 128.7 (C19), 128.6 (C18), 127.5 (d, *J* = 7.6 Hz, C13), 126.7, 126.5 (C1 and C3), 122.9 (C5), 122.1 (C4), 119.3 (C9), 115.1 (d, *J* = 21 Hz, C14), 112.1 (C7), 110.7 (C2), 61.3 (O-CH_2), 48.8 (C16), 14.0 (CH_3); **^{19}F NMR** (376 MHz, $CDCl_3$) δ: -115.9; **HRMS (ESI):** m/z calcd for $C_{27}H_{21}Cl_2FN_3O_2$ $[M+H]^+$: 508.0990; found: 508.0990.

6-Chloro-3-(1-(4-chlorobenzyl)-4-(4-fluorophenyl)-1*H*-imidazol-5-yl)-1*H*-indole-2-carboxylic acid (87)

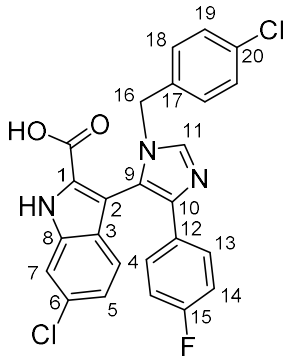

To a stirring solution of **118** (66 mg, 0.13 mmol) in ethanol (1 mL) was added 2 M NaOH (aq, 1 mL). The mixture was heated to reflux for 3 h before being cooled, poured over ice and acidified with 3 M HCl. The mixture was then extracted into EtOAc (3 x 10 mL), washed with brine, dried over Na_2SO_4, filtered, and concentrated *in vacuo* to give the title compound as a yellow oil (62 mg, >98%) used without further purification.

IR (neat film, ν_{max}, cm^{-1}): 3404 (w), 1704 (s), 1592 (w), 1565 (w), 1510 (m), 1493 (m), 1433 (m), 1361 (s), 1327 (m), 1222 (s), 1162 (m), 1090 (m), 1015 (m); **^{1}H NMR** (400 MHz, MeOD) δ: 8.28 (s, 1H, H11), 7.46 (d, *J* = 1.7 Hz, 1 H, H7), 7.39 – 7.35 (m, 2 H), 7.00 (d, *J* = 8.4 Hz, 2 H), 6.88 – 6.84 (m, 3 H), 6.80 – 6.78 (m, 3 H), 5.11 (d, *J* = 15.2 Hz, 1 H, H16), 4.99 (d, *J* = 15.2 Hz, H16); **^{13}C NMR** (101 MHz, MeOD) δ: 162.0 (d, *J* = 248 Hz, C15), 162.7 (C=O), 137.2 (2C), 136.8 (C10, C11, C8), 136.4 (C17), 134.5 (C20), 133.3 (C6), 130.7 (C19), 128.9 (d, *J* = 3.2 Hz, C12), 128.8 (C18), 128.1 (C1), 127.8 (d, *J* = 8.2 Hz, C13), 126.0 (C3), 121.4, 121.3, 121.0 (C4, C5, C9), 114.6 (d, *J* = 22 Hz, C14), 111.8 (C7), 107.6 (C2), 48.9 (C16); **^{19}F NMR** (376 MHz, MeOD) δ: -116.4; **HRMS (ESI):** m/z calcd for $C_{25}H_{15}Cl_2FN_3O_2$ $[M-H]^-$: 478.0531; found: 478.0518.

4-((3,4-difluorobenzyl)oxy)benzonitrile (121)

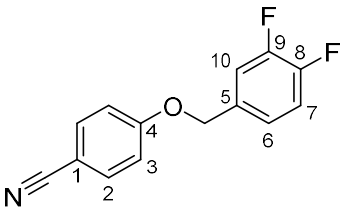

To a stirring solution of 4-cyanophenol (0.50 g, 4.2 mmol) in acetone (50 mL), were added potassium carbonate (2.10 g, 15.2 mmol) and 3,4-difluorobenzylbromide (0.49 mL, 3.8 mmol). The reaction was

heated to 65 °C for 6 h before cooling and concentrating *in vacuo*. The reaction was then diluted in dichloromethane (20 mL), washed with H_2O (2 x 10 mL), dried over Na_2SO_4, filtered, and concentrated *in vacuo* to give the title compound as a white amorphous solid (0.910 g, 98%) used without further purification.

R_f: 0.22 (9:1 PE 40-60:EtOAc); **IR** (neat film, ν_{max}, cm^{-1}): 3053 (w), 2905 (w), 2219 (m, CN), 1603 (m), 1519 (m), 1506 (m), 1438 (m), 1383 (w), 1291 (m), 1248 (s), 1170 (m), 1116 (m), 1001 (m); **^{1}H NMR** (400 MHz, $CDCl_3$) δ: 7.60 (d, *J* = 8.9 Hz, 2H, H2), 7.12 – 7.28 (m, 3H, H6, H7 and H10), 7.00 (d, *J* = 8.9 Hz, 2H, H3), 5.06 (s, 2H, CH_2); **^{13}C NMR** (101 MHz, $CDCl_3$) δ: 161.5 (C4), 150.6 (dd, *J* = 250, 26 Hz, C-F), 150.5 (dd, *J* = 250, 26 Hz, C-F), 134.1 (C2), 132.7 (dd, *J* = 5.4, 3.9 Hz, C5), 123.4 (dd, *J* = 6.5, 3.7 Hz, C6), 119.0 (C≡N), 117.6 (d, *J* = 18.6 Hz, C7/10), 116.5 (d, *J* = 18.6 Hz, C7/10), 115.5 (C3), 104.7 (C1), 69.0 (d, *J* = 1.3 Hz, CH_2); **^{19}F NMR** (376 MHz, $CDCl_3$) δ: -138.86 (d, *J* = 21.0 Hz), -137.66 (d, *J* = 21.0 Hz); **HRMS (ESI):** m/z calcd for $C_{14}H_{10}F_2NO$ $[M+H]^+$: 246.0725; found 246.0734.

(4-((3,4-difluorobenzyl)oxy)phenyl)methanamine (122)

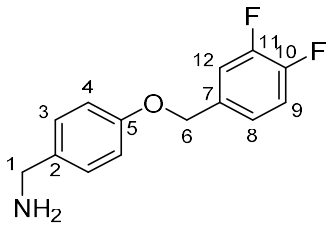

To a stirring solution of **121** (0.90 g, 3.67 mmol) in tetrahydrofuran (25 mL) cooled to 0 °C, was added lithium aluminium hydride (0.836 g, 22 mmol). The reaction was stirred at r.t. for 15 h before cooling to 0 °C and quenching with H_2O (2 mL), followed by 15% NaOH (1 mL), and H_2O (2 mL). The mixture was stirred for a further 2 h before filtering and concentrating *in vacuo* to give the title compound as a yellow oil (0.807 g, 88%) used without further purification.

IR (neat film, ν_{max}, cm^{-1}): 3304 (w), 2928 (w), 2869 (w), 1610 (m), 1584 (m), 1509 (s), 1462 (m), 1435 (m), 1381 (m), 1285 (s), 1236 (s), 1210 (s), 1176 (m), 1114 (m), 1020 (w); **^{1}H NMR** (400 MHz, $CDCl_3$) δ: 7.31 – 7.25 (m, 3 H,), 7.22 – 7.14 (m, 2 H,), 6.96 – 6.91 (m, 2 H,), 5.02 (s, 2 H, H6), 3.83 (s, 2 H, H1), 1.64 (br s, 2 H, NH_2); **^{13}C NMR** (101 MHz, $CDCl_3$) δ: 157.3 (C5), 150.5 (dd, *J* = 250, 49 Hz, C-F), 150.4 (dd, *J* = 250, 49 Hz, C-F), 136.2 (C3), 134.2 – 134.1 (m, C7), 128.4 (C2), 123.2 (dd, *J* = 6.4, 3.7 Hz, C8), 117.3 (d, *J* = 17.4 Hz, C9 or C12), 116.4 (d, *J* = 17.4 Hz, C9 or C12), 114.9 (C4), 68.8 (C6), 45.9 (C1); **^{19}F NMR** (376 MHz, $CDCl_3$) δ: -138.3 (d, *J* = 21 Hz), -140.0 (d, *J* = 21 Hz); **HRMS (ESI):** m/z calcd for $C_{14}H_{14}F_2NO$ $[M+H]^+$: 250.1038; found 250.1046.

Ethyl 6-chloro-3-(1-(4-((3,4-difluorobenzyl)oxy)benzyl)-4-(4-fluorophenyl)-1*H*-imidazol-5-yl)-1*H*-indole-2-carboxylate (123)

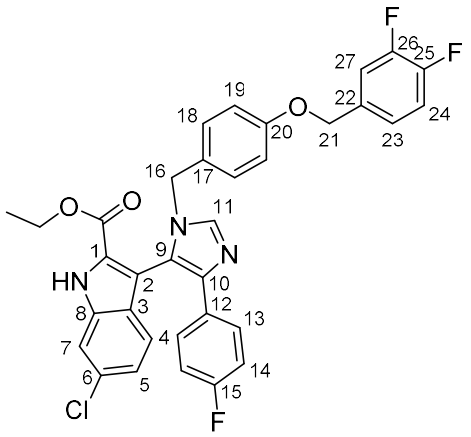

To a stirring solution of **112** (100 mg, 0.4 mmol) in ethanol (2 mL) was added **122** (99 mg, 0.4 mmol). The reaction was stirred at r.t. for 30 mins before **116** (115.7 mg, 0.4 mmol) and triethylamine (56 µL, 0.4 mmol) were added. The reaction was then heated to 50 °C for 3 h before cooling to r.t., stirring for a further 16 h, and concentrating *in vacuo*. The residue was then purified by silica gel chromatography (7:3 to 1:1 Hex/EtOAc) to give the title compound as a yellow oil (160 mg, 65%).

R_f: 0.23 (6:4 EtOAc/Hex); **IR** (neat film, ν_{max}, cm^{-1}): 3038 (w), 1706 (m), 1669 (m), 1612 (m), 1513 (s), 1435 (m), 1308 (m), 1290 (m), 1233 (s), 1199 (s), 1178 (s), 1137 (m), 1117 (m), 1061 (w), 1023 (w); **^{1}H NMR** (400 MHz, $CDCl_3$) δ: 10.81 (br s, 1 H, -NH), 8.57 (s, 1 H, H11), 7.54 (s, 1 H, H7), 7.34 – 7.40 (m, 2 H, H13), 7.08 – 7.22 (m, 3H, H23, H24, H27), 6.97 – 7.02 (m, 2 H, H4, H5), 6.75 – 6.88 (m, 4H, H18 and H14), 6.66 (d, *J* = 8.6 Hz, 2H, H19), 4.83 - 4.96 (m, 4H, 2 x CH_2), 4.06 – 4.20 (m, 2H, CH_2), 1.11 (t, *J* = 7.1 Hz, 3H, CH_3); **^{13}C NMR** (101 MHz, $CDCl_3$) δ: 162.6 (d, *J* = 250 Hz, C15), 160.5 (C=O), 159.2 (C12), 158.7 (C20), 151.5 (dd, *J* = 37, 13 Hz, C25), 149.1 (dd, *J* = 37, 13 Hz, C26), 136.6 (C8), 136.2 (C11), 135.0 (C10), 133.6 (m, C22), 132.4 (C6), 129.6 (C18), 128.3 (d, *J* = 8.1 Hz, C13), 127.7 (C1), 126.3 (C3), 126.2 (C17), 123.5 (m, C23), 123.4 (C5), 121.4 (C4), 121.1 (C9), 117.5 (d, *J* = 17.5 Hz, C24), 116.5 (d, *J* = 17.5 Hz, C27), 115.9 (d, *J* = 21.5 Hz, C14), 115.2 (C19), 112.8 (C7), 107.5 (C2), 68.9 (C21), 61.7 (-**C**H_2-CH_3), 50.4 (C16), 14.1 (CH_3); **^{19}F NMR** (376 MHz, $CDCl_3$) δ: -116.26, -137.21 (d, *J* = 21.0 Hz), -138.69 (d, *J* = 21.0 Hz); **HRMS (ESI):** m/z calcd for $C_{34}H_{26}ClF_3N_3O_3$ $[M+H]^+$: 616.1610; found: 616.1599.

6-Chloro-3-(1-(4-((3,4-difluorobenzyl)oxy)benzyl)-4-(4-fluorophenyl)-1*H*-imidazol-5-yl)-1*H*-indole-2-carboxylic acid (110)

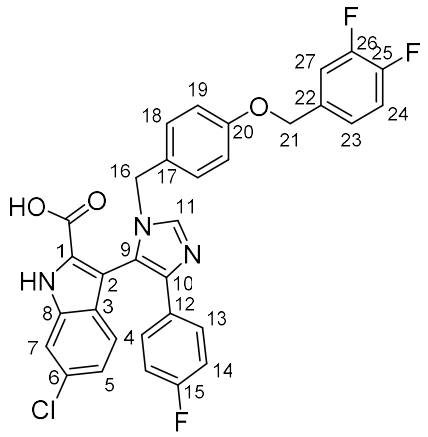

To a stirring solution of **123** (76 mg, 0.12 mmol) in ethanol (1 mL) was added 2 M NaOH (aq, 1 mL). The mixture was heated to reflux for 3 h before being cooled, poured over ice and acidified with 3 M HCl. The mixture was then extracted into EtOAc (3 x 10 mL), washed with brine, dried over Na_2SO_4, filtered, and concentrated *in vacuo* to give the title compound as a yellow solid (53 mg, 73%) used without further purification.

IR (neat film, ν_{max}, cm^{-1}): 1700 (w), 1612 (m), 1513 (s), 1437 (m), 1369 (m), 1325 (m), 1289 (m), 1241 (s), 1177 (m), 1115 (m); **^{1}H NMR** (400 MHz, MeOD) δ: 8.44 (s, 1 H, H11), 7.48 (d, *J* = 1.6 Hz, 1 H, H7), 7.40 – 7.35 (m, 2 H, H13), 7.30 – 7.15 (m, 3 H, H23, H24, H27), 6.89 (t, *J* = 8.7 Hz, 2 H, H18), 6.84 (dd, *J* = 8.6, 1.6 Hz, 1H, H5), 6.78 – 6.75 (m, 3 H, H4 and 14), 6.62 (d, *J* = 8.7 Hz, 2 H, H19), 5.12 (d, *J* = 14.7 Hz, 1 H, H16), 4.94 (d, *J* = 14.7 Hz, 1 H, H16), 4.86 (m, 2 H, H21); **^{13}C NMR** (101 MHz, MeOD) δ: 162.8 (C=O), 162.1 (d, *J* = 250 Hz, C15), 158.2 (2C, C12 and C20), 151.4 (C25), 148.4 (C26), 136.6 (C11), 136.4 (C8), 134.7, 131.2, 130.5, 128.9, 128.0 (d, *J* = 8 Hz), 127.8 (2C), 126.1, 123.5 (m), 121.3, 121.1, 116.9 (d, *J* = 18 Hz,), 116.0 (d, *J* = 17.5 Hz,), 115.2, 114.9 (d, *J* = 22 Hz), 114.5, 111.8 (C7), 107.1 (C2), 68.3 (C21), 49.6 (C16); **^{19}F NMR** (376 MHz, MeOD) δ: -117.0, -141.5 (d, *J* = 21 Hz), -143.0 (d, *J* = 21 Hz); **HRMS (ESI):** m/z calcd for $C_{32}H_{20}ClF_3N_3O_3$ $[M-H]^-$: 586.1151; found: 586.1134.

***tert*-Butyl (2-(2-(2-(4-(3-(4-cyano-3-(trifluoromethyl)phenyl)-5,5-dimethyl-4-oxo-2-thioxoimidazolidin-1-yl)-2-fluorobenzamido)ethoxy)ethoxy)ethyl)carbamate (124)**

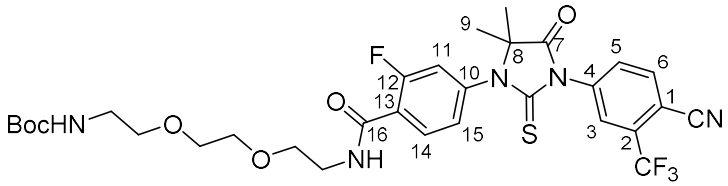

To a stirring solution of **2** (15 mg, 0.03 mmol) in DMF (159 µl) were added HATU (15.16 mg, 0.04 mmol) and DIPEA (6.95 µl, 0.04 mmol). The reaction was stirred for *ca*. 10 mins at 25 °C before **36** (9.90 mg, 0.04 mmol) was added. The reaction was stirred for a further 3 h before being dissolved in EtOAc (5 mL) and H_2O (3 mL), extracted into EtOAc (3 x 5 mL), dried over $MgSO_4$ and concentrated *in vacuo*. The residue was then purified by flash column chromatography (0 to 100% EtOAc/Heptane) to give the title compound (17.00 mg, 75%) as a yellow oil.

R_f: 0.30 (80% EtOAc/Hex); **IR** (neat film, ν_{max}, cm^{-1}): 3361 (w, NH), 2931 (w, CH), 2865 (w, CH), 1758 (m, C=O), 1702 (m, C=O), 1659 (m, C=O), 1619 (m), 1528 (m), 1499 (m), 1434 (m), 1413 (m), 1366 (m), 1311 (s), 1288 (m), 1219 (m), 1176 (s), 1135 (s), 1056 (m); **^{1}H NMR** (500 MHz, $CDCl_3$) δ: 8.24 (t, J = 7.5 Hz, 1 H, H14), 7.99 (d, J = 8.3 Hz, 1 H, H6), 7.95 (d, J = 1.9 Hz, 1 H, H3), 7.83 (dd, J = 8.3, 2.0 Hz, 1 H, H5), 7.22 – 7.26 (m, 1 H, H15), 7.15 – 7.19 (m, 1 H, H11), 4.99 (s, 1 H, NH), 3.74 – 3.62 (m, 8 H, 4x CH_2), 3.55 (t, J = 5.2 Hz, 2 H, CH_2), 3.38 – 3.27 (m, 2 H, CH_2), 1.62 (s, 6 H, H9), 1.43 (s, 9 H, 3x CH_3); **^{13}C NMR** (126 MHz, $CDCl_3$) δ: 179.7 (C=S), 174.5 (C7), 162.2 (C=O), 160.4 (d, *J* = 250 Hz, C12), 156.1 (Boc-C=O), 139.0 (d, *J* = 11 Hz, C13), 136.8 (C1), 135.3 (C6), 133.7 (q, *J* = 33 Hz, C2), 133.3 (C14), 132.1 (C5), 127.1 (q, *J* = 3.5 Hz, C3), 126.1 (d, *J* = 3 Hz, C15), 122.9 (d, *J* = 13 Hz, C10), 121.8 (q, *J* = 275 Hz, CF_3), 118.0 (d, *J* = 28 Hz, C11), 114.7 (-C≡N), 110.4 (C4), 79.5 (boc-qC), 70.4, 70.3, 70.2, 69.6 (4x O-CH_2), 66.6 (C8), 40.5, 39.9 (2x N-CH_2), 28.4 (3x CH_3), 23.9 (C9); **^{19}F NMR** (471 MHz, $CDCl_3$) δ: -62.96, -111.31; **HRMS (ESI):** m/z calcd for $C_{31}H_{36}F_4N_5O_6S$ $[M+H]^+$: 682.2317; found: 682.2308.

***N*-(2-(2-(2-aminoethoxy)ethoxy)ethyl)-4-(3-(4-cyano-3-(trifluoromethyl)phenyl)-5,5-dimethyl-4-oxo-2-thioxoimidazolidin-1-yl)-2-fluorobenzamide (125)**

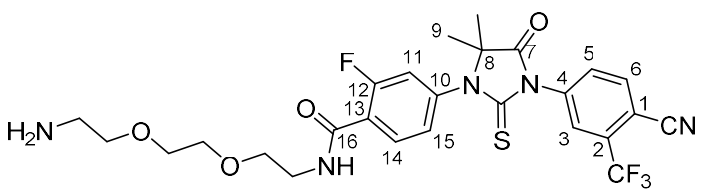

To a stirring solution of **124** (15 mg, 0.02 mmol) in dichloromethane (110 µl) was added 2,2,2-trifluoroacetic acid (251 mg, 2.20 mmol). The reaction was stirred at 25 °C for 2 h before concentrating and dissolving in sat. *aq*. $NaHCO_3$ (5 mL) and extracting into EtOAc (3 x 10 mL), drying over $MgSO_4$, filtering and concentrating *in vacuo* to give the title compound (11.00 mg, 86 %) as a colourless oil used without further purification.

IR (neat film, ν_{max}, cm^{-1}): 3350 (w, NH), 2919 (w, CH), 2849 (w, CH), 1757 (m, C=O), 1655 (m, C=O), 1620 (m), 1534 (m), 1499 (m), 1438 (m), 1413 (m), 1311 (s), 1219 (m), 1177 (m), 1133 (s), 1056 (m); **^{1}H NMR** (500 MHz, $CDCl_3$) δ: 8.21 (t, *J* = 8.3 Hz, 1 H, H14), 7.99 (d, *J* = 8.3 Hz, 1 H, H6), 7.95 (d, *J* = 1.5 Hz, 1 H, H3), 7.83 (dd, *J* = 8.2, 1.8 Hz, 1 H, H5), 7.28 – 7.37 (m, 1 H, NH), 7.23 (dd, *J* = 8.3, 1.8 Hz, 1 H, H15), 7.16 (d, *J* = 10.3 Hz, 1 H, H11), 3.72 – 3.62 (m, 8 H, 4x CH_2), 3.58 – 3.50 (m, 2 H, CH_2), 2.96 – 2.80 (m, 2 H, CH_2), 1.61 (s, 6 H, H9); **^{13}C NMR** (126 MHz, $CDCl_3$) δ: 179.8 (C=S), 174.5 (C7), 162.3 (C=O), 160.4 (d, *J* = 250 Hz, C12), 138.9 (d, *J* = 11 Hz, C13), 136.8 (C1), 135.3 (C6), 133.7 (q, *J* = 33 Hz, C2), 133.2 (C14), 132.1 (C5), 127.1 (q, *J* = 3.5 Hz, C3), 126.1 (C15), 123.1 (d, *J* = 11.6 Hz, C10), 121.9 (q, *J* = 275 Hz, CF_3), 118.0 (d, *J* = 28 Hz, C11), 114.7 (-C≡N), 110.4 (C4), 72.4, 70.4, 70.2, 69.6 (4x O-CH_2), 66.6 (C8), 41.3, 39.9 (2x N-CH_2), 23.8 (C9); **^{19}F NMR** (471 MHz, $CDCl_3$) δ: -61.99, -110.42; **HRMS (ESI):** m/z calcd for $C_{26}H_{28}F_4N_5O_4S$ $[M+H]^+$: 582.1793; found: 582.1793.

6-Chloro-3-(1-(4-chlorobenzyl)-4-(4-fluorophenyl)-1*H*-imidazol-5-yl)-*N*-(2-(2-(2-(4-(3-(4-cyano-3-(trifluoromethyl)phenyl)-5,5-dimethyl-4-oxo-2-thioxoimidazolidin-1-yl)-2-fluorobenzamido)ethoxy)ethoxy)ethyl)-1*H*-indole-2-carboxamide (PROTAC-12)

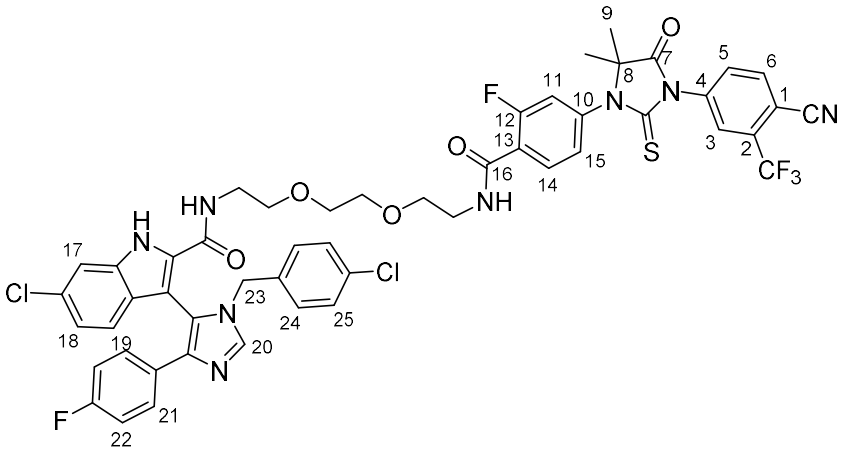

To a stirring solution of **87** (8.0 mg, 0.017 mmol) in DMF (0.1 mL), were added HATU (7.6 mg, 0.020 mmol), DIPEA (3.5 µL, 0.020 mmol), and a solution of **125** (10.7 mg, 0.018 mmol) in DMF (0.1 mL). The reaction was stirred for 18 h before being diluted with EtOAc (5 mL) and H_2O (3 mL), extracted into

EtOAc (2 x 5 mL), washed with brine (5 mL), dried over Na_2SO_4, filtered, and concentrated *in vacuo.* The residue was then purified by silica gel chromatography (1 to 3% MeOH/DCM) to give the title compound as a yellow oil (7 mg, 41%).

R_f: 0.51 (5% MeOH/DCM); **IR** (neat film, ν_{max}, cm^{-1}): 3388 (w), 3259 (w), 2924 (w), 2873 (w), 1758 (m), 1654 (s), 1621 (m), 1538 (s), 1523 (s), 1495 (s), 1439 (s), 1411 (s), 1311 (s), 1220 (s), 1178 (s), 1140 (s), 1057 (w); **^{1}H NMR** (500 MHz, $CDCl_3$) δ: 9.89 (s, 1 H, NH), 8.19 (t, *J* = 8.1 Hz, 1 H, H14), 7.98 (d, *J* = 8.1 Hz, 1 H, H6), 7.94 (d, *J* = 1.6 Hz, 1 H, H3), 7.82 – 7.79 (m, 2 H, H5, H20), 7.51 – 7.38 (m, 4 H), 7.20 (dd, *J* = 7.2 Hz, 1 H, H15), 7.13 – 7.00 (m, 4 H), 6.83 (t, *J* = 8.3 Hz, 2 H), 6.68 (d, *J* = 8.3 Hz, 2 H), 6.24 – 6.20 (m, 1 H), 4.84 (d, *J* = 15.1 Hz, 1 H, H23), 4.72 (d, *J* = 15.1 Hz, 1 H, H23), 1.59 (s, 6 H, H9); **^{13}C NMR** (126 MHz, $CDCl_3$) δ: 179.7 (C=S), 174.4 (C7), 162.4 (C=O), 162.2 (d, *J* = 250 Hz, C-F), 160.3 (d, *J* = 250 Hz, C-F), 160.0 (C=O), 140.6, 139.0, 138.9 (d, *J* = 11 Hz, C13), 136.8, C1), 135.4, 135.3 (C5), 134.2 (2C), 134.0, 133.7 (q, *J* = 35 Hz, C2), 133.1 (d, *J* = 3 Hz, C14), 132.1 (C5), 131.5, 130.0, 129.6 (2C), 128.8, 128.6, 127.5 (d, *J* = 8 Hz), 127.1 (q, *J* = 5 Hz, C3), 126.7, 126.1 (d, *J* = 3.5 Hz, C15), 125.9, 123.3, 123.2, 123.1, 122.8, 121.4, 120.4, 118.0 (d, *J* = 30 Hz, C11), 118.0, 117.7, 115.4 (d, *J* = 22 Hz), 114.7 (-C≡N), 112.3, 110.4 (d, *J* = 2 Hz, C4), 104.4, 70.4, 70.2, 69.6, 69.2 (4x O-CH_2), 66.6 (C8), 48.9 (C23), 39.9, 39.2 (2x N-CH_2), 23.8 (C9); **^{19}F NMR** (471 MHz, $CDCl_3$) δ: -62.0, -110.4, -114.5; **HRMS (ESI):** m/z calcd for $C_{51}H_{42}Cl_2F_5N_8O_5S$ $[M+H]^+$: 1043.2291; found: 1043.2301.

6-Chloro-3-(1-(4-chlorobenzyl)-4-(4-fluorophenyl)-1*H*-imidazol-5-yl)-*N*-(1-(4-(3-(4-cyano-3-(trifluoromethyl)phenyl)-5,5-dimethyl-4-oxo-2-thioxoimidazolidin-1-yl)-2-fluorophenyl)-1-oxo-5,7,10-trioxa-2-azadodecan-12-yl)-1*H*-indole-2-carboxamide (PROTAC-13)

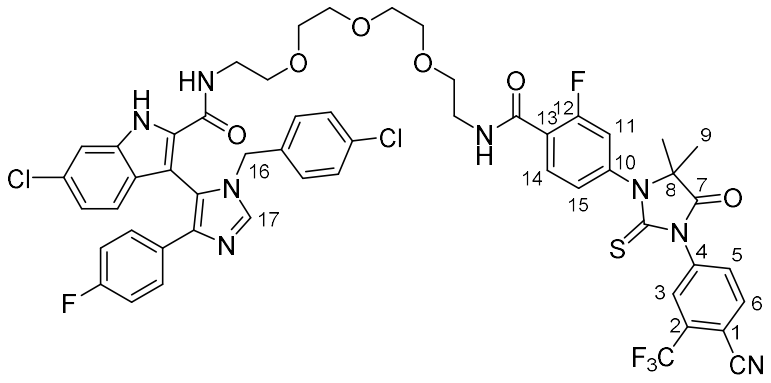

To a stirring solution of **87** (6.5 mg, 0.014 mmol) in DMF (0.1 mL), were added HATU (6.2 mg, 0.016 mmol), DIPEA (2.8 µL, 0.016 mmol), and a solution of **94** (9.3 mg, 0.015 mmol) in DMF (0.1 mL). The

reaction was stirred for 5 h before being diluted with EtOAc (5 mL) and H_2O (3 mL), extracted into EtOAc (2 x 5 mL), washed with brine (5 mL), dried over Na_2SO_4, filtered, and concentrated *in vacuo.* The residue was then purified by silica gel chromatography (1 to 3% MeOH/DCM) to give the title compound as a yellow oil (8.6 mg, 59%).

R_f: 0.20 (5% MeOH/DCM); **IR** (neat film, ν_{max}, cm^{-1}): 3237 (w), 2917 (w), 1759 (m), 1726 (w), 1654 (m), 1620 (m), 1538 (m), 1523 (m), 1496 (m), 1439 (s), 1409 (s), 1311 (s), 1219 (s), 1178 (m), 1140 (s), 1092 (m), 1057 (m), 1015 (w); **^{1}H NMR** (500 MHz, $CDCl_3$) δ: 10.06 (br s, 1 H, NH), 8.21 (t, *J* = 7.6 Hz, 1 H, H14), 7.97 (d, *J* = 8.2 Hz, 1 H, H6), 7.93 (d, *J* = 1 Hz, 1 H, H3), 7.89 (s, 1 H, H17), 7.81 (dd, *J* = 8.1, 2 Hz, 1 H, H5), 7.50 – 7.45 (m, 3 H), 7.31 – 7.27 (m, 1 H), 7.21 (dd, *J* = 8.4, 1.6 Hz, 1 H, H15), 7.14 (dd, *J* = 11.7, 2 Hz, 1 H, H11), 7.09 – 7.02 (m, 4 H), 6.83 (t, *J* = 8.6 Hz, 2 H), 6.69 (d, *J* = 8.3 Hz, 2 H), 6.20 (d, *J* = 5.0 Hz, 1 H), 4.84 (d, *J* = 15.6 Hz, 1 H, H16), 4.77 (d, *J* = 15.6 Hz, 1 H, H16), 3.71 – 3.57 (m, 8 H, 4x CH_2), 3.56 – 3.47 (m, 2 H, CH_2), 3.43 – 3.33 (m, 4 H, 2x CH_2), 3.27 – 3.18 (m, 2 H, CH_2), 1.59 (s, 6 H, H9); **^{13}C NMR** (126 MHz, $CDCl_3$) δ: 179.8 (C=S), 174.5 (C7), 162.2 (C=O), 162.0 (d, *J* = 275 Hz, C-F), 160.3 (d, *J* = 275 Hz, C-F), 160.1 (C=O), 140.5, 139.2, 138.9 (d, *J* = 11 Hz, C13), 136.8 (C1), 135.5, 135.3 (C5), 134.2, 134.1 (2C), 133.7 (q, *J* = 33 Hz, C2), 133.2 (d, *J* = 3 Hz, C14), 132.1 (C5), 131.4, 129.9, 129.6 (2C), 128.8, 128.6, 127.4 (d, *J* = 8 Hz), 127.1 (q, *J* = 5 Hz, C3), 126.7, 126.1 (d, *J* = 3.5 Hz, C15), 125.9, 123.2, 123.1, 123.0, 122.7, 121.4, 120.4, 118.0 (d, *J* = 26 Hz, C11), 117.9 (2C), 115.4 (d, *J* = 22 Hz), 114.7 (-C≡N), 112.3, 110.4 (C4), 104.5, 70.5, 70.4 (2C), 70.3, 69.6, 69.1 (6x O-CH_2), 66.6 (C7), 48.8 (C16), 39.9, 39.3 (2x N-CH_2), 23.8 (C9); **^{19}F NMR** (471 MHz, $CDCl_3$) δ: -62.0, -110.3, -114.7; **HRMS (ESI):** m/z calcd for $C_{53}H_{46}Cl_2F_5N_8O_6S$ $[M+H]^+$: 1087.2553; found: 1087.2501.

6-Chloro-*N*-(2-(2-(2-(4-(3-(4-cyano-3-(trifluoromethyl)phenyl)-5,5-dimethyl-4-oxo-2-thioxoimidazolidin-1-yl)-2-fluorobenzamido)ethoxy)ethoxy)ethyl)-3-(1-(4-((3,4-difluorobenzyl)oxy)benzyl)-4-(4-fluorophenyl)-1*H*-imidazol-5-yl)-1*H*-indole-2-carboxamide (PROTAC-14)

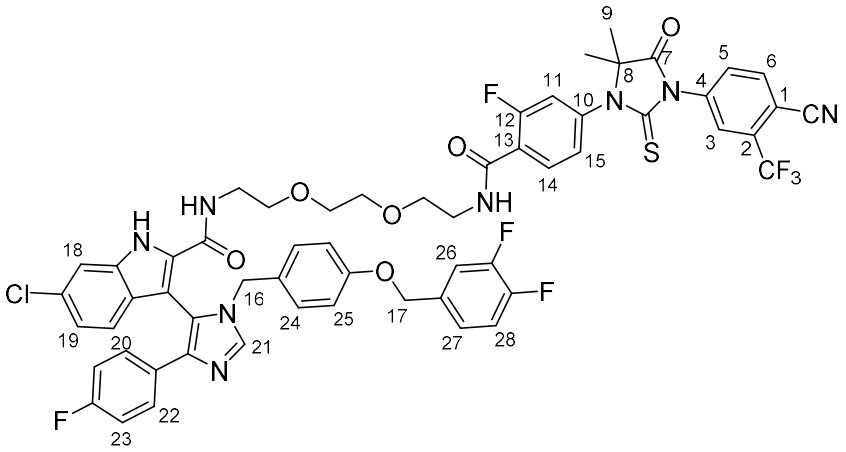

To a stirring solution of **110** (10.1 mg, 0.017 mmol) in DMF (0.1 mL), were added HATU (7.8 mg, 0.020 mmol), DIPEA (3.6 µL, 0.020 mmol), and a solution of **125** (11.0 mg, 0.019 mmol) in DMF (0.1 mL). The reaction was stirred for 18 h before being diluted with EtOAc (5 mL) and H_2O (3 mL), extracted into EtOAc (2 x 5 mL), washed with brine (5 mL), dried over Na_2SO_4, filtered, and concentrated *in vacuo.* The residue was then purified by silica gel chromatography (1 to 3% MeOH/DCM) to give the title compound as a yellow oil (10.8 mg, 55%).

R_f: 0.52 (5% MeOH/DCM); **IR** (neat film, ν_{max}, cm^{-1}): 3383 (w), 3239 (w), 2928 (w), 2876 (w), 1758 (m), 1729 (w), 1648 (m), 1619 (m), 1538 (m), 1520 (s), 1497 (s), 1436 (s), 1412 (s), 1309 (s), 1287 (s), 1218 (s), 1177 (s), 1139 (s), 1113 (s), 1056 (m), 1013 (w); **^{1}H NMR** (500 MHz, $CDCl_3$) δ: 9.99 (br s, 1 H, NH), 8.18 (t, *J* = 8.2 Hz, 1 H, H14), 7.97 (d, *J* = 8.1 Hz, 1 H, H6), 7.94 (d, *J* = 1.6 Hz, 1 H, H3), 7.82 – 7.80 (m, 2 H, H5, H21), 7.51 – 7.40 (m, 4 H), 7.21 – 6.99 (m, 7 H), 6.82 (t, *J* = 8.8 Hz, 2 H), 6.69 – 6.64 (m, 3 H), 6.25 (t, *J* = 4.6 Hz, 1 H, NH), 4.86 (s, 2 H, H17), 4.77 (d, *J* = 14.8 Hz, 1 H, H16), 4.70 (d, *J* = 14.8 Hz, 1 H, H16), 3.73 – 3.61 (m, 4 H, 2x CH_2), 3.55 – 3.30 (m, 6 H, 3x CH_3), 3.25 – 3.19 (m, 2 H, CH_2), 1.58 (s, 6 H, H9); **^{13}C NMR** (126 MHz, $CDCl_3$) δ: 179.7 (C=S), 174.4 (C7), 162.3 (C=O), 162.0 (d, *J* = 250 Hz, C-F), 160.3 (d, *J* = 250 Hz, C12), 160.2 (C=O), 158.1 (O-ArC), 150.3 (dd, *J* = 250, 40 Hz, C-F), 150.2 (dd, *J* = 250, 40 Hz, C-F), 140.5, 138.9, 138.8, 136.8 (C1), 135.5, 135.3 (C5), 133.7 (q, *J* = 34 Hz, C2), 133.7, 133.6 (2C), 133.1 (d, *J* = 3 Hz, C14), 132.1 (C5), 131.3, 130.0, 129.8, 129.7, 128.8, 128.1, 127.4 (d, *J* = 8 Hz), 127.1 (q, *J* = 5 Hz, C3), 126.9, 126.0 (d, *J* = 3.2 Hz, C15), 125.9, 123.3 – 123.2 (m, 3C), 122.6, 121.6, 120.5, 117.9 (d, *J* = 26 Hz, C11), 117.9, 117.5, 117.3, 116.4 (d, *J* = 16 Hz), 115.4 (d, *J* = 22 Hz), 114.9, 114.7 (-C≡N), 112.2, 110.5 (d, *J* = 2 Hz, C4), 104.8, 70.4, 70.2, 69.6, 69.2, 68.8 (5x O-CH_2), 66.6 (C8), 49.1 (C16), 39.9, 39.2

(2x N-CH_2), 23.8 (C9); **^{19}F NMR** (471 MHz, $CDCl_3$) δ: -62.0, -110.4, -114.7, -137.1 (d, *J* = 20.5 Hz), -138.6 (d, *J* = 20.5 Hz); **HRMS (ESI):** m/z calcd for $C_{58}H_{47}ClF_7N_8O_6S$ $[M+H]^+$: 1151.2911; found: 1151.2892.

6-Chloro-*N*-(1-(4-(3-(4-cyano-3-(trifluoromethyl)phenyl)-5,5-dimethyl-4-oxo-2-thioxoimidazolidin-1-yl)-2-fluorophenyl)-1-oxo-5,8,11-trioxa-2-azatridecan-13-yl)-3-(1-(4-((3,4-difluorobenzyl)oxy)benzyl)-4-(4-fluorophenyl)-1*H*-imidazol-5-yl)-1*H*-indole-2-carboxamide (PROTAC-15)

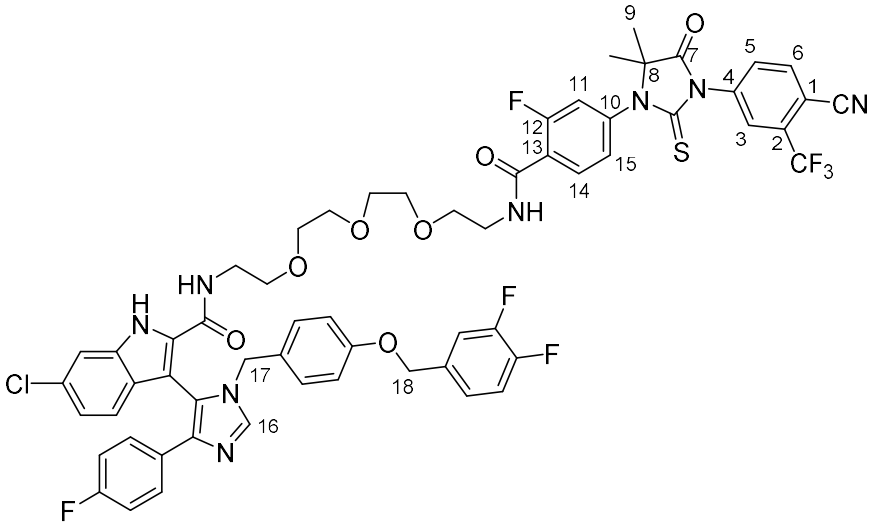

To a stirring solution of **110** (7.9 mg, 0.0135 mmol) in DMF (0.1 mL), were added HATU (6.2 mg, 0.016 mmol), DIPEA (2.8 µL, 0.016 mmol), and a solution of **94** (9.3 mg, 0.015 mmol) in DMF (0.1 mL). The reaction was stirred for 5 h before being diluted with EtOAc (5 mL) and H_2O (3 mL), extracted into EtOAc (2 x 5 mL), washed with brine (5 mL), dried over Na_2SO_4, filtered, and concentrated *in vacuo.* The residue was then purified by silica gel chromatography (1 to 3% MeOH/DCM) to give the title compound as a yellow oil (7.0 mg, 44%).

R_f: 0.23 (5% MeOH/DCM); **IR** (neat film, ν_{max}, cm^{-1}): 3369 (w), 3227 (w), 2920 (w), 1758 (m), 1728 (w), 1654 (m), 1619 (m), 1538 (m), 1521 (s), 1437 (s), 1411 (s), 1310 (s), 1288 (s), 1219 (s), 1177 (s), 1141 (s), 1057 (m); **^{1}H NMR** (500 MHz, $CDCl_3$) δ: 9.87 (br s, 1 H, NH), 8.20 (t, *J* = 8.3 Hz, 1 H, H14), 7.97 (d, *J* = 8.1 Hz, 1 H, H6), 7.94 (d, *J* = 1.5 Hz, 1 H, H3), 7.87 (s, 1 H, H16), 7.81 (dd, *J* = 8.3, 1.8 Hz, 1 H, H5), 7.51 – 7.43 (m, 3 H), 7.29 – 7.27 (m, 1 H, NH), 7.22 – 6.99 (m, 7 H), 6.82 (t, *J* = 8.8 Hz, 2 H), 6.69 – 6.64 (m, 4 H), 6.23 – 6.19 (m, 1 H, NH), 4.86 (s, 2 H, H17), 4.76 (s, 2 H, H16), 3.69 – 3.17 (m, 16 H, 8x CH_2), 1.58 (s, 6 H, H9); **^{13}C NMR** (126 MHz, $CDCl_3$) δ: 179.8 (C=S), 174.5 (C7), 162.2 (C=O), 162.0 (d, *J* = 250 Hz, C-F), 160.3 (d, *J* = 250 Hz, C12), 160.2 (C=O), 158.1 (O-ArC), 150.3 (dd, *J* = 250, 40 Hz, C-F), 150.2 (dd, *J* = 250, 40 Hz, C-F), 140.4, 139.1, 138.9 (d, *J* = 11 Hz, C13), 136.8 (C1), 135.5, 135.3 (C5), 133.7 (q, *J* = 34

Hz, C2), 133.7, 133.6 (2C), 133.2 (d, *J* = 3 Hz, C14), 132.1 (C5), 131.2, 129.9, 129.8 (2C), 128.8, 128.1, 127.4 (d, *J* = 8 Hz), 127.1 (q, *J* = 4 Hz, C3), 126.9, 126.0 (d, *J* = 3 Hz, C15), 125.9, 123.3 – 123.2 (m, 3C), 122.6, 121.6, 120.4, 118.0 (d, *J* = 26 Hz, C11), 117.9, 117.5, 117.3, 116.4 (d, *J* = 16 Hz), 115.4 (d, *J* = 23 Hz), 114.9, 114.7 (-C≡N), 112.1, 110.5 (C4), 104.9, 70.5, 70.4 (2C), 70.3, 69.6, 69.2, 68.8 (7x O-CH_2), 66.6 (8), 49.1 (C16), 39.9, 39.3 (2x N-CH_2), 23.8 (C9); **^{19}F NMR** (471 MHz, $CDCl_3$) δ: -61.9, -110.3, -114.9, -137.2 (d, *J* = 21.3 Hz), -138.6 (d, *J* = 21.3 Hz); **HRMS (ESI):** m/z calcd for $C_{60}H_{51}ClF_7N_8O_6S$ $[M+H]^+$: 1195.3173; found: 1195.3119 .

***tert*-butyl (*S*)-(1-(4-bromophenyl)ethyl)carbamate (127)**

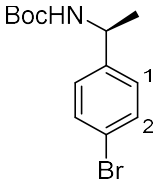

Following the reported procedure,[235] to a stirring solution of (*S*)-(−)-1-(4-bromophenyl)ethylamine (0.55 mL, 3.7 mmol) in EtOAc (1.8 mL) and water (1.8 mL) cooled to 0 °C, were added sodium hydrogen carbonate (0.30 g, 3.6 mmol) and Boc_2O (1.04 mL, 4.5 mmol). The reaction mixture was stirred at r.t. for 3 h before filtering. The white solid was suspended in hexane (3 mL) and water (3 mL) for 30 mins before filtering to give the title compound as a white amorphous solid (1.07 g, 97%).

R_f: 0.76 (6:4 Hex:EtOAc); **IR** (neat film, ν_{max}, cm^{-1}): 3380 (m, NH), 2979 (m, CH), 1680 (s), 1508 (s), 1487 (m), 1443 (m), 1389 (w), 1364 (m), 1343 (m), 1309 (m), 1294 (w), 1244 (m), 1166 (s), 1094 (m), 1059 (s), 1007 (s); **^{1}H NMR** (400 MHz, CDCl3) δ: 7.44 (d, J = 8.4 Hz, 2 H, H2), 7.17 (d, J = 8.4 Hz, 2 H, H1), 4.78 – 4.73 (br d, 2 H, NH and -CH-), 1.41 – 1.40 (br m, 12 H, 4 x CH_3); **^{13}C NMR** (101 MHz, CDCl3) δ: 155.0 (C=O), 143.3 (C-Br), 131.6 (C2), 127.6 (C1), 120.8 (ArC), 79.6 (O-**C**-$(CH_3)_3$), 49.7 (-CH-), 28.4 (3 x CH_3), 22.6 (CH_3); **$[\alpha]_D^{25}$:** -71.8 (c = 0.22, MeOH).

The spectroscopic data are in agreement with those previously reported in the literature for the title compound.[352]

***tert*-Butyl (*S*)-(1-(4-(4-methylthiazol-5-yl)phenyl)ethyl)carbamate (128)**

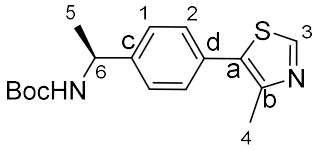

Following the reported procedure,[235] to a stirring solution of **127** (0.976 g, 4.9 mmol) in *N*,*N*-dimethylacrylamide (2.5 mL) were added 4-methylthiazole (1.11 mL, 9.9 mmol), potassium acetate (2.22 g, 9.9 mmol), and palladium acetate (5.0 mg, 0.05 mmol). The reaction mixture was heated to 90 °C for 18 h before cooling and filtering. H_2O (2 mL) was added to the filtrate and the mixture was stirred for a further 4 h at r.t. before filtering to give the title compound as a white amorphous solid (1.23 g, 79%).

R_f: 0.24 (7:3 Hex:EtOAc); **IR** (neat film, ν_{max}, cm^{-1}): 3381 (m, NH), 3052 (w, CH), 2978 (w, CH), 2924 (w, CH), 1677 (s), 1510 (s), 1450 (m), 1406 (m), 1392 (m), 1366 (m), 1310 (m), 1294 (m), 1247 (s), 1166 (s), 1100 (w), 1059 (s), 1003 (m); **^{1}H NMR** (400 MHz, CDCl3) δ: 8.67 (s, 1 H, H3), 7.41 (d, J = 8.3 Hz, 2 H, H2), 7.35 (d, J = 8.3 Hz, 2 H, H1), 4.84 (br s, H6), 2.53 (s, 3 H, H4), 1.48 – 1.43 (m, 12 H, H5 and 3 x CH_3); **^{13}C NMR** (101 MHz, CDCl3) δ: 155.2 (C=O), 150.3 (C3), 148.6 (Cb), 144.1 (Cc), 131.8 (Ca), 130.8 (Cd), 129.6 (C2), 126.3 (C1), 79.7 (-C-(CH_3)$_3$), 50.0 (C6), 28.5 (3 x CH_3), 22.8 (C5), 16.2 (C4); **$[\alpha]_D^{25}$:** -87.2 (c = 0.18, MeOH).

The spectroscopic data are in agreement with those previously reported in the literature for the title compound.[235]

(*S*)-1-(4-(4-methylthiazol-5-yl)phenyl)ethanamine hydrochloride (129)

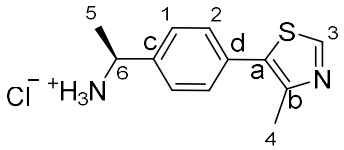

Following the reported procedure,[235] acetyl chloride (0.7 mL, 9.8 mmol) was carefully added to methanol (1.8 mL) cooled to 0 °C, to this **128** (1.213 g, 3.8 mmol) was then added. The slurry was stirred at r.t. for 2 h before concentrating *in vacuo* to give the title compound as a yellow amorphous powder (0.69 g, 70%).

IR (neat film, ν_{max}, cm^{-1}): 3400 (m, NH), 2912 (w, CH), 1704 (w), 1641 (w), 1536 (w), 1417 (w), 1365 (w), 1290 (w), 1226 (w), 1048 (m), 1024 (s), 994 (s); **^{1}H NMR** (400 MHz, d6-DMSO) δ: 9.22 (s, 1 H, H3), 8.79 (br s, 3 H, NH_3), 7.68 (d, *J* = 7.8 Hz, 2 H, H2), 7.57 (d, *J* = 7.8 Hz, 2 H, H1), 4.47 – 4.41 (m, 1 H, H6), 2.49 (s, 3 H, H4), 1.56 (d, *J* = 6.2 Hz, H5); **^{13}C NMR** (101 MHz, d6-DMSO) δ: 153.0 (C3), 147.5 (Cb), 140.0 (Cc), 131.8 (Ca), 131.4 (Cd), 129.6 (C1), 128.1 (C2), 50.1 (C6), 21.2 (C5), 15.9 (C4); **$[\alpha]_D^{25}$:** -2.73 (c = 0.367, MeOH).

The spectroscopic data are in agreement with those previously reported in the literature for the title compound.[235]

(2*S*,4*R*)-4-hydroxy-2-(methoxycarbonyl)pyrrolidin-1-ium chloride (131)

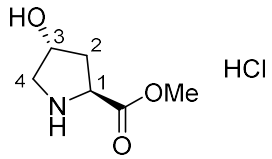

Following a modified version of the reported procedure,[353] to a stirring solution of *L*-hydroxyproline (2.54 g, 19.4 mmol) in methanol (18 mL) was slowly added acetyl chloride (1.94 mL, 27.4 mmol). The reaction mixture was heated to reflux for 7 h before cooling. Diethyl ether (10 mL) was added to induce precipitation and the slurry was filtered and washed with diethyl ether (5 mL) to give the title compound as a white amorphous powder (3.02 g, 87%).

R_f: 0.28 (12% MeOH/DCM 1% NEt_3); **IR** (neat film, ν_{max}, cm^{-1}): 3379 (m, NH), 3323 (w), 3022 (m, CH), 2948 (s, CH), 2749 (w), 2599 (w), 1738 (s, C=O) , 1592 (m), 1438 (m), 1422 (m), 1390 (m), 1346 (w), 1284 (m), 1265 (m), 1218 (s), 1181 (s), 1073 (s); **^{1}H NMR** (400 MHz, d6-DMSO) δ: 5.59 (br s, 1 H, NH), 4.50 – 4.42 (m, 2 H, H1 and H3), 3.77 (s, 3 H, CH_3), 3.38 – 3.34 (m, 2 H and overlapping H_2O, H4 and OH), 3.08 (dt, J = 12.1, 1.2 Hz, 1 H, H4), 2.23 – 2.06 (m, 2 H, H2); **^{13}C NMR** (101 MHz, d6-DMSO) δ: 169.6 (C=O), 68.9 (C1), 57.9 (C3), 53.6 (C4), 53.5 (CH_3), 37.4 (C2); **$[\alpha]_D^{25}$:** -24.9 (c = 1.0, MeOH, lit**.** **$[\alpha]_D$** = -25.3[354]).

The spectroscopic data are in agreement with those previously reported in the literature for the title compound.[353]

(2*S*,4*R*)-1-((*R*)-2-((*tert*-butoxycarbonyl)amino)-3,3-dimethylbutanoyl)-4-hydroxypyrrolidine-2-carboxylic acid (134)

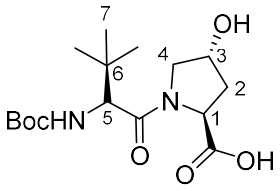

Following the reported procedure,[235] to a stirring solution of (*S*)-*N*-Boc-2-amino-3,3-dimethylbutyric acid (0.715 g, 3.1 mmol) in DMF (7.1 mL) were added HATU (1.25 g, 3.3 mmol) and DIPEA (2.0 mL, 10.2 mmol). The reaction mixture was stirred at r.t. for 15 mins before **131** (0.676 g, 3.7 mmol) was added.

The mixture was then stirred for a further 18 h before diluting in water (10 mL) and extracting into EtOAc (4 x 20 mL). The combined organics were then washed with 5% citric acid (aq., 2 x 10 mL), sat. $NaHCO_3$ (2 x 10 mL), brine (2 x 10 mL), before being dried over Na_2SO_4, filtered and concentrated *in vacuo*. The crude product was then dissolved in THF (5 mL) and water (2.5 mL) and lithium hydroxide monohydrate (1.30 g, 31 mmol) was added. The slurry was stirred at r.t. for 18 h before concentrating *in vacuo*. The residue was diluted with ice water (10 mL) and the pH adjusted to 2 with 3M HCl. After stirring for a further 30 mins the slurry was filtered to give the title compound as a white amorphous powder (0.748 g, 70%) used without further purification.

IR (neat film, ν_{max}, cm^{-1}): 3323 (br m, OH), 2971 (m, CH), 2869 (w, CH), 1686 (br m, C=O), 1625 (s), 1508 (m), 1439 (m), 1394 (m), 1368 (m), 1333 (w), 1247 (m), 1166 (s), 1082 (w), 1057 (w), 1013 (w); **^{1}H NMR** (400 MHz, d6-DMSO) δ: 6.46 (d, *J* = 9.3 Hz, 1 H, NH), 4.33 (br s, 1 H, H3), 4.27 (t, *J* = 8.2 Hz, 1 H, H1), 4.16 (d, *J* = 9.3 Hz, 1 H, H5), 3.66 – 3.57 (m, 2 H, H4), 2.14 – 2.09 (m, 1 H, H2'), 1.91 – 1.85 (m, 1 H, H2''), 1.38 (s, 9 H, Boc-CH_3), 0.94 (s, 9 H, 3 x CH_3); **^{13}C NMR** (101 MHz, d6-DMSO) δ: 173.7 (acid C=O), 170.4 (amide C=O), 155.8 (Boc-C=O), 78.6 (O-**C**-$(CH_3)_3$), 69.2 (C3), 58.6 (C5), 58.2 (C1), 56.5 (C4), 37.7 (C2), 35.8 (C6), 28.6 (Boc-CH_3), 26.7 (CH_3); **$[\alpha]_D^{25}$:** -27.1 (c = 0.188, MeOH).

The spectroscopic data are in agreement with those previously reported in the literature for the title compound.[235]

tert-butyl((*S*)-1-((2*S*,4*R*)-4-hydroxy-2-(((*S*)-1-(4-(4-methylthiazol-5-yl)phenyl)ethyl)carbamoyl) pyrrolidine-1-yl)-3,3-dimethyl-1-oxobutan-2-yl)carbamate (135)

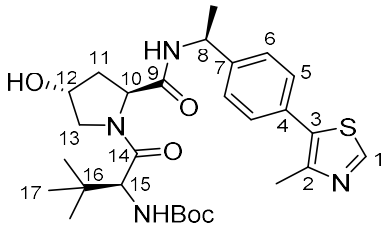

Following a reported procedure,[235] to a stirring solution of **134** (0.748 g, 2.17 mmol) in DMF (7.5 mL) were added HATU (0.991 g, 2.61 mmol) and DIPEA (1.27 mL, 6.51 mmol). The reaction mixture was stirred at r.t. for 15 mins before **129** (0.608 g, 2.39 mmol) was added. The mixture was then stirred for a further 18 h before diluting in water (10 mL) and extracting into EtOAc (4 x 20 mL). The combined organics were then washed with brine (2 x 10 mL), before being dried over Na_2SO_4, filtered and concentrated *in vacuo*. The residue was purified through silica gel column chromatography (1:20 MeOH/DCM) to give the title compound as a white amorphous solid (1.082 g, 90%).

R_f: 0.40 (6% MeOH/DCM); **IR** (neat film, ν_{max}, cm^{-1}): 3288 (w, NH), 2969 (w, CH), 2932 (w, CH), 2876 (w, CH), 1680 (s, C=O), 1631 (s), 1538 (m), 1501 (m), 1433 (m), 1365 (s), 1237 (m), 1165 (s), 1085 (m), 1050 (m), 1012 (m); **^{1}H NMR** (400 MHz, $CDCl_3$) δ: 8.69 (s, 1 H, H1), 7.63 (d, *J* = 7.7 Hz, NH), 7.43 – 7.37 (m, 4 H, Ar-H), 5.28 (d, *J* = 8.8 Hz, 1 H, Boc-NH), 5.09 (quin, *J* = 7.4 Hz, 1 H, H8), 4.77 (t, *J* = 8.3 Hz, 1 H, H10), 4.52 (br s, 1 H, H12), 4.24 (d, *J* = 9.1 Hz, 1 H, H13), 3.61 (dd, *J* = 11.5, 3.6 Hz, 1 H, H13'), 2.54 – 2.51 (m, 4 H, Ar-CH_3 and H11), 2.10 – 2.03 (m, 1 H, H11'), 1.49 (d, *J* = 7.4 Hz, 3 H, ali-CH_3), 1.43 (s, 9 H, Boc-CH_3), 1.04 (s, 9 H, 3 x CH_3); **^{13}C NMR** (101 MHz, $CDCl_3$) δ: 172.8 (C14), 169.6 (C9), 156.5 (Boc C=O), 150.3 (C1), 148.5 (C2), 143.2 (C7), 131.6 (C3), 130.8 (C4), 129.6 (C5), 126.4 (C6), 80.5 (Boc-qC), 70.0 (C12), 59.0 (C15), 58.2 (C10), 56.5 (C13), 48.9 (C8), 35.2 (C11), 34.8 (C16), 28.3 (Boc-CH_3), 26.4 (3 x CH_3), 22.3 (ali-CH_3), 16.0 (Ar-CH_3); **$[\alpha]_D^{25}$:** -151.9 (c = 0.052, MeOH).

Data are in accordance with those reported previously in literature.[235]

(2*S*,4*R*)-1-((*S*)-2-amino-3,3-dimethylbutanoyl)-4-hydroxy-*N*-((*S*)-1-(4-(4-methylthiazol-5-yl)phenyl)ethyl)pyrrolidine-2-carboxamide (136)

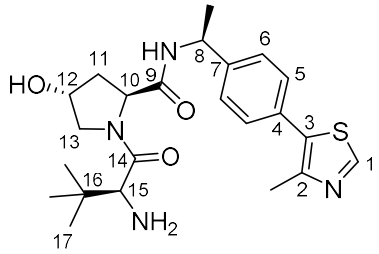

Following a reported procedure,[235] to a stirring solution of **135** (0.112 g, 0.206 mmol) in dichloromethane (1 mL) was added trifluoroacetic acid (0.25 mL). The reaction mixture was stirred at r.t. for 3 h before concentrating *in vacuo*. The residue was then dissolved in $NaHCO_3$ (15 mL) and extracted into dichloromethane (3 x 20 mL). The combined organic was dried over Na_2SO_4, filtered and concentrated *in vacuo*. The residue was purified through silica gel column chromatography (1:19:0.2 MeOH/DCM/NEt_3) to give the title compound as a colourless oil (59 mg, 65%).

R_f: 0.40 (6% MeOH/DCM); **IR** (neat film, ν_{max}, cm^{-1}): 3333 (w, NH), 3280 (w, NH), 2947 (w, CH), 2869 (w, CH), 1693 (s, C=O), 1603 (s), 1548 (m), 1437 (m), 1413 (m), 1370 (m), 1318 (w), 1258 (w), 1224 (m), 1202 (m), 1079 (w), 1013 (w); **^{1}H NMR** (400 MHz, $CDCl_3$) δ: 8.68 (s, 1 H, H1), 7.85 (d, *J* = 7.6 Hz, 1 H, NH), 7.41 – 7.37 (m, 4 H, Ar-H), 5.08 (quin, *J* = 6.8 Hz, 1 H, H8), 4.78 (t, *J* = 7.7 Hz, 1 H, H10), 4.48 (br s, 1 H, H12), 3.76 (d, *J* = 11.2 Hz, 1 H, H13), 3.60 (dd, *J* = 11.2, 3.9 Hz, 1 H, H13'), 3.37 (s, 1 H, H15), 2.85 (br s, 2 H, NH_2), 2.53 (s, 3 H, Ar-CH_3), 2.42 – 2.36 (m, 1 H, H11), 2.13 – 2.07 (m, 1 H, H11'), 1.50 (d, *J* = 6.8 Hz, 3 H, ali-CH_3), 1.01 (s, 9 H, 3 x CH_3); **^{13}C NMR** (101 MHz, $CDCl_3$) δ: 174.1 (C14), 170.2 (C9), 150.3

(C1), 148.4 (C2), 143.5 (C7), 131.6 (C3), 130.7 (C4), 129.5 (C5), 126.4 (C6), 69.9 (C12), 60.5 (C15), 58.6 (C10), 56.5 (C13), 48.9 (C8), 36.4 (C11), 35.7 (C16), 26.2 (3 x CH_3), 22.3 (ali-CH_3), 16.1 (Ar-CH_3); **$[\alpha]_D^{25}$:** -112.8 (c = 0.18, MeOH).

Data are in accordance with those reported previously in literature[235].

(2*S*,4*R*)-1-((*S*)-2-(6-aminohexanamido)-3,3-dimethylbutanoyl)-4-hydroxy-*N*-((*S*)-1-(4-(4-methylthiazol-5-yl)phenyl)ethyl)pyrrolidine-2-carboxamide (138)

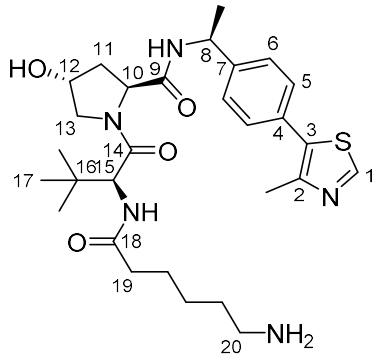

To a stirring solution of **47** (39 mg, 0.17 mmol) in DMF (0.75 mL) were added HATU (77.6 mg, 0.20 mmol) and DIPEA (79 µL, 0.41 mmol). The reaction mixture was stirred at r.t. for 15 mins before **136** (75 mg, 0.17 mmol) was added. The mixture was then stirred for a further 16 h before diluting in water (5 mL) and extracting into EtOAc (4 x 10 mL). The combined organics were then washed with brine (2 x 5 mL), before being dried over Na_2SO_4, filtered and concentrated *in vacuo*. The residue was purified through silica gel column chromatography (DCM to 1:9 MeOH/DCM) to give the crude compound which was then dissolved in a mixture of dichloromethane (0.2 mL) and trifluoroacetic acid (30 µL). The reaction mixture was stirred at r.t. for 3 h before concentrating *in vacuo*. The residue was then dissolved in $NaHCO_3$ (1 mL) and extracted into dichloromethane (3 x 5 mL). The combined organic was dried over Na_2SO_4, filtered and concentrated *in vacuo*. The residue was purified through silica gel column chromatography (1:9:0.2 MeOH/DCM/NEt_3) to give the title compound as a yellow oil (8 mg, 80%).

R_f: 0.09 (1:9:0.2 MeOH/DCM/NEt_3); **IR** (neat film, ν_{max}, cm^{-1}): 3284 (m, NH), 2964 (w, CH), 2869 (w, CH), 1625 (br m, C=O), 1539 (w), 1449 (w), 1413 (w), 1375 (w), 1228 (w), 1201 (w), 1082 (w); **^{1}H NMR** (400 MHz, $CDCl_3$) δ: 8.66 (s, 1 H, H1), 7.87 (d, *J* = 7.6 Hz, 1 H, NH), 7.41 – 7.34 (m, 4 H, Ar-H), 7.11 (d, *J* = 8.5 Hz, 1 H, NH), 5.10 – 5.07 (m, 1 H, H8), 4.74 – 4.70 (m, 1 H, H10), 4.62 – 4.58 (m, 1 H, H15), 4.50 – 4.43 (m, 1 H, H12), 4.01 (d, *J* = 9.9 Hz, 1 H, H13), 3.63 (d, *J* = 9.9 Hz, 1 H, H13'), 2.87 (br s, 2 H, H20), 2.49 (s, 3 H, aryl-CH_3), 2.26 – 2.22 (m, 4 H, CH_2 and H11), 1.61 – 1.26 (m, 11 H, alkyl-CH_3 and 4 x CH_2), 1.05 (s, 9 H, 3 x CH_3); **^{13}C NMR** (101 MHz, $CDCl_3$) δ: 174.1 (C14), 171.7 (C18), 170.3 (C9), 150.3 (C1), 148.4 (C2),

143.6 (C7), 131.6 (C3), 130.7 (C4), 129.4 (C5), 126.4 (C6), 69.9 (C12), 59.0 (C15), 57.9 (C10), 57.3 (C13), 48.8 (C8), 40.1 (C20), 38.6 (C11), 35.5 (C16), 35.4 (C19), 28.4 (CH_2), 26.6 (C17), 25.6 (CH_2), 24.8 (CH_2), 22.4 (ali-CH_3), 16.1 (Aryl-CH_3); **HRMS**: *m/z* $[M+H]^+$ calculated for $C_{29}H_{44}N_5O_4S$: 558.3109; Found: 558.3118; **$[\alpha]_D^{25}$:** -89.167 (c = 0.12, MeOH).

***tert*-Butyl (6-((6-(((*S*)-1-((2*S*,4*R*)-4-hydroxy-2-(((*S*)-1-(4-(4-methylthiazol-5-yl)phenyl)ethyl)carbamoyl)pyrrolidin-1-yl)-3,3-dimethyl-1-oxobutan-2-yl)amino)-6-oxohexyl)amino)-6-oxohexyl)carbamate (139)**

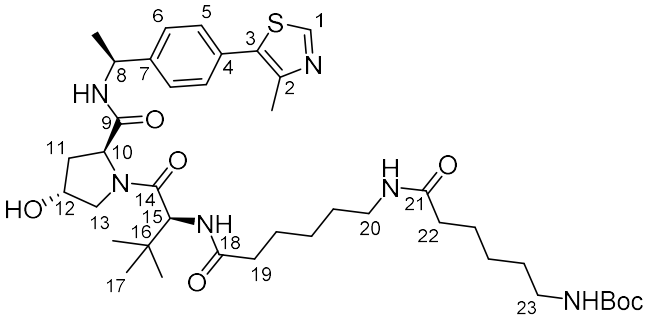

To a stirring solution of **47** (3.3 mg, 0.014 mmol) in DMF (0.1 mL) were added HATU (6 mg, 0.016 mmol) and DIPEA (6.1 µL, 0.031 mmol). The reaction mixture was stirred at r.t. for 15 mins before **138** (8 mg, 0.014 mmol) was added. The mixture was then stirred for a further 16 h before diluting in water (5 mL) and extracting into EtOAc (4 x 10 mL). The combined organics were then washed with brine (2 x 5 mL), before being dried over Na_2SO_4, filtered and concentrated *in vacuo*. The residue was purified through silica gel column chromatography (DCM to 1:9 MeOH/DCM) to give the title compound as a colourless oil (8 mg, 73%).

R_f: 0.18 (6% MeOH/DCM); **IR** (neat film, ν_{max}, cm^{-1}): 3289 (w, NH), 2927 (m, CH), 2865 (w, CH), 1686 (s, C=O), 1630 (s, C=O), 1533 (s), 1452 (m), 1366 (m), 1272 (m), 1249 (m), 1167 (s), 1086 (w); **^{1}H NMR** (400 MHz, CDCl3) δ: 8.71 (s, 1 H, C1), 7.47 – 7.38 (m, 5 H, Ar-H and, NH), 6.63 (br s, 1 H, NH), 6.06 (br s, 1 H, NH), 5.11 (quin, *J* = 7.3 Hz, 1 H, H8), 4.73 (t, *J* = 7.8 Hz, 1 H, H10), 4.59 (d, *J* = 8.4 Hz, 1 H, H15), 4.53 (br s, 1 H, H12), 4.12 (d, *J* = 10.1 Hz, 1 H, H13), 3.63 (d, *J* = 11.0 Hz, 1 H, H13'), 3.22 – 3.11 (m, 6 H, 3 x CH_2), 2.54 (s, 3 H, Ar-CH_3), 2.46 – 2.32 (m, 3 H, H11 and CH_2), 2.27 – 2.16 (m, 5 H, H11' and 2 x CH_2), 1.70 – 1.61 (m, 4 H, 2 x CH_2), 1.48 – 1.45 (m, 12 H, ali-CH_3 and Boc CH_3), 1.41 – 1.30 (m, 6 H, 3 x CH_3), 1.06 (s, 9 H, 3 x CH_3); **^{13}C NMR** (101 MHz, CDCl3) δ: 173.2 (C18), 172.2 (C14), 170.3 (C21), 169.8 (C9), 150.3 (C1), 148.5 (C2), 143.2 (C7), 131.6 (C3), 130.9 (C4), 129.6 (C5), 126.4 (C6), 79.2 (Boc qC), 70.0 (C12), 58.4 (C15), 57.7 (C10), 56.8 (C13), 48.8 (C8), 40.3, 39.1 (C20 and C23), 36.6, 36.0 (C19 and C22), 35.7 (C11), 34.9 (C16), 29.8 (CH_2), 29.7 (CH_2), 29.1 (CH_2), 28.4 (Boc CH_3), 26.5 (3 x CH_3), 26.3 (CH_2), 25.3

(CH_2), 24.9 (CH_2), 22.2 (ali-CH_3), 16.1 (Ar-CH_3); **HRMS**: *m/z* $[M+Na]^+$ calculated for $C_{40}H_{62}N_6O_7S$: 793.4293; Found: 793.4301; **$[\alpha]_D^{25}$:** -50.0 (c = 0.04, MeOH).

(2*S*,4*R*)-1-((*S*)-2-(6-(6-aminohexanamido)hexanamido)-3,3-dimethylbutanoyl)-4-hydroxy-*N*-((*S*)-1-(4-(4-methylthiazol-5-yl)phenyl)ethyl)pyrrolidine-2-carboxamide (140)

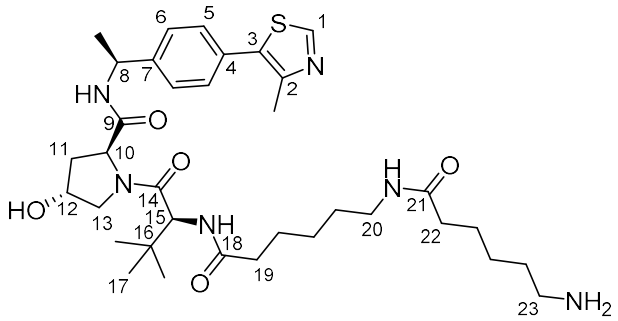

To a stirring solution of **139** (8 mg, 0.010 mmol) in dichloromethane (0.2 mL) was added trifluoroacetic acid (30 µL). The reaction mixture was stirred at r.t. for 3 h before concentrating *in vacuo*. The residue was then dissolved in $NaHCO_3$ (1 mL) and extracted into dichloromethane (3 x 5 mL). The combined organic was dried over Na_2SO_4, filtered and concentrated *in vacuo*. The residue was purified through silica gel column chromatography (1:9:0.2 MeOH/DCM/NEt_3) to give the title compound as a yellow oil (5 mg, 71%).

R_f: 0.06 (1:9:0.2 MeOH/DCM/NEt_3); **IR** (neat film, ν_{max}, cm^{-1}): 3264 (w, NH), 2959 (m, CH), 2920 (m, CH), 2854 (w, CH), 1630 (br s, C=O), 1536 (m), 1445 (m), 1417 (m), 1375 (m), 1260 (m), 1200 (w), 1086 (m), 1016 (m); **^{1}H NMR** (500 MHz, CDCl3) δ: 8.67 (s, 1 H, H1), 7.64 (d, *J* = 7.9 Hz, 1 H, NH), 7.41 – 7.36 (m, 4 H, Ar-H), 6.70 – 6.64 (br m, 2 H, 2 x NH), 5.09 (quin, *J* = 7.3 Hz, 1 H, H8), 4.71 (t, *J* = 7.8 Hz, 1 H, H10), 4.58 (d, *J* = 8.7 Hz, 1 H, H15), 4.50 (s, 1 H, H12), 4.01 (d, *J* = 10.5 Hz, 1 H, H13), 3.66 – 3.58 (m, 1 H, H13'), 3.23 – 3.16 (m, 2 H, CH_2-N), 2.87 (m, 2 H, CH_2-N), 2.52 (s, 3 H, aryl-CH_3), 2.39 – 2.32 (m, 1 H, H11), 2.27 – 2.12 (m, 5 H, H11' and 2 x CH_2), 1.65 – 1.54 (m, 6 H, 3 x CH_2), 1.50 – 1.46 (m, 5 H, alky-CH_3 and CH_2), 1.39 – 1.37 (m, 2 H, CH_2), 1.33 – 1.28 (m, 2 H, CH_2), 1.04 (s, 9 H, H17); **^{13}C NMR** (126 MHz, CDCl3) δ: 173.9 (C18), 173.5 (C14), 171.8 (C21), 170.1 (C9), 150.3 (C1), 148.5 (C2), 143.4 (C7), 131.6 (C3), 130.8 (C4), 129.5 (C5), 126.4 (C6), 69.8 (C12), 58.9 (C15), 57.7 (C10), 57.1 (C13), 48.8 (C8), 40.4, 39.0 (C20 and C23), 36.3, 35.9 (C19 and C22), 35.8 (C11), 35.3 (C16), 29.7 (CH_2), 28.9 (CH_2), 26.6 (C17), 26.1, 25.6, 25.0, 24.8 (CH_3), 22.3 (ali-CH_3), 16.1 (Ar-CH_3); **HRMS**: *m/z* $[M+H]^+$ calculated for $C_{35}H_{55}N_6O_5S$: 671.3949; Found: 671.3946; **$[\alpha]_D^{25}$:** 57.5 (c = 0.04, MeOH).

(2*S*,4*R*)-1-((*S*)-2-(6-(6-(4-(3-(4-cyano-3-(trifluoromethyl)phenyl)-5,5-dimethyl-4-oxo-2-thioxoimidazolidin-1-yl)-2-fluorobenzamido)hexanamido)hexanamido)-3,3-dimethylbutanoyl)-4-hydroxy-*N*-((*S*)-1-(4-(4-methylthiazol-5-yl)phenyl)ethyl)pyrrolidine-2-carboxamide (PROTAC-16)

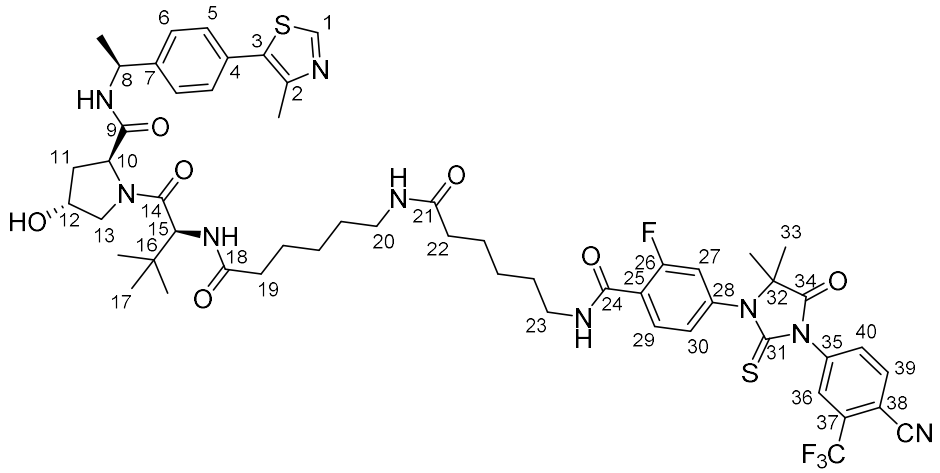

To a stirring solution of **2** (2.8 mg, 0.00625 mmol) in DMF (0.2 mL) were added HATU (2.85 mg, 0.0075 mmol) and DIPEA (1.3 µL, 0.0075 mmol). The reaction mixture was stirred at r.t. for 15 mins before **140** (4.4 mg, 0.0066 mmol) was added. The mixture was then stirred for a further 16 h before diluting in water (5 mL) and extracting into EtOAc (4 x 10 mL). The combined organics were then washed with brine (2 x 5 mL), before being dried over Na_2SO_4, filtered and concentrated *in vacuo*. The residue was purified through silica gel column chromatography (1:19 MeOH/DCM) to give the title compound as a colourless oil (3.0 mg, 45%).

R_f: 0.24 (7% MeOH/DCM); **IR** (neat film, ν_{max}, cm^{-1}): 3290 (w, NH), 2925 (m, CH), 2853 (w, CH), 1756 (m, C=O), 1724 (w, C=O), 1644 (s, C=O), 1622 (s, C=O), 1535 (m), 1500 (m), 1437 (s), 1412 (s), 1373 (m), 1311 (s), 1264 (m), 1219 (m), 1177 (m), 1140 (m), 1056 (w), 1015 (w); **^{1}H NMR** (500 MHz, $CDCl_3$) δ: 8.68 (s, 1 H, H1), 8.21 (t, *J* = 8.3 Hz, 1 H, H29), 7.99 (d, *J* = 8.3 Hz, 1 H, H39), 7.95 (d, *J* = 1.7 Hz, 1 H, H36), 7.82 (dd, *J* = 8.3, 1.9 Hz, 1 H, H40), 7.41 – 7.36 (m, 5 H, H5, H6 and NH), 7.24 (dd, *J* = 8.2, 1.9 Hz, 1 H, H30), 7.16 (dd, *J* = 11.6, 1.9 Hz, 1 H, H27), 6.84 – 6.80 (m, 1 H, NH), 6.25 (d, *J* = 8.7 Hz, 1 H, NH), 5.77 (t, *J* = 5.3 Hz, 1 H, NH), 5.08 (quin, *J* = 6.9 Hz, 1 H, H8), 4.74 (t, *J* = 8.2 Hz, 1 H, H10), 4.57 (d, *J* = 8.2 Hz, 1 H, H15), 4.51 (s, 1 H, H12), 4.12 (d, *J* = 11.9 Hz, 1 H, H13), 3.58 (dd, *J* = 11.9, 3.4, 1 H, H13'), 3.51 – 3.49 (m, 2 H, CH_2-N), 3.23 – 3.19 (m, 2 H, CH_2-N), 2.53 – 2.51 (m, 4 H, Ar-CH_3 and H11), 2.24 – 2.11 (m, 5 H, H11' and 2 x CH_2), 1.71 – 1.61 (m, 8 H, 2 x CH_3 and CH_2), 1.51 – 1.38 (m, 9 H, CH_3-C8), 1.33 – 1.27 (m, 4 H, 2 x CH_2); **^{13}C NMR** (126 MHz, $CDCl_3$) δ: 179.8 (C31), 174.5 (C34), 173.8, 173.1, 172.3, 169.7 (amide C=O), 162.3 (C24), 160.3 (d, *J* = 250 Hz, CF), 150.3, 148.5, 143.1, 140.0 (C25, d, *J* = 11.1 Hz), 136.8 (C38), 135.3 (C39), 133.7 (C37, q, *J* = 33.8 Hz), 133.3 (C29), 132.1 (C40), 131.6, 130.9, 129.6, 127.1 (C36, q, *J* = 6 Hz), 126.4, 126.2 (C30), 122.9 (C28), 121.9 (q, *J* = 273 Hz, CF_3), 118.0 (C27, d, *J* = 26 Hz), 114.8 (C≡N), 110.5 (C35), 70.0 (C12), 66.7 (C20), 58.4 (C15), 57.7 (C10), 56.8 (C13), 48.9 (C8), 39.9,

39.1 (C20 and C23), 36.4, 36.0 (C19 and C22), 35.6 (C11), 34.9 (C16), 29.7, 29.1, 26.5 (C17), 26.4, 26.0, 25.1, 24.9 (C33), 23.9, 22.3 (ali-CH_3), 16.1 (Ar-CH_3); **^{19}F NMR** (471 MHz, $CDCl_3$) δ: -63.0, -111.5; **HRMS**: (ESI) *m/z* $[M+H]^+$ calculated for $C_{55}H_{65}F_4N_9O_7S_2Na$: 1126.4277; Found: 1126.4311.

4-((6-(((*S*)-1-((2*S*,4*R*)-4-hydroxy-2-(((*S*)-1-(4-(4-methylthiazol-5-yl)phenyl)ethyl)carbamoyl)pyrrolidin-1-yl)-3,3-dimethyl-1-oxobutan-2-yl)amino)-6-oxohexyl)amino)-4-oxobutanoic acid (141)

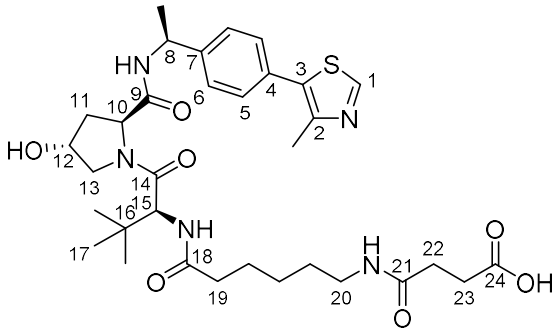

To a stirring solution of **138** (31 mg, 0.055 mmol) in tetrahydrofuran (0.3 mL) was added succinic anhydride (11 mg, 0.11 mmol). The reaction mixture was stirred at r.t. for 24 h before concentrating *in vacuo*. The residue was purified through silica gel column chromatography (1:9:0.1 MeOH/DCM/acetic acid) to give the title compound as a white amorphous solid (30 mg, 83%).

R_f: 0.08 (1:9:0.1 MeOH/DCM/acetic acid); **IR** (neat film, ν_{max}, cm^{-1}): 2929 (m, CH), 1713 (s, C=O), 1614 (s, C=O), 1547 (m), 1416 (m), 1330 (w), 1233 (m), 1205 (m), 1170 (m); **^{1}H NMR** (400 MHz, $CDCl_3$) δ: 8.87 (s, 1 H, H1), 7.45 – 7.41 (m, 4 H, Ar-H), 5.02 – 4.96 (m, 1 H, H8), 4.62 (s, 1 H, H10), 4.59 – 4.55 (m, 1 H, H15), 4.43 – 4.42 (m, 1 H, H12), 3.88 (d, *J* = 11.1 Hz, 1 H, H13), 3.75 (dd, *J* = 10.9, 4.0 Hz, 1 H, H13'), 3.16 (t, *J* = 7.0 Hz, 2 H, H20), 2.59 – 2.56 (m, 2 H, CH_2), 2.48 – 2.44 (m, 5 H, Ar-CH_3 and CH_2), 2.33 – 2.26 (m, 2 H, H23), 2.23 – 2.17 (m, 1 H, H11), 1.98 – 1.92 (m, 1 H, H11'), 1.65 – 1.61 (m, 2 H, CH_2), 1.54 – 1.48 (m, 5 H, ali-CH_3 and CH_2), 1.38 – 1.31 (m, 2 H, CH_2), 1.04 (s, 9 H, 3 x CH_3); **^{13}C NMR** (101 MHz, MeOD) δ: 175.2 (C24), 174.6 (C18), 173.1 (C21), 171.8 (C9), 170.9 (C21), 151.5 (C1), 147.7 (C2), 144.3 (C7), 132.0 (C3), 130.1 (C4), 129.1 (C5), 126.2 (C6), 69.6 (C12), 59.2 (C15), 57.6 (C10), 56.6 (C13), 48.7 (C8), 38.9 (C20), 37.4 (C11), 35.1 (C23), 35.1 (C16), 30.3, 28.8, 28.6, 26.1 (4 x CH_2), 25.6 (C17), 25.2 (CH_2), 21.0 (ali-CH_3), 14.4 (Ar-CH_3); **HRMS**: (ESI) *m/z* $[M+Na]^+$ calculated for $C_{33}H_{47}N_5O_7SNa$: 680.3088; Found: 680.3120; **$[\alpha]_D^{25}$:** 875.0 (c = 0.06, MeOH).

***tert*-Butyl (1-(6-chloro-3-(1-(4-chlorobenzyl)-4-(4-fluorophenyl)-1*H*-imidazol-5-yl)-1*H*-indol-2-yl)-1-oxo-5,8,11,14,17-pentaoxa-2-azanonadecan-19-yl)carbamate (142)**

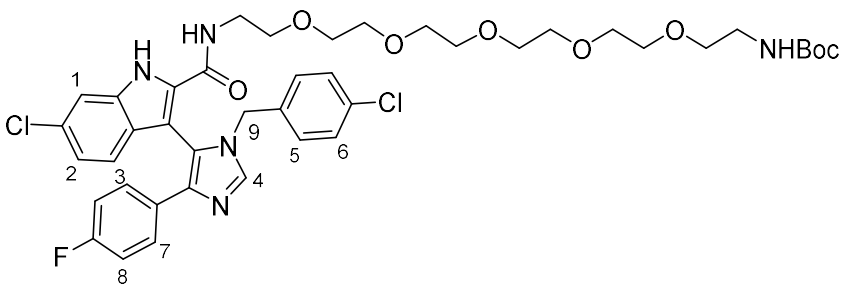

To a stirring solution of **87** (11 mg, 0.023 mmol) in DMF (0.1 mL), were added HATU (10 mg, 0.027 mmol) and DIPEA (4.7 µL, 0.027 mmol). The reaction was stirred at r.t. for *ca*. 15 mins before **30** (10 mg, 0.025 mmol) was added. The reaction was stirred for a further 18 h before being diluted with EtOAc (5 mL) and H_2O (3 mL), extracted into EtOAc (2 x 5 mL), washed with brine (5 mL), dried over Na_2SO_4, filtered, and concentrated *in vacuo.* The residue was then purified by silica gel chromatography (2% MeOH/DCM) to give the title compound as a yellow oil (10 mg, 53%).

R_f: 0.09 (2% MeOH/DCM); **IR** (neat film, ν_{max}, cm^{-1}): 2921 (m), 1752 (m), 1654 (s), 1619 (m), 1538 (m), 1509 (s), 1439 (s), 1407 (s), 1365 (m), 1312 (s), 1250 (s), 1220 (s), 1179 (s), 1138 (s), 1054 (m); **^{1}H NMR** (400 MHz, $CDCl_3$) δ: 10.10 (br s, 1 H, NH), 7.90 (s, 1 H, H4), 7.51 – 7.46 (m, 3 H, H1 H7), 7.10 – 7.04 (m, 4 H, H2, H3, H6), 6.83 (t, *J* = 8.7 Hz, 2 H, H8), 6.71 (d, *J* = 8.7 Hz, 2 H, H5), 6.31 (br s, 1 H, NH), 5.09 (br s, 1 H, NH), 4.86 (d, *J* = 15.3 Hz, 1 H, H9), 4.79 (d, *J* = 15.3 Hz, 1 H, H9), 3.68 – 3.19 (m, 24 H, 12x CH_2), 1.42 (s, 9 H, 3x CH_3); **^{13}C NMR** (101 MHz, $CDCl_3$) δ: 161.4 (d, *J* = 250 Hz, C-F), 160.1 (C=O), 156.1 (Boc C=O), 140.5, 139.1 (C11), 135.6, 134.1, 134.0, 131.3, 130.0, 129.7, 128.8 (C6), 128.6 (C5), 127.4 (d, *J* = 8 Hz, C7), 126.7, 122.6 (C2), 121.4 (C3), 118.1, 115.3 (d, *J* = 22 Hz, C8), 112.3 (C1), 104.8, 79.2 (boc-qC), 70.6 – 70.1 (overlapping 9C), 69.1, 48.8 (C9), 40.3, 39.3 (2x N-CH_2), 28.4 (3x CH_3); **^{19}F NMR** (471 MHz, $CDCl_3$) δ: -114.8; **HRMS (ESI):** m/z calcd for $C_{42}H_{50}Cl_2FN_5O_8Na$ $[M+Na]^+$: 864.2912; found: 864.2943.

6-Chloro-3-(1-(4-chlorobenzyl)-4-(4-fluorophenyl)-1*H*-imidazol-5-yl)-*N*-(1-(4-(3-(4-cyano-3-(trifluoromethyl)phenyl)-5,5-dimethyl-4-oxo-2-thioxoimidazolidin-1-yl)-2-fluorophenyl)-1-oxo-5,8,11,14,17-pentaoxa-2-azanonadecan-19-yl)-1*H*-indole-2-carboxamide (PROTAC-17)

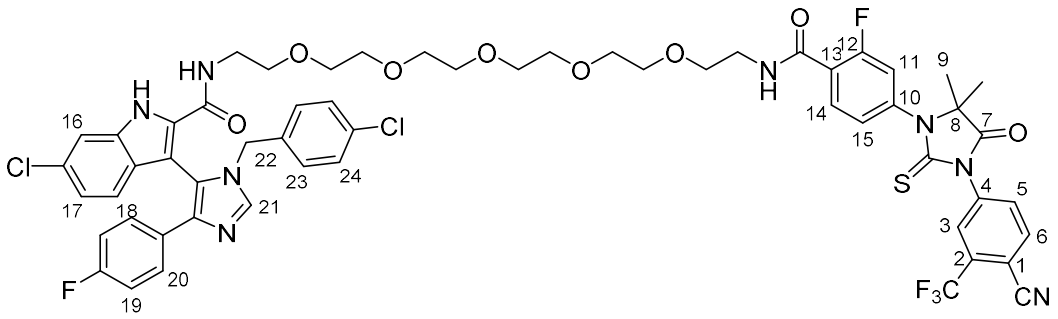

To a stirring solution of **142** (8 mg, 0.009 mmol) in dichloromethane (0.4 mL) was added trifluoroacetic acid (0.1 mL). The reaction mixture was stirred for 2 h before being quenched with $NaHCO_3$ (sat. aq.), extracted into dichloromethane (3x 5 mL), washed with brine (5 mL), dried over Na_2SO_4, filtered and concentrated *in vacuo*. The crude residue was taken directly through with no further purification. To a stirring solution of **2** (3 mg, 0.0067 mmol) in DMF (0.1 mL), were added HATU (3 mg, 0.008 mmol), DIPEA (1.4 µL, 0.008 mmol), and a solution of crude **142** (5 mg, 0.0067 mmol) in DMF (0.1 mL). The reaction was stirred for 18 h before being diluted with EtOAc (5 mL) and H_2O (3 mL), extracted into EtOAc (2 x 5 mL), washed with brine (5 mL), dried over Na_2SO_4, filtered, and concentrated *in vacuo.* The residue was then purified by silica gel chromatography (5% MeOH/DCM) to give the title compound as a yellow oil (4 mg, 51%).

R_f: 0.20 (5% MeOH/DCM); **IR** (neat film, ν_{max}, cm^{-1}): 2988 (w, CH), 2921 (w, CH), 1760 (w, C=O), 1654 (m, C=O), 1617 (m), 1541 (m), 1522 (m), 1496 (m), 1438 (s), 1411 (s) ,1312 (s), 1221 (s), 1179 (m), 1136 (s), 1088 (s); **^{1}H NMR** (500 MHz, $CDCl_3$) δ: 9.99 (br s, 1 H, NH), 8.22 (t, *J* = 8.3 Hz, 1 H, H14), 8.00 – 7.90 (m, 3 H), 7.83 (dd, *J* = 8.6, 2.0 Hz, 1 H, H5), 7.52 – 7.47 (m, 3 H), 7.25 – 7.03 (m, 7 H), 6.84 (t, *J* = 8.9 Hz, 2 H, H19), 6.72 (d, *J* = 8.6 Hz, 2 H, H23), 6.32 (br s, 1 H, NH), 4.87 (d, *J* = 15.2 Hz, 1 H, H22), 4.80 (d, *J* = 15.2 Hz, 1 H, H22), 3.72 – 3.20 (m, 24 H, 12x CH_2), 1.61 (s, 6 H, H9); **^{13}C NMR** (126 MHz, $CDCl_3$) δ: 179.8 (C=S), 174.5 (C7), 162.2 (C=O), 162.0 (d, *J* = 250 Hz, C-F), 160.3 (d, *J* = 250 Hz, C-F), 160.0 (C=O), 139.0 (2C), 138.9 (d, *J* = 11 Hz, C13), 136.8 (C1), 135.4, 135.3 (C5), 134.2, 134.1, 134.0, 133.7 (q, *J* = 33 Hz, C2), 133.2 (d, *J* = 3 Hz, C14), 132.1 (C5), 131.3, 130.1, 129.5, 129.1, 128.8, 128.7, 127.4 (d, *J* = 8 Hz), 127.1 (q, *J* = 5 Hz, C3), 126.7, 126.1 (d, *J* = 3.5 Hz, C15), 125.1, 123.1, 123.0, 122.9, 122.7, 121.3, 120.7, 118.6, 118.2, 118.0 (d, *J* = 26 Hz, C11), 115.4 (d, *J* = 22 Hz), 114.7 (-C≡N), 112.2, 110.5 (C4), 104.7, 70.5 – 70.3, 69.5, 69.1 (overlapping O-CH_2), 66.6 (C8), 48.9 (C22), 40.0, 39.3 (2x N-CH_2), 23.8 (C9); **^{19}F NMR**

(471 MHz, $CDCl_3$) δ: -63.0, -111.2, -115.8; **HRMS (ESI):** m/z calcd for $C_{57}H_{53}Cl_2F_5N_8O_8SNa$ $[M+Na]^+$: 1197.2896; found: 1197.2943.

2,2-Dimethyl-4-oxo-3,8,11,14-tetraoxa-5-azahexadecan-16-yl methanesulfonate (144)

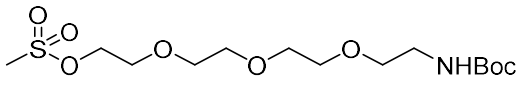

To a stirring solution of **143** (120 mg, 0.41 mmol) in Et_2O (0.5 mL) cooled to 0 °C, were added triethylamine (74 µL, 0.53 mmol), and methanesulfonyl chloride (41 µL, 0.53 mmol). The reaction was stirred at r.t. for 5 h before being diluted with brine (5 mL), extracted into Et_2O (3 x 10 mL) and dried over Na_2SO_4, filtered, and concentrated *in vacuo* to give the title compound as a colourless oil (134 mg, 88%) used without further purification.

R_f: 0.67 (9:1 DCM:MeOH); **IR** (neat film, ν_{max}, cm^{-1}): 3368 (w, NH), 2976 (w, CH), 2873 (w, CH), 1707 (m, C=O), 1511 (m), 1454 (m), 1391 (w), 1350 (m), 1274 (m), 1247 (m), 1200 (s), 1102 (s), 1016 (m); **^{1}H NMR** (400 MHz, $CDCl_3$) δ: 5.02 (br s, 1 H, NH), 4.41 – 4.38 (m, 2 H), 3.80 – 3.78 (m, 2 H), 3.69 – 3.63 (m, 8 H), 3.56 – 3.54 (m, 2 H), 3.32 (br m, 2 H), 3.09 (s, 3 H, CH_3), 1.46 (s, 9 H, 3x CH_3); **^{13}C NMR** (101 MHz, $CDCl_3$) δ: 156.0 (C=O), 79.2 (qC), 70.7, 70.5, 70.2, 69.2, 69.0 (overlapping O-CH_2), 52.6 (CH_2-OMs), 40.4 (N-CH_2), 37.7 (S-CH_3), 28.4 (3x CH_3).

Data are in accordance with those reported previously in literature.[348]

Methyl (*S*)-3-(4-((2,2-dimethyl-4-oxo-3,8,11,14-tetraoxa-5-azahexadecan-16-yl)oxy)phenyl)-2-(3,3-diphenylpropanamido)propanoate (145)

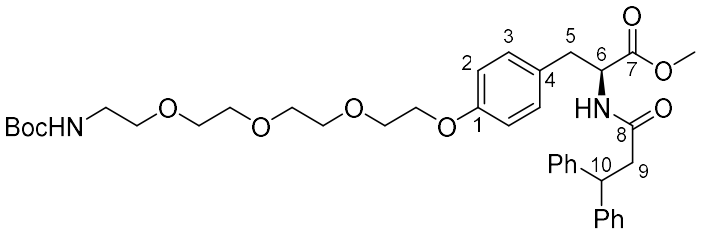

To a stirring solution of **86** (47 mg, 0.12 mmol) in DMF (0.5 mL), were added potassium carbonate (32 mg, 0.23 mmol), and **144** (65 mg, 0.18 mmol). The reaction was heated to 80 °C for 5 h before being cooled, diluted with H_2O (2 mL), extracted into EtOAc (3 x 10 mL), washed with brine (5 mL), dried over Na_2SO_4, filtered, and concentrated *in vacuo*. The residue was then purified by silica gel chromatography (1:1 to 45:55 Hex:EtOAc) to give the title compound as a yellow oil (31 mg, 39%).

R_f: 0.31 (7:3 EtOAc:Hex); **IR** (neat film, ν_{max}, cm^{-1}): 3338 (w), 2921 (m), 1742 (m), 1708 (m), 1653 (m), 1611 (w), 1511 (s), 1451 (m), 1365 (m), 1247 (s), 1173 (s), 1110 (s); **^{1}H NMR** (400 MHz, $CDCl_3$) δ: 7.34 – 7.20 (m, 10 H, Ar-H), 6.74 (d, *J* = 8.6 Hz, 2 H, H3), 6.66 (d, *J* = 8.6 Hz, 2 H, H2), 5.87 (d, *J* = 7.5 Hz, 1 H, NH), 5.07 (br s, 1 H, NH), 4.80 – 4.76 (m, 1 H, H6), 4.62 (t, *J* = 8.0 Hz, 1 H, H10), 4.11 (t, *J* = 4.5 Hz, 2 H, O-CH_2), 3.87 (t, *J* = 4.5 Hz, 2 H, O-CH_2), 3.77 – 3.75 (m, 2 H, O-CH_2), 3.72 – 3.62 (m, 9 H, OMe and 3x O-CH_2), 3.55 (t, *J* = 4.9 Hz, 2 H, O-CH_2), 3.33 – 3.31 (m, 2 H, N-CH_2), 2.97 – 2.84 (m, 4 H, H5 and H9), 1.46 (s, 9 H, 3x CH_3); **^{13}C NMR** (101 MHz, $CDCl_3$) δ: 171.8 (C7), 170.3 (C8), 157.8 (C1), 156.0 (Boc-C=O), 143.8, 143.6, 130.2 (C3), 128.6 (2C), 128.0, 127.8, 127.7, 126.6 (C4), 126.5, 114.5 (C2), 79.2 (qC), 70.8, 70.6 (2C), 70.5, 70.2, 69.8, 67.3 (7x O-CH_2), 53.1 (C6), 52.2 (OMe), 47.1 (C10), 43.0 (C9), 40.4 (N-CH_2), 37.0 (C5), 28.4 (3x CH_3); **HRMS (ESI):** m/z calcd for $C_{38}H_{50}N_2O_9Na$ $[M+Na]^+$: 701.3408; found: 701.3424; **$[\alpha]_D^{25}$** 1.0° (c = 0.1, MeOH).

Methyl (*S*)-3-(4-(2-(2-(2-(2-aminoethoxy)ethoxy)ethoxy)ethoxy)phenyl)-2-(3,3-diphenylpropanamido)propanoate (146)

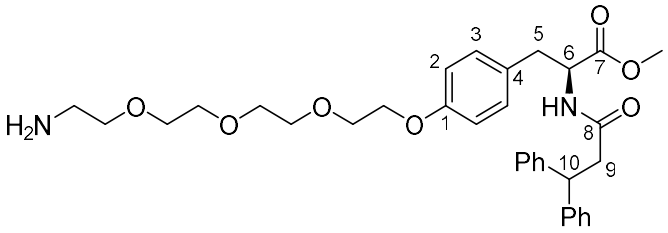

To a stirring solution of **145** (28 mg, 0.041 mmol) in dichloromethane (0.4 mL) was added trifluoroacetic acid (0.1 mL). The reaction was stirred for 3 h at r.t. before being concentrated, diluted with sat. aq. $NaHCO_3$ (2 mL), extracted into dichloromethane (3 x 10 mL), dried over Na_2SO_4, filtered, and concentrated *in vacuo* to give the title compound as a yellow oil (21.3 mg, 89%) used without further purification.

IR (neat film, ν_{max}, cm^{-1}): 2913 (m), 1743 (m), 1650 (m), 1611 (m), 1542 (m), 1511 (s), 1450 (m), 1247 (s), 1123 (s), 1066 (s); **^{1}H NMR** (400 MHz, $CDCl_3$) δ: 7.34 – 7.18 (m, 10 H, Ar-H), 6.75 (d, *J* = 8.7 Hz, 2 H, H3), 6.65 (d, *J* = 8.7 Hz, 2 H, H2), 6.00 (d, *J* = 7.4 Hz, 1 H, NH), 4.81 – 4.77 (m, 1 H, H6), 4.62 (t, *J* = 7.5 Hz, 1 H, H10), 4.11 (t, *J* = 4.6 Hz, 2 H, O-CH_2), 3.87 (t, *J* = 4.6 Hz, 2 H, O-CH_2), 3.76 – 3.66 (m, 11 H, OMe and 4x O-CH_2), 3.54 (t, *J* = 4.8 Hz, 2 H, O-CH_2), 3.00 – 2.80 (m, 6 H, N-CH_2, H5 and H9), 2.26 (br s, 2 H, NH_2); **^{13}C NMR** (101 MHz, $CDCl_3$) δ: 171.8 (C7), 170.4 (C8), 157.7 (C1), 143.8, 143.6, 130.3 (C3), 128.6 (2C), 128.0, 127.9, 127.7, 126.6 (C4), 126.5, 114.5 (C2), 72.8, 70.8, 70.6 (2C), 70.3, 69.7, 67.4 (7x O-CH_2), 53.1 (C6), 52.2 (OMe), 47.1 (C10), 42.9 (C9), 41.6 (N-CH_2), 37.0 (C5); **HRMS (ESI):** m/z calcd for $C_{33}H_{43}N_2O_7$ $[M+H]^+$: 579.3065; found: 579.3070; **$[\alpha]_D^{25}$** 2.0° (c = 0.1, MeOH).

Methyl (*S*)-3-(4-((1-(4-(3-(4-cyano-3-(trifluoromethyl)phenyl)-5,5-dimethyl-4-oxo-2-thioxoimidazolidin-1-yl)-2-fluorophenyl)-1-oxo-5,8,11-trioxa-2-azatridecan-13-yl)oxy)phenyl)-2-(3,3-diphenylpropanamido)propanoate (PROTAC-18)

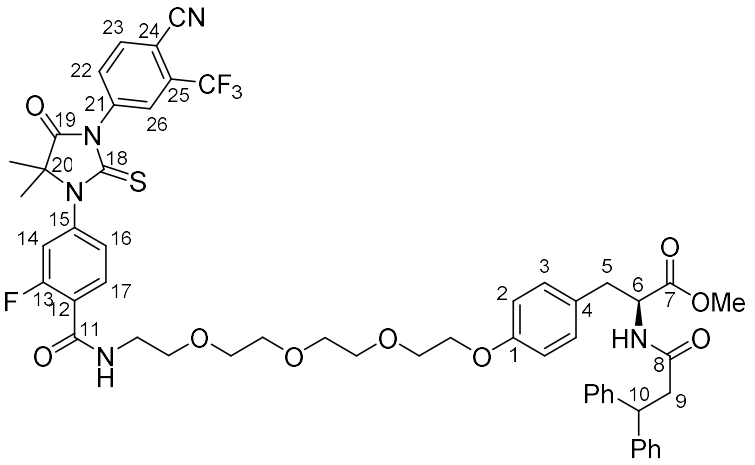

To a stirring solution of **2** (14 mg, 0.031 mmol) in DMF (0.3 mL), were added HATU (14 mg, 0.037 mmol) and DIPEA (6.5 µL, 0.037 mmol). The reaction was stirred at r.t. for *ca*. 15 mins before **146** (20 mg, 0.034 mmol) was added. The reaction was stirred for a further 5 h before being diluted with EtOAc (5 mL) and H_2O (3 mL), extracted into EtOAc (2 x 5 mL), washed with brine (5 mL), dried over Na_2SO_4, filtered, and concentrated *in vacuo.* The residue was then purified by silica gel chromatography (2% MeOH/DCM) to give the title compound as a yellow oil (22.3 mg, 65%).

R_f: 0.35 (5% MeOH/DCM); **IR** (neat film, ν_{max}, cm^{-1}): 2920 (w), 1751 (m), 1653 (m), 1619 (m), 1532 (m), 1508 (m), 1498 (m), 1438 (s), 1411 (m), 1311 (s), 1248 (m), 1219 (s), 1177 (m), 1136 (s), 1056 (m); **^{1}H NMR** (400 MHz, $CDCl_3$) δ: 8.23 (t, *J* = 8.3 Hz, 1 H, H17), 8.01 – 7.97 (m, 2 H, H23 and H26), 7.84 (dd, *J* = 8.2, 1.8 Hz, 1 H, H22), 7.33 – 7.14 (m, 13 H, 10x Ar-H, H14, H16, NH overlapping $CHCl_3$), 6.73 (d, *J* = 8.7 Hz, 2 H, H3), 6.65 (d, *J* = 8.7 Hz, 2 H, H2), 5.91 (d, *J* = 7.8 Hz, 1 H, NH), 4.80 – 4.75 (m, 1 H, H6), 4.61 (t, *J* = 7.8 Hz, 1 H, H10), 4.08 (t, *J* = 4.5 Hz, 2 H, O-CH_2), 3.84 (t, *J* = 4.7 Hz, 2 H, O-CH_2), 3.74 – 3.66 (m, 15 H, OMe and 6x CH_2), 3.00 – 2.88 (m, 3 H, H5 and H9), 2.85 – 2.81 (m, 1 H, H9), 1.61 (s, 6 H, 2x CH_3); **^{13}C NMR** (101 MHz, $CDCl_3$) δ: 179.8 (C=S), 174.5 (C19), 171.8 (C7), 170.4 (C8), 162.2 (d, *J* = 3.2 Hz, C11), 160.4 (d, *J* = 250 Hz, C13), 157.7 (C1), 143.8, 143.6, 138.9 (d, *J* = 10 Hz, C12), 136.8 (C24), 135.3 (C23), 133.9 (C25), 133.2 (d, *J* = 3.6 Hz, C17), 132.1 (C22), 130.2, 128.6 (2C), 128.0, 127.9, 127.6, 127.1 (d, *J* = 5.6 Hz, C26), 126.6, 126.5, 126.1 (d, *J* = 2.9 Hz, C16), 123.1 (d, *J* = 12.5 Hz, C15), 119.1 (q, *J* = 273 Hz, CF_3), 118.0 (d, *J* = 25.6 Hz, C14), 114.7 (C2), 114.5 (-C≡N), 110.4 (d, *J* = 4.4 Hz, C21), 70.8, 70.6, 70.4, 69.7, 69.5, 67.3, 66.6 (7x O-CH_2), 53.1 (C6), 52.2 (OMe), 47.1 (C10), 42.9 (C9), 40.0 (N-CH_2), 37.0 (C5), 23.8 (2x CH_3); **^{19}F NMR** (376 MHz, $CDCl_3$) δ: -62.0, -110.3; **HRMS (ESI):** m/z calcd for $C_{53}H_{53}F_4N_5O_9SNa$ $[M+Na]^+$: 1034.3392; found: 1034.3415; **$[\alpha]_D^{25}$** 9.0° (c = 0.1, MeOH).

(*S*)-3-(4-((1-(4-(3-(4-cyano-3-(trifluoromethyl)phenyl)-5,5-dimethyl-4-oxo-2-thioxoimidazolidin-1-yl)-2-fluorophenyl)-1-oxo-5,8,11-trioxa-2-azatridecan-13-yl)oxy)phenyl)-2-(3,3-diphenylpropanamido)propanoic acid (PROTAC-19)

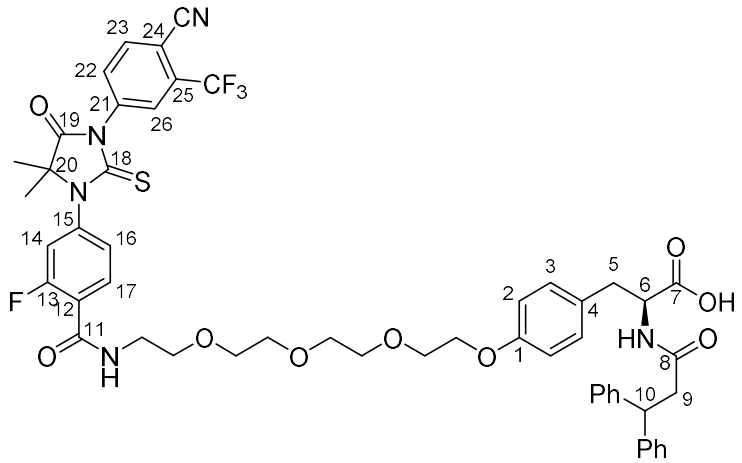

To a stirring solution of **PROTAC-18** (18 mg, 0.0178 mmol) in acetic acid (0.5 mL) was added HCl (1 M, 0.5 mL). The reaction was heated to 100 °C for 3 h before being cooled and concentrated to give the title compound as a yellow oil (12 mg, 67%) used without further purification.

IR (neat film, ν_{max}, cm^{-1}): 3325 (w, NH), 2927 (m, CH), 2853 (w, CH), 1755 (m, C=O), 1724 (m, C=O), 1708 (m, C=O), 1654 (m), 1619 (m), 1538 (m), 1514 (m), 1498 (m), 1440 (s), 1411 (s), 1311 (s), 1250 (m), 1219 (s), 1178 (s), 1139 (s), 1056 (m); **^{1}H NMR** (400 MHz, $CDCl_3$) δ: 8.19 (t, *J* = 8.3 Hz, 1 H, H17), 7.98 (d, *J* = 8.2 Hz, H23), 7.94 (d, *J* = 1.9 Hz, H26), 7.81 (dd, *J* = 8.3, 1.9 Hz, H22), 7.32 – 7.13 (m, 13 H, 10x Ar-H, H14, H16, NH overlapping $CHCl_3$), 6.72 – 6.62 (m, 4 H, H2 and H3), 6.01 (d, *J* = 7.1 Hz, 1 H, NH), 4.75 – 4.71 (m, 1 H, H6), 4.63 – 4.60 (m, 1 H, H10), 4.06 (t, *J* = 4.5 Hz, 2 H, O-CH_2), 3.82 – 3.80 (m, 2 H, O-CH_2), 3.72 – 3.53 (m, 12 H, 6x CH_2), 3.01 – 2.89 (m, 3 H, H5 and H9), 2.85 – 2.81 (m, 1 H, H9), 1.60 (s, 6 H, 2x CH_3); **^{13}C NMR** (101 MHz, $CDCl_3$) δ: 179.8 (C=S), 174.4 (C19), 172.3 (C7), 170.9 (C8), 162.6 (d, *J* = 3.2 Hz, C11), 160.4 (d, *J* = 250 Hz, C13), 157.8 (C1), 143.7, 143.5, 139.2 (d, *J* = 10.6 Hz, C12), 136.8 (C24), 135.3 (C23), 133.7 (q, *J* = 34 Hz, C25), 133.3 (d, *J* = 2.9 Hz, C17), 132.1 (C22), 130.4 (C3), 128.7, 128.6, 128.0 (2C), 127.6, 127.0 (q, *J* = 4.8 Hz, C26), 126.7, 126.6, 126.2 (d, *J* = 3.3 Hz, C16), 122.5 (d, *J* = 11.3 Hz, C15), 121.8 (q, *J* = 273 Hz, CF_3), 118.0 (d, *J* = 26.1 Hz, C14), 114.7 (C2), 114.5 (-C≡N), 110.5 (d, *J* = 2.3 Hz, C21), 70.9, 70.7, 70.6, 70.3, 69.7, 69.2, 67.5 (7x O-CH_2), 66.6 (C20), 53.3 (C6), 47.2 (C10), 43.0 (C9), 40.2 (N-CH_2), 36.6 (C5), 23.8 (2x CH_3); **^{19}F NMR** (376 MHz, $CDCl_3$) δ: -62.9, -111.0; **HRMS (ESI):** m/z calcd for $C_{52}H_{50}F_4N_5O_9S$ [M-H]-: 996.3271; found: 996.3300; **$[\alpha]_D^{20}$** 32.5° (c = 0.08, MeOH).

Methyl (*S*)-3-(4-(2-(tert-butoxy)-2-oxoethoxy)phenyl)-2-(3,3-diphenylpropanamido)propanoate (147)

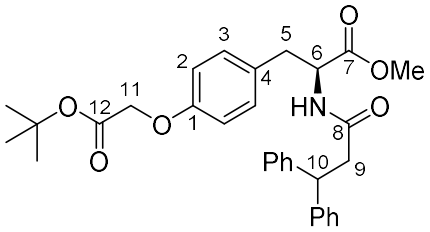

To a stirring solution of **86** (315 mg, 0.78 mmol) in DMF (2 mL), were added potassium carbonate (216 mg, 1.56 mmol), and *tert*-butyl bromoacetate (162 µL, 1.09 mmol). The reaction was heated to 80 °C for 6 h before being cooled, diluted with H_2O (2 mL), extracted into EtOAc (3 x 10 mL), washed with brine (5 mL), dried over Na_2SO_4, filtered, and concentrated *in vacuo*. The residue was then purified by silica gel chromatography (1:1 Hex:EtOAc) to give the title compound as a yellow oil (320 mg, 79%).

R_f: 0.31 (7:3 Hex:EtOAc); **IR** (neat film, ν_{max}, cm^{-1}): 2980 (w), 1746 (m), 1711 (m), 1661 (m), 1510 (m), 1438 (m), 1367 (m), 1308 (m), 1216 (s), 1152 (s), 1080 (m); **^{1}H NMR** (400 MHz, $CDCl_3$) δ: 7.34 – 7.21 (m, 10 H, Ar-H overlapped $CDCl_3$), 6.73 (d, *J* = 8.7 Hz, 2 H, H3), 6.66 (d, *J* = 8.7 Hz, 2 H, H2), 5.83 (d, *J* = 7.5 Hz, 1 H, NH), 4.81 – 4.77 (m, 1 H, H6), 4.64 – 4.60 (m, 1 H, H10), 4.49 (s, 2 H, H11), 3.66 (s, 3 H, OMe), 2.97 – 2.84 (m, 4 H, H5 and H9), 1.51 (s, 9 H, 3x CH_3); **^{13}C NMR** (101 MHz, $CDCl_3$) δ: 171.7 (C7), 170.3 (C8), 168.0 (C12), 157.0 (C1), 143.8, 143.6, 130.3 (C3), 128.6 (2C), 128.5, 128.0, 127.6, 126.7 (C4), 126.5, 114.6 (C2), 82.4 (qC), 65.7 (C11), 53.1 (C6), 52.2 (OMe), 47.1 (C10), 43.0 (C9), 36.9 (C5), 28.1 (3x CH_3); **HRMS (ESI):** m/z calcd for $C_{31}H_{35}NO_6Na$ $[M+Na]^+$: 540.2356; found: 540.2356; **$[\alpha]_D^{20}$** 4.1° (c = 0.54, MeOH).

(*S*)-2-(4-(2-(3,3-diphenylpropanamido)-3-methoxy-3-oxopropyl)phenoxy)acetic acid (148)

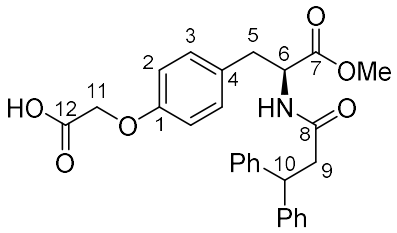

To a stirring solution of **147** (128 mg, 0.25 mmol) in dichloromethane (0.8 mL) was added trifluoroacetic acid (0.2 mL). The reaction was stirred for 3 h at r.t. before being concentrated *in vacuo* to give the title compound as a yellow oil (110 mg, 96%) used without further purification.

R_f: 0.50 (7:3 EtOAc:Hex); **IR** (neat film, ν_{max}, cm^{-1}): 3355 (m), 2948 (w), 1735 (s), 1647 (m), 1611 (m), 1542 (m), 1510 (s), 1438 (m), 1375 (w), 1213 (s), 1179 (s), 1121 (w), 1079 (m), 1019 (s); **^{1}H NMR** (400 MHz, $CDCl_3$) δ: 7.30 – 7.19 (m, 10 H, Ar-H overlapping $CDCl_3$), 6.77 (d, *J* = 8.7 Hz, 2 H, H3), 6.68 (d, *J* = 8.7 Hz, 2 H, H2), 6.21 (d, *J* = 7.9 Hz, 1 H, NH), 4.83 – 4.78 (m, 1 H, H6), 4.65 (s, 2 H, H11), 4.56 (t, *J* = 8.2 Hz, 1 H, H10), 3.69 (s, 3 H, OMe), 3.06 – 2.81 (m, 4 H, H5 and H9); **^{13}C NMR** (101 MHz, $CDCl_3$) δ: 172.4, 172.1, 171.7 (3x C=O), 156.5 (C1), 143.2, 143.0, 130.5 (C3), 128.8, 128.7 (2C), 127.9, 127.6, 126.8 (C4), 126.7, 114.7 (C2), 64.8 (C11), 53.3 (C6), 52.5 (OMe), 47.3 (C10), 42.8 (C9), 36.9 (C5); **HRMS (ESI):** m/z calcd for $C_{31}H_{35}NO_6Na$ $[M-H]^-$: 460.1765; found: 460.1760; **$[\alpha]_D^{20}$** 10.9° (c = 0.32, MeOH).

Methyl (S)-3-(4-((2,2-dimethyl-4,18-dioxo-3,8,11,14-tetraoxa-5,17-diazanonadecan-19-yl)oxy)phenyl)-2-(3,3-diphenylpropanamido)propanoate (149)

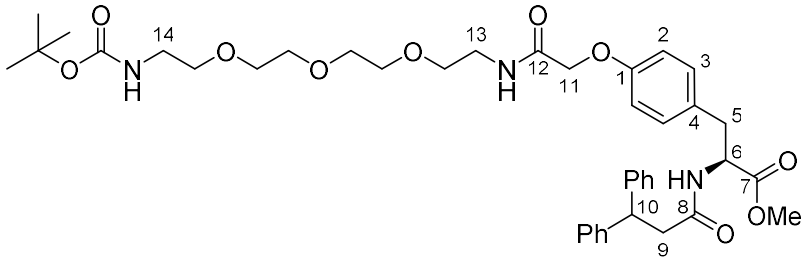

To a stirring solution of **148** (25 mg, 0.054 mmol) in DMF (0.4 mL), were added HATU (23 mg, 0.059 mmol) and DIPEA (10.4 µL, 0.059 mmol). The reaction was stirred at r.t. for *ca*. 15 mins before **92** (17 mg, 0.059 mmol) was added. The reaction was stirred for a further 4 h before being diluted with EtOAc (5 mL) and H_2O (3 mL), extracted into EtOAc (2 x 5 mL), washed with brine (5 mL), dried over Na_2SO_4, filtered, and concentrated *in vacuo.* The residue was then purified by silica gel chromatography (1 to 5% MeOH/DCM) to give the title compound as a yellow oil (21 mg, 53%).

R_f: 0.26 (6% MeOH/DCM); **IR** (neat film, ν_{max}, cm^{-1}): 3310 (w), 2926 (w), 2865 (w), 1742 (m), 1706 (m), 1656 (s), 1536 (s), 1510 (s), 1450 (m), 1366 (m), 1274 (m), 1246 (s), 1175 (s), 1122 (s); **^{1}H NMR** (400 MHz, $CDCl_3$) δ: 7.34 – 7.20 (m, 10 H, Ar-H overlapping $CDCl_3$), 7.02 (br s, 1 H, NH), 6.74 (d, *J* = 8.7 Hz, 2 H, H3), 6.68 (d, *J* = 8.7 Hz, 2 H, H2), 5.92 (d, *J* = 6.7 Hz, 1 H, NH), 5.05 (br s, 1 H, NH), 4.81 – 4.77 (m, 1 H, H6), 4.62 (t, *J* = 7.6 Hz, 1 H, H10), 4.46 (s, 2 H, H11), 3.68 – 3.51 (m, 17 H, 7x CH_2 and OMe), 3.30 (q, *J* = 5.5 Hz, 2 H, N-CH_2), 3.01 – 2.82 (m, 4 H, H5 and H9), 1.46 (s, 9 H, 3x CH_3); **^{13}C NMR** (101 MHz, $CDCl_3$) δ: 171.7, 170.4, 168.2 (3x C=O), 156.3 (C1), 156.0 (Boc-C=O), 143.8, 143.6, 130.5 (C3), 129.3, 128.6 (2C), 128.0, 127.6, 126.6 (C4), 126.5, 114.7 (C2), 79.2 (qC), 70.5, 70.3, 70.2 (2C), 69.8 (overlapping O-CH_2), 67.4 (C11), 53.1 (C6), 52.3 (OMe), 47.1 (C10), 42.9 (C9), 40.3, 38.8 (2x N-CH_2), 36.9 (C5), 28.4 (3x

CH_3); **HRMS (ESI):** m/z calcd for $C_{40}H_{53}N_3O_{10}Na$ $[M+Na]^+$: 758.3623; found: 758.3608; **$[\alpha]_D^{20}$** 10.0° (c = 0.06, MeOH).

Methyl (*S*)-3-(4-((14-amino-2-oxo-6,9,12-trioxa-3-azatetradecyl)oxy)phenyl)-2-(3,3-diphenylpropanamido)propanoate (150)

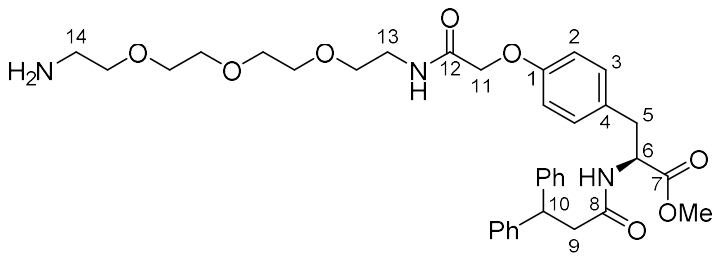

To a stirring solution of **149** (19 mg, 0.026 mmol) in dichloromethane (0.4 mL) was added trifluoroacetic acid (0.1 mL). The reaction was stirred for 3 h at r.t. before being concentrated, diluted with sat. aq. $NaHCO_3$ (2 mL), extracted into dichloromethane (3 x 10 mL), dried over Na_2SO_4, filtered, and concentrated *in vacuo* to give the title compound as a yellow oil (16 mg, >98%) used without further purification.

IR (neat film, ν_{max}, cm^{-1}): 3345 (m), 2920 (m), 1740 (m), 1650 (s), 1611 (m), 1542 (m), 1510 (s), 1446 (m), 1350 (m), 1242 (m), 1101 (m); **^{1}H NMR** (400 MHz, $CDCl_3$) δ: 7.34 – 7.18 (m, 10 H, Ar-H overlapping $CDCl_3$), 6.74 (d, *J* = 8.7 Hz, 2 H, H3), 6.67 (d, *J* = 8.7 Hz, 2 H, H2), 6.09 (d, *J* = 7.6 Hz, 1 H, NH), 4.82 – 4.77 (m, 1 H, H6), 4.62 (t, *J* = 8.0 Hz, 1 H, H10), 4.46 (s, 2 H, H11), 3.68 – 3.50 (m, 19 H, 8x CH_2 and OMe), 3.01 – 2.91 (m, 3 H, H5 and H9), 2.88 – 2.83 (m, 1 H, H9), 1.87 (br s, 2 H, NH_2); **^{13}C NMR** (101 MHz, $CDCl_3$) δ: 171.7, 170.4, 168.3 (3x C=O), 156.3 (C1), 143.8, 143.6, 130.5 (C3), 129.3, 128.6 (2C), 128.0, 127.6, 126.6 (C4), 126.5, 114.7 (C2), 70.6, 70.5, 70.3, 70.2, 69.8 (overlapping O-CH_2), 67.4 (C11), 53.1 (C6), 52.3 (OMe), 47.1 (C10), 42.9 (C9), 38.8, 38.6 (2x N-CH_2), 36.9 (C5); **HRMS (ESI):** m/z calcd for $C_{35}H_{46}N_3O_8$ $[M+H]^+$: 636.3280; found: 636.3294; **$[\alpha]_D^{20}$** 18.9° (c = 0.09, MeOH).

Methyl (*S*)-3-(4-((1-(4-(3-(4-cyano-3-(trifluoromethyl)phenyl)-5,5-dimethyl-4-oxo-2-thioxoimidazolidin-1-yl)-2-fluorophenyl)-1,15-dioxo-5,8,11-trioxa-2,14-diazahexadecan-16-yl)oxy)phenyl)-2-(3,3-diphenylpropanamido)propanoate (PROTAC-20)

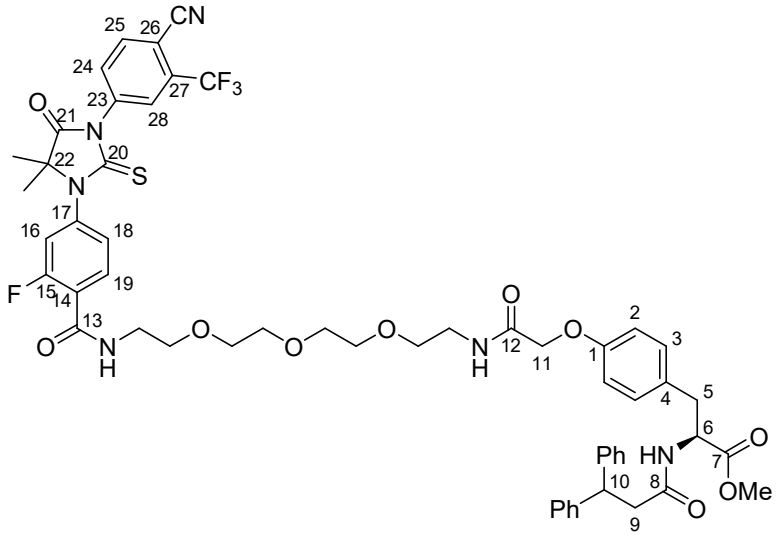

To a stirring solution of **2** (10 mg, 0.023 mmol) in DMF (0.2 mL), were added HATU (10 mg, 0.027 mmol) and DIPEA (4.8 µL, 0.027 mmol). The reaction was stirred at r.t. for *ca*. 15 mins before **150** (16 mg, 0.025 mmol) was added. The reaction was stirred for a further 8 h before being diluted with EtOAc (5 mL) and H_2O (3 mL), extracted into EtOAc (2 x 5 mL), washed with brine (5 mL), dried over Na_2SO_4, filtered, and concentrated *in vacuo.* The residue was then purified by silica gel chromatography (2% MeOH/DCM) to give the title compound as a yellow oil (14 mg, 58%).

R_f: 0.32 (5% MeOH/DCM); **IR** (neat film, ν_{max}, cm^{-1}): 3300 (w), 2920 (w), 2865 (w), 1751 (m), 1657 (s), 1620 (m), 1537 (m), 1507 (s), 1439 (s), 1413 (s), 1311 (s), 1218 (s), 1177 (s), 1136 (s), 1056 (m); **^{1}H NMR** (400 MHz, $CDCl_3$) δ: 8.22 (t, *J* = 8.3 Hz, 1 H, H19), 7.98 (d, *J* = 8.3 Hz, 1 H, H25), 7.95 (d, *J* = 1.9 Hz, 1 H, H28), 7.82 (dd, *J* = 8.3, 1.9 Hz, 1 H, H22), 7.31 – 7.14 (m, 13 H, 10x Ar-H, H16, H18, NH overlapping $CHCl_3$), 6.99 (t, *J* = 5.5 Hz, 1 H, NH), 6.71 (d, *J* = 8.7 Hz, 2 H, H3), 6.66 (d, *J* = 8.7 Hz, 2 H, H2), 5.92 (d, *J* = 6.7 Hz, 1 H, NH), 4.78 – 4.75 (m, 1 H, H6), 4.60 (t, *J* = 7.9 Hz, H10), 4.42 (s, 2 H, H11), 3.68 – 3.57 (m, 17 H, 7x CH_2 and OMe), 3.54 (t, *J* = 5.3 Hz, 2 H, N-CH_2), 2.98 – 2.82 (m, 4 H, H5 and H9), 1.60 (s, 6 H, 2x CH_3); **^{13}C NMR** (101 MHz, $CDCl_3$) δ: 179.8 (C20), 174.4 (C21), 171.7 (C7), 170.4 (C8), 168.2 (C12), 162.1 (d, *J* = 3.0 Hz, C13), 160.3 (d, *J* = 250 Hz, C15), 156.2 (C1), 143.8, 143.5, 139.0 (d, *J* = 10.7 Hz, C14), 136.8 (C24), 135.3 (C25), 133.7 (q, *J* = 33.5 Hz, C27), 133.3 (d, *J* = 3.5 Hz, C19), 132.1 (C24), 130.5 (C3), 129.3, 128.6 (2C), 128.0, 127.6, 127.1 (q, *J* = 4.8 Hz, C28), 126.6 (C4), 126.5, 126.1 (d, *J* = 3.1 Hz, C18), 122.9 (d, *J* = 12 Hz, C17), 121.8 (q, *J* = 275 Hz, CF_3), 118.0 (d, *J* = 26.0 Hz, C16), 114.7 (2C, C2 and -C≡N), 110.4 (q, *J* = 2.1 Hz, C23), 70.5, 70.4, 70.3, 69.7, 69.5, 67.4 (O-CH_2), 66.6 (C22), 64.1 (C11), 53.1 (C6), 52.3

(OMe), 47.1 (C10), 42.9 (C9), 39.9, 38.8 (2x N-CH_2), 36.9 (C5), 23.8 (2x CH_3); **^{19}F NMR** (376 MHz, $CDCl_3$) δ: -62.9, -111.3; **HRMS (ESI):** m/z calcd for $C_{55}H_{56}F_4N_6O_{10}SNa$ $[M+Na]^+$: 1091.3607; found: 1091.3649; **$[\alpha]_D^{20}$** 8.3° (c = 0.06, MeOH).

1*H*-indol-3-yl acetate (156)

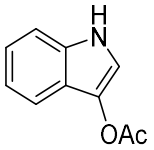

Following a modified version of a reported procedure,[312] to a stirring solution of indole (0.358 g, 3.06 mmol) and sodium hydroxide (0.123 g, 3.06 mmol) in methanol (30 mL) were added iodine (0.777 g, 3.06 mmol) and a solution of potassium iodide (0.507 g, 3.06 mmol) in H_2O (6 mL). The reaction was stirred in the dark at r.t. for 3 h before H_2O (20 mL) was added and the precipitate was filtered, washed with H_2O (10 mL), and dried *in vacuo*. The crude solid was then dissolved in acetic acid (16 mL) and silver acetate (0.714 g, 4.28 mmol) was added. The reaction was heated to 90 °C for 1 h before being cooled, filtered and concentrated *in vacuo*. The residue was then purified by silica gel chromatography (9:1 to 4:1 PE/EtOAc) to give the title compound as an amorphous white solid (0.180 g, 34%).

R_f: 0.40 (8:2 PE/EtOAc); **IR** (neat film, ν_{max}, cm^{-1}): 3341 (s, NH), 3120 (w, CH), 1744 (s, C=O), 1626 (w), 1581 (w), 1550 (w), 1490 (w), 1459 (m), 1428 (m), 1370 (m), 1349 (m), 1312 (m), 1244 (m), 1210 (s), 1125 (m), 1098 (m), 1071 (m), 1009 (m); **^{1}H NMR** (400 MHz, $CDCl_3$) δ : 7.85 (br s, 1 H, NH), 7.56 (d, *J* = 7.9 Hz, 1 H), 7.36 (d, *J* = 2.8 Hz, 1 H), 7.33 (d, *J* = 8.1 Hz, 1 H), 7.24 – 7.20 (m, 1 H), 7.16 – 7.12 (m, 1 H), 2.37 (s, 3 H, CH_3); **^{13}C NMR** (101 MHz, $CDCl_3$) δ : 168.7 (C=O), 133.1, 130.6, 122.8, 120.0, 119.9, 117.5, 113.3, 111.3, 21.0 (CH_3).

Data are in accordance with those reported previously in literature.[310]

(*E*)-2-(4-methoxybenzylidene)indolin-3-one (159)

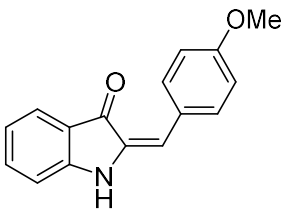

Following a reported procedure.[311] To a stirring solution of 4-ethynylanisole (110 mg, 0.50 mmol), 6-iodoaniline (66.1 mg, 0.5 mmol), $Pd(PPh_3)_4$ (29 mg, 0.025 mmol) and triethylamine (0.418 mL, 3 mmol) in toluene (1 mL); a pre-stirred mixture (30 °C, 1.5 h) of acetic anhydride (94.5 µL, 1 mmol) and formic acid (38 µL, 1 mmol) was added dropwise. The reaction mixture was stirred at r.t. for 2 h then heated to 70 °C for 15 h before being cooled, filtered and concentrated *in vacuo*. The residue was then purified by silica gel chromatography (19:1 to 4:1 PE/EtOAc) to give the title compound as an amorphous orange solid (55 mg, 44%).

R_f: 0.25 (9:1 PE 40-60/EtOAc); **IR** (neat film, ν_{max}, cm^{-1}): 3428 (w, NH), 2931 (w, CH), 1603 (m, C=O), 1509 (m), 1499 (m), 1455 (m), 1431 (m), 1351 (m), 1286 (m), 1245 (s), 1178 (s), 1113 (m), 1025 (s); **^{1}H NMR** (400 MHz, $CDCl_3$) δ : 8.27 (br s, 1 H, NH), 7.62 – 7.58 (m, 3 H), 7.38 (dd, *J* = 7.9, 0.9 Hz, 1 H), 7.17 (dt, *J* = 7.0, 1.1 Hz, 1 H), 7.11 (dt, *J* = 7.8, 1.0 Hz, 1 H), 7.00 – 6.97 (m, 2 H), 6.72 (dd, *J* = 2.1, 0.9 Hz, 1 H), 3.86 (s, 3 H, OMe); **^{13}C NMR** (101 MHz, $CDCl_3$) δ : 159.4, 138.0, 136.6, 129.4, 126.5, 125.2, 121.9, 120.3, 120.2, 114.5, 110.7, 98.8, 55.4 (OMe).

Data are in accordance with those reported previously in literature.[311]

2-(4-bromobenzylidene)indolin-3-one (152)

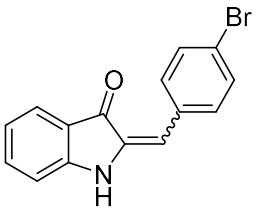

156 (0.172 g, 0.982 mmol) was dissolved in sodium hydroxide (1.5 M, aq, 5.4 mL, 8.05 mmol) and heated to 100 °C for 15 mins. The reaction mixture was then cooled to 0 °C and a solution of 4-bromobenzaldehyde (0.182 g, 0.982 mmol) in methanol (0.98 mL) was slowly added. The reaction was stirred at 0 °C for a further 30 mins then warmed to r.t. and stirred for 48 h, before being acidified with 1 M HCl, extracted into EtOAc (3 x 20 mL), dried over Na_2SO_4, filtered, and concentrated to give the title compound as a very dark yellow amorphous solid (0.271 g, 92%) which required no further purification.

R_f: 0.17 (5% EtOAc/PE 40-60); **IR** (neat film, ν_{max}, cm^{-1}): 3267 (w, NH), 2928 (w, CH), 2857 (w, CH), 1698 (s, C=O), 1618 (s), 1485 (s), 1467 (s), 1375 (m), 1314 (m), 1248 (m), 1212 (m), 1133 (m), 1073 (w), 1008 (m); **^{1}H NMR** (400 MHz, d6-DMSO) δ : 9.85 (s, 1 H, NH), 7.70 – 7.65 (m, 4 H), 7.60 (d, *J* = 7.4 Hz, 1 H), 7.57 – 7.53 (m, 1 H), 7.14 (d, *J* = 8.1 Hz, 1 H), 6.94 (t, *J* = 7.4 Hz, 1 H), 6.60 (s, 1 H); **^{13}C NMR** (101 MHz,

d6-DMSO) δ : 186.8 (C=O), 154.6, 137.0, 135.2, 133.9, 132.3, 132.1, 124.6, 121.9, 120.4, 120.4, 113.0, 109.7.

Data are in accordance with those reported previously in literature.[311]

2-((*tert*-butoxycarbonyl)amino)ethyl methanesulfonate (164)

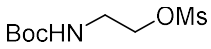

To a stirring solution of 2-(*N*-*tert*-butoxycarbonylamino)ethanol (0.26 mL, 1.55 mmol) in dichloromethane (2 mL) cooled to 0 °C, were added DIPEA (0.324 mL, 1.86 mmol) and methanesulfonyl chloride (0.13 mL, 1.71 mmol). The reaction was warmed to r.t. and stirred for 3 h before being diluted with H_2O (10 mL), extracted into dichloromethane (3 x 15 mL), dried over Na_2SO_4, filtered, and concentrated *in vacuo* to give the title compound (0.370 g, >98%) as a colourless oil which required no further purification.

^{1}H NMR (400 MHz, $CDCl_3$) δ : 4.91 (br s, 1 H, NH), 4.28 (t, *J* = 5.6 Hz, 2 H, CH_2-O), 3.47 (q, *J* = 5.6 Hz, 2 H, CH_2-N), 3.03 (s, 3 H, CH_3), 1.44 (s, 9 H, 3 x CH_3); **^{13}C NMR** (101 MHz, $CDCl_3$) δ : 155.7 (C=O), 80.0 (Cq), 68.9 (CH_2-O), 40.0 (CH_2-N), 37.4 (CH_3), 28.3 (3 x CH_3).

Data are in accordance with those reported previously in literature[355].

2-[*bis*(*tert*-butoxycarbonyl)amino]ethyl bromide (172)

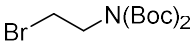

To a stirring solution of di-*tert*-butyl-iminodicarboxylate (0.545 g, 2.5 mmol) in a mixture of tetrahydrofuran (15 mL) and DMF (5 mL) was added sodium hydride (0.105 g, 2.63 mmol). The reaction was heated to 65 °C for 2.5 h before 1,2-dibromoethane (0.97 mL, 11.3 mmol) was added, the reaction was then stirred at 65 °C for a further 3 h. The reaction was then cooled to 0 °C, ether (25 mL) and H_2O (20 mL) were added. The organic was washed with H_2O (2 x 20 mL), dried over $MgSO_4$, filtered and concentrated *in vacuo*. The residue was then purified by silica gel chromatography (2% to 10% Ether/PE 40-60) to give the title compound as a colourless oil (0.243 g, 30%).

R_f: 0.88 (7:3 PE/EtOAc); **IR** (neat film, ν_{max}, cm^{-1}): 1770 (m, C=O), 1760 (m, C=O), 1523 (m), 1460 (w), 1391 (w), 1365 (w), 1222 (w), 1142 (s), 1097 (s); **^{1}H NMR** (400 MHz, $CDCl_3$) δ : 3.95 (t, *J* = 7.4 Hz, 2 H, CH_2-N), 3.45 (t, *J* = 7.4 Hz, 2 H, CH_2-Br), 1.50 (s, 18 H, 6 x CH_3); **^{13}C NMR** (101 MHz, $CDCl_3$) δ : 152.1 (C=O), 82.9 (qC), 47.3 (C-N), 29.0 (C-Br), 28.0 (CH_3); **HRMS (ESI):** Mass not found.

***tert*-Butyl (2-(1*H*-indol-1-yl)ethyl)carbamate (174)**

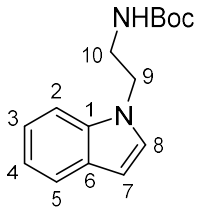

To a stirring solution of indole (0.20 g, 1.71 mmol) in DMF (6 mL) cooled to 0 °C was added NaH (60% w/w, 75 mg, 1.88 mmol). The reaction was stirred for 30 mins before being warmed to r.t. and a solution of **167** (0.509 g, 1.88 mmol) in DMF (2 mL) was added dropwise. The reaction mixture was stirred for a further 18 h at r.t. before being heated to 80 °C for 1 h. The mixture was then cooled, quenched with NH_4Cl (aq. sat. 10 mL), extracted into EtOAc (3x 20 mL), dried over Na_2SO_4, filtered and concentrated *in vacuo*. The residue was then purified by silica gel chromatography (9:1 PE/EtOAc) to give the title compound as a yellow oil (125 mg, 27%).

R_f: 0.20 (9:1 PE/EtOAc); **IR** (neat film, ν_{max}, cm^{-1}): 3341 (w, NH), 2976 (w, CH), 2931 (w, CH), 1705 (s, C=O), 1512 (s), 1464 (m), 1394 (m), 1365 (m), 1270 (m), 1249 (m), 1169 (s); **^{1}H NMR** (400 MHz, $CDCl_3$) δ : 7.63 (dt, *J* = 7.9, 1.0 Hz, 1 H, H5), 7.36 (d, *J* = 8.2 Hz, 1 H, H2), 7.23 – 7.19 (m, 1 H, H3), 7.13 – 7.08 (m, 2 H, H8 and H4), 6.52 (dd, *J* = 3.1, 0.6 Hz 1 H, H7), 4.53 (br s, 1 H, NH), 4.28 (t, *J* = 5.7 Hz, 2 H, H9), 3.50 (q, *J* = 6.0 Hz, 2 H, H10), 1.44 (s, 9 H, 3x CH_3); **^{13}C NMR** (101 MHz, $CDCl_3$) δ : 155.9 (C=O), 136.0 (C1), 128.6 (C6), 127.9 (C8), 121.7 (C3), 121.0 (C5), 119.5 (C4), 109.3 (C2), 101.6 (C7), 79.7 (qC), 45.9 (C9), 40.9 (C10), 28.3 (CH_3); **HRMS (ESI):** m/z calcd for $C_{15}H_{20}N_2O_2Na$ $[M+Na]^+$: 283.1417; found: 283.1418.

4-Bromo-2,6-difluoroaniline (181)

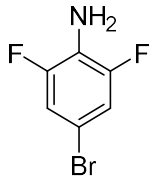

To a stirring solution of 2,6-difluoroaniline (1.29 g, 10 mmol) in acetonitrile (20 mL) was added *N*-bromosuccinimide (1.78 g, 10 mmol). The reaction was stirred at r.t. for 18 h then diluted with hexane (25 mL) and water (25 mL). The aqueous was extracted with hexane (3 x 25 mL), and the combined organics were dried over $MgSO_4$, filtered, and concentrated *in vacuo*. The residue was then purified

by silica gel chromatography (8:2 PE/DCM) to give the title compound as an off-white amorphous powder (1.22 g, 59%).

R_f: 0.27 (8:2 PE/DCM); **^{1}H NMR** (400 MHz, $CDCl_3$) δ : 6.99 (dd, *J* = 6.3, 1.2 Hz, 2 H, C-H), 3.73 (br s, 2 H, NH_2); **^{13}C NMR** (101 MHz, $CDCl_3$) δ : 151.9 (dd, *J* = 244, 8.9 Hz, C-F), 123.7 (t, *J* = 16.2 Hz, -C-NH_2), 115.1 – 114.7 (m, C-H), 107.2 (t, *J* = 11.7 Hz, -C-Br); **^{19}F NMR** (376 MHz, $CDCl_3$) δ : - 130.70.

Data are in accordance with those reported previously in literature.[356]

5-Bromo-1,3-difluoro-2-nitrosobenzene (178)

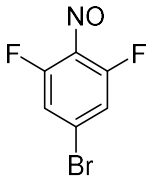

To a stirring solution of **181** (0.146 g, 0.70 mmol) in chloroform (1 mL) was added a solution of Oxone™ (0.432 g, 1.4 mmol) in water (2.8 mL). The reaction mixture was stirred vigorously at r.t. for 18 h before being extracted into chloroform (3 x 10 mL), washed with 1 M HCl (2bx 5 mL), $NaHSO_4$ (sat. aq. 2 x 5 mL), water (2 x 5 mL), and brine (5 mL). The organics were then dried over Na_2SO_4, filtered, and concentrated *in vacuo* to give the title compound as an off-white amorphous powder (135 mg, 87%) used without further purification.

IR (neat film, ν_{max}, cm^{-1}): 3060 (w, CH), 2919 (w, CH), 1601 (s, NO), 1483 (m), 1432 (s), 1293 (m), 1276 (s), 1193 (m), 1075 (m), 1060 (s); **^{1}H NMR** (400 MHz, $CDCl_3$) δ : 7.34 (d, *J* = 8.2 Hz, 2 H); **^{13}C NMR** (101 MHz, $CDCl_3$) δ : 153.3 (dd, *J* = 273, 5 Hz, C-F), 145.5 (t, *J* = 8.3 Hz, C-NO), 130.6 (t, *J* = 12.3 Hz, C-Br), 117.0 (dd, *J* = 23, 4 Hz, C-H).

Data are in accordance with those reported previously in literature.[357]

Ethyl 4-amino-3,5-difluorobenzoate (183)

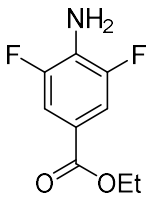

To a stirring solution of **179** (70 mg, 0.40 mmol) in ethanol (1.5 mL) was added conc. H_2SO_4 (50 µL). The reaction was heated to reflux for 18 h before being cooled to rt, neutralised with $NaHCO_3$, extracted into dichloromethane (3 x 20 mL), dried over $MgSO_4$, filtered, and concentrated to give the title compound as an off-white amorphous powder (66 mg, 81%).

R_f: 0.59 (7:3 PE 40-60/EtOAc); **^{1}H NMR** (400 MHz, $CDCl_3$) δ : 7.57 – 7.49 (m, 2H, ArC-H), 4.33 (q, *J* = 7.2 Hz, 2H, CH_2), 4.12 (s, 2H, NH_2), 1.37 (t, *J* = 7.2 Hz, 3H, CH_3); **^{13}C NMR** (101 MHz, $CDCl_3$) δ : 165.1 (C=O), 150.7 (dd, *J* = 240, 8.2 Hz, C-F), 128.8 (t, *J* = 16.4 Hz, -C-NH_2), 118.6 (t, *J* = 8.2 Hz, -**C**-COOEt), 112.8 – 112.4 (m, C-H), 61.0 (CH_2), 14.3 (CH_3); **^{19}F NMR (**376 MHz, $CDCl_3$) δ : -133.9.

Data are in accordance with those reported previously in literature.[285]

Ethyl (*E*)-4-((4-bromo-2,6-difluorophenyl)diazenyl)-3,5-difluorobenzoate (182)

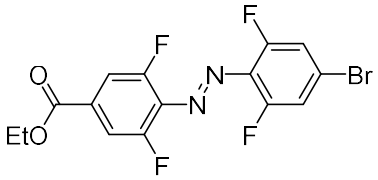

To a stirring solution of **178** (64 mg, 0.288 mmol) in a mixture of toluene (1 mL), acetic acid (1 mL) and TFA (0.2 mL) was added **183** (58 mg, 0.288 mmol). The reaction was stirred in the dark at r.t. for 5 days before concentrating *in vacuo*. The residue was then purified by silica gel chromatography (1 to 5% EtOAc/PE 40-60) to give the title compound as a red amorphous powder as a mixture of two isomers (32 mg, 27%, isomer ratio 1:0.25).

R_f: 0.15 (3% EtOAc/PE 40-60); **IR** (neat film, ν_{max}, cm^{-1}): 3084 (w, CH), 2984 (w, CH), 1716 (s, C=O), 1597 (m), 1574 (s), 1484 (m), 1465 (m), 1432 (s), 1370 (m), 1336 (s), 1304 (m), 1233 (s), 1193 (s), 1173 (m), 1083 (m), 1053 (s), 1013 (s); **^{1}H NMR** (400 MHz, $CDCl_3$) δ : 7.73 (d, *J* = 8.9 Hz, 2 H, major isomer), 7.56 (d, *J* = 8.0 Hz, minor isomer), 7.30 (d, *J* = 8.3 Hz, 2 H, major isomer), 7.09 – 7.06 (m, minor isomer), 4.43 (q, *J* = 7.1 Hz, 2 H, CH_2, major isomer), 4.38 (q, *J* = 7.1 Hz, minor isomer), 1.43 (t, *J* = 7.1 Hz, 3 H, CH_3, major isomer), 1.38 (t, *J* = 7.1 Hz, minor isomer); **^{13}C NMR** (101 MHz, $CDCl_3$) δ : 163.8 (t, *J* = 3.0 Hz, C=O, major), 163.6 (t, *J* = 3.0 Hz, C=O, minor), 155.7 (dd, *J* = 265, 5 Hz, C-F, major), 154.9 (dd, *J* = 260, 3.6 Hz, C-F, major), 151.6 (dd, *J* = 260, 5.5 Hz, C-F, minor), 151.2 (dd, *J* = 255, 5 Hz, C-F, minor), 134.8 (t, *J* = 16 Hz, minor), 134.4 (t, *J* = 10 Hz, major), 133.3 (t, *J* = 10 Hz. major), 132.4 (t, *J* = 9 Hz, minor), 130.9 (t, *J* = 17 Hz, minor), 130.6 (t, *J* = 9.6 Hz, major), 125.1 (t, *J* = 12 Hz, major), 122.6 (t, *J* = 11.1 Hz, minor), 116.9 – 116.7 (m, major), 116.4 – 116.1 (m, minor), 114.0 – 113.8 (m, major), 113.6 – 113.4 (m, minor),

62.1 (CH_2), 14.2 (CH_3); **^{19}F NMR (**376 MHz, $CDCl_3$) δ : -117.4 (t, *J* = 5.6 Hz, minor), -118.1 (t, *J* = 5.6 Hz, minor), -118.1 (s, major), -120.0 (s, major).

Data are in accordance with those reported previously in literature[358].

Ethyl (*E*)-4-((4-acetamido-2,6-difluorophenyl)diazenyl)-3,5-difluorobenzoate (188)

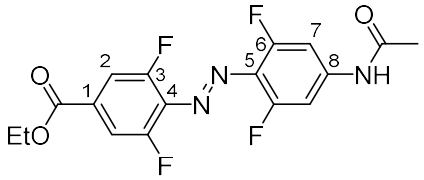

To a stirring solution of **182** (29 mg, 0.072 mmol) in degassed 1,4-dioxane (0.9 mL) were added acetamide (12.7 mg, 0.215 mmol), XantPhos (8.3 mg, 0.014 mmol), Cs_2CO_3 (58.2 mg, 0.18 mmol) and finally $Pd_2(dba)_3$ (6.5 mg, 0.0072 mmol). The reaction mixture was heated to 90 °C for 1 h before being cooled, diluted with EtOAc (5 mL) and brine (5 mL), extracted into EtOAc (3 x 5 mL), dried over Na_2SO_4, filtered and concentrated *in vacuo*. The residue was then purified by silica gel chromatography (7:3 PE 40-60/EtOAc) to give the title compound as a red amorphous powder as a mixture of two isomers (30 mg, >98%, isomer ratio 1:0.3).

R_f: 0.15 (7:3 PE 40-60/EtOAc); **IR** (neat film, ν_{max}, cm^{-1}): 3557 (w, NH), 3063 (w, CH), 3007 (w, CH), 1709 (m, C=O), 1692 (m, C=O), 1603 (s), 1576 (m), 1541 (s), 1480 (m), 1427 (s), 1370 (s), 1336 (s), 1280 (m), 1250 (s), 1202 (m), 1152 (s), 1095 (m), 1055 (s), 1016 (s); **^{1}H NMR** (400 MHz, $CDCl_3$) δ : 7.71 (d, *J* = 8.8 Hz, 2 H, H2, major), 7.56 – 7.53 (m, minor), 7.36 (d, *J* = 11.2 Hz, 2 H, H7, major), 7.15 (d, *J* = 9.7 Hz, minor), 4.42 (q, *J* = 7.1 Hz, 2 H, CH_2, major), 4.37 (q, *J* = 7.1 Hz, minor), 2.24 (s, 3 H, Acetyl-CH_3, major), 2.16 (s, minor), 1.42 (t, *J* = 7.1 Hz, 3 H, CH_3, major), 1.38 (t, *J* = 7.1 Hz, minor); **^{13}C NMR** (101 MHz, $CDCl_3$) δ : 168.6 (N-C=O, major), 168.4 (N-C=O, minor), 164.0 (t, *J* = 3 Hz, O-C=O, major), 163.7 (t, *J* = 3 Hz, O-C=O, minor), 156.9 (dd, *J* = 250, 6 Hz, C6, major), 154.8 (dd, *J* = 250, 6 Hz, C3, major), 152.2 (dd, *J* = 250, 6 Hz, C-F, minor), 151.3 (dd, *J* = 250, 6 Hz, C-F, minor), 142.0 (t, *J* = 13.8 Hz, C8, major), 140.1 (t, *J* = 12.7 Hz, minor), 135.1 (t, *J* = 15.5 Hz, minor), 134.8 (t, *J* = 11 Hz, C4, major), 132.4 (t, *J* = 7.8 Hz, C1, major), 131.9 (t, *J* = 8.5 Hz, minor), 127.7 (t, *J* = 9 Hz, C5, major), 113.9 – 113.7 (m, C-H, C2, major), 113.6 – 113.4 (m, minor), 103.1 (dd, *J* = 25.7, 2.9 Hz, C-H, C7, major), 102.9 – 102.7 (m, minor), 62.0 (CH_2), 24.9 (ester-CH_3, major), 24.7 (Ac-CH_3), 14.2 (ester-CH_3, minor); **^{19}F NMR (**376 MHz, $CDCl_3$) δ : -116.8 (s, major), -117.2 (t, *J* = 5 Hz, minor), -118.2 (t, *J* = 5 Hz, minor), - 120.7 (s, major); **HRMS (ESI):** m/z calcd for $C_{17}H_{14}F_4N_3O_3$ $[M+H]^+$: 384.0966; found: 384.0965.

(*E*)-4-((4-(ethoxycarbonyl)-2,6-difluorophenyl)diazenyl)-3,5-difluorobenzoic acid (191)

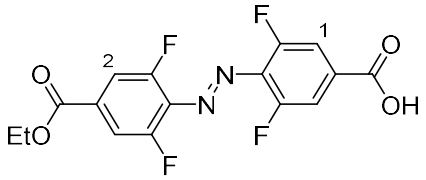

To a stirring solution of **179** (0.124 g, 0.72 mmol) in a mixture of dichloromethane (1.7 mL) and acetone (0.33 mL) was added a solution of Oxone™ (0.881 g, 1.43 mmol) in H_2O (0.7 mL). The reaction was stirred vigorously for 18 h before being extracted into EtOAc (3 x 20 mL), washed with brine (5 mL), dried over Na_2SO_4, filtered and concentrated to give the crude product which was used immediately. To a stirring solution of crude **192** (70 mg, 0.374 mmol) in a mixture of toluene (1 mL), acetic acid (1 mL) and TFA (0.2 mL) was added **183** (60 mg, 0.299 mmol). The reaction was stirred in the dark at r.t. for 5 days before concentrating *in vacuo*. The residue was then purified by silica gel chromatography (2:1:97 MeOH/AcOH/DCM) to give the title compound as a red amorphous powder as a mixture of two isomers (32 mg, 27%, isomer ratio 1:0.25).

R_f: 0.55 (5% MeOH/DCM); **IR** (neat film, ν_{max}, cm^{-1}): 2922 (br w, OH), 2827 (w, CH), 1692 (s, C=O), 1623 (s, C=O), 1587 (s), 1537 (m), 1452 (m), 1417 (s), 1338 (s), 1277 (s), 1237 (s), 1146 (m), 1085 (w), 1051 (m), 1019 (w); Only major isomer reported; **^{1}H NMR** (400 MHz, $CDCl_3$) δ : 7.80 (dd, *J* = 17.6, 8.9 Hz, 2H, H1), 7.63 – 7.58 (m, 2H, H2), 4.46 (q, *J* = 7.2 Hz, 2H, CH_2), 1.46 (t, *J* = 7.2 Hz, 3H, CH_3); **^{13}C NMR** (101 MHz, $CDCl_3$) δ : 170.3, 163.7 (t, *J* = 3 Hz), 155.1 (dd, *J* = 250, 6 Hz, CF), 155.0 (dd, *J* = 250, 6 Hz, CF), 146.7, 134.1 (t, *J* = 15.5 Hz), 130.6 (t, *J* = 13 Hz), 130.0 (t, *J* = 16 Hz), 114.6 – 113.9 (m, C2), 113.5 – 112.6 (m, C1), 62.3 (CH_2), 14.2 (CH_3); **^{19}F NMR (**376 MHz, $CDCl_3$) δ : -120.3 (d, *J* = 5 Hz), -133.7; **HRMS (ESI):** m/z calcd for $C_{16}H_8F_4N_2O_4$ $[M-H]^-$: 369.0504; Found: 369.0501.

***tert*-Butyl (2-(4-(3-(4-cyano-3-(trifluoromethyl)phenyl)-5,5-dimethyl-4-oxo-2-thioxoimidazolidin-1-yl)-2-fluorobenzamido)ethyl)carbamate (194)**

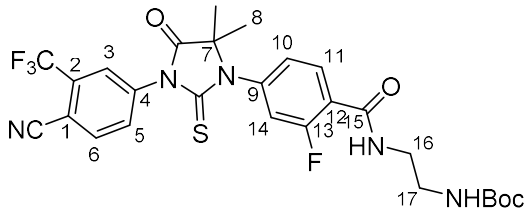

To a stirring solution of **2** (18 mg, 0.040 mmol) in DMF (0.3 mL) were added HATU (23 mg, 0.060 mmol) and DIPEA (10.4 µL, 0.060 mmol). The reaction mixture was stirred at r.t. for 15 mins before **193** (10

mg, 0.060 mmol) was added. The mixture was then stirred for a further 16 h before diluting in water (5 mL) and extracting into EtOAc (3 x 10 mL). The combined organics were then washed with 10% LiCl (2 x 5 mL), and brine (2 x 5 mL), before being dried over Na_2SO_4, filtered and concentrated *in vacuo*. The residue was purified through silica gel column chromatography (6:4 to 7:3 EtOAc/PE 40-60) to give the title compound as a colourless oil (22 mg, 92%).

R_f: 0.36 (7:3 EtOAc/PE 40-60); **IR** (neat film, ν_{max}, cm-1): 2925 (w, CH), 1759 (m, C=O), 1708 (m, C=O), 1659 (m), 1621 (m), 1530 (m), 1500 (m), 1439 (s), 1409 (s), 1369 (m), 1312 (s), 1284 (m), 1219 (m), 1177 (s), 1137 (s), 1054 (w); **^{1}H NMR (400** MHz, $CDCl_3$) δ : 8.26 (t, *J* = 8.5 Hz, 1 H, H6), 8.01 (d, *J* = 8.4 Hz, 1 H, H11), 7.97 (d, *J* = 1.6 Hz, 1 H, H14), 7.85 (dd, *J* = 8.4, 1.6 Hz, 1 H, H10), 7.31 (br s, 1 H, NH), 7.26 (dd, *J* = 8.4, 1.8 Hz, 1 H, H5), 7.17 (dd, *J* = 11.3, 1.6 Hz, 1 H, H3), 4.99 (br s, 1 H, NH), 3.65 – 3.62 (m, 2 H, CH_2), 3.44 – 3.40 (m, 2 H, CH_2), 1.63 (s, 6 H, 2 x CH_3), 1.45 (s, 9 H, 3 x CH_3);**^{13}C NMR** (101 MHz, $CDCl_3$) δ : 179.7 (C=S), 174.5 (cyclic C=O), 161.9 (d, *J* = 274 Hz, C13), 159.7 (C15), 156.8 (Boc C=O), 139.1 (d, *J* = 10.5 Hz, C12), 136.8 (C1), 135.3 (C6), 133.7 (q, *J* = 33 Hz, C2), 133.2 (C11), 132.2 (C5), 127.1 (q, *J* = 5.2 Hz, C3), 126.1 (C10), 122.6 (q, *J* = 250 Hz, CF_3), 121.1 (C9), 118.0 (d, *J* = 26 Hz, C14), 114.7 (-C≡N), 110.4 (q, *J* = 2.1 Hz, C4), 79.9 (Boc-qC), 66.6 (C7), 41.4 (CH_2), 40.0 (CH_2), 28.3 (Boc CH_3), 23.9 (C8); **^{19}F NMR (**376 MHz, $CDCl_3$) δ : -62.0, -109.9; **HRMS (ESI):** m/z calcd for $[M+Na]^+$: 616.1612; found: 616.1630.

***N*-(2-aminoethyl)-4-(3-(4-cyano-3-(trifluoromethyl)phenyl)-5,5-dimethyl-4-oxo-2-thioxoimidazolidin-1-yl)-2-fluorobenzamide (177)**

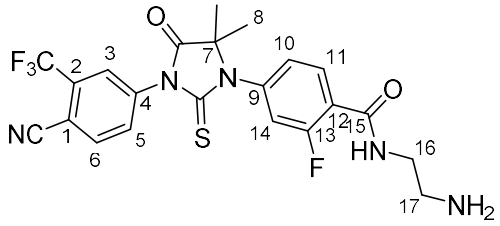

To a stirring solution of **194** (22 mg, 0.037 mmol) in dichloromethane (1 mL) was added trifluoroacetic acid (0.25 mL). The reaction was stirred for 3 h at r.t. before being concentrated, diluted with sat. aq. $NaHCO_3$ (2 mL), extracted into dichloromethane (3 x 10 mL), dried over Na_2SO_4, filtered, and concentrated *in vacuo* to give the title compound as a yellow oil (18 mg, >98%) used without further purification.

IR (neat film, ν_{max}, cm^{-1}): 2921 (w, CH), 2851 (w, CH), 1756 (m, C=O), 1727 (w), 1655 (m), 1619 (m), 1533 (m), 1498 (m), 1433 (s), 1411 (s), 1308 (s), 1284 (s), 1218 (s), 1176 (s), 1132 (s), 1055 (m); **^{1}H NMR** (400 MHz, $CDCl_3$) δ : 8.23 (t, *J* = 8.5 Hz, 1 H, H6), 7.97 (d, *J* = 8.5 Hz, 1 H, H11), 7.93 (s, 1 H, H14), 7.80

(dd, *J* = 8.1, 1.5 Hz, 1 H, H10), 7.24 – 7.17 (m, 2 H, NH and H5), 7.13 (dd, *J* = 11.4, 1.5 Hz, H3), 3.55 (q, *J* = 5.5 Hz, 2 H, CH_2), 3.00 – 2.96 (m, 2 H, CH_2), 1.72 (br s, 2 H, NH_2), 1.59 (s, 6 H, 2 x CH_3); **^{13}C NMR** (101 MHz, $CDCl_3$) δ : 179.7 (C=S), 174.4 (cyclic C=O), 162.3 (d, *J* = 2.7 Hz, C15), 160.4 (d, *J* = 250 Hz, C13), 139.0 (d, *J* = 10.5 Hz, C12), 136.8 (C1), 135.3 (C6), 133.7 (q, *J* = 34 Hz, C2), 133.3 (d, *J* = 3.3 Hz, C11), 132.1 (C5), 127.1 (q, *J* = 4.3 Hz, C3), 126.1 (d, *J* = 3.2 Hz, C10), 123.0 (q, *J* = 250 Hz, CF_3), 120.5 (C9), 118.0 (d, *J* = 26 Hz, C14), 114.7 (-C≡N), 110.4 (q, *J* = 2.1 Hz, C4), 66.6 (C7), 42.5 (CH_2), 41.0 (CH_2), 23.9 (C8); **^{19}F NMR** (376 MHz, $CDCl_3$) δ : -62.0, -110.4; **HRMS (ESI):** m/z calcd for $C_{22}H_{20}F_4N_5O_2S$ $[M+H]^+$: 494.1268; found: 494.1288.

Ethyl 4-((*E*)-(2,6-difluoro-4-((1-((2*S*,4*R*)-4-hydroxy-2-((4-(4-methylthiazol-5-yl)benzyl)carbamoyl) pyrrolidin-1-yl)-3,3-dimethyl-1-oxobutan-2-yl)carbamoyl)phenyl)diazenyl)-3,5-difluorobenzoate (195)

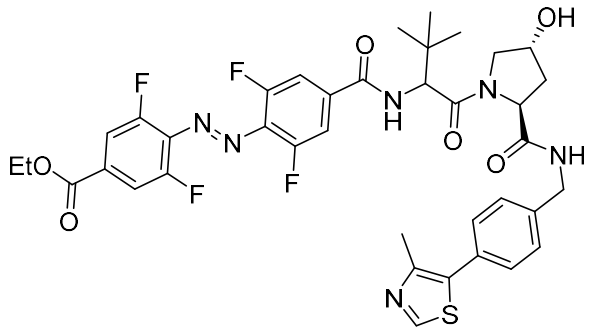

To a stirring solution of **191** (8 mg, 0.022 mmol) in DMF (0.1 mL) were added HATU (9.9 mg, 0.026 mmol) and DIPEA (9.4 µL, 0.054 mmol). The reaction mixture was stirred at r.t. for 15 mins before **154** (13.2 mg, 0.026 mmol) was added. The mixture was then stirred for a further 16 h before diluting in water (5 mL) and extracting into EtOAc (3 x 10 mL). The combined organics were then washed with brine (2 x 5 mL), before being dried over Na_2SO_4, filtered and concentrated *in vacuo*. The residue was purified through silica gel column chromatography (DCM to 4% MeOH/DCM) to give the title compound as an orange oil (11 mg, 65%).

R_f: 0.29 (4% MeOH/DCM); **IR** (neat film, ν_{max}, cm^{-1}): 3395 (w, NH), 2961 (w, CH), 2865 (w, CH), 1703 (s, C=O), 1668 (m), 1627 (s), 1574 (m), 1532 (m), 1431 (s), 1365 (s), 1334 (m), 1232 (s), 1089 (m), 1048 (m), 1016 (m); **^{1}H NMR** (400 MHz, $CDCl_3$) δ : Mixture of cis and trans isomers, 8.69 (s, 1 H), 7.75 – 7.73 (m, 1 H), 7.55 – 7.47 (m, 2 H), 7.39 – 7.33 (m, 4 H), 7.15 – 7.07 (m, 1 H), 6.89 (d, *J* = 9.0 Hz, 0.7 H), 6.75 (d, *J* = 9.0 Hz, 0.3 H), 4.76 – 4.67 (m, 2 H), 4.62 – 4.57 (m, 2 H), 4.45 – 4.33 (m, 3 H), 4.08 – 4.01 (m, 1 H), 3.74 – 3.71 (m, 1H), 2.59 – 2.54 (m, 1 H), 2.52 – 2.51 (m, 3 H), 2.15 – 2.10 (m, 1H), 1.43 (t, *J* = 7.2 Hz, 2 H), 1.36 (t, *J* = 7.2 Hz, 1 H), 1.02 (s, 6 H), 0.98 (s, 3H); **^{13}C NMR** (101 MHz, $CDCl_3$) δ : Only major

isomer reported; 171.2, 170.4, 164.3, 163.7, 155.2 (dd, *J* = 260, 4 Hz, C-F), 155.0 (dd, *J* = 260, 4 Hz, C-F), 150.4, 148.5, 137.9, 137.0, 134.1, 133.7, 133.4, 131.5, 131.1, 129.6, 128.1, 114.0 – 113.8 (m, 1C), 111.9 – 111.7 (m, 1C), 70.2, 62.2, 58.7, 58.2, 56.8, 43.3, 36.0, 35.8, 26.5, 16.0, 14.2; **^{19}F NMR (**376 MHz, $CDCl_3$) δ : -118.3, -119.4; **HRMS (ESI):** m/z calcd for $C_{38}H_{38}F_4N_6O_6SNa$ $[M+Na]^+$: 805.2402; Found 805.2407.

(2*S*,4*R*)-1-((*S*)-2-(4-((*E*)-(4-((2-(4-(3-(4-cyano-3-(trifluoromethyl)phenyl)-5,5-dimethyl-4-oxo-2-thioxoimidazolidin-1-yl)-2-fluorobenzamido)ethyl)carbamoyl)-2,6-difluorophenyl)diazenyl)-3,5-difluorobenzamido)-3,3-dimethylbutanoyl)-4-hydroxy-*N*-(4-(4-methylthiazol-5-yl)benzyl)pyrrolidine-2-carboxamide (azoPROTAC1)

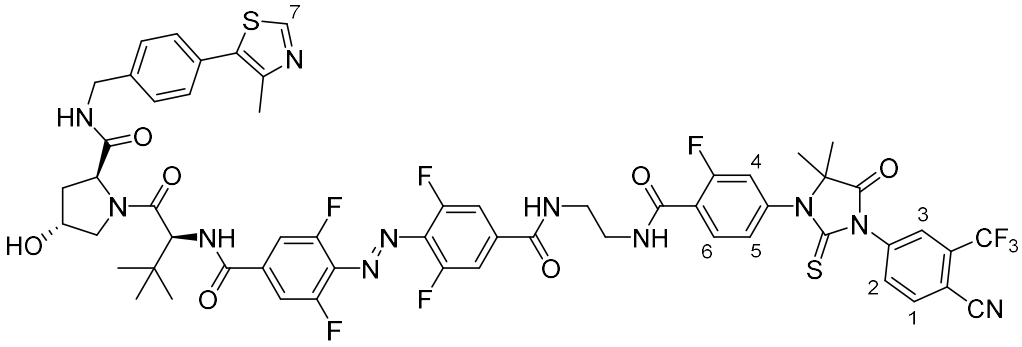

To a stirring solution of **195** (4.2 mg, 0.0055 mmol) in a mixture of THF and H_2O (2:1, 1 mL) was added lithium hydroxide (0.5 mg, 0.011 mmol). The reaction was stirred at r.t. for 3 h before acidifying to pH 3 with 1 M HCl and extracting into EtOAc (3 x 10 mL). The combined organics were washed with brine (5 mL), dried over Na_2SO_4, filtered, and concentrated *in vacuo*. The crude residue was directly dissolved in DMF (0.1 mL) and cooled to 0 °C, before HATU (2.51 mg, 0.0066 mmol) and DIPEA (1.1 µL, 0.0066 mmol) were added. The reaction mixture was stirred for 15 mins before **177** (3.3 mg, 0.0066 mmol) was added. The mixture was then warmed to r.t. and stirred for a further 16 h before diluting in water (5 mL) and extracting into EtOAc (3 x 10 mL). The combined organics were then washed with brine (2 x 5 mL), before being dried over Na_2SO_4, filtered and concentrated *in vacuo*. The residue was purified through silica gel column chromatography (1 to 5% MeOH/DCM) to give the title compound as an orange oil (5.2 mg, 78%).

R_f: 0.39 (6% MeOH/DCM); **IR** (neat film, ν_{max}, cm^{-1}): 3360 (w, NH), 2926 (w, CH), 2857 (w, CH), 1757 (w), 1655 (s), 1633 (s), 1571 (m), 1537 (m), 1498 (m), 1430 (s), 1312 (s), 1221 (m), 1179 (m), 1141 (m), 1052 (m); **^{1}H NMR** (700 MHz, $CDCl_3$) δ : 8.71 (s, 1 H, H7), 8.32 (t, *J* = 8.4 Hz, 1 H, H1), 8.02 (d, *J* = 8.2 Hz, 1 H, H6), 7.97 (d, *J* = 2.0 Hz, 1 H, H4), 7.85 (dd, *J* = 8.3, 2.0 Hz, 1 H, H5), 7.69 (t, *J* = 4.6 Hz, 1 H, NH), 7.59

(d, *J* = 9.1 Hz, 2 H), 7.49 (d, *J* = 8.7 Hz, 2 H), 7.43 – 7.35 (m, 5 H), 7.31 (dd, *J* = 8.5, 2.1 Hz, 1 H), 7.23 – 7.19 (m, 1 H), 7.15 (t, *J* = 5.6 Hz, 1 H, NH), 6.83 (d, *J* = 8.9 Hz, 1 H), 4.78 – 4.75 (m, 1 H), 4.70 – 4.59 (m, 3 H), 4.39 (dd, *J* = 15.1, 5.3 Hz, 1 H), 4.10 (d, *J* = 11.1 Hz, 1 H), 3.88 – 3.84 (m, 1 H), 3.78 – 3.74 (m, 3 H), 3.69 – 3.68 (m, 1 H), 3.04 (br s, 1 H), 2.65 – 2.61 (m, 1 H), 2.55 (s, 3 H, CH_3), 1.89 – 1.87 (m, 1 H), 1.64 (s, 6 H, 2x CH_3), 1.04 (s, 9 H, 3x CH_3); **^{13}C NMR** (176 MHz, $CDCl_3$) δ : 179.8 (C=S), 174.4 (cyclic C=O), 171.3, 170.4, 164.5, 164.4, 161.8, 160.6 (d, *J* = 250 Hz, C-F), 155.4 (dd, *J* = 260, 4 Hz, C-F), 155.2 (dd, *J* = 260, 4 Hz, C-F), 150.4, 148.5, 139.8 (d, *J* = 10.5 Hz), 137.9, 137.6, 136.7, 135.4, 133.9, 133.7, 133.4, 133.2, 133.1, 132.1, 131.5, 131.2, 129.6, 128.2, 127.1, 126.5, 121.8 (q, *J* = 250 Hz, CF_3), 121.7, 118.2 (d, *J* = 26 Hz, C14), 114.7 (-C≡N), 111.8 – 111.7 (m, 1C), 111.5 – 111.3 (m, 1C), 110.5, 68.0, 66.7, 58.6, 58.2, 56.8, 43.4, 42.5, 40.1, 35.9, 35.7, 26.5, 23.9, 16.1; **^{19}F NMR (**376 MHz, $CDCl_3$) δ : -62.0, -109.7, -117.3 (d, *J* = 134 Hz), -118.4 (d, *J* = 38 Hz); Mixture of cis and trans, only major isomer reported; **HRMS (ESI):** m/z calcd for $C_{58}H_{51}F_8N_{11}O_7S_2Na$ $[M+Na]^+$: 1252.3179; found: 1252.3190.

***tert*-Butyl (2-(4-bromophenoxy)ethyl)carbamate (198)**

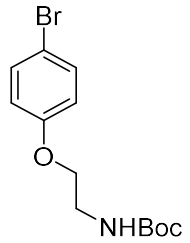

Following a literature procedure,[359] to a stirring solution of 4-bromophenol (1.00 g, 5.8 mmol) in DMF (15 mL) were added potassium carbonate (6.99 g, 50.6 mmol) and 2-(boc-amino)ethyl bromide (1.08 g, 4.82 mmol). The reaction mixture was stirred at 65 °C for 24 h before being cooled to r.t., diluted with H_2O (50 mL) and extracted into EtOAc (3x 100 mL). The organics were washed with brine (50 mL), dried over Na_2SO_4, filtered and concentrated *in vacuo*. The residue was purified through silica gel column chromatography (5% EtOAc/PE 40-60) to give the title compound as a colourless oil (1.50 g, 98%).

R_f: 0.10 (5% EtOAc/PE 40-60); **IR** (neat film, ν_{max}, cm^{-1}): 3346 (w, NH), 2974 (w, CH), 2884 (w, CH), 1686 (m), 1588 (w), 1515 (m), 1488 (s), 1392 (w), 1366 (m), 1282 (m), 1241 (s), 1170 (s), 1111 (w), 1067 (m), 1003 (w); **^{1}H NMR** (400 MHz, $CDCl_3$) δ : 7.37 (d, *J* = 9.1 Hz, 2 H), 6.77 (d, *J* = 9.1 Hz, 2 H), 4.97 (br s, 1 H), 3.98 (t, *J* = 5.2 Hz, 2 H), 3.52 (q, *J* = 5.2 Hz, 2 H), 1.45 (s, 9 H); **^{13}C NMR** (101 MHz, $CDCl_3$) δ : 157.7, 155.1, 132.3, 117.2, 116.2, 79.7, 67.4, 40.0, 28.4.

Data are in accordance with those reported previously in literature.[359]

2-((4-(2-((*tert*-butoxycarbonyl)amino)ethoxy)phenyl)amino)-2-methylpropanoic acid (199)

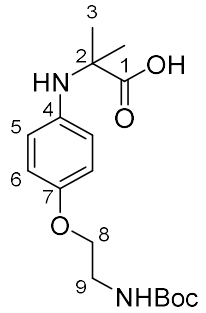

To a stirring solution of **198** (0.516 g, 1.63 mmol) in a mixture of DMF (7.2 mL) and H_2O (1.8 mL) were added aminoisobutyric acid (0.202 g, 1.96 mmol), potassium carbonate (0.901 g, 6.52 mmol), copper (I) iodide (47 mg, 0.245 mmol), and 2-acetylcyclohexanone (42 µL, 0.33 mmol). The reaction mixture was heated to 90 °C for 18 h, then cooled, diluted with H_2O (20 mL), and washed with EtOAc (3 x 20 mL). The aqueous was then acidified with citric acid to pH 3, then extracted with EtOAc (3 x 20 mL), washed with brine (25 mL), dried over $MgSO_4$, filtered, and concentrated *in vacuo*. The residue was purified through silica gel column chromatography (1 to 6% MeOH/DCM) to give the title compound as a white amorphous solid (0.123 g, 22%).

R_f: 0.20 (6% MeOH/DCM); **IR** (neat film, ν_{max}, cm^{-1}): 2971 (w, CH), 1687 (s), 1615 (s), 1557 (m), 1515 (s), 1462 (m), 1431 (m), 1401 (m), 1366 (s), 1306 (m), 1261 (s), 1173 (s), 1111 (w), 1056 (w); **^{1}H NMR** (400 MHz, MeOD) δ : 7.13 (d, *J* = 8.3 Hz, 2 H, Ar-H), 6.95 (d, *J* = 8.3 Hz, 2 H, Ar-H), 3.99 (t, *J* = 5.3 Hz, 2 H, H8), 3.41 (t, *J* = 5.3 Hz, 2 H, H9), 1.44 (s, 9 H, Boc-CH_3), 1.41 (s, 6 H, H3); **^{13}C NMR** (101 MHz, MeOD) δ : 176.1 (C1), 157.2, 157.1 (C7 and Boc C=O), 130.2 (C4), 123.7, 114.9 (C5 and C6), 78.8 (Boc-qC), 67.0 (C8), 63.7 (C2), 39.5 (C9), 27.3 (Boc-CH_3), 22.9 (C3); **HRMS (ESI):** m/z calcd for $C_{17}H_{25}N_2O_5$ $[M-H]^-$: 337.1763; Found: 337.1762.

Methyl 2-((4-(2-((tert-butoxycarbonyl)amino)ethoxy)phenyl)amino)-2-methylpropanoate (200)

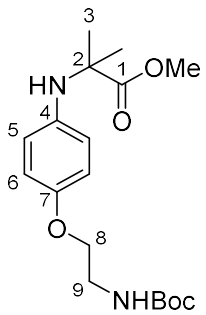

To a stirring solution of **199** (84 mg, 0.25 mmol) in DMF (1.5 mL) were added potassium carbonate (51.4 mg, 138.2 mmol) and iodomethane (23 µL, 0.372 mmol). The reaction mixture was heated to 45 °C for 4 h before cooling and concentrating *in vacuo*. The residue was purified through silica gel column chromatography (9:1 to 8:2 PE 40-60/EtOAc) to give the title compound as a colourless oil (52 mg, 59%).

R_f: 0.60 (1:1 PE 40-60/EtOAc); **IR** (neat film, ν_{max}, cm^{-1}): 3387 (w, NH), 2977 (w, CH), 2936 (w, CH), 1697 (m, C=O), 1508 (s), 1465 (m), 1383 (m), 1365 (m), 1272 (m), 1238 (s), 1165 (s), 1143 (s), 1067 (w); **^{1}H NMR** (400 MHz, $CDCl_3$) δ : 6.73 (d, *J* = 8.9 Hz, 2 H, Ar-H), 6.62 (d, *J* = 8.9 Hz, 2 H, Ar-H), 4.98 (br s, 1 H, NH), 3.94 (t, *J* = 5.0 Hz, 2 H, H8), 3.69 (s, 3 H, OMe), 3.48 (q, *J* = 5.0 Hz, 2 H, H9), 1.49 (s, 6 H, H3), 1.44 (s, 9 H, Boc-CH_3); **^{13}C NMR** (101 MHz, $CDCl_3$) δ : 176.8 (C1), 155.9 (Boc-C=O), 152.7 (C7), 139.3 (C4), 119.5, 115.1 (C5 and C6), 79.4 (Boc-qC), 67.6 (C8), 58.4 (C2), 52.3 (OMe), 40.2 (C9), 28.4 (Boc-CH_3), 26.3 (C3); **HRMS (ESI):** m/z calcd for $C_{18}H_{28}N_2O_5Na$ $[M+Na]^+$: 375.1896; Found: 375.1883.

***tert*-Butyl (2-(4-(3-(4-cyano-3-(trifluoromethyl)phenyl)-5,5-dimethyl-4-oxo-2-thioxoimidazolidin-1-yl)phenoxy)ethyl)carbamate (201)**

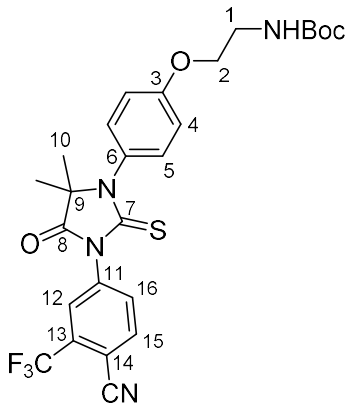

To a stirring solution of **200** (40 mg, 0.114 mmol) in DMF (0.5 mL) was added **5** (39 mg, 0.17 mmol). The reaction mixture was heated to 90 °C for 7 h, before being cooled, diluted with H_2O (5 mL) and extracted with EtOAc (3 x 15 mL). The organics were washed with brine (10 mL), dried over $MgSO_4$, filtered and concentrated *in vacuo*. The residue was purified through silica gel column chromatography (15% Acetone/Hexane) to give the title compound as a colourless oil (60 mg, 96%).

R_f: 0.14 (15% Acetone/Hexane); **IR** (neat film, ν_{max}, cm^{-1}): 3380 (w, NH), 2979 (w, CH), 2873 (w, CH), 1755 (m, C=O), 1707 (s, C=O), 1612 (w), 1504 (s), 1440 (s), 1389 (m), 1365 (m), 1310 (s), 1286 (s), 1246 (s), 1195 (s), 1169 (s), 1137 (s), 1055 (m), 1003 (w); **^{1}H NMR** (400 MHz, $CDCl_3$) δ : 7.98 – 7.96 (m, 2 H, H12, H15), 7.84 (dd, *J* = 8.2, 2.2 Hz, 1 H, H16), 7.21 (d, *J* = 9.2 Hz, 2 H, H5), 7.03 (d, *J* = 9.2 Hz, 2 H, H4),

4.98 (br s, 1 H, NH), 4.07 (t, *J* = 5.1 Hz, 2 H, H2), 3.56 (q, *J* = 5.1 Hz, 2 H, H1), 1.57 (s, 6 H, H10), 1.46 (s, 9 H, Boc-CH_3); **^{13}C NMR** (101 MHz, $CDCl_3$) δ : 180.2 (C7), 175.0 (C8), 159.3 (C3), 155.8 (Boc-C=O), 137.2 (C14), 135.2 (C15), 133.6 (q, *J* = 34 Hz, C13), 132.2 (C16), 130.7 (C6), 127.7 (C5), 127.1 (q, *J* = 4.7 Hz, C12), 121.9 (q, *J* = 273 Hz, CF_3), 115.5 (C4), 114.8 (-C≡N), 110.2 (q, *J* = 2.1 Hz, C11), 79.7 (Boc-qC), 67.5 (C2), 66.3 (C9), 40.0 (C1), 28.4 (Boc-CH_3), 23.6 (C10); **^{19}F NMR** (376 MHz, $CDCl_3$) δ: -61.9; **HRMS (ESI):** m/z calcd for $C_{26}H_{27}N_4O_4F_3SNa$ $[M+Na]^+$: 571.1603; Found: 571.1604.

4-(3-(4-(2-aminoethoxy)phenyl)-4,4-dimethyl-5-oxo-2-thioxoimidazolidin-1-yl)-2-(trifluoromethyl)benzonitrile (202)

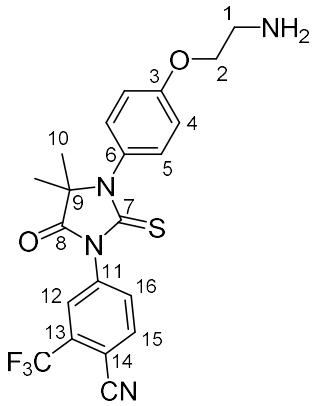

To a stirring solution of **201** (50 mg, 0.09 mmol) in dichloromethane (0.8 mL) was added TFA (0.2 mL). The reaction mixture was stirred at r.t. for 4 h before being quenched with $NaHCO_3$ (sat. aq.). The mixture was then extracted into dichloromethane (3 x 10 mL), washed with brine (5 mL), dried over Na_2SO_4, filtered and concentrated *in vacuo* to give the title compound as a white amorphous solid (45 mg, 98%) which was used without further purification.

IR (neat film, ν_{max}, cm^{-1}): 2928 (w, CH), 1753 (m, C=O), 1709 (m), 1666 (w), 1611 (w), 1504 (m), 1431 (s), 1364 (m), 1309 (s), 1282 (s), 1246 (s), 1222 (m), 1192 (s), 1169 (s), 1132 (s), 1054 (m), 1002 (w); **^{1}H NMR** (400 MHz, MeOD) δ : 7.98 (m, 2 H, H12, H15), 7.84 (dd, *J* = 8.4, 1.9 Hz, 1 H, H16), 7.20 (d, *J* = 8.9 Hz, 2 H, H5), 7.04 (d, *J* = 8.9 Hz, 2 H, H4), 4.04 (t, *J* = 5.2 Hz, 2 H, H2), 3.13 (br s, 2 H, H1), 1.57 (s, 6 H, H10); **^{13}C NMR** (101 MHz, MeOD) δ : 180.1 (C7), 175.1 (C8), 159.7 (C3), 137.2 (C14), 135.2 (C15), 133.5 (q, *J* = 34 Hz, C13), 132.2 (C16), 130.6 (C6), 127.4 (C5), 127.1 (q, *J* = 4.7 Hz, C12), 121.9 (q, *J* = 273 Hz, CF_3), 115.6 (C4), 114.8 (-C≡N), 110.1 (q, *J* = 2.2 Hz, C11), 70.5 (C2), 66.3 (C9), 41.4 (C1), 23.6 (C10); **^{19}F NMR** (376 MHz, $CDCl_3$) δ: -62.0; **HRMS (ESI):** m/z calcd for $C_{21}H_{19}F_3N_4O_2S$ $[M+H]^+$: 449.1254; Found: 449.1259.

(2*S*,4*R*)-1-((*S*)-2-(4-((*E*)-(4-((2-(4-(3-(4-cyano-3-(trifluoromethyl)phenyl)-5,5-dimethyl-4-oxo-2-thioxoimidazolidin-1-yl)phenoxy)ethyl)carbamoyl)-2,6-difluorophenyl)diazenyl)-3,5-difluorobenzamido)-3,3-dimethylbutanoyl)-4-hydroxy-*N*-(4-(4-methylthiazol-5-yl)benzyl)pyrrolidine-2-carboxamide (azoPROTAC2)

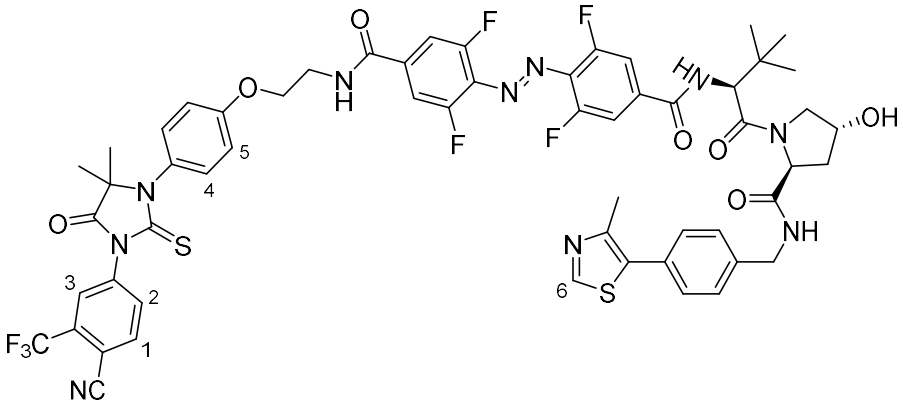

To a stirring solution of **195** (11.7 mg, 0.015 mmol) in a mixture of THF and H_2O (2:1, 1 mL) was added lithium hydroxide (1.3 mg, 0.030 mmol). The reaction was stirred at r.t. for 3 h before acidifying to pH 3 with 1 M HCl and extracting into EtOAc (3 x 10 mL). The combined organics were washed with brine (5 mL), dried over Na_2SO_4, filtered, and concentrated *in vacuo*. The crude residue was directly dissolved in DMF (0.2 mL) and cooled to 0 °C, before HATU (7.5 mg, 0.0197 mmol) and DIPEA (3.4 µL, 0.0197 mmol) were added. The reaction mixture was stirred for 15 mins before **202** (9.4 mg, 0.021 mmol) was added. The mixture was then warmed to r.t. and stirred for a further 16 h before diluting in water (5 mL) and extracting into EtOAc (3 x 10 mL). The combined organics were then washed with brine (2 x 5 mL), before being dried over Na_2SO_4, filtered and concentrated *in vacuo*. The residue was purified through silica gel column chromatography (1 to 4% MeOH/DCM) to give the title compound as an orange oil (8 mg, 47%).

R_f: 0.40 (5% MeOH/DCM); **IR** (neat film, ν_{max}, cm^{-1}): 3345 (w, NH), 2922 (w, CH), 1754 (w, C=O), 1720 (w, C=O), 1653 (m, C=O), 1625 (m), 1575 (m), 1511 (m), 1428 (s), 1371 (m), 1312 (m), 1286 (m), 1246 (m), 1193 (m), 1173 (m), 1138 (m), 1049 (m); Mixture of cis and trans, only major isomer reported; **^{1}H NMR** (500 MHz, $CDCl_3$) δ : 8.68 (s, 1 H, H6), 8.00 – 7.95 (m, 2H), 7.85 - 7.82 (m, 1 H), 7.49 (dd, *J* = 21.0, 9.0 Hz, 1 H), 7.40 – 7.31 (m, 6 H), 7.26 – 7.24 (m, 1 H), 7.23 – 7.18 (m, 2 H), 7.15 – 7.01 (m, 3 H), 6.75 – 6.69 (m, 2 H), 4.75 – 4.53 (m, 4 H), 4.37 – 4.30 (m, 1 H), 4.16 (t, *J* = 5.3 Hz, 2 H), 4.00 (d, *J* = 11.4 Hz, 1 H), 3.88 – 3.78 (m, 2 H), 3.72 – 3.64 (m, 1 H), 2.50 (s, 3 H, CH_3), 2.49 – 2.44 (m, 1 H), 2.10 – 2.06 (m, 1 H), 1.56 (s, 6 H, 2x CH_3), 0.98 (s, 9 H, 3x CH_3); **^{13}C NMR** (126 MHz, $CDCl_3$) δ : 180.2 (C=S), 175.0 (cyclic C=O), 171.2, 170.5, 164.4, 164.3, 160.0, 151.4 (d, *J* = 260 Hz, C-F), 151.2 (d, *J* = 260 Hz, C-F), 150.4, 148.5, 137.8, 137.1, 136.4, 135.7, 135.2, 134.1, 133.7, 133.6 (q, *J* = 26 Hz), 132.2, 131.5, 131.1, 130.8,

129.6, 128.1, 128.0, 127.1 (q, *J* = 4.9 Hz), 121.9 (q, *J* = 275 Hz, CF_3), 115.6, 114.8 (-C≡N), 111.8 – 111.3 (m, 2C), 110.2, 70.2, 66.6, 66.3, 58.7, 58.2, 56.8, 43.3, 39.7, 36.0, 35.7, 26.5, 23.6, 16.0; **^{19}F NMR** (376 MHz, $CDCl_3$) δ: -62.0, -117.1 (dt, *J* = 59, 5.6 Hz), -118.2; **HRMS (ESI):** m/z calcd for $C_{57}H_{52}F_7N_{10}O_7S_2$ $[M+H]^+$: 1185.3345; Found: 1185.3355.

Ethyl (*E*)-4-((2,6-difluoro-4-hydroxyphenyl)diazenyl)benzoate (209)

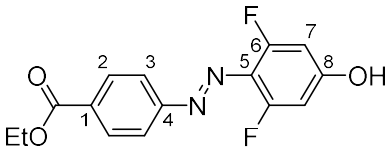

To a stirring solution of ethyl 4-aminobenzoate (0.50 g, 3.0 mmol) in a mixture of acetic acid (3 mL) and conc. H_2SO_4 (0.4 mL) cooled to 0 °C, was very slowly added a solution of sodium nitrite (0.29 g, 4.2 mmol) in H_2O (0.6 mL). The reaction was stirred at 0 °C for 30 mins before being very slowly added to a 0 °C solution of 3,5-difluorophenol (0.398 g, 3.06 mmol) and NaOH (2.52 g, 63 mmol) in H_2O (2 mL). The solution was then stirred for 30 mins, then filtered, and the solid washed with cold H_2O to yield the title compound as an amorphous dark brown solid (0.75 g, 82%).

IR (neat film, ν_{max}, cm^{-1}): 3358 (w, NH), 3075 (w, CH), 1687 (s, C=O), 1623 (s), 1590 (m), 1527 (m), 1470 (m), 1440 (m), 1353 (m), 1285 (s), 1229 (m), 1155 (s), 1108 (m), 1053 (m), 1011 (w); **^{1}H NMR** (400 MHz, d-DMSO) δ : 11.41 (s, 1 H, OH), 8.12 – 8.08 (m, 2 H, H2), 7.85 – 7.81 (m, 2 H, H3), 6.68 (d, *J* = 12 Hz, 2 H, H7), 4.33 (q, *J* = 7.1 Hz, 2 H, CH_2), 1.32 (t, *J* = 7.1 Hz, 3 H, CH_3); **^{13}C NMR** (101 MHz, $CDCl_3$) δ : 165.8 (C=O), 162.7 (C8), 157.6 (dd, *J* = 260, 8 Hz, C6), 155.8 (C4), 131.9 (C1), 130.9 (C2), 122.6 (C5), 122.4 (C3), 100.9 (dd, *J* = 23, 3 Hz, C7), 61.5 (CH_2), 14.6 (CH_3); **^{19}F NMR (**376 MHz, $CDCl_3$) δ : -118.4; **HRMS (ESI):** m/z calcd for $C_{15}H_{13}F_2N_2O_3$ $[M+H]^+$: 307.0889; Found: 307.0888.

Ethyl (*E*)-4-((4-(2-(*tert*-butoxy)-2-oxoethoxy)-2,6-difluorophenyl)diazenyl)benzoate (210)

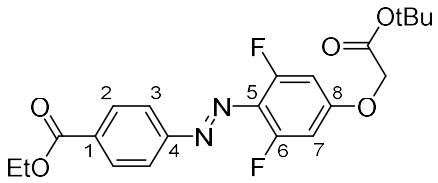

To a stirring solution of **209** (73 mg, 0.238 mmol) in DMF (1.5 mL) were added *tert*-butyl bromoacetate (42.2 µL, 0.286 mmol), potassium carbonate (66 mg, 0.477 mmol) and a catalytic amount of potassium iodide. The reaction was heated to 100 °C for 18 h before being cooled, diluted with water (3 mL), extracted into DCM (3 x 10 mL) then into EtOAc (3 x 10 mL), dried over Na_2SO_4, filtered, and

concentrated *in vacuo*. The residue was purified through silica gel column chromatography (9:1 PE 40-60/EtOAc) to give the title compound as an amorphous orange solid (92 mg, 92%).

R_f: 0.55 (8:2 PE 40-60/EtOAc); **IR** (neat film, ν_{max}, cm^{-1}): 2982 (w, CH), 1752 (m, C=O), 1718 (m, C=O), 1625 (m), 1582 (w), 1445 (w), 1369 (m), 1275 (m), 1231 (m), 1146 (s), 1105 (m), 1059 (m); **^{1}H NMR** (400 MHz, $CDCl_3$) δ : 8.18 (d, *J* = 8.6 Hz, 2 H, H2), 7.91 (d, *J* = 8.6 Hz, 2 H, H3), 6.60 (d, *J* = 10.7 Hz, 2 H, H7), 4.57 (s, 2 H, CH_2), 4.41 (q, *J* = 7.1 Hz, 2 H, Et-CH_2), 1.51 (s, 9 H, 3x CH_3), 1.43 (t, *J* = 7.1 Hz, 3 H, Et-CH_3); **^{13}C NMR** (101 MHz, $CDCl_3$) δ : 166.5 (*t*Bu-O-C=O), 166.0 (Ar-C=O), 160.1 (d, *J* = 260 Hz, C6), 156.2 (C8), 155.8 (C4), 132.4 (C1), 130.5 (C2), 122.5 (C5), 122.4 (C3), 99.6 (dd, *J* = 24.5, 2.8 Hz, C7), 83.3 (qC), 66.0 (CH_2), 61.3 (CH_2-CH_3), 28.0 (3x CH_3), 14.3 (CH_3); **^{19}F NMR (**376 MHz, $CDCl_3$) δ : -116.6; **HRMS (ESI):** m/z calcd for $C_{21}H_{23}F_2N_2O_5$ $[M+H]^+$: 421.1570; Found: 421.1566.

(*E*)-2-(4-((4-(ethoxycarbonyl)phenyl)diazenyl)-3,5-difluorophenoxy)acetic acid (211)

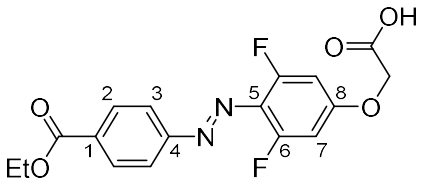

To a stirring solution of **210** (30 mg, 0.071 mmol) in dichloromethane (1 mL) was added TFA (0.5 mL). The reaction was stirred at r.t. for 3 h before being concentrated *in vacuo*. The residue was purified through silica gel column chromatography (3 to 5% MeOH/DCM + 1% AcOH) to give the title compound as an amorphous orange solid (16 mg, 62%).

R_f: 0.23 (5% MeOH/DCM + 1% AcOH); **IR** (neat film, ν_{max}, cm^{-1}): 1718 (s, C=O), 1700 (s, C=O), 1629 (s), 1623 (s), 1540 (m), 1435 (m), 1363 (m), 1300 (m), 1278 (s), 1167 (m), 1101 (m), 1066 (m); Mixture of cis and trans isomers, only major reported; **^{1}H NMR** (400 MHz, d-DMSO) δ : 8.15 (d, *J* = 8.5 Hz, 2 H, H2), 7.90 (d, *J* = 8.5 Hz, 2 H, H3), 7.00 (d, *J* = 11.7 Hz, 2 H, H7), 4.83 (s, 2 H, CH_2), 4.36 (q, *J* = 7.0 Hz, 2 H, Et-CH_2), 1.36 (t, *J* = 7.0 Hz, 3 H, Et-CH_3); **^{13}C NMR** (101 MHz, d-DMSO) δ : 169.7 (acid C=O), 165.6 (Ar-C=O), 162.0 (C8), 157.1 (dd, *J* = 260, 7.7 Hz, C6), 155.7 (C4), 132.3 (C1), 131.0 (C2), 130.7 (C5), 122.8 (C3), 100.6 (dd, *J* = 23.8, 2.4 Hz, C7), 66.3 (CH_2), 61.6 (Et-CH_2), 14.6 (CH_3); **^{19}F NMR (**376 MHz, $CDCl_3$) δ : -117.4; **HRMS (ESI):** m/z calcd for $C_{17}H_{13}F_2N_2O_5$ $[M-H]^-$: 363.0798; Found: 363.0788.

Ethyl 4-((*E*)-(2,6-difluoro-4-(2-(((*S*)-1-((2*S*,4*R*)-4-hydroxy-2-((4-(4-methylthiazol-5-yl)benzyl)carbamoyl)pyrrolidine-1-yl)-3,3-dimethyl-1-oxobutan-2-yl)amino)-2-oxoethoxy)phenyl)diazenyl)benzoate (212)

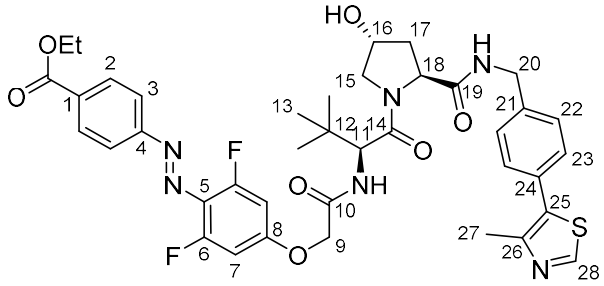

To a stirring solution of **211** (14 mg, 0.038 mmol) in DMF (0.5 mL) were added HATU (17.5 mg, 0.046 mmol) and DIPEA (16.5 µL, 0.095 mmol). The reaction mixture was stirred at r.t. for 15 mins before **154** (21.4 mg, 0.042 mmol) was added. The mixture was then stirred for a further 6 h before diluting in water (5 mL) and extracting into EtOAc (3 x 10 mL). The combined organics were then washed with brine (2 x 5 mL), before being dried over Na_2SO_4, filtered and concentrated *in vacuo*. The residue was purified through silica gel column chromatography (DCM to 4% MeOH/DCM) to give the title compound as an orange oil (20 mg, 68%).

R_f: 0.30 (5% MeOH/DCM); **IR** (neat film, ν_{max}, cm^{-1}): 3374 (w, NH), 2957 (w, CH), 1716 (m, C=O), 1672 (m, C=O), 1623 (s), 1581 (m), 1523 (m), 1480 (m), 1436 (m), 1407 (m), 1369 (m), 1350 (m), 1273 (s), 1226 (m), 1152 (s), 1097 (m), 1058 (m), 1014 (m); Mixture of cis and trans isomers, only major reported; **^{1}H NMR** (400 MHz, $CDCl_3$) δ : 8.67 (s, 1 H, H28), 8.17 (d, *J* = 8.5 Hz, 2 H, H2), 7.90 (d, *J* = 8.5 Hz, 2 H, H3), 7.38 – 7.32 (m, 4 H, H22, H23), 7.24 – 7.20 (m, 1 H, NH), 6.92 (d, *J* = 8.7 Hz, 1 H, NH), 6.65 (d, *J* = 10.5 Hz, 2 H, H7), 4.73 – 4.68 (m, 1 H), 4.61 – 4.52 (m, 4 H), 4.44 – 4.30 (m, 4 H), 4.02 – 3.95 (m, 1 H), 3.69 – 3.65 (m, 1 H), 2.56 – 2.47 (m, 4 H), 2.14 – 2.10 (m, 1 H), 1.42 (t, *J* = 7.2 Hz, 3 H, Et-CH_2), 0.95 (s, 9 H, H13); **^{13}C NMR** (101 MHz, $CDCl_3$) δ : 170.9, 170.5, 166.9, 166.0, 165.6, 157.4 (dd, *J* = 260, 9 Hz, C-F), 155.6, 150.4, 148.5, 137.9, 132.6 (C1), 131.1 (C2), 130.5 (C5), 130.3, 129.5, 128.1, 122.5 (C3), 118.4, 100.0 – 99.7 (m, C7), 70.2, 67.5, 61.3, 58.7, 57.1, 56.8, 43.3, 36.1, 35.4, 26.3 (C27), 16.0 (C13), 14.3 (Et-CH_3); **^{19}F NMR (**376 MHz, $CDCl_3$) δ : -116.8; **HRMS (ESI):** m/z calcd for $C_{40}H_{44}F_2N_5O_7S$ $[M+H]^+$: 776.2923; Found: 776.2879.

(2*S*,4*R*)-1-((*S*)-2-(2-(4-((*E*)-(4-((2-(4-(3-(4-cyano-3-(trifluoromethyl)phenyl)-5,5-dimethyl-4-oxo-2-thioxoimidazolidin-1-yl)phenoxy)ethyl)carbamoyl)phenyl)diazenyl)-3,5-difluorophenoxy)acetamido)-3,3-dimethylbutanoyl)-4-hydroxy-*N*-(4-(4-methylthiazol-5-yl)benzyl)pyrrolidine-2-carboxamide (azoPROTAC3)

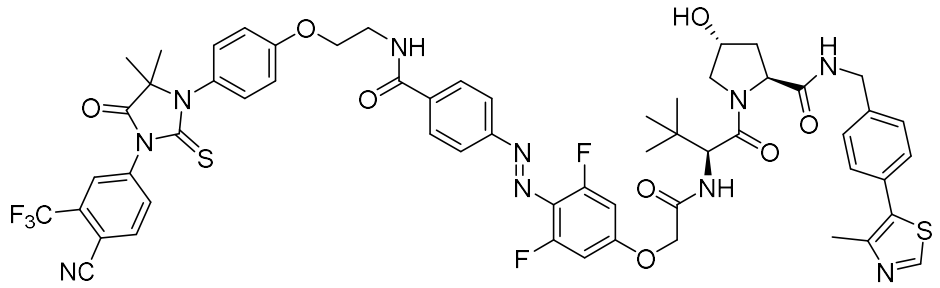

To a stirring solution of **212** (16 mg, 0.0206 mmol) in a mixture of THF and H_2O (2:1, 1 mL) was added lithium hydroxide (1.7 mg, 0.0412 mmol). The reaction was stirred at r.t. for 3 h before acidifying to pH 3 with 1 M HCl and extracting into EtOAc (3 x 10 mL). The combined organics were washed with brine (5 mL), dried over Na_2SO_4, filtered, and concentrated *in vacuo*. The crude residue was directly dissolved in DMF (0.2 mL) and cooled to 0 °C, before HATU (10.2 mg, 0.0268 mmol) and DIPEA (4.7 µL, 0.0268 mmol) were added. The reaction mixture was stirred for 15 mins before **202** (12.0 mg, 0.0268 mmol) was added. The mixture was then warmed to r.t. and stirred for a further 16 h before diluting in water (5 mL) and extracting into EtOAc (3 x 10 mL). The combined organics were then washed with brine (2 x 5 mL), before being dried over Na_2SO_4, filtered and concentrated *in vacuo*. The residue was purified through silica gel column chromatography (1 to 5% MeOH/DCM) to give the title compound as a colourless oil (7 mg, 30%).

R_f: 0.31 (5% MeOH/DCM); **IR** (neat film, ν_{max}, cm^{-1}): 3348 (w, NH), 2922 (w, CH), 2855 (w, CH), 1759 (m, C=O), 1708 (m, C=O), 1666 (m, C=O), 1626 (s), 1581 (m), 1538 (m), 1512 (s), 1436 (s), 1353 (m), 1311 (s), 1247 (m), 1222 (m), 1194 (m), 1166 (s), 1142 (s), 1055 (m); Mixture of cis and trans isomers, only major reported; **^{1}H NMR** (500 MHz, $CDCl_3$) δ : 8.68 (s, 1 H), 7.98 – 7.90 (m, 4 H), 7.84 (dt, *J* = 8.2, 2.2 Hz, 1 H), 7.73 (d, *J* = 8.6 Hz, 1 H), 7.39 – 7.33 (m, 4 H), 7.25 – 7.17 (m, 3 H), 7.10 – 7.03 (m, 3H), 6.96 (d, *J* = 8.4 Hz, 1 H), 6.70 – 6.61 (m, 2 H), 6.39 (d, *J* = 8.6 Hz, 1 H), 4.73 (t, *J* = 7.8 Hz, 1 H), 4.61 – 4.53 (m, 4 H), 4.39 – 4.34 (m, 2 H), 4.25 (t, *J* = 5 Hz, 2 H), 4.04 (d, *J* = 11.6 Hz, 1 H), 3.97 – 3.93 (m, 2 H), 3.68 – 3.64 (m, 1 H), 2.62 – 2.50 (m, 4 H), 2.18 – 2.13 (m, 1 H), 1.58 (s, 6 H, 2x CH_3), 0.94 (s, 9 H, 3x CH_3); **^{13}C NMR** (126 MHz, $CDCl_3$) δ : 180.2, 175.0, 171.0, 170.3, 166.9, 166.8, 166.5, 159.2, 157.5 (dd, *J* = 260, 8 Hz, C-F), 157.2, 155.0, 150.4, 148.5, 137.9, 137.1, 136.3, 135.2, 133.6 (q, *J* = 34 Hz), 131.3 (d, *J* = 50 Hz), 131.1, 130.8, 129.6, 128.2, 128.0, 127.8, 127.1 (q, *J* = 5 Hz), 122.9, 121.8 (q, *J* = 275 Hz), 118.9, 115.6, 114.8, 110.2 (m), 100.0 – 99.7 (m), 70.3, 67.6, 67.0, 66.3, 58.5, 57.1, 56.7, 43.3, 39.6, 35.8, 35.3, 26.3, 23.6, 16.0; **^{19}F NMR (**376 MHz, $CDCl_3$) δ : -62.0, -115.9; **HRMS (ESI):** m/z calcd for $C_{58}H_{57}F_5N_{10}O_8S_2$ $[M+2H]^{2+}$: 590.1856; Found: 590.1861.

4-acetoxybenzoic acid (214)

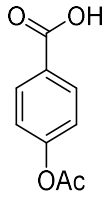

Following a literature procedure,[360] to a stirring solution of 4-hydroxybenzoic acid (1.00 g, 7.24 mmol) in pyridine (7 mL) was added acetic anhydride (0.75 mL, 7.97 mmol). The reaction mixture was heated to reflux for 2 h before being cooled to r.t. and poured over $NaHCO_3$ (sat. aq. 30 mL). The solution was then acidified to pH 2 with conc. HCl and the precipitate was filtered, washed with H_2O, and dried *in vacuo* to give the title compound as a white amorphous solid (1.25 g, 96%) used without further purification.

R_f: 0.31 (1:1 PE/EtOAc); **IR** (neat film, ν_{max}, cm^{-1}): 2839 (br w, OH), 2674 (w, CH), 1753 (s, C=O), 1682 (s, C=O), 1605 (m), 1508 (w), 1429 (m), 1373 (m), 1317 (m), 1290 (m), 1222 (s), 1204 (s), 1168 (s), 1129 (m), 1104 (w), 1018 (m); **^{1}H NMR** (400 MHz, CDCl3) δ: 8.15 – 8.12 (m, 2 H), 7.23 – 7.19 (m, 2 H), 2.35 (s, 3 H); **^{13}C NMR** (101 MHz, CDCl3) δ: 169.9, 168.8, 154.9, 131.8, 126.8, 121.7, 21.2.

Data are in accordance with those reported previously in literature.[360]

4-(6-methoxy-2-(4-methoxyphenyl)benzo[*b*]thiophene-3-carbonyl)phenyl acetate (216)

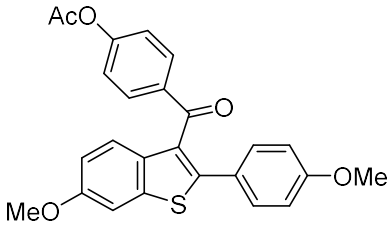

To a stirring solution of **214** (0.347 g, 1.93 mmol) in dichloromethane (6 mL) cooled to 0 °C were dropwise added oxalyl chloride (0.49 mL, 5.78 mmol), followed by a few drops of DMF. The reaction mixture was warmed to r.t. and stirred for 1 h before concentrating *in vacuo* to give the acyl chloride as a white solid. This was then dissolved in dichloromethane (10 mL) and cooled to 0 °C, 6-methoxy-2-(4-methoxyphenyl)-benzo[*b*]thiophene (0.417 g, 1.54 mmol) was added followed by $AlCl_3$ (0.386 g, 2.90 mmol) in three portions, over 5 mins. The reaction was warmed to r.t. and stirred for 1 h before being carefully quenched with ice-water, followed by 1 M HCl. The reaction was separated and the aqueous further extracted with dichloromethane (2 x 30 mL). The combined organics were dried over Na_2SO_4, filtered and concentrated *in vacuo*. The residue was purified through silica gel column

chromatography (7:3 PE 40-60/DCM to DCM) to give the title compound as a yellow amorphous solid (0.29 g, 35%).

R_f: 0.23 (3:1 DCM/PE 40-60); **^{1}H NMR** (400 MHz, $CDCl_3$) δ: 7.81 – 7.78 (m, 2 H), 7.59 (d, *J* = 8.9 Hz, 1 H), 7.33 – 7.29 (m, 3 H), 7.02 – 6.97 (m, 3 H), 6.77 – 6.74 (m, 2 H), 3.89 (s, 3 H), 3.75 (s, 3H), 2.27 (s, 3 H); **^{13}C NMR** (101 MHz, $CDCl_3$) δ: 193.1, 168.6, 159.9, 157.7, 154.3, 144.1, 140.0, 135.0, 133.7, 131.5, 130.4, 130.0, 125.7, 124.1, 121.5, 114.9, 114.1, 104.5, 55.6, 55.3, 21.1.

Data are in accordance with those reported previously in literature.[317]

(4-hydroxyphenyl)(6-methoxy-2-(4-methoxyphenyl)benzo[b]thiophen-3-yl)methanone (217)

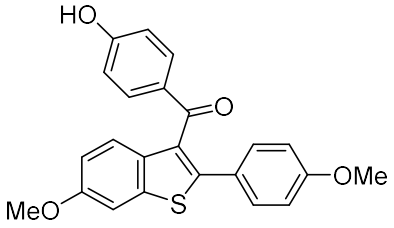

To a stirring solution of **216** (0.29 g, 0.67 mmol) in a mixture of EtOH (7 mL) and water (3 mL) was added sodium acetate (0.275 g, 3.35 mmol). The reaction mixture was heated to 90 °C and stirred for 12 h before cooling and concentrating *in vacuo*. The residue was dissolved in EtOAc (15 mL) and water (10 mL), separated and the aqueous extracted with EtOAc (2 x 15 mL). The combined organics were dried over Na_2SO_4, filtered and concentrated *in vacuo* to give the title compound as a yellow oil (0.234 g, 89%) used without further purification.

R_f: 0.48 (5% MeOH/DCM); **IR** (neat film, ν_{max}, cm^{-1}): 3307 (br w, OH), 2952 (w, CH), 1630 (m), 1602 (s), 1573 (m), 1535 (m), 1499 (m), 1474 (m), 1438 (m), 1351 (w), 1294 (m), 1252 (s), 1225 (m), 1178 (m), 1162 (m), 1076 (w), 1030 (m); **^{1}H NMR** (400 MHz, $CDCl_3$) δ: 7.74 – 7.70 (m, 2 H), 7.53 (d, *J* = 9.1 Hz, 1 H), 7.35 – 7.31 (m, 3 H), 6.96 (dd, *J* = 9.1, 2.4 Hz, 1 H), 6.77 – 6.66 (m, 4 H), 5.73 (s, 1 H), 3.88 (s, 3 H), 3.74 (s, 3 H); **^{13}C NMR** (101 MHz, $CDCl_3$) δ: 193.3 (C=O), 160.3, 159.7, 157.6, 142.8, 140.0, 133.9, 132.7, 130.5, 130.4, 130.3, 126.0, 124.0, 115.2, 114.8, 114.1, 104.5, 55.6, 55.3.

Data are in accordance with those reported previously in literature[317].

(4-(2-(ethylamino)ethoxy)phenyl)(6-methoxy-2-(4-methoxyphenyl)benzo[*b*]thiophen-3-yl)methanone (218)

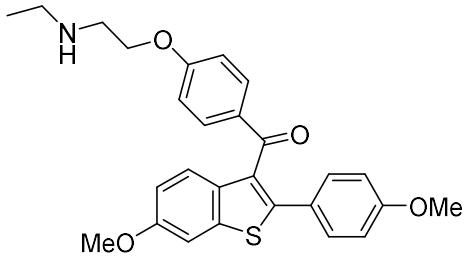

To a stirring solution of **217** (0.229 g, 0.59 mmol) in acetonitrile (10 mL) were added 1,2-dibromoethane (0.102 mL, 1.18 mmol) and Cs_2CO_3 (0.287 mg, 0.88 mmol). The reaction mixture was heated to 80 °C and stirred for 14 h before being cooled, filtered, washed with acetonitrile (10 mL) and concentrated *in vacuo*. The residue was dissolved in DMF (6 mL) and ethylamine (2.95 mL, 2 M, THF) was added. The reaction mixture was heated to 80 °C for 14 h before being cooled, diluted with EtOAc (20 mL) and brine (15 mL). The layers were separated and the aqueous extracted with EtOAc (2 x 15 mL). The combined organics were dried over Na_2SO_4, filtered and concentrated. The residue was purified through silica gel column chromatography (DCM to 9:1 DCM/MeOH) to give the title compound as a yellow amorphous solid (0.29 g, 35%).

R_f: 0.28 (1:9 MeOH/DCM); **^{1}H NMR** (400 MHz, $CDCl_3$) δ: 7.75 (d, *J* = 8.9 Hz, 2 H), 7.52 (d, *J* = 9.1 Hz, 1 H), 7.35 – 7.31 (m, 3 H), 6.95 (dd, *J* = 9.1, 2.4 Hz, 1 H), 6.77 – 6.73 (m, 4 H), 4.11 (t, *J* = 5.1 Hz, 2 H), 3.88 (s, 3 H), 3.74 (s, 3 H), 3.06 (t, *J* = 5.1 Hz, 2 H), 2.81 (q, *J* = 7.2 Hz, 2 H), 1.19 (t, *J* = 7.2 Hz, 3 H); **^{13}C NMR** (101 MHz, $CDCl_3$) δ: 193.2, 162.5, 159.7, 157.6, 142.5, 140.1, 133.9, 132.3, 130.7, 130.4, 130.3, 126.0, 124.0, 114.8, 114.2, 114.1, 104.5, 66.2, 55.6, 55.2, 47.5, 43.8, 13.9.

Data are in accordance with those reported previously in literature.[317]

(4-(2-(ethylamino)ethoxy)phenyl)(6-hydroxy-2-(4-hydroxyphenyl)benzo[*b*]thiophen-3-yl)methanone (219)

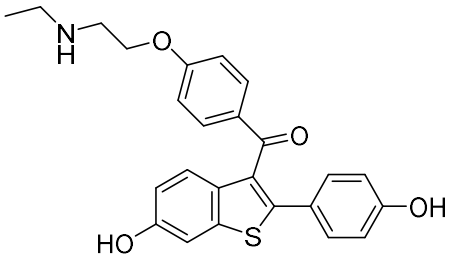

To a stirring solution of **218** (0.080 g, 0.173 mmol) in dichloromethane (3 mL) cooled to 0 °C was dropwise added boron tribromide (1 M in DCM, 0.69 mL, 0.693 mmol). The reaction mixture was warmed to rt. and stirred for 2 h before being quenched with MeOH (0.25 mL) and concentrated *in vacuo*. The residue was dissolved in $NaHCO_3$ (sat. aq.) and extracted into EtOAc (3 x 20 mL), dried over Na_2SO_4, filtered and concentrated. The residue was purified through silica gel column chromatography (9:1 to 8:1 DCM/MeOH) to give the title compound as a yellow amorphous solid (0.055 g, 73%).

R_f: 0.14 (15% MeOH/DCM); **IR** (neat film, ν_{max}, cm^{-1}): 3186 (br m, OH), 2970 (w, CH), 2888 (w, CH), 1633 (m), 1594 (s), 1569 (m), 1536 (m), 1502 (m), 1465 (m), 1419 (m), 1354 (m), 1306 (m), 1250 (s)< 1226 (s), 1165 (s), 1133 (m), 1107 (m), 1078 (m), 1039 (s); **^{1}H NMR** (400 MHz, $CDCl_3$) δ: 7.71 (d, *J* = 8.8 Hz, 2 H), 7.42 (d, *J* = 8.9 Hz, 1 H), 7.26 (d, *J* = 2.3 Hz, 1 H), 7.19 – 7.15 (m, 2 H), 6.88 – 6.85 (m, 3 H), 6.63 – 6.59 (m, 2 H), 4.16 (t, *J* = 5.1 Hz, 2 H), 3.15 (t, *J* = 5.1 Hz, 2 H), 2.88 (q, *J* = 7.3 Hz, 2 H), 1.21 (t, *J* = 7.3 Hz, 3 H); **^{13}C NMR** (101 MHz, $CDCl_3$) δ: 194.1 (C=O), 162.7, 157.9, 155.4, 142.7, 140.0, 132.8, 132.1, 130.8, 130.0, 129.7, 124.6, 123.3, 115.1, 114.7, 113.9, 106.5, 65.2, 47.9, 43.1, 11.7.

Data are in accordance with those reported previously in literature.[317]

(2*S*,4*R*)-1-((*S*)-2-(4-((*Z*)-(4-(ethyl(2-(4-(6-hydroxy-2-(4-hydroxyphenyl)benzo[*b*]thiophene-3-carbonyl)phenoxy)ethyl)carbamoyl)-2,6-difluorophenyl)diazenyl)-3,5-difluorobenzamido)-3,3-dimethylbutanoyl)-4-hydroxy-*N*-(4-(4-methylthiazol-5-yl)benzyl)pyrrolidine-2-carboxamide (azoPROTAC4)

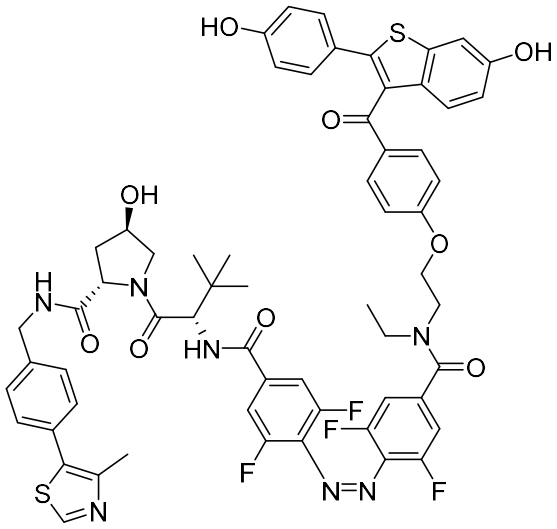

To a stirring solution of **195** (7 mg, 0.0089 mmol) in a mixture of THF and H_2O (2:1, 1 mL) was added lithium hydroxide (0.7 mg, 0.0178 mmol). The reaction was stirred at r.t. for 3 h before acidifying to

pH 3 with 1 M HCl and extracting into EtOAc (3 x 10 mL). The combined organics were washed with brine (5 mL), dried over Na_2SO_4, filtered, and concentrated *in vacuo*. The crude residue was directly dissolved in DMF (0.2 mL) and cooled to 0 °C, before HATU (4.4 mg, 0.0116 mmol) and DIPEA (2.0 µL, 0.0116 mmol) were added. The reaction mixture was stirred for 15 mins before **219** (5.0 mg, 0.0116 mmol) was added. The mixture was then warmed to r.t. and stirred for a further 16 h before diluting in water (5 mL) and extracting into EtOAc (3 x 10 mL). The combined organics were then washed with brine (2 x 5 mL), before being dried over Na_2SO_4, filtered and concentrated *in vacuo*. The residue was purified through silica gel column chromatography (5% MeOH/DCM) to give the title compound as a red amorphous solid (3.5 mg, 35%).

R_f: 0.25 (5% MeOH/DCM); Mixture of cis and trans isomers, only major reported; **^{1}H NMR** (500 MHz, MeOD) δ : 7.82 – 7.38 (m, 10 H), 7.29 – 7.00 (m, 5 H), 6.91 – 6.80 (m, 3 H), 6.65 – 6.58 (m, 2 H), 4.65 – 4.50 (m, 4 H), 4.42 – 4.23 (m, 2 H), 4.16 – 3.70 (m, 5 H), 3.56 – 3.42 (m, 2 H), 2.47 (s, 3 H), 2.27 – 2.03 (m , 2 H), 1.19 – 1.06 (m, 12 H); **^{13}C NMR** (126 MHz, MeOD) δ : 194.2, 173.0, 170.5, 168.8, 165.1, 161.9, 157.8, 155.4, 155.3 (dd, *J* = 260, 4 Hz, C-F), 154.9 (dd, *J* = 260, 4 Hz, C-F), 151.4, 150.1, 147.6, 142.8, 140.0, 138.9, 132.9, 132.1, 131.9, 130.1, 130.0, 129.8, 129.2, 129.0, 128.9, 128.1, 127.8, 127.5, 124.6, 123.4, 115.0, 114.7, 113.9, 111.9 – 111.7 (m, 1C), 106.4, 70.1, 69.7, 67.5, 59.5, 58.5, 56.8, 45.2, 42.3, 37.6, 35.8, 25.6, 14.4, 13.0; **^{19}F NMR (**376 MHz, MeOD) δ : -74.0 (m), -121.2 (m); **HRMS (ESI):** m/z calcd for $C_{61}H_{56}F_4N_7O_9S_2$ $[M+H]^+$: 1170.3512; Found: 1170.3513.

4-Fluoroisobenzofuran-1,3-dione (225)

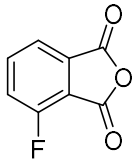

Following a reported procedure;[361] a stirring solution of 3-fluorophthalic acid (0.500 g, 2.7 mmol) in acetic anhydride (4 mL) was refluxed at 140 °C for 2 h. The reaction mixture was then concentrated *in vacuo* to give the title compound as an off-white amorphous solid (0.448 g, 90%).

^{1}H NMR (400 MHz, $CDCl_3$) δ: 7.97 – 7.92 (m, 1H), 7.85 (d, *J* = 7.7 Hz, 1 H), 7.57 (t, *J* = 8.6 Hz, 1 H); **^{13}C NMR** (101 MHz, $CDCl_3$) δ: 161.6 (d, *J* = 2.9 Hz, C=O), 158.8 (d, *J* = 2.2 Hz, C=O), 158.5 (d, *J* = 275 Hz, C-F), 139.0 (d, *J* = 7.7 Hz), 133.3, 124.0 (d, *J* = 19 Hz), 122.0 (d, *J* = 4.2 Hz), 117.7 (d, *J* = 13.4 Hz); **^{19}F NMR (**376 MHz, $CDCl_3$) δ : -108.4.

Data are in accordance with those reported previously in literature.[361]

2-(2,6-dioxopiperidin-3-yl)-4-fluoroisoindoline-1,3-dione (223)

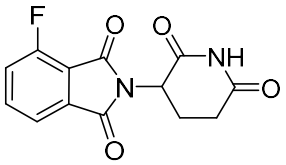

Following a reported procedure;[362] to a stirring solution of **225** (50 mg, 0.3 mmol) in acetic acid (1 mL) were added *rac*-*α*-aminoglutarimide hydrochloride (54.3 mg, 0.33 mmol) and potassium acetate (91.1 mg, 0.95 mmol). The reaction mixture was heated to 90 °C and stirred for 15 h. The reaction was then cooled to r.t., diluted with H_2O (5 mL), extracted into EtOAc (3 x 10 mL), washed with brine (5 mL), dried over Na_2SO_4, filtered and concentrated *in vacuo*. The residue was purified through silica gel column chromatography (1% MeOH/DCM) to give the title compound as a white amorphous solid (80 mg, 96%).

R_f: 0.57 (5% MeOH/DCM); **IR** (neat film, ν_{max}, cm^{-1}): 3275 (w, NH), 3087 (w, CH), 2920 (w, CH), 1779 (m, C=O), 1703 (s, C=O), 1623 (m), 1610 (m), 1479 (m), 1384 (s), 1350 (m), 1327 (m), 1300 (m), 1256 (s), 1199 (s), 1115 (m), 1018 (m); **^{1}H NMR** (400 MHz, d-DMSO) δ: 11.13 (s, 1 H, NH), 7.96 – 7.91 (m, 1 H), 7.77 (d, *J* = 7.4 Hz, 1 H), 7.72 (t, *J* = 9.1 Hz, 1 H), 5.14 (dd, *J* = 12.8, 5.5 Hz, 1 H), 2.92 -2.83 (m, 1 H), 2.61 – 2.54 (m, 1 H), 2.52 – 2.44 (m, 1 H, overlapping DMSO), 2.07 – 2.03 (m, 1 H); **^{13}C NMR** (101 MHz, d-DMSO) δ: 173.2, 170.1, 166.6 (d, *J* = 3 Hz), 164.4, 157.3 (d, *J* = 260 Hz, C-F), 138.5 (d, *J* = 7.9 Hz), 133.9 (d, *J* = 1.5 Hz), 123.5 (d, *J* = 19 Hz), 120.5 (d, *J* = 3.8 Hz), 117.5 (d, *J* = 12 Hz), 49.5, 31.3, 22.3; **^{19}F NMR (**376 MHz, $CDCl_3$) δ : -114.7.

Data are in accordance with those reported previously in literature.[363]

***tert*-Butyl (2-((2-(2,6-dioxopiperidin-3-yl)-1,3-dioxoisoindolin-4-yl)amino)ethyl)carbamate (227)**

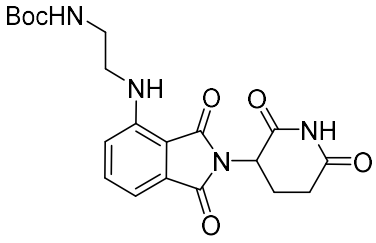

Following a reported procedure;[364] to a stirring solution of **223** (25 mg, 0.091 mmol) in DMF (0.5 mL) were added *N*-Boc-ethylenediamine (16 mg, 0.010 mmol) and DIPEA (31.5 µL, 0.181 mmol). The reaction mixture was heated to 90 °C and stirred for 15 h. The reaction was then cooled to r.t., diluted with H_2O (5 mL), extracted into EtOAc (3 x 10 mL), washed with brine (5 mL), dried over Na_2SO_4, filtered and concentrated *in vacuo*. The residue was purified through silica gel column chromatography (30 to 50% EtOAc/PE 40-60) to give the title compound as a yellow amorphous solid (22 mg, 58%).

R_f: 0.28 (1:1 PE 40-60/EtOAc); **IR** (neat film, ν_{max}, cm^{-1}): 3365 (w, NH), 3000 (w, CH), 1732 (m, C=O), 1714 (s, C=O), 1697 (s, C=O), 1623 (m), 1511 (m), 1482 (w), 1408 (m), 1368 (m), 1320 (m), 1290 (m), 1260 (m), 1209 (m), 1171 (m), 1131 (m), 1111 (m), 1080 (m), 1022 (m); **^{1}H NMR** (400 MHz, d6-DMSO) δ: 11.07 (s, 1 H, NH), 7.56 (t, *J* = 7.7 Hz, 1 H), 7.12 (d, *J* = 8.7 Hz, 1 H), 7.02 – 6.97 (m, 2 H), 6.69 (t, *J* = 6.2 Hz, 1 H, NH), 5.03 (dd, *J* = 12.8, 5.6 Hz, 1 H), 3.40 – 3.33 (m, 2 H, overlapping H_2O), 3.10 (q, *J* = 5.6 Hz, 2 H), 2.91 – 2.82 (m, 1 H), 2.65 – 2.44 (m, 2 H, overlapping DMSO), 2.04 – 1.96 (m, 1 H), 1.34 (s, 9 H, 3x CH_3); **^{13}C NMR** (101 MHz, d6-DMSO) δ: 173.3, 170.5, 169.2, 167.8, 156.3, 146.8, 136.6, 132.7, 117.5, 110.9, 109.7, 78.2, 49.0, 42.0, 40.1, 31.4, 28.6, 22.6.

Data are in accordance with those reported previously in literature.[364]

tert-Butyl (1-(2-(2,6-dioxopiperidin-3-yl)-1,3-dioxoisoindolin-4-yl)azetidin-3-yl)carbamate (228)

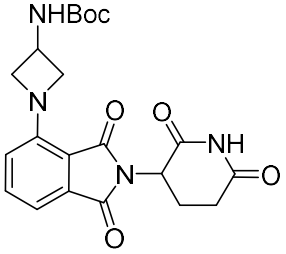

To a stirring solution of **223** (50 mg, 0.181 mmol) in DMF (1 mL) were added *tert*-butyl *N*-(azetidin-3-yl)carbamate hydrochloride (41.6 mg, 0.199 mmol) and DIPEA (101 µL, 0.579 mmol). The reaction mixture was heated to 90 °C and stirred for 15 h. The reaction was then cooled to r.t., diluted with H_2O (5 mL), extracted into EtOAc (3 x 10 mL), washed with brine (5 mL), dried over Na_2SO_4, filtered and concentrated *in vacuo*. The residue was purified through silica gel column chromatography (1:1 EtOAc/PE 40-60) to give the title compound as a yellow amorphous solid (77 mg, >98%).

R_f: 0.23 (1:1 PE 40-60/EtOAc); **IR** (neat film, ν_{max}, cm^{-1}): 2929 (w, CH), 1701 (s, C=O), 1618 (w), 1575 (w), 1542 (w), 1489 (m), 1470 (m), 1396 (m), 1364 (m), 1323 (m), 1260 (m), 1197 (m), 1163 (m), 1121 (m), 1065 (w), 1032 (w); **^{1}H NMR** (400 MHz, d6-DMSO) δ: 11.13 (s, 1 H), 7.58 – 7.54 (m, 2 H), 7.11 (d, *J* = 7.0 Hz, 1 H), 6.77 (d, *J* = 8.4 Hz, 1 H), 5.04 (dd, *J* = 12.8, 5.5 Hz, 1 H), 4.43 – 4.40 (m, 2 H), 4.36 – 4.32 (m, 1 H), 3.95 – 3.92 (m, 2 H), 2.90 – 2.82 (m, 1 H), 2.59 – 2.52 (m, 2 H), 2.00 – 1.96 (m, 1 H), 1.38 (s, 9 H); **^{13}C NMR** (101 MHz, d6-DMSO) δ: 173.3, 170.5, 167.6, 166.9, 155.4, 148.1, 135.4, 133.7, 120.6, 112.3, 110.7, 78.7, 61.3, 49.1, 41.0, 31.4, 28.6, 22.5.

Data are in accordance with those reported previously in literature.[365]

***tert*-Butyl 4-(2-(2,6-dioxopiperidin-3-yl)-1,3-dioxoisoindolin-4-yl)piperazine-1-carboxylate (229)**

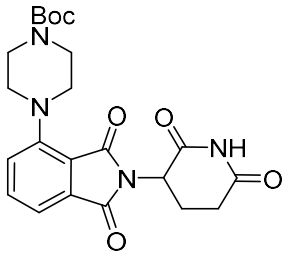

To a stirring solution of **223** (25 mg, 0.091 mmol) in DMF (0.5 mL) were added 1-Boc-piperazine (16 mg, 0.010 mmol) and DIPEA (31.5 µL, 0.181 mmol). The reaction mixture was heated to 90 °C and stirred for 15 h. The reaction was then cooled to r.t., diluted with H_2O (5 mL), extracted into EtOAc (3 x 10 mL), washed with brine (5 mL), dried over Na_2SO_4, filtered and concentrated *in vacuo*. The residue was purified through silica gel column chromatography (30 to 50% EtOAc/PE 40-60) to give the title compound as a yellow amorphous solid (34 mg, 84%).

R_f: 0.24 (1:1 PE 40-60/EtOAc); **IR** (neat film, ν_{max}, cm^{-1}): 2915 (w, CH), 1699 (s, C=O), 1616 (w), 1540 (w), 1403 (m), 1362 (m), 1329 (m), 1267 (m), 1243 (m), 1197 (m), 1174 (m), 1131 (m), 1041 (m), 1006 (m); **^{1}H NMR** (400 MHz, d6-DMSO) δ: 11.08 (s, 1 H), 7.70 (t, *J* = 7.4 Hz, 1 H), 7.38 – 7.32 (m, 2 H), 5.11 – 5.06 (m, 1 H), 3,49 (br s, 4 H), 3,23 (br s, 3 H), 2.91 – 2.80 (m, 1 H), 2.60 – 2.52 (m, 2 H), 2.02 – 1.99 (m, 1 H), 1.41 (s, 9 H); **^{13}C NMR** (101 MHz, d6-DMSO) δ: 173.3, 170.4, 167.5, 166.8, 154.3, 150.0, 136.4, 134.0, 124.4, 117.4, 115.7, 79.5, 50.8, 49.3, 43.4, 31.4, 28.5, 22.5.

Data are in accordance with those reported previously in literature.[366]

4-((2-aminoethyl)amino)-2-(2,6-dioxopiperidin-3-yl)isoindoline-1,3-dione (220)

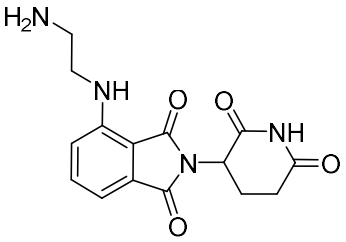

To a stirring solution of **227** (18 mg, 0.043 mmol) in dichloromethane (0.5 mL) was added trifluoroacetic acid (0.5 mL). The reaction was stirred for 3 h at r.t. before being concentrated, diluted with sat. aq. $NaHCO_3$ (2 mL), extracted into dichloromethane (3 x 10 mL), dried over Na_2SO_4, filtered, and concentrated *in vacuo* to give the title compound as a yellow oil (14 mg, >98%)

R_f: 0.35 (1:9:0.1 MeOH/DCM/NEt_3); **IR** (neat film, ν_{max}, cm^{-1}): 3383 (w, NH), 2976 (w, CH), 2917 (w, CH), 1720 (m, C=O), 1697 (s, C=O), 1626 (m), 1604 (m), 1513 (m), 1464 (m), 1405 (m), 1360 (m), 1325 (m),

1256 (m), 1198 (m), 1164 (m), 1110 (m), 1086 (m), 1042 (m), 1020 (m); **^{1}H NMR** (400 MHz, MeOD) δ: 7.58 (t, *J* = 7.9 Hz, 1 H), 7.13 – 7.09 (m, 2 H), 5.06 (dd, *J* = 13, 5.8 Hz, 1 H), 3.54 (t, *J* = 6.5 Hz, 2 H), 3.34 (s, 2 H), 3.02 (t, *J* = 6.5 Hz, 2 H), 2.91 – 2.66 (m, 3 H), 2.14 – 2.07 (m, 1 H); **^{13}C NMR** (101 MHz, MeOD) δ: 173.2, 170.3, 169.2, 167.8, 146.4, 135.6, 132.6, 116.5, 111.1, 110.6, 48.8, 42.0, 39.3, 30.8, 22.4.

Data are in accordance with those reported previously in literature.[364]

5.4. General Biological procedures

5.4.1. Cell proliferation assay protocol

LNCaP and PC3 cells were grown in Roswell Park Memorial Institute 1640 (RPMI-1640) medium with 10% fetal calf serum (FCS) and 1% glutamax. The cells were seeded in a 96-well black-walled clear flat-bottom polystyrene plate (2,000 cells/well) and incubated at 37 °C in a 5% CO_2 atmosphere for 24 h. The two cell lines were treated with varying concentrations of PROTACs (from 10 mM stock solution in DMSO) in triplicate for five days in RPMI-1640 with 10% FCS and 1% glutamax, and a final DMSO concentration of 1%. The plates were monitored using an Essen Bioscience Incucyte live-cell analysis system which analysed the plates every 4 h to calculate pIC_{50} values based on confluence.

5.4.2. CETSA protocol for AR degradation assay run with Dr Joseph Shaw

This protocol was run as previously reported.[174] LNCaP cells were grown in RPMI-1640 medium with L-glutamine and 10% FCS. PROTACs (from 10 mM stock solution in DMSO) in triplicate were dosed into 384-well PCR plate using a hp Tecan D3000e digital dispenser. LNCaP cells were seeded to 3.5 x 10^7 cells/mL and 5 µL was added to each well using a Multidrop Combi dispenser. The plate was incubated for either 1 h or 4.5 h, and then AR levels were quantified using AlphaScreen® technology as follows. 2x SureFire Lysis Buffer (20 µL/well) was added and following 10 mins incubation, samples were briefly clarified. Samples were mixed and 3 µL of lysate was transferred to a 384-well ProxiPlate. A solution of 1x ImmunoAssay Buffer was prepared containing 0.08 µg/mL Dako Mouse anti-AR antibody, 0.15 µg/mL Merck Millipore Rabbit anti-AR antibody, 120 µg/mL Anti-mouse IgG Alpha Donor beads and 30 µg/mL Anti-rabbit IgG AlphaLISA Acceptor beads. 6 µL of this solution was added to the lysate in the ProxiPlate under subdued light. The plate was then sealed and incubated for 16 h in the dark before analysis using an EnVision plate reader. Data was plotted in GraphPad Prism 6 to fit a nonlinear regression and determine 50% effective concentrations (EC_{50}) by Dr Joseph Shaw.

5.4.3. Expression and purification of MDM2 (6-125) with Rohan Eapen

As previously reported.[367] A gene encoding for MDM2 (6-125) was cloned into a pRSETa vector. The plasmid was transformed into the *E. coli* expression cell line, C41(DE3). Colonies were picked and grown in 2xYT medium (Formedium), supplemented with ampicillin (50 µg/ mL) at 37 °C, and shaken at 180 rpm in an orbital incubator until an OD600 = 0.6 was achieved. Cultures were then induced with 0.5 mM IPTG, and the temperature was lowered to 25 °C for overnight incubation. Cells were pelleted and resuspended in lysis buffer (50 mM Tris-HCl, 500 mM NaCl, 20 mM Imidazole, 1 mM DTT, 0.1% (v/v) Tween 20, 1 SigmaFAST EDTA-free protease inhibitor (Sigma), pH 8.5). Lysozyme and DNase were added, and cells were lysed by sonication on ice (20 cycles, 10 seconds on, 10 seconds off). Lysate was centrifuged at 40000 x g for 1 h at 4 °C. Supernatant containing the His-tagged protein was diluted to 100 mL with buffer A (20 mM Tris-HCl, 500 mM NaCl, 1 mM DTT, pH 8.5) and loaded onto a 5 mL HisTrap Excel column. The column was washed with 20 column volumes (CV) of buffer A + 20 mM Imidazole and then eluted in 5 CV of buffer B (20 mM Tris-HCl, 500 mM NaCl, 500 mM Imidazole, 1 mM DTT, pH 8.5). Eluted proteins were desalted using a Centripure P25 column (Generon) into phosphate buffered saline (PBS) + 1 mM DTT, pH 7.4. 100 units of thrombin (Sigma, T4648) were added to the desalted protein and allowed to cleave overnight at 4 °C. Protein was then diluted with buffer C (20 mM Bis-Tris, 1mM DTT, pH 6.5) to approximately 30 mM NaCl in the protein sample. Protein was then loaded onto a MonoS column and eluted with a linear gradient over 20 CV using buffer D (20 mM Bis-Tris, 1 M NaCl, 1mM DTT, pH 6.5). Eluted protein fractions were pooled and analysed for purity by SDS PAGE and the correct mass was confirmed by mass spectrometry.

5.4.4. Competition fluorescence polarisation procedure

Competition fluorescence polarisation was carried out using MDM2 and a 5-TAMRA-labelled tracer peptide in a similar fashion as previously described.[175] The dissociation constant of the tracer peptide was previously described by Lau *et al*.[175]. Stock solutions of small molecule/peptide inhibitors in DMSO (50/10 mM) were diluted in assay buffer (1 × PBS + 0.01% (v/v) Tween 20 + 3% (v/v) DMSO) to a top concentration of 3 mM for small molecules and 10 µM for peptides, then 2/3-fold serial dilutions were made to give a 20-point titration. A stock solution of FP tracer (1 mM) was diluted in assay buffer to a concentration of 200 nM (final assay concentration of 50 nM). MDM2 was diluted in assay buffer to a concentration of 380 nM (final assay concentration of 95 nM). Dilutions of small molecule/peptide inhibitors (20 µL), FP tracer (10 µL) and MDM2 (10 µL) were added to a 384-well plate (OptiPlate™ - 384 F, Perkin Elmer) and incubated at r.t. for 1 hour. Titrations were conducted in triplicate. Fluorescence polarisation was measured using a BMG ClarioStar plate reader using an excitation filter

at 540 nm and emission filter at 590 nm, with a 20 nm bandwidth. Graphs were plotted using GraphPad Prism 7.0 and analysed using the following equation:

$$r = r_0 + (r_b + r_0) \times \frac{2\sqrt{(d^2 - 3e}\cos(\theta/3) - 9}{3K_{d1} + 2\sqrt{(d^2 - 3e)}\cos(\theta/3) - d}$$

$$d = K_{d1} + K_{d2} + [L]_{st} + [L]_t - [P]_t$$

$$e = K_{d1}([L]_t - [P]_t) + K_{d2}([L]_{st} - [P]_t) + K_{d1}K_{d2}$$

$$\theta = \cos^{-1}\left(\frac{-2d^3 + 9de - 27f}{2\sqrt{(d^2 - 3e)^3}}\right)$$

$$f = -K_{d1}K_{d2}[P]_t$$

Where, r is anisotropy measured, r_0 is anisotropy of free peptide, r_b is anisotropy of MDM2:5-TAMRA peptide complex, K_{d1} is apparent dissociation constant of 5-TAMRA peptide to MDM2, K_{d2} is dissociation constant of non-labelled ligand to MDM2, $[P]_t$ is MDM2 concentration, $[L]_t$ is non-labelled ligand concentration and $[L]_{st}$ is 5-TAMRA peptide concentration.

5.4.5. CETSA protocol for target engagement run by Dr Joseph Shaw

This protocol was run as previously reported.[174] Using the same LNCaP cell-line, dosing procedure, and endpoint as previously described for the CETSA AR degradation assay with the following modifications. For the antagonist binding mode: following the PROTAC dosing, a 2x DHT dose response (1 nM total concentration) was prepared in media and 5 µL was added to each well. Following the assay time-course, both agonist and antagonist binding modes were heat shocked at 46 °C for 3 mins, followed by a 3 mins cool at 25 °C using a Veriti SimpliAmp (ThermoFisher) prior to addition of SureFire Lysis Buffer and subsequent AlphaScreen® endpoint read-out and analysis previously described.

5.4.6. Differential Scanning Fluorimetry (DSF) with Rohan Eapen

For computationally predicted MDM2 binders: stock solutions of small molecules in DMSO (50 mM) were diluted to concentrations of 5 mM, 1 mM and 200 µM in assay buffer (1 × PBS + 0.01% (v/v) Tween 20 + 10% (v/v) DMSO). **For literature MDM2 binders**: stock solutions of small molecules in

DMSO (20 mM) were diluted to concentrations of 800 µM, 400 µM and 200 µM in assay buffer (1 × PBS + 0.01% (v/v) Tween 20 + 10% (v/v) DMSO).

A combined solution of MDM2 and SYPRO-Orange (Thermo Fisher) was prepared by diluting stock MDM2 and SYPRO-Orange in assay buffer to a concentration of 40 µM and 10x respectively (final assay concentration of 20 µM and 5x). Stocks of small molecules (10 µL), and SYPRO-Orange/MDM2 (10 µL) were diluted into a 96-well plate. Each sample was run in triplicate. Thermal melt curves were attained using a Bio-Rad CFX Connect, measuring fluorescence intensity at 568 nm over a temperature range of 25 – 95 °C at a step ramp rate of 0.5 °C per 30 seconds. Fluorescence intensity curves were plotted and analysed using GraphPad Prism 7.0 software to determine the melting temperature (T_m) of each thermal ramp using the following equation.

$$Y = A + \frac{B - A}{1 + e^{\left(\frac{-H}{R}\right)\times\left(\frac{1}{x}-\frac{1}{t}\right)+\left(\frac{C}{R}\times\ln\left(\frac{x}{t}\right)+\frac{t}{x}-1\right)}}$$

Where, *Y* is the observed fluorescence intensity of SYPRO Orange, *A* is the fluorescence intensity of SYPRO-Orange in the presence of non-native protein, *B* is the fluorescence intensity of SYPRO-Orange in the presence of native protein, *H* is the enthalpy of protein unfolding, *C* is the heat capacity of protein unfolding, *R* is the gas constant (8.314 J.mol^{-1}) and *t* is the melting temperature (T_m). Data are plotted as the average ΔT_m of MDM2 with each small molecule compound, at their respective concentrations compared to apo MDM2 (5% (v/v) DMSO).

5.4.7. AR degradation by AlphaScreen® of MDM2 PROTACs run by Dr Andreas Hock

Using a very similar method to the CETSA AlphaScreen® AR degradation protocol previously described. LNCaP cells were grown in RPMI-1640 medium with L-glutamine and 10% FCS. PROTACs (from 10 mM stock solution in DMSO) in triplicate were dosed into 384-well PCR plates using a hp Tecan D3000e digital dispenser. LNCaP cells were seeded to 7,500 cells/well using a Multidrop Combi dispenser. The plates were incubated for 16 h and the endogenous AR levels were quantified using AlphaScreen® technology and fitted using GraphPad Prism 6 as previously described, to give qAC_{50} values corresponding to 50% AR degradation.

5.4.8. AR degradation imaging assay run by Dr Andreas Hock

LNCaP cells were grown in RPMI-1640 medium containing 10% FCS and 1% glutamine. Cells were plated on Perkin-Elmer 384-well Cell Carrier Ultra plates at 12,000 cells per well (40 µL). PROTACs

(from 10 mM stock solution in DMSO) were dosed using Echo 555 dispenser, and the plates incubated for 16 h before fixing with 4% paraformaldehyde (final concentration) for 30 mins and stained for AR and FKBP5 as follows. The plates were washed 3 x with PBS using a Biotek washer before incubating with anti-AR N terminal (mouse) antibody (1:1000), diluted in modified blocking buffer for 2 h at r.t. The plates were then washed with PBS and incubated with anti-mouse secondary antibody- 488 (1:500) and DRAQ5 (1:2000) diluted in modified blocking buffer for 45 mins at r.t. Finally, the plates were washed with 3 x PBS and sealed with black plate seals. The plates were imaged on the CellInsight and analysed using Columbus and Genedata software by Dr Andreas Hock.

5.4.9. Photoswitchable PROTAC AR degradation protocol run with Dr Andreas Hock

Using the same protocol as described previously with minor modifications. LNCaP cells were grown in RPMI-1640 medium containing 10% FCS and 1% glutamine. Cells were plated on Perkin-Elmer 384-well Cell Carrier Ultra plates at 12,000 cells per well (40 µL).

For azoPROTAC1: PROTAC (10 mM stock solution in DMSO) was dosed at top concentration of 30 µM generating a 7-point dose response curve. After dosing, the plate was then irradiated with either 415 nm or 530 nm Thorlab mounted LEDs for 10 mins and the plate incubated for 24 h prior to fixing, staining and analysing on the CellInsight as described previously.

For azoPROTAC1 and azoPROTAC2: PROTAC (10 mM stock solution in DMSO) was irradiated with 530 nm LEDs for 30 mins prior to being dosed on the assay plate at a top concentration of 30 µM, to generate a 14-point two-fold dilution dose-response curve. The 530 nm irradiated plates were directly placed in a dark incubator after dosing, whilst the remaining plates were irradiated for 10 mins with 415 nm LEDs. The plates were then incubated for 6 h, before being fixed and stained as described previously.

6. References

1 A. Hershko, *Angew. Chemie - Int. Ed.*, 2005, **44**, 5932–5943.

2 A. Hershko and G. Tomkins, *Biol. Chem.*, 1971, **246**, 710–714.

3 A. Ciehanover, Y. Hod and A. Hershko, *Biochem. Biophys. Res. Commun.*, 1978, **81**, 1100–1105.

4 K. D. Wilkinson, M. K. Urban and A. L. Haas, *J. Biol. Chem.*, 1980, **255**, 7529–7532.

5 A. Hershko, A. Ciechanover, H. Heller, A. L. Haas and I. A. Rose, *Proc. Natl. Acad. Sci.*, 1980, **77**, 1783–1786.

6 A. Ciechanover, H. Heller, R. Katz-Etzion and A. Hershko, *Proc. Natl. Acad. Sci.*, 1981, **78**, 761–765.

7 A. Hershko, A. Ciechanover and I. A. Rose, *J. Biol. Chem.*, 1981, **256**, 1525–1528.

8 A. Hershko, H. Heller, S. Elias and A. Ciechanover, *J. Biol. Chem.*, 1983, **258**, 8206–8214.

9 A. Hershko, H. Heller, E. Eytan and Y. Reiss, *J. Biol. Chem.*, 1986, **261**, 11992–11999.

10 A. Hershko, *J. Biol. Chem.*, 1988, **263**, 15237–15240.

11 D. L. Buckley and C. M. Crews, *Angew. Chemie - Int. Ed.*, 2014, **53**, 2312–2330.

12 A. Hershko and A. Ciechanover, *Annu. Rev. Biochem.*, 1998, **67**, 425–479.

13 M. Toure and C. M. Crews, *Angew. Chemie - Int. Ed.*, 2016, **55**, 1966–1973.

14 J. S. Schneekloth and C. M. Crews, *ChemBioChem*, 2005, **6**, 40–46.

15 K. M. Sakamoto, K. B. Kim, A. Kumagai, F. Mercurio, C. M. Crews and R. J. Deshaies, *Proc. Natl. Acad. Sci. U. S. A.*, 2001, **98**, 8554–9.

16 K. M. Sakamoto, *Mol. Cell. Proteomics*, 2003, **2**, 1350–1358.

17 J. S. Schneekloth, F. N. Fonseca, M. Koldobskiy, A. Mandal, R. Deshaies, K. Sakamoto and C. M. Crews, *J. Am. Chem. Soc.*, 2004, **126**, 3748–3754.

18 A. R. Schneekloth, M. Pucheault, H. S. Tae and C. M. Crews, *Bioorg. Med. Chem. Lett.*, 2008, **18**, 5904–5908.

19 T. W. Corson, N. Aberle and C. M. Crews, *ACS Chem. Biol.*, 2008, **3**, 677–692.

20 T. K. Neklesa, J. D. Winkler and C. M. Crews, *Pharmacol. Ther.*, 2017, **174**, 138–144.

21 D. L. Buckley, K. Raina, N. Darricarrere, J. Hines, J. L. Gustafson, I. E. Smith, A. H. Miah, J. D. Harling and C. M. Crews, *ACS Chem. Biol.*, 2015, **10**, 1831–1837.

22 G. E. Winter, D. L. Buckley, J. Paulk, J. M. Roberts, A. Souza, S. Dhe-Paganon and J. E. Bradner, *Science*, 2015, **348**, 1376–1381.

23 J. Lu, Y. Qian, M. Altieri, H. Dong, J. Wang, K. Raina, J. Hines, J. D. Winkler, A. P. Crew, K. Coleman and C. M. Crews, *Chem. Biol.*, 2015, **22**, 755–763.

24 D. P. Bondeson, A. Mares, I. E. D. Smith, E. Ko, S. Campos, A. H. Miah, K. E. Mulholland, N. Routly, D. L. Buckley, J. L. Gustafson, N. Zinn, P. Grandi, S. Shimamura, G. Bergamini, M. Faelth-Savitski, M. Bantscheff, C. Cox, D. A. Gordon, R. R. Willard, J. J. Flanagan, L. N. Casillas, B. J. Votta, W. den Besten, K. Famm, L. Kruidenier, P. S. Carter, J. D. Harling, I. Churcher and C. M. Crews, *Nat. Chem. Biol.*, 2015, **11**, 611–617.

25 B. Zhou, J. Hu, F. Xu, Z. Chen, L. Bai, E. Fernandez-Salas, M. Lin, L. Liu, C.-Y. Yang, Y. Zhao, D. McEachern, S. Przybranowski, B. Wen, D. Sun and S. Wang, *J. Med. Chem.*, 2018, **61**, 2, 462-481.

26 C. P. Tinworth, H. Lithgow, L. Dittus, Z. I. Bassi, S. E. Hughes, M. Muelbaier, H. Dai, I. E. D. Smith, W. J. Kerr, G. A. Burley, M. Bantscheff and J. D. Harling, *ACS Chem. Biol.*, 2019, **14**, 342–347.

27 G. Xue, J. Chen, L. Liu, D. Zhou, Y. Zuo, T. Fu and Z. Pan, *Chem. Commun.*, 2020, **56**, 1521-1524.

28 A. Testa, S. J. Hughes, X. Lucas, J. E. Wright and A. Ciulli, *Angew. Chemie Int. Ed.*, 2020, **59**, 1727–1734.

29 C. Maniaci, S. J. Hughes, A. Testa, W. Chen, D. J. Lamont, S. Rocha, D. R. Alessi, R. Romeo and A. Ciulli, *Nat. Commun.*, 2017, **8**, 830.

30 M. Girardini, C. Maniaci, S. J. Hughes, A. Testa and A. Ciulli, *Bioorg. Med. Chem.*, 2019, **27**, 2466–2479.

31 Y. Wang, X. Jiang, F. Feng, W. Liu and H. Sun, *Acta Pharm. Sin. B*, 2020, **10**, 2, 207-238.

32 H. Pei, Y. Peng, Q. Zhao and Y. Chen, *RSC Adv.*, 2019, **9**, 16967–16976.

33 Y. Zou, D. Ma and Y. Wang, *Cell Biochem. Funct.*, 2019, **37**, 21–30.

34 M. S. Gadd, A. Testa, X. Lucas, K.-H. Chan, W. Chen, D. J. Lamont, M. Zengerle and A. Ciulli, *Nat. Chem. Biol.*, 2017, **13**, 514–521.

35 D. P. Bondeson, B. E. Smith, G. M. Burslem, A. D. Buhimschi, J. Hines, S. Jaime-Figueroa, J. Wang,

B. D. Hamman, A. Ishchenko and C. M. Crews, *Cell Chem. Biol.*, 2018, **25**, 78-87.e5.

36 C. M. Olson, B. Jiang, M. A. Erb, Y. Liang, Z. M. Doctor, Z. Zhang, T. Zhang, N. Kwiatkowski, M. Boukhali, J. L. Green, W. Haas, T. Nomanbhoy, E. S. Fischer, R. A. Young, J. E. Bradner, G. E. Winter and N. S. Gray, *Nat. Chem. Biol.*, 2018, **14**, 163–170.

37 G. M. Burslem, B. E. Smith, A. C. Lai, S. Jaime-Figueroa, D. C. McQuaid, D. P. Bondeson, M. Toure, H. Dong, Y. Qian, J. Wang, A. P. Crew, J. Hines and C. M. Crews, *Cell Chem. Biol.*, 2018, **25**, 67-77.e3.

38 D. A. DeGoey, H.-J. Chen, P. B. Cox and M. D. Wendt, *J. Med. Chem.*, 2018, **61**, 2636–2651.

39 X. Sun, J. Wang, X. Yao, W. Zheng, Y. Mao, T. Lan, L. Wang, Y. Sun, X. Zhang, Q. Zhao, J. Zhao, R.-P. Xiao, X. Zhang, G. Ji and Y. Rao, *Cell Discov.*, 2019, **5**, 10.

40 S. D. Edmondson, B. Yang and C. Fallan, *Bioorg. Med. Chem. Lett.*, 2019, **29**, 1555–1564.

41 L. Zhang, B. Riley-Gillis, P. Vijay and Y. Shen, *Mol. Cancer Ther.*, 2019, **18**, 1302-1311.

42 J. Ferlay, I. Soerjomataram, R. Dikshit, S. Eser, C. Mathers, M. Rebelo, D. M. Parkin, D. Forman and F. Bray, *Int. J. Cancer*, 2015, **136**, E359–E386.

43 W. Gao, C. E. Bohl and J. T. Dalton, *Chem. Rev.*, 2005, **105**, 3352–3370.

44 M. E. Tan, J. Li, H. E. Xu, K. Melcher and E. Yong, *Acta Pharmacol. Sin.*, 2015, **36**, 3–23.

45 I. D. Cockshott, *Clin. Pharmacokinet.*, 2004, **43**, 855–878.

46 V. Pelekanou and E. Castanas, *J. Cell. Biochem.*, 2016, **2234**, 2224–2234.

47 T. Chandrasekar, J. C. Yang, A. C. Gao and C. P. Evans, *Transl. Androl. Urol.*, 2015, **4**, 365–80.

48 T. Visakorpi, E. Hyytinen, P. Koivisto, M. Tanner, R. Keinänen, C. Palmberg, a Palotie, T. Tammela, J. Isola and O. P. Kallioniemi, *Nat. Genet.*, 1995, **9**, 401–406.

49 Q. Wang, W. Li, Y. Zhang, X. Yuan, K. Xu, J. Yu, Z. Chen, R. Beroukhim, H. Wang, M. Lupien, T. Wu, M. M. Regan, C. A. Meyer, J. S. Carroll, A. K. Manrai, O. A. Jänne, S. P. Balk, R. Mehra, B. Han, A. M. Chinnaiyan, M. A. Rubin, L. True, M. Fiorentino, C. Fiore, M. Loda, P. W. Kantoff, X. S. Liu and M. Brown, *Cell*, 2009, **138**, 245–256.

50 C. D. Chen, D. S. Welsbie, C. Tran, S. H. Baek, R. Chen, R. Vessella, M. G. Rosenfeld and C. L. Sawyers, *Nat. Med.*, 2004, **10**, 33–39.

51 C. Tran, S. Ouk, N. J. Clegg, Y. Chen, P. A. Watson, V. Arora, J. Wongvipat, P. M. Smith-Jones, D.

Yoo, A. Kwon, T. Wasielewska, D. Welsbie, C. D. Chen, C. S. Higano, T. M. Beer, D. T. Hung, H. I. Scher, M. E. Jung and C. L. Sawyers, *Science*, 2009, **324**, 787–790.

52 J. Schalken and J. M. Fitzpatrick, *BJU Int.*, 2016, **117**, 215–225.

53 J. El-Amm, N. Patel, A. Freeman and J. B. Aragon-Ching, *Clin. Med. Insights Oncol.*, 2013, **7**, 235–245.

54 J. D. Joseph, N. Lu, J. Qian, J. Sensintaffar, G. Shao, D. Brigham, M. Moon, E. C. Maneval, I. Chen, B. Darimont and J. H. Hager, *Cancer Discov.*, 2013, **3**, 1020–1029.

55 M. D. Balbas, M. J. Evans, D. J. Hosfield, J. Wongvipat, V. K. Arora, P. A. Watson, Y. Chen, G. L. Greene, Y. Shen and C. L. Sawyers, *Elife*, 2013, **2013**, 1–21.

56 C. K. Osborne, A. Wakeling and R. I. Nicholson, *Br. J. Cancer*, 2004, **90**, S2–S6.

57 T. M. Willson, B. R. Henke, T. M. Momtahen, P. S. Charifson, K. W. Batchelor, D. B. Lubahn, L. B. Moore, B. B. Oliver, H. R. Sauls, J. A. Triantafillou, S. G. Wolfe and P. G. Baer, *J. Med. Chem.*, 1994, **37**, 1550–1552.

58 L. Wang, V. S. Guillen, N. Sharma, K. Flessa, J. Min, K. E. Carlson, W. Toy, S. Braqi, B. S. Katzenellenbogen, J. A. Katzenellenbogen, S. Chandarlapaty and A. Sharma, *ACS Med. Chem. Lett.*, 2018, **9**, 803–808.

59 G. L. Beretta and N. Zaffaroni, *Front. Chem.*, 2019, **7**, 369.

60 R. H. Bradbury, N. J. Hales, A. A. Rabow, G. E. Walker, D. G. Acton, D. M. Andrews, P. Ballard, N. A. N. Brooks, N. Colclough, A. Girdwood, U. J. Hancox, O. Jones, D. Jude, S. A. Loddick and A. A. Mortlock, *Bioorg. Med. Chem. Lett.*, 2011, **21**, 5442–5445.

61 R. H. Bradbury, D. G. Acton, N. L. Broadbent, A. N. Brooks, G. R. Carr, G. Hatter, B. R. Hayter, K. J. Hill, N. J. Howe, R. D. O. Jones, D. Jude, S. G. Lamont, S. A. Loddick, H. L. McFarland, Z. Parveen, A. A. Rabow, G. Sharma-Singh, N. C. Stratton, A. G. Thomason, D. Trueman, G. E. Walker, S. L. Wells, J. Wilson and J. M. Wood, *Bioorg. Med. Chem. Lett.*, 2013, **23**, 1945–1948.

62 A. Omlin, R. J. Jones, R. van der Noll, T. Satoh, M. Niwakawa, S. A. Smith, J. Graham, M. Ong, R. D. Finkelman, J. H. M. Schellens, A. Zivi, M. Crespo, R. Riisnaes, D. Nava-Rodrigues, M. D. Malone, C. Dive, R. Sloane, D. Moore, J. J. Alumkal, A. Dymond, P. A. Dickinson, M. Ranson, G. Clack, J. de Bono and T. Elliott, *Invest. New Drugs*, 2015, **33**, 679–690.

63 M. T. Schweizer, K. Haugk, J. S. McKiernan, R. Gulati, H. H. Cheng, J. L. Maes, R. F. Dumpit, P. S. Nelson, B. Montgomery, J. S. McCune, S. R. Plymate and E. Y. Yu, *PLoS One*, 2018, **13**, e0198389.

64 J. L. Gustafson, T. K. Neklesa, C. S. Cox, A. G. Roth, D. L. Buckley, H. S. Tae, T. B. Sundberg, D. B. Stagg, J. Hines, D. P. McDonnell, J. D. Norris and C. M. Crews, *Angew. Chemie Int. Ed.*, 2015, **54**, 9659–9662.

65 S. Ponnusamy, C. C. Coss, T. Thiyagarajan, K. Watts, D.-J. Hwang, Y. He, L. A. Selth, I. J. McEwan, C. B. Duke, J. Pagadala, G. Singh, R. W. Wake, C. Ledbetter, W. D. Tilley, T. Moldoveanu, J. T. Dalton, D. D. Miller and R. Narayanan, *Cancer Res.*, 2017, **77**, 6282 LP – 6298.

66 D.-J. Hwang, Y. He, S. Ponnusamy, M. L. Mohler, T. Thiyagarajan, I. J. McEwan, R. Narayanan and D. D. Miller, *J. Med. Chem.*, 2019, **62**, 491–511.

67 S. Ponnusamy, Y. He, D.-J. Hwang, T. Thiyagarajan, R. Houtman, V. Bocharova, B. G. Sumpter, E. Fernandez, D. Johnson, Z. Du, L. M. Pfeffer, R. H. Getzenberg, I. J. McEwan, D. D. Miller and R. Narayanan, *Clin. Cancer Res.*, 2019, **25**, 6764 LP – 6780.

68 R. Narayanan, S. Ponnusamy and D. D. Miller, *Oncoscience*, 2017, **4**, 175–177.

69 Y. Itoh, M. Ishikawa, M. Naito and Y. Hashimoto, *J. Am. Chem. Soc.*, 2010, **132**, 5820–5826.

70 Y. Itoh, R. Kitaguchi, M. Ishikawa, M. Naito and Y. Hashimoto, *Bioorg. Med. Chem.*, 2011, **19**, 6768–6778.

71 N. Shibata, K. Nagai, Y. Morita, O. Ujikawa, N. Ohoka, T. Hattori, R. Koyama, O. Sano, Y. Imaeda, H. Nara, N. Cho and M. Naito, *J. Med. Chem.*, 2018, **61**, 543–575.

72 M. Naito, N. Ohoka and N. Shibata, *Drug Discov. Today Technol.*, 2019, **31**, 35–42.

73 A. M. Hunter, E. C. LaCasse and R. G. Korneluk, *Apoptosis*, 2007, **12**, 1543–1568.

74 J. Salami, S. Alabi, R. R. Willard, N. J. Vitale, J. Wang, H. Dong, M. Jin, D. P. McDonnell, A. P. Crew, T. K. Neklesa and C. M. Crews, *Commun. Biol.*, 2018, **1**, 100.

75 X. Han, C. Wang, C. Qin, W. Xiang, E. Fernandez-Salas, C.-Y. Yang, M. Wang, L. Zhao, T. Xu, K. Chinnaswamy, J. Delproposto, J. Stuckey and S. Wang, *J. Med. Chem.*, 2019, **62**, 941–964.

76 X. Han, L. Zhao, W. Xiang, C. Qin, B. Miao, T. Xu, M. Wang, C.-Y. Yang, K. Chinnaswamy, J. Stuckey and S. Wang, *J. Med. Chem.*, 2019, **62**, 11218–11231.

77 T. Neklesa, L. B. Snyder, R. R. Willard, N. Vitale, J. Pizzano, D. A. Gordon, M. Bookbinder, J. Macaluso, H. Dong, C. Ferraro, G. Wang, J. Wang, C. M. Crews, J. Houston, A. P. Crew and I. Taylor, *J. Clin. Oncol.*, 2019, **37**, 259.

78 A. Mullard, *Nat. Rev. Drug Discov.*, 2019, **18**, 895–895.

79 P. Braun and A. C. Gingras, *Proteomics*, 2012, **12**, 1478–1498.

80 H. Yin and A. D. Hamilton, *Angew. Chemie - Int. Ed.*, 2005, **44**, 4130–4163.

81 J. P. Overington, B. Al-Lazikani and A. L. Hopkins, *Nat. Rev. Drug Discov.*, 2006, **5**, 993–6.

82 J. Eder, R. Sedrani and C. Wiesmann, *Nat. Rev. Drug Discov.*, 2014, **13**, 577–587.

83 S. Jones and J. M. Thornton, *Proc. Natl. Acad. Sci.*, 1996, **93**, 13–20.

84 P. J. Hajduk, J. R. Huth and C. Tse, *Drug Discov. Today*, 2005, **10**, 1675–1682.

85 N. Tsomaia, *Eur. J. Med. Chem.*, 2015, **94**, 459–470.

86 D. E. Scott, A. R. Bayly, C. Abell and J. Skidmore, *Nat. Rev. Drug Discov.*, 2016, **15**, 533–550.

87 M. R. Arkin and J. A. Wells, *Nat. Rev. Drug Discov.*, 2004, **3**, 301–317.

88 T. Clackson and J. Wells, *Science*, 1995, **267**, 383–386.

89 M. J. Gorczynski, J. Grembecka, Y. Zhou, Y. Kong, L. Roudaia, M. G. Douvas, M. Newman, I. Bielnicka, G. Baber, T. Corpora, J. Shi, M. Sridharan, R. Lilien, B. R. Donald, N. A. Speck, M. L. Brown and J. H. Bushweller, *Chem. Biol.*, 2007, **14**, 1186–1197.

90 D. B. Kitchen, H. Decornez, J. R. Furr and J. Bajorath, *Nat. Rev. Drug Discov.*, 2004, **3**, 935–949.

91 G. Bhardwaj, V. K. Mulligan, C. D. Bahl, J. M. Gilmore, P. J. Harvey, O. Cheneval, G. W. Buchko, S. V. S. R. K. Pulavarti, Q. Kaas, A. Eletsky, P.-S. Huang, W. A. Johnsen, P. J. Greisen, G. J. Rocklin, Y. Song, T. W. Linsky, A. Watkins, S. A. Rettie, X. Xu, L. P. Carter, R. Bonneau, J. M. Olson, E. Coutsias, C. E. Correnti, T. Szyperski, D. J. Craik and D. Baker, *Nature*, 2016, **538**, 329–335.

92 J. A. Wells and C. L. McClendon, *Nature*, 2007, **450**, 1001–1009.

93 B. C. Raimundo, J. D. Oslob, A. C. Braisted, J. Hyde, R. S. McDowell, M. Randal, N. D. Waal, J. Wilkinson, C. H. Yu and M. R. Arkin, *J. Med. Chem.*, 2004, **47**, 3111–3130.

94 A. C. Braisted, J. D. Oslob, W. L. Delano, J. Hyde, R. S. McDowell, N. Waal, C. Yu, M. R. Arkin and B. C. Raimundo, *J. Am. Chem. Soc.*, 2003, **125**, 3714–3715.

95 M. R. Arkin, R. S. McDowell, M. Randal, W. L. DeLano, J. Hyde, T. N. Luong, J. D. Oslob, D. R. Raphael, L. Taylor, J. Wang, J. A. Wells and A. C. Braisted, *Proc. Natl. Acad. Sci. U. S. A.*, 2003, **100**, 1603–8.

96 P. Chène, *Nat. Rev. Cancer*, 2003, **3**, 102–109.

97 M. Wade, Y.-C. Li and G. M. Wahl, *Nat. Rev. Cancer*, 2013, **13**, 83–96.

98 D. P. Lane, *Nature*, 1992, **358**, 15–16.

99 A. J. Levine and M. Oren, *Nat. Rev. Cancer*, 2009, **9**, 749–758.

100 J. Momand, G. Zambetti, D. Olson, D. George and A. Levine, *Cell*, 1992, **69**, 1237–1245.

101 S. M. Picksley and D. P. Lane, *BioEssays*, 1993, **15**, 689–690.

102 D. Michael and M. Oren, *Semin. Cancer Biol.*, 2003, **13**, 49–58.

103 J. D. Oliner, K. W. Kinzler, P. S. Meltzer, D. L. George and B. Vogelstein, *Nature*, 1992, **358**, 80–83.

104 C. J. Brown, S. Lain, C. S. Verma, A. R. Fersht and D. P. Lane, *Nat. Rev. Cancer*, 2009, **9**, 862–873.

105 S. M. Mendrysa, K. A. O'Leary, M. K. McElwee, J. Michalowski, R. N. Eisenman, D. A. Powell and M. E. Perry, *Genes Dev.*, 2006, **20**, 16–21.

106 S. M. Mendrysa, M. K. McElwee, J. Michalowski, K. A. O'Leary, K. M. Young and M. E. Perry, *Mol. Cell. Biol.*, 2003, **23**, 462–472.

107 L. T. Vassilev, *Science*, 2004, **303**, 844–848.

108 Y. Zhao, A. Aguilar, D. Bernard and S. Wang, *J. Med. Chem.*, 2015, **58**, 1038–1052.

109 M. Andreeff, K. R. Kelly, K. Yee, S. Assouline, R. Strair, L. Popplewell, D. Bowen, G. Martinelli, M. W. Drummond, P. Vyas, M. Kirschbaum, S. P. Iyer, V. Ruvolo, G. M. Nogueras González, X. Huang, G. Chen, B. Graves, S. Blotner, P. Bridge, L. Jukofsky, S. Middleton, M. Reckner, R. Rueger, J. Zhi, G. Nichols and K. Kojima, *Clin. Cancer Res.*, 2016, **22**, 868–876.

110 R. P. Wurz and V. J. Cee, *J. Med. Chem.*, 2019, **62**, 445–447.

111 Y. Li, J. Yang, A. Aguilar, D. McEachern, S. Przybranowski, L. Liu, C.-Y. Yang, M. Wang, X. Han and S. Wang, *J. Med. Chem.*, 2019, **62**, 448–466.

112 D. J. Craik, D. P. Fairlie, S. Liras and D. Price, *Chem. Biol. Drug Des.*, 2013, **81**, 136–147.

113 A. Schmidtko, J. Lötsch, R. Freynhagen and G. Geisslinger, *Lancet*, 2010, **375**, 1569–1577.

114 L. L. Nielsen, A. A. Young and D. G. Parkes, *Regul. Pept.*, 2004, **117**, 77–88.

115 P. Wojcik and L. Berlicki, *Bioorg. Med. Chem. Lett.*, 2016, **26**, 707–713.

116 L. Nevola and E. Giralt, *Chem. Commun.*, 2015, **51**, 3302–3315.

117 L. Pauling, R. B. Corey and H. R. Branson, *Proc. Natl. Acad. Sci.*, 1951, **37**, 205–211.

118 J. M. Baldwin, *Prog. Biophys. Mol. Biol.*, 1976, **29**, 225–320.

119 G. N. Ramachandran, C. Ramakrishnan and V. Sasisekharan, *J. Mol. Biol.*, 1963, **7**, 95–99.

120 P. C. Lyu, P. J. Gans and N. R. Kallenbach, *J. Mol. Biol.*, 1992, **223**, 343–350.

121 A. D. De Araujo, H. N. Hoang, W. M. Kok, F. Diness, P. Gupta, T. A. Hill, R. W. Driver, D. A. Price, S. Liras and D. P. Fairlie, *Angew. Chemie - Int. Ed.*, 2014, **53**, 6965–6969.

122 Y. H. Lau, P. de Andrade, Y. Wu and D. R. Spring, *Chem. Soc. Rev.*, 2015, **44**, 91–102.

123 Y. H. Lau, P. de Andrade, S.-T. Quah, M. Rossmann, L. Laraia, N. Sköld, T. J. Sum, P. J. E. Rowling, T. L. Joseph, C. Verma, M. Hyvönen, L. S. Itzhaki, A. R. Venkitaraman, C. J. Brown, D. P. Lane and D. R. Spring, *Chem. Sci.*, 2014, **5**, 1804–1809.

124 J. Vagner, H. Qu and V. J. Hruby, *Curr. Opin. Chem. Biol.*, 2008, **12**, 292–296.

125 R. P. Cheng, S. H. Gellman and W. F. Degrado, *Chem. Rev.*, 2001, **101**, 3219–3232.

126 S. H. Gellman, *Acc. Chem. Res.*, 1998, **31**, 173–180.

127 Q. Chu, R. E. Moellering, G. J. Hilinski, Y.-W. Kim, T. N. Grossmann, J. T.-H. Yeh and G. L. Verdine, *Med. Chem. Commun.*, 2015, **6**, 111–119.

128 C. T. Walsh, L. D. Zydowsky and F. D. McKeon, *J. Biol. Chem.*, 1992, **267**, 13115–13118.

129 A. M. Felix, E. P. Heimer, C.-T. Wang, T. J. Lambros, A. Fournier, T. F. Mowles, S. Maines, R. M. Campbell, B. B. Wegrzynski, V. Toome, D. Fry and V. S. Madison, *Int. J. Pept. Protein Res.*, 2009, **32**, 441–454.

130 J. W. Taylor, *Biopolymers*, 2002, **66**, 49–75.

131 D. Y. Jackson, D. S. King, J. Chmielewski, S. Singh and P. G. Schultz, *J. Am. Chem. Soc.*, 1991, **113**, 9391–9392.

132 S. J. Miller, H. E. Blackwell and R. H. Grubbs, *J. Am. Chem. Soc.*, 1996, **118**, 9606–9614.

133 S. J. Miller and R. H. Grubbs, *J. Am. Chem. Soc.*, 1995, **117**, 5855–5856.

134 H. E. Blackwell and R. H. Grubbs, *Angew. Chemie - Int. Ed.*, 1998, **37**, 3281–3284.

135 C. E. Schafmeister, J. Po and G. L. Verdine, *J. Am. Chem. Soc.*, 2000, **122**, 5891–5892.

136 L. D. Walensky, *Science*, 2004, **305**, 1466–1470.

137 R. E. Moellering, M. Cornejo, T. N. Davis, C. Del Bianco, J. C. Aster, S. C. Blacklow, A. L. Kung, D. G. Gilliland, G. L. Verdine and J. E. Bradner, *Nature*, 2009, **462**, 182–188.

138 T. N. Grossmann, J. T.-H. Yeh, B. R. Bowman, Q. Chu, R. E. Moellering and G. L. Verdine, *Proc. Natl. Acad. Sci.*, 2012, **109**, 17942–17947.

139 P. M. Cromm, S. Schaubach, J. Spiegel, A. Fürstner, T. N. Grossmann and H. Waldmann, *Nat. Commun.*, 2016, **7**, 11300.

140 S. Cantel, A. L. C. Isaad, M. Scrima, J. J. Levy, R. D. DiMarchi, P. Rovero, J. A. Halperin, A. M. D'Ursi, A. M. Papini and M. Chorev, *J. Org. Chem.*, 2008, **73**, 5663–5674.

141 M. Scrima, A. Le Chevalier-Isaad, P. Rovero, A. M. Papini, M. Chorev and A. M. D'Ursi, *European J. Org. Chem.*, 2010, 446–457.

142 J. E. Moses and A. D. Moorhouse, *Chem. Soc. Rev.*, 2016, **45**, 6888–6888.

143 S. A. Kawamoto, A. Coleska, X. Ran, H. Yi, C. Y. Yang and S. Wang, *J. Med. Chem.*, 2012, **55**, 1137–1146.

144 J. Iegre, J. S. Gaynord, N. S. Robertson, H. F. Sore, M. Hyvönen and D. R. Spring, *Adv. Ther.*, 2018, **1**, 1800052.

145 Y. H. Lau, Y. Wu, M. Rossmann, B. X. Tan, P. De Andrade, Y. S. Tan, C. Verma, G. J. McKenzie, A. R. Venkitaraman, M. Hyvönen and D. R. Spring, *Angew. Chemie - Int. Ed.*, 2015, **54**, 15410–15413.

146 M. Pazgier, M. Liu, G. Zou, W. Yuan, C. Li, C. Li, J. Li, J. Monbo, D. Zella, S. G. Tarasov and W. Lu, *Proc. Natl. Acad. Sci.*, 2009, **106**, 4665–4670.

147 C. J. Brown, S. T. Quah, J. Jong, A. M. Goh, P. C. Chiam, K. H. Khoo, M. L. Choong, M. A. Lee, L. Yurlova, K. Zolghadr, T. L. Joseph, C. S. Verma and D. P. Lane, *ACS Chem. Biol.*, 2013, **8**, 506–512.

148 Y. S. Chang, B. Graves, V. Guerlavais, C. Tovar, K. Packman, K.-H. To, K. A. Olson, K. Kesavan, P. Gangurde, A. Mukherjee, T. Baker, K. Darlak, C. Elkin, Z. Filipovic, F. Z. Qureshi, H. Cai, P. Berry, E. Feyfant, X. E. Shi, J. Horstick, D. A. Annis, A. M. Manning, N. Fotouhi, H. Nash, L. T. Vassilev and T. K. Sawyer, *Proc. Natl. Acad. Sci.*, 2013, **110**, E3445–E3454.

149 J. Momand and G. P. Zambetti, *J. Cell. Biochem.*, 1997, **64**, 343–352.

150 D. Shi and W. Gu, *Genes Cancer*, 2012, **3**, 240–248.

151 S. Shangary and S. Wang, *Clin. Cancer Res.*, 2008, **14**, 5318 LP – 5324.

152 L. Buetow and D. T. Huang, *Nat. Rev. Mol. Cell Biol.*, 2016, **17**, 626–642.

153 WO2010099238A1, 2010.

154 R. Wong and S. J. Dolman, *J. Org. Chem.*, 2007, **72**, 3969–3971.

155 H. Munch, J. S. Hansen, M. Pittelkow, J. B. Christensen and U. Boas, *Tetrahedron Lett.*, 2008, **49**, 3117–3119.

156 H. A. Staab, *Angew. Chemie Int. Ed. English*, 1962, **1**, 351–367.

157 Y. Jin, D. Watkins, N. N. Degtyareva, K. D. Green, M. N. Spano, S. Garneau-Tsodikova and D. P. Arya, *Med. Chem. Commun.*, 2016, **7**, 164–169.

158 M. J. Hynes and J. A. Maurer, *Angew. Chemie Int. Ed.*, 2012, **51**, 2151–2154.

159 A. Bouzide and G. Sauve, *Org. Lett.*, 2002, 8781–8783.

160 M. K. Muller, K. Petkau and L. Brunsveld, *Chem. Commun.*, 2011, **47**, 310–312.

161 E. Valeur and M. Bradley, *Chem. Soc. Rev.*, 2009, **38**, 606–631.

162 B. B. Mollet, M. Comellas-Aragones, A. J. H. Spiering, S. H. M. Sontjens, E. W. Meijer and P. Y. W. Dankers, *J. Mater. Chem. B*, 2014, **2**, 2483–2493.

163 M. B. Andrus, T. M. Turner, E. P. Updegraff, Z. E. Sauna and S. V Ambudkar, *Tetrahedron Lett.*, 2001, **42**, 3819–3822.

164 I. de Feijter, O. J. G. M. Goor, S. I. S. Hendrikse, M. Comellas-Aragonès, S. H. M. Söntjens, S. Zaccaria, P. P. K. H. Fransen, J. W. Peeters, L.-G. Milroy and P. Y. W. Dankers, *Synlett*, 2015, **26**, 2707–2713.

165 T. Suzuki, S. Hisakawa, Y. Itoh, N. Suzuki, K. Takahashi, M. Kawahata, K. Yamaguchi, H. Nakagawa and N. Miyata, *Bioorg. Med. Chem. Lett.*, 2007, **17**, 4208–4212.

166 A. Favre, J. Grugier, A. Brans, B. Joris and J. Marchand-Brynaert, *Tetrahedron*, 2012, **68**, 10818–10826.

167 Y. H. Lau, PhD Thesis, University of Cambridge, 2014.

168 Y. Wu, PhD Thesis, University of Cambridge, 2016.

169 N. Fischer, E. D. Goddard-Borger, R. Greiner, T. M. Klapötke, B. W. Skelton and J. Stierstorfer,

J. Org. Chem., 2012, **77**, 1760–1764.

170 E. B. Askew, R. T. Gampe, T. B. Stanley, J. L. Faggart and E. M. Wilson, *J. Biol. Chem.* , 2007, **282**, 25801–25816.

171 D. M. Molina, R. Jafari, M. Ignatushchenko, T. Seki, E. A. Larsson, C. Dan, L. Sreekumar, Y. Cao and P. Nordlund, *Science*, 2013, **341**, 84 LP – 87.

172 D. Matulis, J. K. Kranz, F. R. Salemme and M. J. Todd, *Biochemistry*, 2005, **44**, 5258–5266.

173 J. Shaw, I. Dale, P. Hemsley, L. Leach, N. Dekki, J. P. Orme, V. Talbot, A. J. Narvaez, M. Bista, D. Martinez Molina, M. Dabrowski, M. J. Main and D. Gianni, *SLAS Discov. Adv. Sci. Drug Discov.*, 2018, **24**, 121–132.

174 J. Shaw, M. Leveridge, C. Norling, J. Karén, D. M. Molina, D. O'Neill, J. E. Dowling, P. Davey, S. Cowan, M. Dabrowski, M. Main and D. Gianni, *Sci. Rep.*, 2018, **8**, 163.

175 Y. H. Lau, P. de Andrade, S.-T. Quah, M. Rossmann, L. Laraia, N. Sköld, T. J. Sum, P. J. E. Rowling, T. L. Joseph, C. Verma, M. Hyvönen, L. S. Itzhaki, A. R. Venkitaraman, C. J. Brown, D. P. Lane and D. R. Spring, *Chem. Sci.*, 2014, **5**, 1804–1809.

176 M. E. Jung, S. Ouk, D. Yoo, C. L. Sawyers, C. Chen, C. Tran and J. Wongvipat, *J. Med. Chem.*, 2010, **53**, 2779–2796.

177 P. S. Jadhavar, S. A. Ramachandran, E. Riquelme, A. Gupta, K. P. Quinn, D. Shivakumar, S. Ray, D. Zende, A. K. Nayak, S. K. Miglani, B. D. Sathe, M. Raja, O. Farias, I. Alfaro, S. Belmar, J. Guerrero, S. Bernales, S. Chakravarty, D. T. Hung, J. N. Lindquist and R. Rai, *Bioorg. Med. Chem. Lett.*, 2016, **26**, 5222–5228.

178 WO2016118666A1, 2016.

179 P. G. Dougherty, J. Wen, X. Pan, A. Koley, J.-G. Ren, A. Sahni, R. Basu, H. Salim, G. Appiah Kubi, Z. Qian and D. Pei, *J. Med. Chem.*, 2019, **62**, 10098–10107.

180 L. D. Lavis, *ACS Chem. Biol.*, 2008, **3**, 203–206.

181 C. Bechara and S. Sagan, *FEBS Lett.*, 2013, **587**, 1693–1702.

182 D. J. Mitchell, D. T. Kim, L. Steinman, C. G. Fathman and J. B. Rothbard, *J. Pept. Res.*, 2000, **56**, 318–325.

183 S. G. Patel, E. J. Sayers, L. He, R. Narayan, T. L. Williams, E. M. Mills, R. K. Allemann, L. Y. P. Luk, A. T. Jones and Y.-H. Tsai, *Sci. Rep.*, 2019, **9**, 6298.

184 Y. Wu, A. Kaur, E. Fowler, M. M. Wiedmann, R. Young, W. R. J. D. Galloway, L. Olsen, H. F. Sore, A. Chattopadhyay, T. T.-L. Kwan, W. Xu, S. J. Walsh, P. de Andrade, M. Janecek, S. Arumugam, L. S. Itzhaki, Y. H. Lau and D. R. Spring, *ACS Chem. Biol.*, 2019, **14**, 526–533.

185 H. Lebraud, D. J. Wright, C. N. Johnson and T. D. Heightman, *ACS Cent. Sci.*, 2016, **2**, 927–934.

186 K. Sharma, A. V Strizhak, E. Fowler, X. Wang, W. Xu, C. Hatt Jensen, Y. Wu, H. F. Sore, Y. H. Lau, M. Hyvönen, L. S. Itzhaki and D. R. Spring, *Org. Biomol. Chem.*, 2019, **17**, 8014–8018.

187 R. P. Wurz, K. Dellamaggiore, H. Dou, N. Javier, M.-C. Lo, J. D. McCarter, D. Mohl, C. Sastri, J. R. Lipford and V. J. Cee, *J. Med. Chem.*, 2018, **61**, 453–461.

188 Y. Jiang, Q. Deng, H. Zhao, M. Xie, L. Chen, F. Yin, X. Qin, W. Zheng, Y. Zhao and Z. Li, *ACS Chem. Biol.*, 2018, **13**, 628–635.

189 Y. Dai, N. Yue, J. Gong, C. Liu, Q. Li, J. Zhou, W. Huang and H. Qian, *Eur. J. Med. Chem.*, 2020, **187**, 111967.

190 Y. Zhao, A. Aguilar, D. Bernard and S. Wang, *J. Med. Chem.*, 2015, **58**, 1038–1052.

191 P. Matsson and J. Kihlberg, *J. Med. Chem.*, 2017, **60**, 1662–1664.

192 Y. Fang, G. Liao and B. Yu, *Acta Pharm. Sin. B*, 2020, DOI: 10.1016/j.apsb.2020.01.003.

193 B. Vu, P. Wovkulich, G. Pizzolato, A. Lovey, Q. Ding, N. Jiang, J.-J. Liu, C. Zhao, K. Glenn, Y. Wen, C. Tovar, K. Packman, L. Vassilev and B. Graves, *ACS Med. Chem. Lett.*, 2013, **4**, 466–469.

194 Q. Ding, Z. Zhang, J.-J. Liu, N. Jiang, J. Zhang, T. M. Ross, X.-J. Chu, D. Bartkovitz, F. Podlaski, C. Janson, C. Tovar, Z. M. Filipovic, B. Higgins, K. Glenn, K. Packman, L. T. Vassilev and B. Graves, *J. Med. Chem.*, 2013, **56**, 5979–5983.

195 Y. Rew, D. Sun, F. Gonzalez-Lopez De Turiso, M. D. Bartberger, H. P. Beck, J. Canon, A. Chen, D. Chow, J. Deignan, B. M. Fox, D. Gustin, X. Huang, M. Jiang, X. Jiao, L. Jin, F. Kayser, D. J. Kopecky, Y. Li, M.-C. Lo, A. M. Long, K. Michelsen, J. D. Oliner, T. Osgood, M. Ragains, A. Y. Saiki, S. Schneider, M. Toteva, P. Yakowec, X. Yan, Q. Ye, D. Yu, X. Zhao, J. Zhou, J. C. Medina and S. H. Olson, *J. Med. Chem.*, 2012, **55**, 4936–4954.

196 D. Sun, Z. Li, Y. Rew, M. Gribble, M. D. Bartberger, H. P. Beck, J. Canon, A. Chen, X. Chen, D. Chow, J. Deignan, J. Duquette, J. Eksterowicz, B. Fisher, B. M. Fox, J. Fu, A. Z. Gonzalez, F. Gonzalez-Lopez De Turiso, J. B. Houze, X. Huang, M. Jiang, L. Jin, F. Kayser, J. Liu, M.-C. Lo, A. M. Long, B. Lucas, L. R. McGee, J. McIntosh, J. Mihalic, J. D. Oliner, T. Osgood, M. L. Peterson, P. Roveto, A. Y. Saiki, P. Shaffer, M. Toteva, Y. Wang, Y. C. Wang, S. Wortman, P. Yakowec, X.

Yan, Q. Ye, D. Yu, M. Yu, X. Zhao, J. Zhou, J. Zhu, S. H. Olson and J. C. Medina, *J. Med. Chem.*, 2014, **57**, 1454–1472.

197 W. L. Gluck, M. M. Gounder, R. Frank, F. Eskens, J. Y. Blay, P. A. Cassier, J.-C. Soria, S. Chawla, V. de Weger, A. J. Wagner, D. Siegel, F. De Vos, E. Rasmussen and H. A. Henary, *Invest. New Drugs*, 2019, DOI: 10.1007/s10637-019-00840-1.

198 P. Holzer, K. Masuya, P. Furet, J. Kallen, T. Valat-Stachyra, S. Ferretti, J. Berghausen, M. Bouisset-Leonard, N. Buschmann, C. Pissot-Soldermann, C. Rynn, S. Ruetz, S. Stutz, P. Chène, S. Jeay and F. Gessier, *J. Med. Chem.*, 2015, **58**, 6348–6358.

199 S. Jeay, S. Gaulis, S. Ferretti, H. Bitter, M. Ito, T. Valat, M. Murakami, S. Ruetz, D. A. Guthy, C. Rynn, M. R. Jensen, M. Wiesmann, J. Kallen, P. Furet, F. Gessier, P. Holzer, K. Masuya, J. Würthner, E. Halilovic, F. Hofmann, W. R. Sellers and D. Graus Porta, *Elife*, 2015, **4**, e06498.

200 S. Bauer, G. Demetri, S. Jeay, R. Dummer, N. Guerreiro, D. S. Tan, A. Kumar, C. Meille, L. Van Bree, E. Halilovic, J. U. Wuerthner and P. Cassier, *Ann. Oncol.*, 2016, **27**, vi116.

201 S. Wang, W. Sun, Y. Zhao, D. McEachern, I. Meaux, C. Barrière, J. A. Stuckey, J. L. Meagher, L. Bai, L. Liu, C. G. Hoffman-Luca, J. Lu, S. Shangary, S. Yu, D. Bernard, A. Aguilar, O. Dos-Santos, L. Besret, S. Guerif, P. Pannier, D. Gorge-Bernat and L. Debussche, *Cancer Res.*, 2014, **74**, 5855 LP – 5865.

202 M. de Jonge, V. A. de Weger, M. A. Dickson, M. Langenberg, A. Le Cesne, A. J. Wagner, K. Hsu, W. Zheng, S. Macé, G. Tuffal, K. Thomas and J. H. M. Schellens, *Eur. J. Cancer*, 2017, **76**, 144–151.

203 V. A. de Weger, M. de Jonge, M. H. G. Langenberg, J. H. M. Schellens, M. Lolkema, A. Varga, B. Demers, K. Thomas, K. Hsu, G. Tuffal, S. Goodstal, S. Macé and E. Deutsch, *Br. J. Cancer*, 2019, **120**, 286–293.

204 Z. Ding and D. Kihara, *Curr. Protoc. Protein Sci.*, 2018, **93**, e62.

205 C. Rakers, M. Bermudez, B. G. Keller, J. Mortier and G. Wolber, *WIREs Comput. Mol. Sci.*, 2015, **5**, 345–359.

206 B. K. Shoichet, *Nature*, 2004, **432**, 862–865.

207 W. Wang, X. Zhu, X. Hong, L. Zheng, H. Zhu and Y. Hu, *Medchemcomm*, 2013, **4**, 411–416.

208 N. Atatreh, M. A. Ghattas, S. K. Bardaweel, S. Al Rawashdeh and M. Al Sorkhy, *Drug Des. Devel. Ther.*, 2018, **12**, 3741–3752.

209 A. Voet, X. Qing, X. Y. Lee, J. De Raeymaecker, J. Tame, K. Zhang and M. De Maeyer, *J. Receptor. Ligand Channel Res.*, 2014, **7**, 81-92.

210 E. Lionta, G. Spyrou and D. K. V. and Z. Cournia, *Curr. Top. Med. Chem.*, 2014, **14**, 1923–1938.

211 D. Stumpfe and J. Bajorath, *J. Chem. Inf. Model.*, 2020, DOI: 10.1021/acs.jcim.9b01101.

212 A. L. and C. Di Giovanni, *Curr. Med. Chem.*, 2013, **20**, 2839–2860.

213 J. J. Irwin and B. K. Shoichet, *J. Chem. Inf. Model.*, 2005, **45**, 177–182.

214 T. Sterling and J. J. Irwin, *J. Chem. Inf. Model.*, 2015, **55**, 2324–2337.

215 C. M. Dobson, *Nature*, 2004, **432**, 824–828.

216 N. van Hilten, F. Chevillard and P. Kolb, *J. Chem. Inf. Model.*, 2019, **59**, 644–651.

217 J. Lyu, S. Wang, T. E. Balius, I. Singh, A. Levit, Y. S. Moroz, M. J. O'Meara, T. Che, E. Algaa, K. Tolmachova, A. A. Tolmachev, B. K. Shoichet, B. L. Roth and J. J. Irwin, *Nature*, 2019, **566**, 224–229.

218 S. Shangary and S. Wang, *Annu. Rev. Pharmacol. Toxicol.*, 2009, **49**, 223–241.

219 Y. Lu, Z. Nikolovska-Coleska, X. Fang, W. Gao, S. Shangary, S. Qiu, D. Qin and S. Wang, *J. Med. Chem.*, 2006, **49**, 3759–3762.

220 D. R. Spring, *Org. Biomol. Chem.*, 2003, **1**, 3867–3870.

221 W. R. J. D. Galloway, A. Isidro-Llobet and D. R. Spring, *Nat. Commun.*, 2010, **1**, 80.

222 L. Mervin, E. Fowler, S. L. Kidd, N. Mateu, R. S. Eapen, H. F. Sore, L. S. Itzhaki, A. Bender and D. R. Spring, *Bioorg. Med. Chem.*, 2020, Submitted.

223 T. A. Halgren, R. B. Murphy, R. A. Friesner, H. S. Beard, L. L. Frye, W. T. Pollard and J. L. Banks, *J. Med. Chem.*, 2004, **47**, 1750–1759.

224 G. C. Nwokogu, *Encycl. Reagents Org. Synth.*, 2001.

225 F. Sondheimer, Y. Amiel and Y. Gaoni, *J. Am. Chem. Soc.*, 1962, **84**, 270–274.

226 A. Viola and J. H. MacMillan, *J. Am. Chem. Soc.*, 1968, **90**, 6141–6145.

227 H. P. Acharya, K. Miyoshi and Y. Kobayashi, *Org. Lett.*, 2007, **9**, 3535–3538.

228 H.-S. Lin and L. A. Paquette, *Synth. Commun.*, 1994, **24**, 2503–2506.

229 W. Wang, J.-J. Qin, S. Voruganti, K. S. Srivenugopal, S. Nag, S. Patil, H. Sharma, M.-H. Wang, H.

Wang, J. K. Buolamwini and R. Zhang, *Nat. Commun.*, 2014, **5**, 5086.

230 D. F. Veber, S. R. Johnson, H.-Y. Cheng, B. R. Smith, K. W. Ward and K. D. Kopple, *J. Med. Chem.*, 2002, **45**, 2615–2623.

231 M. Giustiniano, S. Daniele, S. Pelliccia, V. La Pietra, D. Pietrobono, D. Brancaccio, S. Cosconati, A. Messere, S. Giuntini, L. Cerofolini, M. Fragai, C. Luchinat, S. Taliani, G. La Regina, F. Da Settimo, R. Silvestri, C. Martini, E. Novellino and L. Marinelli, *J. Med. Chem.*, 2017, **60**, 8115–8130.

232 G. M. Popowicz, A. Czarna, S. Wolf, K. Wang, W. Wang, A. Dömling and T. A. Holak, *Cell Cycle*, 2010, **9**, 1104–1111.

233 A. Twarda-Clapa, S. Krzanik, K. Kubica, K. Guzik, B. Labuzek, C. G. Neochoritis, K. Khoury, K. Kowalska, M. Czub, G. Dubin, A. Dömling, L. Skalniak and T. A. Holak, *J. Med. Chem.*, 2017, **60**, 4234–4244.

234 J. Sisko, M. Mellinger, P. W. Sheldrake and N. H. Baine, *Tetrahedron Lett.*, 1996, **37**, 8113–8116.

235 K. Raina, J. Lu, Y. Qian, M. Altieri, D. Gordon, A. M. Rossi, J. Wang, X. Chen, H. Dong, K. Siu, J. D. Winkler, A. P. Crew, C. M. Crews and K. G. Coleman, *Proc Natl Acad Sci U S A*, 2016, **113**, 7124–7129.

236 B. Wang, L. Fang, H. Zhao, T. Xiang and D. Wang, *Acta Biochim. Biophys. Sin. (Shanghai).*, 2012, **44**, 685–691.

237 C. Tovar, J. Rosinski, Z. Filipovic, B. Higgins, K. Kolinsky, H. Hilton, X. Zhao, B. T. Vu, W. Qing, K. Packman, O. Myklebost, D. C. Heimbrook and L. T. Vassilev, *Proc. Natl. Acad. Sci. U. S. A.*, 2006, **103**, 1888 LP – 1893.

238 L. Meng, R. Mohan, B. H. B. Kwok, M. Elofsson, N. Sin and C. M. Crews, *Proc. Natl. Acad. Sci.*, 1999, **96**, 10403–10408.

239 J. Hines, S. Lartigue, H. Dong, Y. Qian and C. M. Crews, *Cancer Res.*, 2019, **79**, 251-262.

240 A. D. Basso, D. B. Solit, G. Chiosis, B. Giri, P. Tsichlis and N. Rosen, *J. Biol. Chem.* , 2002, **277**, 39858–39866.

241 H. R. Kim, H. S. Kang and H. Do Kim, *IUBMB Life*, 1999, **48**, 429–433.

242 H.-P. Shih, X. Zhang and A. M. Aronov, *Nat. Rev. Drug Discov.*, 2018, **17**, 19–33.

243 M. J. Waring, J. Arrowsmith, A. R. Leach, P. D. Leeson, S. Mandrell, R. M. Owen, G. Pairaudeau,

W. D. Pennie, S. D. Pickett, J. Wang, O. Wallace and A. Weir, *Nat. Rev. Drug Discov.*, 2015, **14**, 475.

244 K. M. Gayvert, N. S. Madhukar and O. Elemento, *Cell Chem. Biol.*, 2016, **23**, 1294–1301.

245 D. G. Rudmann, *Toxicol. Pathol.*, 2012, **41**, 310–314.

246 F. P. Guengerich, *Drug Metab. Pharmacokinet.*, 2011, **26**, 3–14.

247 J. Morstein and D. Trauner, *Curr. Opin. Chem. Biol.*, 2019, **50**, 145–151.

248 K. Hüll, J. Morstein and D. Trauner, *Chem. Rev.*, 2018, **118**, 10710–10747.

249 W. A. Velema, W. Szymanski and B. L. Feringa, *J. Am. Chem. Soc.*, 2014, **136**, 2178–2191.

250 M. M. Lerch, M. J. Hansen, G. M. van Dam, W. Szymanski and B. L. Feringa, *Angew. Chemie Int. Ed.*, 2016, **55**, 10978–10999.

251 P. Paoletti, G. C. R. Ellis-Davies and A. Mourot, *Nat. Rev. Neurosci.*, 2019, **20**, 514–532.

252 M. Ricart-Ortega, J. Font and A. Llebaria, *Mol. Cell. Endocrinol.*, 2019, **488**, 36–51.

253 A. F. Dos Santos, D. R. Q. De Almeida, L. F. Terra, M. S. Baptista and L. Labriola, *J. Cancer Metastasis Treat*, 2019, **5**, 1–20.

254 M. Yang, T. Yang and C. Mao, *Angew. Chemie Int. Ed.*, 2019, **58**, 14066–14080.

255 P. Klán, T. Šolomek, C. G. Bochet, A. Blanc, R. Givens, M. Rubina, V. Popik, A. Kostikov and J. Wirz, *Chem. Rev.*, 2013, **113**, 119–191.

256 A. Y. Vorobev and A. E. Moskalensky, *Comput. Struct. Biotechnol. J.*, 2020, **18**, 27–34.

257 T. Slanina, P. Shrestha, E. Palao, D. Kand, J. A. Peterson, A. S. Dutton, N. Rubinstein, R. Weinstain, A. H. Winter and P. Klán, *J. Am. Chem. Soc.*, 2017, **139**, 15168–15175.

258 J. P. Olson, M. R. Banghart, B. L. Sabatini and G. C. R. Ellis-Davies, *J. Am. Chem. Soc.*, 2013, **135**, 15948–15954.

259 E. Smith and I. Collins, *Future Med. Chem.*, 2015, **7**, 159–183.

260 M. W. H. Hoorens and W. Szymanski, *Trends Biochem. Sci.*, 2018, **43**, 567–575.

261 K. Matsuda and M. Irie, *J. Photochem. Photobiol. C Photochem. Rev.*, 2004, **5**, 169–182.

262 H. Cahová and A. Jäschke, *Angew. Chemie Int. Ed.*, 2013, **52**, 3186–3190.

263 G. S. Hartley, *Nature*, 1937, **140**, 281.

264 M. Zhu and H. Zhou, *Org. Biomol. Chem.*, 2018, **16**, 8434–8445.

265 H. Kaufman, S. M. Vratsanos and B. F. Erlanger, *Science*, 1968, **162**, 1487–1489.

266 J. R. Kumita, O. S. Smart and G. A. Woolley, *Proc. Natl. Acad. Sci.*, 2000, **97**, 3803–3808.

267 S. Kneissl, E. J. Loveridge, C. Williams, M. P. Crump and R. K. Allemann, *ChemBioChem*, 2008, **9**, 3046–3054.

268 L. Albert and O. Vázquez, *Chem. Commun.*, 2019, **55**, 10192–10213.

269 W. J. Deal, B. F. Erlanger and D. Nachmansohn, *Proc. Natl. Acad. Sci.*, 1969, **64**, 1230–1234.

270 A. Damijonaitis, J. Broichhagen, T. Urushima, K. Hüll, J. Nagpal, L. Laprell, M. Schönberger, D. H. Woodmansee, A. Rafiq, M. P. Sumser, W. Kummer, A. Gottschalk and D. Trauner, *ACS Chem. Neurosci.*, 2015, **6**, 701–707.

271 S. Pittolo, X. Gómez-Santacana, K. Eckelt, X. Rovira, J. Dalton, C. Goudet, J.-P. Pin, A. Llobet, J. Giraldo, A. Llebaria and P. Gorostiza, *Nat. Chem. Biol.*, 2014, **10**, 813–815.

272 X. Gómez-Santacana, S. Pittolo, X. Rovira, M. Lopez, C. Zussy, J. A. R. Dalton, A. Faucherre, C. Jopling, J.-P. Pin, F. Ciruela, C. Goudet, J. Giraldo, P. Gorostiza and A. Llebaria, *ACS Cent. Sci.*, 2017, **3**, 81–91.

273 M. Wegener, M. J. Hansen, A. J. M. Driessen, W. Szymanski and B. L. Feringa, *J. Am. Chem. Soc.*, 2017, **139**, 17979–17986.

274 S. B. Levy and B. Marshall, *Nat. Med.*, 2004, **10**, S122.

275 I. Tochitsky, M. A. Kienzler, E. Isacoff and R. H. Kramer, *Chem. Rev.*, 2018, **118**, 10748–10773.

276 T. J. McMillan, E. Leatherman, A. Ridley, J. Shorrocks, S. E. Tobi and J. R. Whiteside, *J. Pharm. Pharmacol.*, 2008, **60**, 969–976.

277 C. Ash, M. Dubec, K. Donne and T. Bashford, *Lasers Med. Sci.*, 2017, **32**, 1909–1918.

278 C. Boulègue, M. Löweneck, C. Renner and L. Moroder, *ChemBioChem*, 2007, **8**, 591–594.

279 A. A. Beharry, L. Wong, V. Tropepe and G. A. Woolley, *Angew. Chemie Int. Ed.*, 2011, **50**, 1325–1327.

280 J. D. Harris, M. J. Moran and I. Aprahamian, *Proc. Natl. Acad. Sci.*, 2018, **115**, 9414–9422.

281 Z. L. Pianowski, *Chem. – A Eur. J.*, 2019, **25**, 5128–5144.

282 A. A. Beharry, O. Sadovski and G. A. Woolley, *J. Am. Chem. Soc.*, 2011, **133**, 19684–19687.

283 S. Samanta, T. M. McCormick, S. K. Schmidt, D. S. Seferos and G. A. Woolley, *Chem. Commun.*, 2013, **49**, 10314–10316.

284 S. Samanta, A. A. Beharry, O. Sadovski, T. M. McCormick, A. Babalhavaeji, V. Tropepe and G. A. Woolley, *J. Am. Chem. Soc.*, 2013, **135**, 9777–9784.

285 D. Bléger, J. Schwarz, A. M. Brouwer and S. Hecht, *J. Am. Chem. Soc.*, 2012, **134**, 20597–20600.

286 R. Siewertsen, H. Neumann, B. Buchheim-Stehn, R. Herges, C. Näther, F. Renth and F. Temps, *J. Am. Chem. Soc.*, 2009, **131**, 15594–15595.

287 M. Hammerich, C. Schütt, C. Stähler, P. Lentes, F. Röhricht, R. Höppner and R. Herges, *J. Am. Chem. Soc.*, 2016, **138**, 13111–13114.

288 J. Calbo, C. E. Weston, A. J. P. White, H. S. Rzepa, J. Contreras-García and M. J. Fuchter, *J. Am. Chem. Soc.*, 2017, **139**, 1261–1274.

289 X.-M. Liu, X.-Y. Jin, Z.-X. Zhang, J. Wang and F.-Q. Bai, *RSC Adv.*, 2018, **8**, 11580–11588.

290 C. Knie, M. Utecht, F. Zhao, H. Kulla, S. Kovalenko, A. M. Brouwer, P. Saalfrank, S. Hecht and D. Bléger, *Chem. – A Eur. J.*, 2014, **20**, 16492–16501.

291 J. B. Trads, J. Burgstaller, L. Laprell, D. B. Konrad, L. de la Osa de la Rosa, C. D. Weaver, H. Baier, D. Trauner and D. M. Barber, *Org. Biomol. Chem.*, 2017, **15**, 76–81.

292 L. Agnetta, M. Bermudez, F. Riefolo, C. Matera, E. Claro, R. Messerer, T. Littmann, G. Wolber, U. Holzgrabe and M. Decker, *J. Med. Chem.*, 2019, **62**, 3009–3020.

293 S. Iamsaard, E. Anger, S. J. Aßhoff, A. Depauw, S. P. Fletcher and N. Katsonis, *Angew. Chemie Int. Ed.*, 2016, **55**, 9908–9912.

294 K. Kumar, C. Knie, D. Bléger, M. A. Peletier, H. Friedrich, S. Hecht, D. J. Broer, M. G. Debije and A. P. H. J. Schenning, *Nat. Commun.*, 2016, **7**, 11975.

295 K. Müller, A. Knebel, F. Zhao, D. Bléger, J. Caro and L. Heinke, *Chem. – A Eur. J.*, 2017, **23**, 5434–5438.

296 S. Castellanos, A. Goulet-Hanssens, F. Zhao, A. Dikhtiarenko, A. Pustovarenko, S. Hecht, J. Gascon, F. Kapteijn and D. Bléger, *Chem. – A Eur. J.*, 2016, **22**, 746–752.

297 D. Samanta, J. Gemen, Z. Chu, Y. Diskin-Posner, L. J. W. Shimon and R. Klajn, *Proc. Natl. Acad. Sci.*, 2018, **115**, 9379–9384.

298 O. S. Bushuyev, A. Tomberg, T. Friščić and C. J. Barrett, *J. Am. Chem. Soc.*, 2013, **135**, 12556–12559.

299 O. S. Bushuyev, T. C. Corkery, C. J. Barrett and T. Friščić, *Chem. Sci.*, 2014, **5**, 3158–3164.

300 C. Petermayer and H. Dube, *Acc. Chem. Res.*, 2018, **51**, 1153–1163.

301 C. Petermayer, S. Thumser, F. Kink, P. Mayer and H. Dube, *J. Am. Chem. Soc.*, 2017, **139**, 15060–15067.

302 C. Petermayer and H. Dube, *J. Am. Chem. Soc.*, 2018, **140**, 13558–13561.

303 D. V Berdnikova, *Chem. Commun.*, 2019, **55**, 8402–8405.

304 L. Greb and J.-M. Lehn, *J. Am. Chem. Soc.*, 2014, **136**, 13114–13117.

305 D. J. van Dijken, P. Kovaříček, S. P. Ihrig and S. Hecht, *J. Am. Chem. Soc.*, 2015, **137**, 14982–14991.

306 S. Helmy, F. A. Leibfarth, S. Oh, J. E. Poelma, C. J. Hawker and J. Read de Alaniz, *J. Am. Chem. Soc.*, 2014, **136**, 8169–8172.

307 M. M. Lerch, S. J. Wezenberg, W. Szymanski and B. L. Feringa, *J. Am. Chem. Soc.*, 2016, **138**, 6344–6347.

308 M. Reynders, B. S. Matsuura, M. Bérouti, D. Simoneschi, A. Marzio, M. Pagano and D. Trauner, *Sci. Adv.*, 2020, **6**, eaay5064.

309 P. Pfaff, K. Samarasinghe, C. M. Crews and E. M. Carreira, *ACS Cent Sci.*, 2019, **5**, 10, 1682-1690.

310 K. Liu, P. Wen, J. Liu and G. Huang, *Synthesis*, 2010, **21**, 3623–3626.

311 R. Li, X. Qi and X.-F. Wu, *Org. Biomol. Chem.*, 2017, **15**, 6905–6908.

312 O. Pitayatanakul, T. Higashino, T. Kadoya, M. Tanaka, H. Kojima, M. Ashizawa, T. Kawamoto, H. Matsumoto, K. Ishikawa and T. Mori, *J. Mater. Chem. C*, 2014, **2**, 9311–9317.

313 P. Y. Choy, C. P. Lau and F. Y. Kwong, *J. Org. Chem.*, 2011, **76**, 80–84.

314 M. M. Heravi, Z. Kheilkordi, V. Zadsirjan, M. Heydari and M. Malmir, *J. Organomet. Chem.*, 2018, **861**, 17–104.

315 R. Dorel, C. P. Grugel and A. M. Haydl, *Angew. Chemie Int. Ed.*, 2019, **58**, 17118–17129.

316 A. Marini, A. Muñoz-Losa, A. Biancardi and B. Mennucci, *J. Phys. Chem. B*, 2010, **114**, 17128–

17135.

317 J. Hu, B. Hu, M. Wang, F. Xu, B. Miao, C.-Y. Yang, M. Wang, Z. Liu, D. F. Hayes, K. Chinnaswamy, J. Delproposto, J. Stuckey and S. Wang, *J. Med. Chem.*, 2019, **62**, 1420–1442.

318 D. Clemett and C. M. Spencer, *Drugs*, 2000, **60**, 379–411.

319 G. E. Winter, D. L. Buckley, J. Paulk, J. M. Roberts, A. Souza, S. Dhe-Paganon and J. E. Bradner, *Science*, 2015, **348**, 1376–1381.

320 R. P. Wurz, K. Dellamaggiore, H. Dou, N. Javier, M.-C. Lo, J. D. McCarter, D. Mohl, C. Sastri, J. R. Lipford and V. J. Cee, *J. Med. Chem.*, 2018, **61**, 2, 453-461.

321 L. De Boni, L. Misoguti, S. C. Zílio and C. R. Mendonça, *ChemPhysChem*, 2005, **6**, 1121–1125.

322 G. Cabré, A. Garrido-Charles, M. Moreno, M. Bosch, M. Porta-de-la-Riva, M. Krieg, M. Gascón-Moya, N. Camarero, R. Gelabert, J. M. Lluch, F. Busqué, J. Hernando, P. Gorostiza and R. Alibés, *Nat. Commun.*, 2019, **10**, 907.

323 M. Izquierdo-Serra, M. Gascón-Moya, J. J. Hirtz, S. Pittolo, K. E. Poskanzer, È. Ferrer, R. Alibés, F. Busqué, R. Yuste, J. Hernando and P. Gorostiza, *J. Am. Chem. Soc.*, 2014, **136**, 8693–8701.

324 M. Gascón-Moya, A. Pejoan, M. Izquierdo-Serra, S. Pittolo, G. Cabré, J. Hernando, R. Alibés, P. Gorostiza and F. Busqué, *J. Org. Chem.*, 2015, **80**, 9915–9925.

325 M. Dong, A. Babalhavaeji, C. V Collins, K. Jarrah, O. Sadovski, Q. Dai and G. A. Woolley, *J. Am. Chem. Soc.*, 2017, **139**, 13483–13486.

326 A. B. Pun, L. M. Campos and D. N. Congreve, *J. Am. Chem. Soc.*, 2019, **141**, 3777–3781.

327 S. Wen, J. Zhou, K. Zheng, A. Bednarkiewicz, X. Liu and D. Jin, *Nat. Commun.*, 2018, **9**, 2415.

328 J. Liu, W. Bu, L. Pan and J. Shi, *Angew. Chemie Int. Ed.*, 2013, **52**, 4375–4379.

329 J.-C. Boyer, C.-J. Carling, B. D. Gates and N. R. Branda, *J. Am. Chem. Soc.*, 2010, **132**, 15766–15772.

330 J. Lai, Y. Zhang, N. Pasquale and K.-B. Lee, *Angew. Chemie Int. Ed.*, 2014, **53**, 14419–14423.

331 X. Sun, J. Shi, X. Fu, Y. Yang and H. Zhang, *Sci. Rep.*, 2018, **8**, 10595.

332 X. Wu, G. Chen, J. Shen, Z. Li, Y. Zhang and G. Han, *Bioconjug. Chem.*, 2015, **26**, 166–175.

333 S. N. Sanders, M. K. Gangishetty, M. Y. Sfeir and D. N. Congreve, *J. Am. Chem. Soc.*, 2019, **141**, 9180–9184.

334 F. Nique, S. Hebbe, C. Peixoto, D. Annoot, J. M. Lefrançois, E. Duval, L. Michoux, N. Triballeau, J. M. Lemoullec, P. Mollat, M. Thauvin, T. Prangé, D. Minet, P. Clément-Lacroix, C. Robin-Jagerschmidt, D. Fleury, D. Guédin and P. Deprez, *J. Med. Chem.*, 2012, **55**, 8225–8235.

335 S. Ushijima, K. Moriyama and H. Togo, *Tetrahedron*, 2012, **68**, 4701–4709.

336 H. Sekiguchi, K. Muranaka, A. Osada, S. Ichikawa and A. Matsuda, *Bioorg. Med. Chem.*, 2010, **18**, 5732–5737.

337 X. Li, S. J. H. Martin, Z. S. Chinoy, L. Liu, B. Rittgers, R. A. Dluhy and G.-J. Boons, *Chem. – A Eur. J.*, 2016, **22**, 11180–11185.

338 H. Marom, K. Miller, Y. Bechor-Bar, G. Tsarfaty, R. Satchi-Fainaro and M. Gozin, *J. Med. Chem.*, 2010, **53**, 6316–6325.

339 J. Picha, M. Budesinsky, K. Machackova, M. Collinsova and J. Jiracek, *J. Pept. Sci.*, 2017, **23**, 202–214.

340 C. Testa, M. Scrima, M. Grimaldi, A. M. D'Ursi, M. L. Dirain, N. Lubin-Germain, A. Singh, C. Haskell-Luevano, M. Chorev, P. Rovero and A. M. Papini, *J. Med. Chem.*, 2014, **57**, 9424–9434.

341 A. Brennauer, M. Keller, M. Freund, G. Bernhardt and A. Buschauer, *Tetrahedron Lett.*, 2007, **48**, 6996–6999.

342 A. C. Biraboneye, S. Madonna, Y. Laras, S. Krantic, P. Maher and J. L. Kraus, *J. Med. Chem.*, 2009, **52**, 4358–4369.

343 C. De Cola, A. Manicardi, R. Corradini, I. Izzo and F. De Riccardis, *Tetrahedron*, 2012, **68**, 499–506.

344 Y. Kim, H. K. Pak, Y. H. Rhee and J. Park, *Chem. Commun.*, 2016, **52**, 6549–6552.

345 X. Sun, X. Li, S. Song, Y. Zhu, Y.-F. Liang and N. Jiao, *J. Am. Chem. Soc.*, 2015, **137**, 6059–6066.

346 J. L. García Ruano, J. Alemán, M. Belén Cid and A. Parra, *Org. Lett.*, 2005, **7**, 179–182.

347 C. N. Rao, D. Lentz and H.-U. Reissig, *Angew. Chemie Int. Ed.*, 2015, **54**, 2750–2753.

348 C. Steinebach, I. Sosič, S. Lindner, A. Bricelj, F. Kohl, Y. L. D. Ng, M. Monschke, K. G. Wagner, J. Krönke and M. Gütschow, *Medchemcomm*, 2019, **10**, 1037–1041.

349 Q. Meng, Z. Wang, J. Cui, Q. Cui, J. Dong, Q. Zhang and S. Li, *J. Med. Chem.*, 2018, **61**, 10901–10909.

350 N. Estrada-Ortiz, C. G. Neochoritis, A. Twarda-Clapa, B. Musielak, T. A. Holak and A. Dömling, *ACS Med. Chem. Lett.*, 2017, **8**, 1025–1030.

351 J. C. Boehm, J. M. Smietana, M. E. Sorenson, R. S. Garigipati, T. F. Gallagher, P. L. Sheldrake, J. Bradbeer, A. M. Badger, J. T. Laydon, J. C. Lee, L. M. Hillegass, D. E. Griswold, J. J. Breton, M. C. Chabot-Fletcher and J. L. Adams, *J. Med. Chem.*, 1996, **39**, 3929–3937.

352 WO2014/4229, 2014.

353 K. S. Lee, J. H. Lim, Y. K. Kang, K. H. Yoo, D. C. Kim, K. J. Shin and D. J. Kim, *Eur. J. Med. Chem.*, 2006, **41**, 1347–1351.

354 A. Lewis, J. Wilkie, T. J. Rutherford and D. Gani, *J. Chem. Soc. Perkin Trans. 1*, 1998, 3777–3794.

355 R. Shyam, N. Charbonnel, A. Job, C. Blavignac, C. Forestier, C. Taillefumier and S. Faure, *ChemMedChem*, 2018, **13**, 1513–1516.

356 J. Moreno, M. Gerecke, L. Grubert, S. A. Kovalenko and S. Hecht, *Angew. Chemie Int. Ed.*, 2016, **55**, 1544–1547.

357 C. R. Opie, N. Kumagai and M. Shibasaki, *Angew. Chemie Int. Ed.*, 2017, **56**, 3349–3353.

358 F. Zhao, L. Grubert, S. Hecht and D. Bléger, *Chem. Commun.*, 2017, **53**, 3323–3326.

359 Y. Yamada, T. Kubota, M. Nishio and K. Tanaka, *J. Am. Chem. Soc.*, 2014, **136**, 6505–6509.

360 Y. Wu, Q. Shi, H. Lei, X. Liu and L. Luan, *Tetrahedron*, 2014, **70**, 3757–3761.

361 P. Nandhikonda and M. D. Heagy, *Org. Lett.*, 2010, **12**, 4796–4799.

362 K. Yang, Y. Song, H. Xie, H. Wu, Y.-T. Wu, E. D. Leisten and W. Tang, *Bioorg. Med. Chem. Lett.*, 2018, **28**, 2493–2497.

363 B. Zhou, J. Hu, F. Xu, Z. Chen, L. Bai, E. Fernandez-Salas, M. Lin, L. Liu, C.-Y. Yang, Y. Zhao, D. McEachern, S. Przybranowski, B. Wen, D. Sun and S. Wang, *J. Med. Chem.*, 2018, **61**, 462–481.

364 WO2017024317, 2017.

365 WO2017197051, 2017.

366 US2018179183, 2018.

367 J. Charoenpattarapreeda, Y. S. Tan, J. Iegre, S. J. Walsh, E. Fowler, R. S. Eapen, Y. Wu, H. F. Sore, C. S. Verma, L. Itzhaki and D. R. Spring, *Chem. Commun.*, 2019, **55**, 7914–7917.

7. Appendices

7.1. Selected NMR Spectra

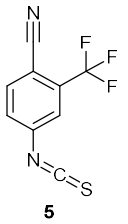

5

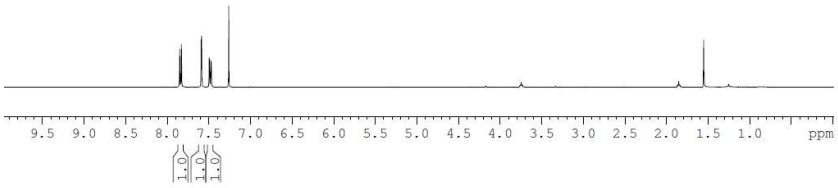

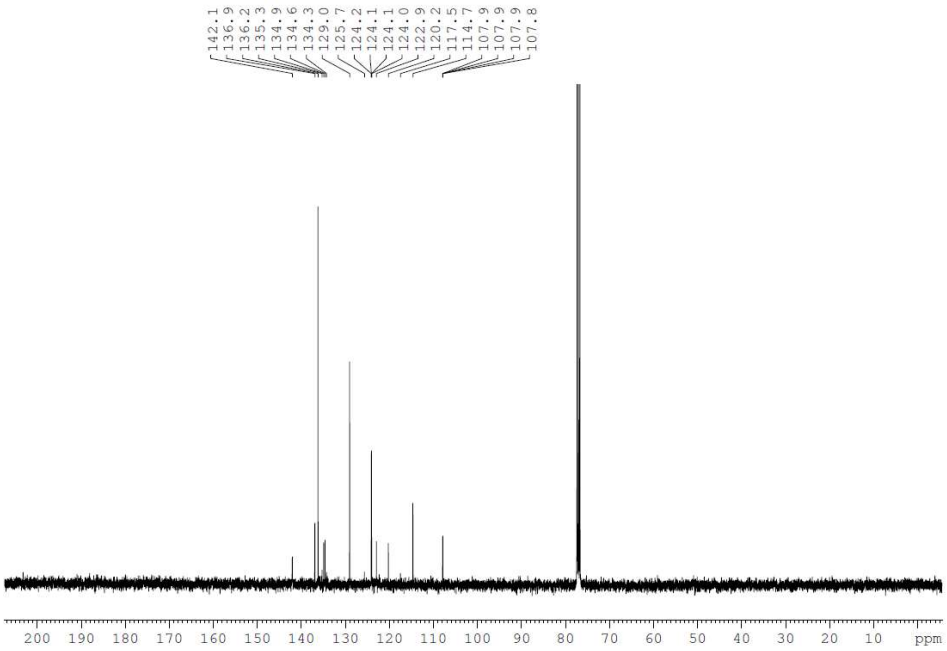

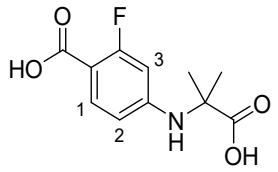
O
F
HO
3
1
2
N
H
O
OH

11

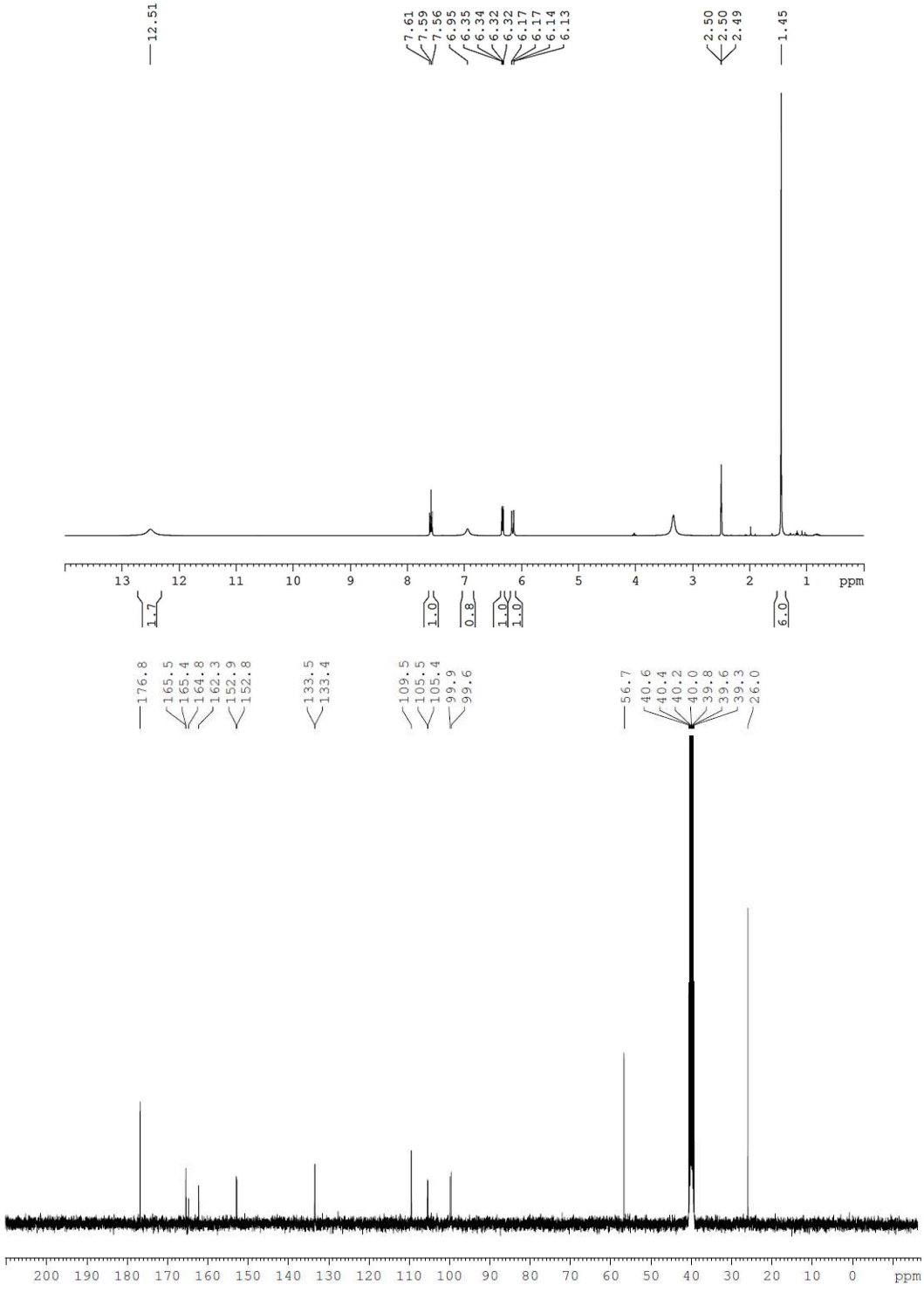
12.51
7.61
7.59
7.56
6.95
6.35
6.34
6.32
6.32
6.17
6.17
6.14
6.13
2.50
2.50
2.49
1.45
ppm
1.7
1.0
0.8
1.0
1.0
6.0
176.8
165.5
165.4
164.8
162.3
152.9
152.8
133.5
133.4
109.5
105.5
105.4
99.9
99.6
56.7
40.6
40.4
40.2
40.0
39.8
39.6
39.3
26.0
ppm

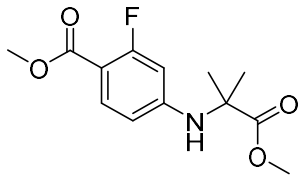

4

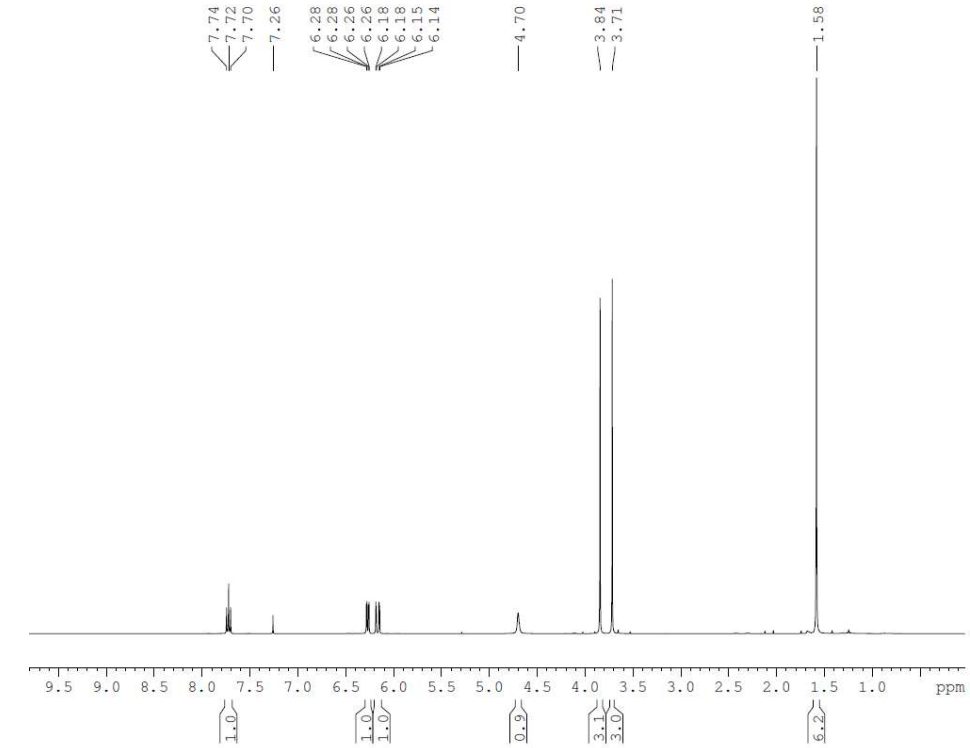
7.74
7.72
7.70
7.26
6.28
6.28
6.26
6.26
6.18
6.18
6.15
6.14
4.70
3.84
3.71
1.58
ppm
1.0
1.0
1.0
0.9
3.1
3.0
6.2

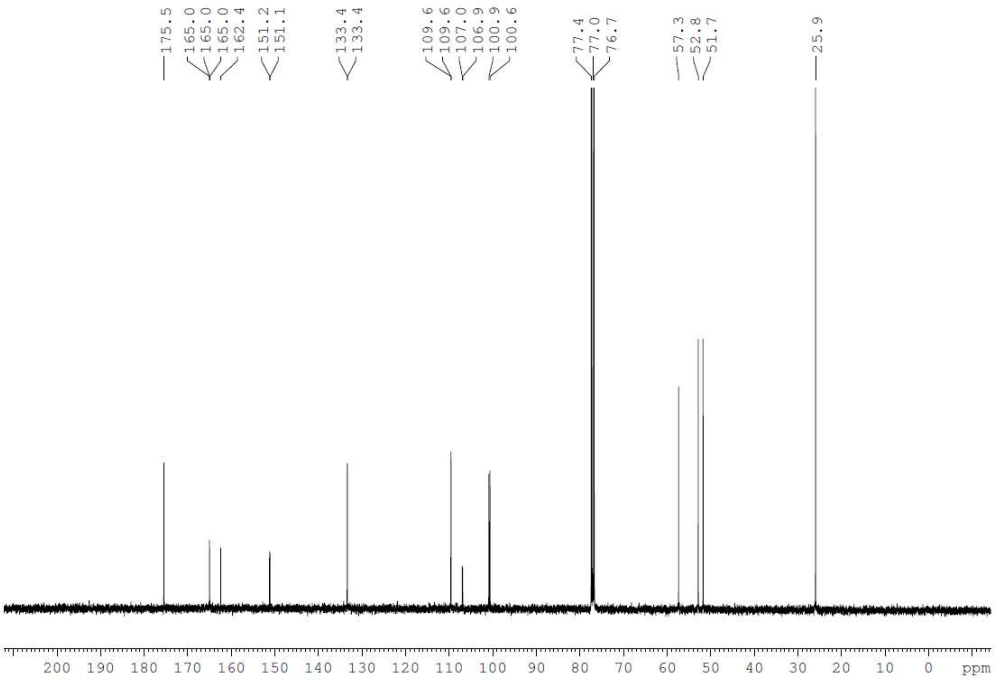
175.5
165.0
165.0
165.0
162.4
151.2
151.1
133.4
133.4
109.6
109.6
107.0
106.9
100.9
100.6
77.4
77.0
76.7
57.3
52.8
51.7
25.9
ppm

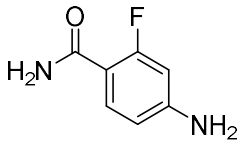
O
F
H2N
NH2

13


8.02
8.00
7.97
7.44
7.43
7.42
7.41
7.36
7.35
7.33
7.32
7.26
6.61
6.26

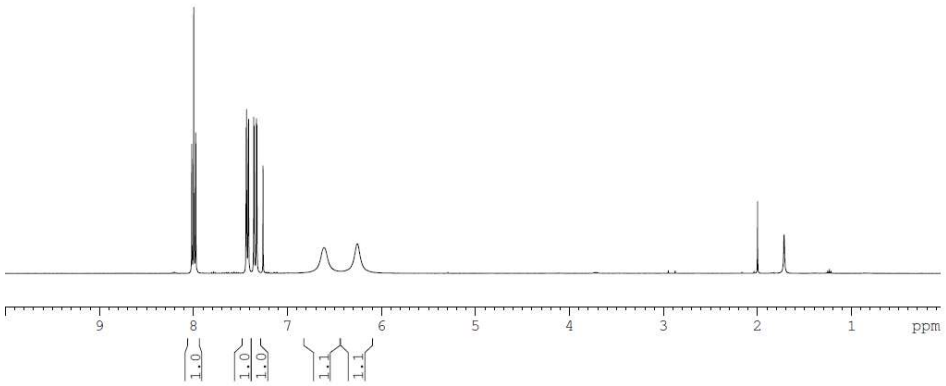
9
8
7
6
5
4
3
2
1
ppm
1.0
1.0
1.0
1.1
1.1

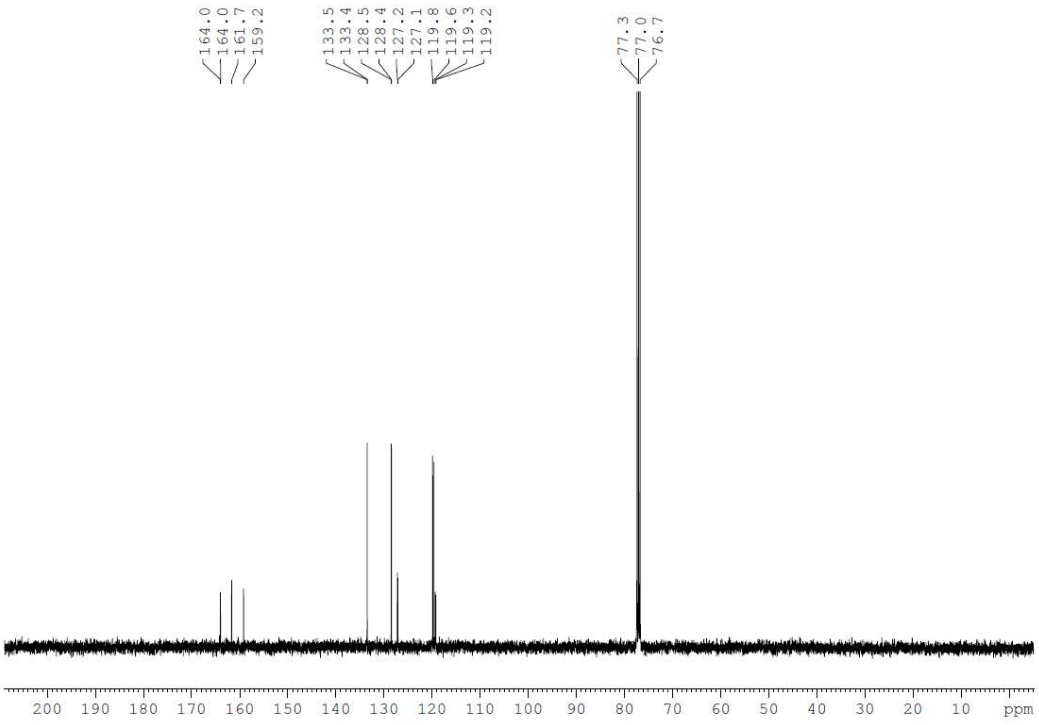
164.0
164.0
161.7
159.2
133.5
133.4
128.5
128.4
127.2
127.1
119.8
119.6
119.3
119.2
77.3
77.0
76.7
200
190
180
170
160
150
140
130
120
110
100
90
80
70
60
50
40
30
20
10
ppm

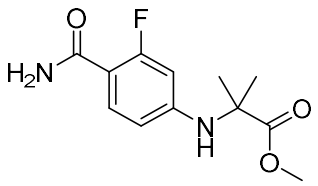
O
F
H2N
N
H
O
O

15

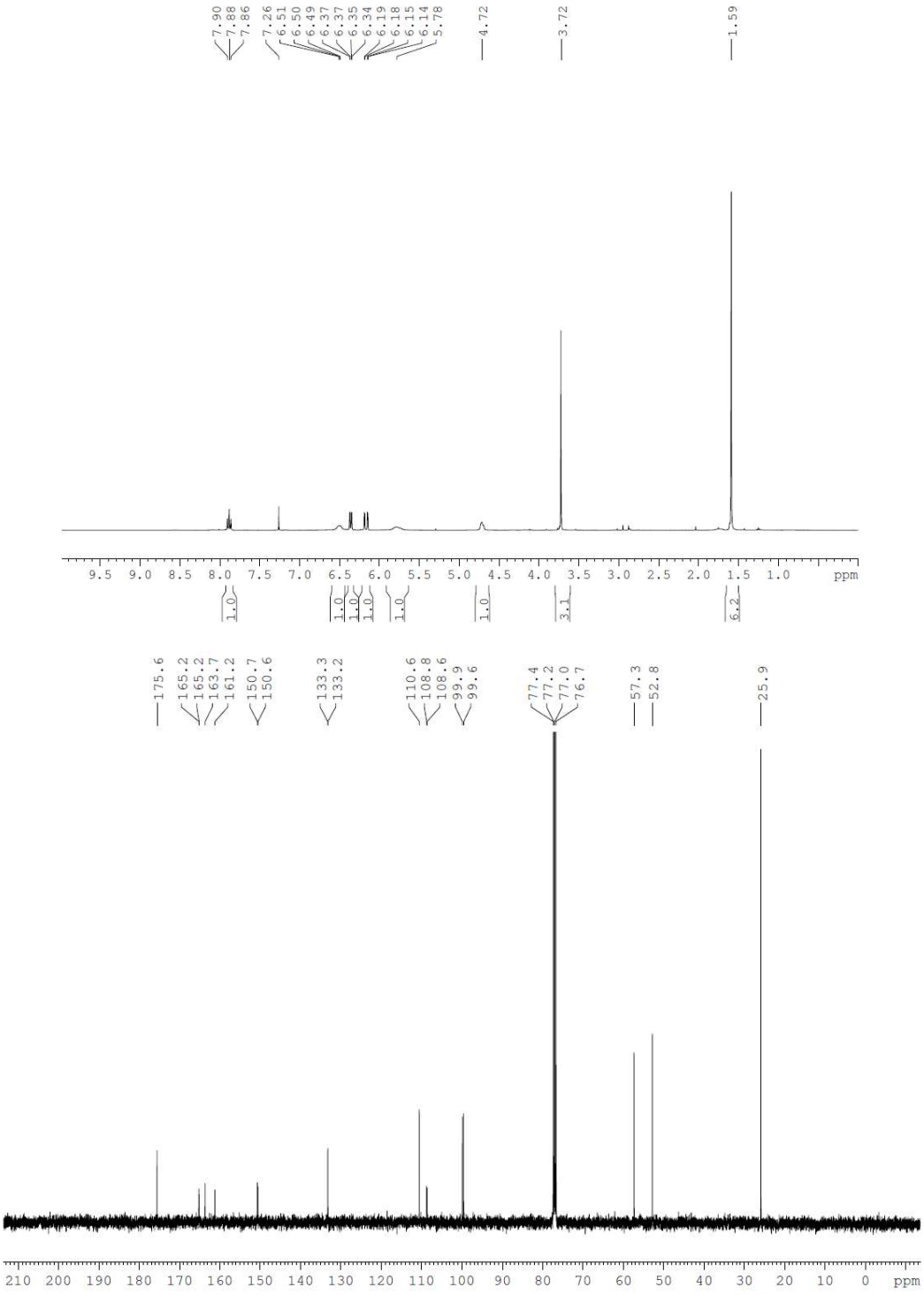
7.90
7.88
7.86
7.26
6.51
6.50
6.49
6.37
6.37
6.35
6.34
6.19
6.18
6.15
6.14
5.78
4.72
3.72
1.59
9.5 9.0 8.5 8.0 7.5 7.0 6.5 6.0 5.5 5.0 4.5 4.0 3.5 3.0 2.5 2.0 1.5 1.0 ppm
1.0
1.0
1.0
1.0
1.0
1.0
3.1
6.2
175.6
165.2
165.2
163.7
161.2
150.7
150.6
133.3
133.2
110.6
108.8
108.6
99.9
99.6
77.4
77.2
77.0
76.7
57.3
52.8
25.9
210 200 190 180 170 160 150 140 130 120 110 100 90 80 70 60 50 40 30 20 10 0 ppm

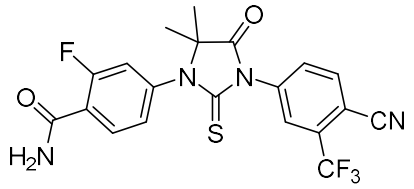
F
O
N
N
O
S
CN
H_2N
CF_3

16

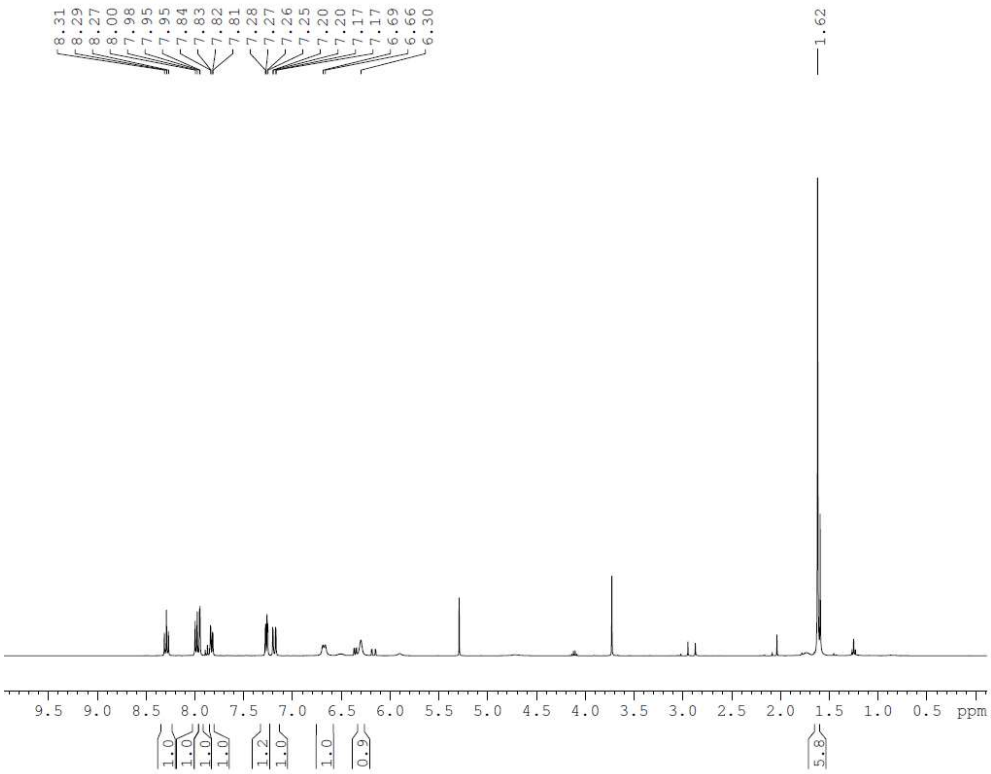
8.31
8.29
8.27
8.00
7.98
7.95
7.95
7.84
7.83
7.82
7.81
7.28
7.27
7.26
7.25
7.20
7.20
7.17
7.17
6.69
6.66
6.30
1.62
9.5 9.0 8.5 8.0 7.5 7.0 6.5 6.0 5.5 5.0 4.5 4.0 3.5 3.0 2.5 2.0 1.5 1.0 0.5 ppm
1.0
1.0
1.0
1.0
1.2
1.0
1.0
0.9
5.8

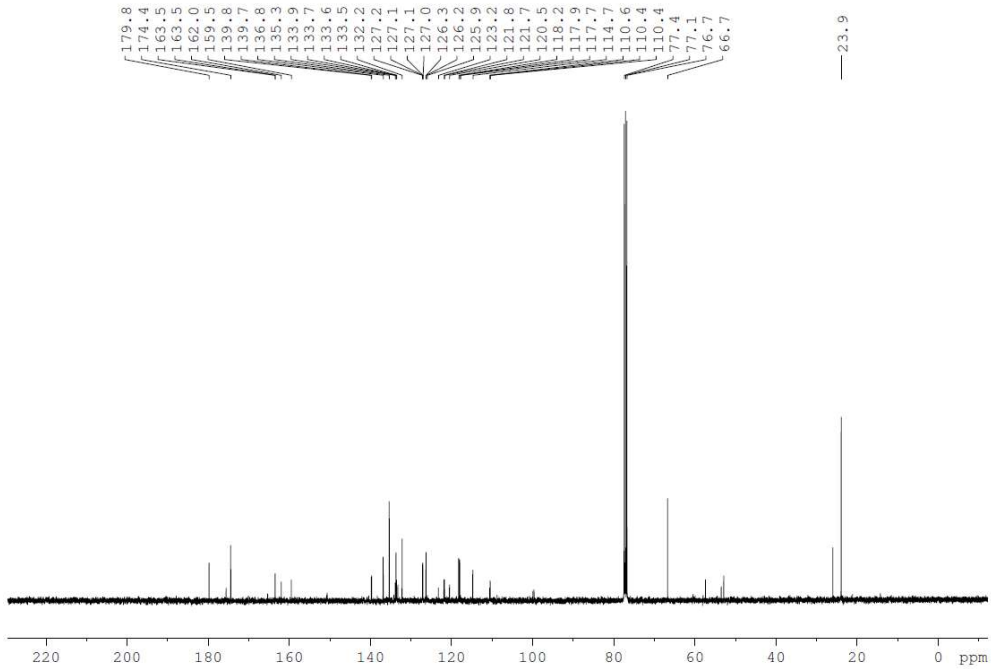
179.8
174.4
163.5
163.5
162.0
159.5
139.8
139.7
136.8
135.3
133.9
133.7
133.6
133.5
132.2
127.2
127.1
127.1
127.0
126.3
126.2
125.9
123.2
121.8
121.7
120.5
118.2
117.9
117.7
114.7
110.6
110.4
110.4
77.4
77.1
76.7
66.7
23.9
220 200 180 160 140 120 100 80 60 40 20 0 ppm

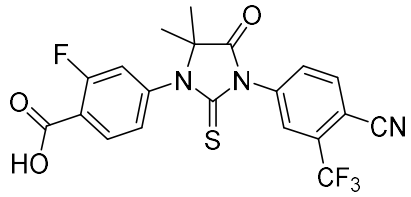
F
O
HO
N
N
O
S
CN
CF3

2

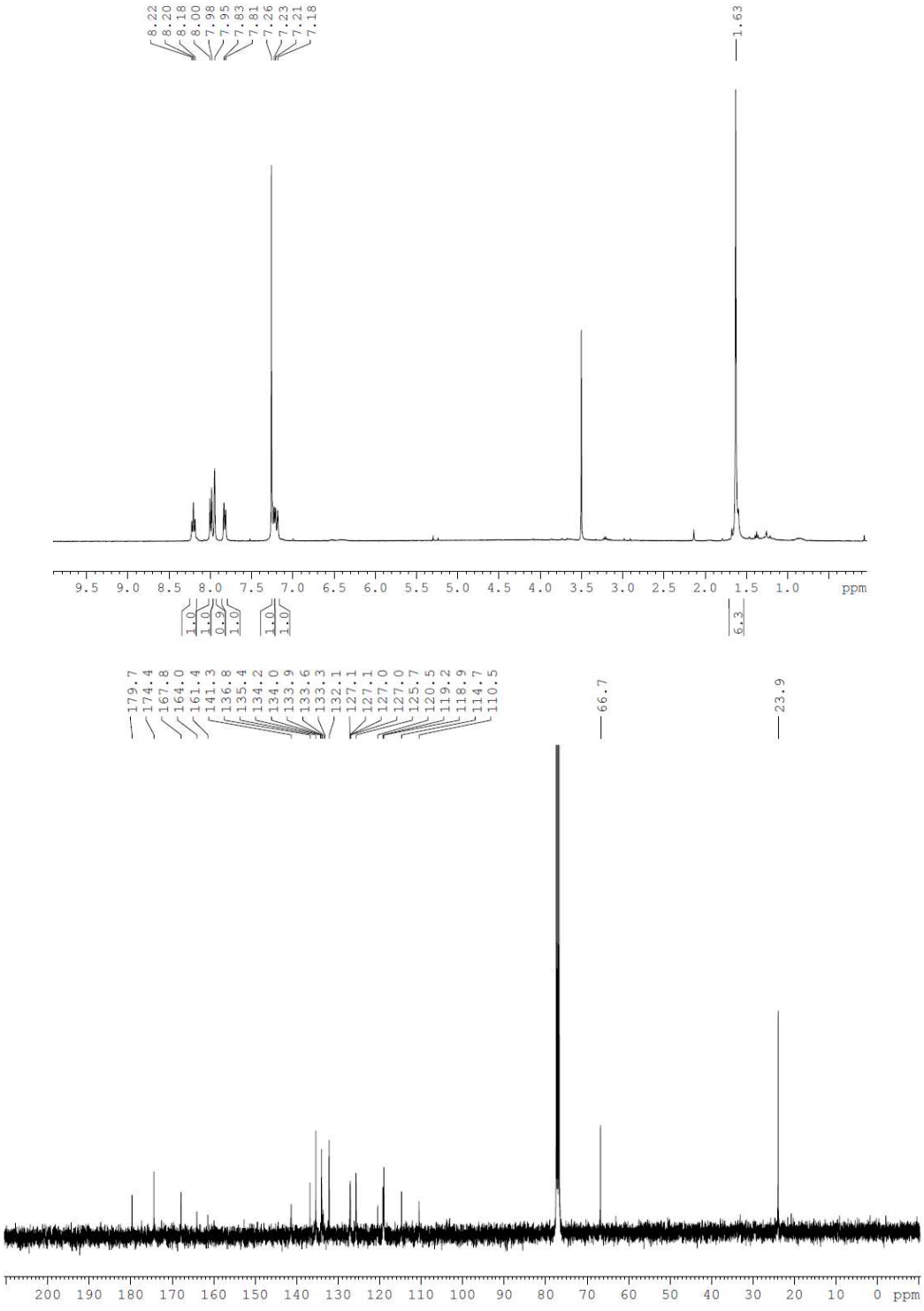
8.22
8.20
8.18
8.00
7.98
7.95
7.83
7.81
7.26
7.23
7.21
7.18
1.63
9.5 9.0 8.5 8.0 7.5 7.0 6.5 6.0 5.5 5.0 4.5 4.0 3.5 3.0 2.5 2.0 1.5 1.0 ppm
1.0
1.0
0.9
1.0
1.0
1.0
6.3
179.7
174.4
167.8
164.0
161.4
141.3
136.8
135.4
134.2
134.0
133.9
133.6
133.3
132.1
127.1
127.1
127.0
127.0
125.7
120.5
119.2
118.9
114.7
110.5
66.7
23.9
200 190 180 170 160 150 140 130 120 110 100 90 80 70 60 50 40 30 20 10 0 ppm

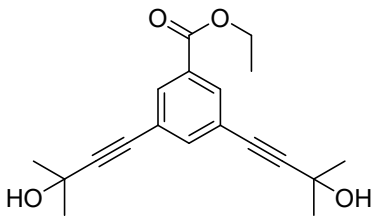
O
O
HO
OH

19

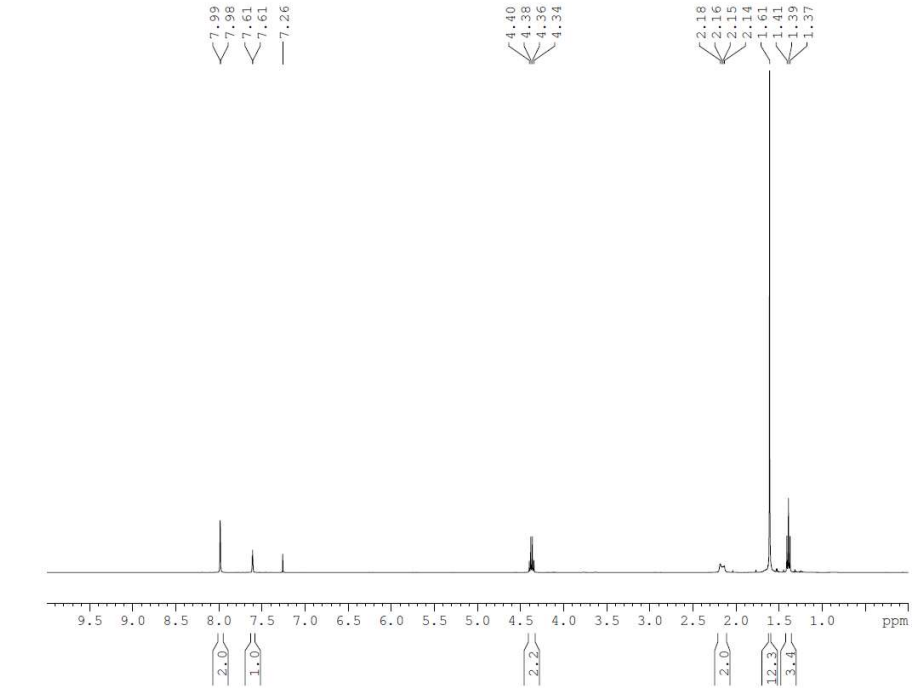
7.99
7.98
7.61
7.61
7.26
4.40
4.38
4.36
4.34
2.18
2.16
2.15
2.14
1.61
1.41
1.39
1.37
9.5 9.0 8.5 8.0 7.5 7.0 6.5 6.0 5.5 5.0 4.5 4.0 3.5 3.0 2.5 2.0 1.5 1.0 ppm
2.0
1.0
2.2
2.0
12.3
3.4

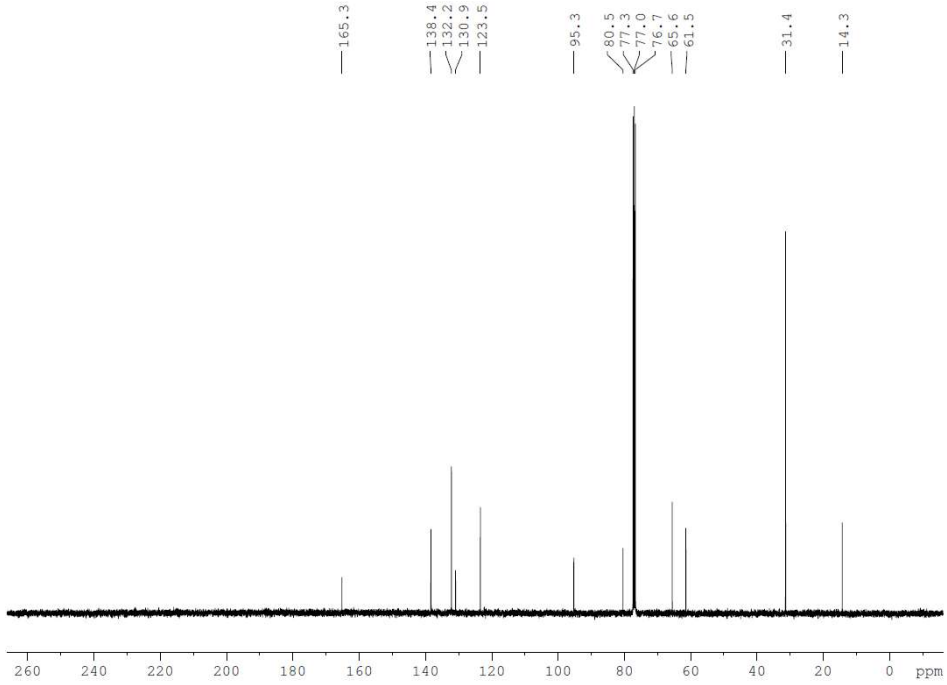
165.3
138.4
132.2
130.9
123.5
95.3
80.5
77.3
77.0
76.7
65.6
61.5
31.4
14.3
260 240 220 200 180 160 140 120 100 80 60 40 20 0 ppm

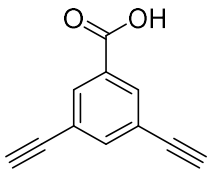
O
OH

6

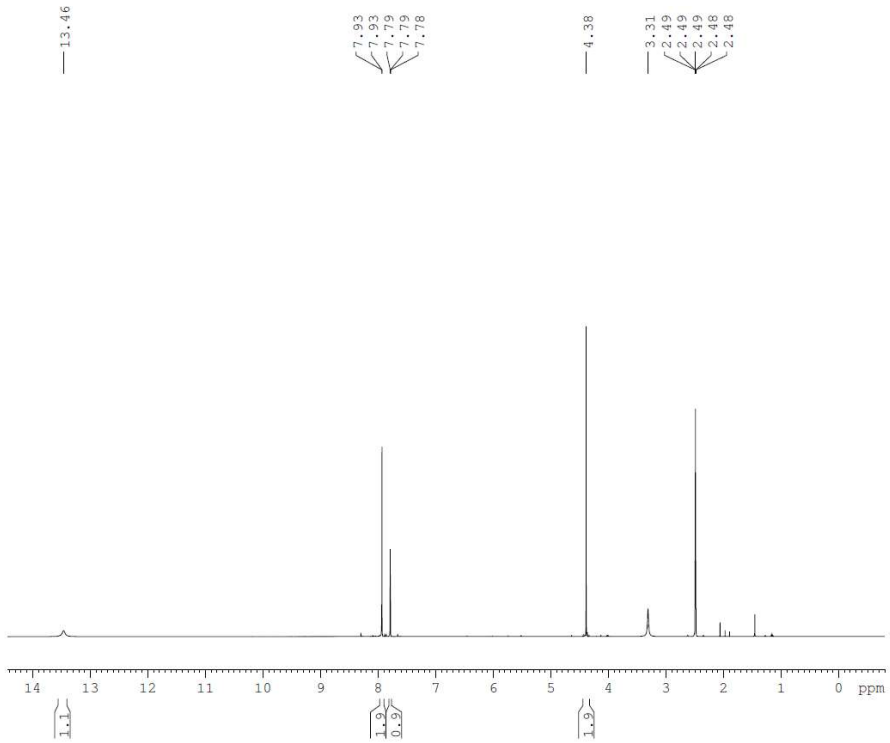
13.46
7.93
7.93
7.79
7.79
7.78
4.38
3.31
2.49
2.49
2.49
2.48
2.48
14 13 12 11 10 9 8 7 6 5 4 3 2 1 0 ppm
1.1
1.9
0.9
1.9

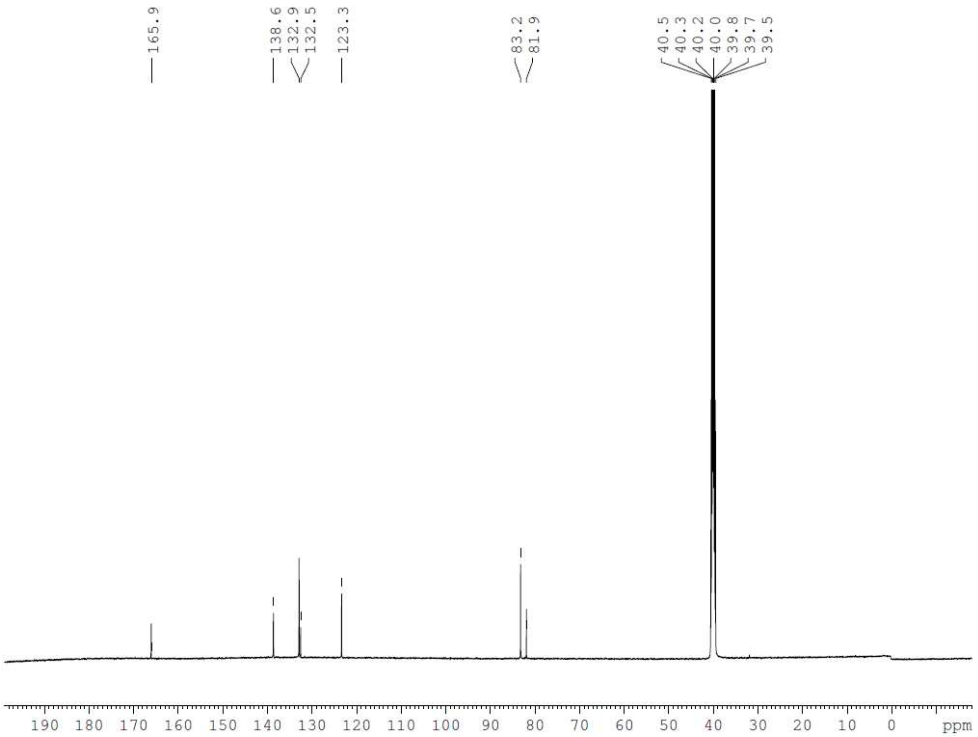
165.9
138.6
132.9
132.5
123.3
83.2
81.9
40.5
40.3
40.2
40.0
39.8
39.7
39.5
190 180 170 160 150 140 130 120 110 100 90 80 70 60 50 40 30 20 10 0 ppm

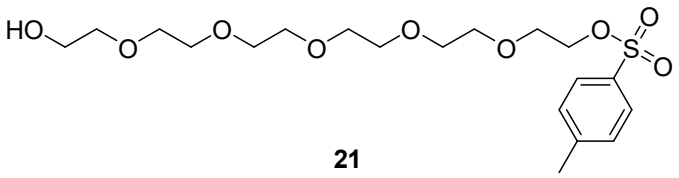

21

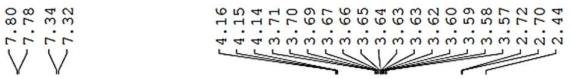
7.80
7.78
7.34
7.32
4.16
4.15
4.14
3.71
3.70
3.69
3.67
3.66
3.65
3.64
3.63
3.63
3.62
3.60
3.59
3.58
3.57
2.72
2.70
2.44

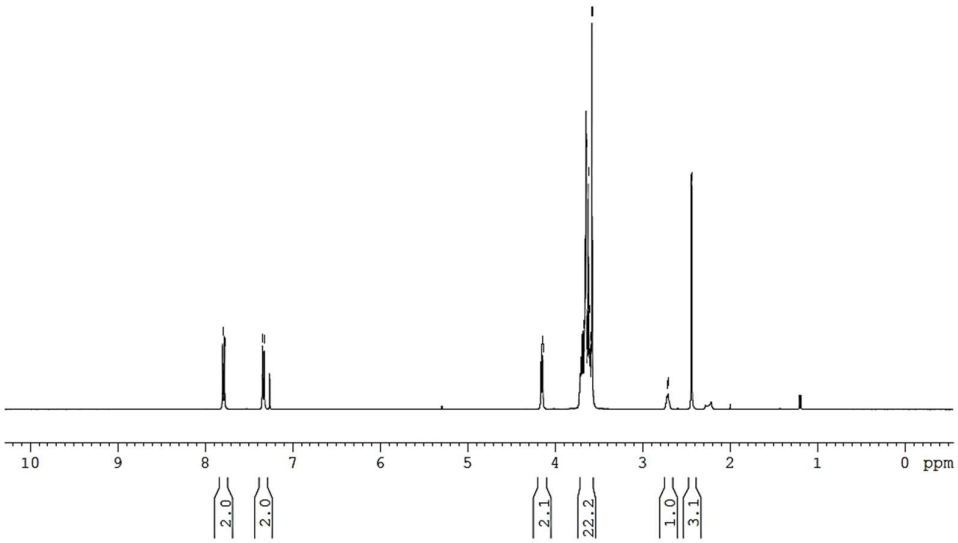
10 9 8 7 6 5 4 3 2 1 0 ppm
2.0
2.0
2.1
22.2
1.0
3.1

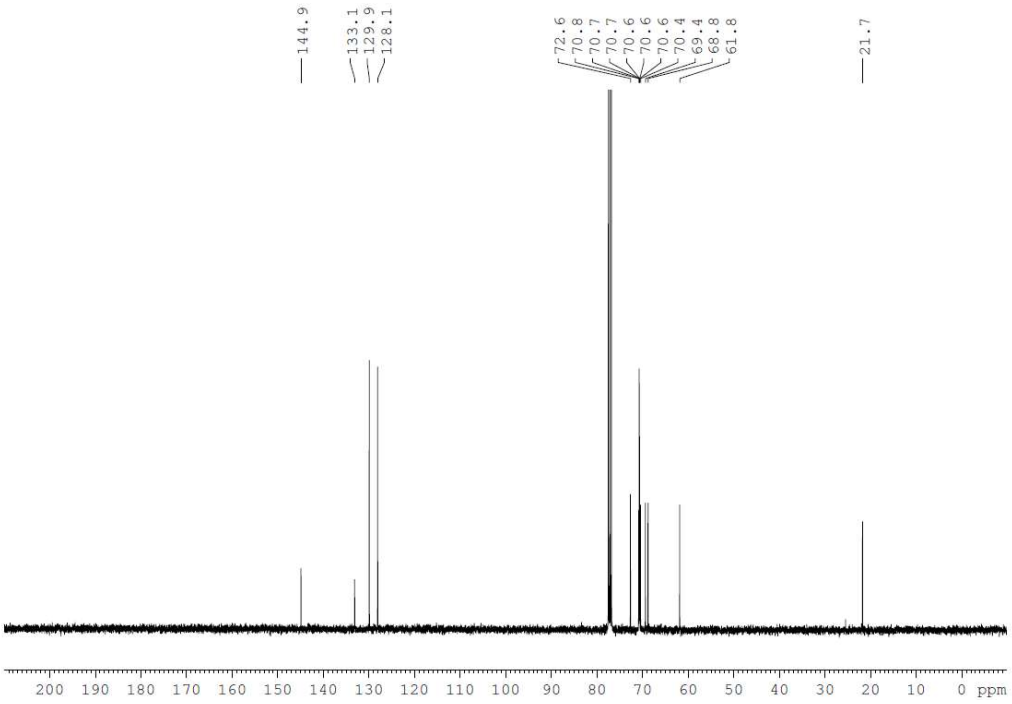
144.9
133.1
129.9
128.1
72.6
70.8
70.7
70.7
70.6
70.6
70.6
70.4
69.4
68.8
61.8
21.7
200 190 180 170 160 150 140 130 120 110 100 90 80 70 60 50 40 30 20 10 0 ppm

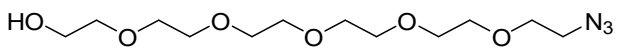

22

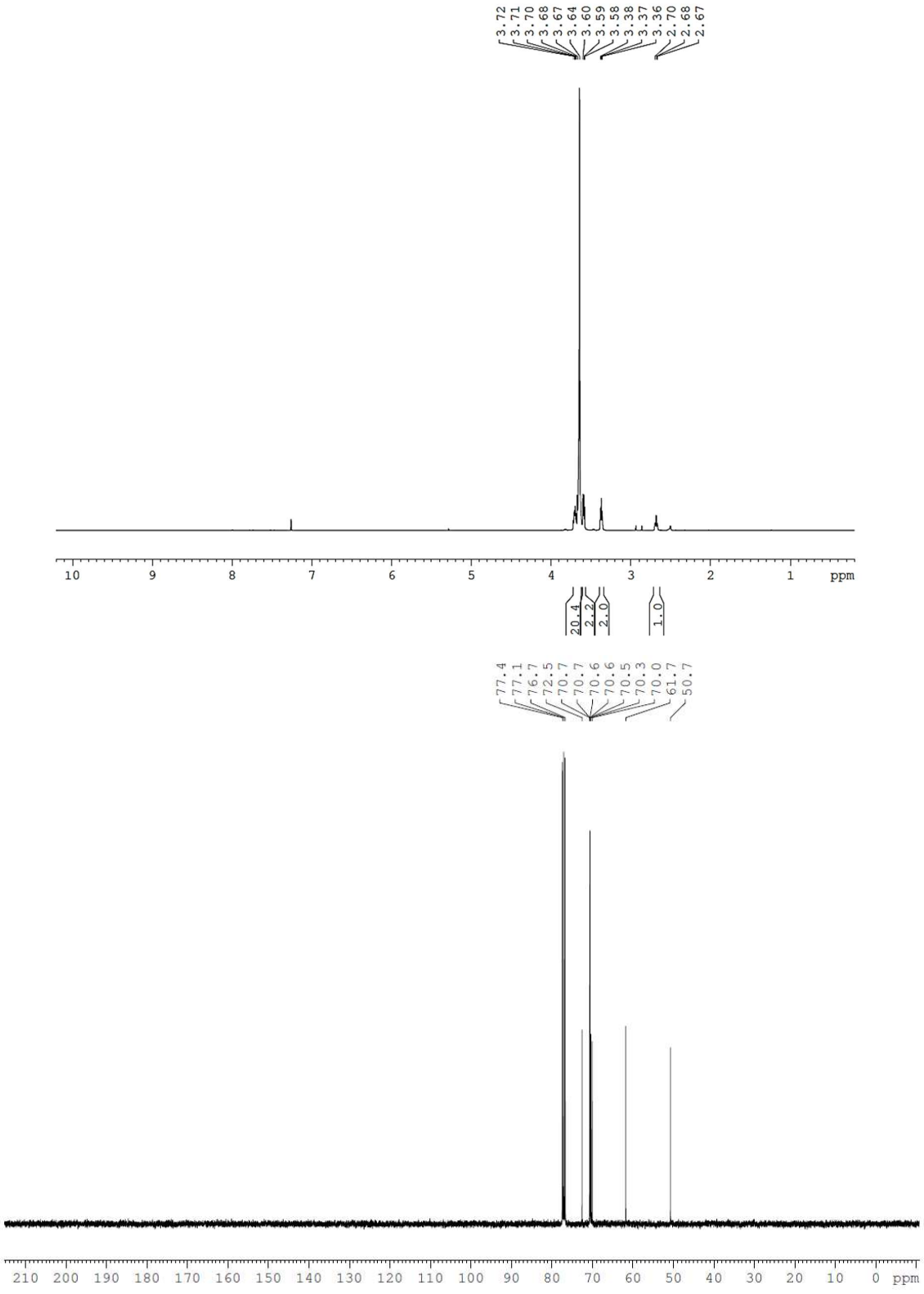
3.72
3.71
3.70
3.68
3.67
3.64
3.60
3.59
3.58
3.38
3.37
3.36
2.70
2.68
2.67
10 9 8 7 6 5 4 3 2 1 ppm
20.4
2.2
2.0
1.0
77.4
77.1
76.7
72.5
70.7
70.7
70.6
70.6
70.5
70.3
70.0
61.7
50.7
210 200 190 180 170 160 150 140 130 120 110 100 90 80 70 60 50 40 30 20 10 0 ppm

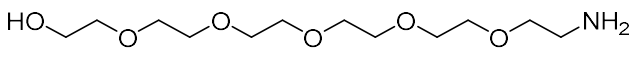
HO
O
O
O
O
O
NH2

23

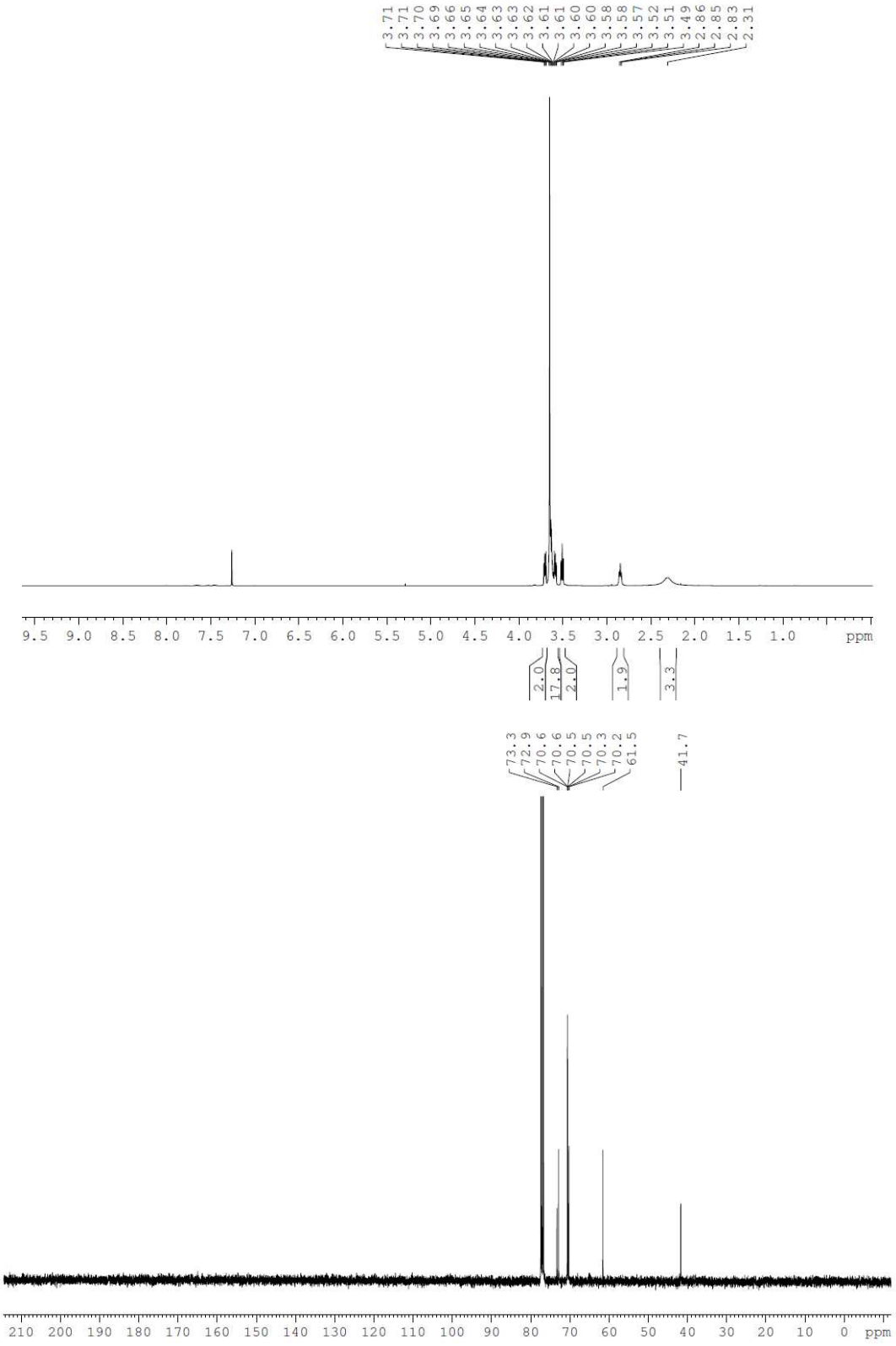
3.71
3.71
3.70
3.69
3.66
3.65
3.64
3.63
3.63
3.62
3.61
3.61
3.60
3.60
3.58
3.58
3.57
3.52
3.51
3.49
2.86
2.85
2.83
2.31
9.5 9.0 8.5 8.0 7.5 7.0 6.5 6.0 5.5 5.0 4.5 4.0 3.5 3.0 2.5 2.0 1.5 1.0 ppm
2.0
17.8
2.0
1.9
3.3
73.3
72.9
70.6
70.6
70.5
70.5
70.3
70.2
61.5
41.7
210 200 190 180 170 160 150 140 130 120 110 100 90 80 70 60 50 40 30 20 10 0 ppm

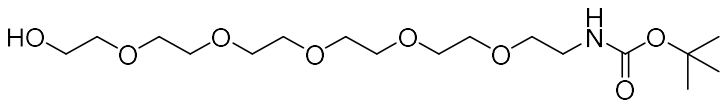

7

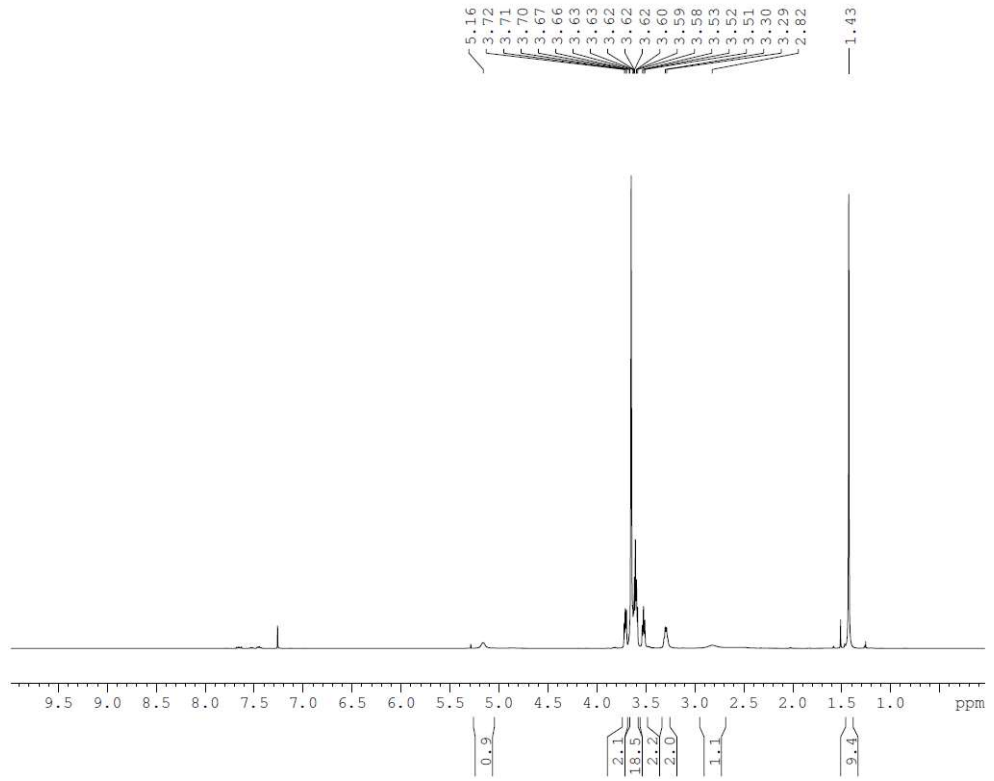
5.16
3.72
3.71
3.70
3.67
3.66
3.63
3.63
3.62
3.62
3.62
3.60
3.59
3.58
3.53
3.52
3.51
3.30
3.29
2.82
1.43
9.5 9.0 8.5 8.0 7.5 7.0 6.5 6.0 5.5 5.0 4.5 4.0 3.5 3.0 2.5 2.0 1.5 1.0 ppm
0.9
2.1
18.5
2.2
2.0
1.1
9.4

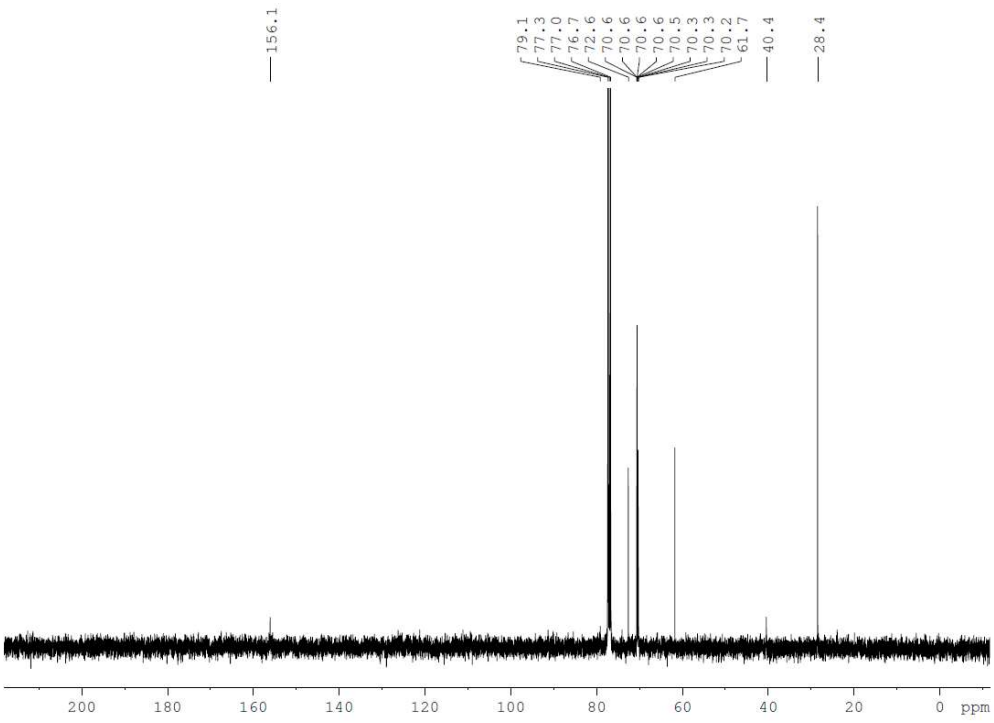
156.1
79.1
77.3
77.0
76.7
72.6
70.6
70.6
70.6
70.6
70.5
70.3
70.3
70.2
61.7
40.4
28.4
200 180 160 140 120 100 80 60 40 20 0 ppm

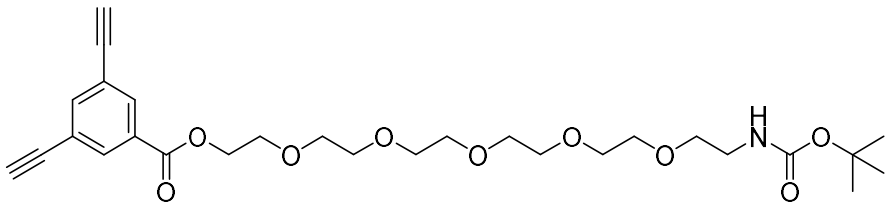

24

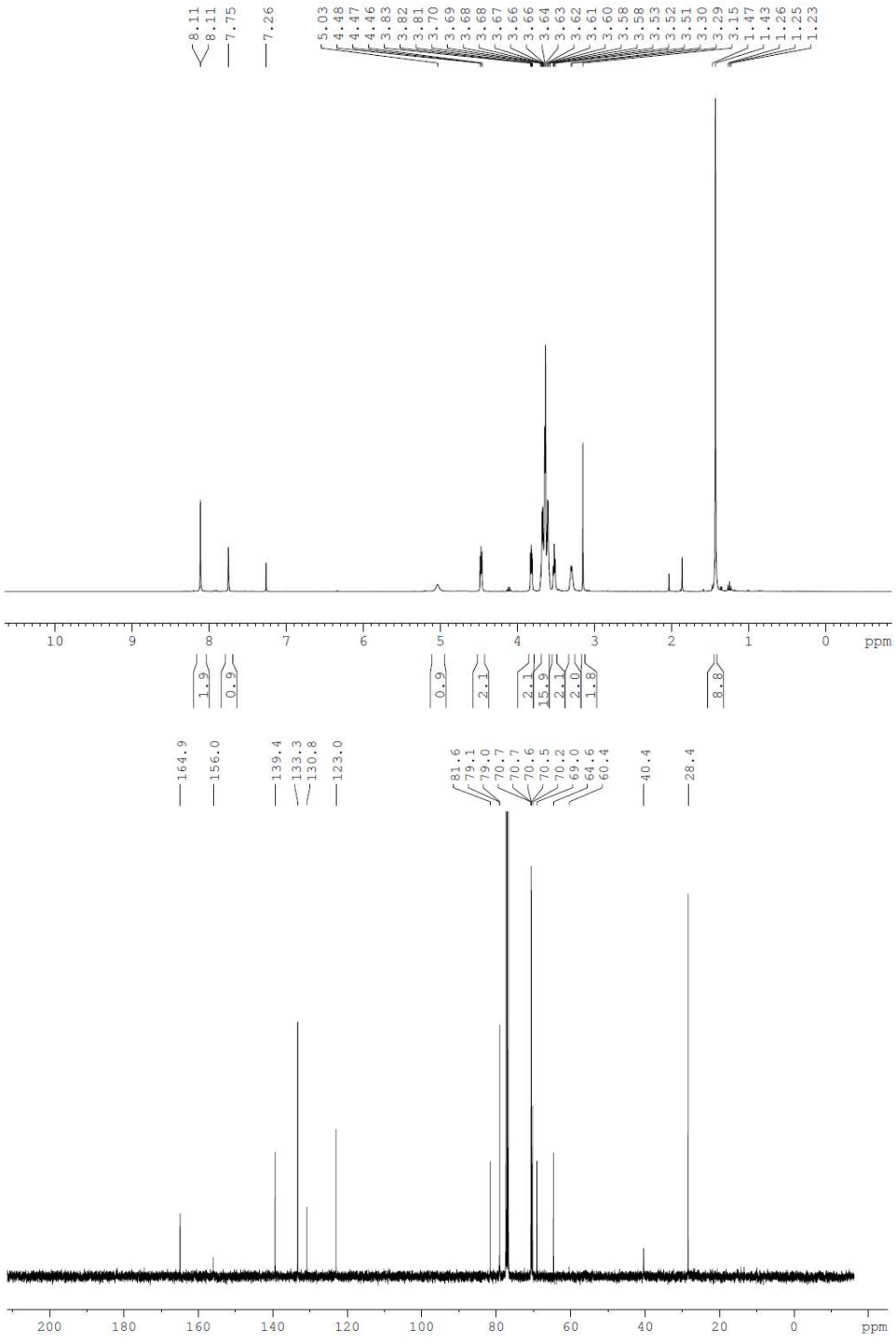
8.11
8.11
7.75
7.26
5.03
4.48
4.47
4.46
3.83
3.82
3.81
3.70
3.69
3.68
3.68
3.67
3.66
3.66
3.64
3.63
3.62
3.61
3.60
3.58
3.58
3.53
3.52
3.51
3.30
3.29
3.15
1.47
1.43
1.26
1.25
1.23
ppm
1.9
0.9
0.9
2.1
2.1
15.9
2.1
2.0
1.8
8.8
164.9
156.0
139.4
133.3
130.8
123.0
81.6
79.1
79.0
70.7
70.7
70.6
70.5
70.2
69.0
64.6
60.4
40.4
28.4
ppm

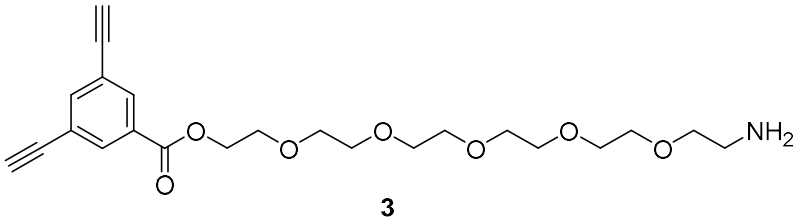

3

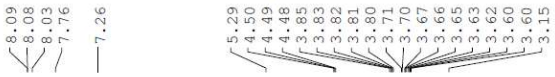
8.09
8.08
8.03
7.76
7.26
5.29
4.50
4.49
4.48
3.85
3.83
3.82
3.81
3.80
3.71
3.70
3.67
3.66
3.65
3.63
3.62
3.60
3.60
3.15

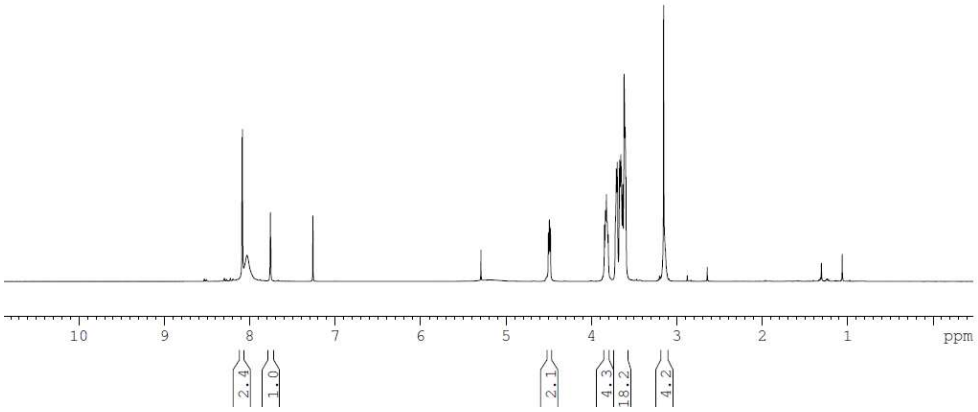
10
9
8
7
6
5
4
3
2
1
ppm
2.4
1.0
2.1
4.3
18.2
4.2

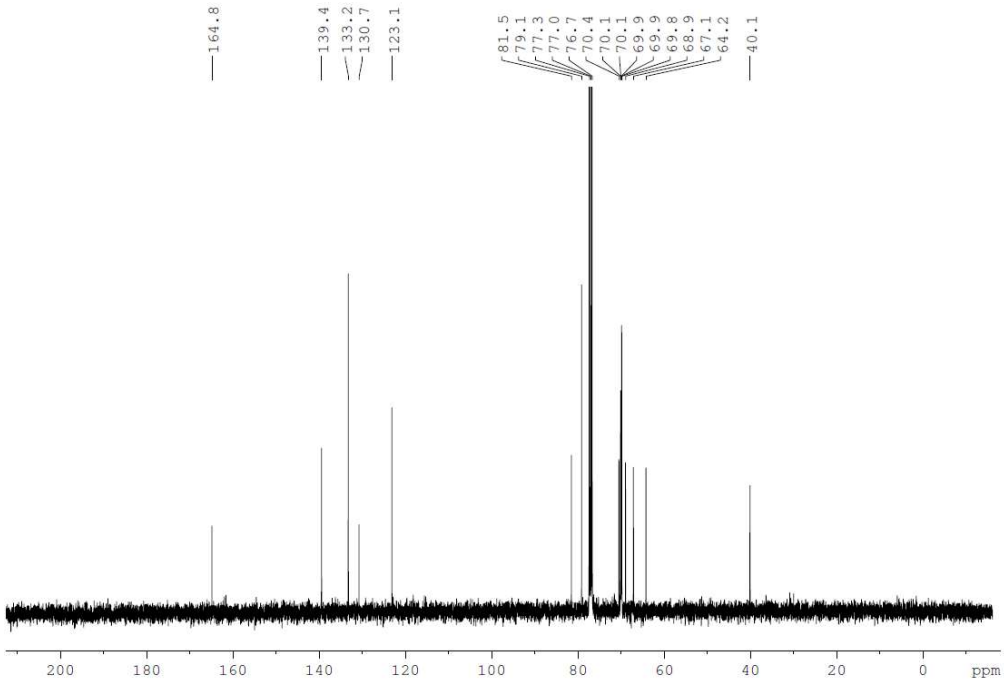
164.8
139.4
133.2
130.7
123.1
81.5
79.1
77.3
77.0
76.7
70.4
70.1
70.1
69.9
69.9
69.8
68.9
67.1
64.2
40.1
200
180
160
140
120
100
80
60
40
20
0
ppm

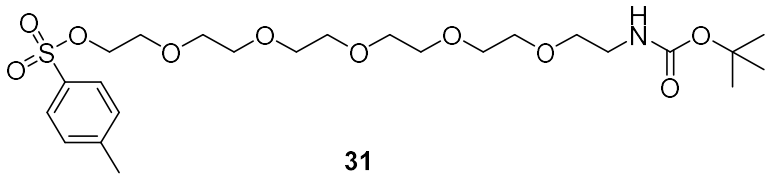

31

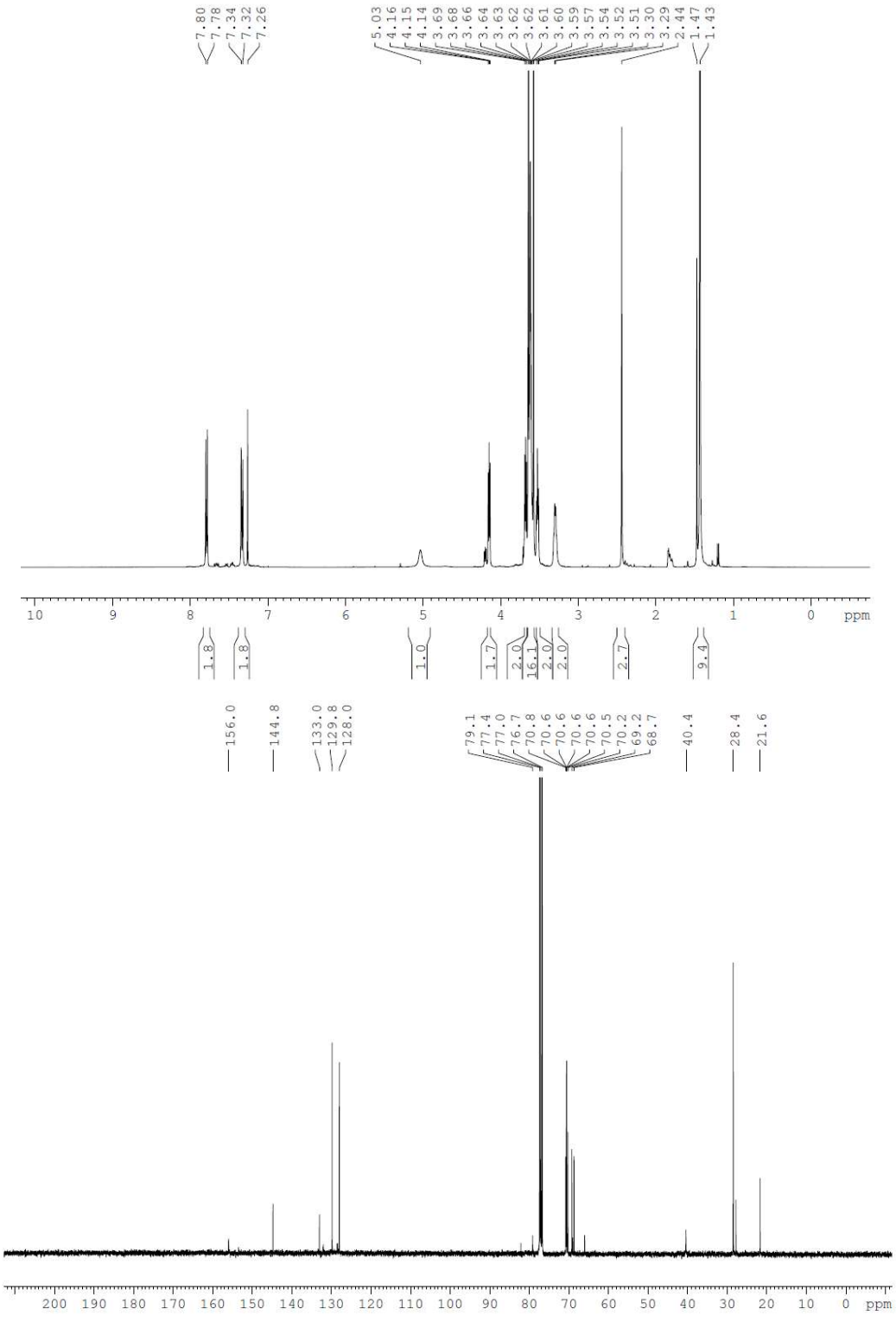
7.80
7.78
7.34
7.32
7.26
5.03
4.16
4.15
4.14
3.69
3.68
3.66
3.64
3.63
3.62
3.62
3.61
3.60
3.59
3.57
3.54
3.52
3.51
3.30
3.29
2.44
1.47
1.43
10 9 8 7 6 5 4 3 2 1 0 ppm
1.8
1.8
1.0
1.7
2.0
16.1
2.0
2.0
2.7
9.4
156.0
144.8
133.0
129.8
128.0
79.1
77.4
77.0
76.7
70.8
70.6
70.6
70.6
70.6
70.5
70.2
69.2
68.7
40.4
28.4
21.6
200 190 180 170 160 150 140 130 120 110 100 90 80 70 60 50 40 30 20 10 0 ppm

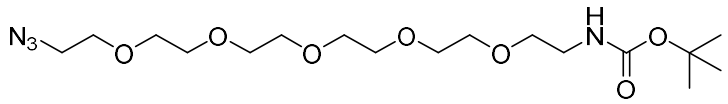

32

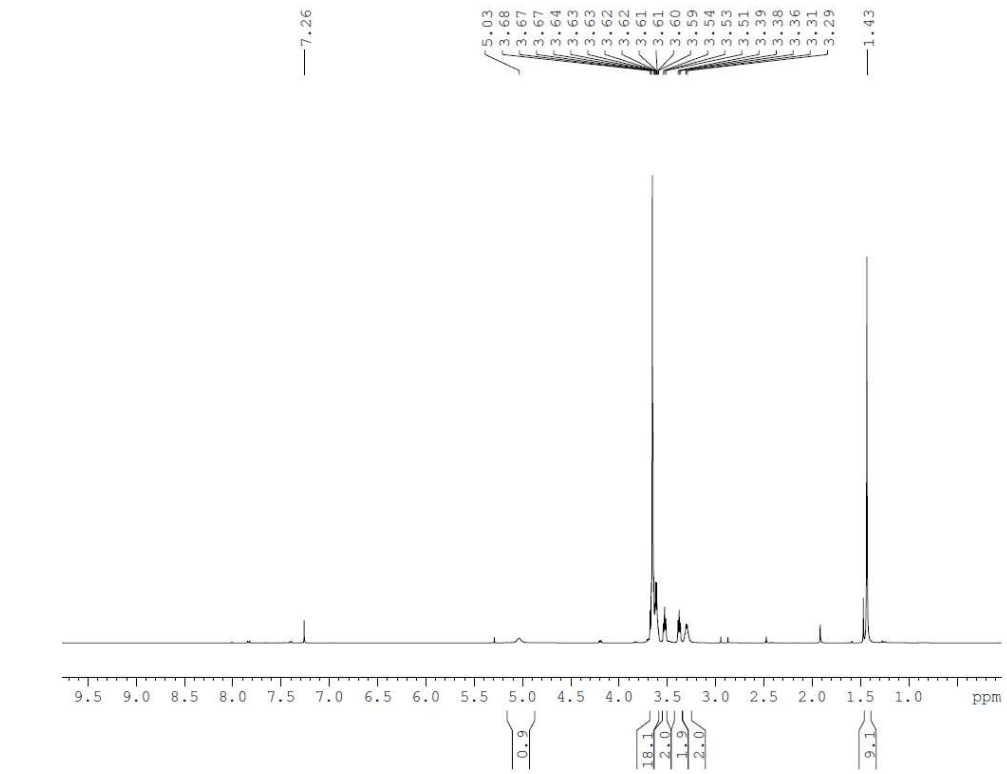
7.26
5.03
3.68
3.67
3.67
3.64
3.63
3.63
3.62
3.62
3.61
3.61
3.60
3.59
3.54
3.53
3.51
3.39
3.38
3.36
3.31
3.29
1.43
9.5 9.0 8.5 8.0 7.5 7.0 6.5 6.0 5.5 5.0 4.5 4.0 3.5 3.0 2.5 2.0 1.5 1.0 ppm
0.9
18.1
2.0
1.9
2.0
9.1

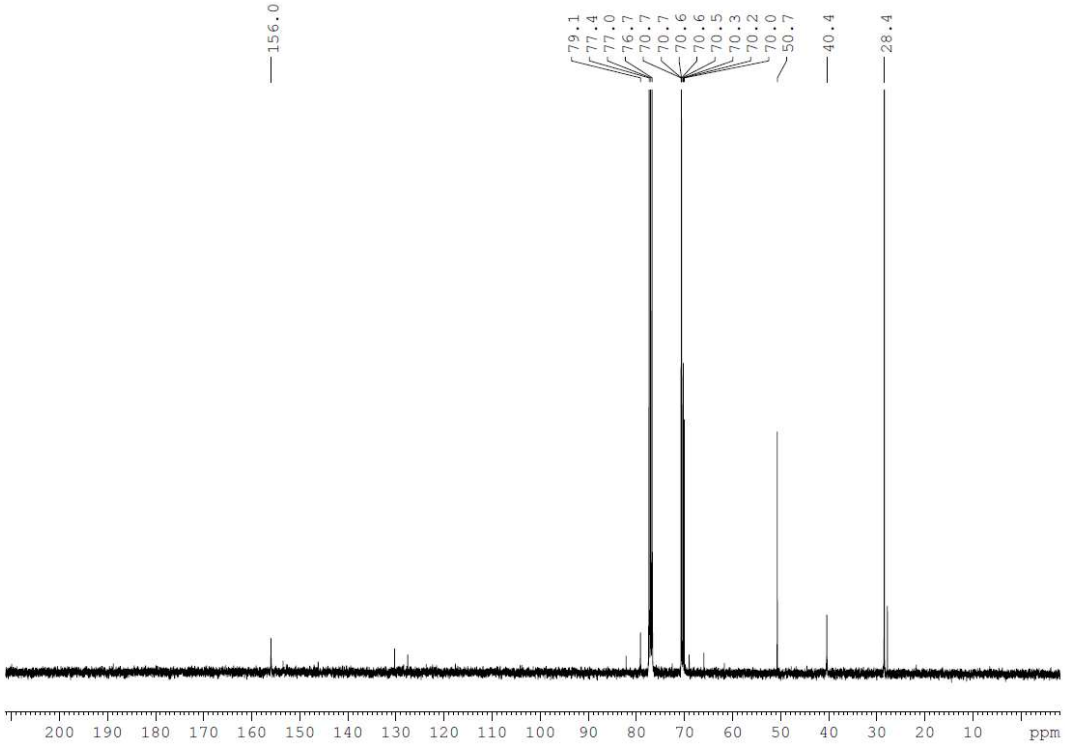
156.0
79.1
77.4
77.0
76.7
70.7
70.7
70.6
70.6
70.5
70.3
70.2
70.0
50.7
40.4
28.4
200 190 180 170 160 150 140 130 120 110 100 90 80 70 60 50 40 30 20 10 ppm

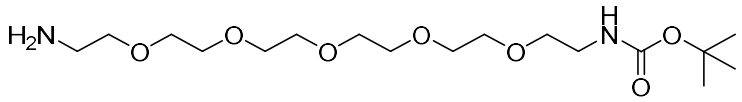

30

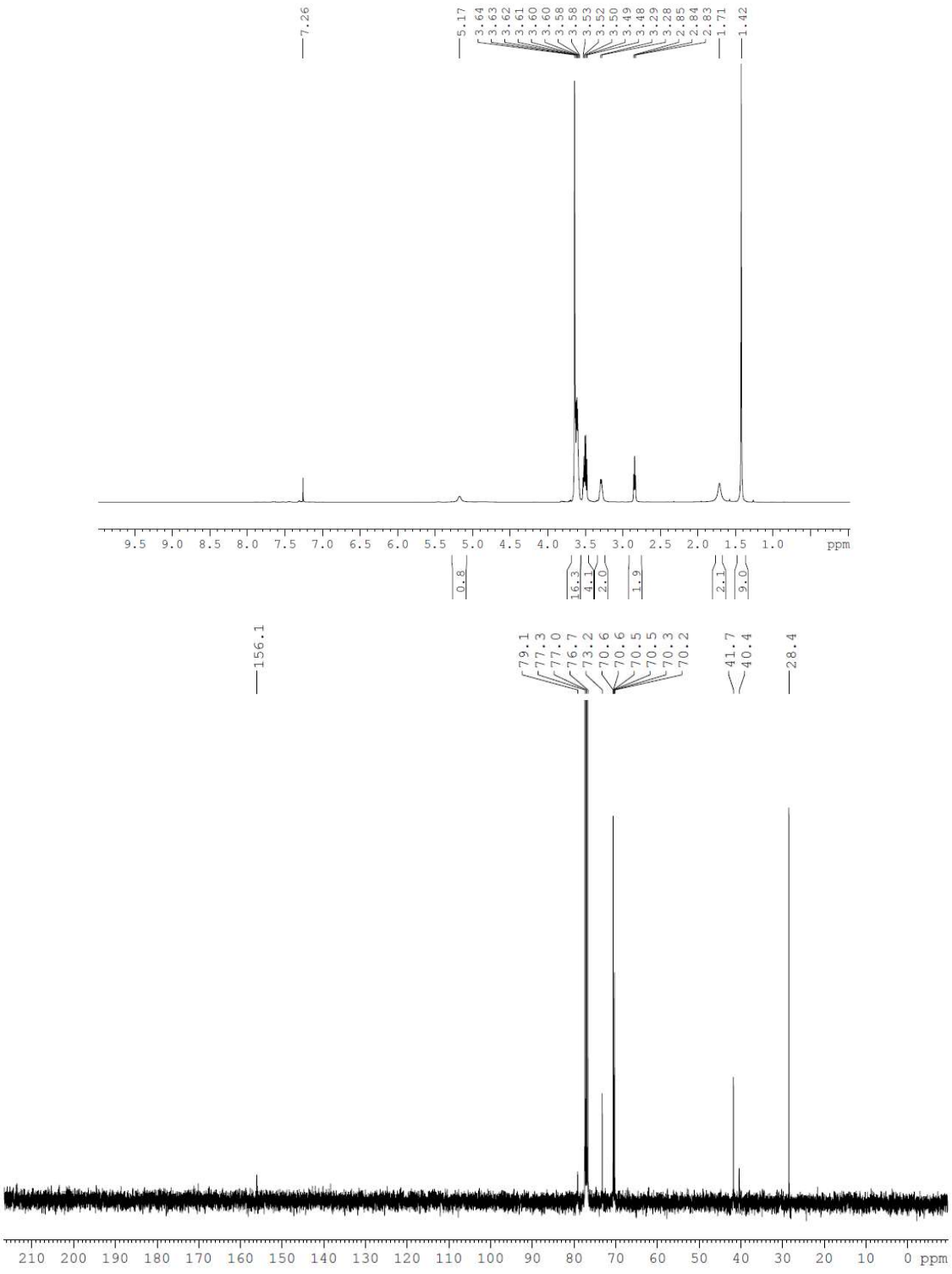
7.26
5.17
3.64
3.63
3.62
3.61
3.60
3.60
3.58
3.58
3.53
3.52
3.50
3.49
3.48
3.29
3.28
2.85
2.84
2.83
1.71
1.42
ppm
0.8
16.3
4.1
2.0
1.9
2.1
9.0
156.1
79.1
77.3
77.0
76.7
73.2
70.6
70.6
70.5
70.5
70.3
70.2
41.7
40.4
28.4
ppm

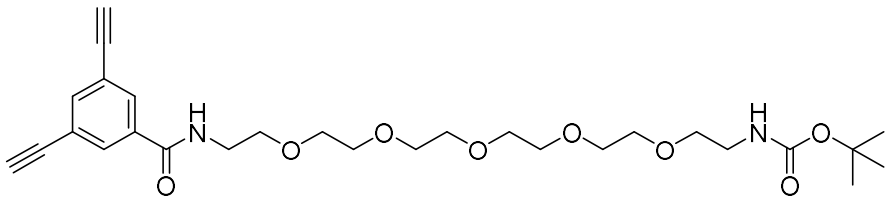

33

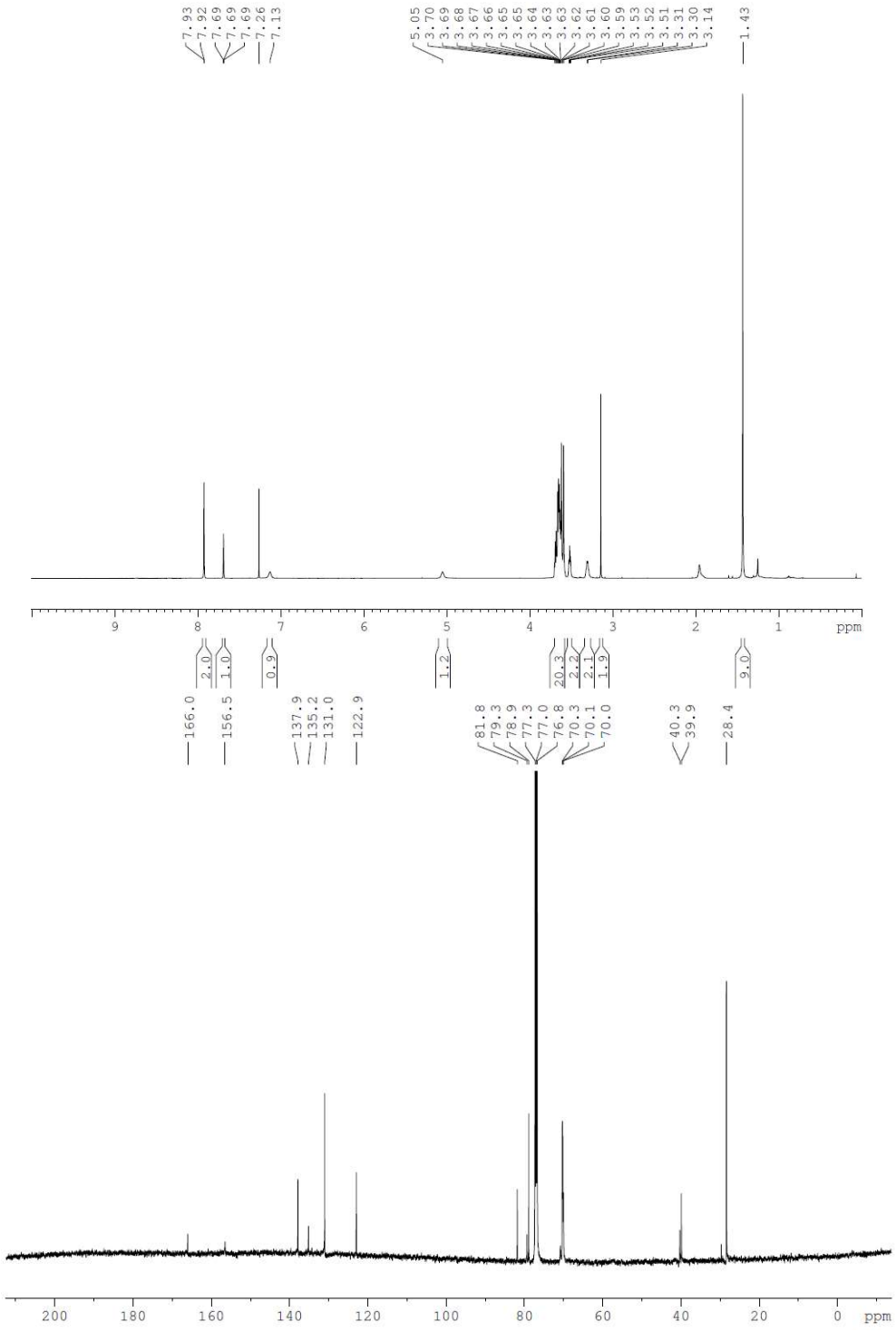
7.93
7.92
7.69
7.69
7.69
7.26
7.13
5.05
3.70
3.69
3.68
3.67
3.66
3.65
3.65
3.64
3.63
3.63
3.62
3.61
3.60
3.59
3.53
3.52
3.51
3.31
3.30
3.14
1.43
ppm
2.0
1.0
0.9
1.2
20.3
2.2
2.1
1.9
9.0
166.0
156.5
137.9
135.2
131.0
122.9
81.8
79.3
78.9
77.3
77.0
76.8
70.3
70.1
70.0
40.3
39.9
28.4
ppm

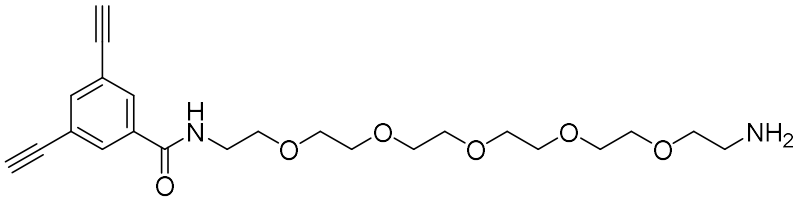

26


8.05
8.04
8.00
7.68
7.68
7.68
7.26
3.75
3.74
3.73
3.67
3.66
3.65
3.65
3.63
3.62
3.62
3.62
3.61
3.61
3.60
3.60
3.59
3.59
3.59
3.58
3.58
3.57
3.56
3.12
2.92
2.91
2.90

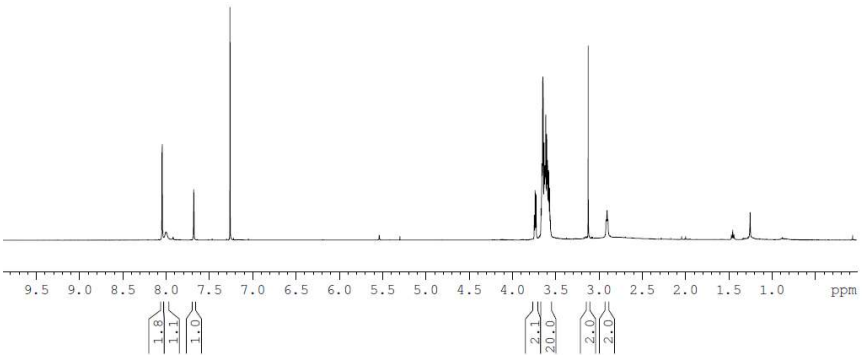
9.5 9.0 8.5 8.0 7.5 7.0 6.5 6.0 5.5 5.0 4.5 4.0 3.5 3.0 2.5 2.0 1.5 1.0 ppm
1.8
1.1
1.0
2.1
20.0
2.0
2.0

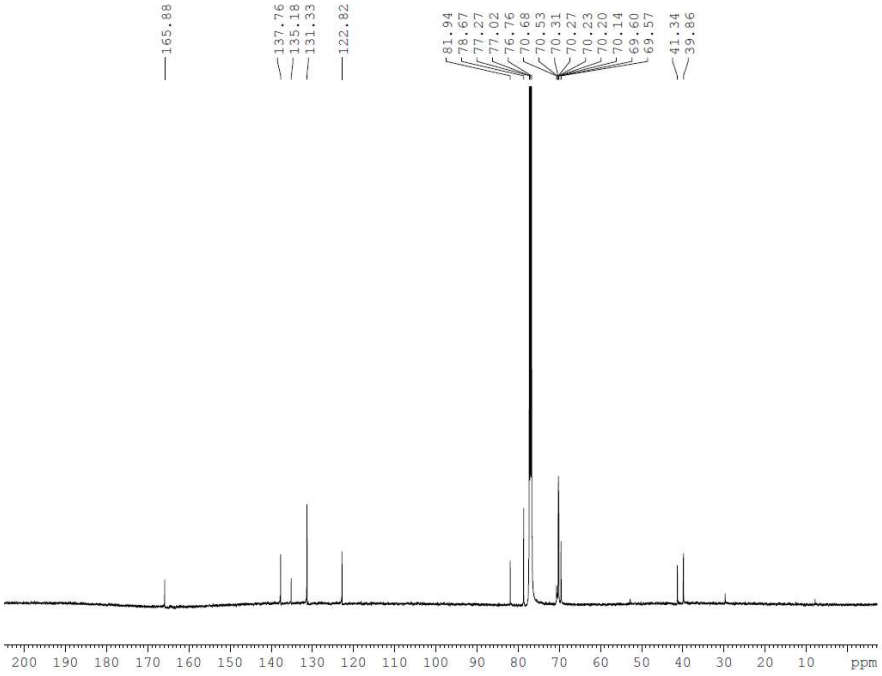
165.88
137.76
135.18
131.33
122.82
81.94
78.67
77.27
77.02
76.76
70.68
70.53
70.31
70.27
70.23
70.20
70.14
69.60
69.57
41.34
39.86
200 190 180 170 160 150 140 130 120 110 100 90 80 70 60 50 40 30 20 10 ppm

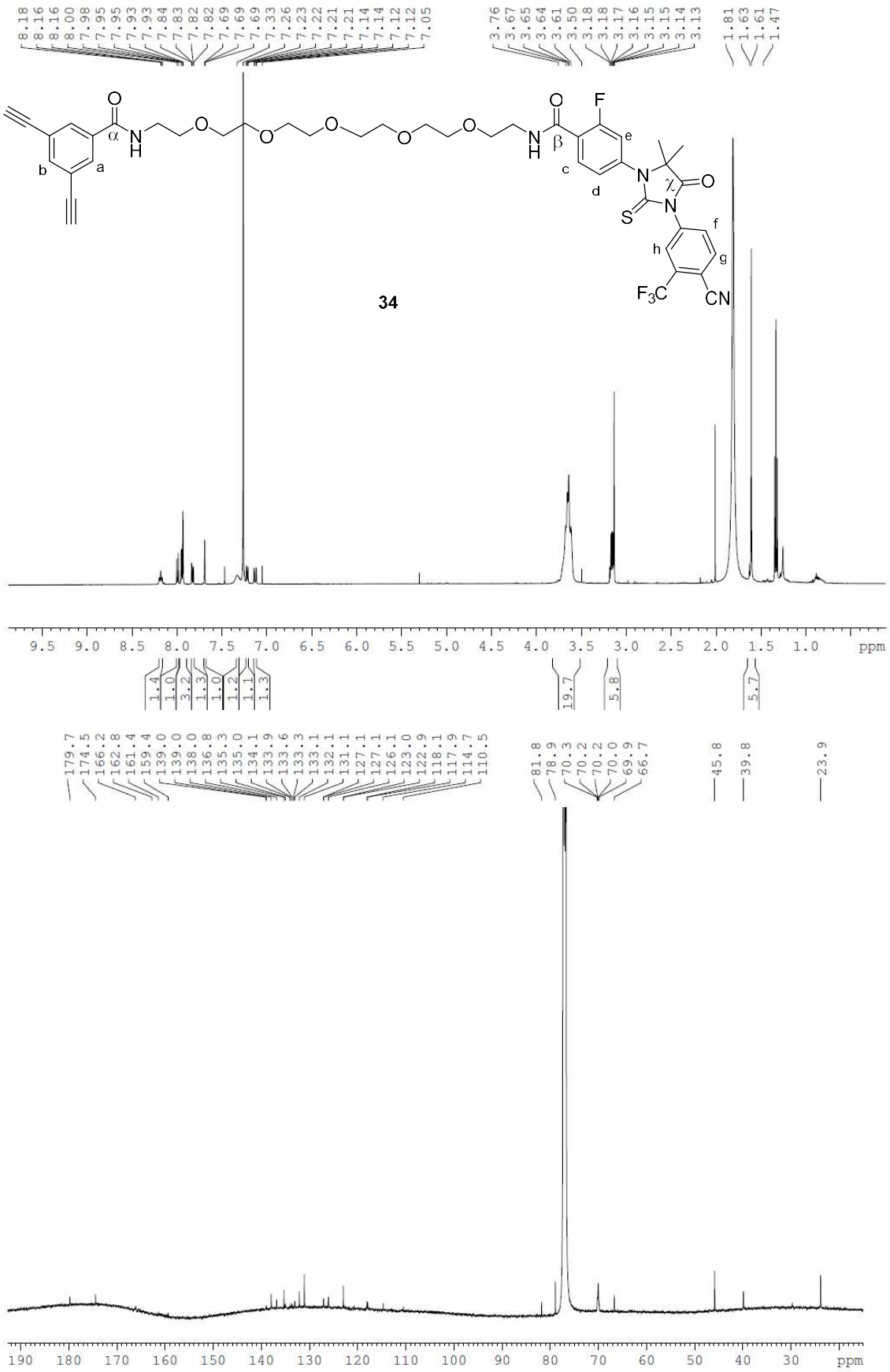
8.18
8.16
8.16
8.00
7.98
7.95
7.95
7.93
7.93
7.84
7.83
7.82
7.82
7.69
7.69
7.69
7.33
7.26
7.23
7.22
7.21
7.21
7.14
7.14
7.12
7.12
7.05
3.76
3.67
3.65
3.64
3.61
3.50
3.18
3.18
3.17
3.16
3.15
3.15
3.14
3.13
1.81
1.63
1.61
1.47
O
α
N
H
O
O
O
O
O
O
N
H
O
β
F
e
c
d
N
χ
O
N
S
f
h
g
F3C
CN
a
b
34
9.5 9.0 8.5 8.0 7.5 7.0 6.5 6.0 5.5 5.0 4.5 4.0 3.5 3.0 2.5 2.0 1.5 1.0 ppm
1.4
1.0
3.2
1.3
1.0
1.2
1.1
1.3
19.7
5.8
5.7
179.7
174.5
166.2
162.8
161.4
159.4
139.0
139.0
138.0
136.8
135.3
135.0
134.1
133.9
133.6
133.3
133.1
132.1
131.1
127.1
127.1
126.1
123.0
122.9
118.1
117.9
114.7
110.5
81.8
78.9
70.3
70.2
70.2
70.0
69.9
66.7
45.8
39.8
23.9
190 180 170 160 150 140 130 120 110 100 90 80 70 60 50 40 30 ppm

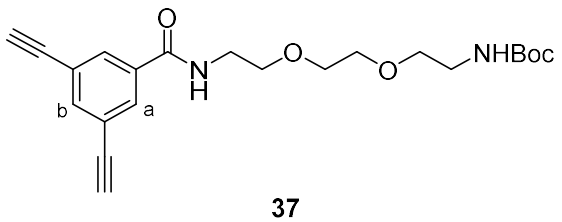
O
N
H
O
O
NHBoc
b
a

37

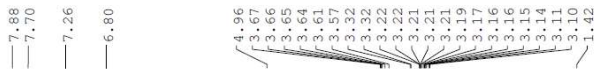
7.88
7.70
7.26
6.80
4.96
3.67
3.66
3.65
3.64
3.61
3.57
3.32
3.22
3.21
3.21
3.19
3.17
3.16
3.15
3.14
3.11
3.10
1.42

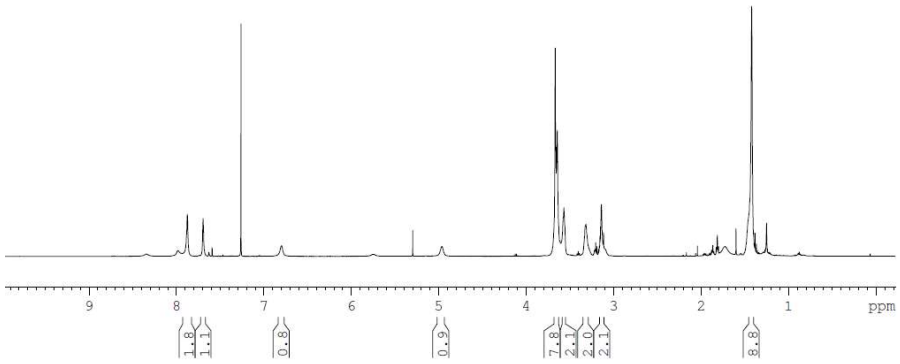
9
8
7
6
5
4
3
2
1
ppm
1.8
1.1
0.8
0.9
7.8
2.1
2.0
2.1
8.8

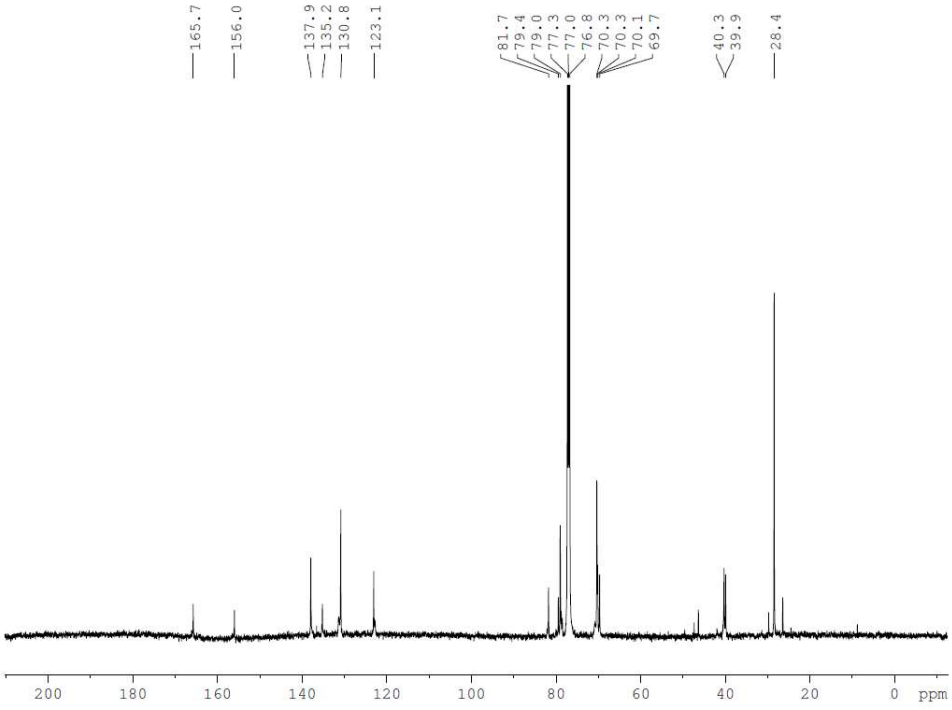
165.7
156.0
137.9
135.2
130.8
123.1
81.7
79.4
79.0
77.3
77.0
76.8
70.3
70.3
70.1
69.7
40.3
39.9
28.4
200
180
160
140
120
100
80
60
40
20
0
ppm

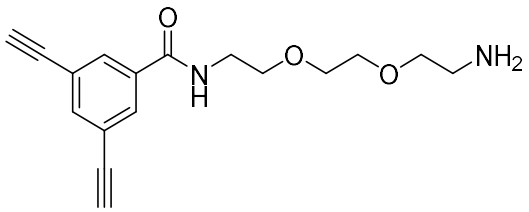

38

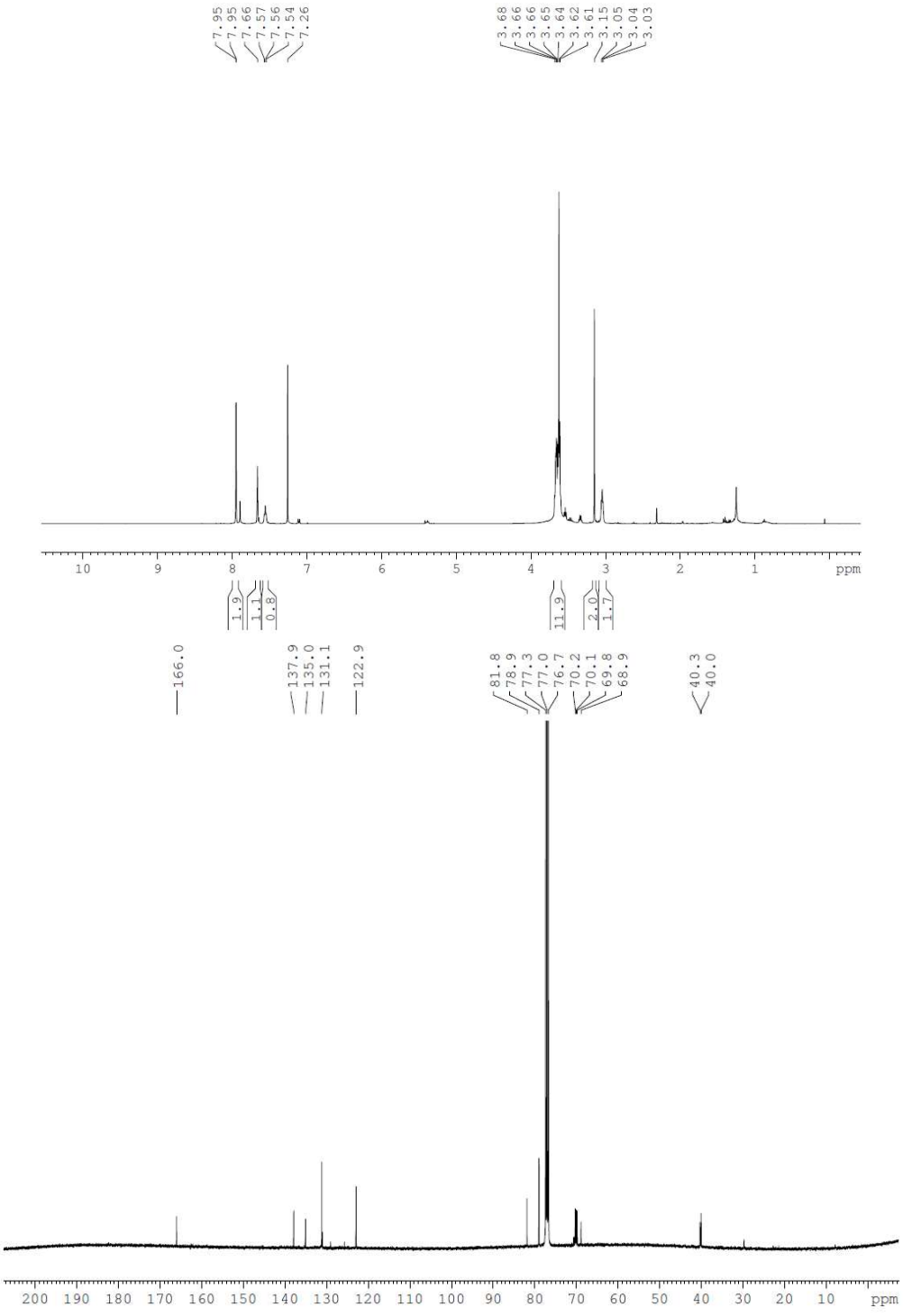
7.95
7.95
7.66
7.57
7.56
7.54
7.26
3.68
3.66
3.66
3.65
3.64
3.62
3.61
3.15
3.05
3.04
3.03
ppm
1.9
1.1
0.8
11.9
2.0
1.7
166.0
137.9
135.0
131.1
122.9
81.8
78.9
77.3
77.0
76.7
70.2
70.1
69.8
68.9
40.3
40.0
ppm

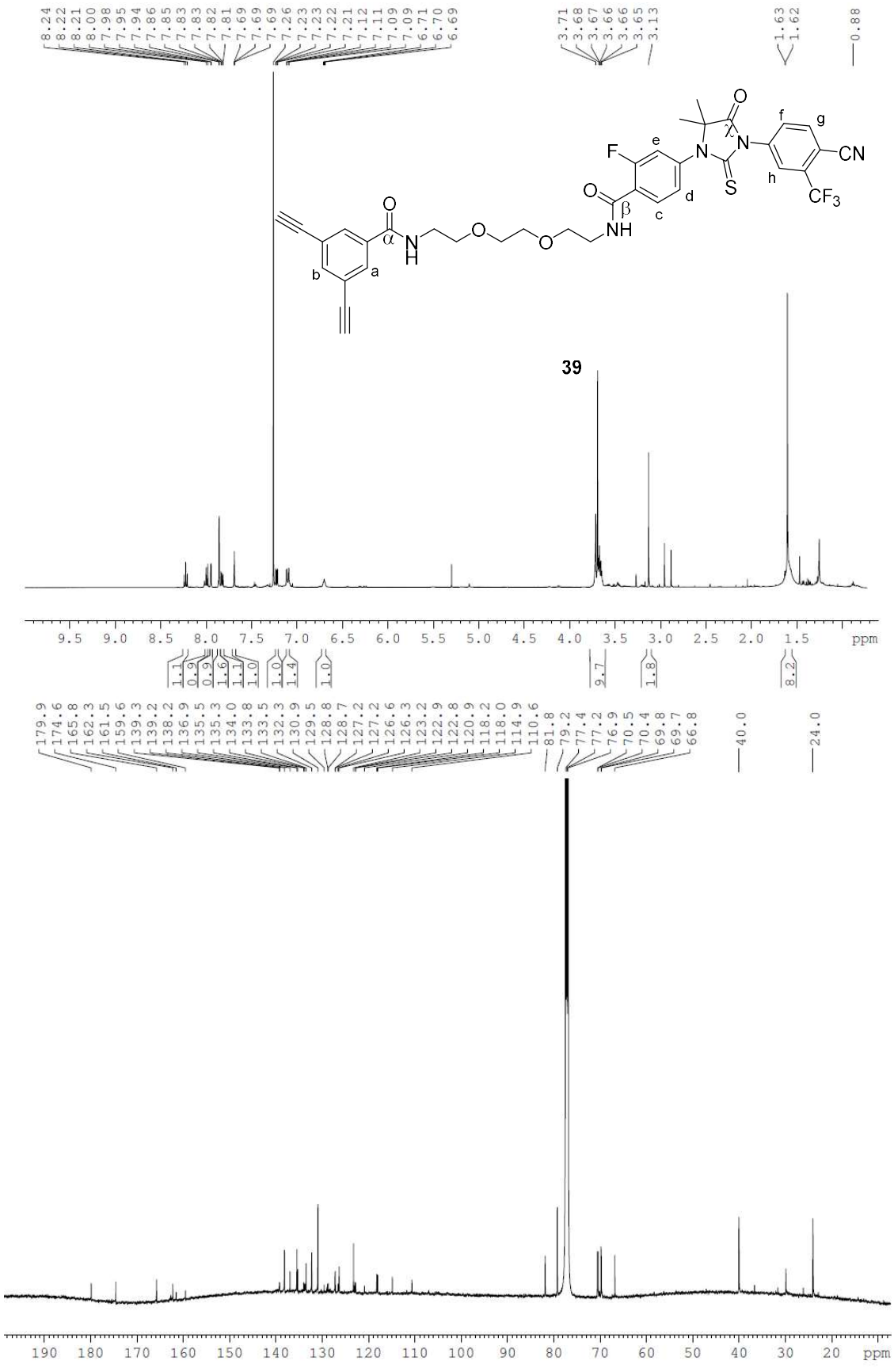
8.24
8.22
8.21
8.00
7.98
7.95
7.94
7.86
7.85
7.83
7.83
7.82
7.81
7.69
7.69
7.69
7.26
7.23
7.23
7.22
7.21
7.12
7.11
7.09
7.09
6.71
6.70
6.69
3.71
3.68
3.67
3.66
3.66
3.65
3.13
1.63
1.62
0.88
39
9.5 9.0 8.5 8.0 7.5 7.0 6.5 6.0 5.5 5.0 4.5 4.0 3.5 3.0 2.5 2.0 1.5 ppm
1.1
0.9
0.9
1.6
1.1
1.0
1.0
1.4
1.0
9.7
1.8
8.2
179.9
174.6
165.8
162.3
161.5
159.6
139.3
139.2
138.2
136.9
135.5
135.3
134.0
133.8
133.5
132.3
130.9
129.5
128.8
128.7
127.2
127.2
126.6
126.3
123.2
122.9
122.8
120.9
118.2
118.0
114.9
110.6
81.8
79.2
77.4
77.2
76.9
70.5
70.4
69.8
69.7
66.8
40.0
24.0
190 180 170 160 150 140 130 120 110 100 90 80 70 60 50 40 30 20 ppm

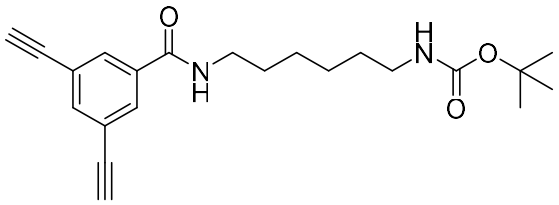

44

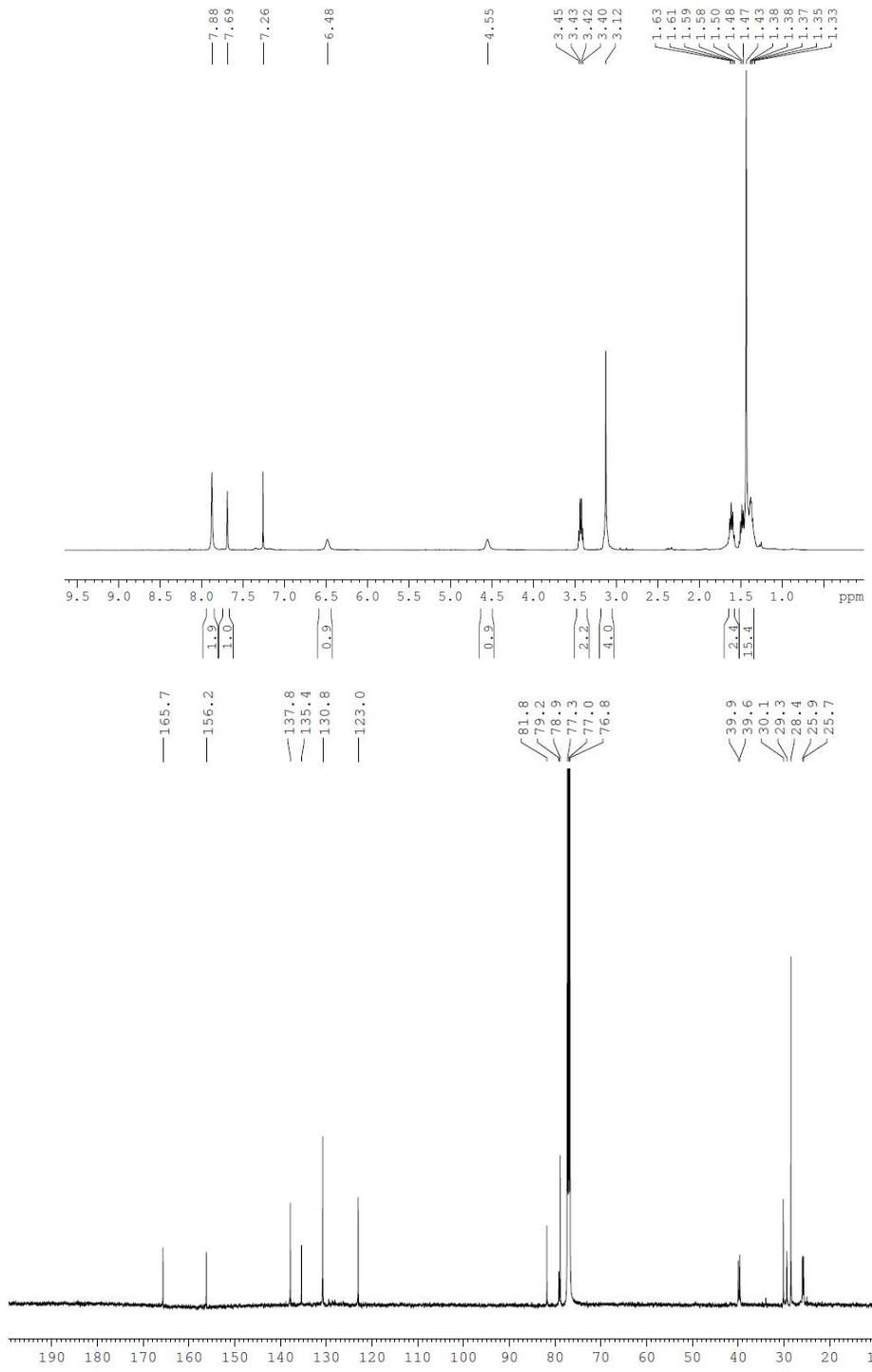
7.88
7.69
7.26
6.48
4.55
3.45
3.43
3.42
3.40
3.12
1.63
1.61
1.59
1.58
1.50
1.48
1.47
1.43
1.38
1.38
1.37
1.35
1.33
ppm
1.9
1.0
0.9
0.9
2.2
4.0
2.4
15.4
165.7
156.2
137.8
135.4
130.8
123.0
81.8
79.2
78.9
77.3
77.0
76.8
39.9
39.6
30.1
29.3
28.4
25.9
25.7
10 ppm

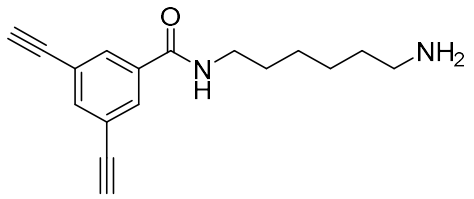
O
N
H
NH2

45

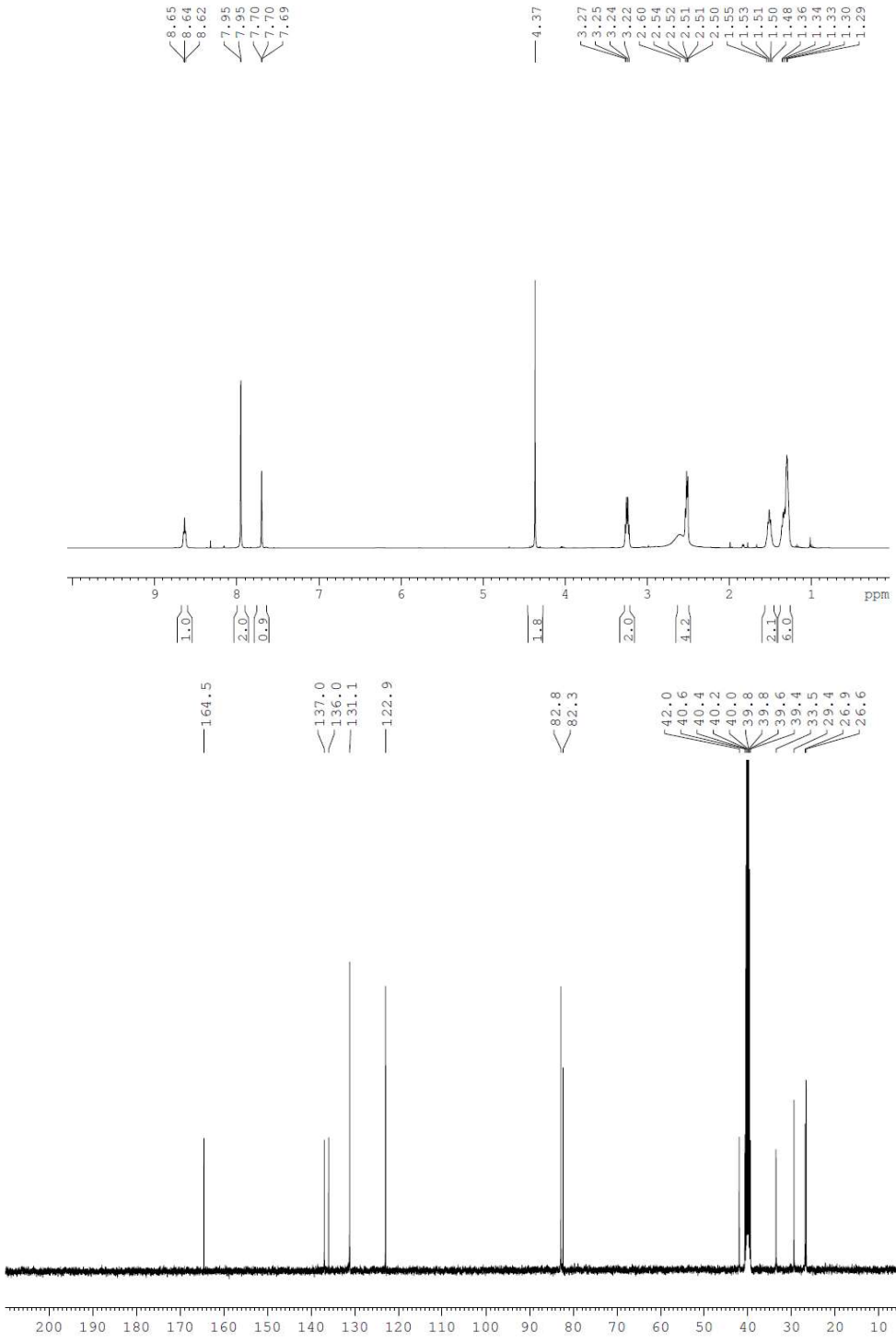
8.65
8.64
8.62
7.95
7.95
7.70
7.70
7.69
4.37
3.27
3.25
3.24
3.22
2.60
2.54
2.52
2.51
2.50
1.55
1.53
1.51
1.50
1.48
1.36
1.34
1.33
1.30
1.29
ppm
1.0
2.0
0.9
1.8
2.0
4.2
2.1
6.0
164.5
137.0
136.0
131.1
122.9
82.8
82.3
42.0
40.6
40.4
40.2
40.0
39.8
39.8
39.6
39.4
33.5
29.4
26.9
26.6
ppm

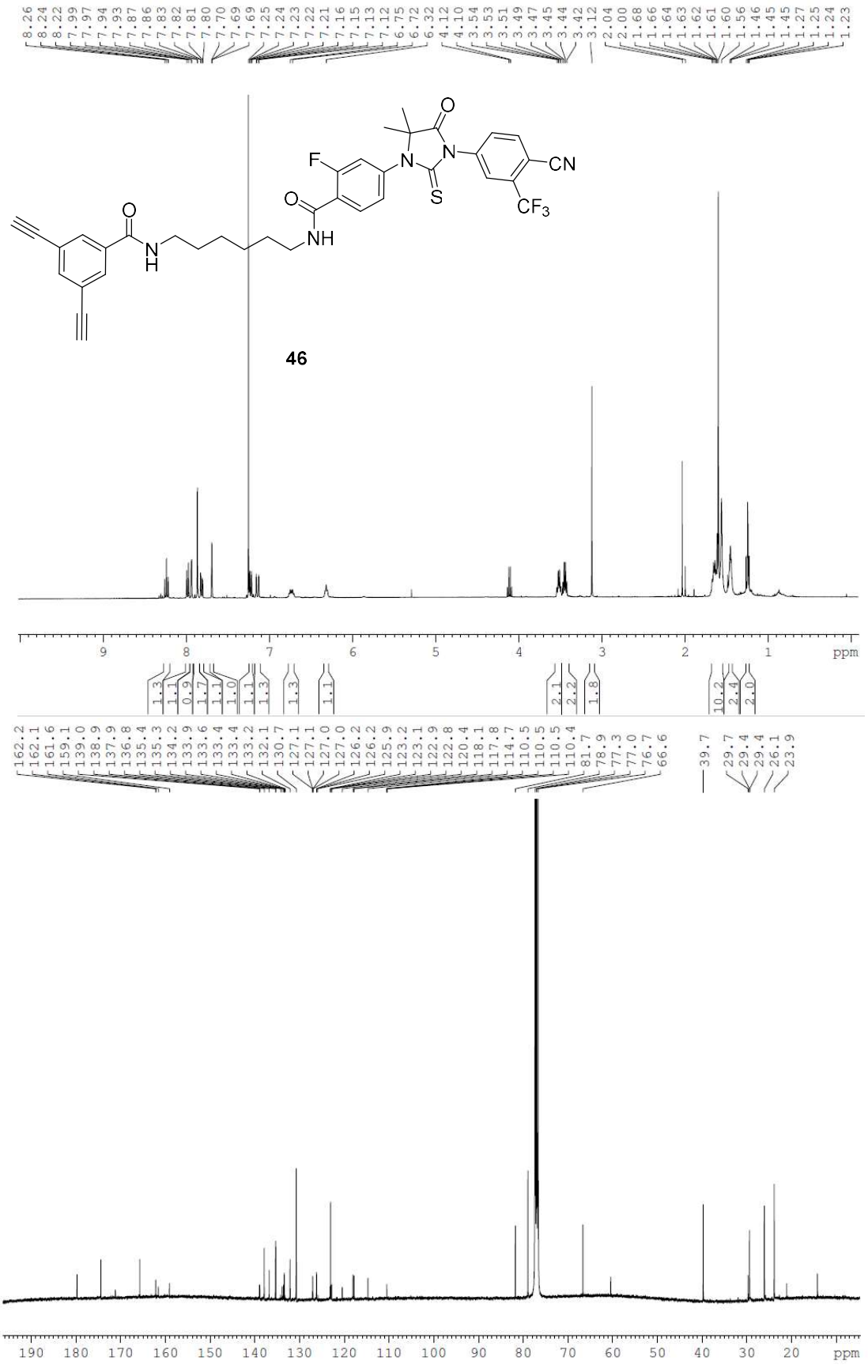
8.26 8.24 8.22 7.99 7.97 7.94 7.93 7.87 7.86 7.83 7.82 7.81 7.80 7.70 7.69 7.69 7.25 7.24 7.23 7.22 7.21 7.16 7.15 7.13 7.12 6.75 6.72 6.32 4.12 4.10 3.54 3.53 3.51 3.49 3.47 3.45 3.44 3.42 3.12 2.04 2.00 1.68 1.66 1.64 1.63 1.62 1.61 1.60 1.56 1.46 1.45 1.45 1.27 1.25 1.24 1.23
O
F
N
N
O
CN
S
CF3
O
NH
N
H
46
9 8 7 6 5 4 3 2 1 ppm
1.3 1.1 0.9 1.7 1.1 1.0 1.1 1.3 1.3 1.1 2.1 2.2 1.8 10.2 2.4 2.0
162.2 162.1 161.6 159.1 139.0 138.9 137.9 136.8 135.4 135.3 134.2 133.9 133.6 133.4 133.4 133.2 132.1 130.7 127.1 127.1 127.0 127.0 126.2 126.2 125.9 123.2 123.1 122.9 122.8 120.4 118.1 117.8 114.7 110.5 110.5 110.4 81.7 78.9 77.3 77.0 76.7 66.6 39.7 29.7 29.4 29.4 26.1 23.9
190 180 170 160 150 140 130 120 110 100 90 80 70 60 50 40 30 20 ppm

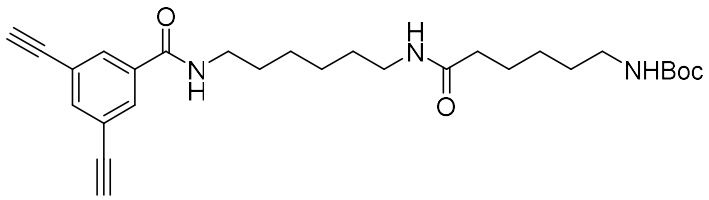
O
H
N
N
H
O
NHBoc

48

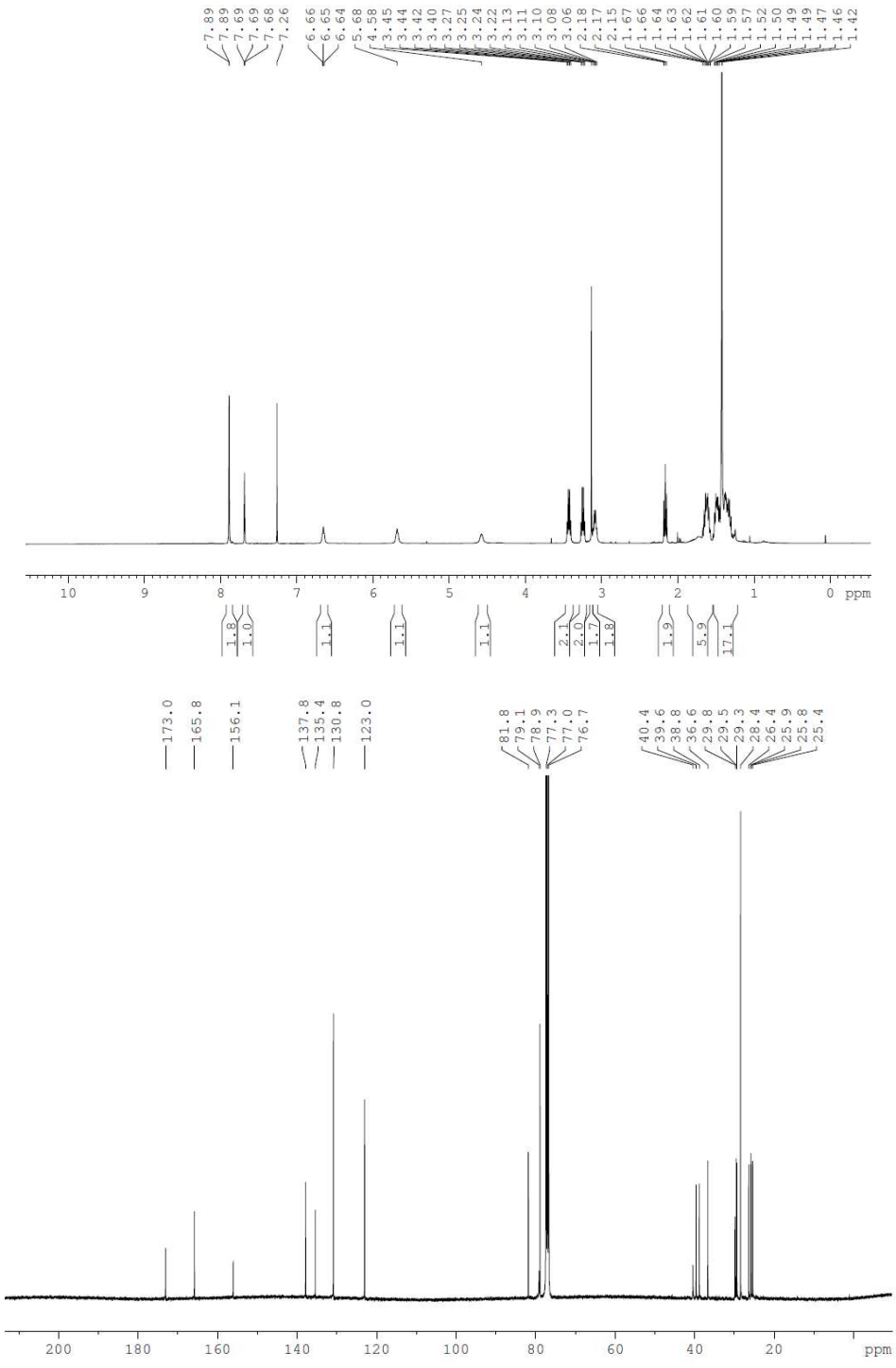
7.89
7.89
7.69
7.69
7.68
7.26
6.66
6.65
6.64
5.68
4.58
3.45
3.44
3.42
3.40
3.27
3.25
3.24
3.22
3.13
3.11
3.10
3.08
3.06
2.18
2.17
2.15
1.67
1.66
1.64
1.63
1.62
1.61
1.60
1.59
1.57
1.52
1.50
1.49
1.49
1.47
1.46
1.42
10
9
8
7
6
5
4
3
2
1
0 ppm
1.8
1.0
1.1
1.1
1.1
2.1
2.0
1.7
1.8
1.9
5.9
17.1
173.0
165.8
156.1
137.8
135.4
130.8
123.0
81.8
79.1
78.9
77.3
77.0
76.7
40.4
39.6
38.8
36.6
29.8
29.5
29.3
28.4
26.4
25.9
25.8
25.4
200
180
160
140
120
100
80
60
40
20
ppm

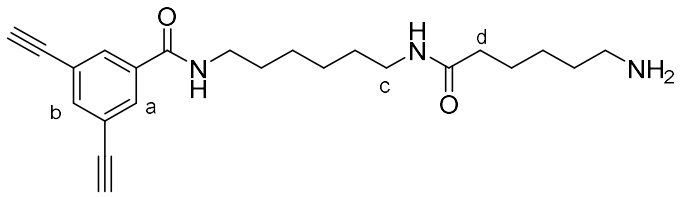
O
H
N
N
H
O
NH2
a
b
c
d

49

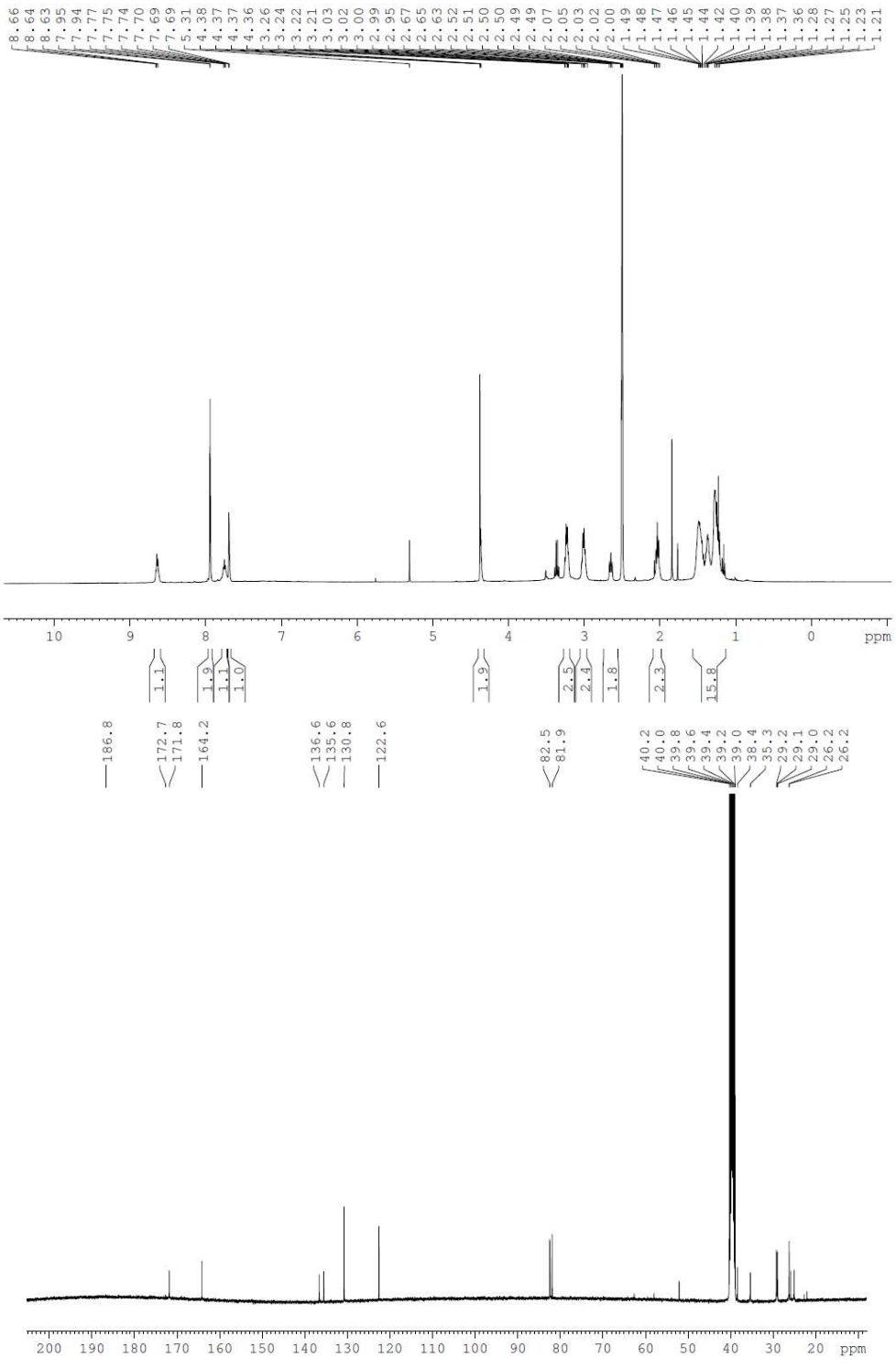
8.66 8.64 8.63 7.95 7.94 7.77 7.75 7.74 7.70 7.69 7.69 5.31 4.38 4.37 4.37 4.36 3.26 3.24 3.22 3.21 3.03 3.02 3.00 2.99 2.95 2.67 2.65 2.63 2.52 2.51 2.50 2.50 2.49 2.49 2.07 2.05 2.03 2.02 2.00 1.49 1.48 1.47 1.46 1.45 1.44 1.42 1.40 1.39 1.38 1.37 1.36 1.28 1.27 1.25 1.23 1.21
10 9 8 7 6 5 4 3 2 1 0 ppm
1.1 1.9 1.1 1.0 1.9 2.5 2.4 1.8 2.3 15.8
186.8 172.7 171.8 164.2 136.6 135.6 130.8 122.6 82.5 81.9 40.2 40.0 39.8 39.6 39.4 39.2 39.0 38.4 35.3 29.2 29.1 29.0 26.2 26.2
200 190 180 170 160 150 140 130 120 110 100 90 80 70 60 50 40 30 20 ppm

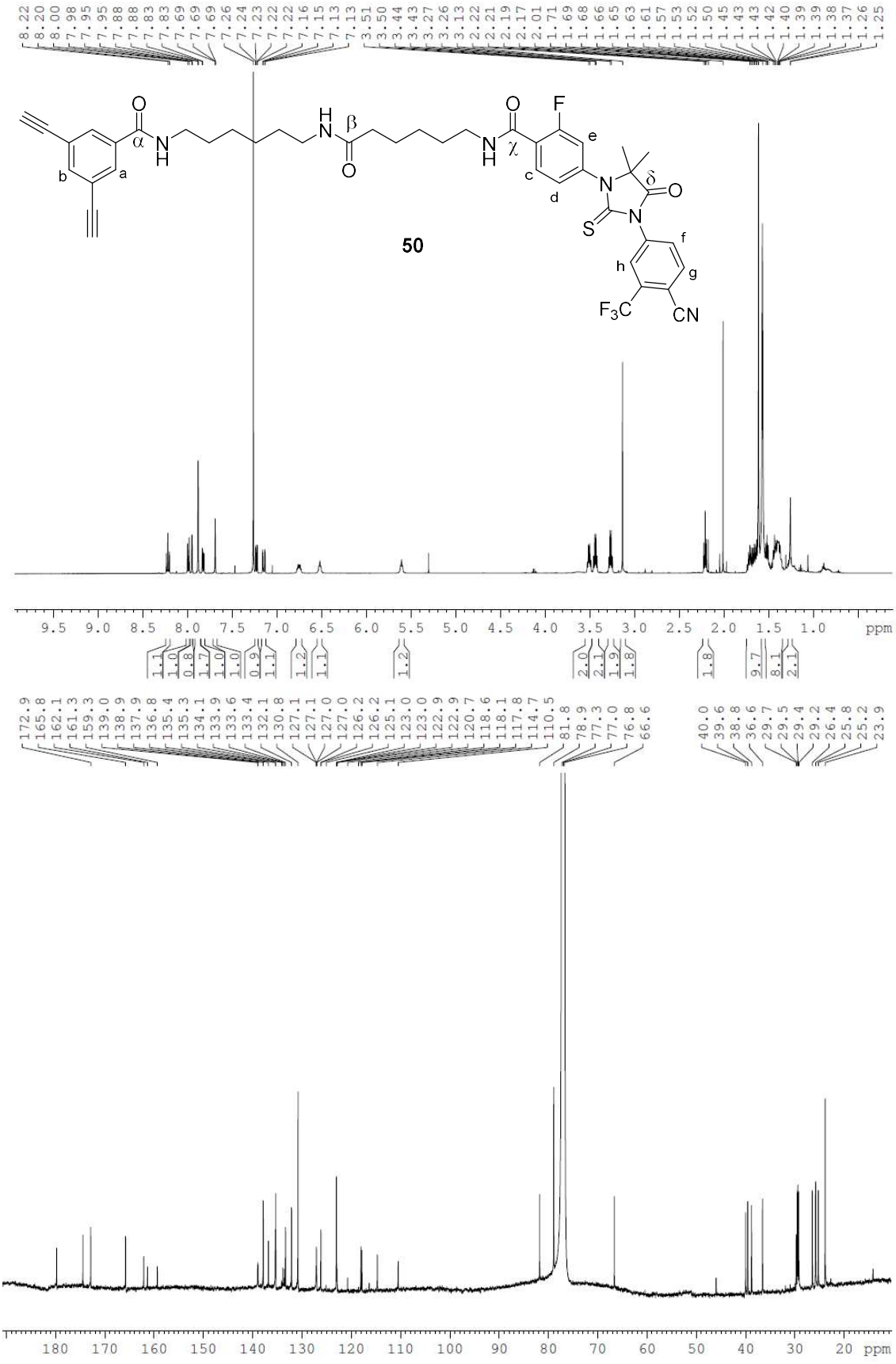
50

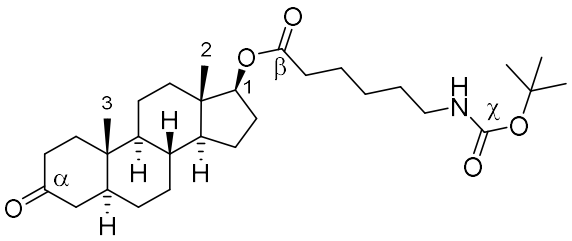
O
2
O
β
1
3
H
H
H
H
α
O
H
N
χ
O
O

52

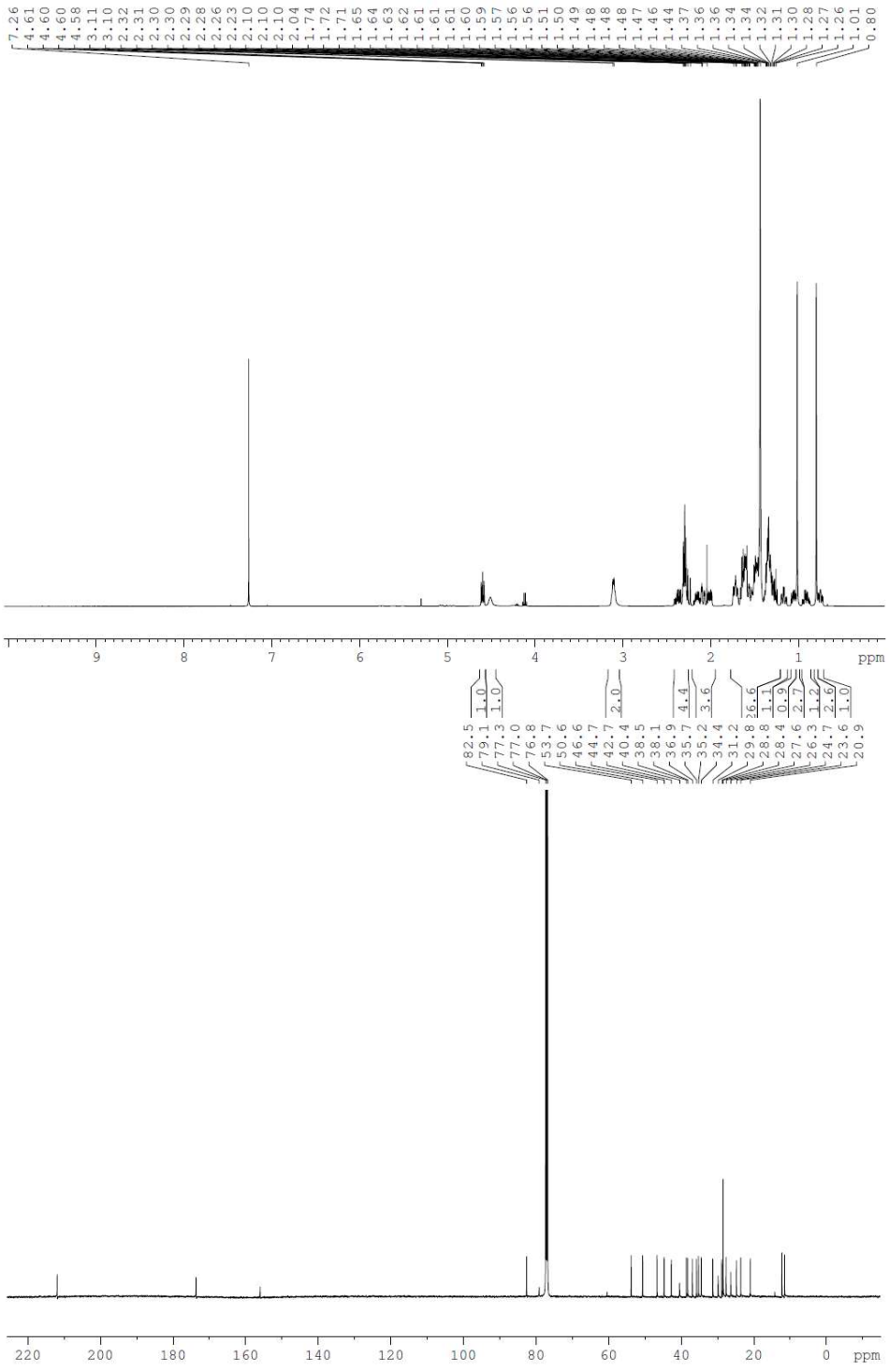
7.26
4.61
4.60
4.60
4.58
3.11
3.10
2.32
2.31
2.30
2.30
2.29
2.28
2.26
2.23
2.10
2.10
2.10
2.04
1.74
1.72
1.71
1.65
1.64
1.63
1.62
1.61
1.61
1.61
1.60
1.59
1.57
1.56
1.56
1.51
1.50
1.49
1.48
1.48
1.48
1.47
1.46
1.44
1.37
1.36
1.36
1.34
1.34
1.32
1.31
1.30
1.28
1.27
1.26
1.01
0.80
9
8
7
6
5
4
3
2
1
ppm
1.0
1.0
2.0
4.4
3.6
16.6
1.1
0.9
2.7
1.2
2.6
1.0
82.5
79.1
77.3
77.0
76.8
53.7
50.6
46.6
44.7
42.7
40.4
38.5
38.1
36.9
35.7
35.2
34.4
31.2
29.8
28.8
28.4
27.6
26.3
24.7
23.6
20.9
220
200
180
160
140
120
100
80
60
40
20
0
ppm

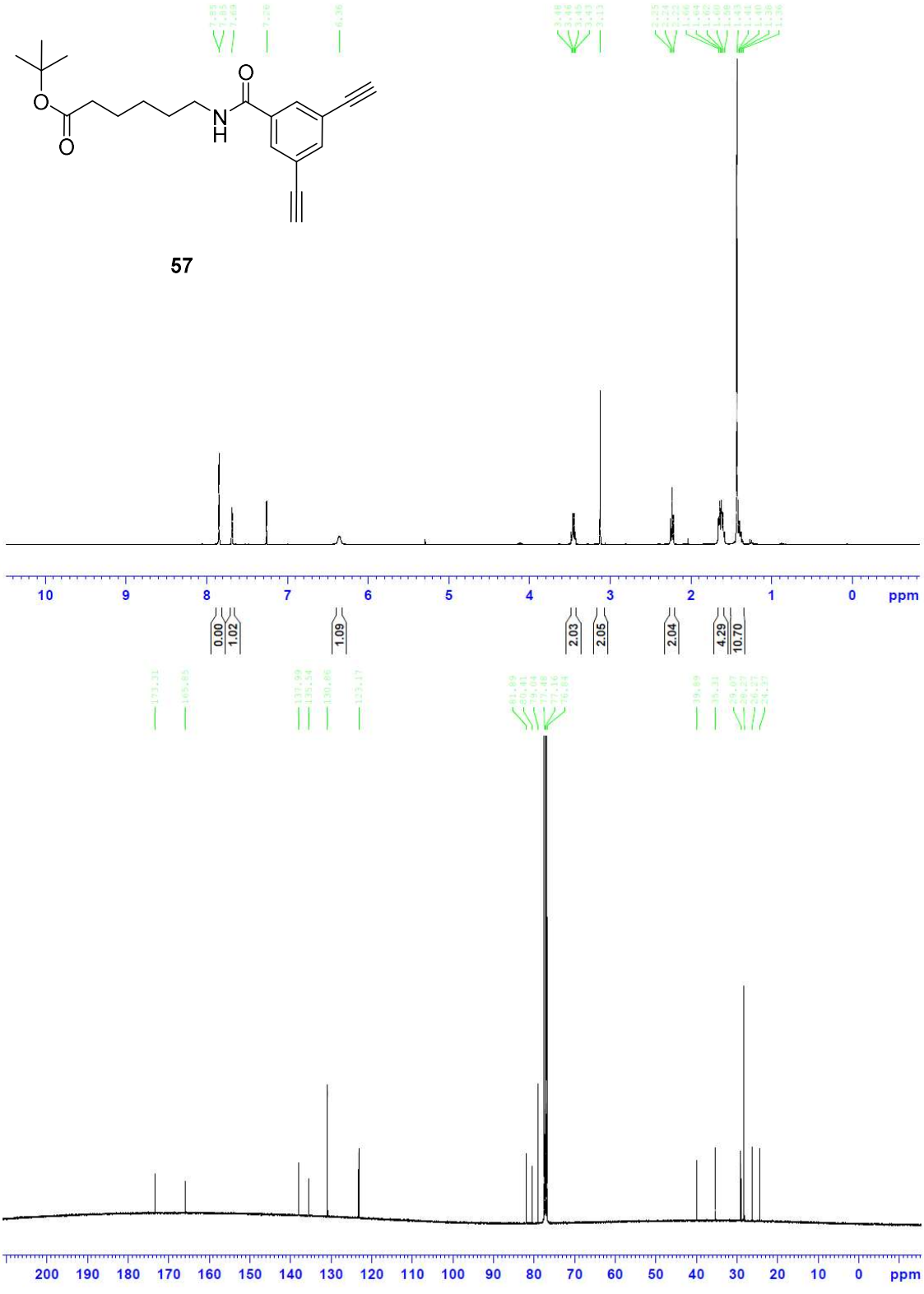
O
O
N
H
O
O
57
10 9 8 7 6 5 4 3 2 1 0 ppm
0.00 1.02 1.09 2.03 2.05 2.04 4.29 10.70
200 190 180 170 160 150 140 130 120 110 100 90 80 70 60 50 40 30 20 10 0 ppm

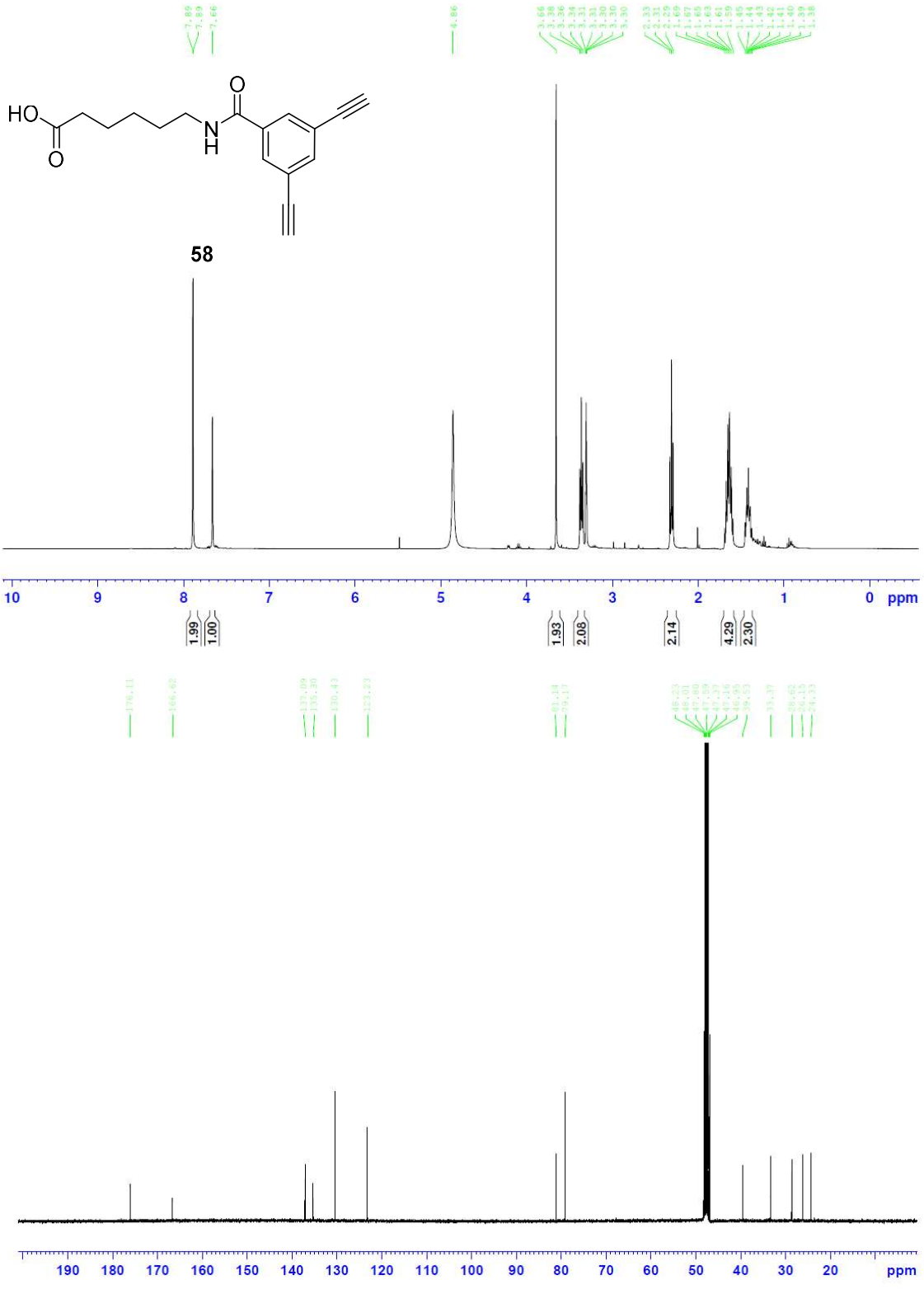
HO
O
N
H
O
58
10
9
8
7
6
5
4
3
2
1
0
ppm
1.99
1.00
1.93
2.08
2.14
4.29
2.30
190
180
170
160
150
140
130
120
110
100
90
80
70
60
50
40
30
20
ppm

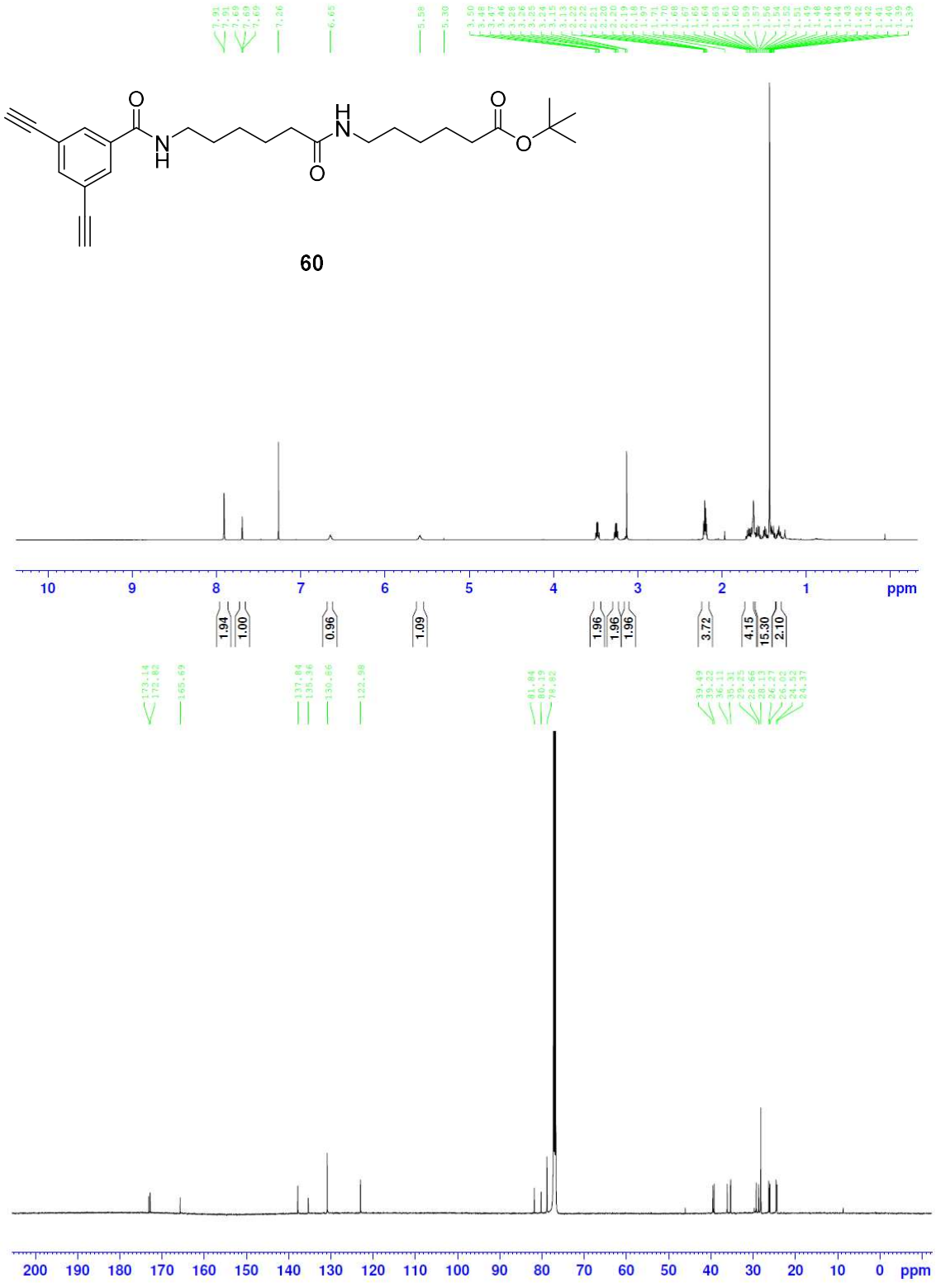

60

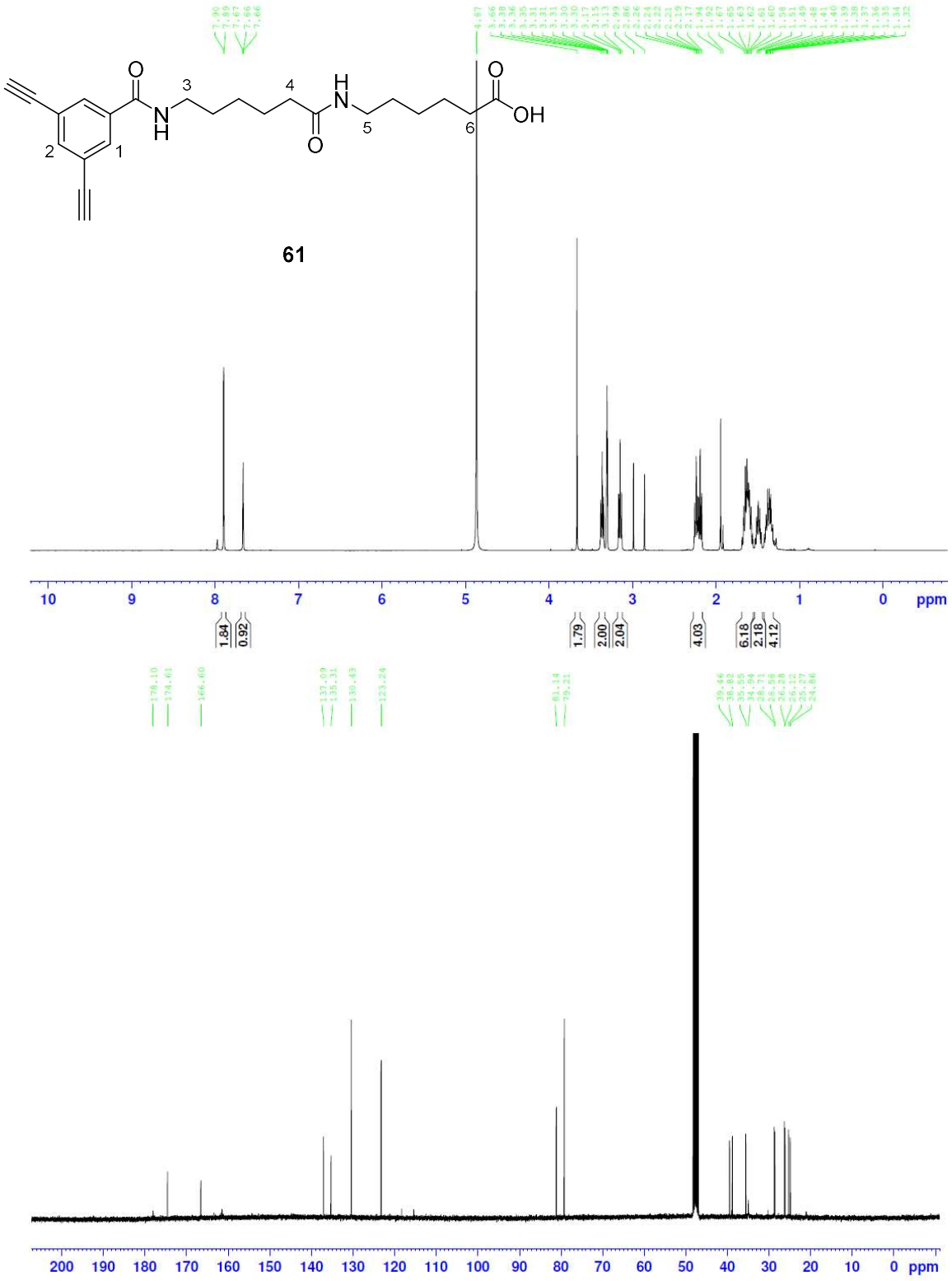
61
ppm
ppm

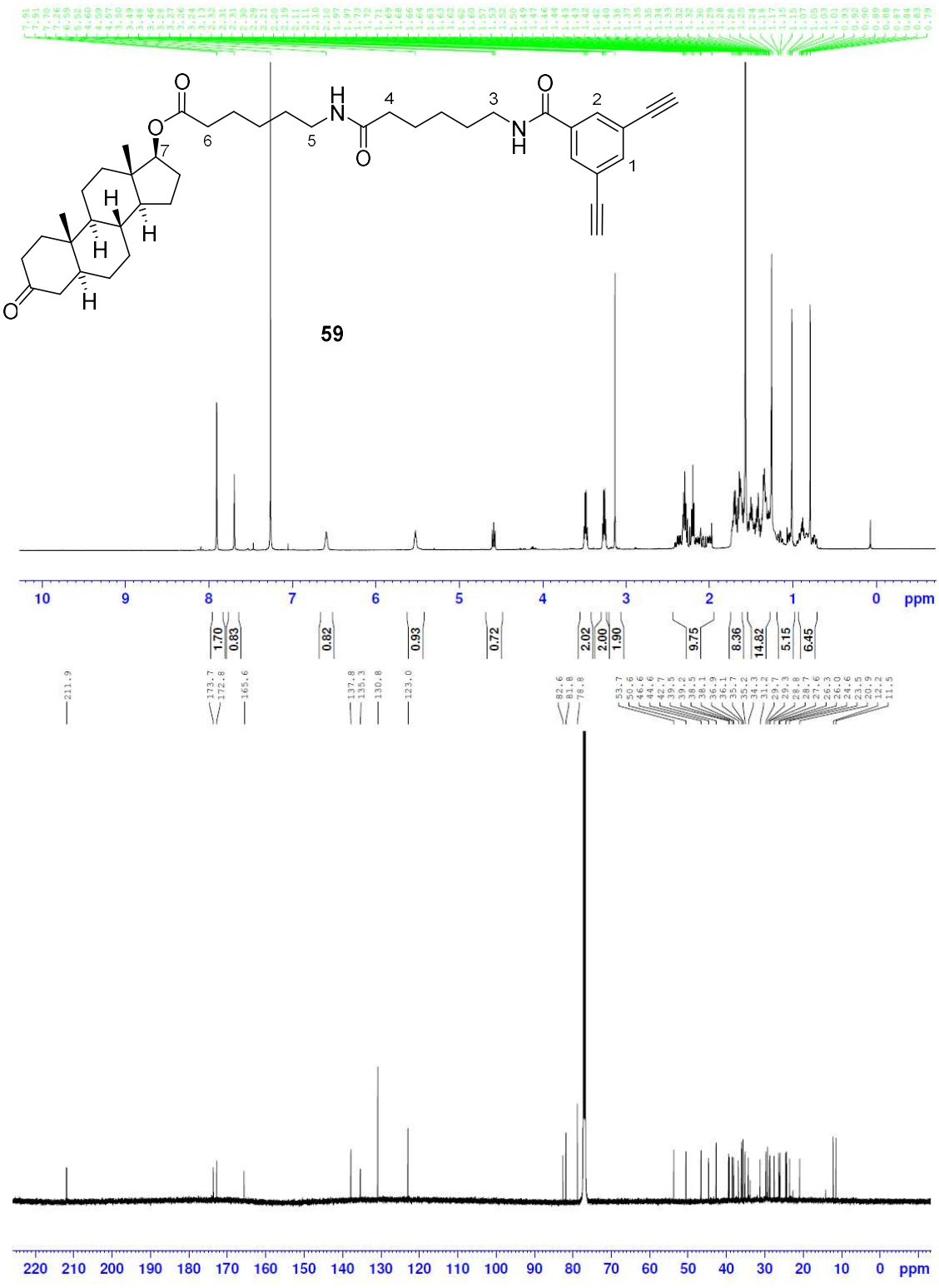
59
10 9 8 7 6 5 4 3 2 1 0 ppm
1.70 0.83 0.82 0.93 0.72 2.02 2.00 1.90 9.75 8.36 14.82 5.15 6.45
220 210 200 190 180 170 160 150 140 130 120 110 100 90 80 70 60 50 40 30 20 10 0 ppm

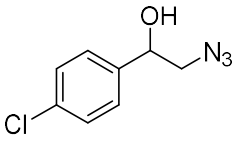
OH
N3
Cl

66

7.36
7.33
7.31
7.29
7.26
4.86
4.84
4.84
4.83
3.47
3.44
3.43
3.42
3.40
2.54
10
9
8
7
6
5
4
3
2
1
0 ppm
2.0
2.0
1.0
2.1
1.0

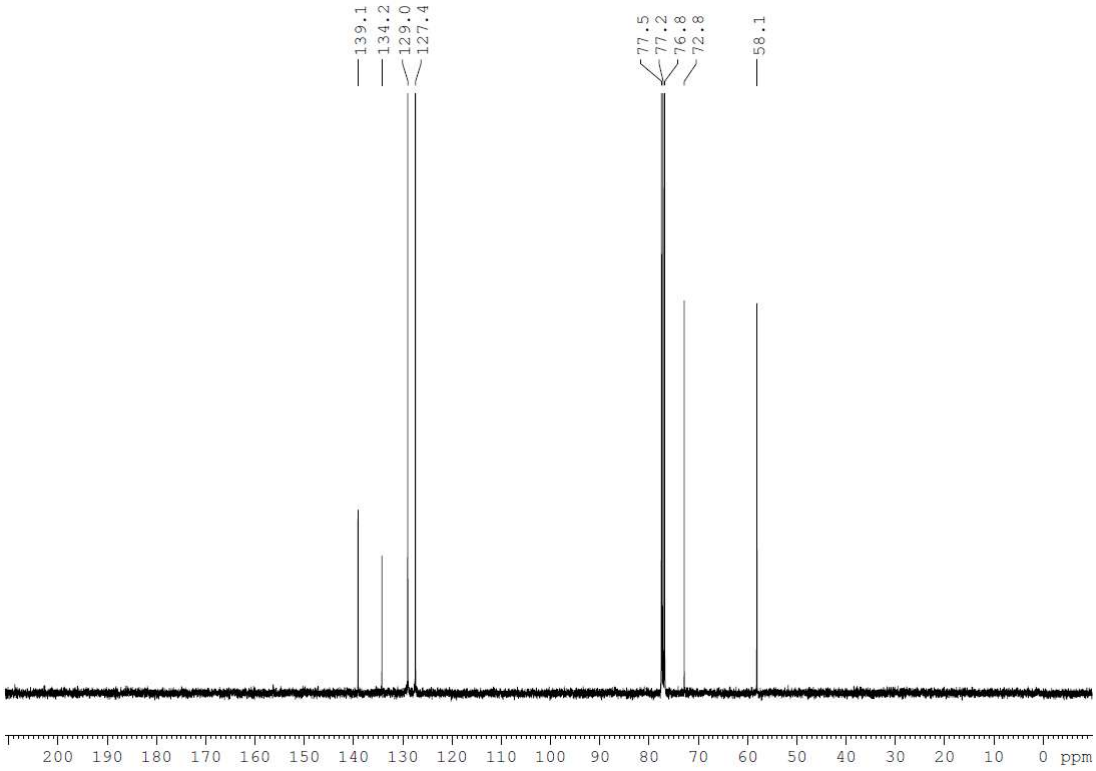
139.1
134.2
129.0
127.4
77.5
77.2
76.8
72.8
58.1
200
190
180
170
160
150
140
130
120
110
100
90
80
70
60
50
40
30
20
10
0 ppm

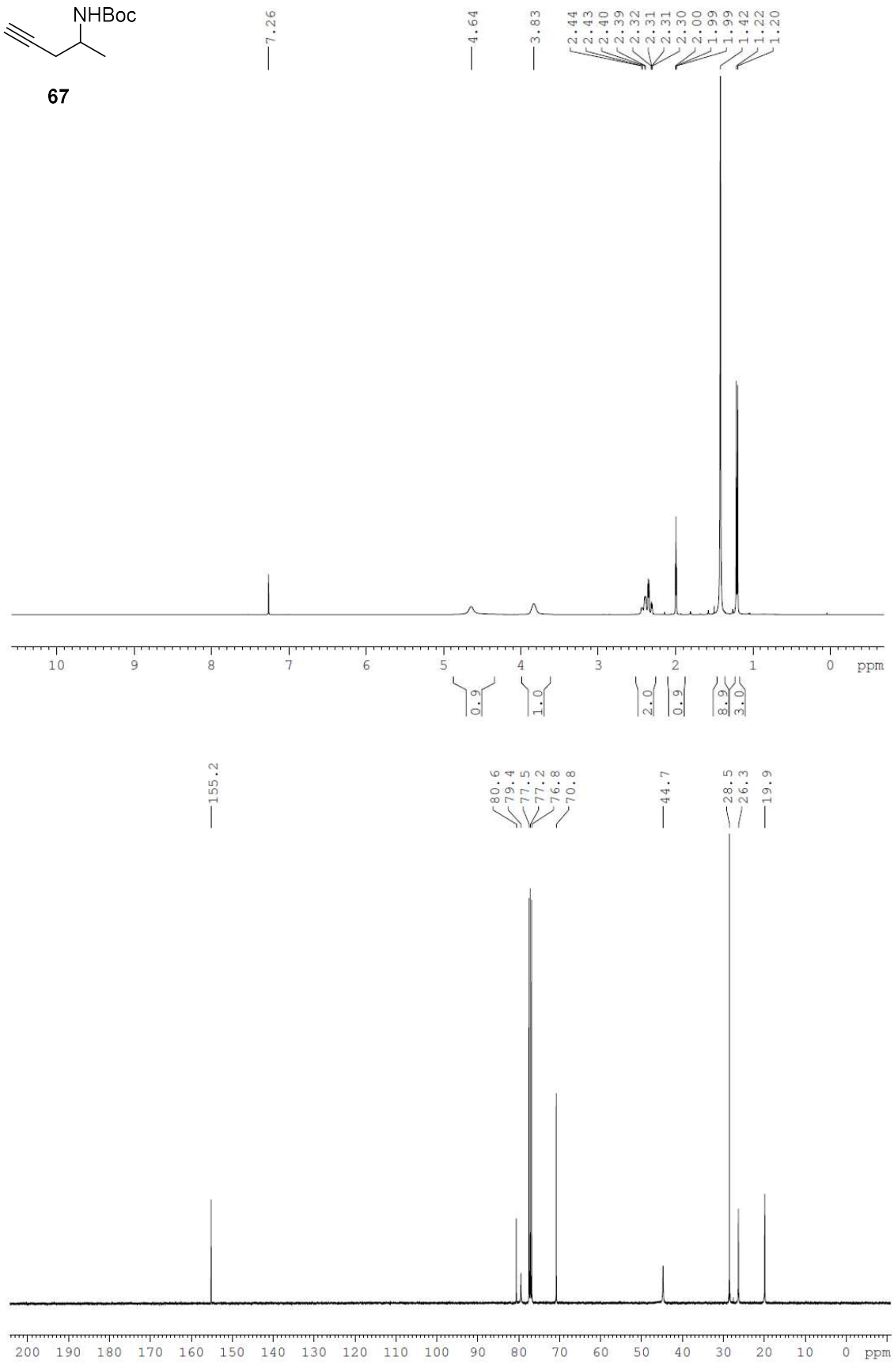
NHBoc
67
7.26
4.64
3.83
2.44
2.43
2.40
2.39
2.32
2.31
2.31
2.30
2.00
1.99
1.99
1.42
1.22
1.20
10 9 8 7 6 5 4 3 2 1 0 ppm
0.9
1.0
2.0
0.9
8.9
3.0
155.2
80.6
79.4
77.5
77.2
76.8
70.8
44.7
28.5
26.3
19.9
200 190 180 170 160 150 140 130 120 110 100 90 80 70 60 50 40 30 20 10 0 ppm

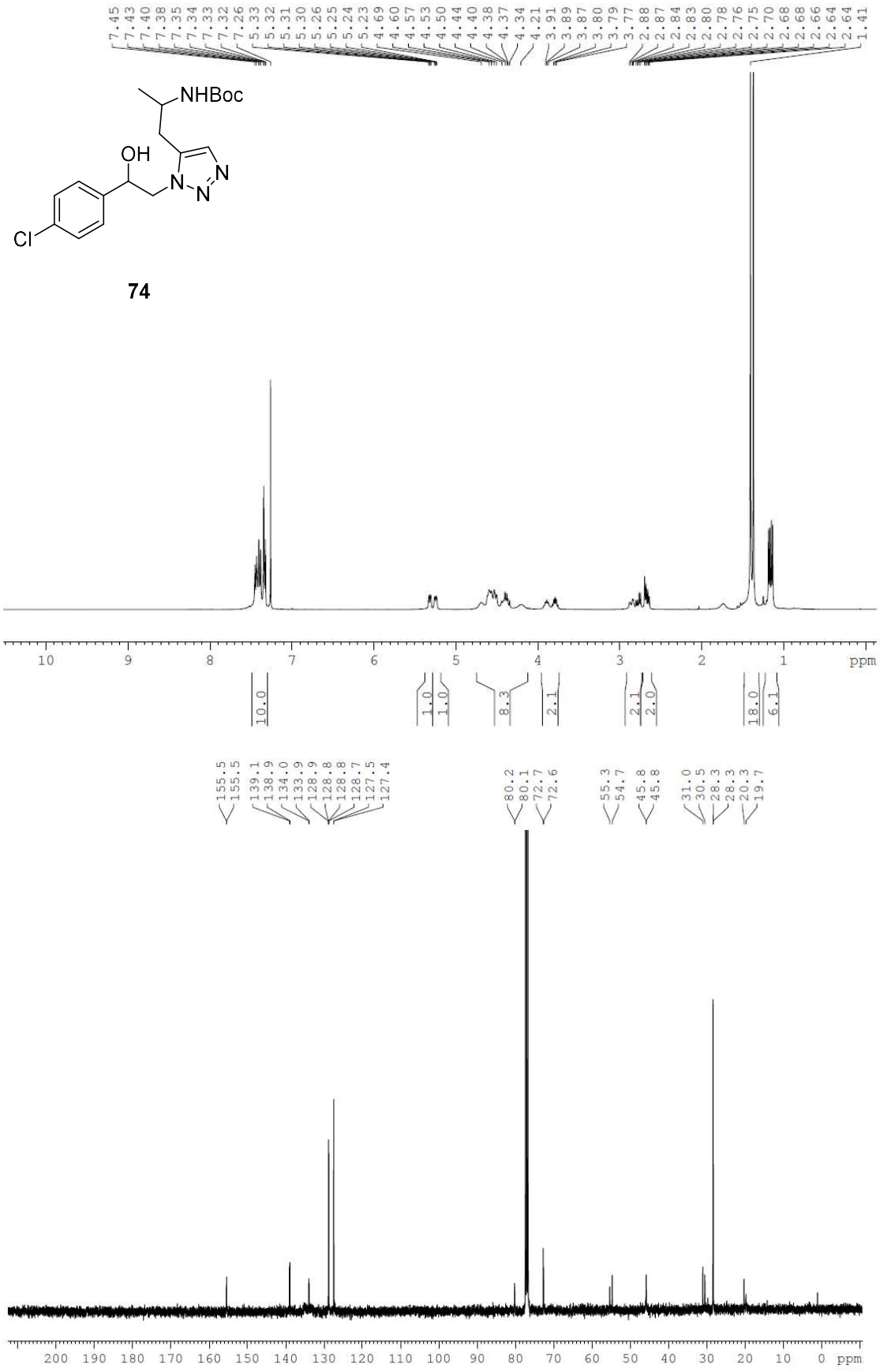
7.45
7.43
7.40
7.38
7.35
7.34
7.33
7.32
7.26
5.33
5.32
5.31
5.30
5.26
5.25
5.24
5.23
4.69
4.60
4.57
4.53
4.50
4.44
4.40
4.38
4.37
4.34
4.21
3.91
3.89
3.87
3.80
3.79
3.77
2.88
2.87
2.84
2.83
2.80
2.78
2.76
2.75
2.70
2.68
2.68
2.66
2.64
2.64
1.41
NHBoc
OH
N
N
N
Cl
74
10
9
8
7
6
5
4
3
2
1
ppm
10.0
1.0
1.0
8.3
2.1
2.1
2.0
18.0
6.1
155.5
155.5
139.1
138.9
134.0
133.9
128.9
128.8
128.8
128.7
127.5
127.4
80.2
80.1
72.7
72.6
55.3
54.7
45.8
45.8
31.0
30.5
28.3
28.3
20.3
19.7
200
190
180
170
160
150
140
130
120
110
100
90
80
70
60
50
40
30
20
10
0
ppm

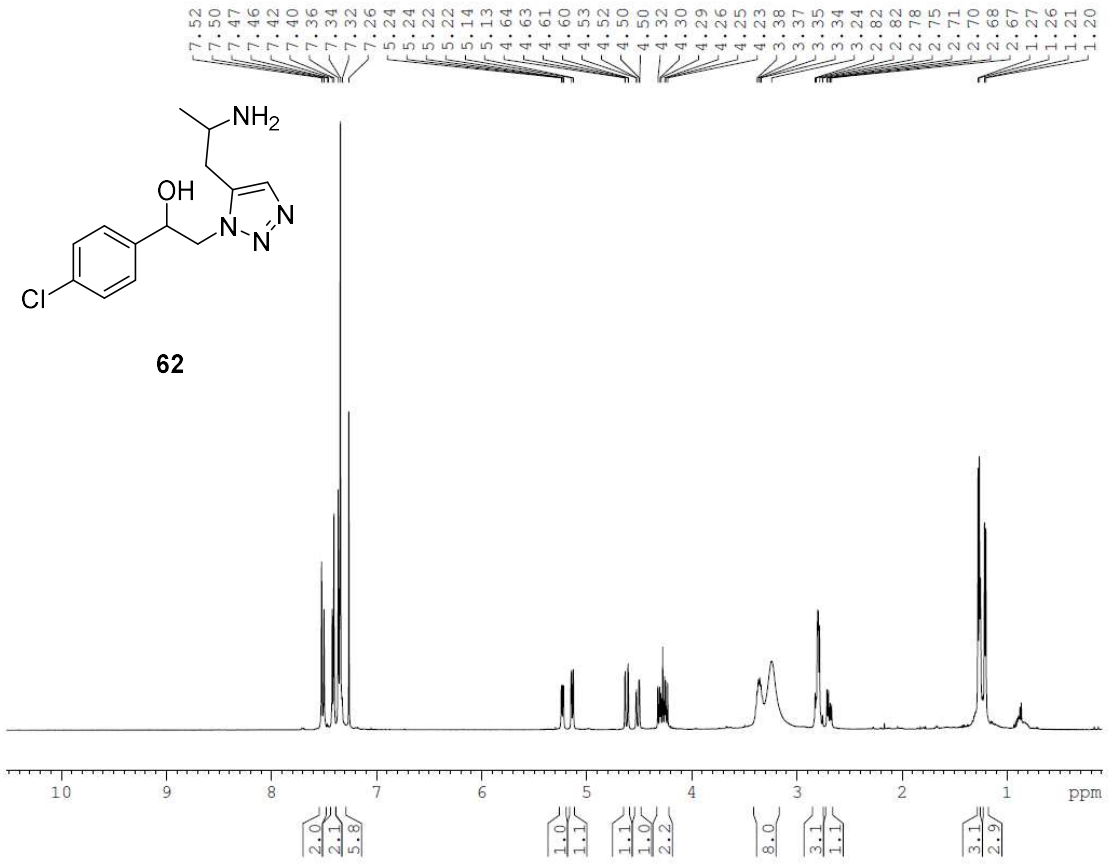
7.52
7.50
7.47
7.46
7.42
7.40
7.36
7.34
7.32
7.26
5.24
5.24
5.22
5.22
5.14
5.13
4.64
4.63
4.61
4.60
4.53
4.52
4.50
4.50
4.32
4.30
4.29
4.26
4.25
4.23
3.38
3.37
3.35
3.34
3.24
2.82
2.78
2.75
2.71
2.70
2.68
2.67
1.27
1.26
1.21
1.20
NH2
OH
N
N
N
Cl
62
10
9
8
7
6
5
4
3
2
1
ppm
2.0
2.1
5.8
1.0
1.1
1.1
1.0
2.2
8.0
3.1
1.1
3.1
2.9

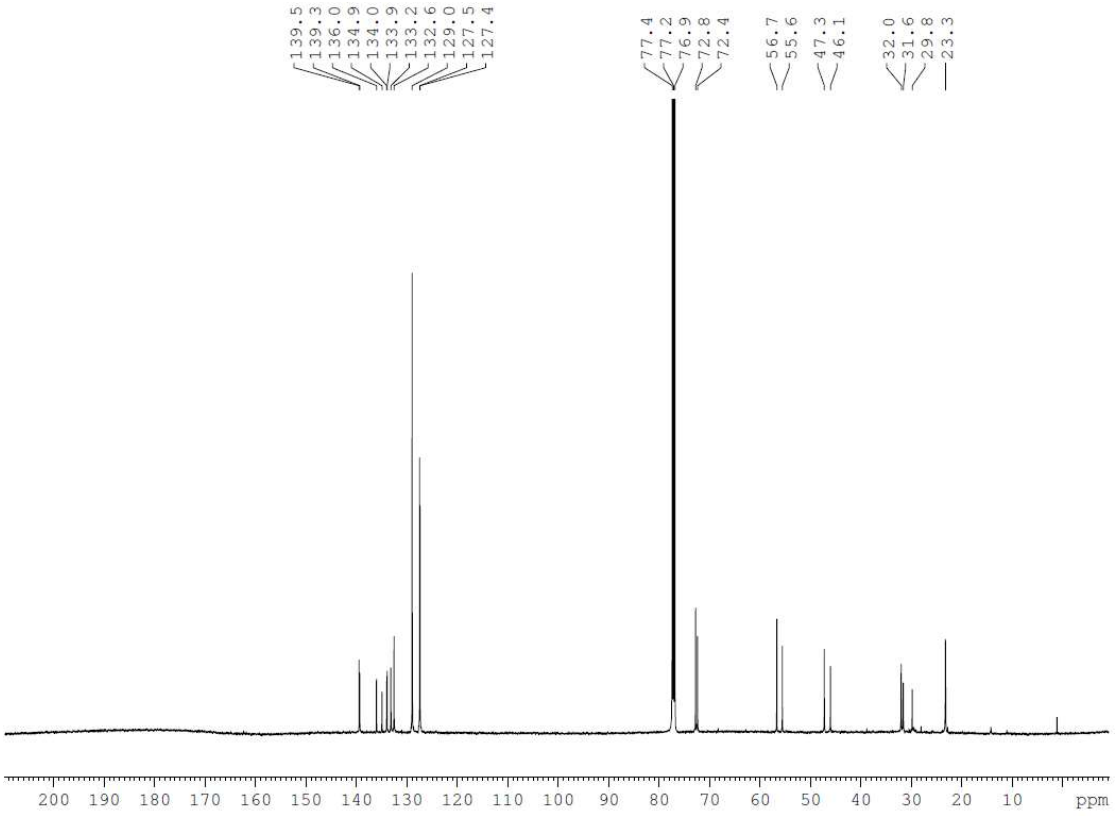
139.5
139.3
136.0
134.9
134.0
133.9
133.2
132.6
129.0
127.5
127.4
77.4
77.2
76.9
72.8
72.4
56.7
55.6
47.3
46.1
32.0
31.6
29.8
23.3
200
190
180
170
160
150
140
130
120
110
100
90
80
70
60
50
40
30
20
10
ppm

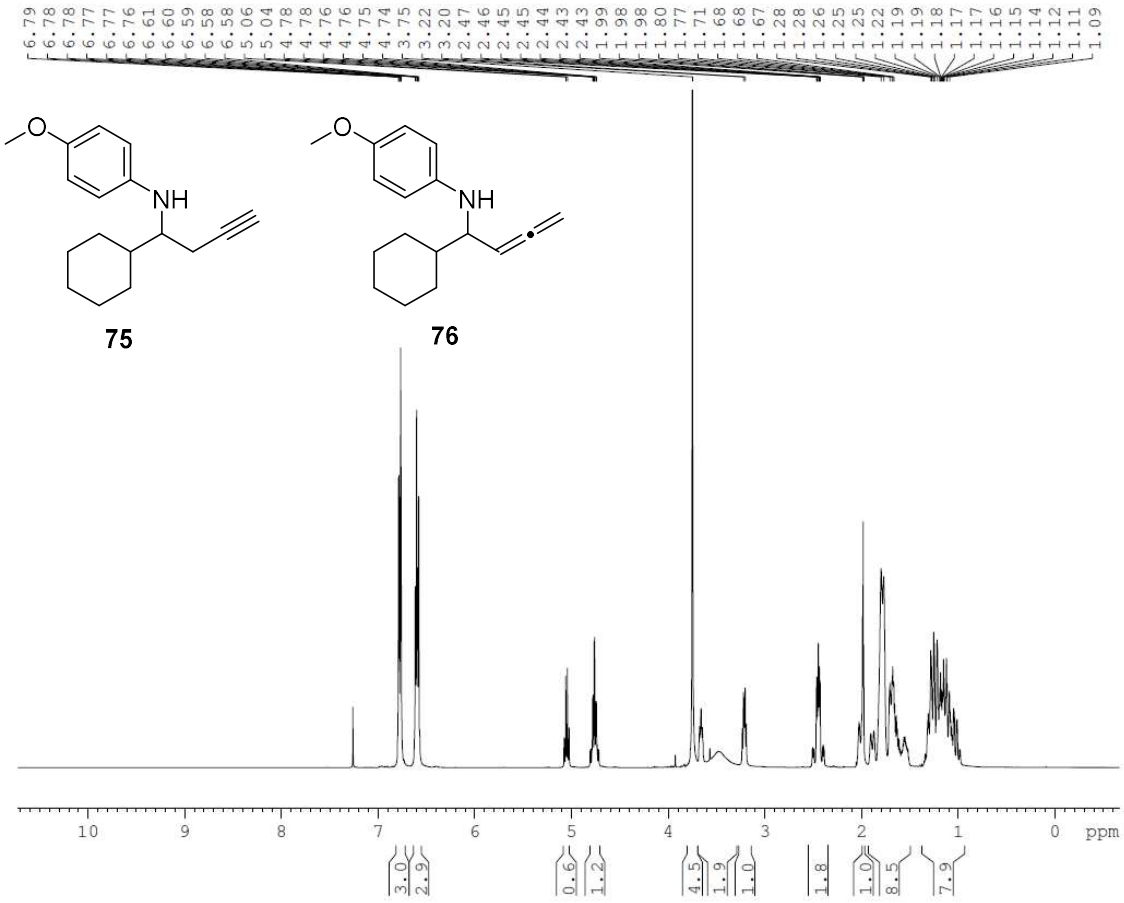
6.79 6.78 6.78 6.77 6.77 6.76 6.61 6.60 6.59 6.58 6.58 5.06 5.04 4.78 4.78 4.76 4.76 4.75 4.74 3.75 3.22 3.20 2.47 2.46 2.45 2.45 2.44 2.43 2.43 1.99 1.98 1.98 1.80 1.77 1.71 1.68 1.67 1.28 1.28 1.26 1.25 1.25 1.22 1.19 1.19 1.18 1.17 1.17 1.16 1.15 1.14 1.12 1.11 1.09
O
NH
75
O
NH
76
10 9 8 7 6 5 4 3 2 1 0 ppm
3.0 2.9 0.6 1.2 4.5 1.9 1.0 1.8 1.0 8.5 7.9

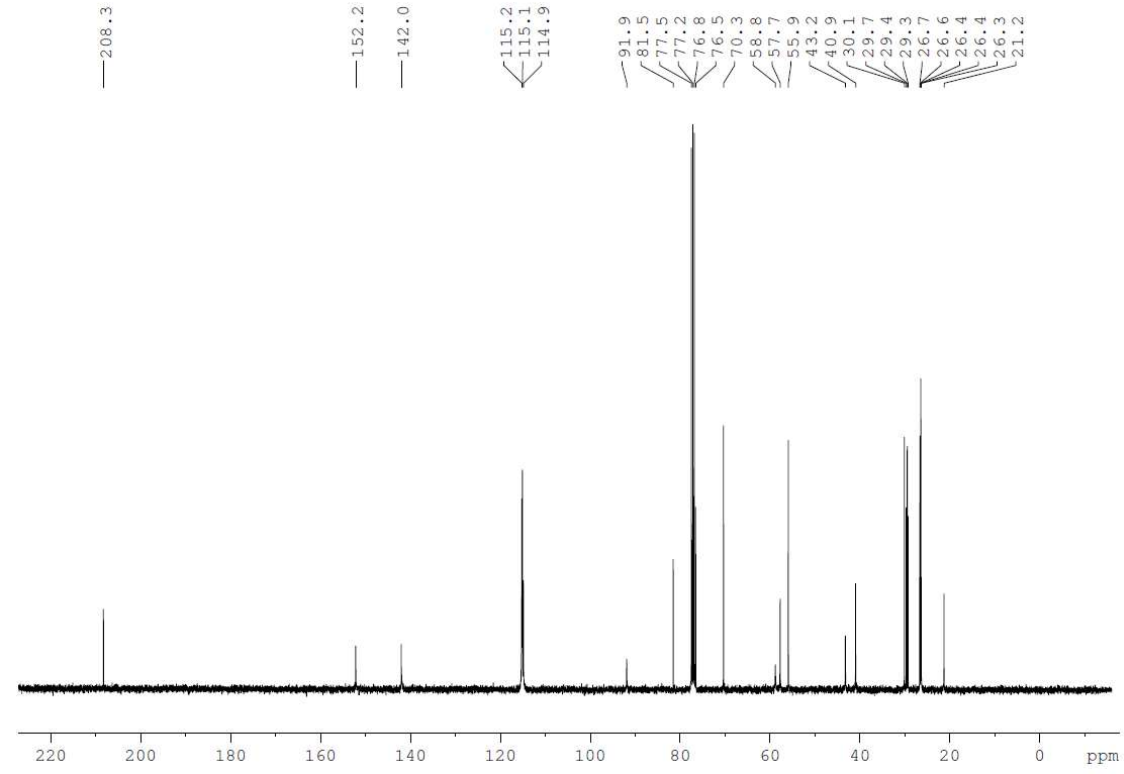
208.3
152.2
142.0
115.2
115.1
114.9
91.9
81.5
77.5
77.2
76.8
76.5
70.3
58.8
57.7
55.9
43.2
40.9
30.1
29.7
29.4
29.3
26.7
26.6
26.4
26.4
26.3
21.2
220 200 180 160 140 120 100 80 60 40 20 0 ppm

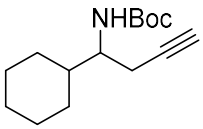
NHBoc

68

7.26
4.63
4.61
3.53
3.52
3.51
3.50
3.49
2.43
2.42
2.42
2.41
1.97
1.96
1.96
1.82
1.78
1.77
1.76
1.73
1.66
1.64
1.63
1.43
1.28
1.28
1.26
1.25
1.25
1.22
1.22
1.19
1.19
1.16
1.14
1.14
1.13
10
9
8
7
6
5
4
3
2
1
0
ppm
0.9
1.0
2.1
1.0
6.3
9.0
3.4
2.3

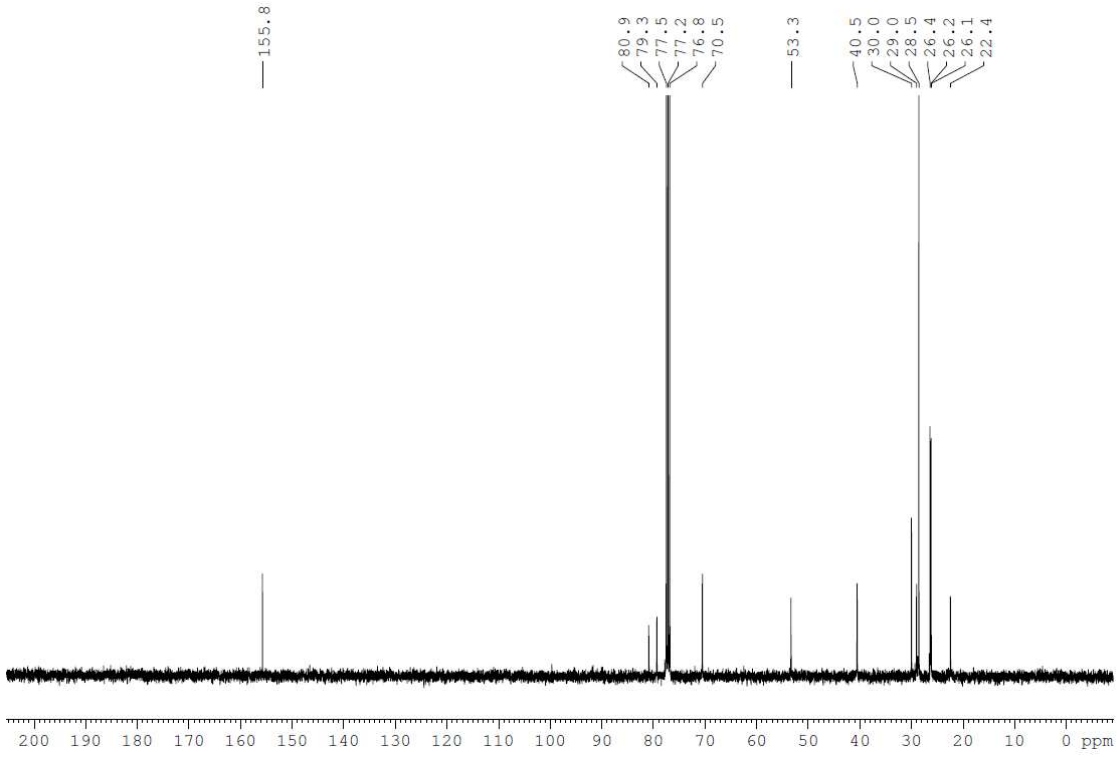
155.8
80.9
79.3
77.5
77.2
76.8
70.5
53.3
40.5
30.0
29.0
28.5
26.4
26.2
26.1
22.4
200
190
180
170
160
150
140
130
120
110
100
90
80
70
60
50
40
30
20
10
0 ppm

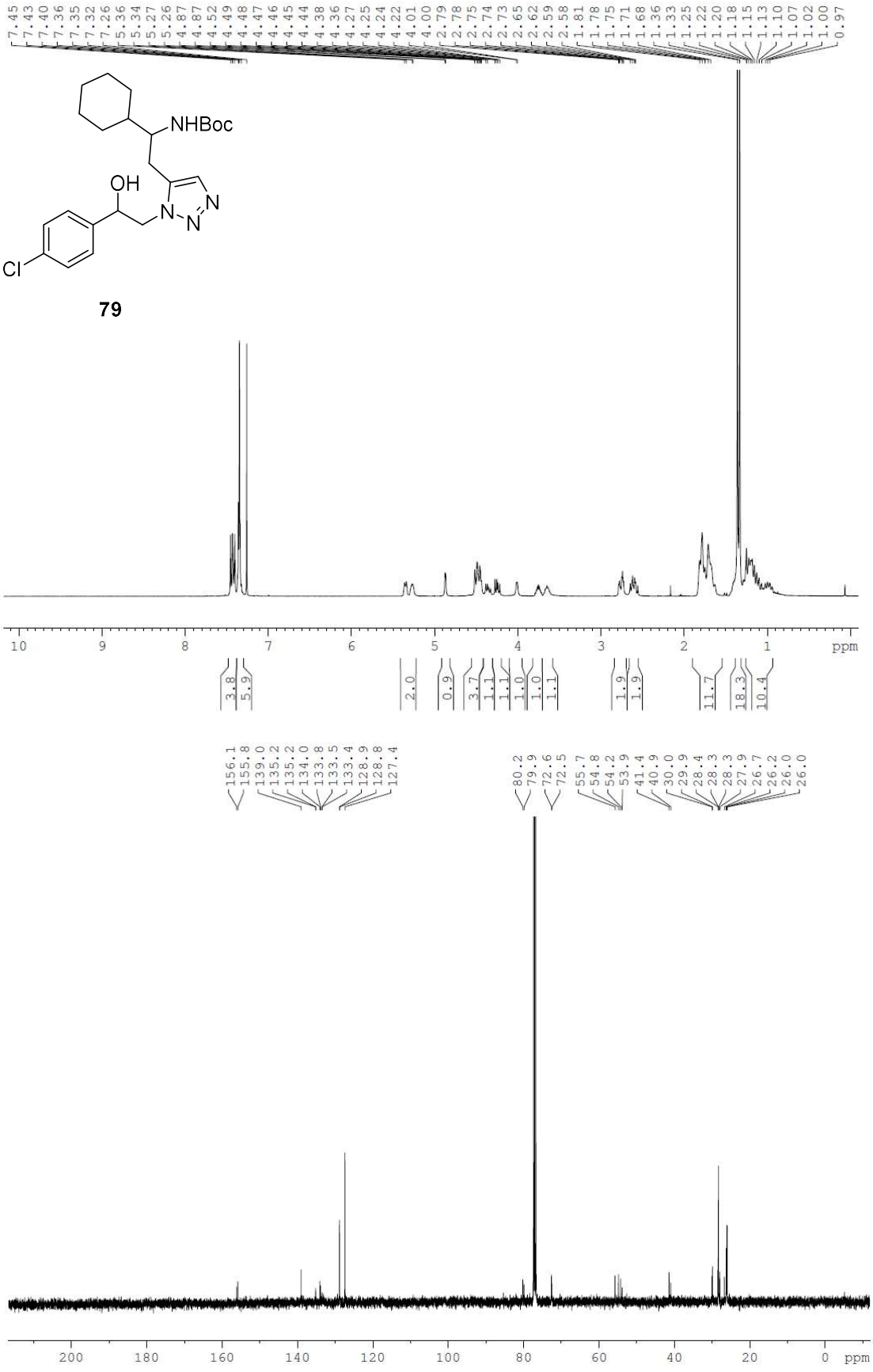
7.45 7.43 7.40 7.36 7.35 7.32 7.26 5.36 5.34 5.27 5.26 4.87 4.87 4.52 4.49 4.48 4.47 4.46 4.45 4.44 4.38 4.36 4.27 4.25 4.24 4.22 4.01 4.00 2.79 2.78 2.75 2.74 2.73 2.65 2.62 2.59 2.58 1.81 1.78 1.75 1.71 1.68 1.36 1.33 1.25 1.22 1.20 1.18 1.15 1.13 1.10 1.07 1.02 1.00 0.97
NHBoc
OH
N
N
N
Cl
79
10 9 8 7 6 5 4 3 2 1 ppm
3.8 5.9 2.0 0.9 3.7 1.1 1.1 1.0 1.0 1.1 1.9 1.9 11.7 18.3 10.4
156.1 155.8 139.0 135.2 135.2 134.0 133.8 133.5 133.4 128.9 128.8 127.4
80.2 79.9 72.6 72.5 55.7 54.8 54.2 53.9 41.4 40.9 30.0 29.9 28.4 28.3 28.3 27.9 26.7 26.2 26.0 26.0
200 180 160 140 120 100 80 60 40 20 0 ppm

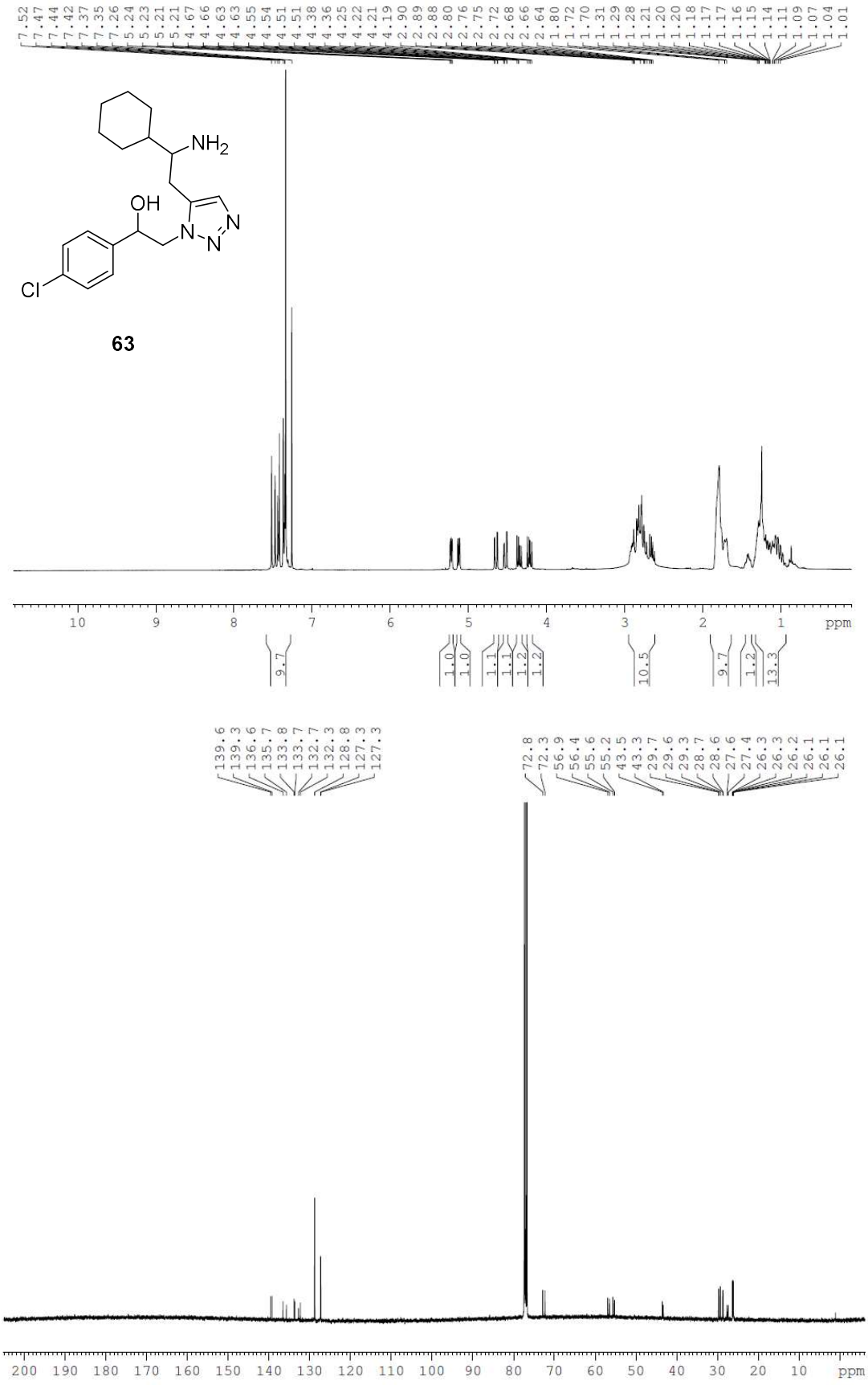
7.52
7.47
7.44
7.42
7.37
7.35
7.26
5.24
5.23
5.21
5.21
4.67
4.66
4.63
4.63
4.55
4.54
4.51
4.51
4.38
4.36
4.25
4.22
4.21
4.19
2.90
2.89
2.88
2.80
2.76
2.75
2.72
2.68
2.66
2.64
1.80
1.72
1.70
1.31
1.29
1.28
1.21
1.20
1.20
1.18
1.17
1.17
1.16
1.15
1.14
1.11
1.09
1.07
1.04
1.01
NH2
OH
N
N
N
Cl
63
10
9
8
7
6
5
4
3
2
1
ppm
9.7
1.0
1.0
1.1
1.1
1.2
1.2
10.5
9.7
1.2
13.3
139.6
139.3
136.6
135.7
133.8
133.7
132.7
132.3
128.8
127.3
127.3
72.8
72.3
56.9
56.4
55.6
55.2
43.5
43.3
29.7
29.6
29.3
28.7
28.6
27.6
27.4
26.3
26.3
26.2
26.1
26.1
26.1
200
190
180
170
160
150
140
130
120
110
100
90
80
70
60
50
40
30
20
10
ppm

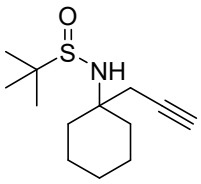
O
S
NH

81

7.26
3.49
2.64
2.63
2.60
2.59
2.42
2.42
2.38
2.38
2.06
2.06
2.05
1.95
1.92
1.78
1.77
1.75
1.75
1.72
1.71
1.70
1.69
1.68
1.66
1.65
1.63
1.60
1.58
1.56
1.55
1.55
1.53
1.53
10 9 8 7 6 5 4 3 2 1 0 ppm
0.9
1.0
1.0
0.9
1.0
9.3
8.9

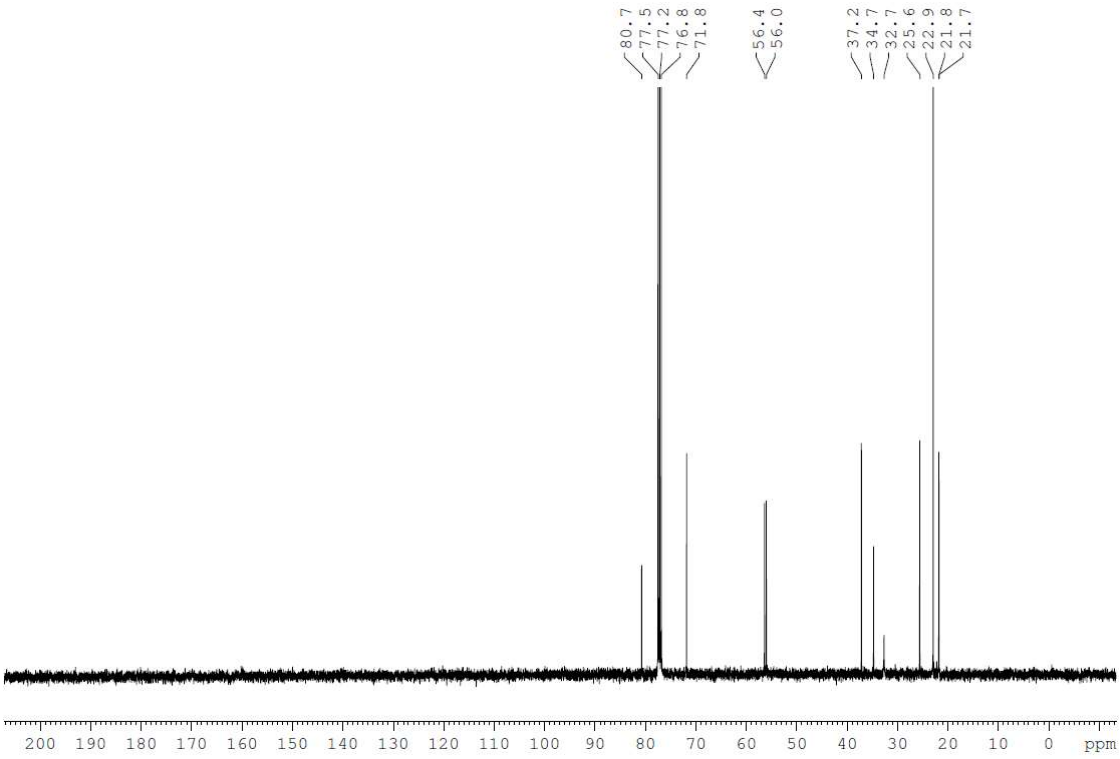
80.7
77.5
77.2
76.8
71.8
56.4
56.0
37.2
34.7
32.7
25.6
22.9
21.8
21.7
200 190 180 170 160 150 140 130 120 110 100 90 80 70 60 50 40 30 20 10 0 ppm

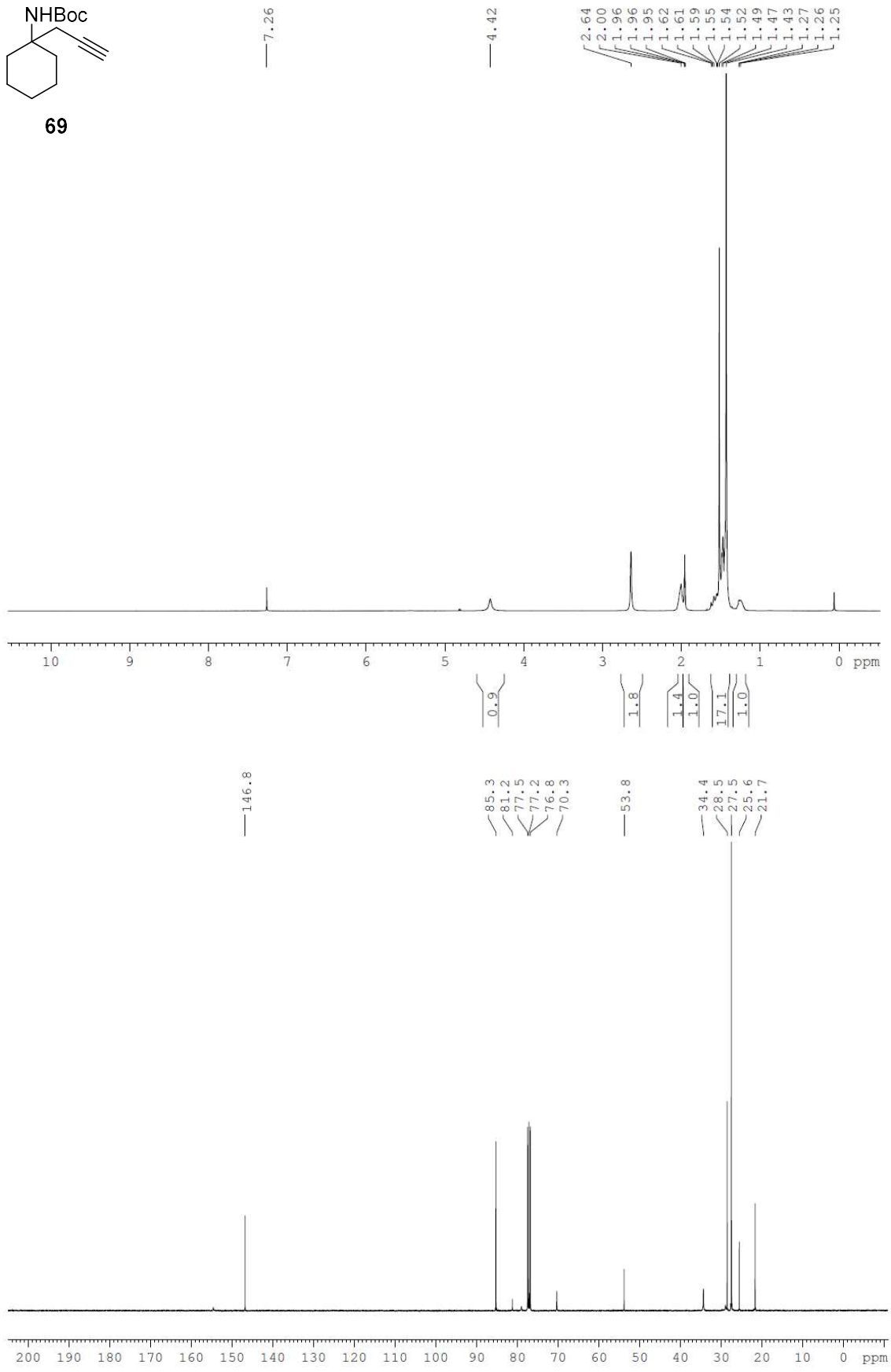
NHBoc
69
7.26
4.42
2.64
2.00
1.96
1.96
1.95
1.62
1.61
1.59
1.55
1.54
1.52
1.49
1.47
1.43
1.27
1.26
1.25
10 9 8 7 6 5 4 3 2 1 0 ppm
0.9
1.8
1.4
1.0
17.1
1.0
146.8
85.3
81.2
77.5
77.2
76.8
70.3
53.8
34.4
28.5
27.5
25.6
21.7
200 190 180 170 160 150 140 130 120 110 100 90 80 70 60 50 40 30 20 10 0 ppm

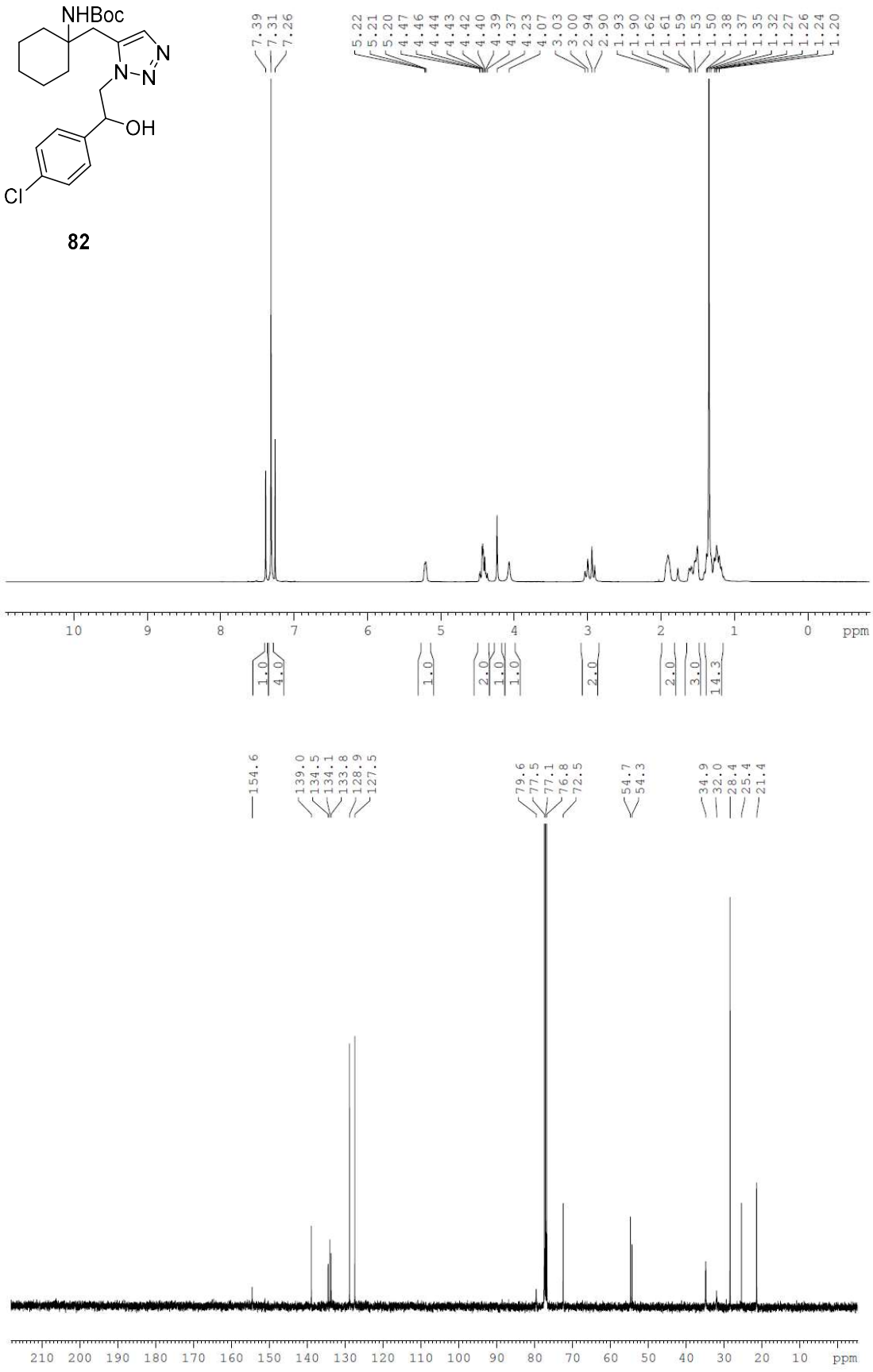
NHBoc
N
N
N
OH
Cl
7.39
7.31
7.26
5.22
5.21
5.20
4.47
4.46
4.44
4.43
4.42
4.40
4.39
4.37
4.23
4.07
3.03
3.00
2.94
2.90
1.93
1.90
1.62
1.61
1.59
1.53
1.50
1.38
1.37
1.35
1.32
1.27
1.26
1.24
1.20
ppm
1.0
4.0
1.0
2.0
1.0
1.0
2.0
2.0
3.0
14.3
154.6
139.0
134.5
134.1
133.8
128.9
127.5
79.6
77.5
77.1
76.8
72.5
54.7
54.3
34.9
32.0
28.4
25.4
21.4
ppm

82

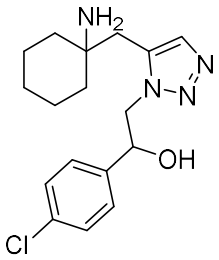
NH2
N
N
N
OH
Cl

64

7.51
7.44
7.43
7.42
7.42
7.41
7.36
7.36
7.35
7.34
7.34
7.33
7.26
5.16
5.16
5.14
5.14
4.69
4.69
4.66
4.65
4.31
4.29
4.27
4.25
3.19
2.83
1.59
1.57
1.56
1.54
1.51
1.49
1.47
1.41
1.39
1.36
1.35
1.24
11 10 9 8 7 6 5 4 3 2 1 ppm
1.0
2.0
2.1
1.0
1.0
1.0
2.1
2.0
11.0

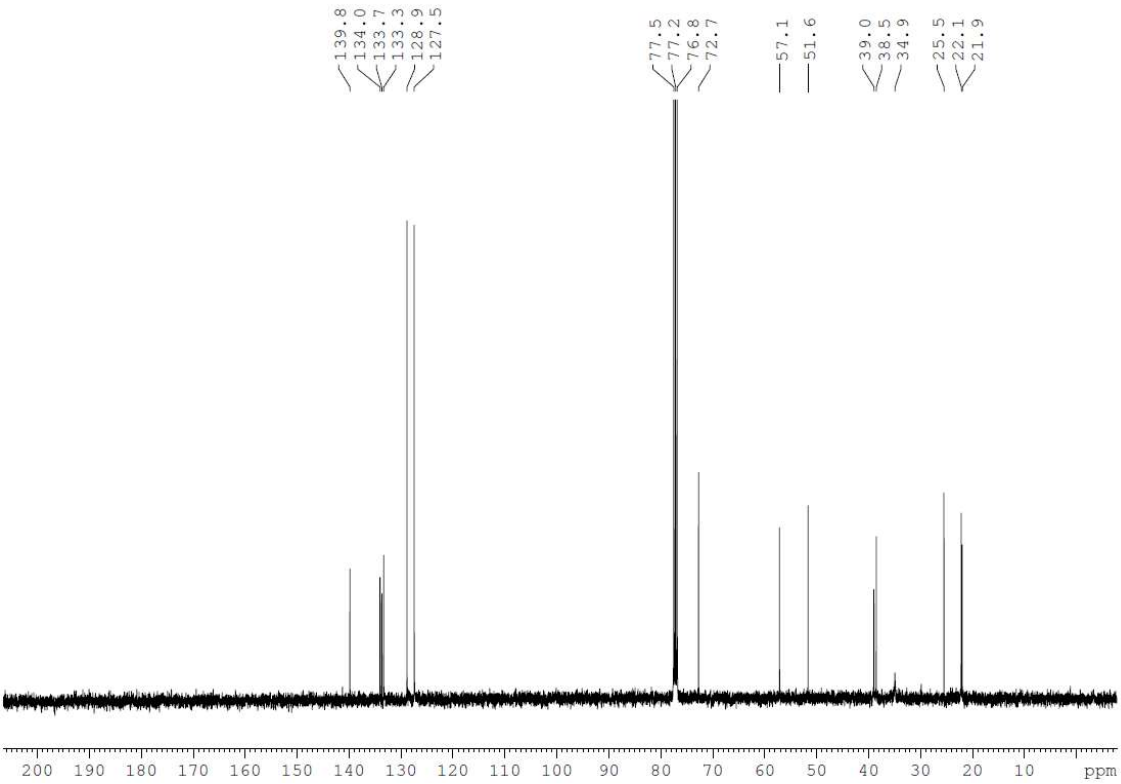
139.8
134.0
133.7
133.3
128.9
127.5
77.5
77.2
76.8
72.7
57.1
51.6
39.0
38.5
34.9
25.5
22.1
21.9
200 190 180 170 160 150 140 130 120 110 100 90 80 70 60 50 40 30 20 10 ppm

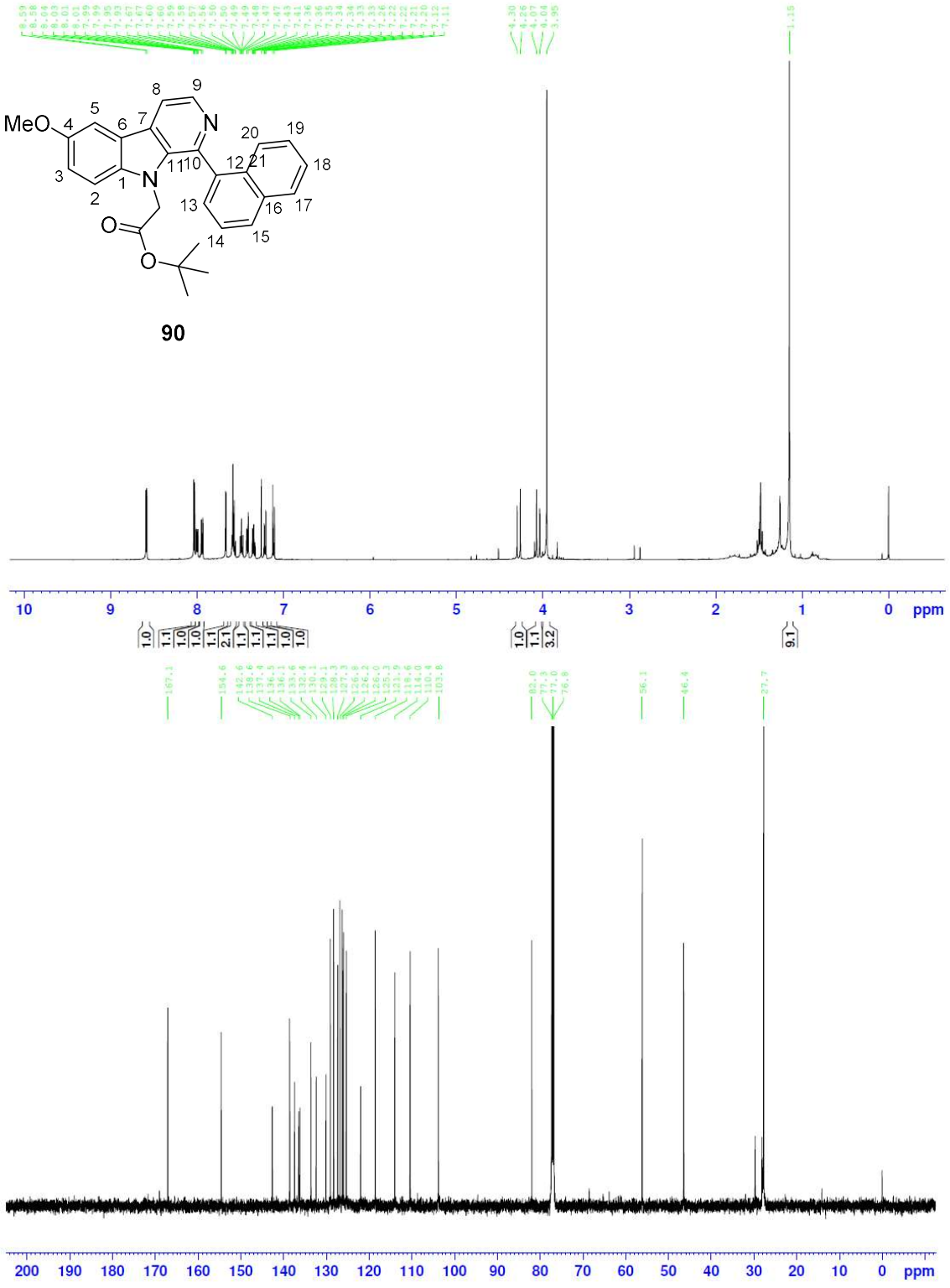

90

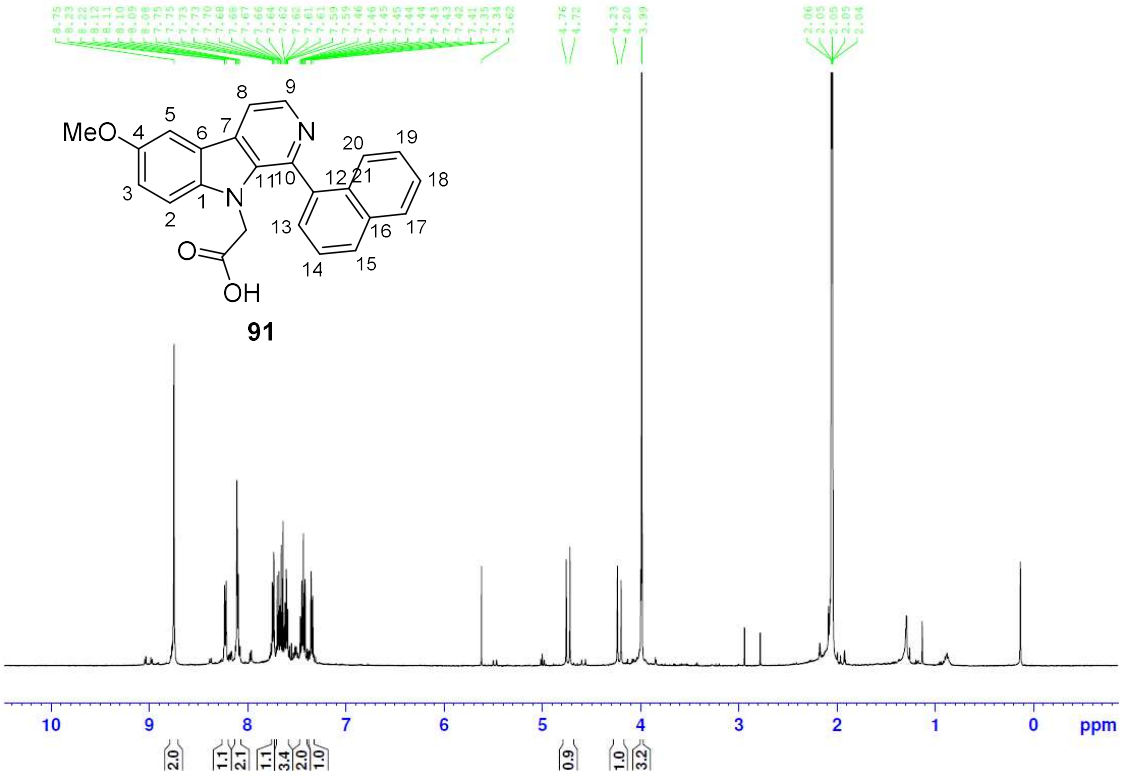

91

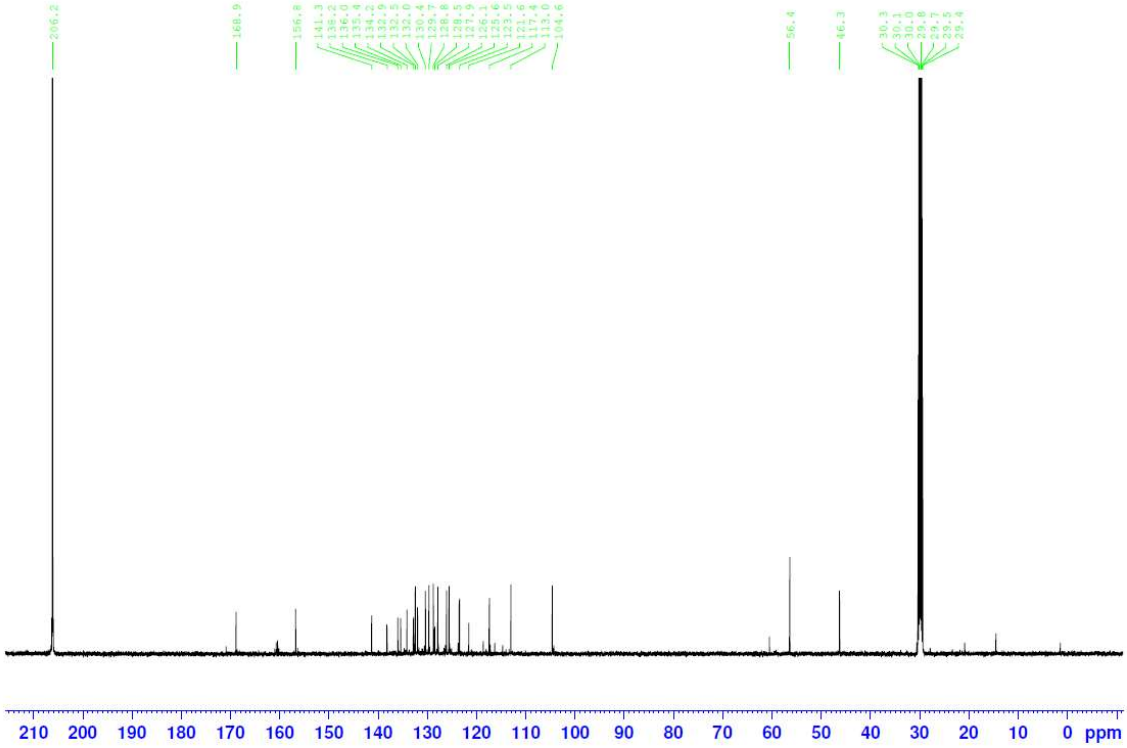

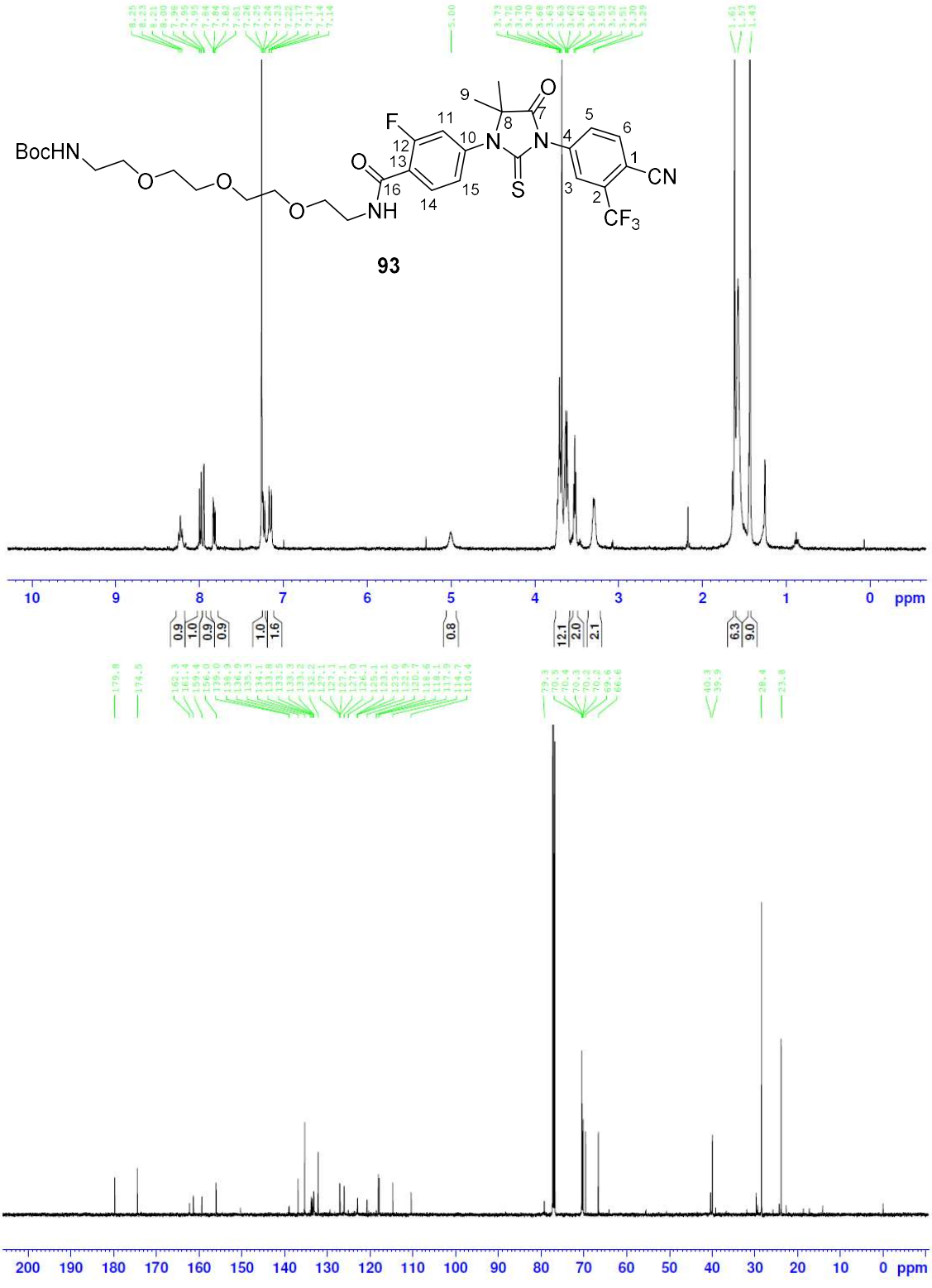
BocHN
O
O
O
NH
F
O
S
N
N
CN
CF3
93
ppm

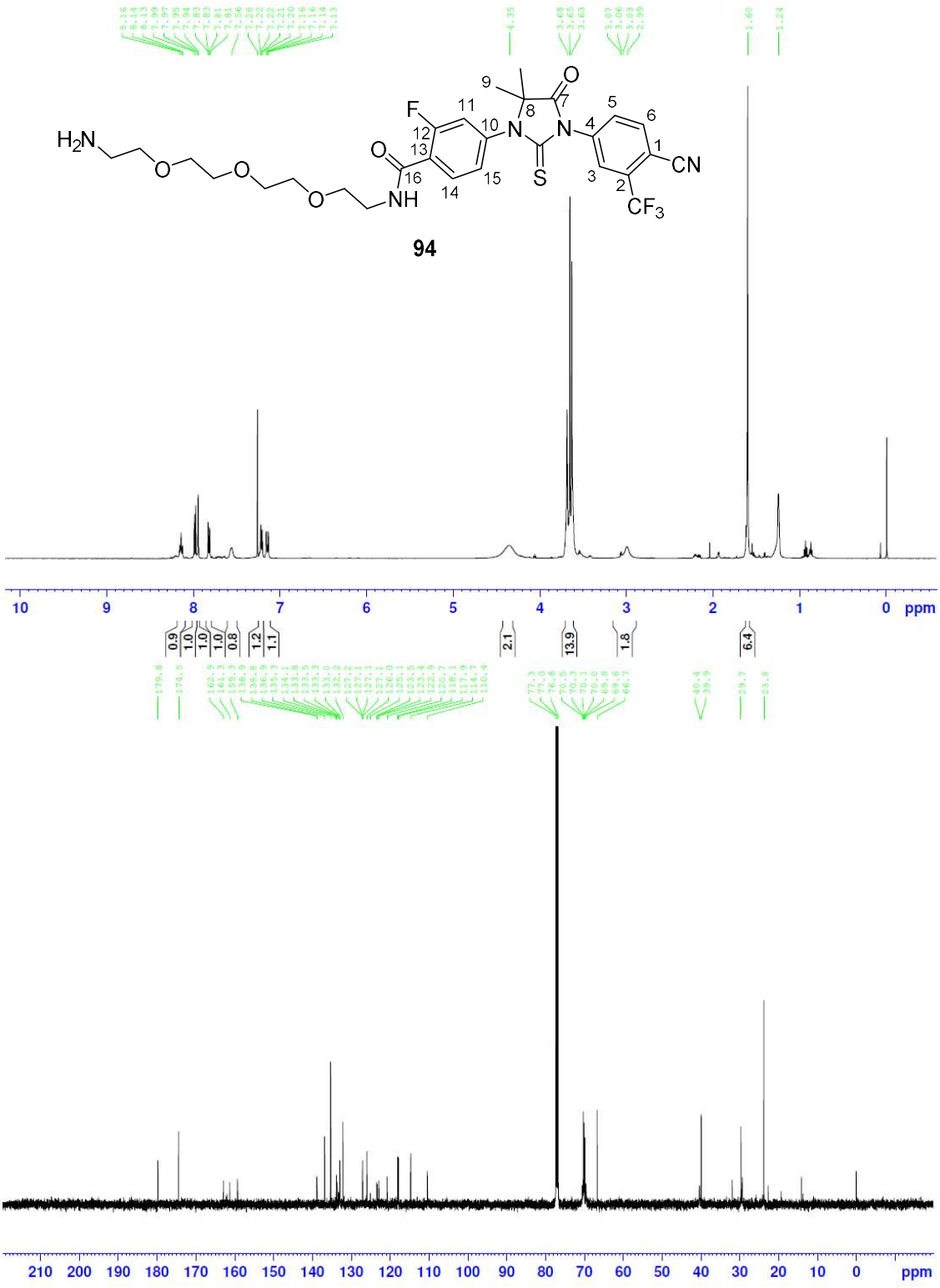
H2N
O
O
O
NH
O
F
9
8
7
O
10
N
N
4
5
6
1
CN
11
12
13
16
14
15
S
3
2
CF3
94
10 9 8 7 6 5 4 3 2 1 0 ppm
210 200 190 180 170 160 150 140 130 120 110 100 90 80 70 60 50 40 30 20 10 0 ppm

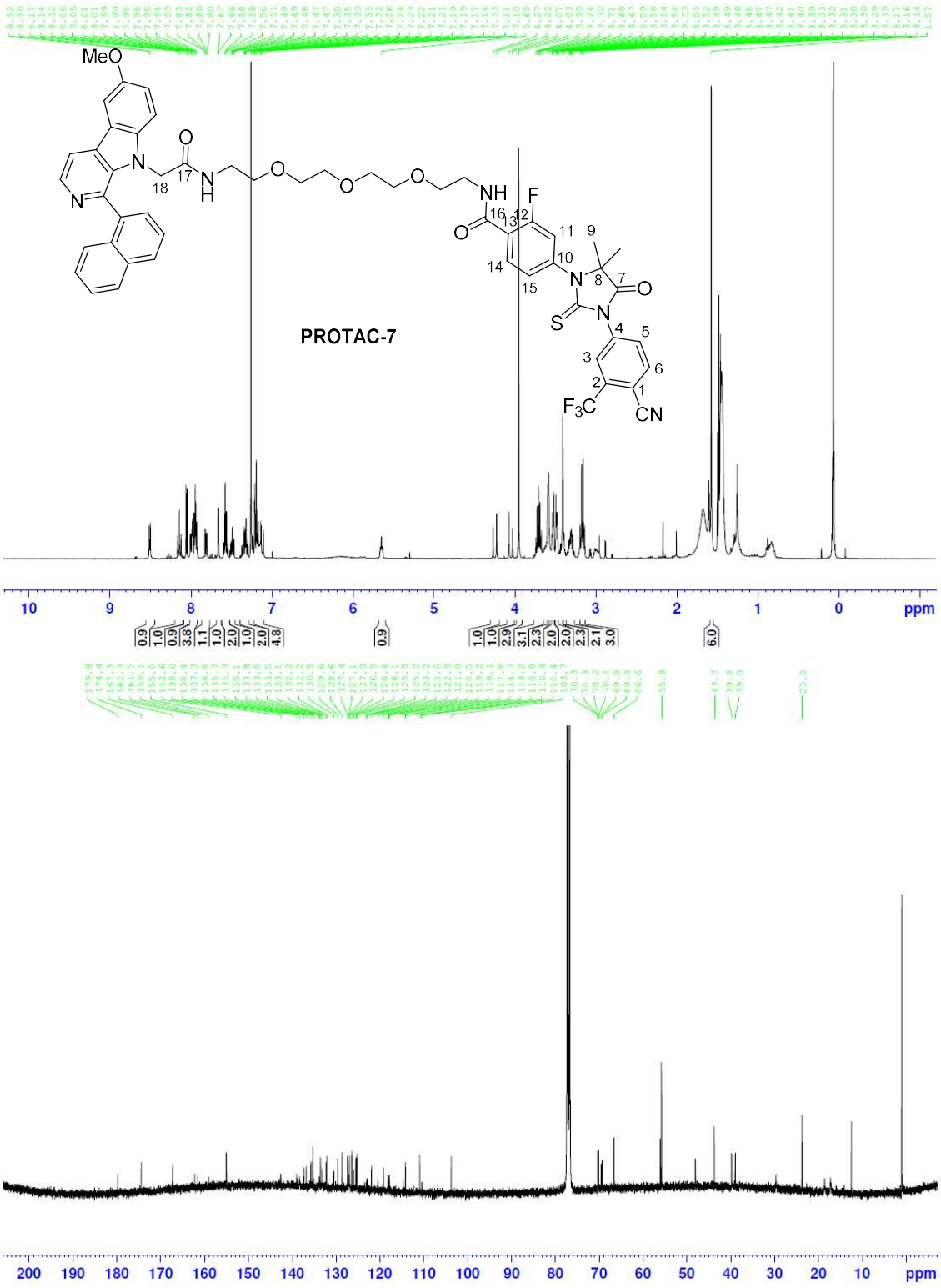
MeO
O
N
N
H
O
O
O
NH
F
O
S
N
O
N
F3C
CN
PROTAC-7
10
9
8
7
6
5
4
3
2
1
0
ppm
200
190
180
170
160
150
140
130
120
110
100
90
80
70
60
50
40
30
20
10
ppm

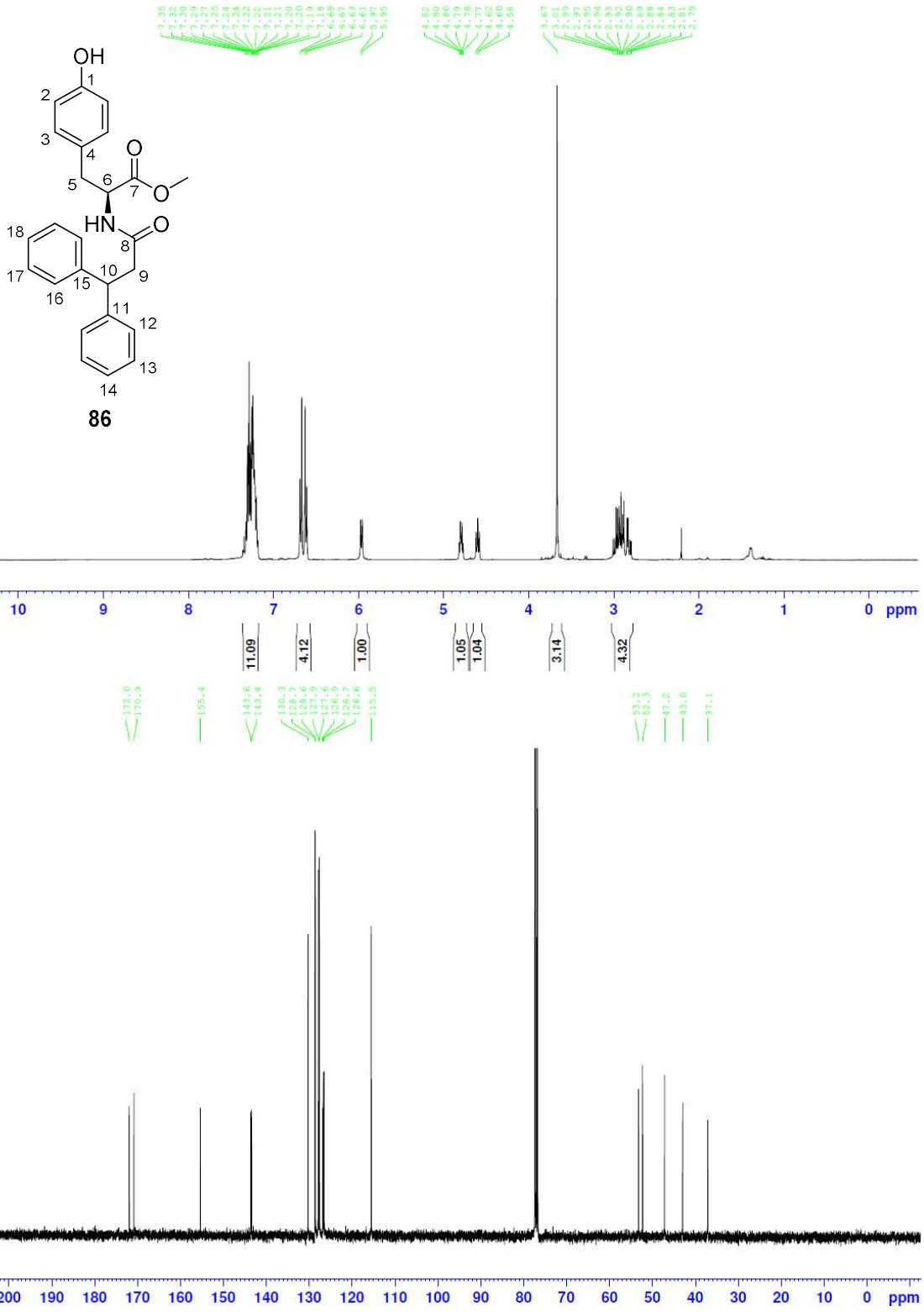
OH
1
2
3
4
5
6
7
O
O
HN
O
8
9
10
11
12
13
14
15
16
17
18
86
10 9 8 7 6 5 4 3 2 1 0 ppm
11.09
4.12
1.00
1.05
1.04
3.14
4.32
200 190 180 170 160 150 140 130 120 110 100 90 80 70 60 50 40 30 20 10 0 ppm

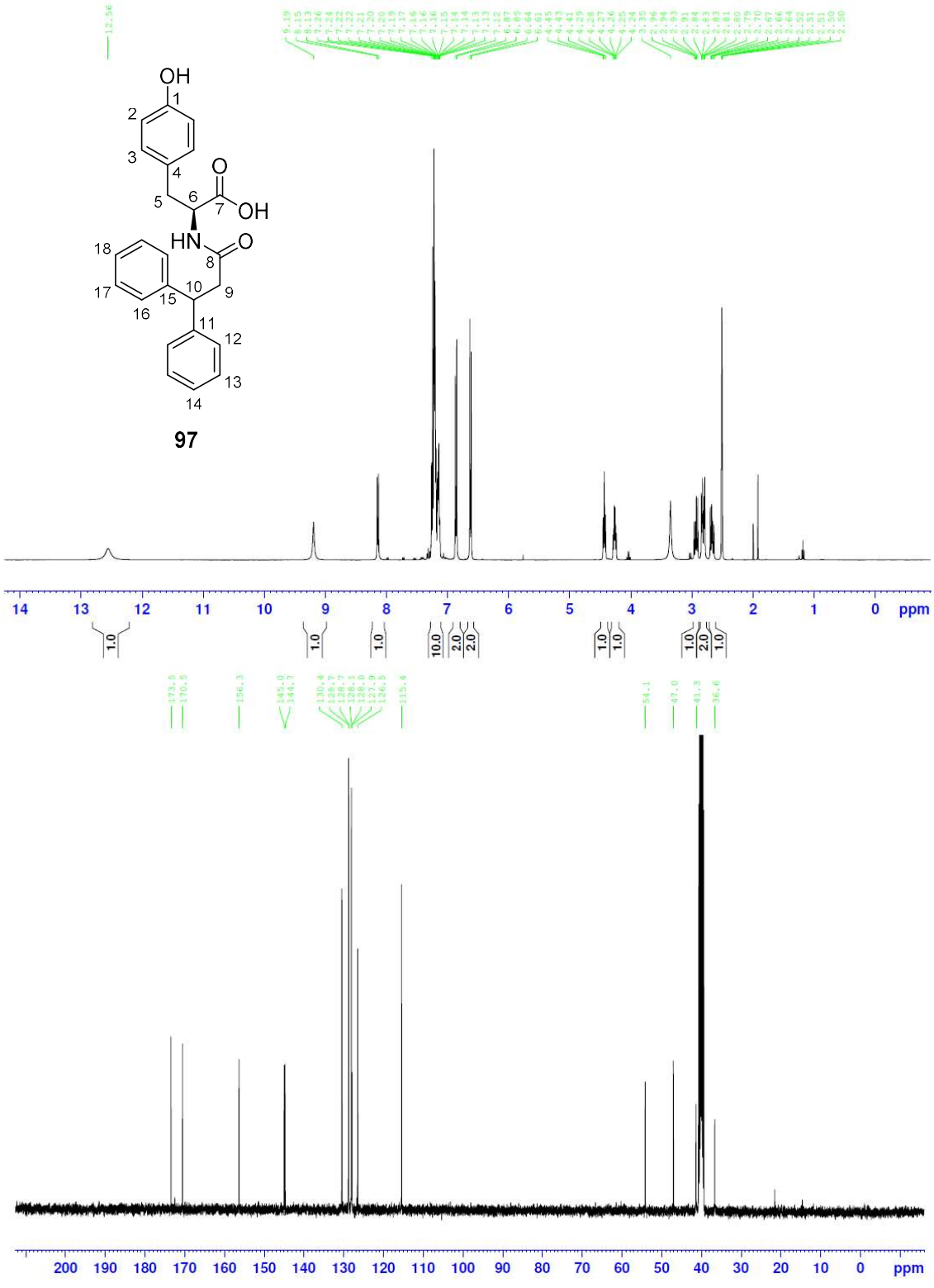
OH
1
2
3
4
5
6
7
OH
O
HN
8
O
18
17
16
15
10
9
11
12
13
14
97
ppm
ppm

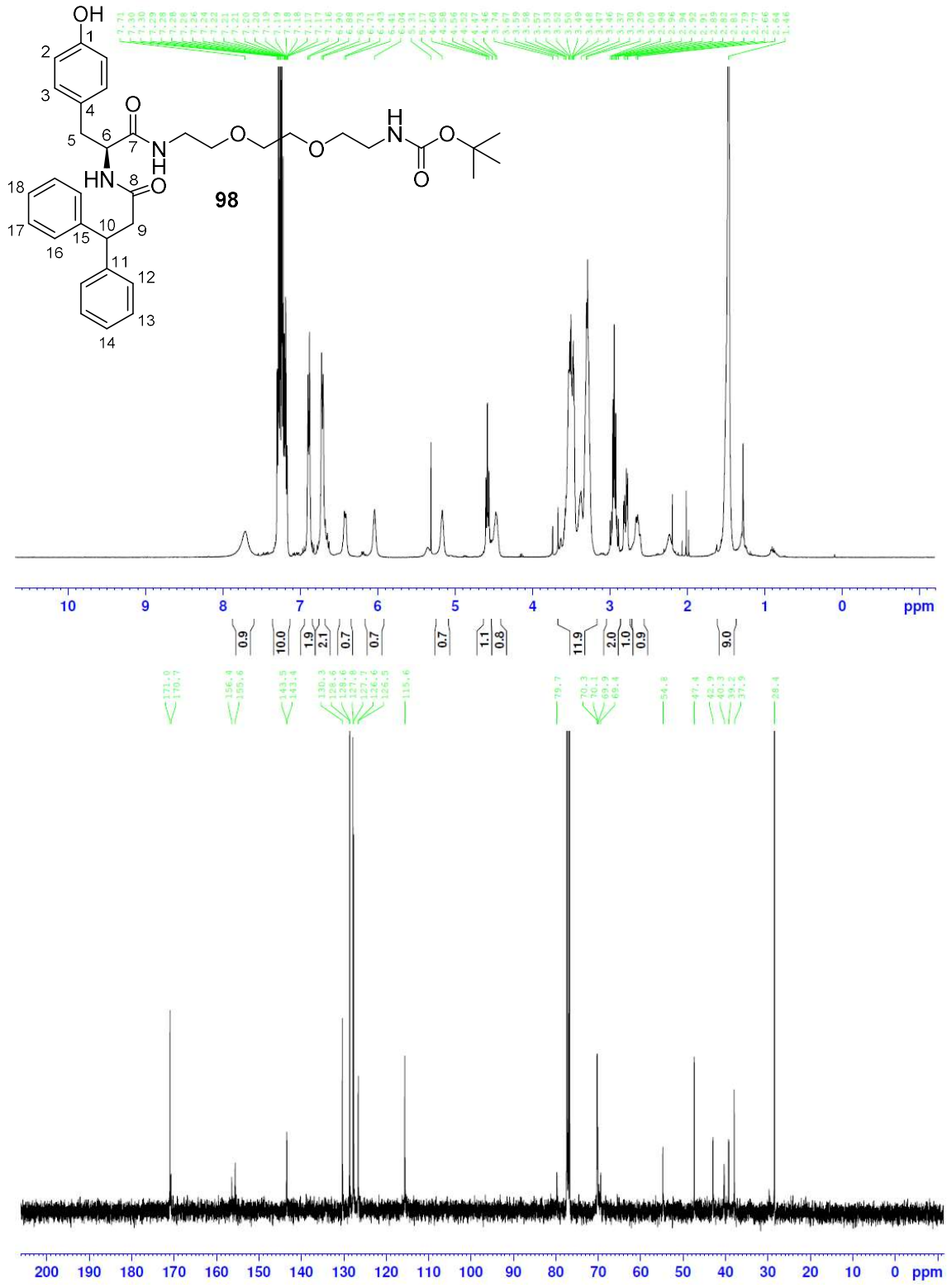
OH
1
2
3
4
5
6
7
8
9
10
11
12
13
14
15
16
17
18
O
N
H
HN
O
O
O
N
H
O
O
98
10 9 8 7 6 5 4 3 2 1 0 ppm
0.9
10.0
1.9
2.1
0.7
0.7
0.7
1.1
0.8
11.9
2.0
1.0
0.9
9.0
200 190 180 170 160 150 140 130 120 110 100 90 80 70 60 50 40 30 20 10 0 ppm

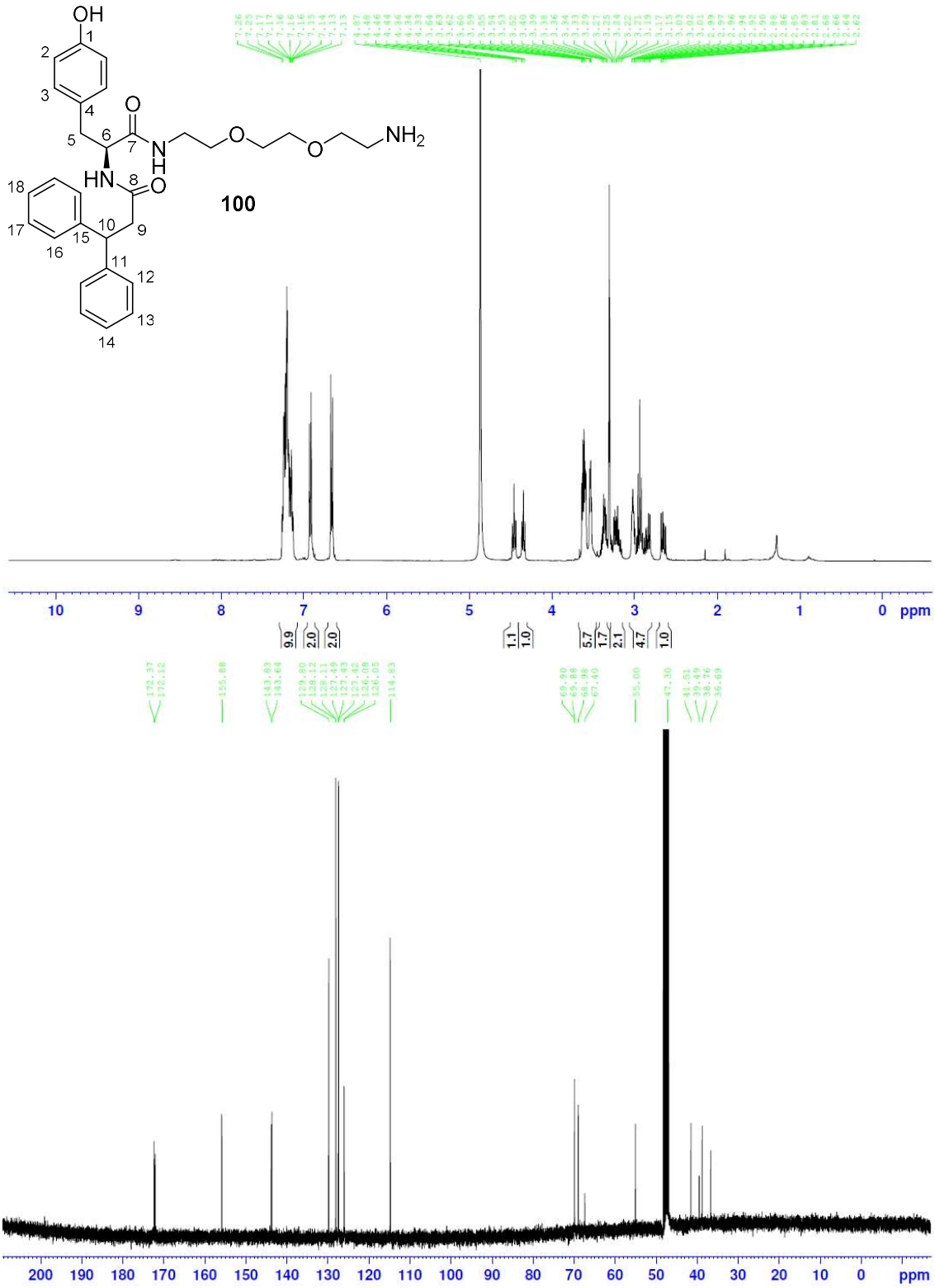
OH
1
2
3
4
5
6
7
O
N
H
HN
8
O
NH2
O
O
18
17
16
15
10
9
11
12
13
14
100
10 9 8 7 6 5 4 3 2 1 0 ppm
9.9
2.0
2.0
1.1
1.0
5.7
1.7
2.1
4.7
1.0
200 190 180 170 160 150 140 130 120 110 100 90 80 70 60 50 40 30 20 10 0 ppm

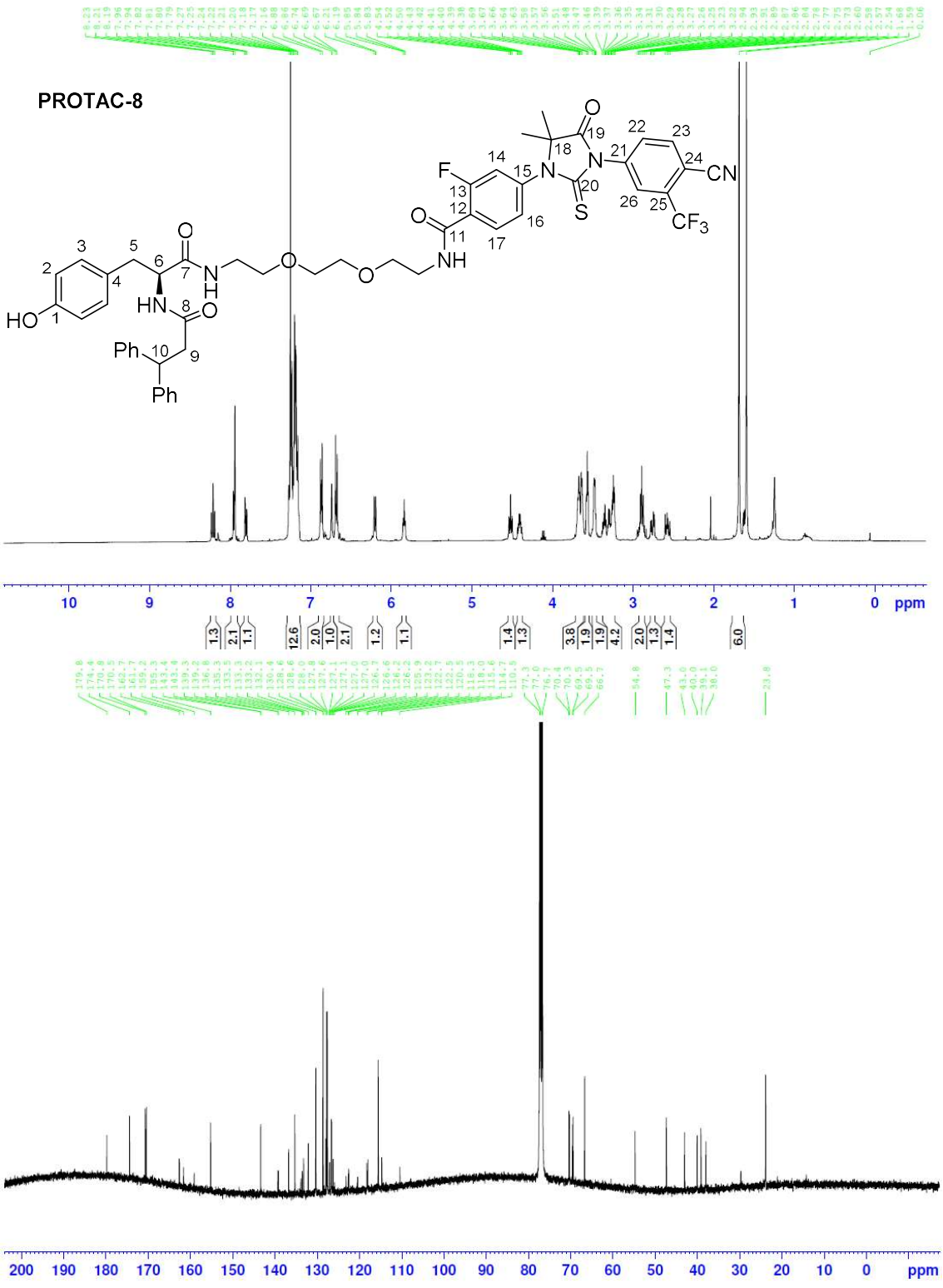
PROTAC-8
HO
HN
NH
NH
O
F
N
S
CN
CF3
Ph
Ph
10
9
8
7
6
5
4
3
2
1
0
ppm
200
190
180
170
160
150
140
130
120
110
100
90
80
70
60
50
40
30
20
10
0
ppm

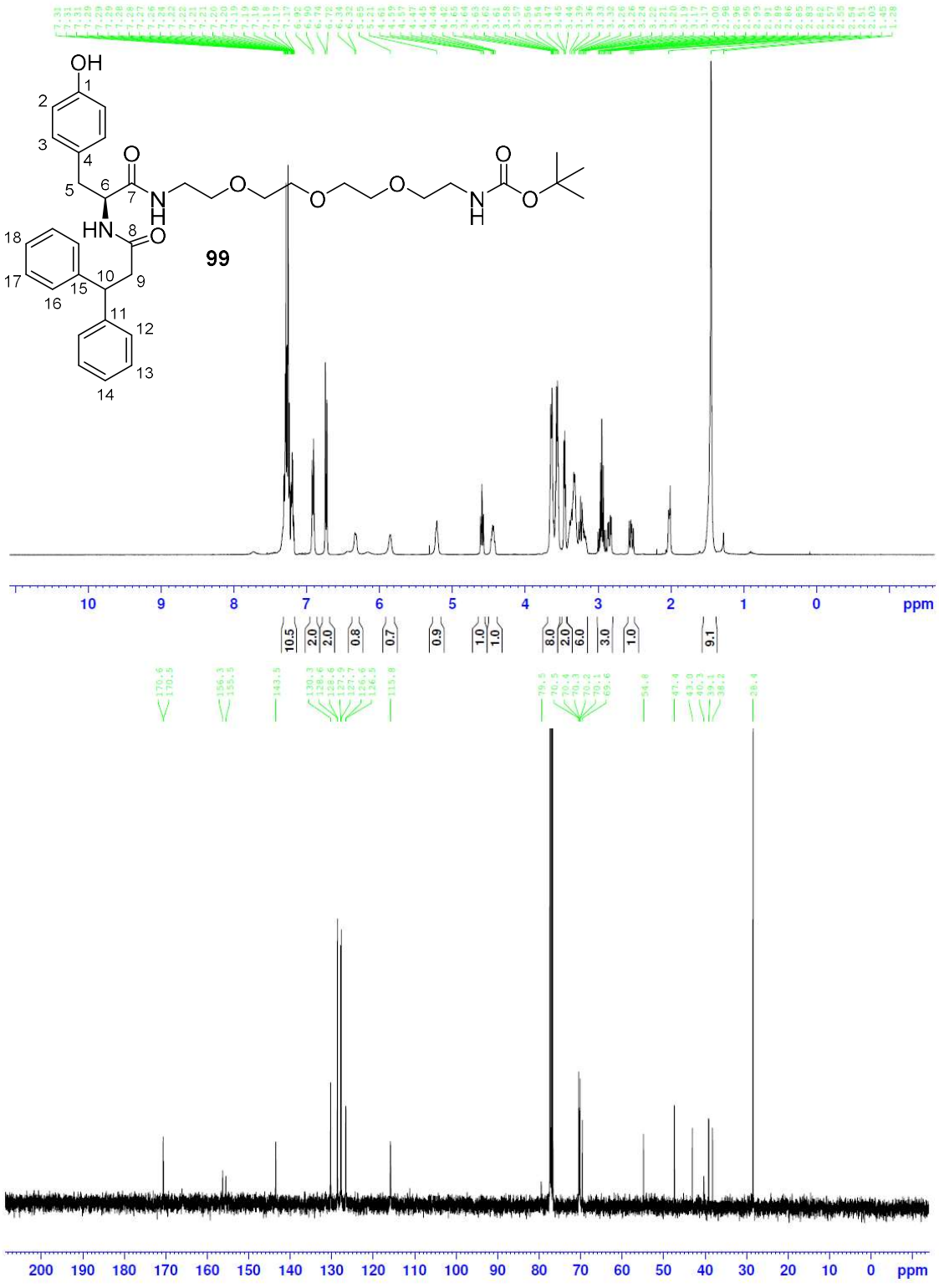
OH
1
2
3
4
5
6
7
O
N
H
HN
8
O
18
17
16
15
10
9
11
12
13
14
99
O
O
O
O
N
H
O
O
10
9
8
7
6
5
4
3
2
1
0
ppm
10.5
2.0
2.0
0.8
0.7
0.9
1.0
1.0
8.0
2.0
6.0
3.0
1.0
9.1
200
190
180
170
160
150
140
130
120
110
100
90
80
70
60
50
40
30
20
10
0
ppm

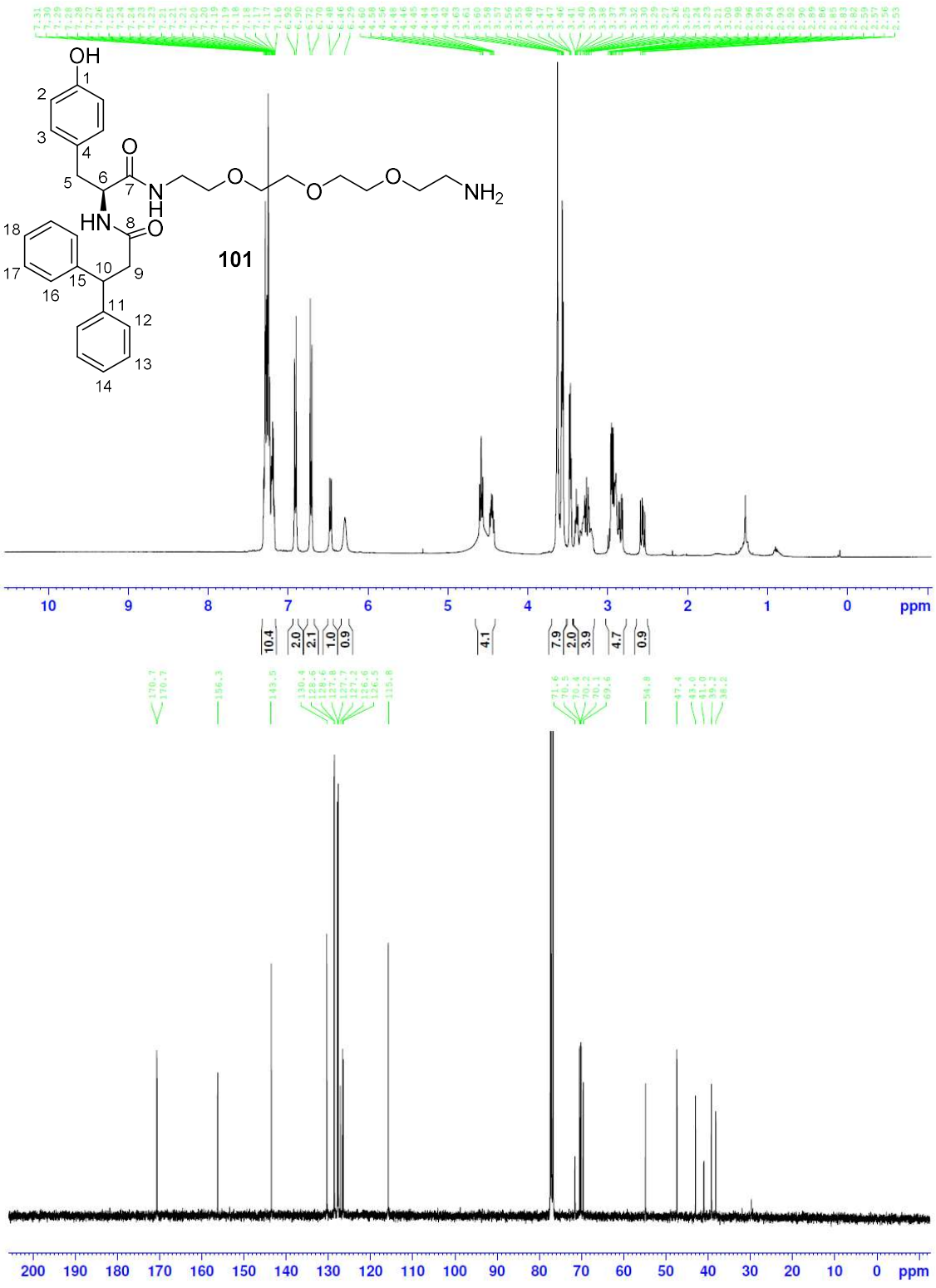
OH
1
2
3
4
5
6
7
N
H
O
HN
8
O
18
17
16
15
10
9
11
12
13
14
101
O
O
O
NH2
10
9
8
7
6
5
4
3
2
1
0
ppm
10.4
2.0
2.1
1.0
0.9
4.1
7.9
2.0
3.9
4.7
0.9
200
190
180
170
160
150
140
130
120
110
100
90
80
70
60
50
40
30
20
10
0
ppm

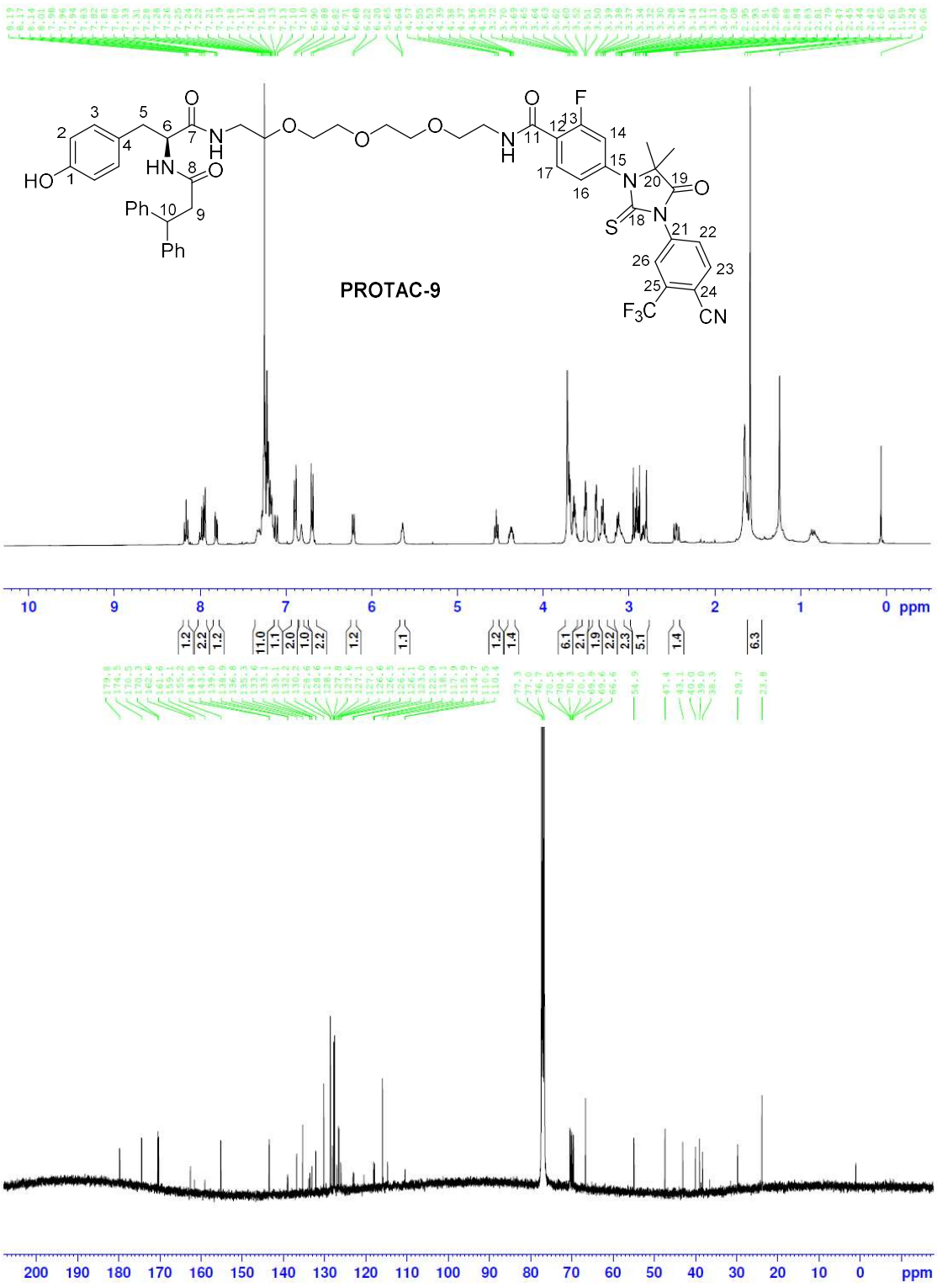
PROTAC-9
10 9 8 7 6 5 4 3 2 1 0 ppm
200 190 180 170 160 150 140 130 120 110 100 90 80 70 60 50 40 30 20 10 0 ppm

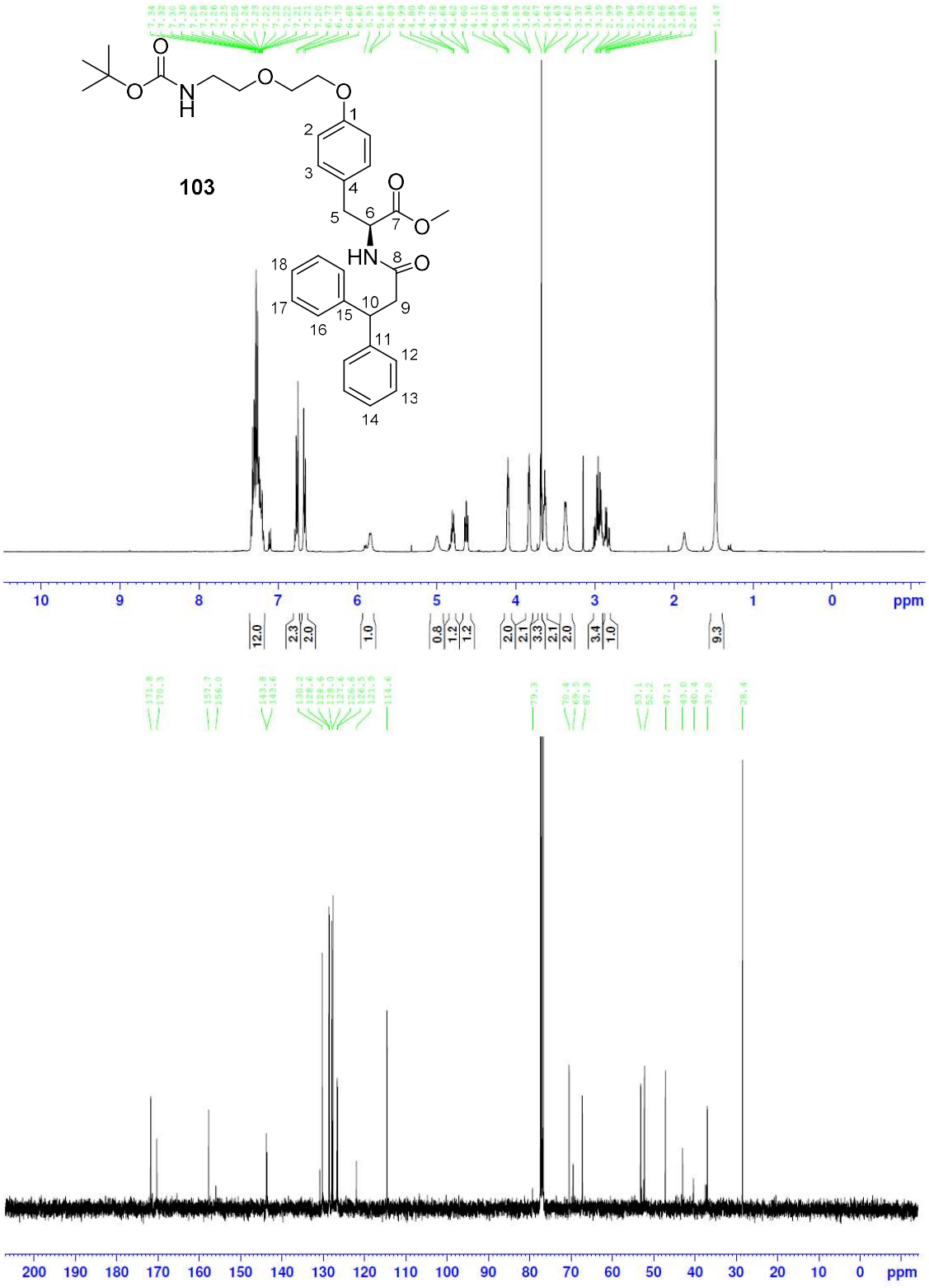
103
10 9 8 7 6 5 4 3 2 1 0 ppm
200 190 180 170 160 150 140 130 120 110 100 90 80 70 60 50 40 30 20 10 0 ppm

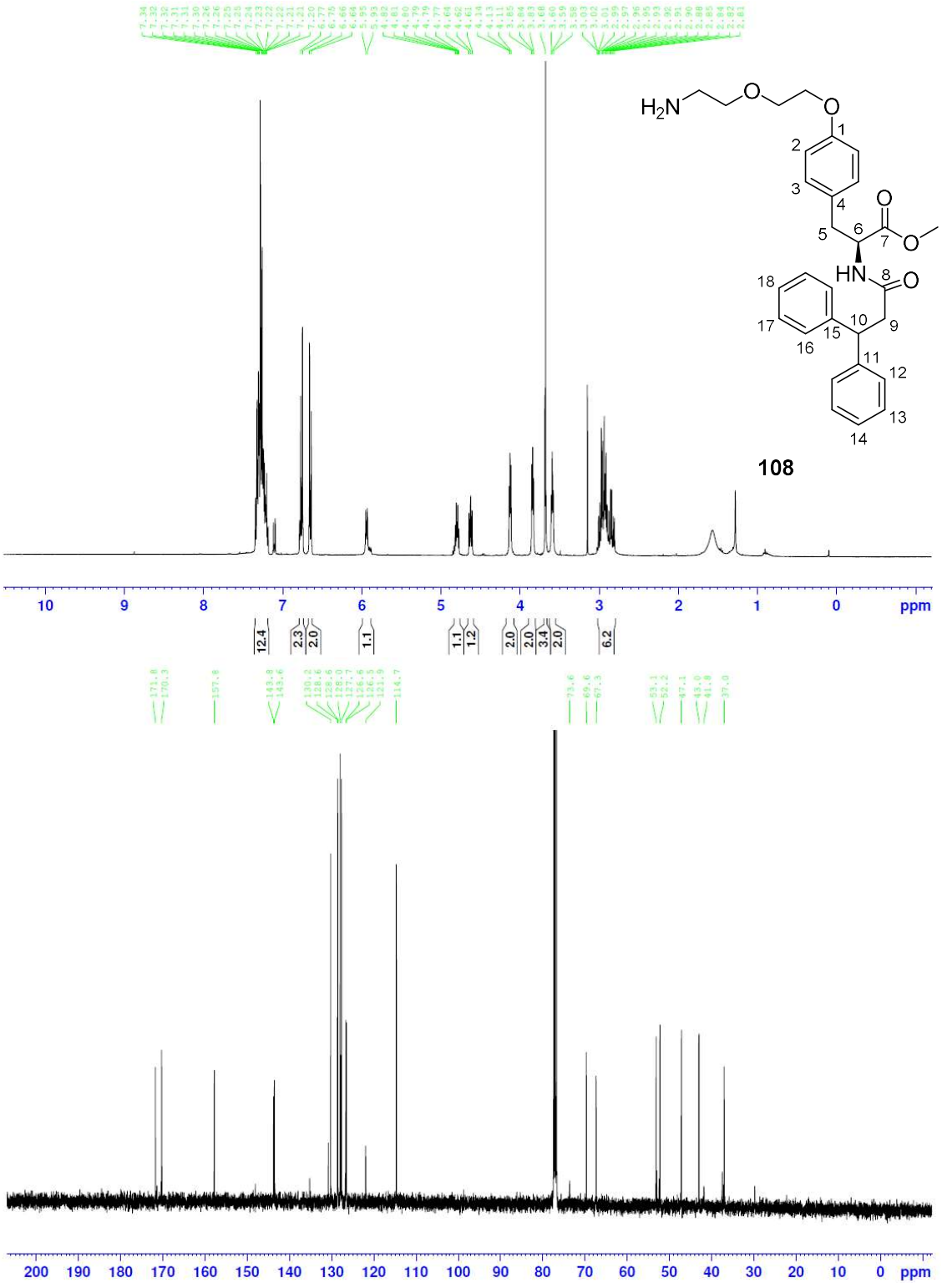
108

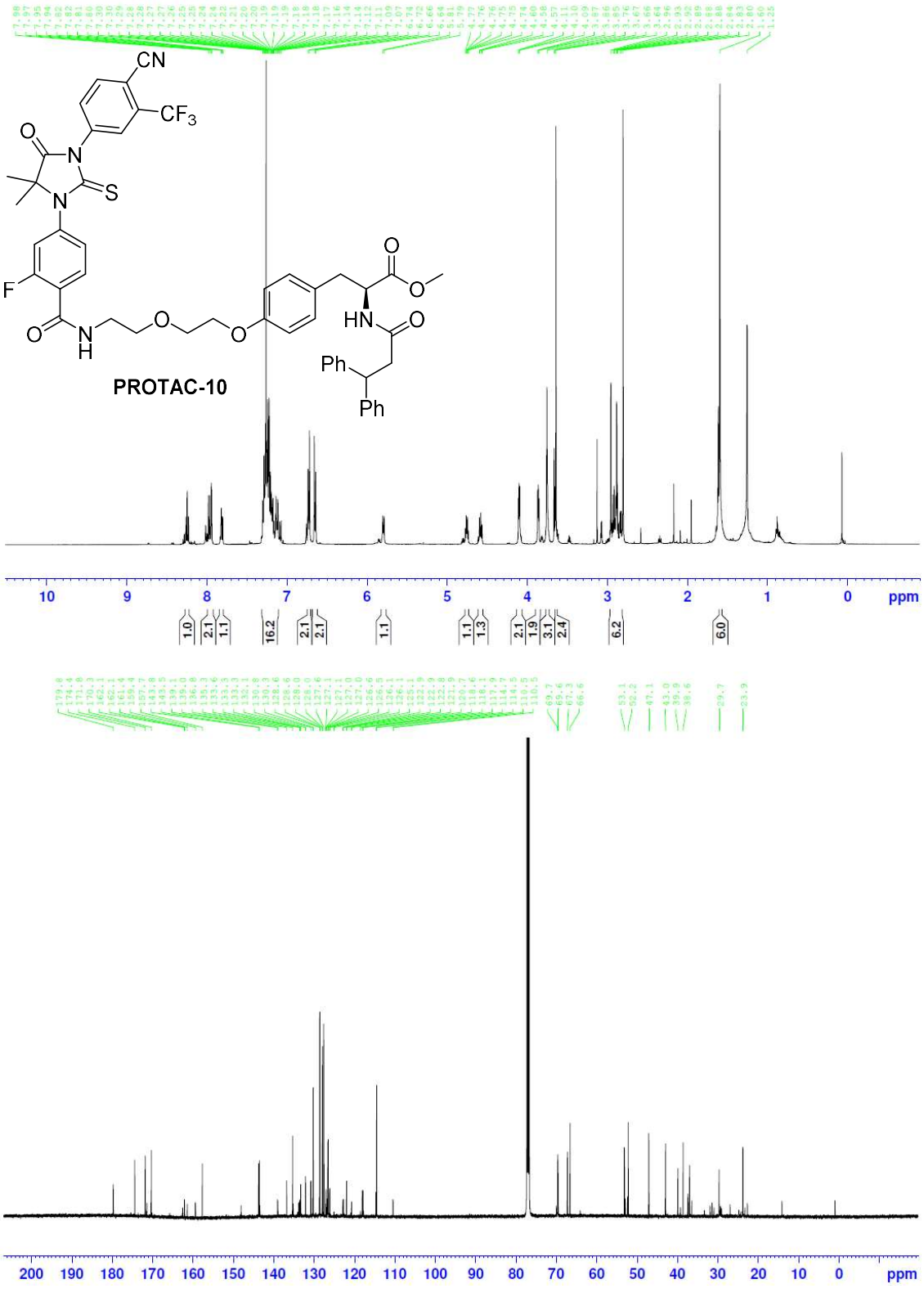
CN
CF3
O
N
S
N
F
O
N
H
O
O
O
HN
O
Ph
Ph
PROTAC-10
10
9
8
7
6
5
4
3
2
1
0
ppm
1.0
2.1
1.1
16.2
2.1
2.1
1.1
1.1
1.3
2.1
1.9
3.1
2.4
6.2
6.0
200
190
180
170
160
150
140
130
120
110
100
90
80
70
60
50
40
30
20
10
0
ppm

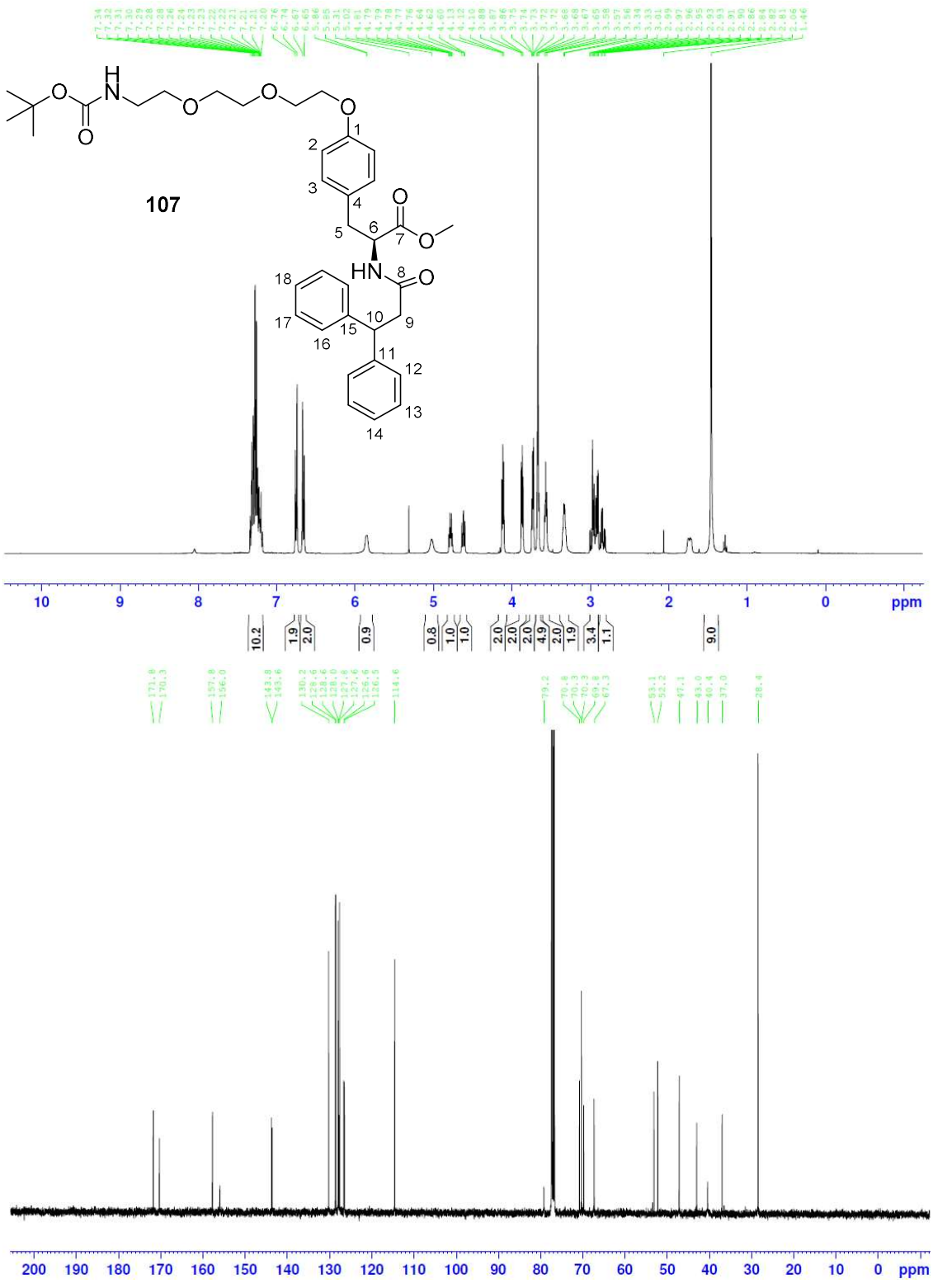
107
10 9 8 7 6 5 4 3 2 1 0 ppm
200 190 180 170 160 150 140 130 120 110 100 90 80 70 60 50 40 30 20 10 0 ppm

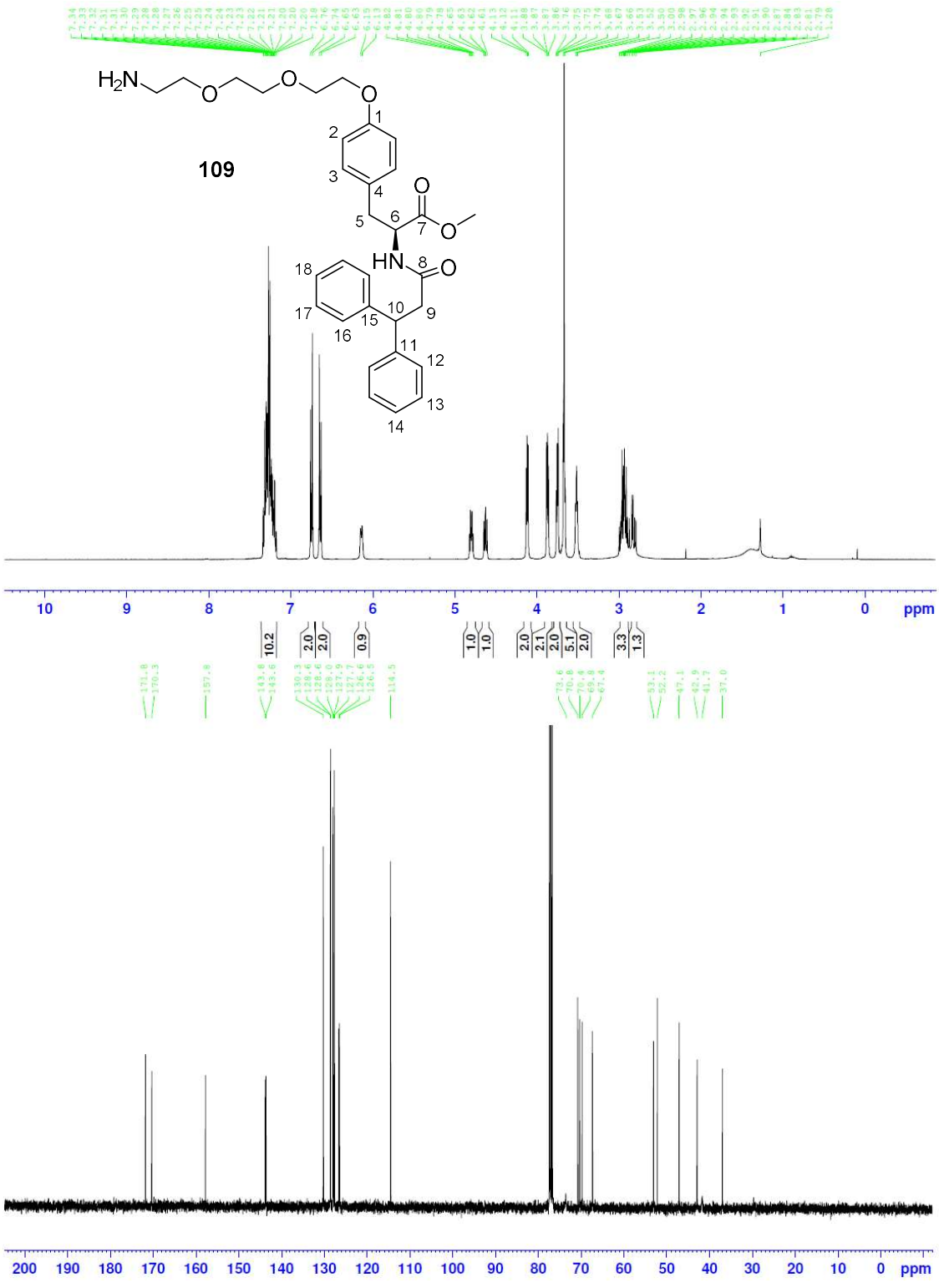
109
10 9 8 7 6 5 4 3 2 1 0 ppm
200 190 180 170 160 150 140 130 120 110 100 90 80 70 60 50 40 30 20 10 0 ppm

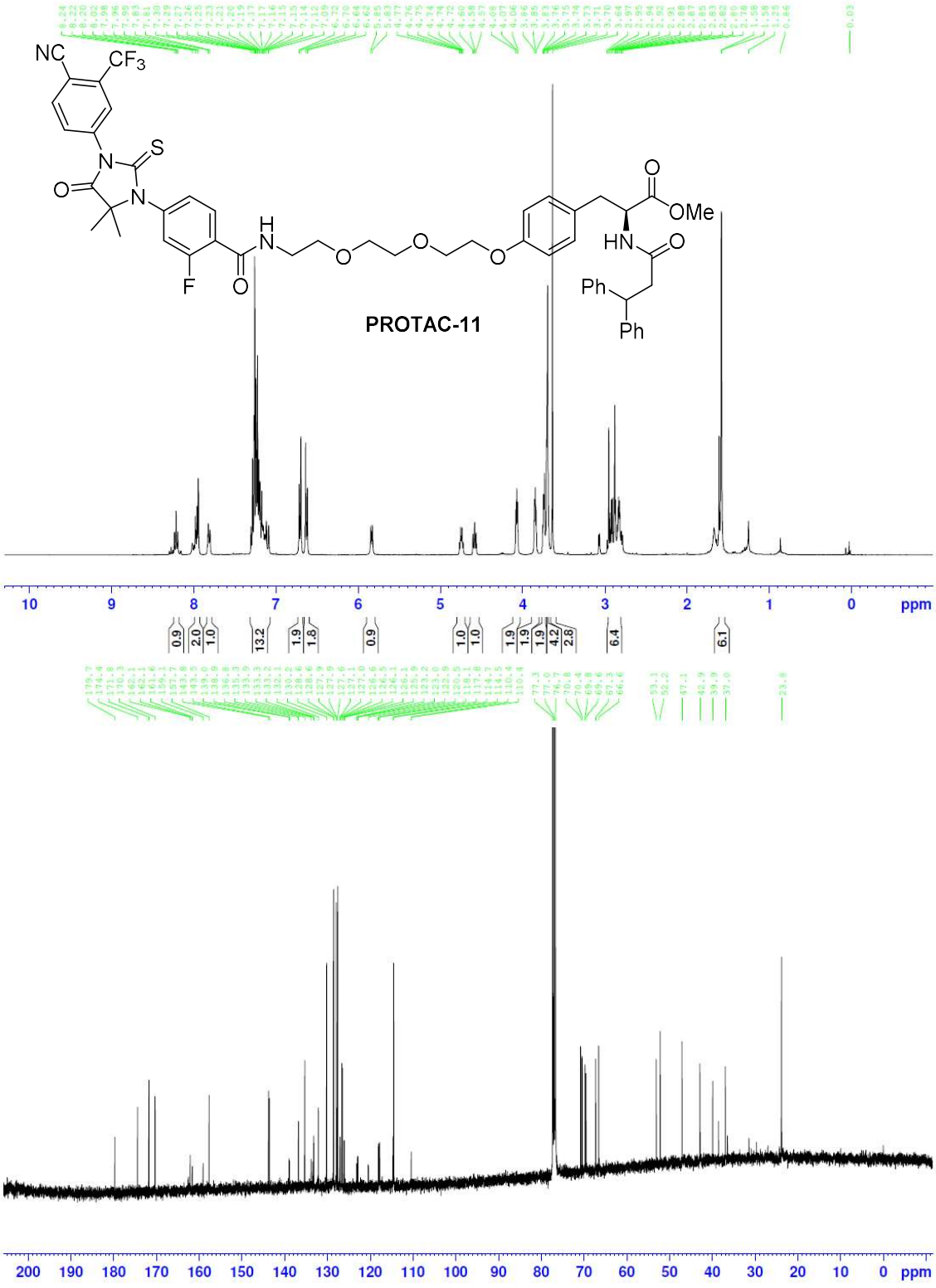
NC
CF3
S
O
N
N
H
N
O
O
O
O
O
OMe
HN
O
F
O
Ph
Ph
PROTAC-11
10 9 8 7 6 5 4 3 2 1 0 ppm
0.9 2.0 1.0 13.2 1.9 1.8 0.9 1.0 1.0 1.9 1.9 1.9 4.2 2.8 6.4 6.1
200 190 180 170 160 150 140 130 120 110 100 90 80 70 60 50 40 30 20 10 0 ppm

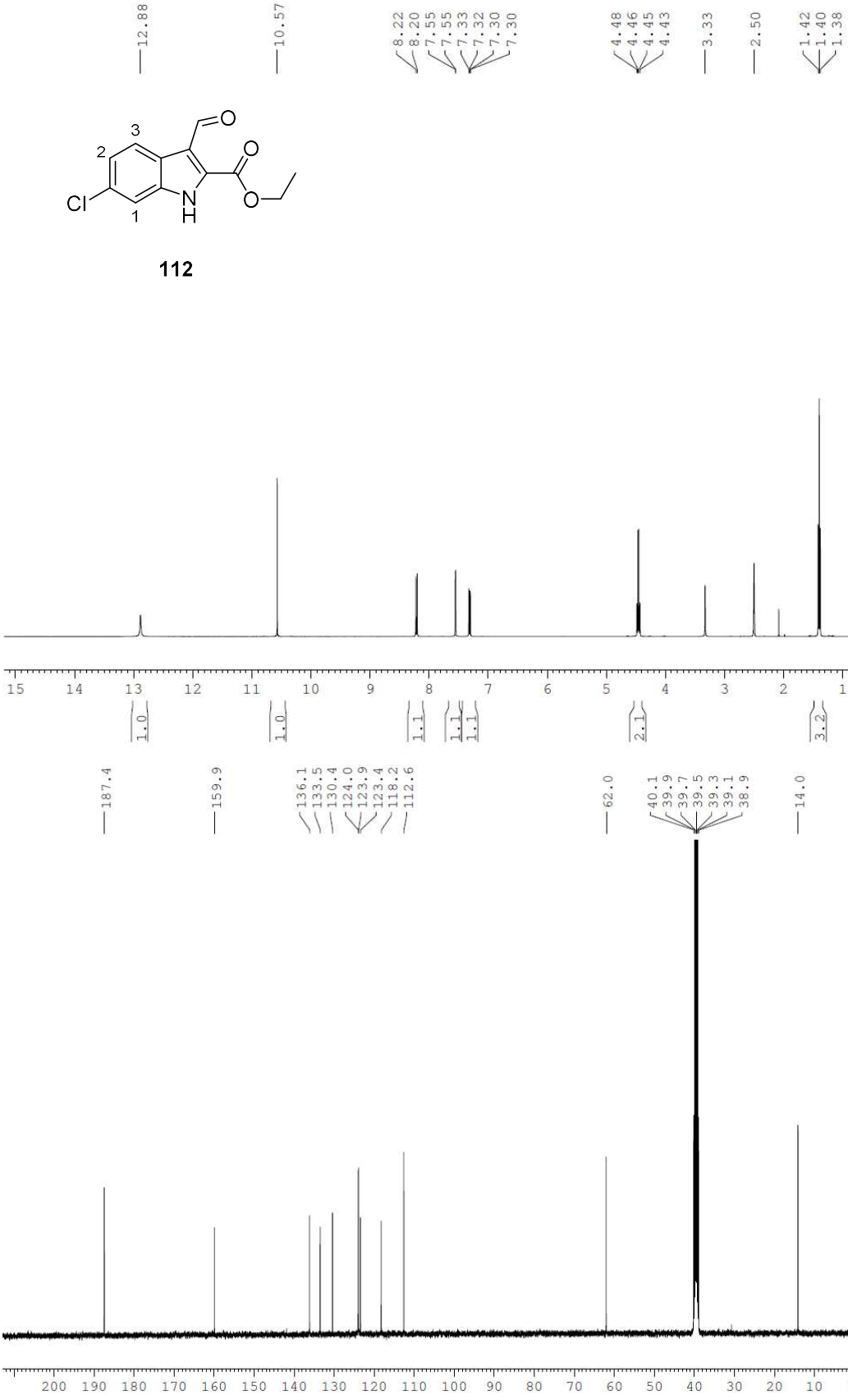
12.88
10.57
8.22
8.20
7.55
7.55
7.33
7.32
7.30
7.30
4.48
4.46
4.45
4.43
3.33
2.50
1.42
1.40
1.38
O
O
O
Cl
N
H
1
2
3
15 14 13 12 11 10 9 8 7 6 5 4 3 2 1 ppm
1.0
1.0
1.1
1.1
1.1
2.1
3.2
187.4
159.9
136.1
133.5
130.4
124.0
123.9
123.4
118.2
112.6
62.0
40.1
39.9
39.7
39.5
39.3
39.1
38.9
14.0
200 190 180 170 160 150 140 130 120 110 100 90 80 70 60 50 40 30 20 10 0 ppm

112

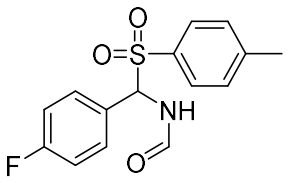
O
O=S
NH
F
O

115

8.16
7.75
7.73
7.45
7.44
7.43
7.42
7.36
7.34
7.16
7.09
7.08
6.34
6.31
2.47
9.5 9.0 8.5 8.0 7.5 7.0 6.5 6.0 5.5 5.0 4.5 4.0 3.5 3.0 2.5 2.0 1.5 1.0 ppm
1.00
1.91
2.02
2.16
2.92
1.06
2.92
164.96
162.44
159.64
145.82
132.81
130.86
130.78
129.95
129.36
116.15
115.93
77.34
77.02
76.70
69.81
21.77
200 190 180 170 160 150 140 130 120 110 100 90 80 70 60 50 40 30 20 10 0 ppm

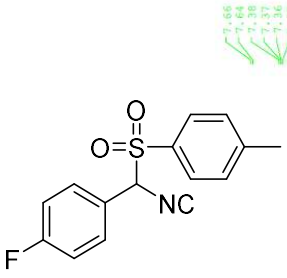

116

7.66
7.64
7.38
7.37
7.36
7.35
7.29
7.14
7.12
7.09
5.62
2.50
10
9
8
7
6
5
4
3
2
1
0 ppm
2.03
4.21
2.21
1.00
3.11

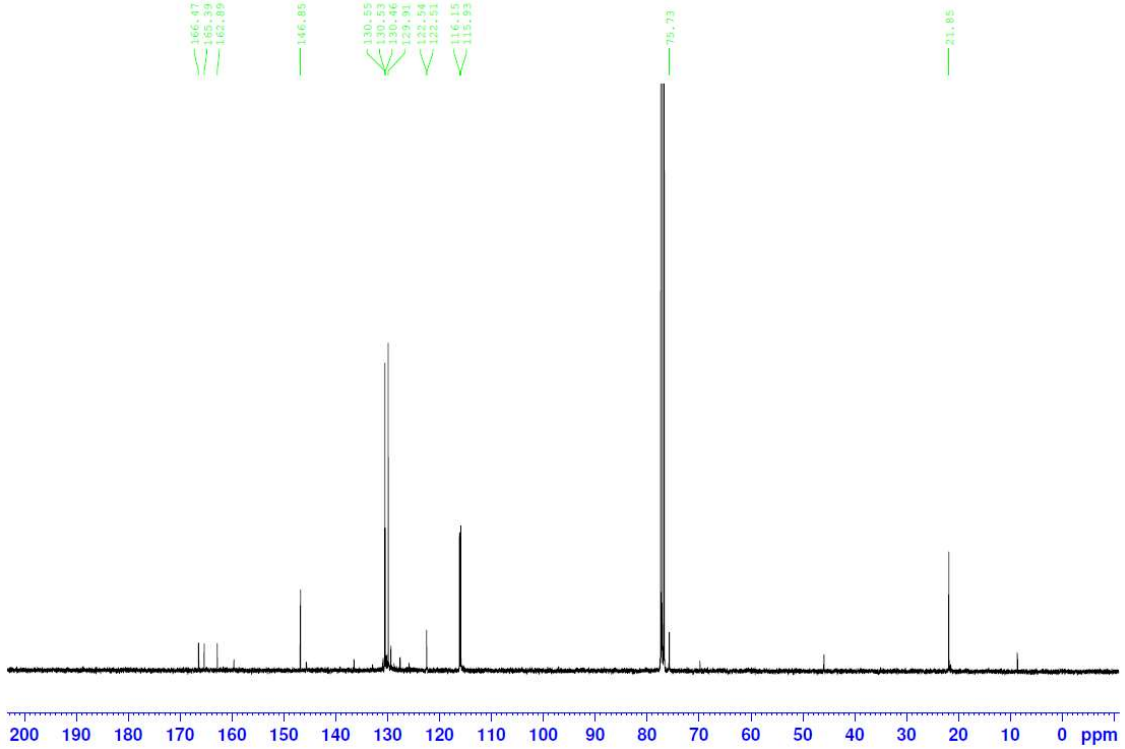
166.47
165.39
162.89
146.85
130.55
130.53
130.46
129.91
122.54
122.51
116.15
115.93
70.73
21.85
200
190
180
170
160
150
140
130
120
110
100
90
80
70
60
50
40
30
20
10
0 ppm

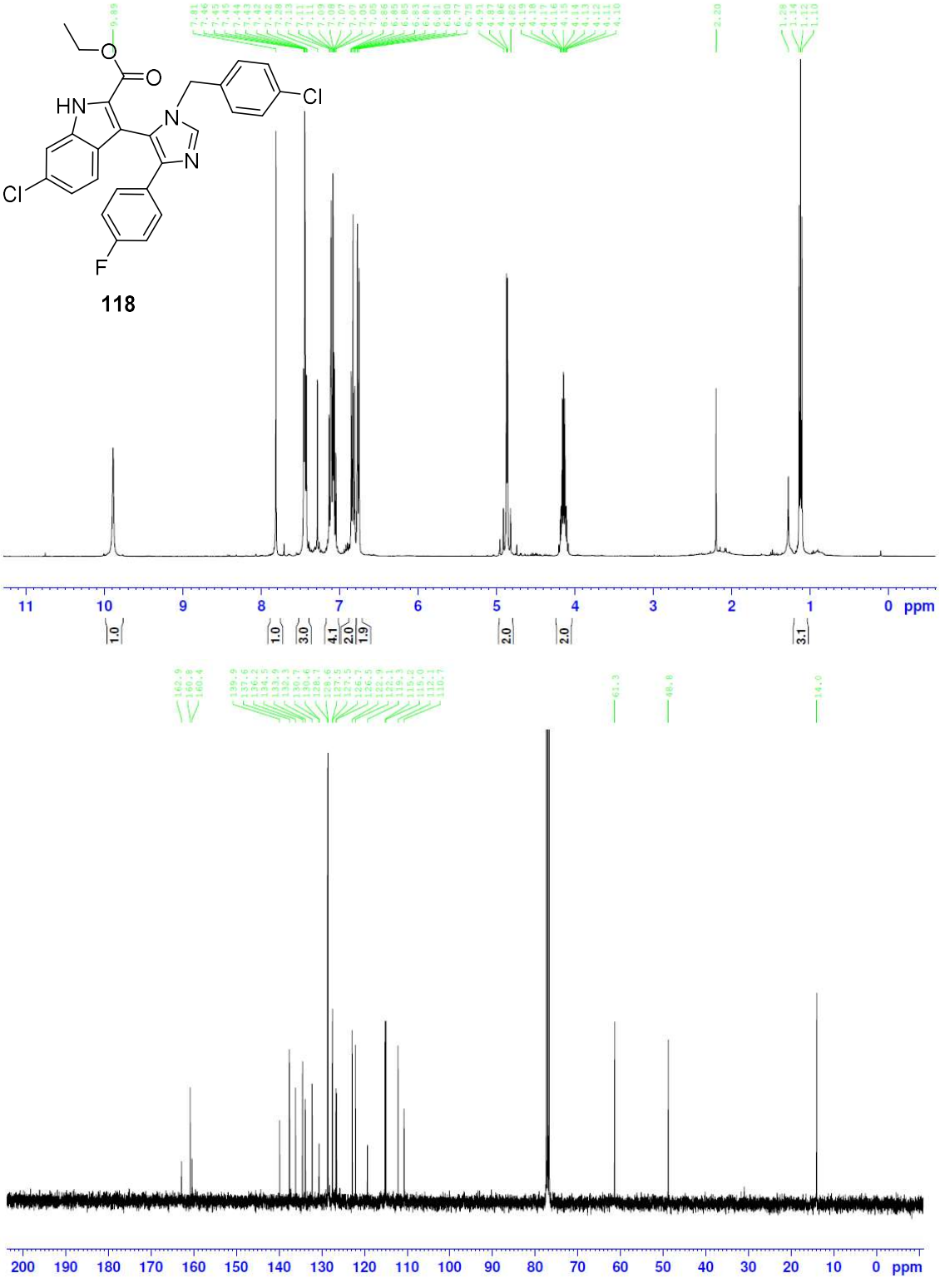
O
O
HN
N
N
Cl
Cl
F
118
11 10 9 8 7 6 5 4 3 2 1 0 ppm
200 190 180 170 160 150 140 130 120 110 100 90 80 70 60 50 40 30 20 10 0 ppm

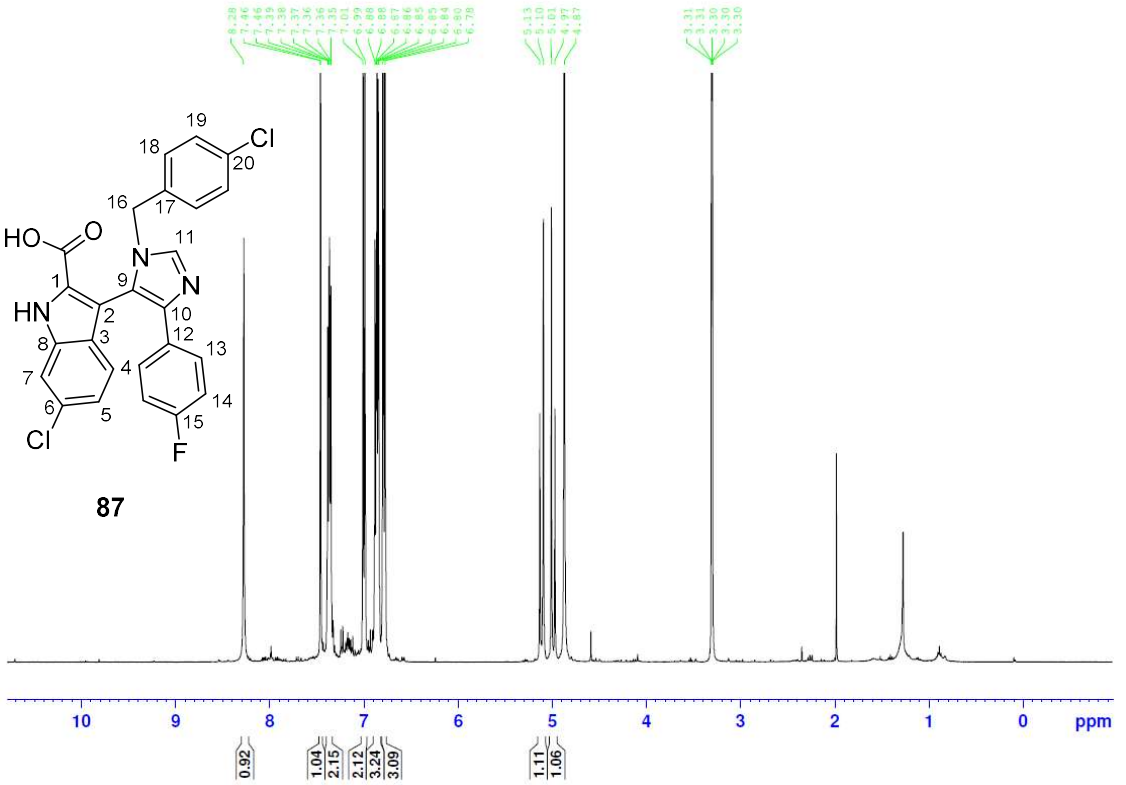
HO
O
HN
N
N
Cl
Cl
F
87
10
9
8
7
6
5
4
3
2
1
0
ppm

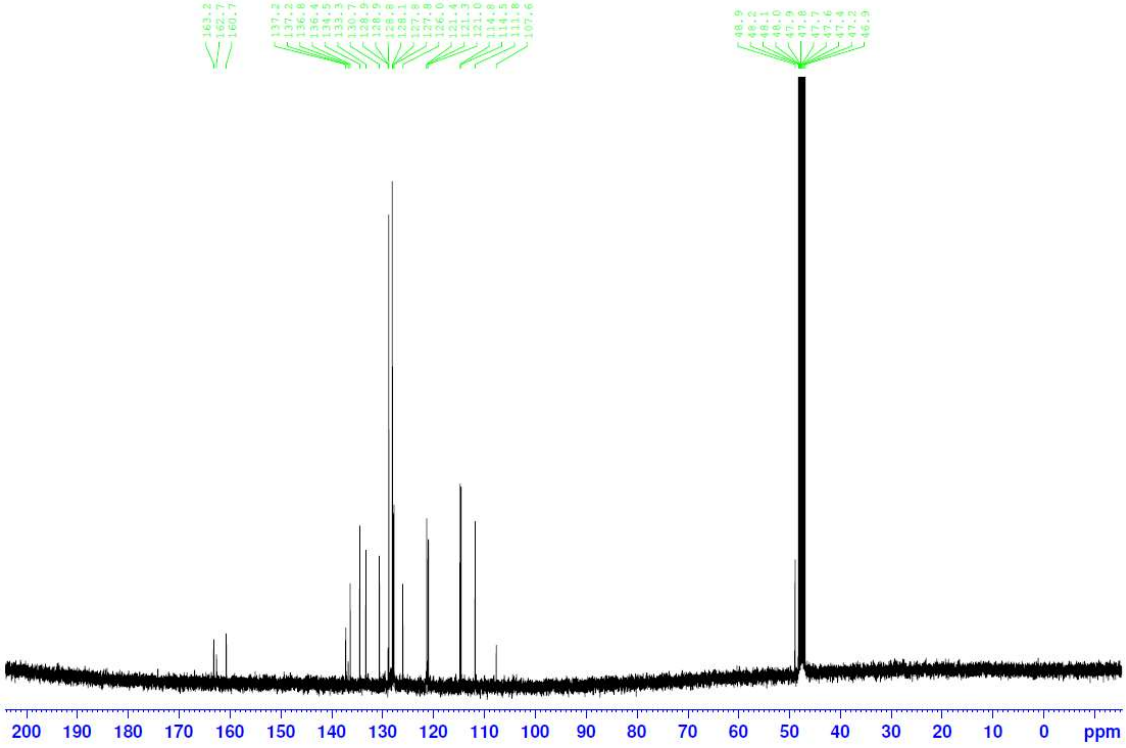
200
190
180
170
160
150
140
130
120
110
100
90
80
70
60
50
40
30
20
10
0
ppm

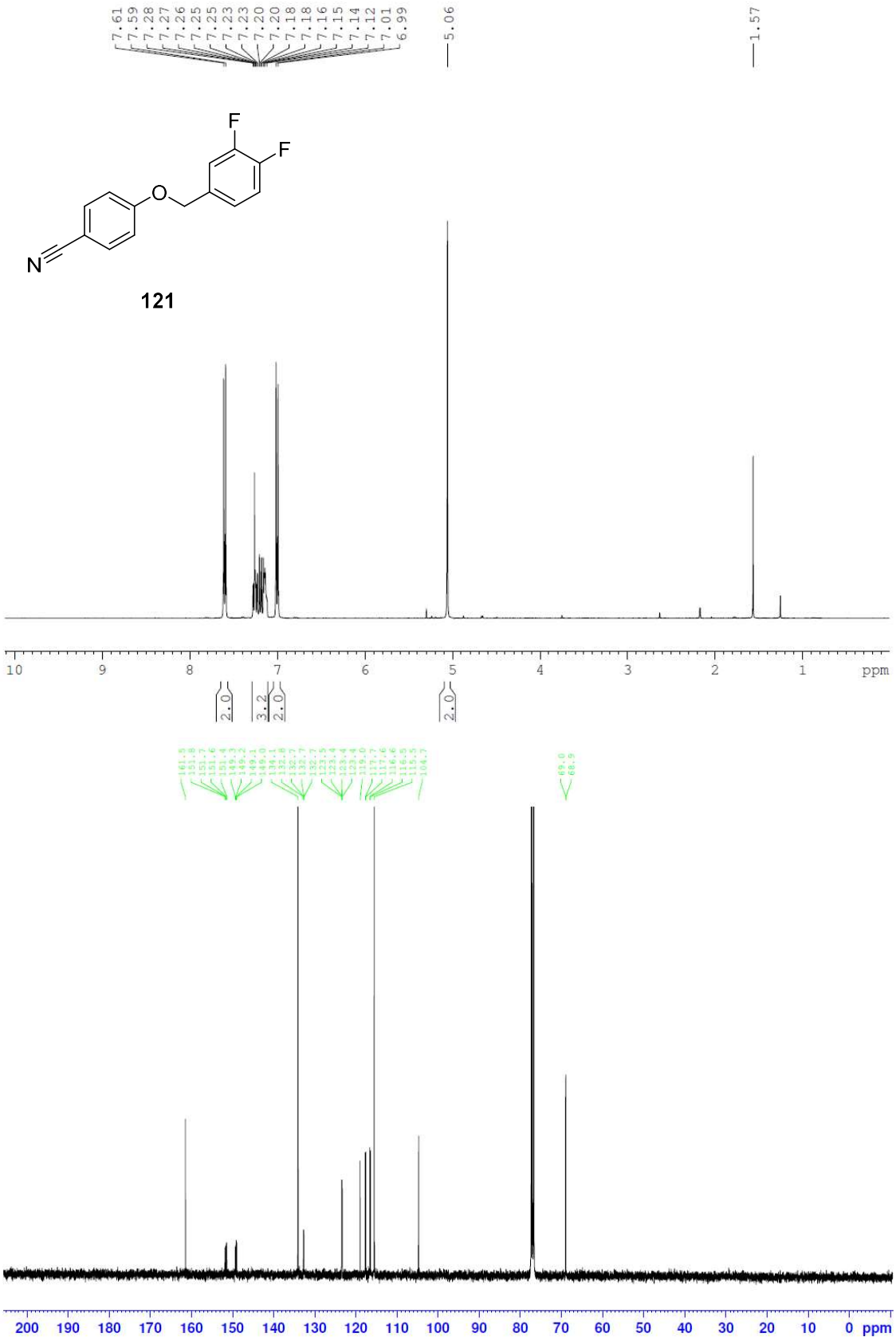
7.61
7.59
7.28
7.27
7.26
7.25
7.25
7.23
7.23
7.20
7.20
7.18
7.18
7.16
7.15
7.14
7.12
7.01
6.99
5.06
1.57
F
F
O
N
121
10
9
8
7
6
5
4
3
2
1
ppm
2.0
3.2
2.0
2.0
161.5
151.8
151.7
151.6
151.4
149.2
149.1
149.0
134.1
132.8
132.7
132.7
132.7
123.5
123.4
123.4
123.4
119.0
117.7
117.6
116.6
116.5
115.5
104.7
69.0
68.9
200
190
180
170
160
150
140
130
120
110
100
90
80
70
60
50
40
30
20
10
0
ppm

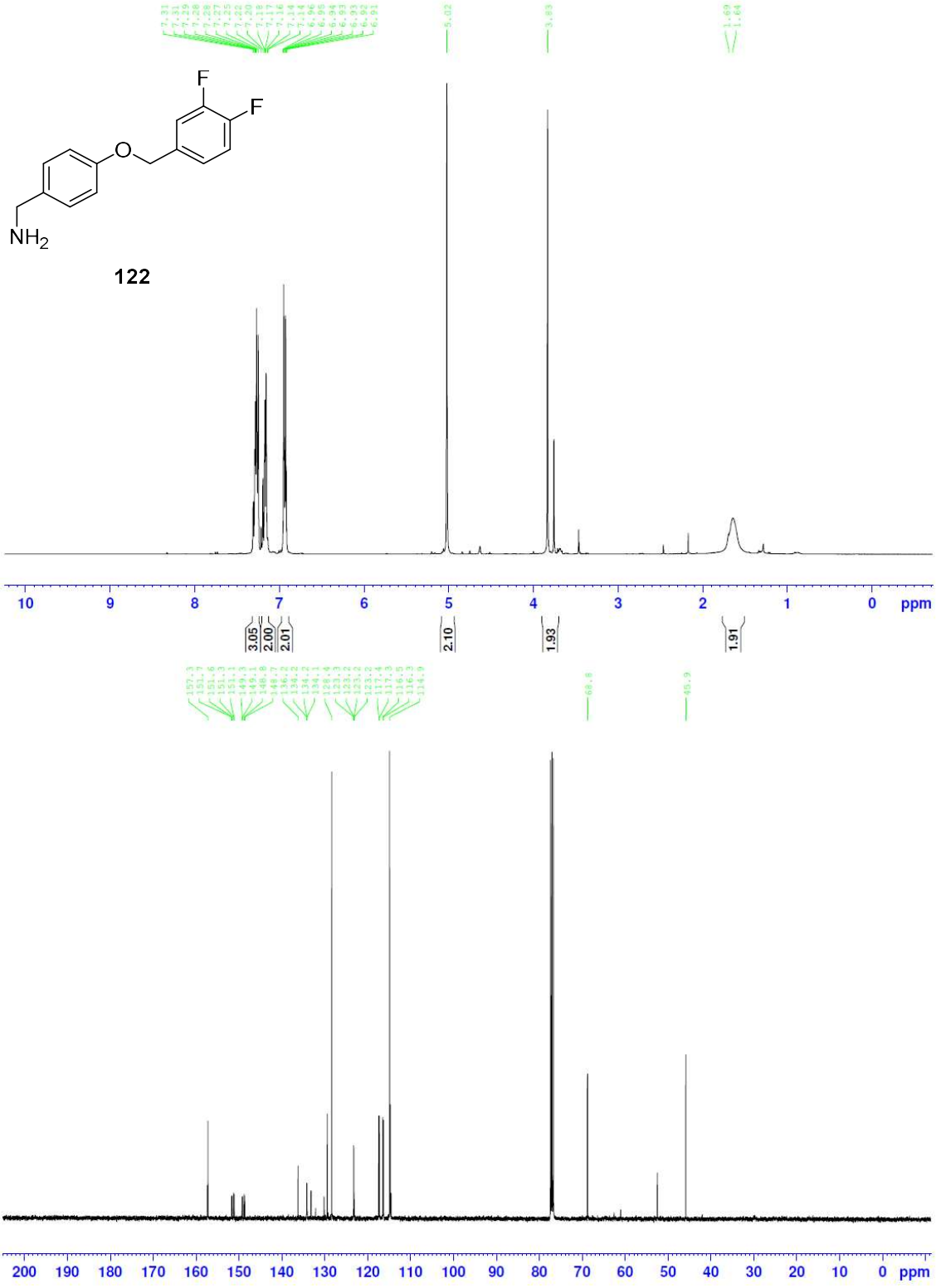
F
F
O
NH2
122
ppm
3.05
2.00
2.01
2.10
1.93
1.91
ppm

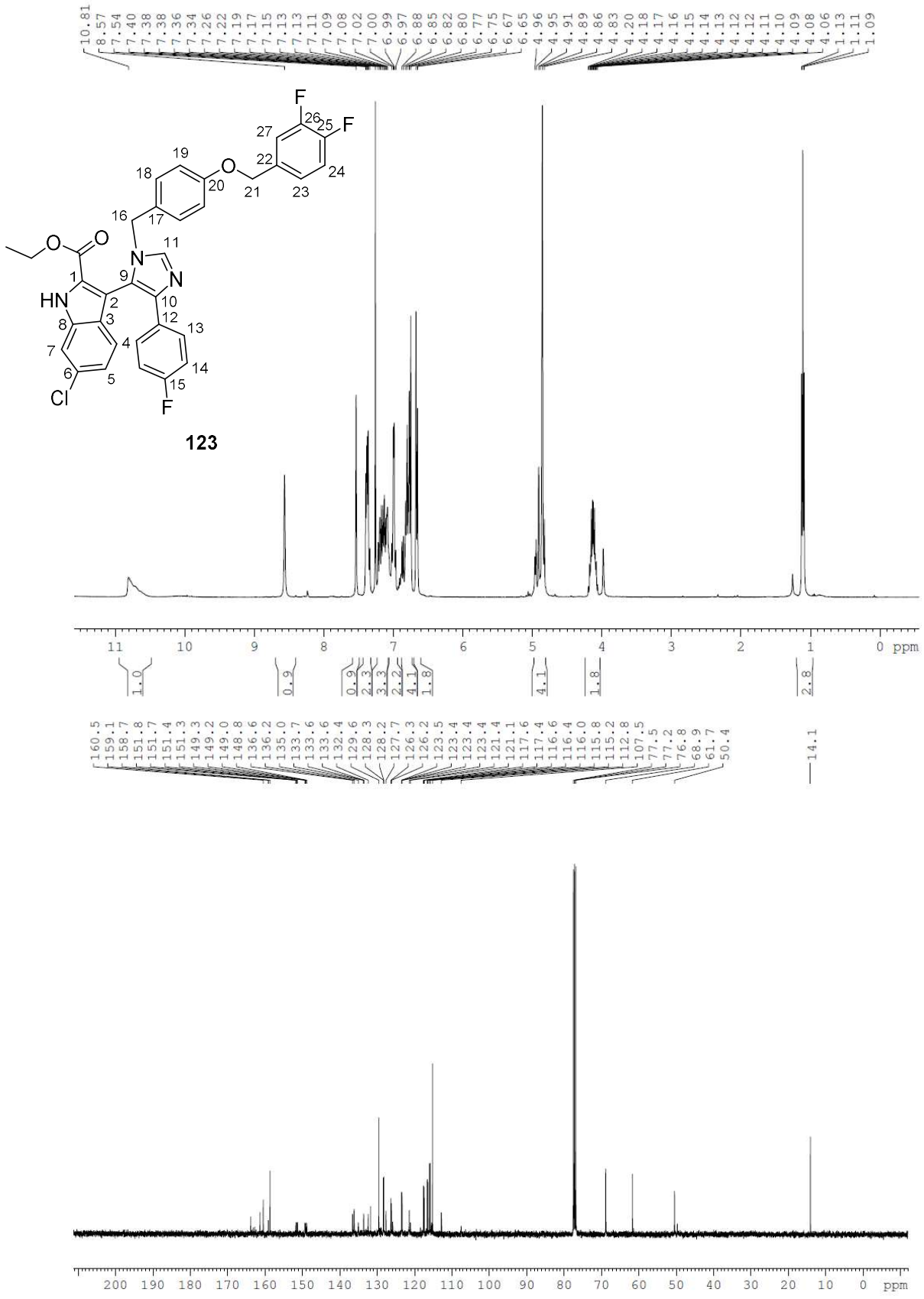
10.81
8.57
7.54
7.40
7.38
7.38
7.36
7.34
7.26
7.22
7.19
7.17
7.15
7.13
7.13
7.11
7.09
7.08
7.02
7.00
6.99
6.97
6.88
6.85
6.82
6.80
6.77
6.75
6.67
6.65
4.96
4.95
4.91
4.89
4.86
4.83
4.20
4.18
4.17
4.16
4.15
4.14
4.13
4.12
4.12
4.11
4.10
4.09
4.08
4.06
1.13
1.11
1.09
F
26
25
F
27
19
18
O
20
22
24
21
23
16
17
11
O
O
N
9
N
1
HN
2
10
8
3
12
13
7
4
14
6
5
15
Cl
F
123
11
10
9
8
7
6
5
4
3
2
1
0 ppm
1.0
0.9
0.9
2.3
3.3
2.2
4.1
1.8
4.1
1.8
2.8
160.5
159.1
158.7
151.8
151.7
151.4
151.3
149.3
149.2
149.0
148.8
136.6
136.2
135.0
133.7
133.6
133.6
132.4
129.6
128.3
128.2
127.7
126.3
126.2
123.5
123.4
123.4
123.4
121.4
121.1
117.6
117.4
116.6
116.4
116.0
115.8
115.2
112.8
107.5
77.5
77.2
76.8
68.9
61.7
50.4
14.1
200
190
180
170
160
150
140
130
120
110
100
90
80
70
60
50
40
30
20
10
0
ppm

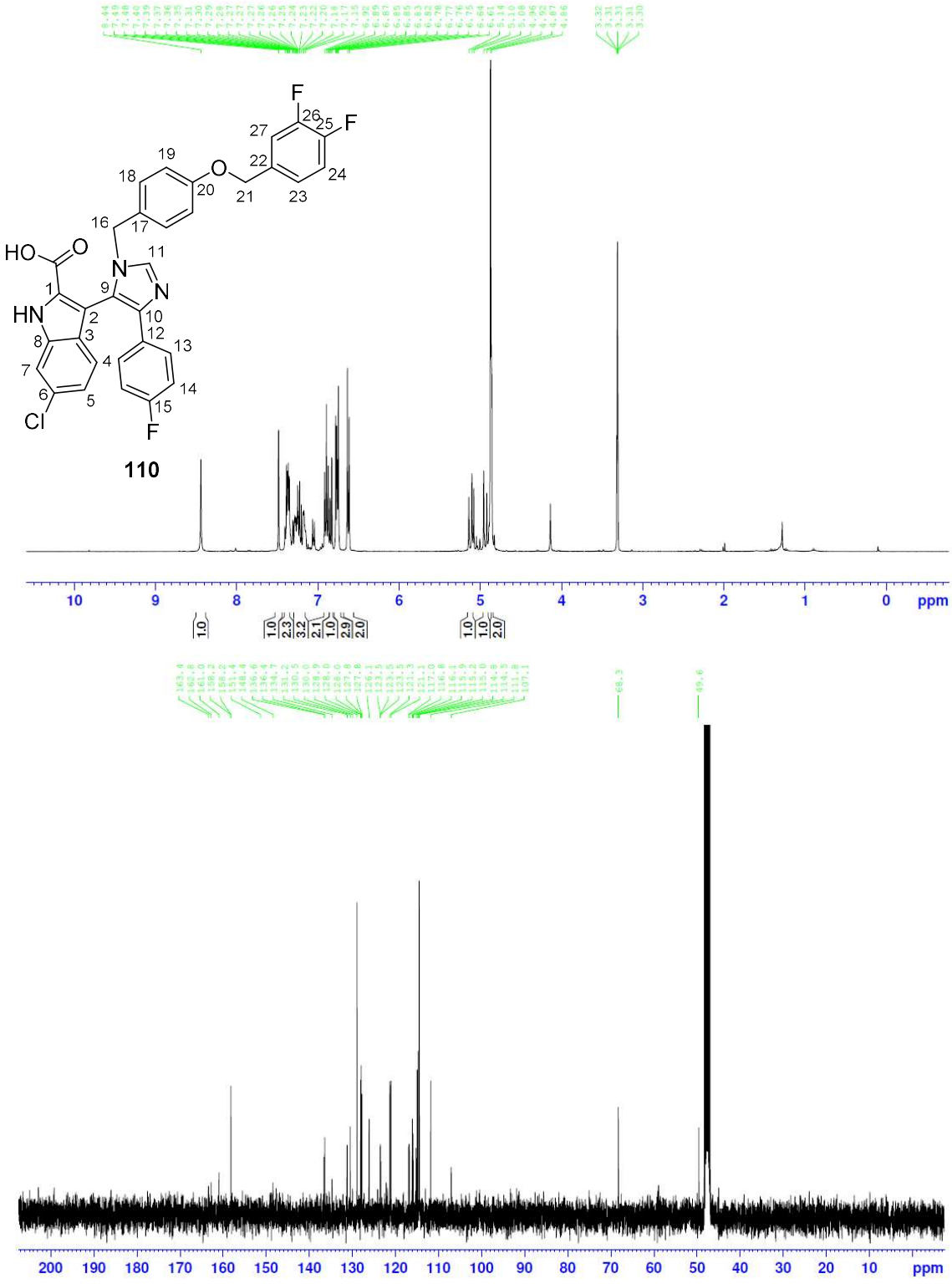
F
26
25
F
27
22
24
19
O
18
20
21
23
16
17
HO
O
11
N
1
9
N
HN
2
10
12
13
8
3
4
7
6
5
14
Cl
15
F
110
10
9
8
7
6
5
4
3
2
1
0
ppm
1.0
1.0
2.3
3.2
2.1
1.0
2.9
2.0
1.0
1.0
2.0
68.3
69.6
200
190
180
170
160
150
140
130
120
110
100
90
80
70
60
50
40
30
20
10
ppm

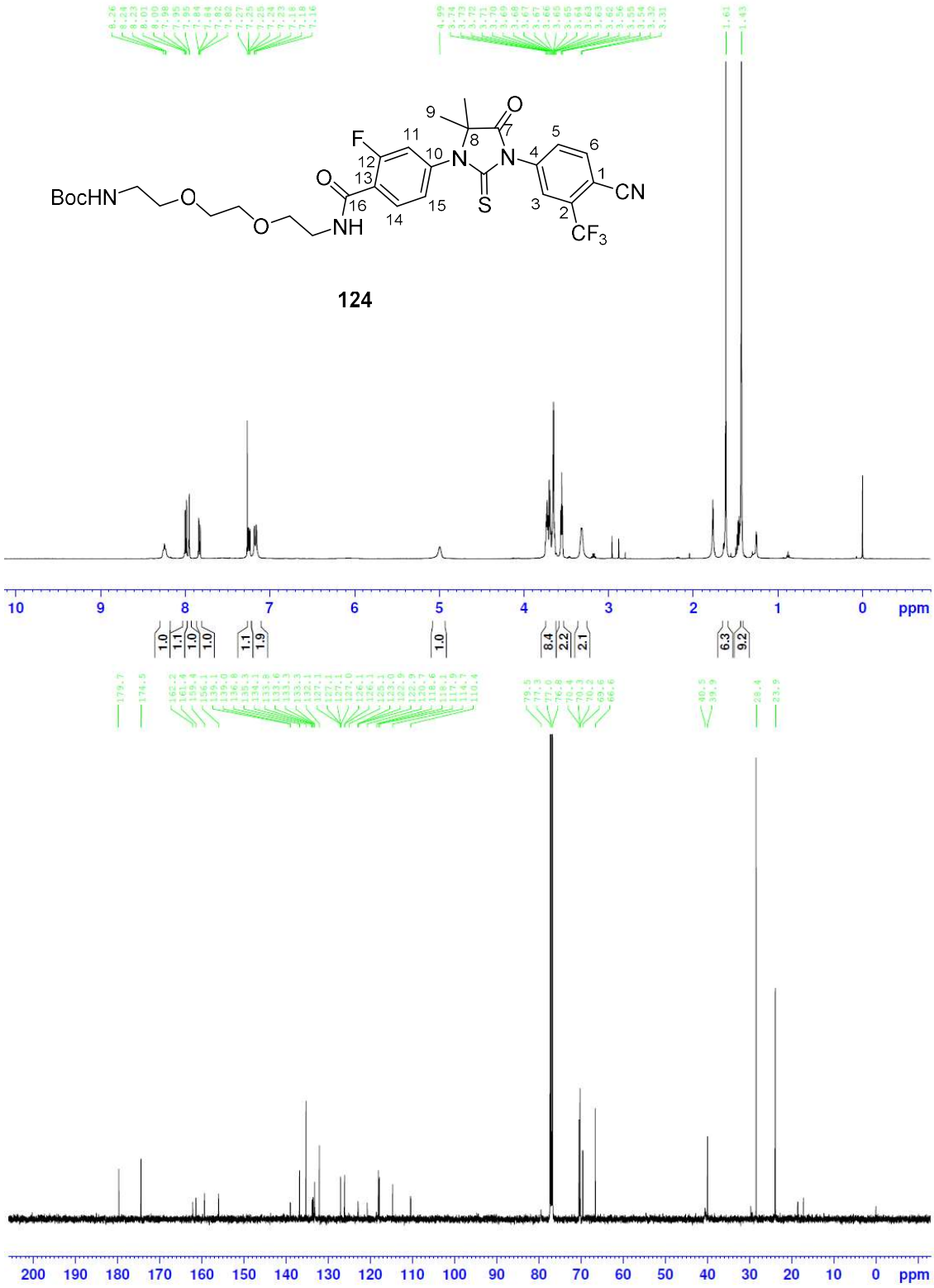

124

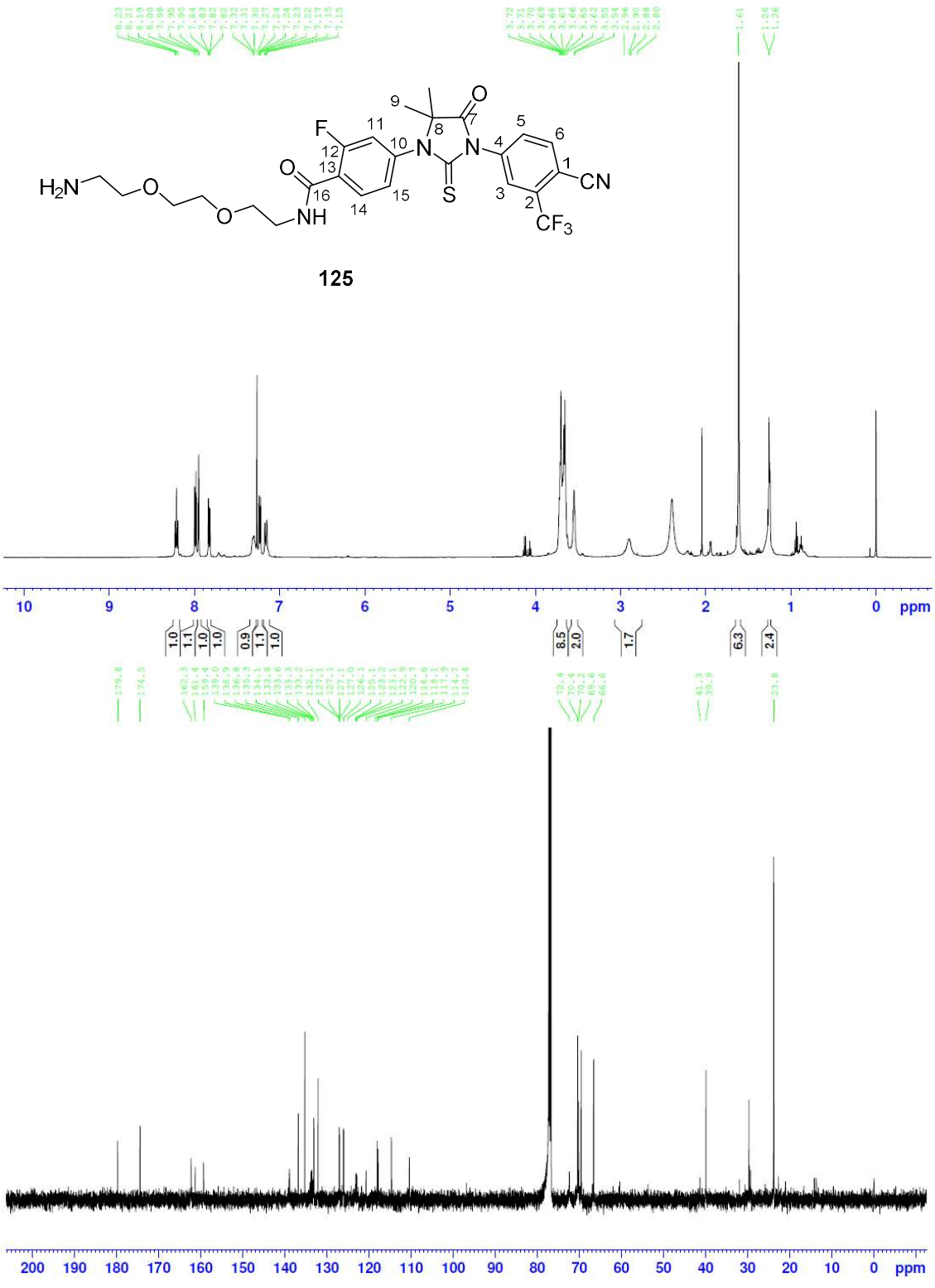
F
O
O
N
N
S
NH
O
CN
CF3
H2N
10
9
8
7
6
5
4
3
2
1
ppm
200
190
180
170
160
150
140
130
120
110
100
90
80
70
60
50
40
30
20
10
0

125

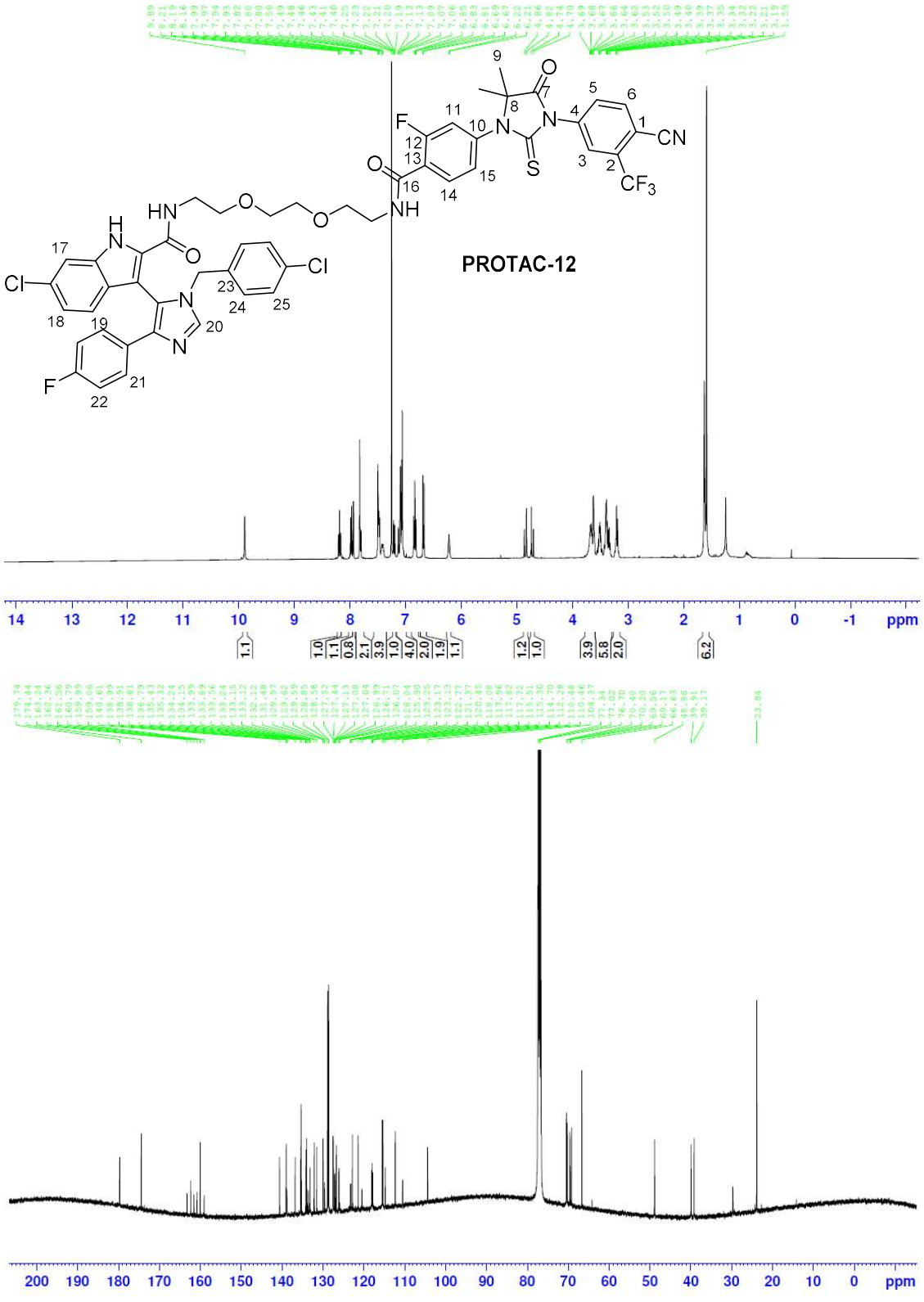
PROTAC-12
14 13 12 11 10 9 8 7 6 5 4 3 2 1 0 -1 ppm
200 190 180 170 160 150 140 130 120 110 100 90 80 70 60 50 40 30 20 10 0 ppm

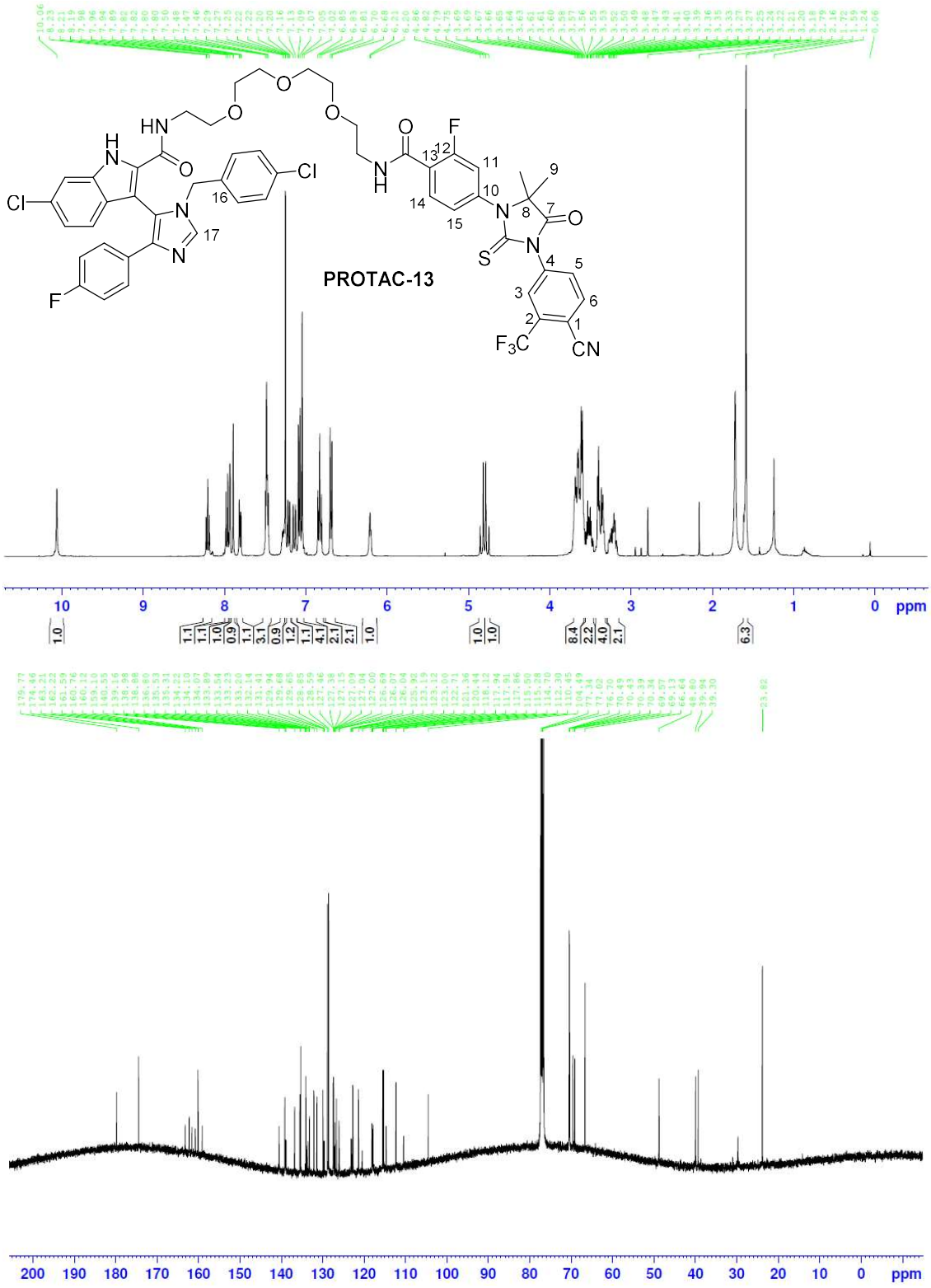
PROTAC-13
ppm
ppm

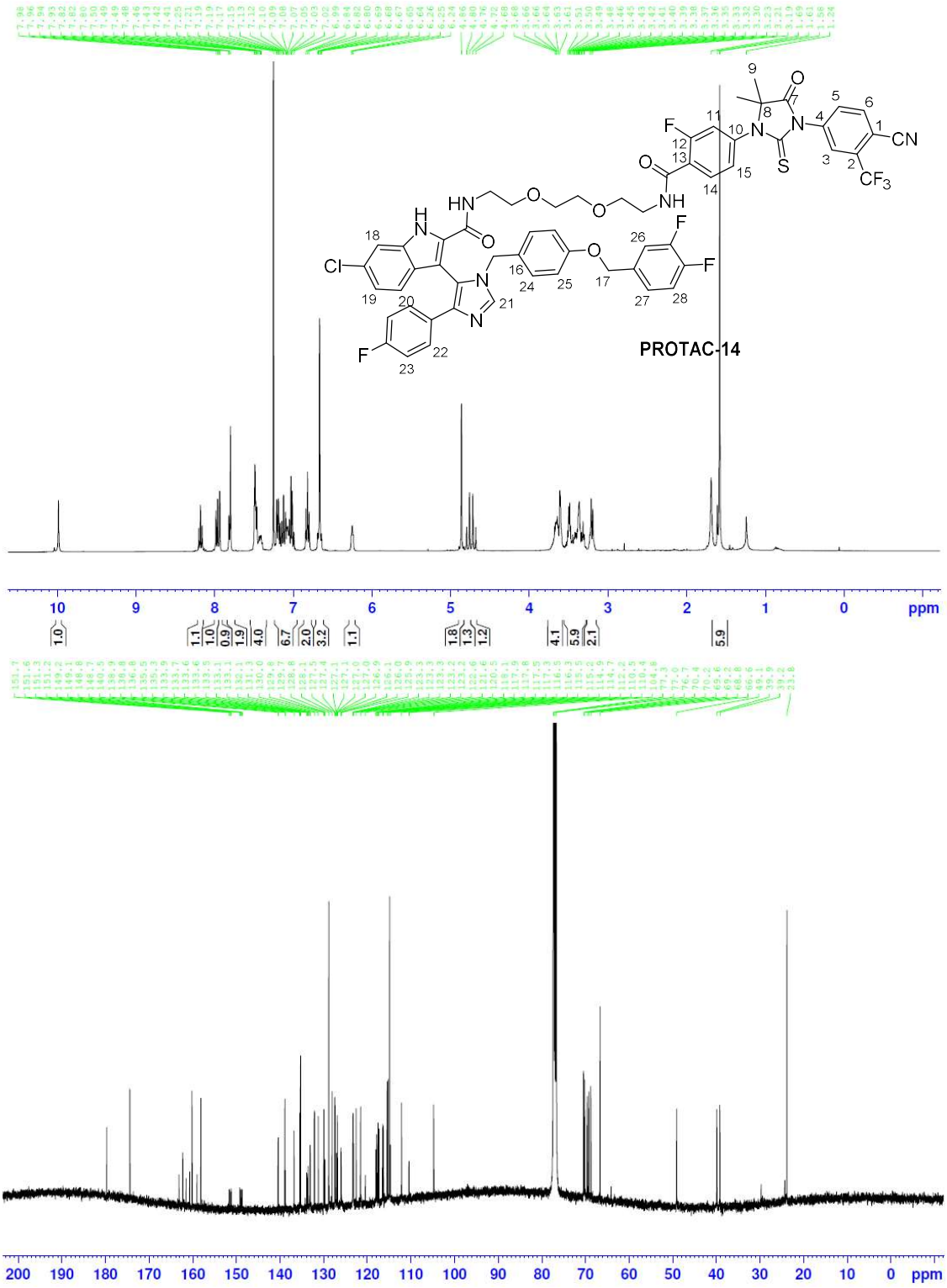
PROTAC-14
ppm
ppm

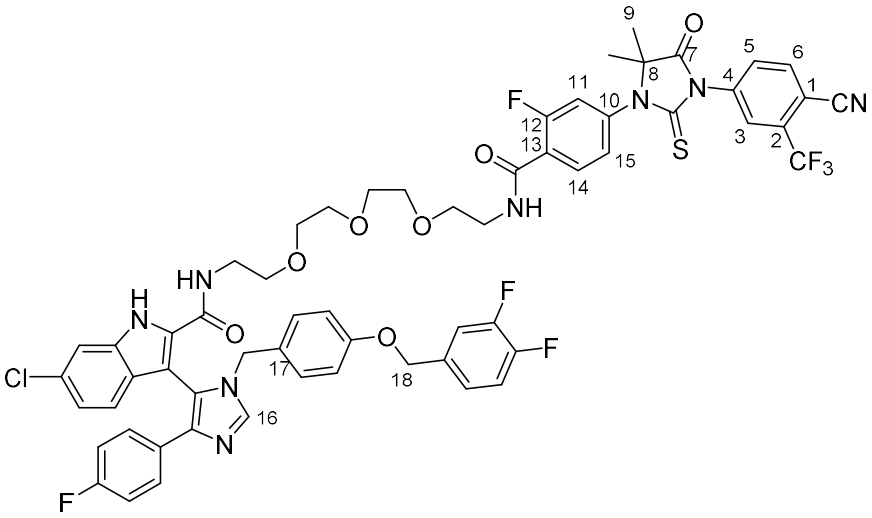
9
O
7
8
5
6
4
1
CN
11
10
N
N
3
2
CF3
F
12
13
S
O
15
14
NH
O
O
O
HN
H
N
O
F
Cl
17
18
F
N
16
N
F

PROTAC-15

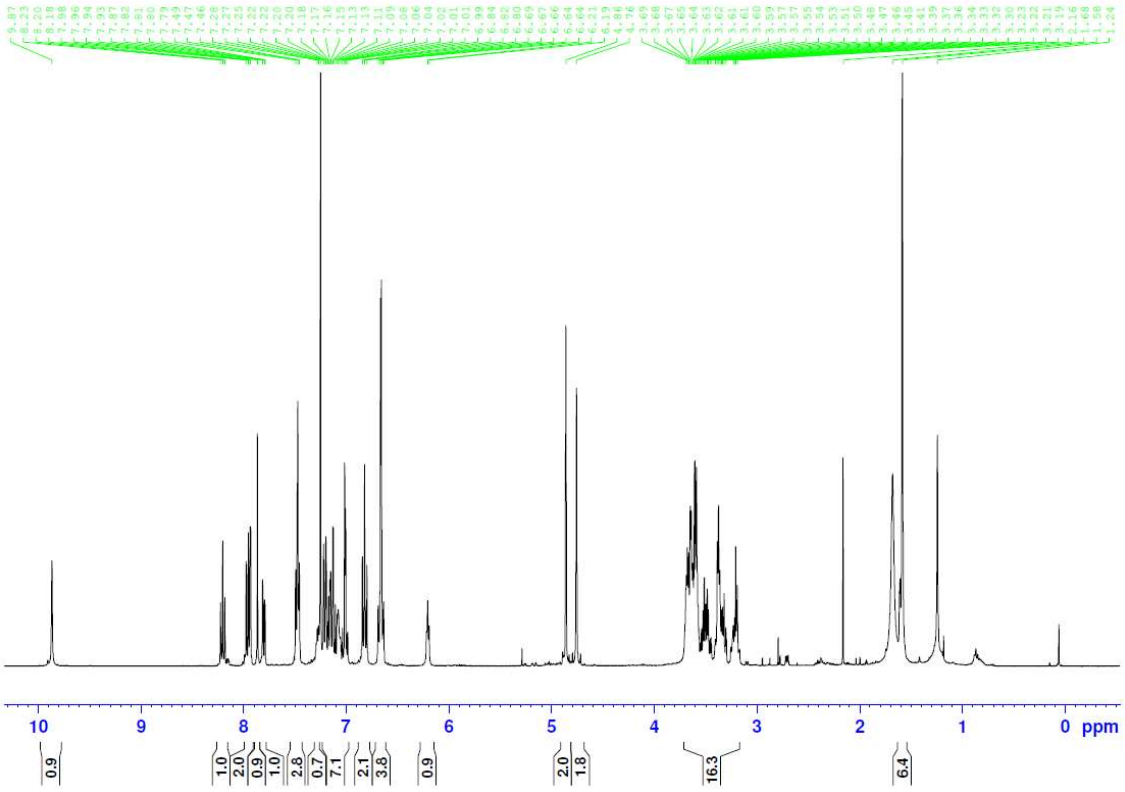
10
9
8
7
6
5
4
3
2
1
0 ppm
0.9
1.0
2.0
0.9
1.0
2.8
0.7
7.1
2.1
3.8
0.9
2.0
1.8
16.3
6.4

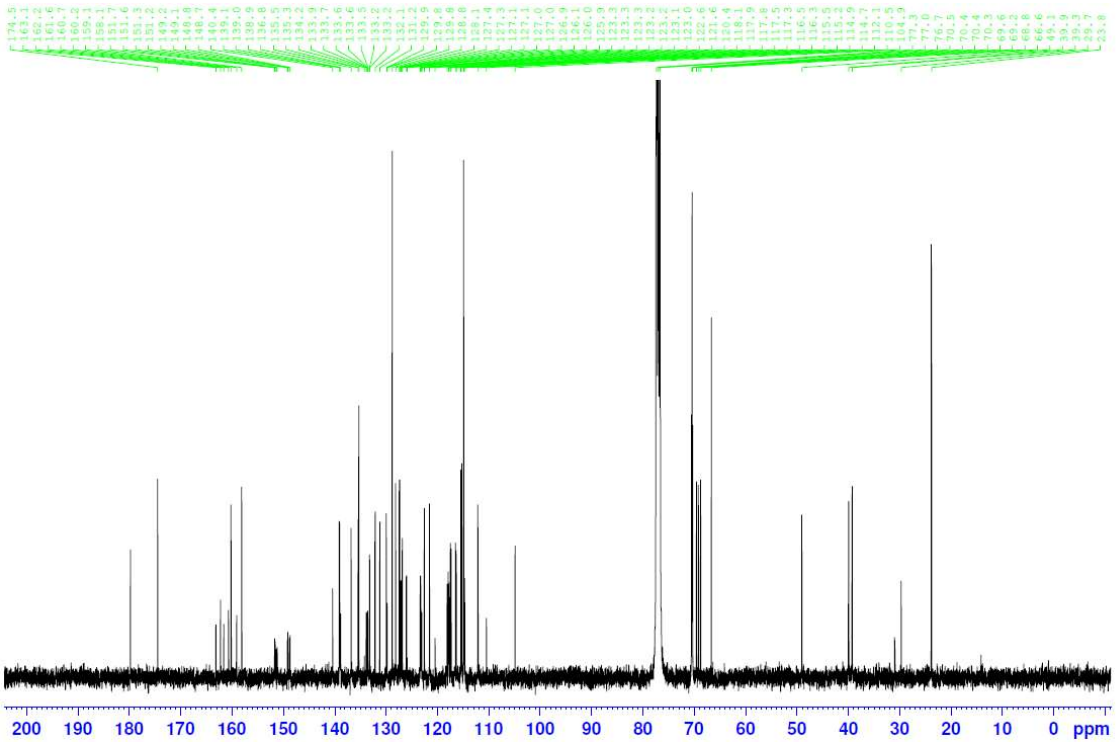
200 190 180 170 160 150 140 130 120 110 100 90 80 70 60 50 40 30 20 10 0 ppm

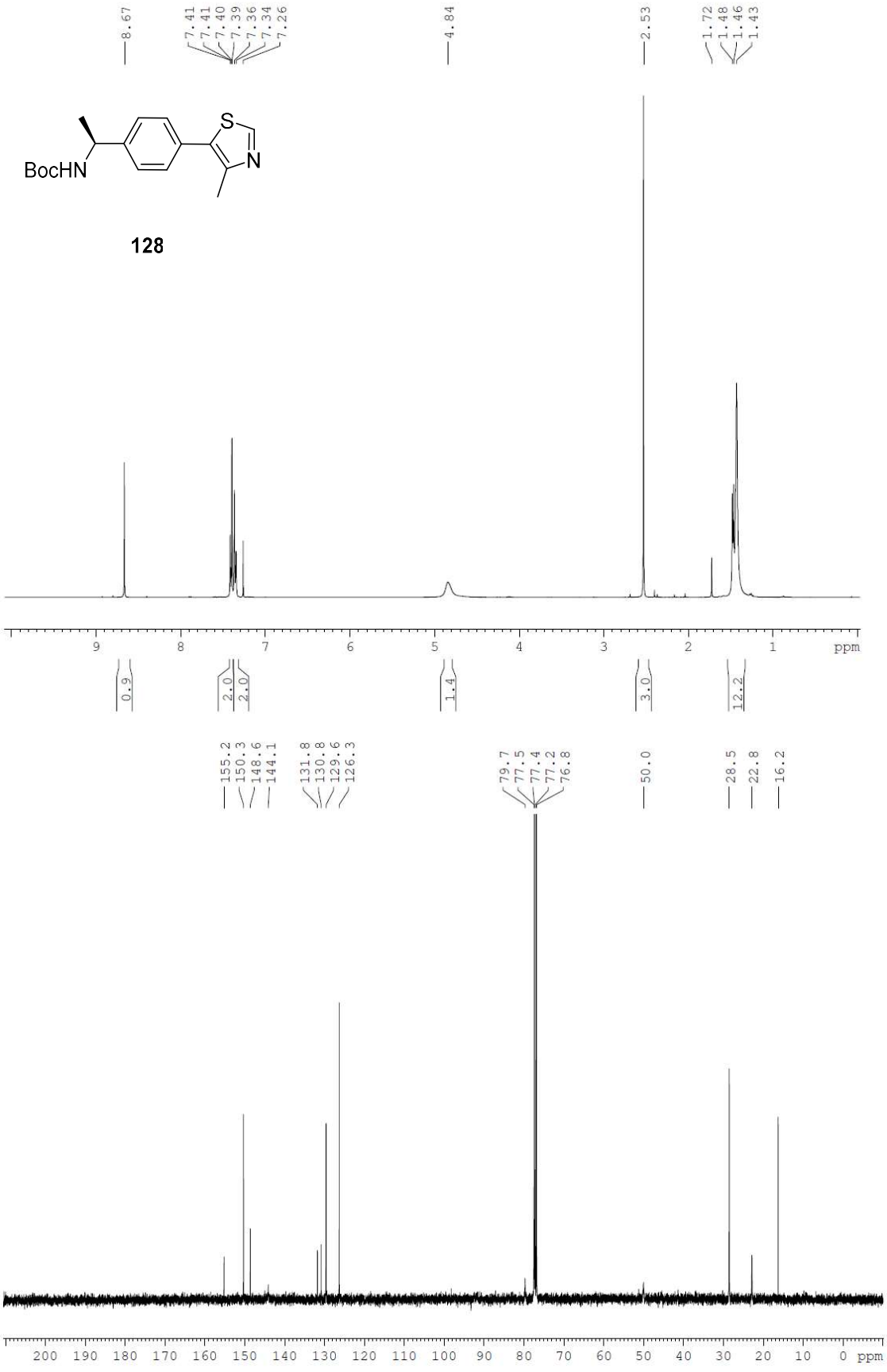
8.67
7.41
7.41
7.40
7.39
7.36
7.34
7.26
4.84
2.53
1.72
1.48
1.46
1.43
BocHN
S
N
9
8
7
6
5
4
3
2
1
ppm
0.9
2.0
2.0
1.4
3.0
12.2
155.2
150.3
148.6
144.1
131.8
130.8
129.6
126.3
79.7
77.5
77.4
77.2
76.8
50.0
28.5
22.8
16.2
200 190 180 170 160 150 140 130 120 110 100 90 80 70 60 50 40 30 20 10 0 ppm

128

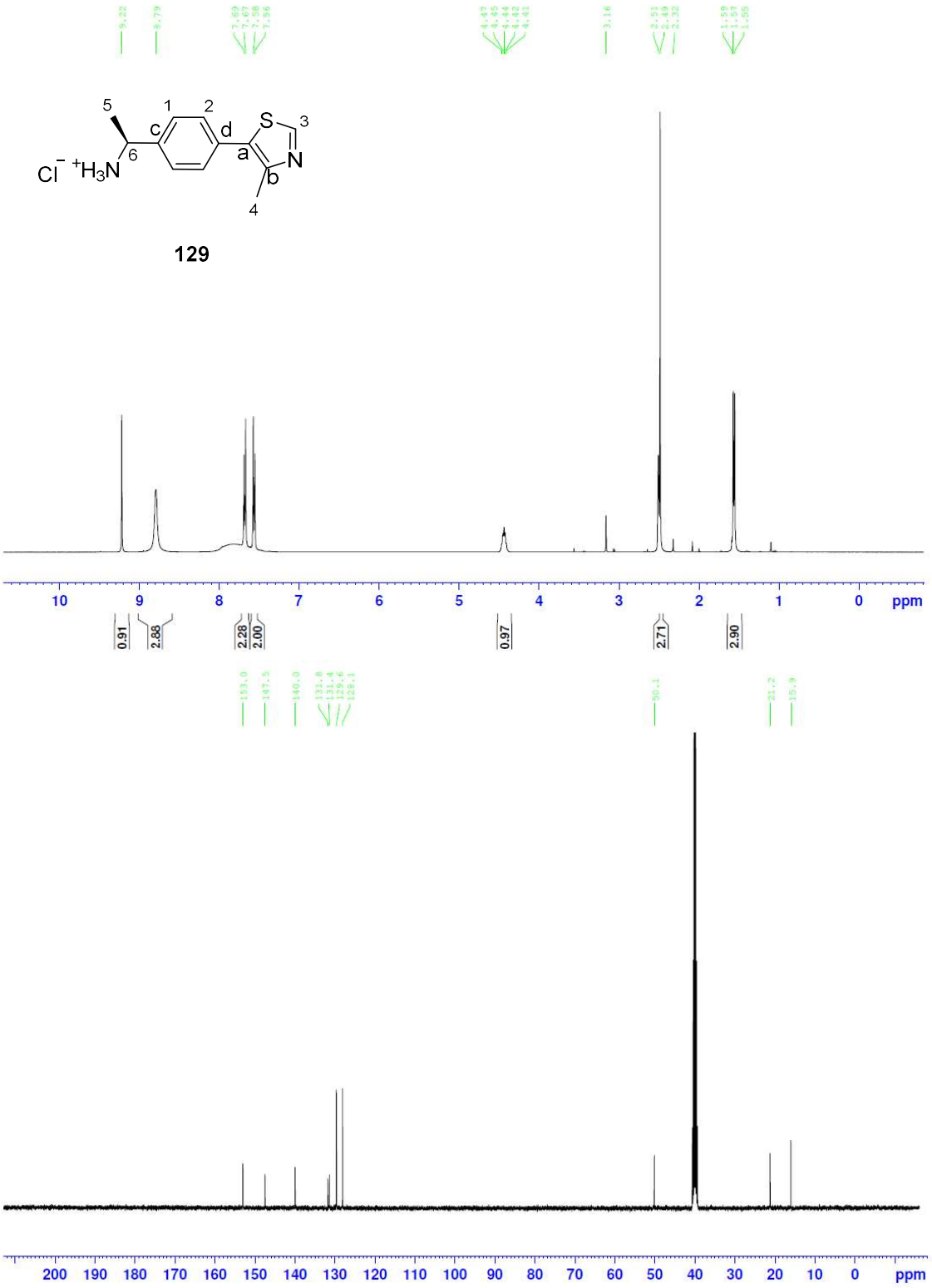
9.22
8.79
7.69
7.67
7.58
7.56
4.47
4.45
4.44
4.42
4.41
3.16
2.51
2.49
2.32
1.59
1.57
1.55
5
1
2
c
d
S
3
6
a
N
b
4
Cl⁻ ⁺H3N
10
9
8
7
6
5
4
3
2
1
0
ppm
0.91
2.88
2.28
2.00
0.97
2.71
2.90
153.0
147.5
140.0
131.8
131.4
129.6
128.1
50.1
21.2
15.9
200
190
180
170
160
150
140
130
120
110
100
90
80
70
60
50
40
30
20
10
0
ppm

129

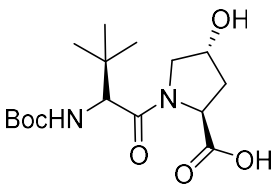
OH
BocHN
N
O
O
OH

134

6.47
6.44
4.33
4.29
4.27
4.24
4.17
4.14
3.66
3.65
3.64
3.63
3.59
3.57
3.46
2.51
2.50
2.14
2.11
2.09
1.91
1.90
1.89
1.88
1.87
1.86
1.85
1.38
0.94
10 9 8 7 6 5 4 3 2 1 0 ppm
0.87
1.09
1.19
1.00
2.07
0.89
1.19
9.14
8.82
173.72
170.43
155.78
78.59
69.25
58.66
58.15
56.48
37.74
35.83
28.64
26.66
200 190 180 170 160 150 140 130 120 110 100 90 80 70 60 50 40 30 20 10 0 ppm

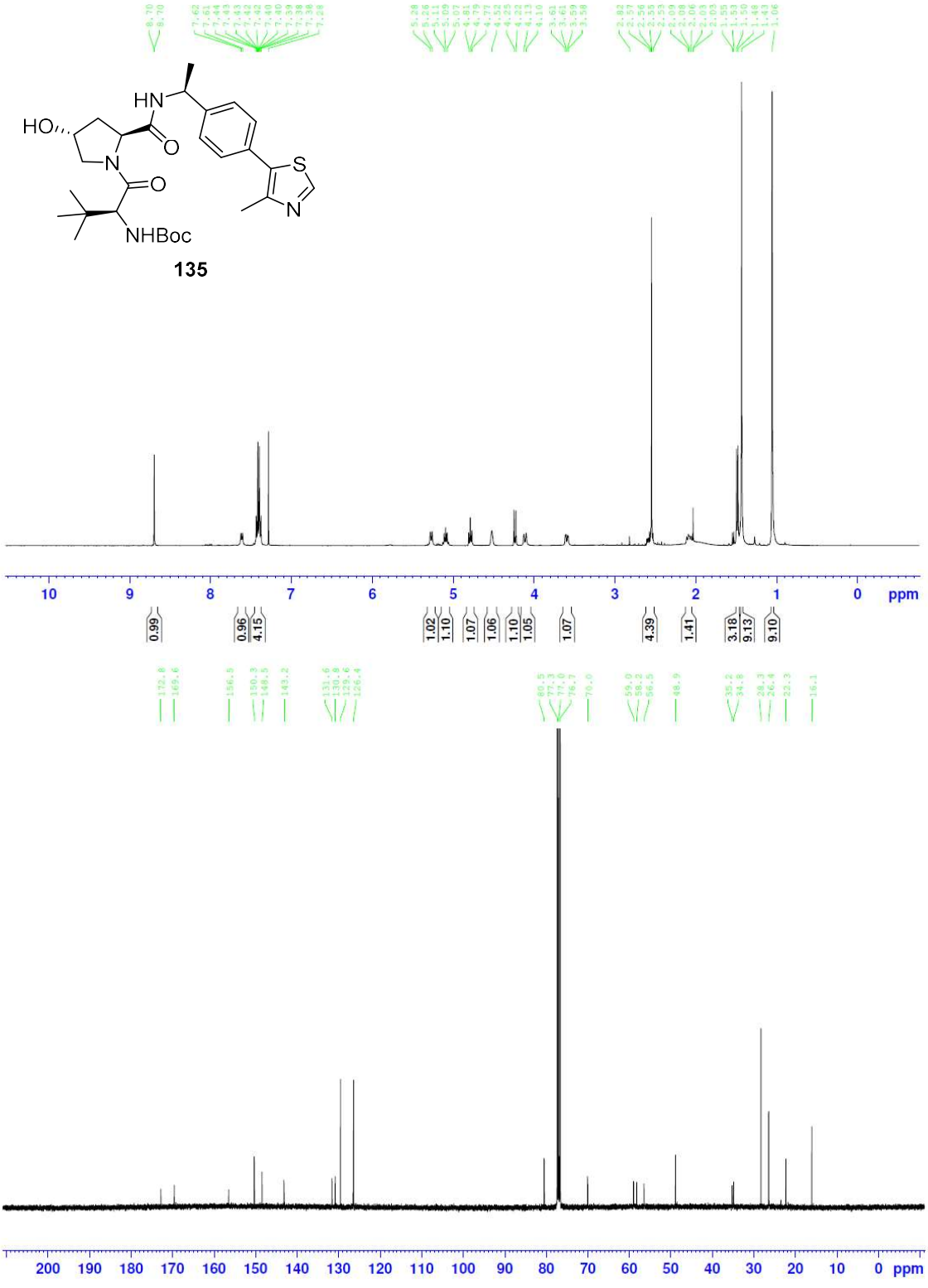
HO
HN
O
N
O
S
N
NHBoc
135
ppm
ppm

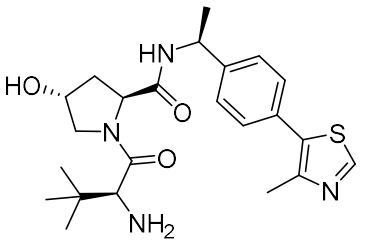
HO
HN
O
N
O
S
N
NH2

136

10 9 8 7 6 5 4 3 2 1 0 ppm
200 190 180 170 160 150 140 130 120 110 100 90 80 70 60 50 40 30 20 10 0 ppm

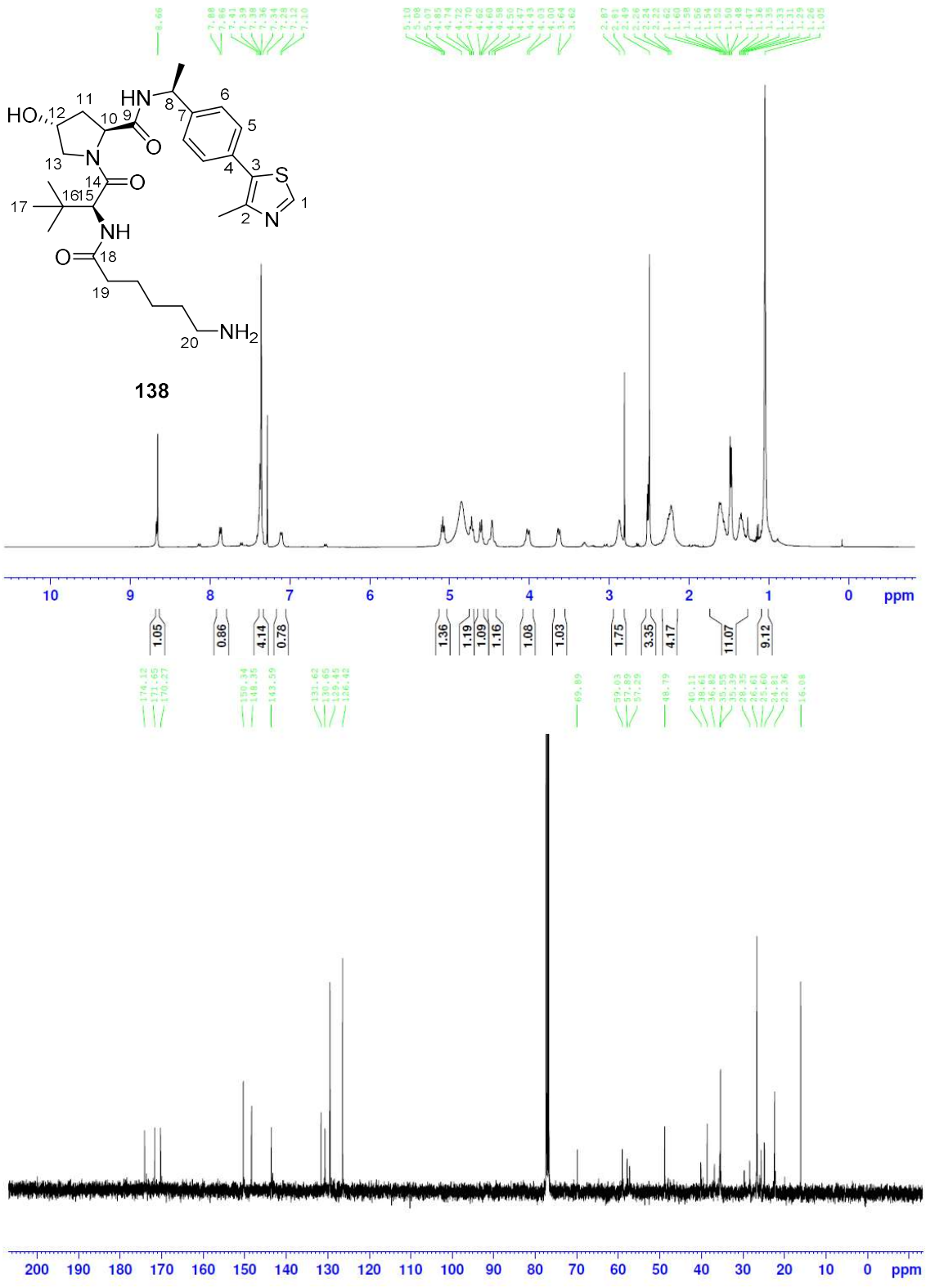
HO
HN
O
N
O
NH
O
NH2
S
N
1
2
3
4
5
6
7
8
9
10
11
12
13
14
15
16
17
18
19
20
138
10 9 8 7 6 5 4 3 2 1 0 ppm
1.05 0.86 4.14 0.78 1.36 1.19 1.09 1.16 1.08 1.03 1.75 3.35 4.17 11.07 9.12
200 190 180 170 160 150 140 130 120 110 100 90 80 70 60 50 40 30 20 10 0 ppm

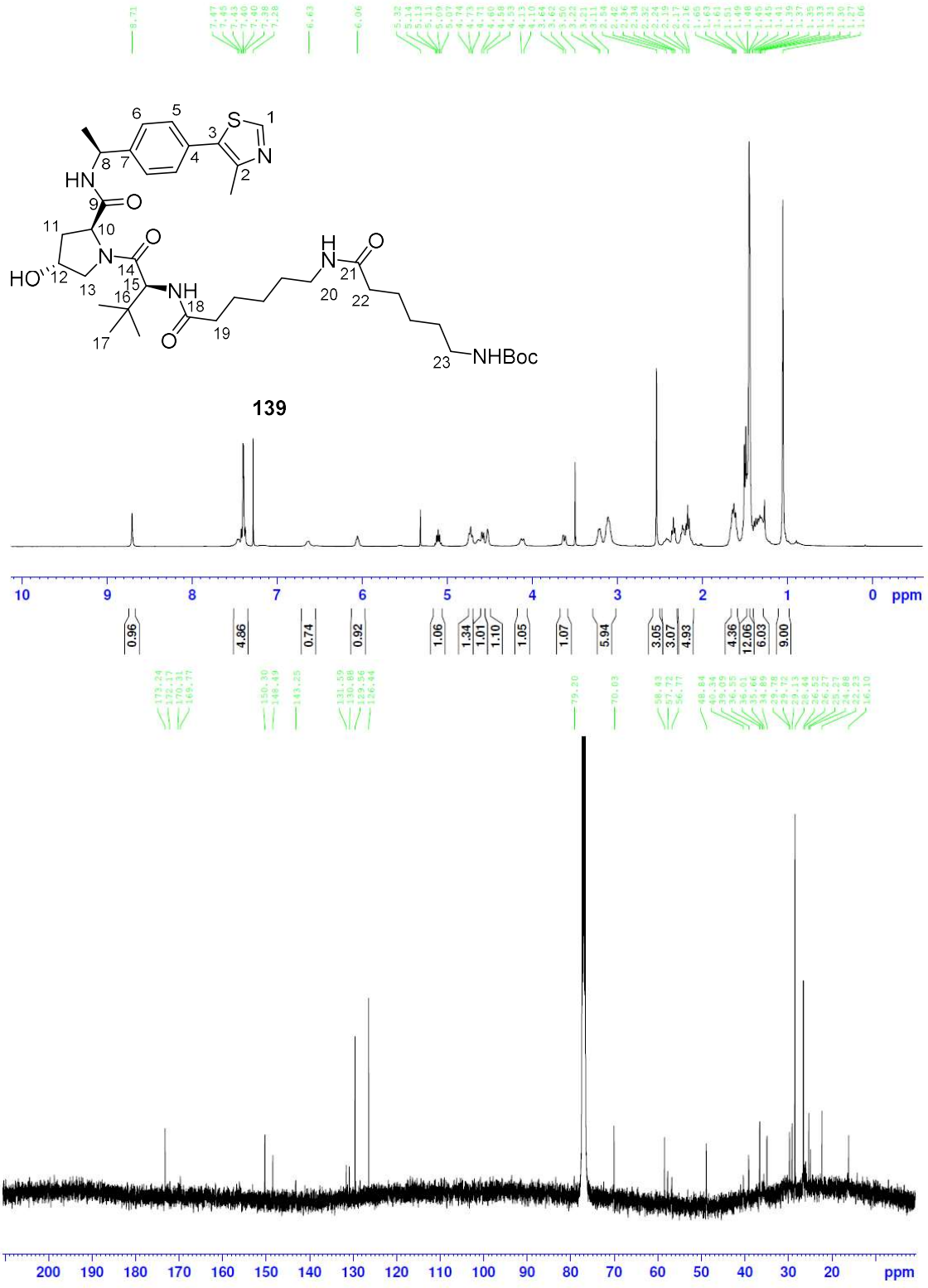
HO
HN
NH
NHBoc
139
ppm
ppm

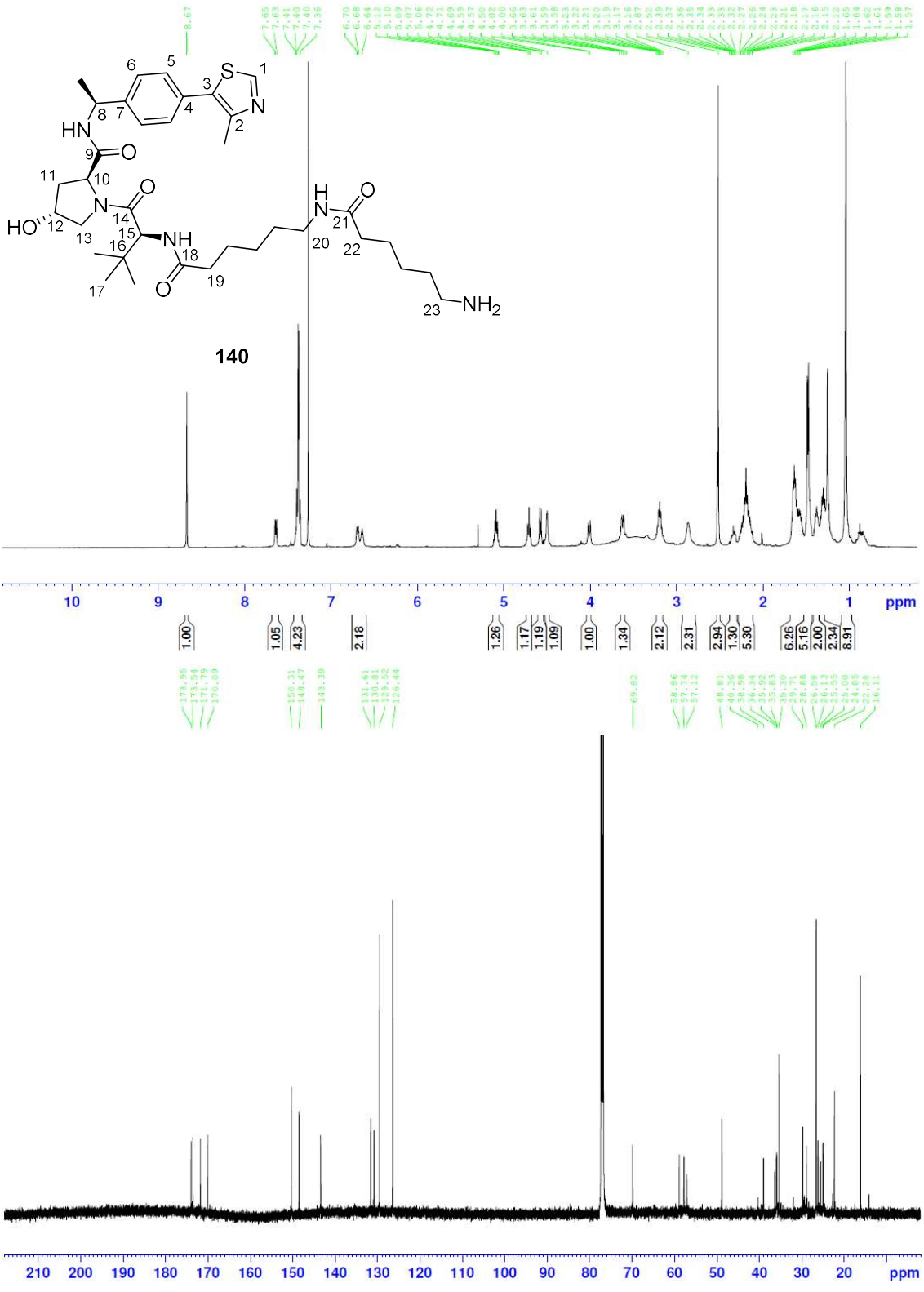
140
ppm
ppm

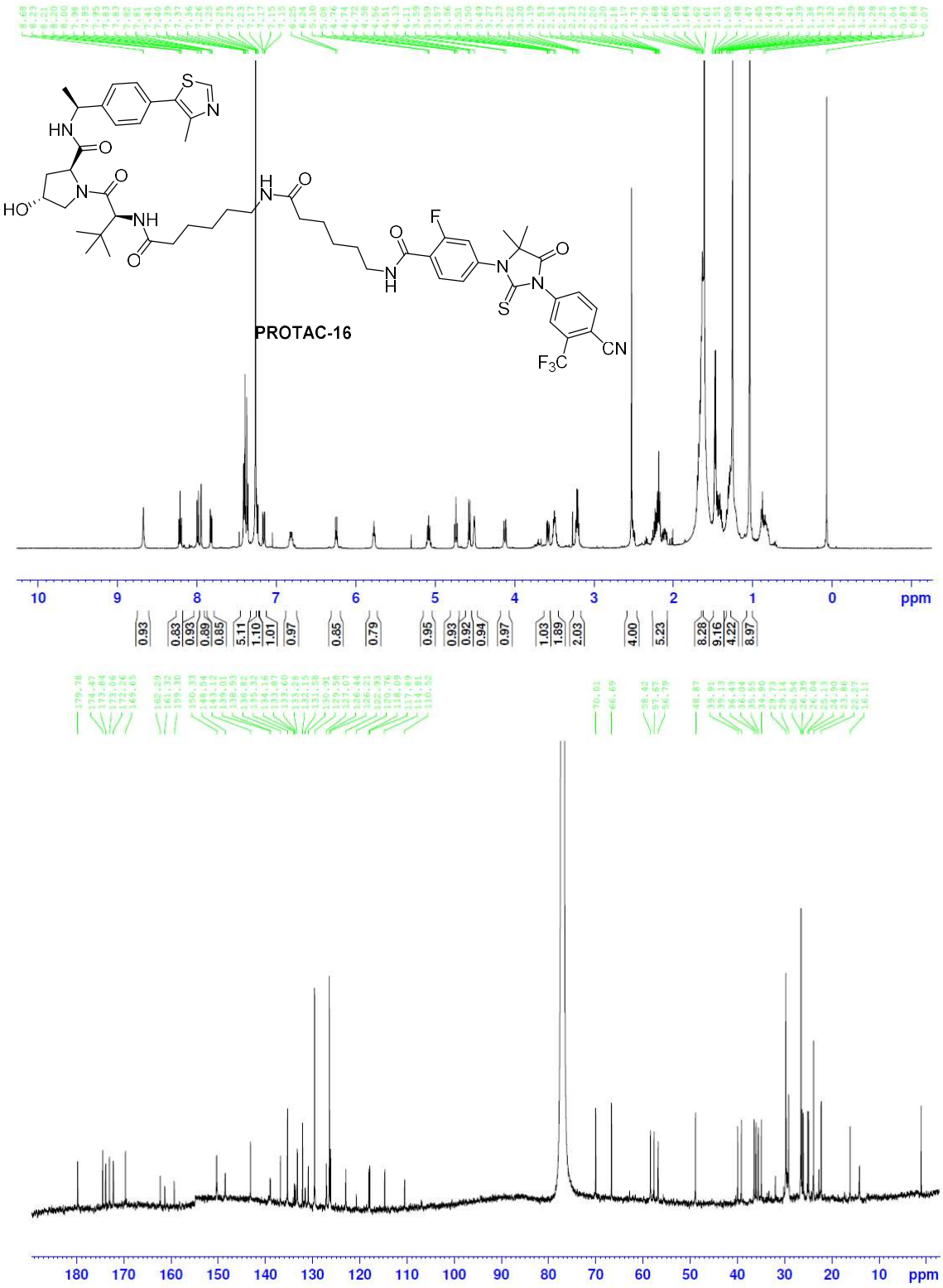
PROTAC-16
HO
HN
NH
S
N
O
F
CN
F_3C
10 9 8 7 6 5 4 3 2 1 0 ppm
180 170 160 150 140 130 120 110 100 90 80 70 60 50 40 30 20 10 ppm

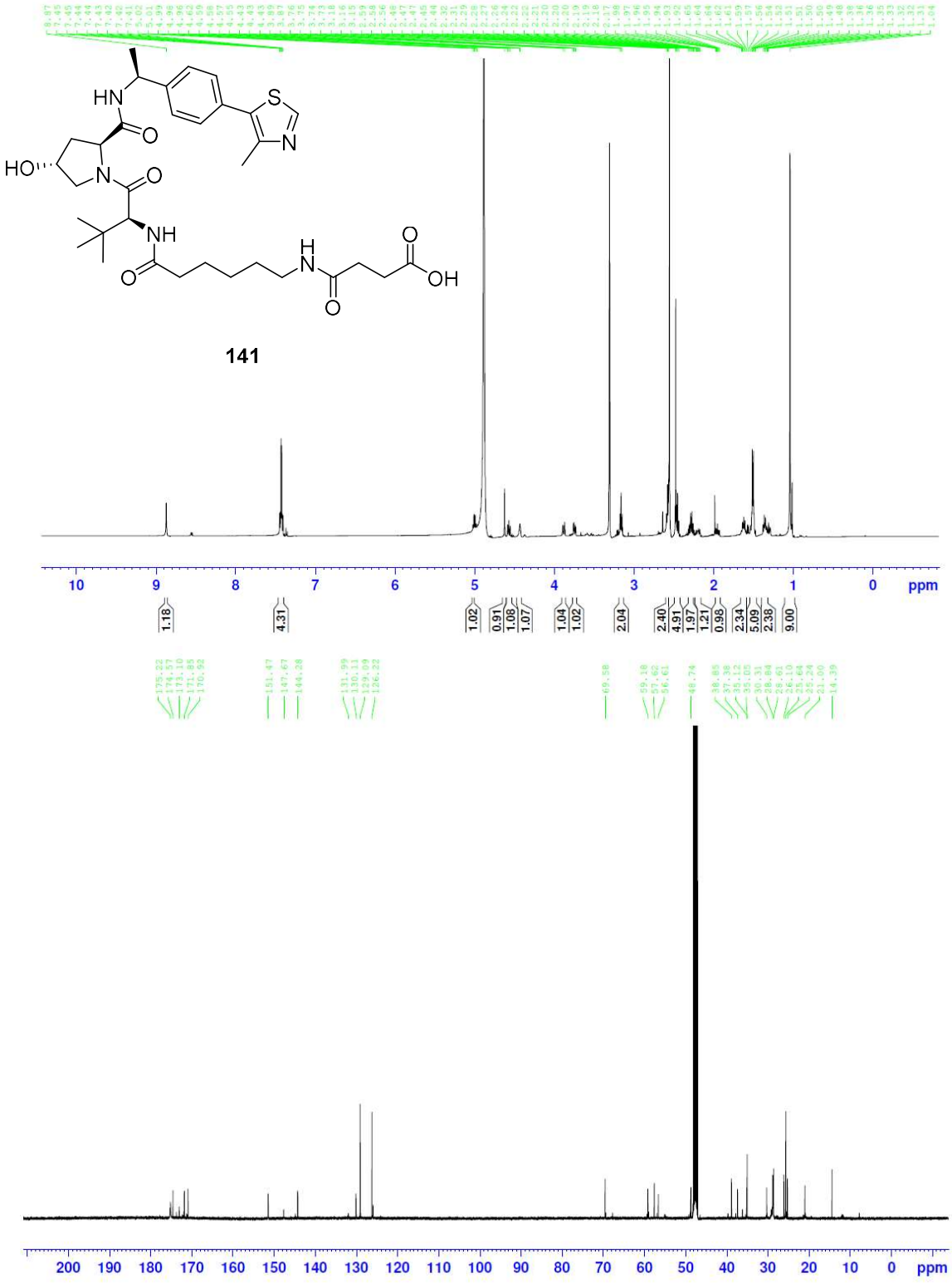
HN
O
S
N
HO
N
O
NH
H
N
O
O
OH
O
141
10 9 8 7 6 5 4 3 2 1 0 ppm
1.18 4.31 1.02 0.91 1.08 1.07 1.04 1.02 2.04 2.40 4.91 1.97 1.21 0.98 2.34 5.09 2.38 9.00
200 190 180 170 160 150 140 130 120 110 100 90 80 70 60 50 40 30 20 10 0 ppm

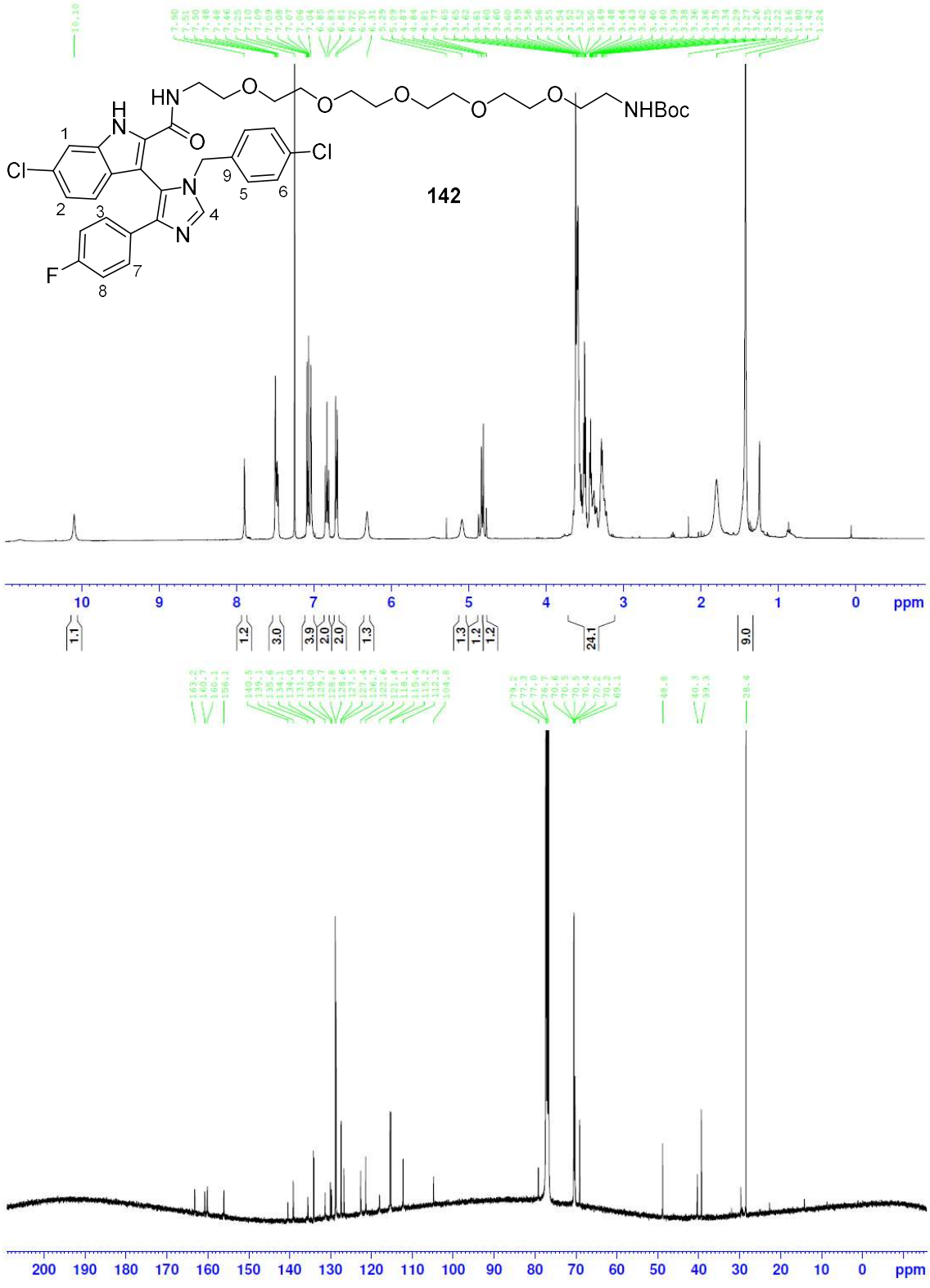
HN
O
O
O
O
O
NHBoc
H
N
O
Cl
Cl
N
N
F
1
2
3
4
5
6
7
8
9
142
10
9
8
7
6
5
4
3
2
1
0
ppm
1.1
1.2
3.0
3.9
2.0
2.0
1.3
1.3
1.2
1.2
24.1
9.0
200
190
180
170
160
150
140
130
120
110
100
90
80
70
60
50
40
30
20
10
0
ppm

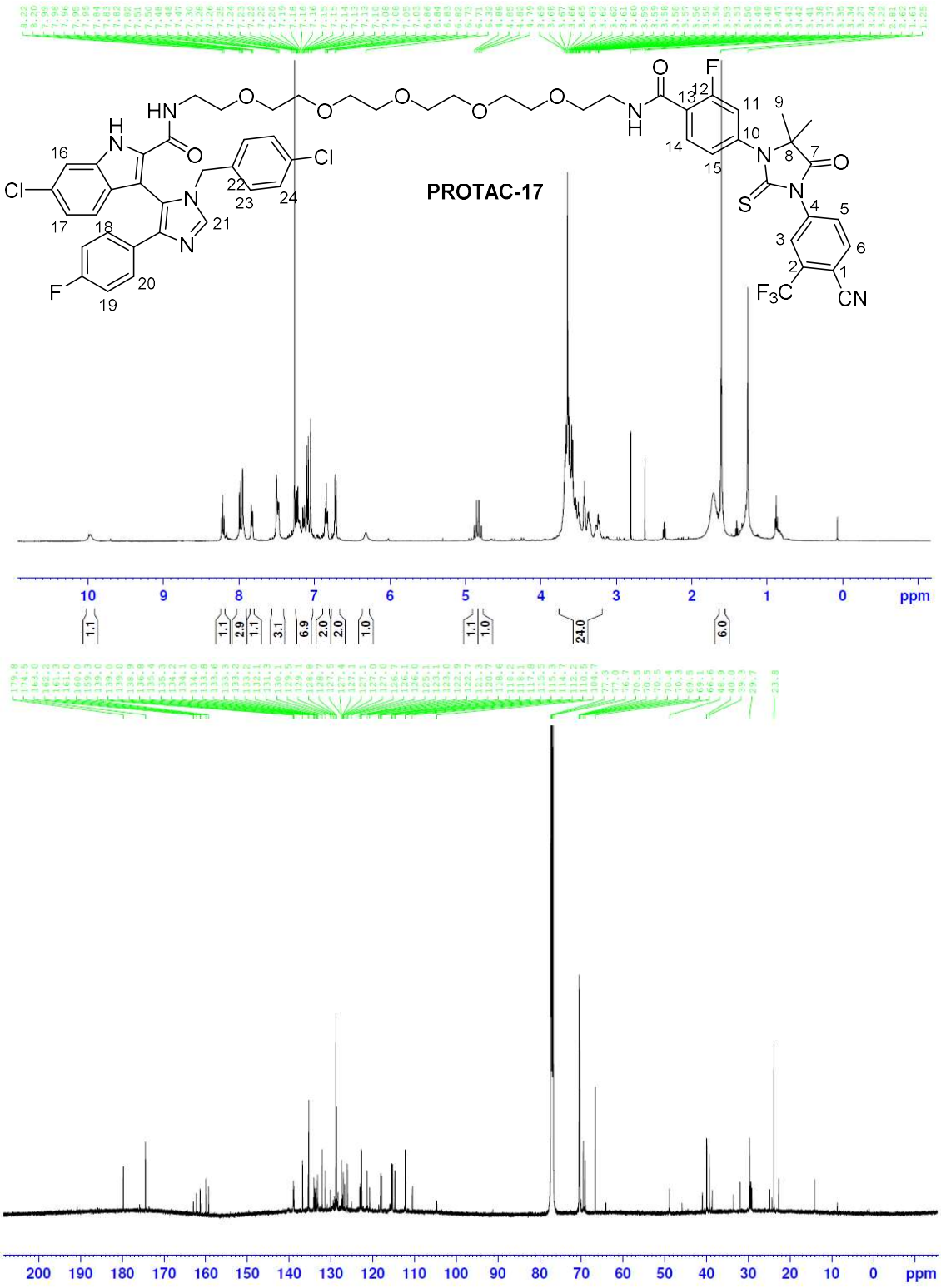
PROTAC-17
ppm
ppm

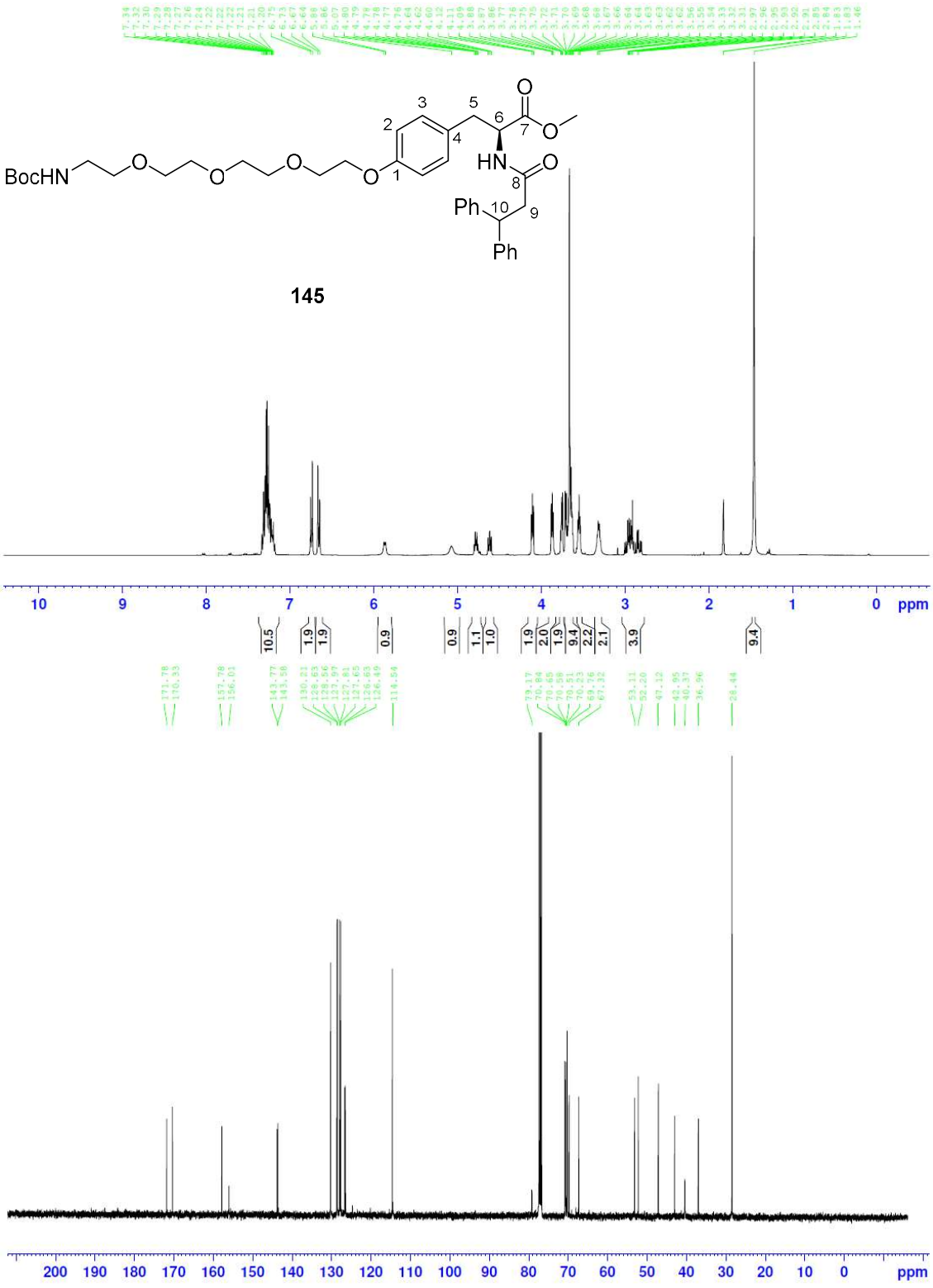
BocHN
O
O
O
O
1
2
3
4
5
6
7
8
9
10
HN
O
O
Ph
Ph
10
9
8
7
6
5
4
3
2
1
0
ppm
200
190
180
170
160
150
140
130
120
110
100
90
80
70
60
50
40
30
20
10
0
ppm

145

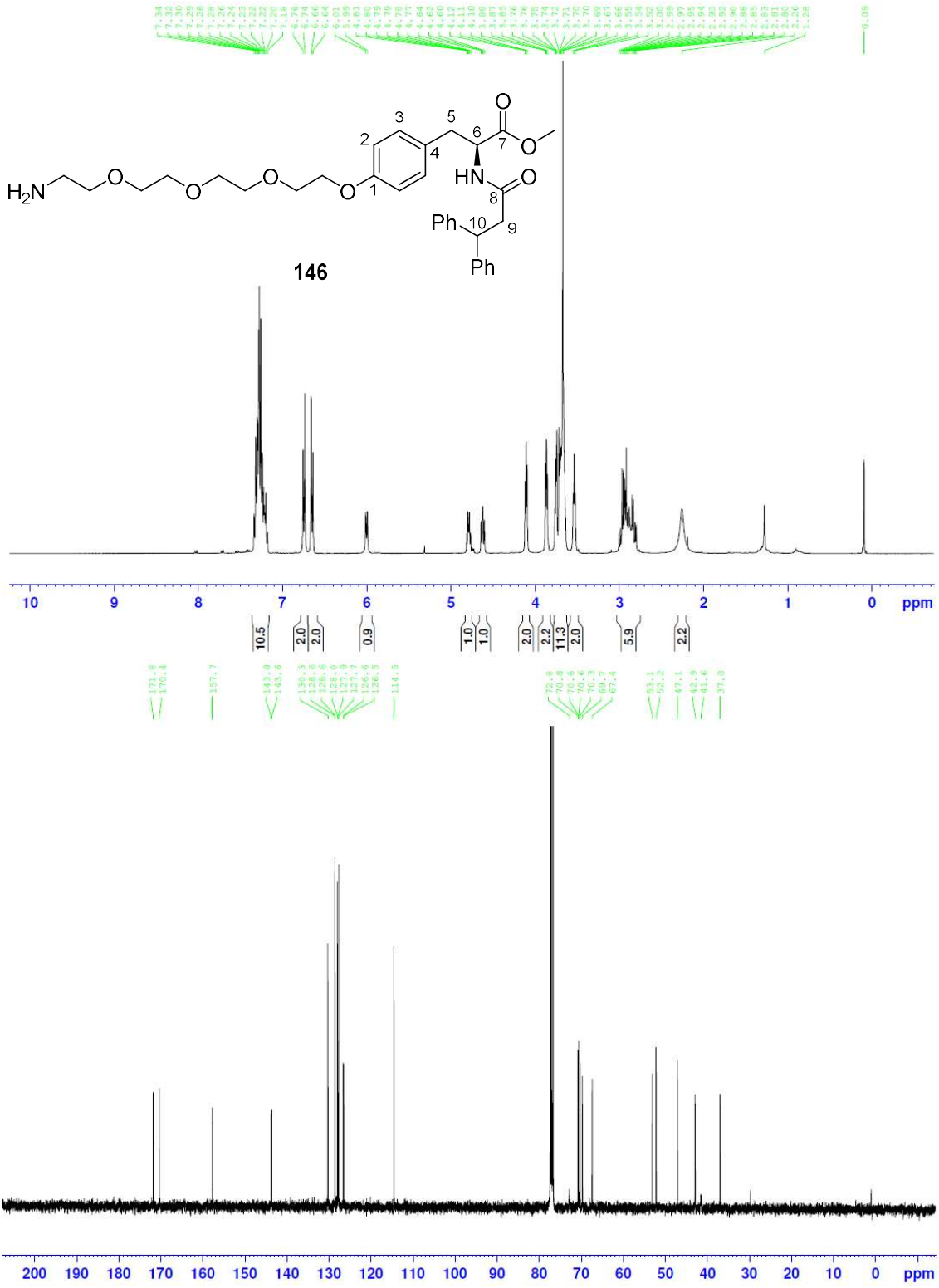
H2N
O
O
O
O
O
1
2
3
4
5
6
7
8
9
10
HN
O
O
Ph
Ph
146
10
9
8
7
6
5
4
3
2
1
0
ppm
200
190
180
170
160
150
140
130
120
110
100
90
80
70
60
50
40
30
20
10
0
ppm

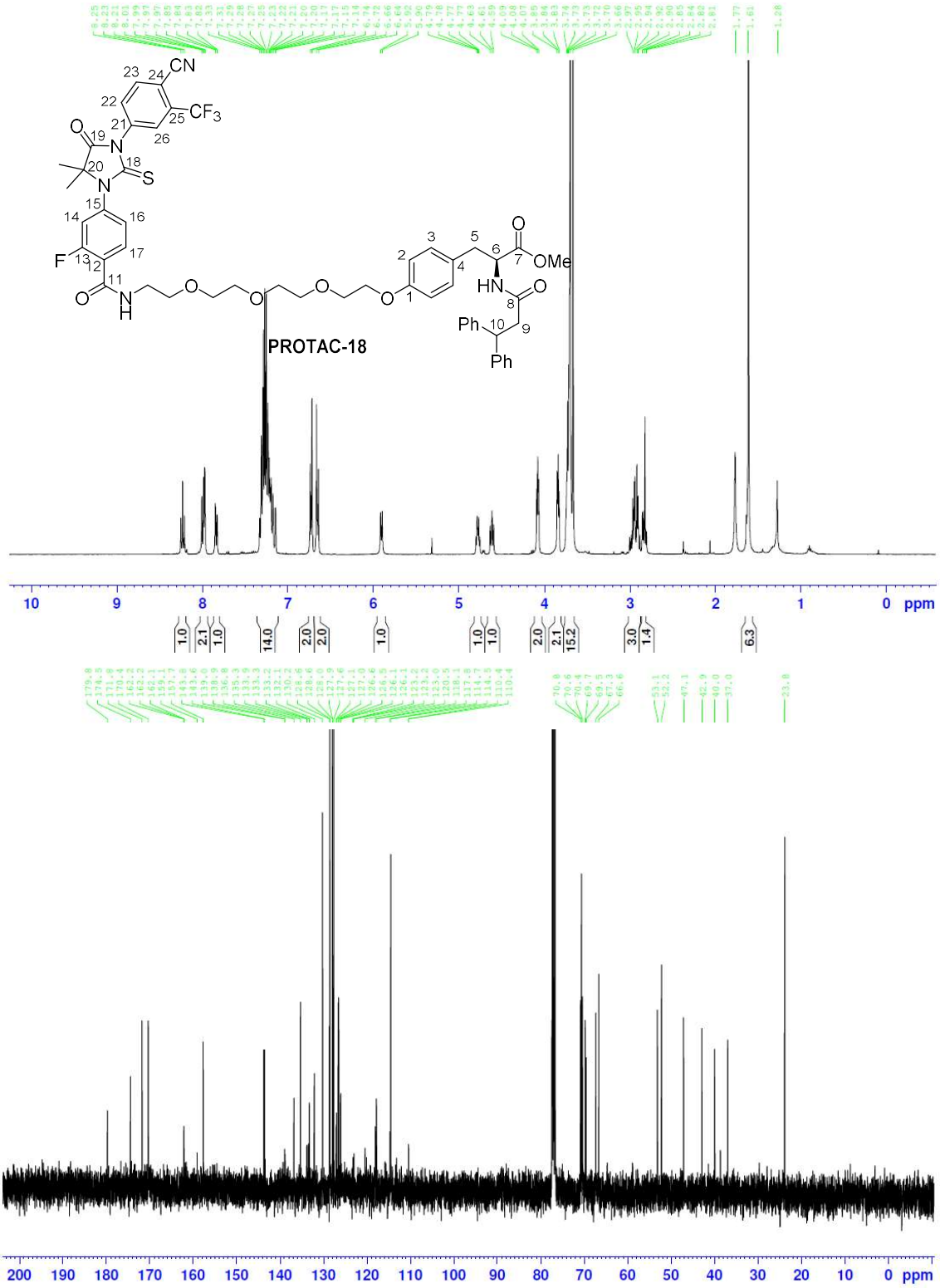
PROTAC-18
10 9 8 7 6 5 4 3 2 1 0 ppm
200 190 180 170 160 150 140 130 120 110 100 90 80 70 60 50 40 30 20 10 0 ppm

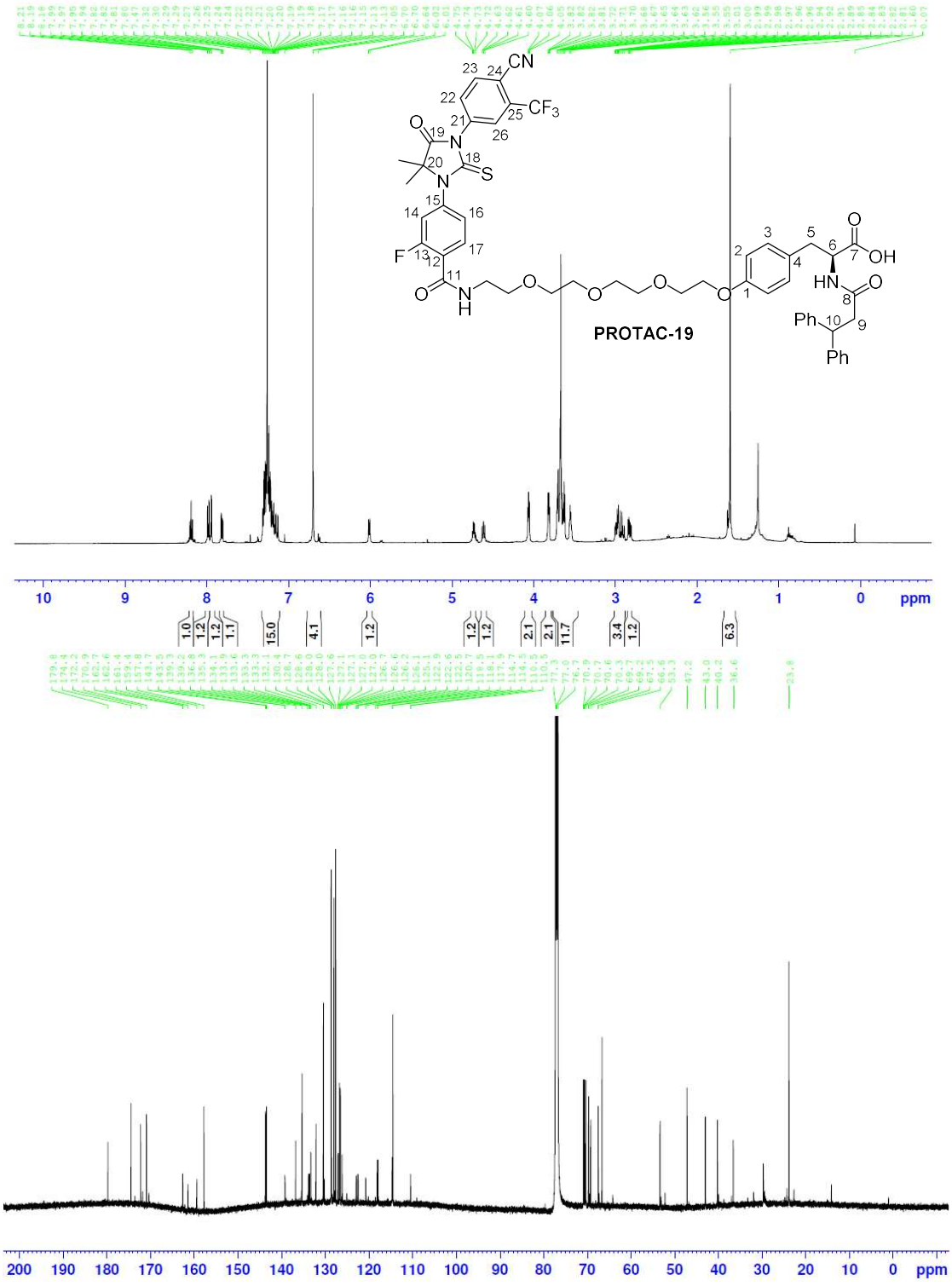
PROTAC-19
10 9 8 7 6 5 4 3 2 1 0 ppm
200 190 180 170 160 150 140 130 120 110 100 90 80 70 60 50 40 30 20 10 0 ppm

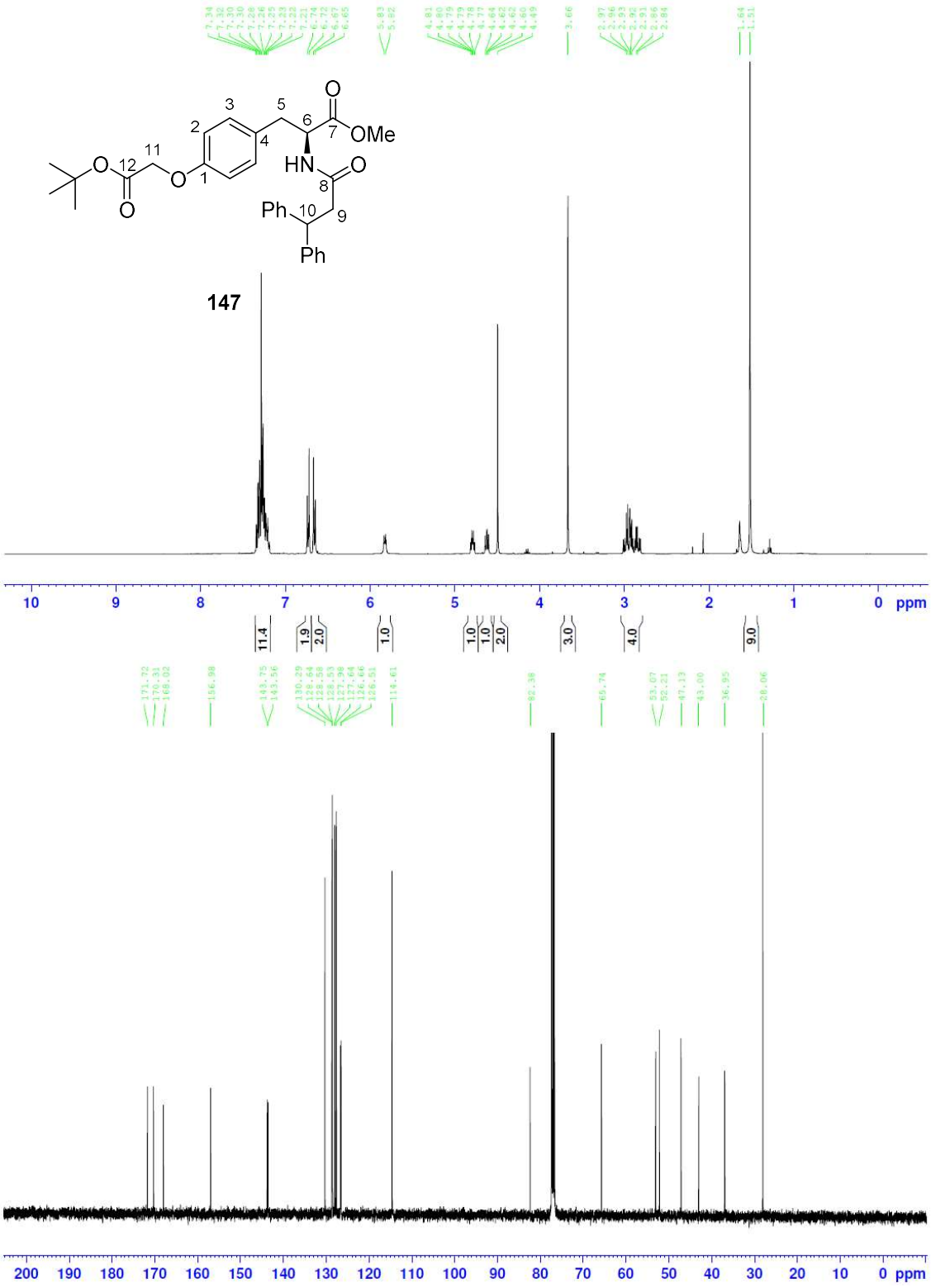
147
ppm
ppm

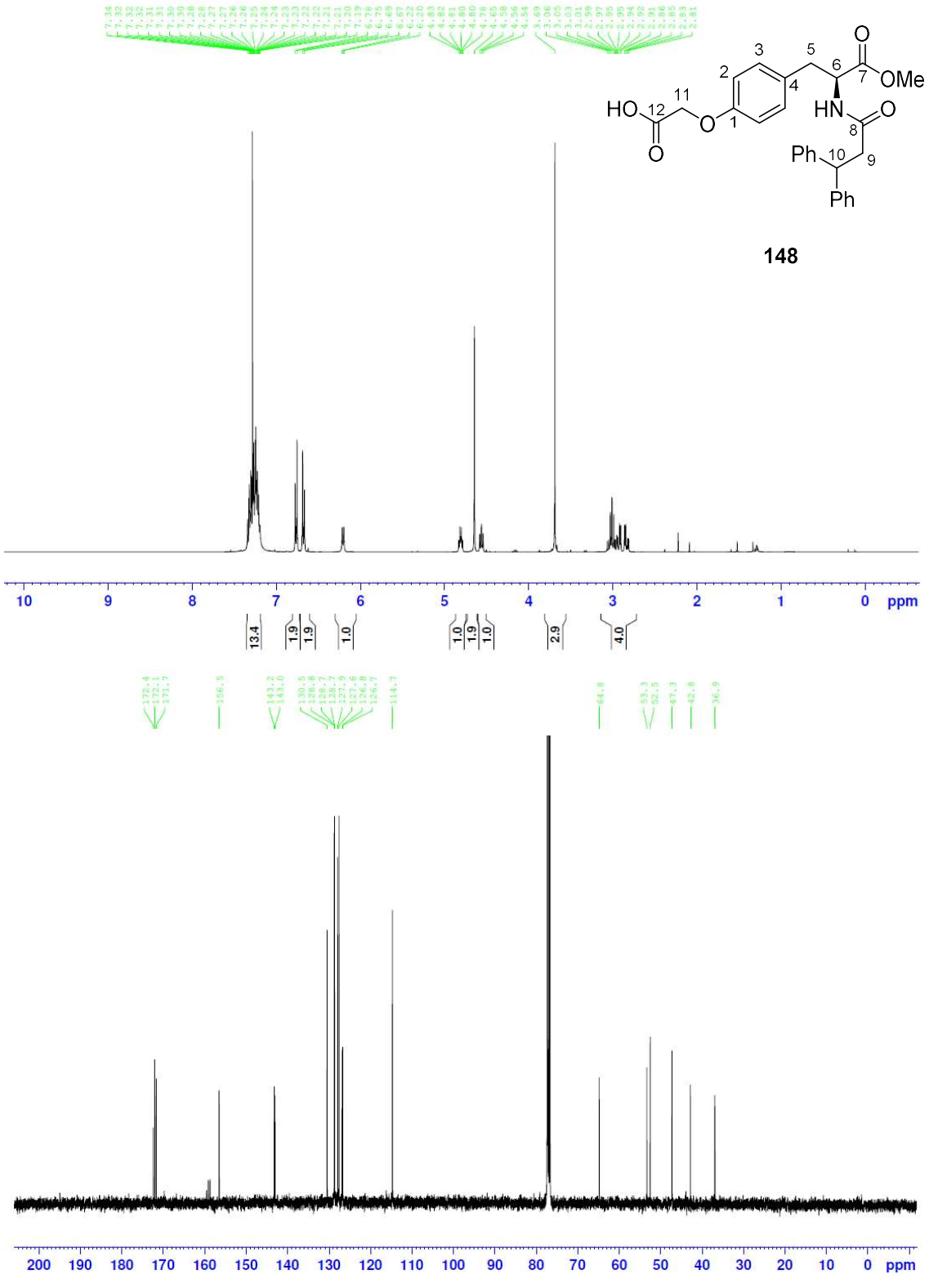
HO
O
O
11
12
O
1
2
3
4
5
6
7
OMe
O
HN
8
O
9
10
Ph
Ph
148
10 9 8 7 6 5 4 3 2 1 0 ppm
13.4
1.9
1.9
1.0
1.0
1.9
1.0
2.9
4.0
200 190 180 170 160 150 140 130 120 110 100 90 80 70 60 50 40 30 20 10 0 ppm

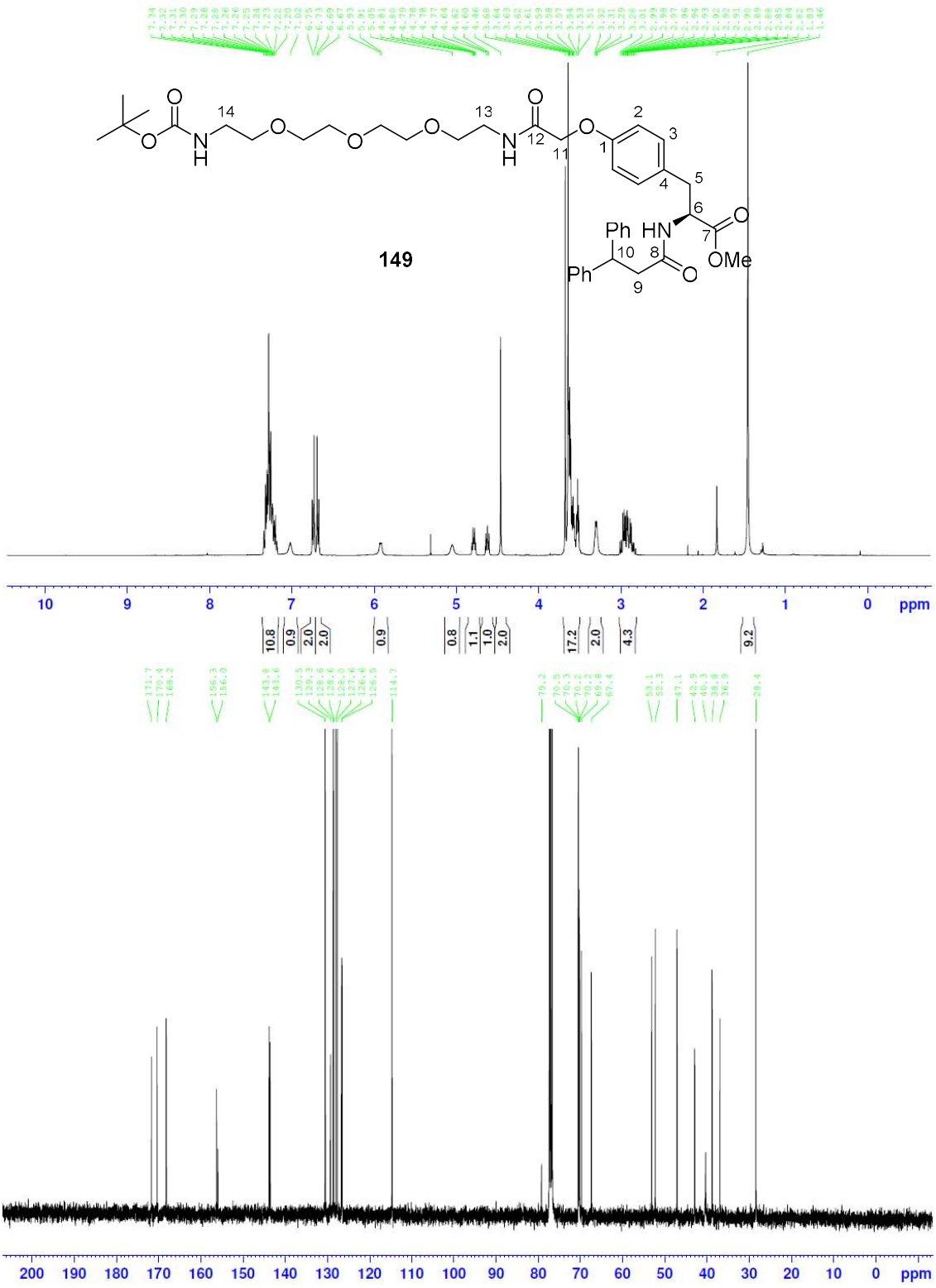
149
Ph HN
OMe
Ph
10.8
0.9
2.0
2.0
0.9
0.8
1.1
1.0
2.0
17.2
2.0
4.3
9.2
ppm

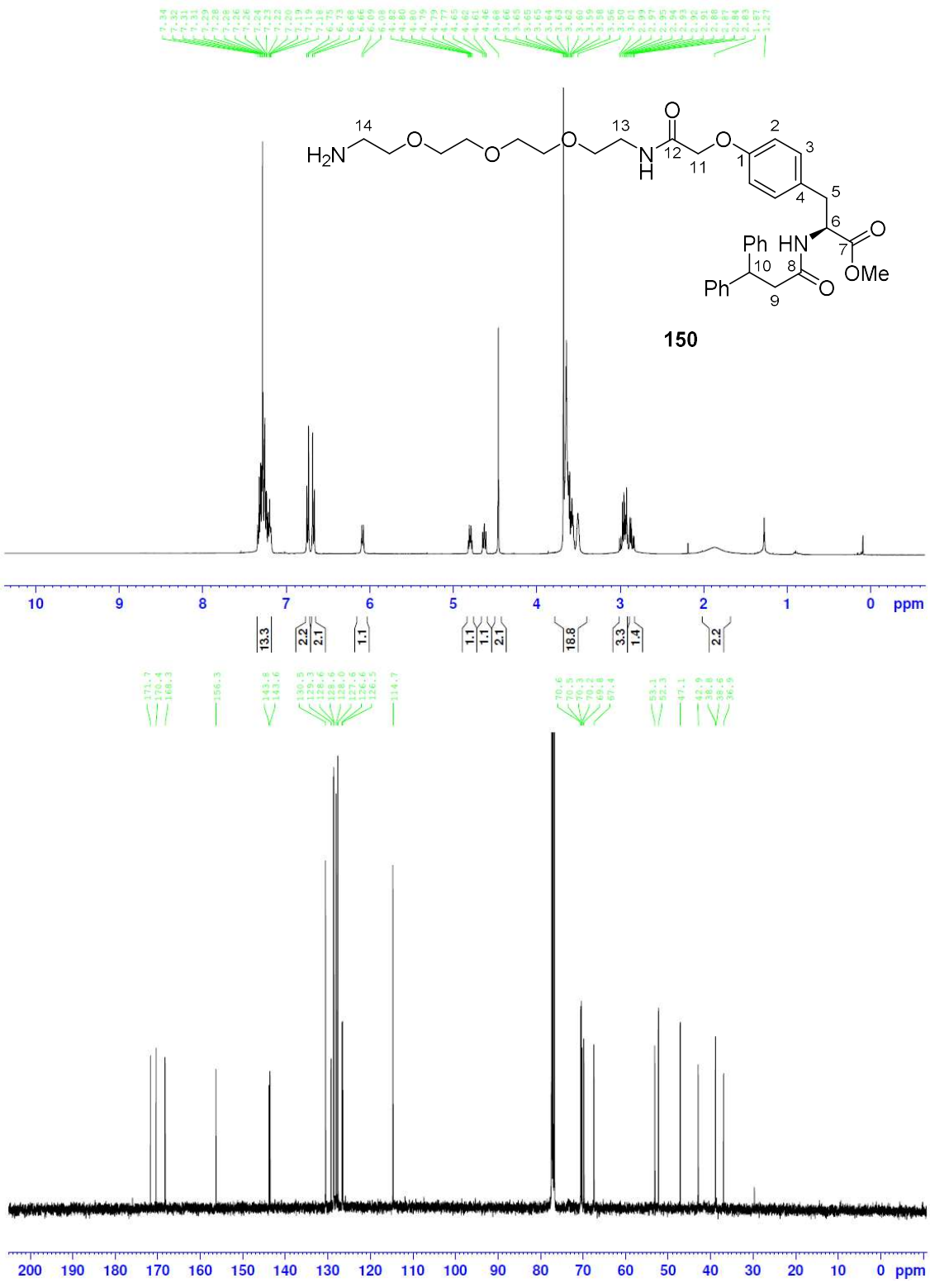
H2N
O
N
H
Ph
HN
OMe
Ph
150
10
9
8
7
6
5
4
3
2
1
0 ppm
200
190
180
170
160
150
140
130
120
110
100
90
80
70
60
50
40
30
20
10
0 ppm

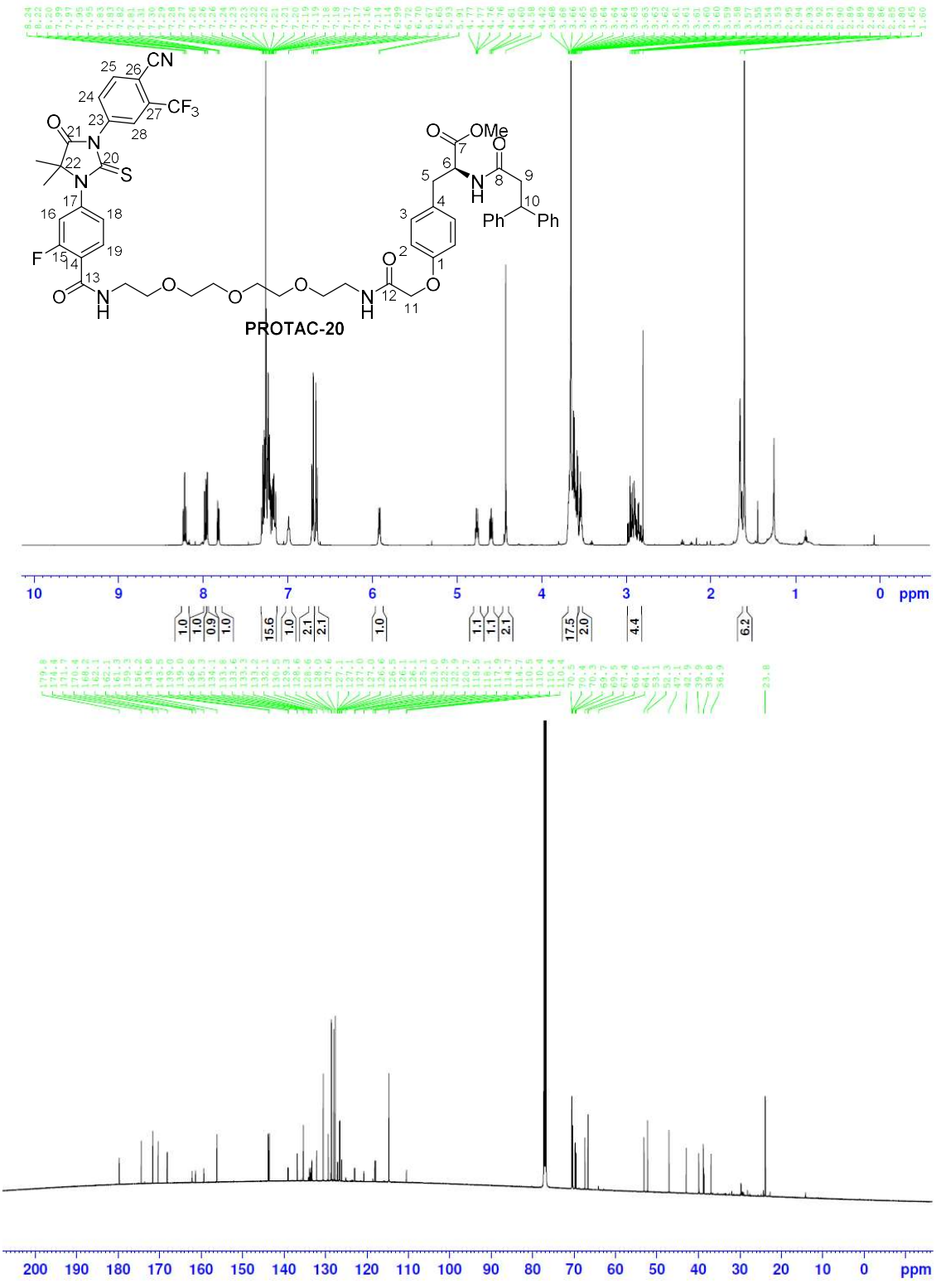
PROTAC-20
ppm
ppm

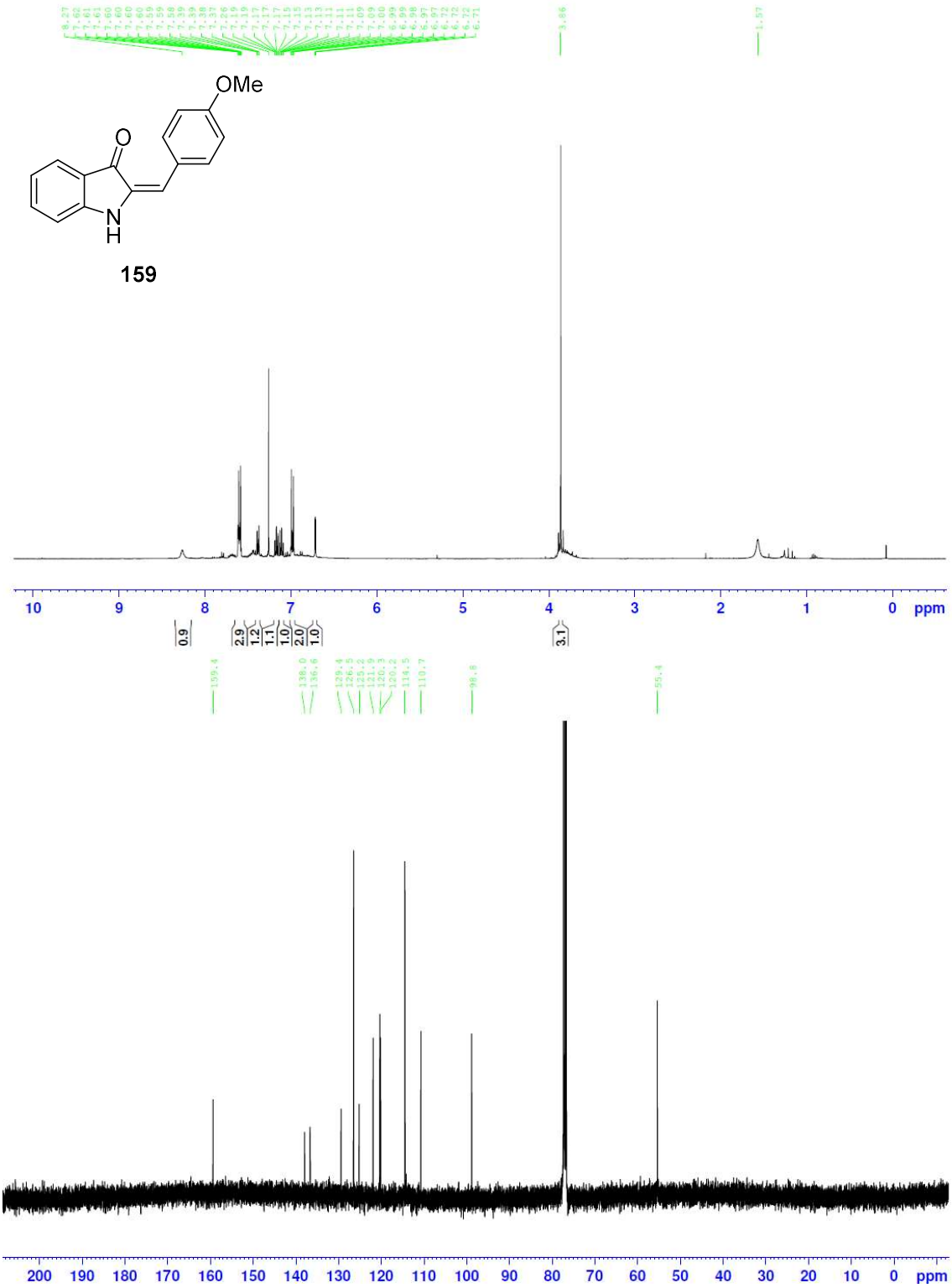
OMe
O
N
H
159
ppm
ppm

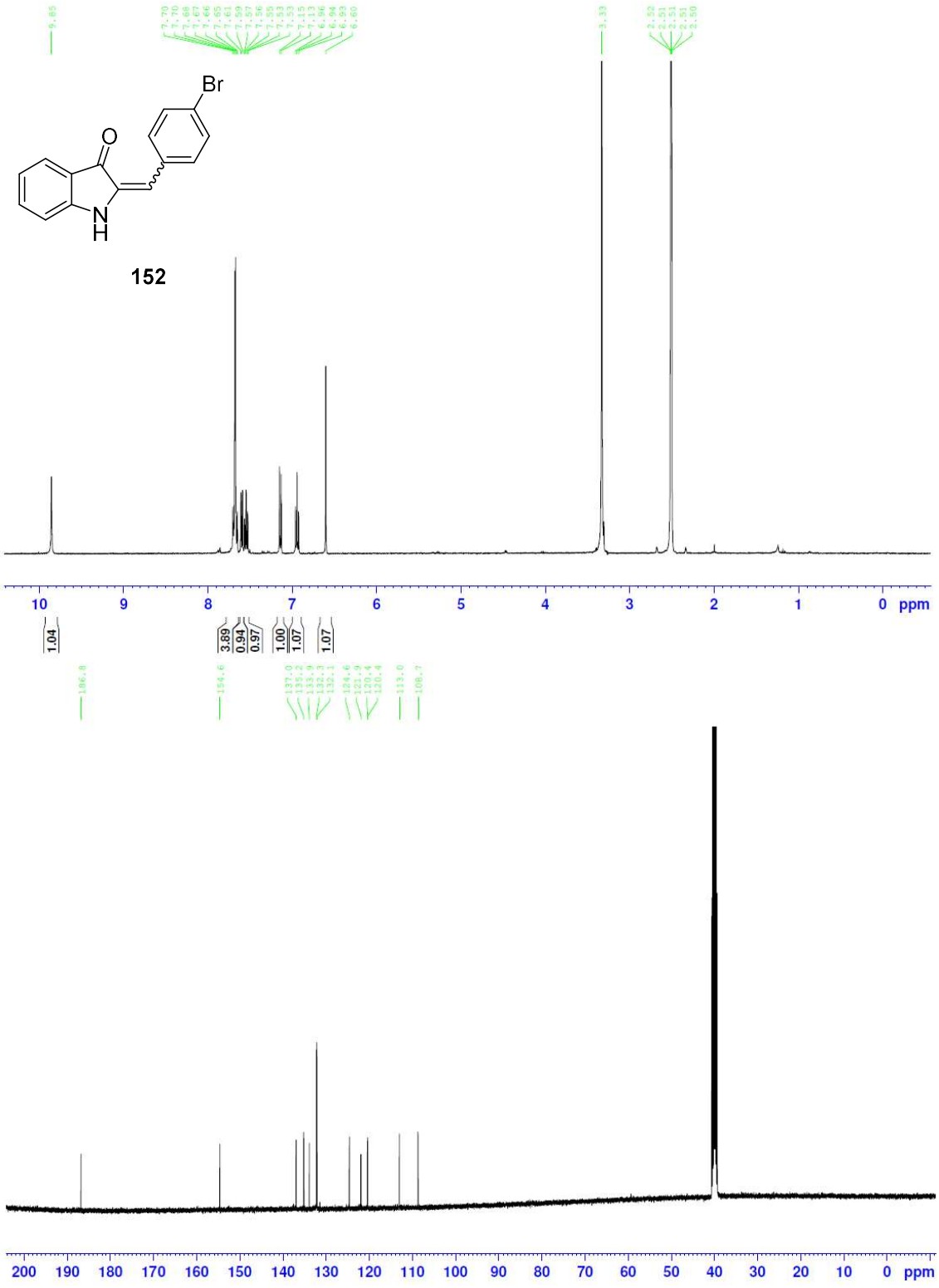
Br
O
N
H
152
10 9 8 7 6 5 4 3 2 1 0 ppm
200 190 180 170 160 150 140 130 120 110 100 90 80 70 60 50 40 30 20 10 0 ppm

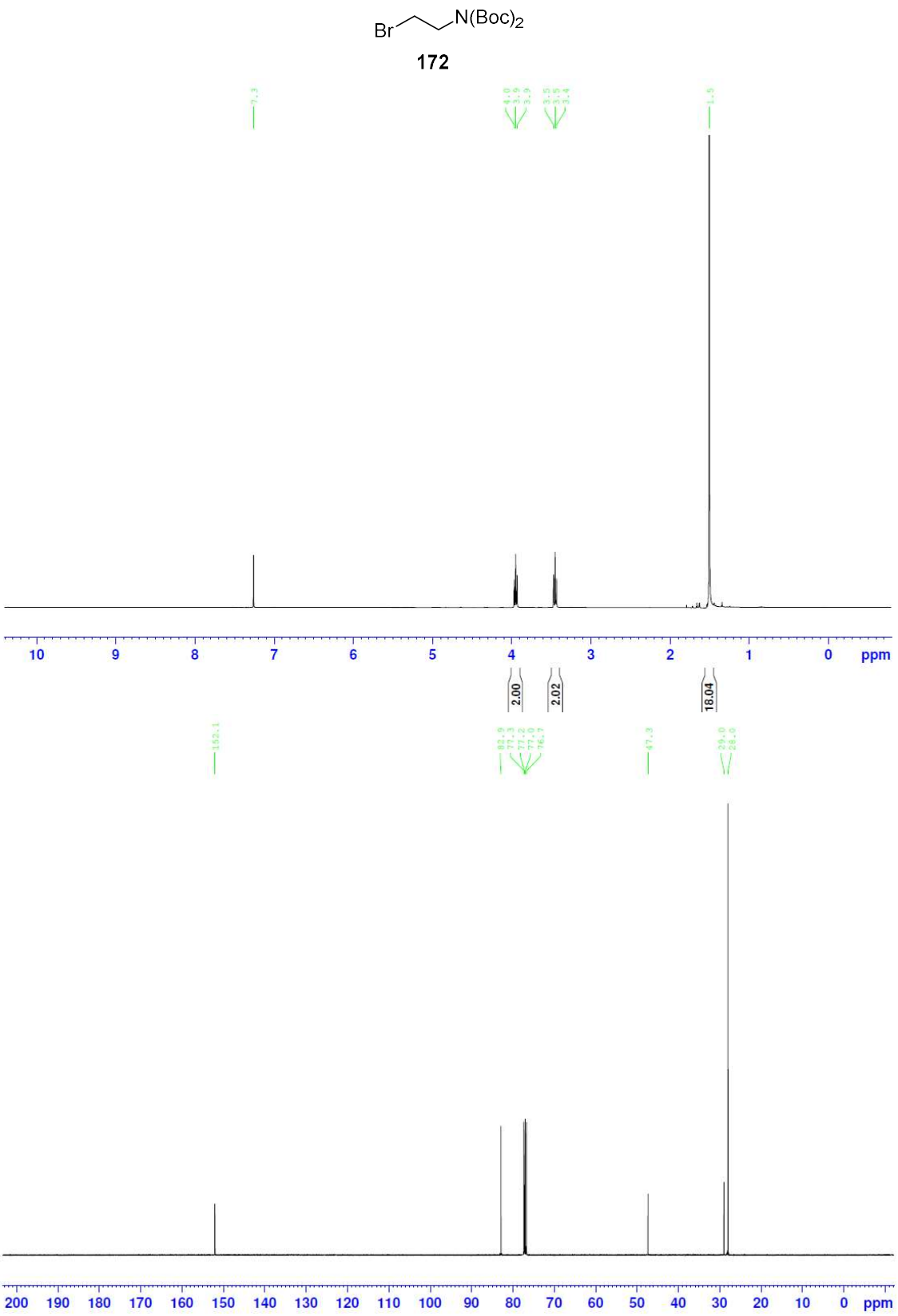
Br
N(Boc)2
172
7.3
4.0
3.9
3.9
3.5
3.5
3.5
3.4
1.5
10
9
8
7
6
5
4
3
2
1
0
ppm
2.00
2.02
18.04
152.1
82.9
77.3
77.2
77.0
76.7
47.3
29.0
28.0
200
190
180
170
160
150
140
130
120
110
100
90
80
70
60
50
40
30
20
10
0
ppm

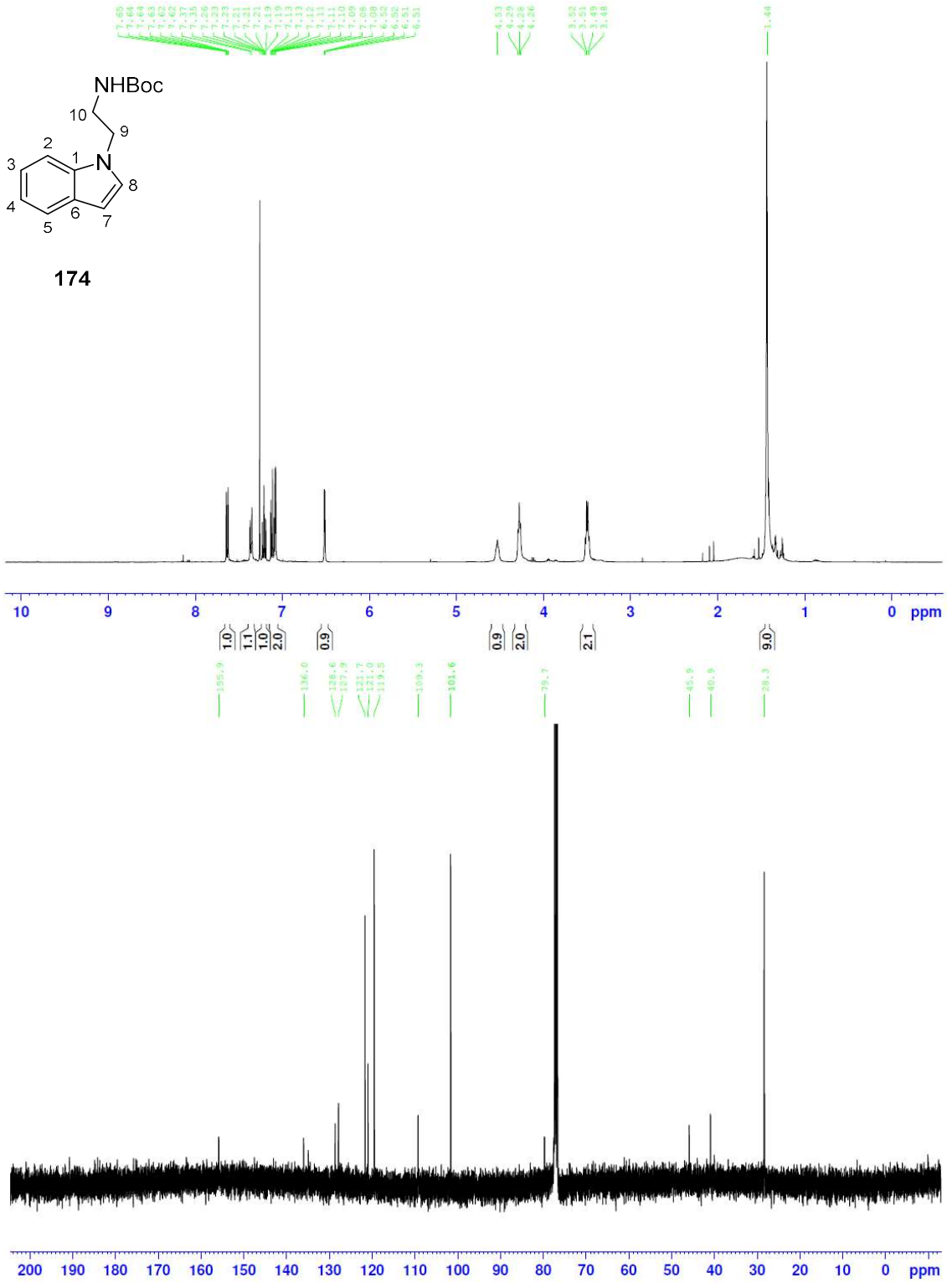
NHBoc
10
9
2
1
N
3
8
4
6
7
5
174
ppm
ppm

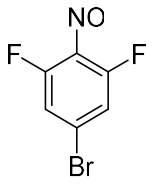
NO
F
F
Br

178

7.35
7.33
7.26
1.25
10
9
8
7
6
5
4
3
2
1
0
ppm
2.0
154.7
154.7
152.0
152.0
145.6
145.5
145.5
130.7
130.6
130.5
117.1
117.1
116.9
116.8
77.3
77.0
76.7
29.7
200
190
180
170
160
150
140
130
120
110
100
90
80
70
60
50
40
30
20
10
0
ppm

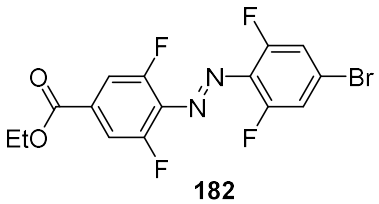
F
F
O
N
Br
EtO
N
F
F

182

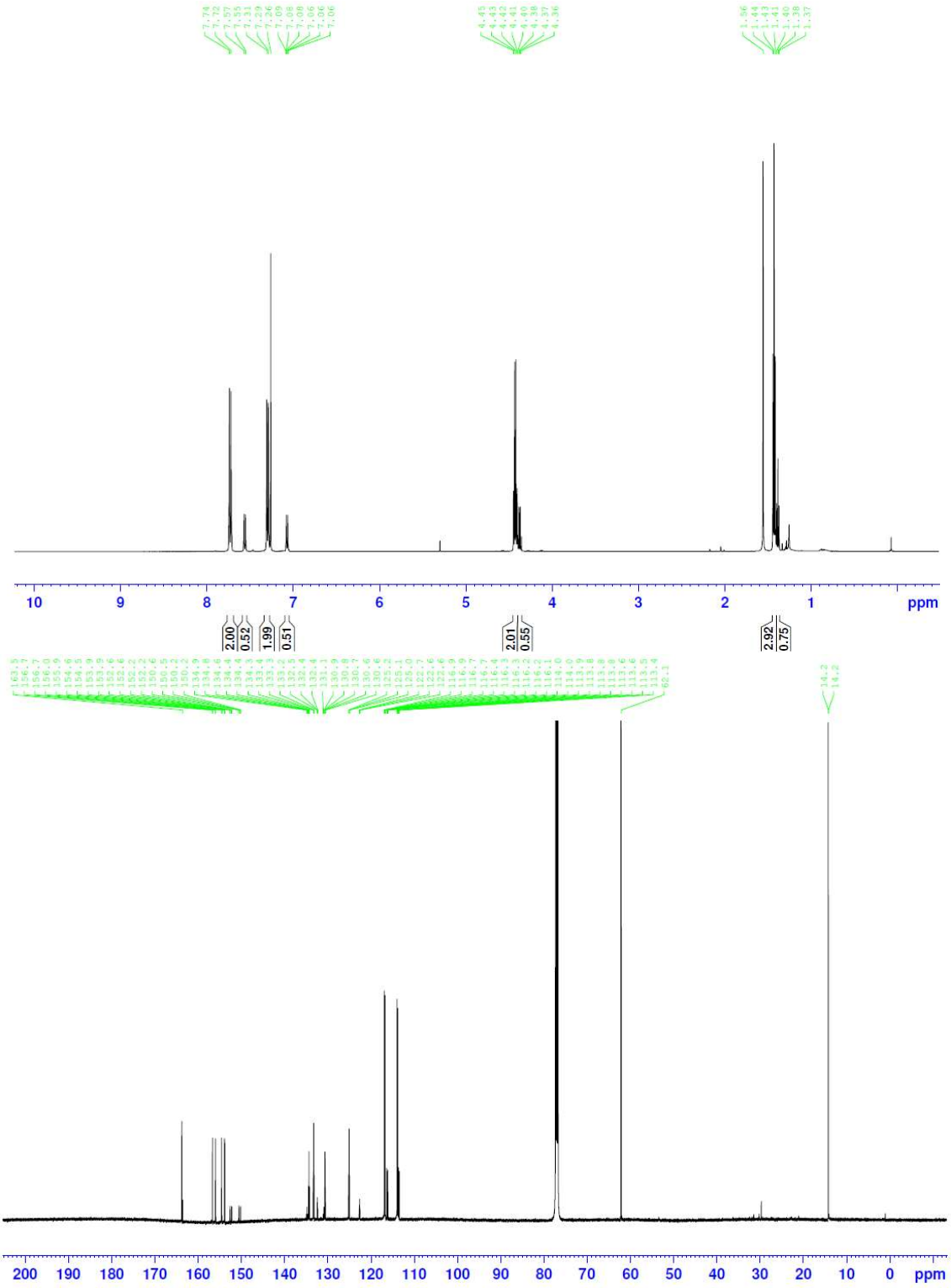
10
9
8
7
6
5
4
3
2
1
ppm
2.00
0.52
1.99
0.51
2.01
0.55
2.92
0.75
200
190
180
170
160
150
140
130
120
110
100
90
80
70
60
50
40
30
20
10
0
ppm

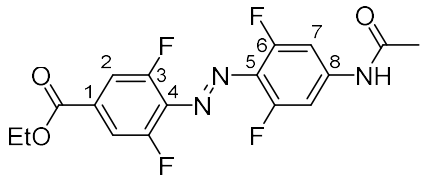
F
O
7
6
2
F
5
8
O
NH
1
3
4
N
N
EtO
F
F

188

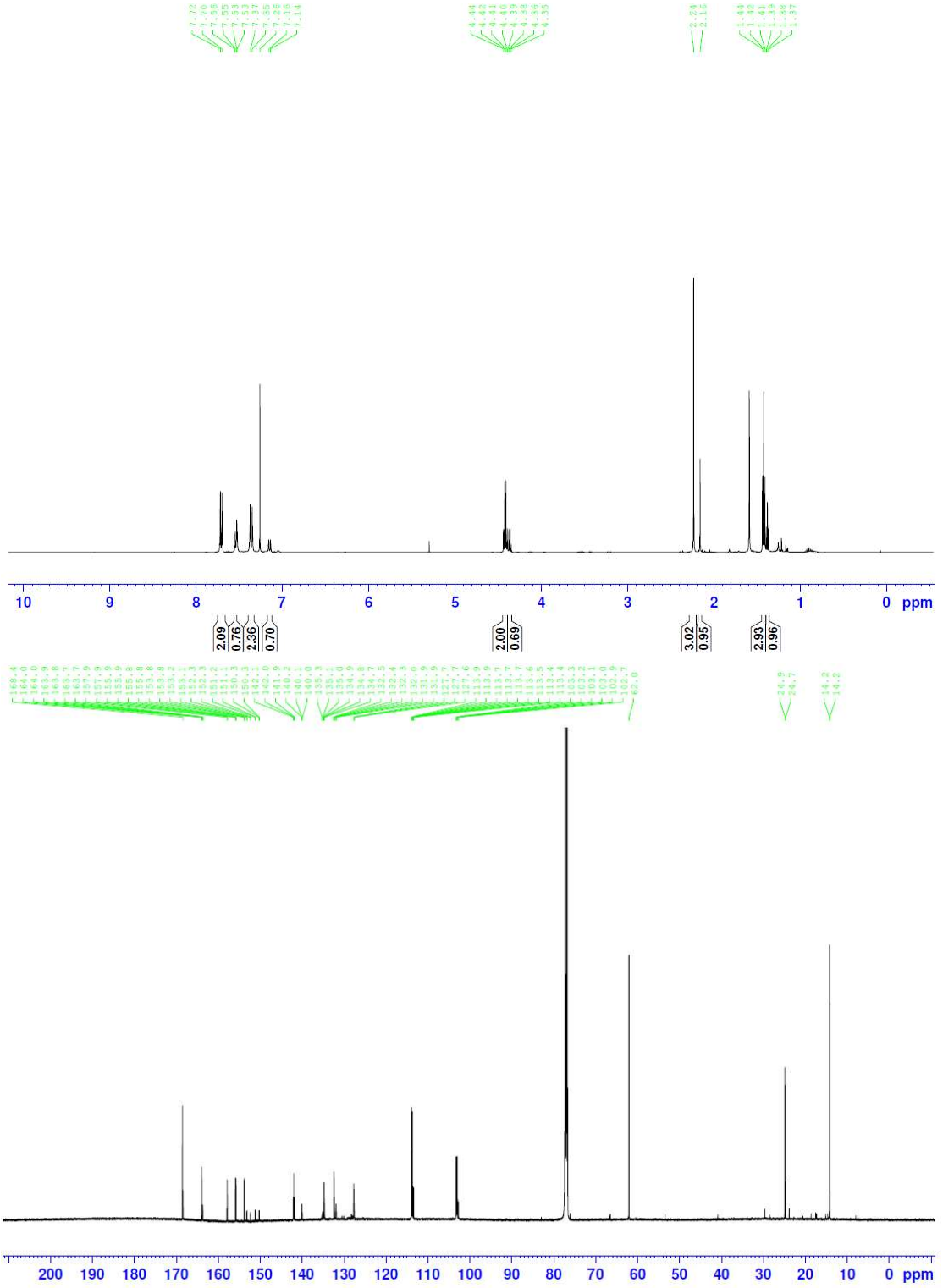
10 9 8 7 6 5 4 3 2 1 0 ppm
200 190 180 170 160 150 140 130 120 110 100 90 80 70 60 50 40 30 20 10 0 ppm

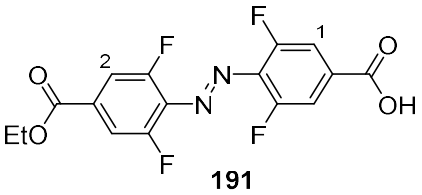
F
1
2
F
O
O
N
N
OH
EtO
F
F

191

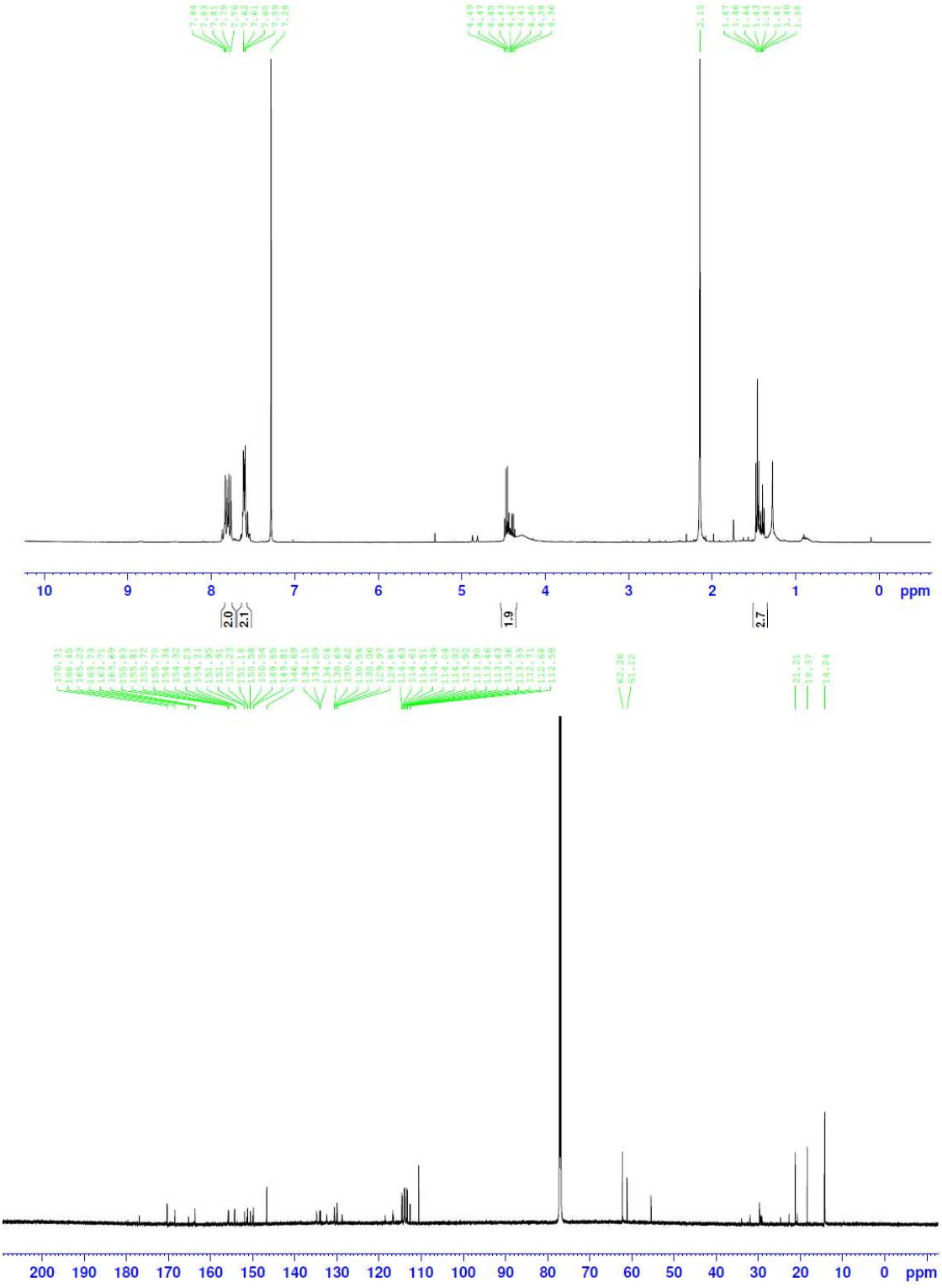
10 9 8 7 6 5 4 3 2 1 0 ppm
2.0
2.1
1.9
2.7
200 190 180 170 160 150 140 130 120 110 100 90 80 70 60 50 40 30 20 10 0 ppm

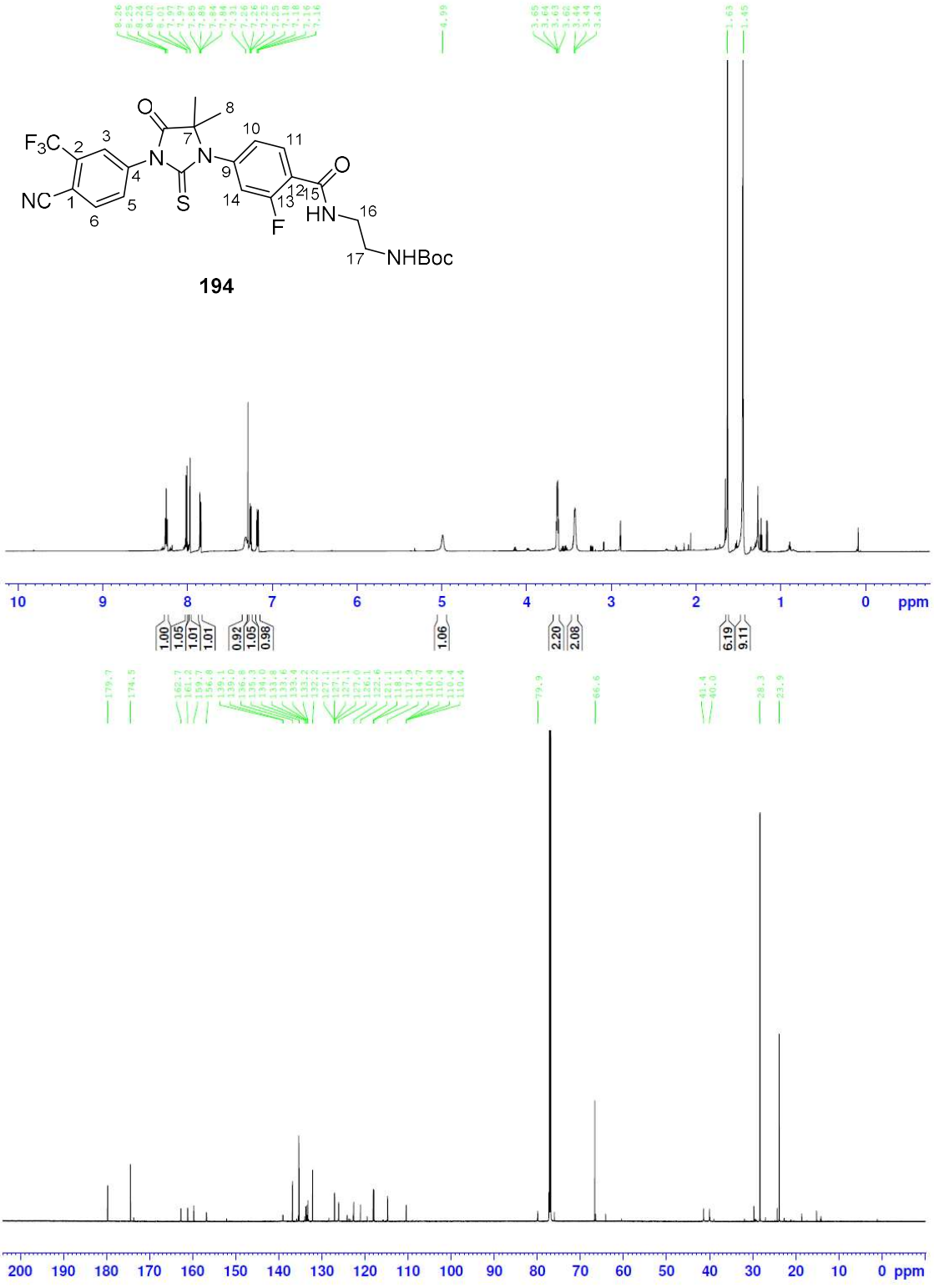
F3C
NC
O
N
S
HN
F
NHBoc
194
ppm

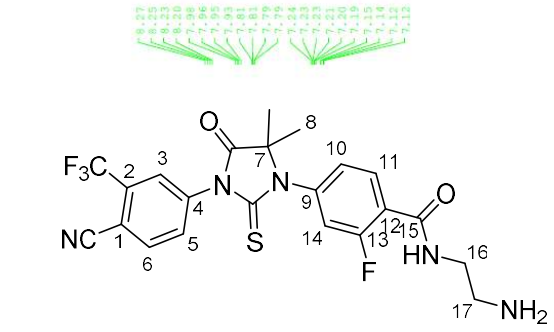
O
8
F3C
2
3
7
10
11
N
N
9
O
4
12
15
NC
1
5
S
14
13
HN
16
6
F
17
NH2

177

10
9
8
7
6
5
4
3
2
1
0
ppm
200
190
180
170
160
150
140
130
120
110
100
90
80
70
60
50
40
30
20
10
0
ppm

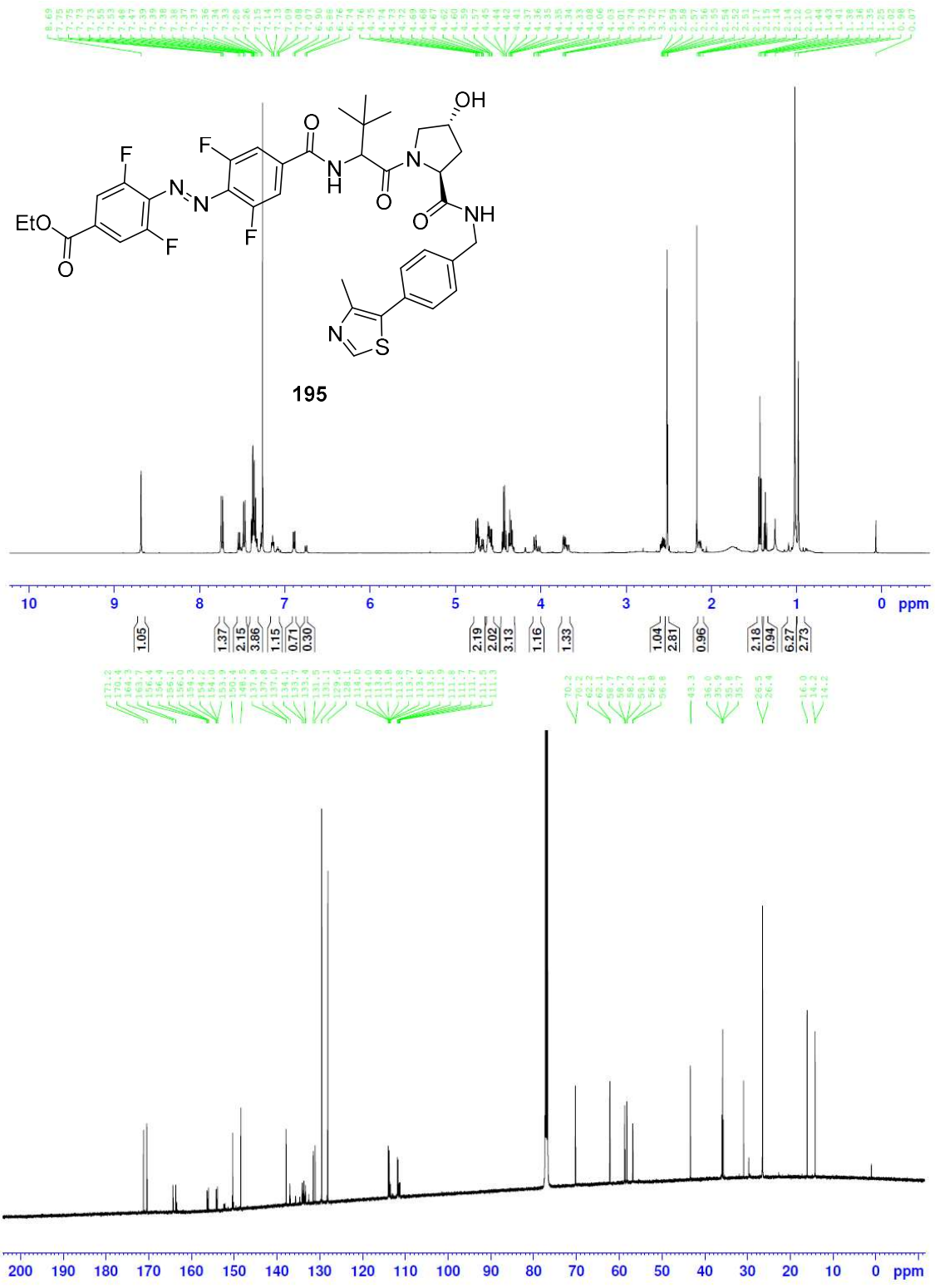
EtO
O
F
F
F
F
N
N
O
N
H
O
N
O
OH
NH
N
S
195
10 9 8 7 6 5 4 3 2 1 0 ppm
200 190 180 170 160 150 140 130 120 110 100 90 80 70 60 50 40 30 20 10 0 ppm

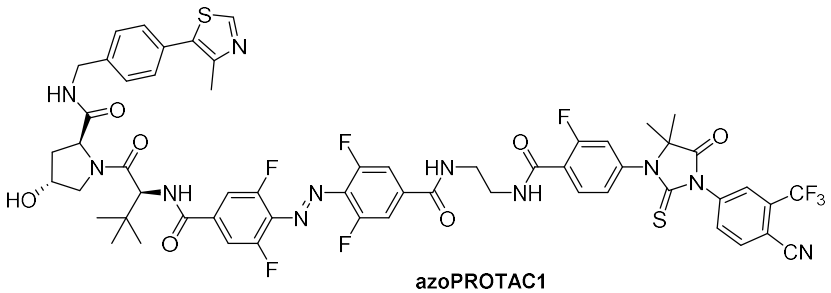

azoPROTAC1

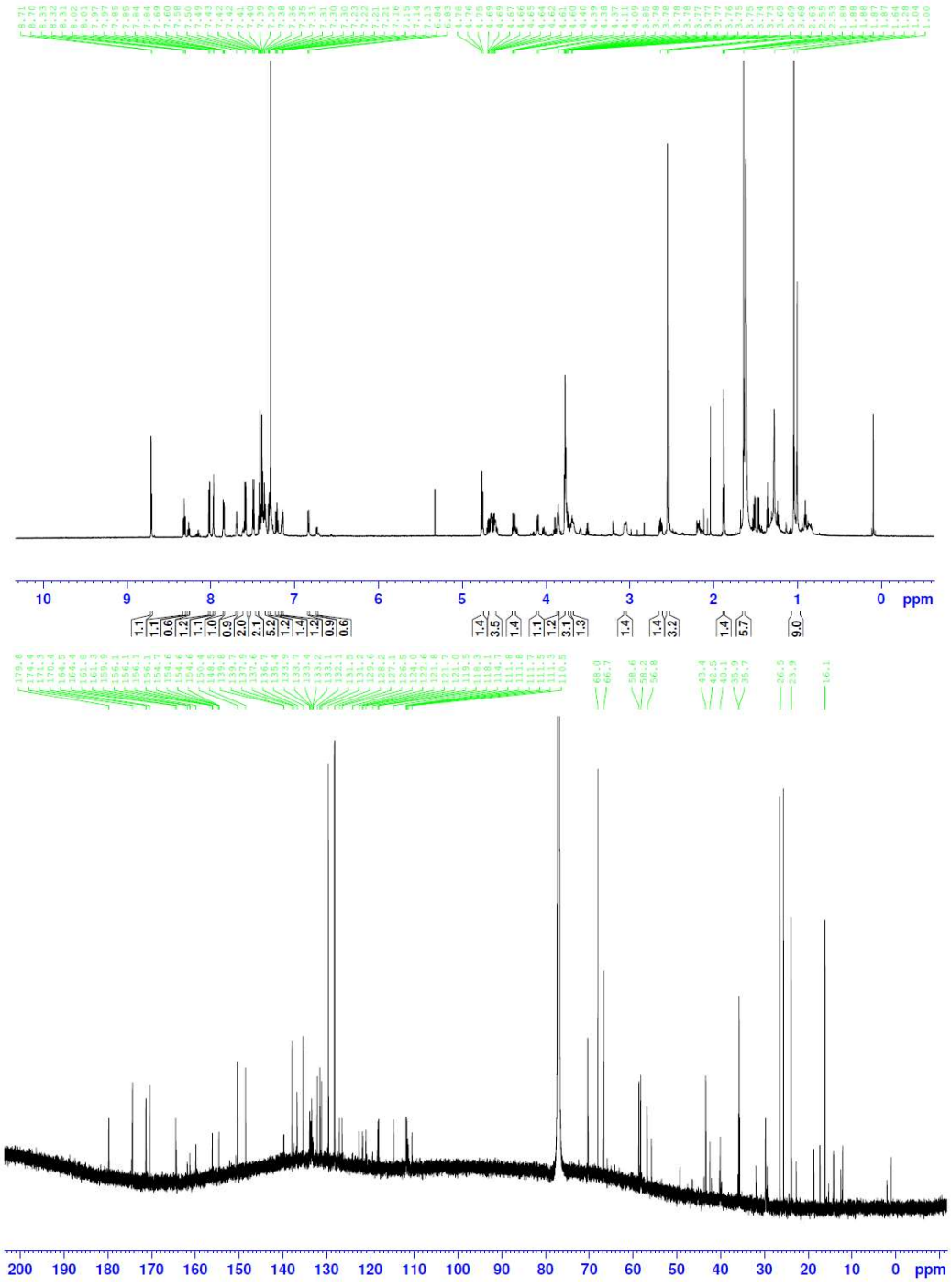

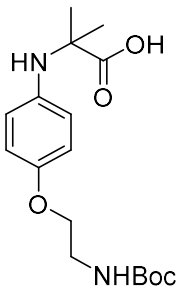
HN
OH
O
O
NHBoc

199

7.14
7.11
6.96
6.94
4.86
4.01
3.96
3.98
3.42
3.41
3.39
3.31
3.31
3.30
3.30
3.30
1.44
1.41
10 9 8 7 6 5 4 3 2 1 0 ppm
2.0
2.0
2.0
2.0
9.0
5.8
176.1
157.2
157.1
130.2
123.7
114.9
78.8
67.0
63.7
39.5
27.3
22.9
200 190 180 170 160 150 140 130 120 110 100 90 80 70 60 50 40 30 20 10 0 ppm

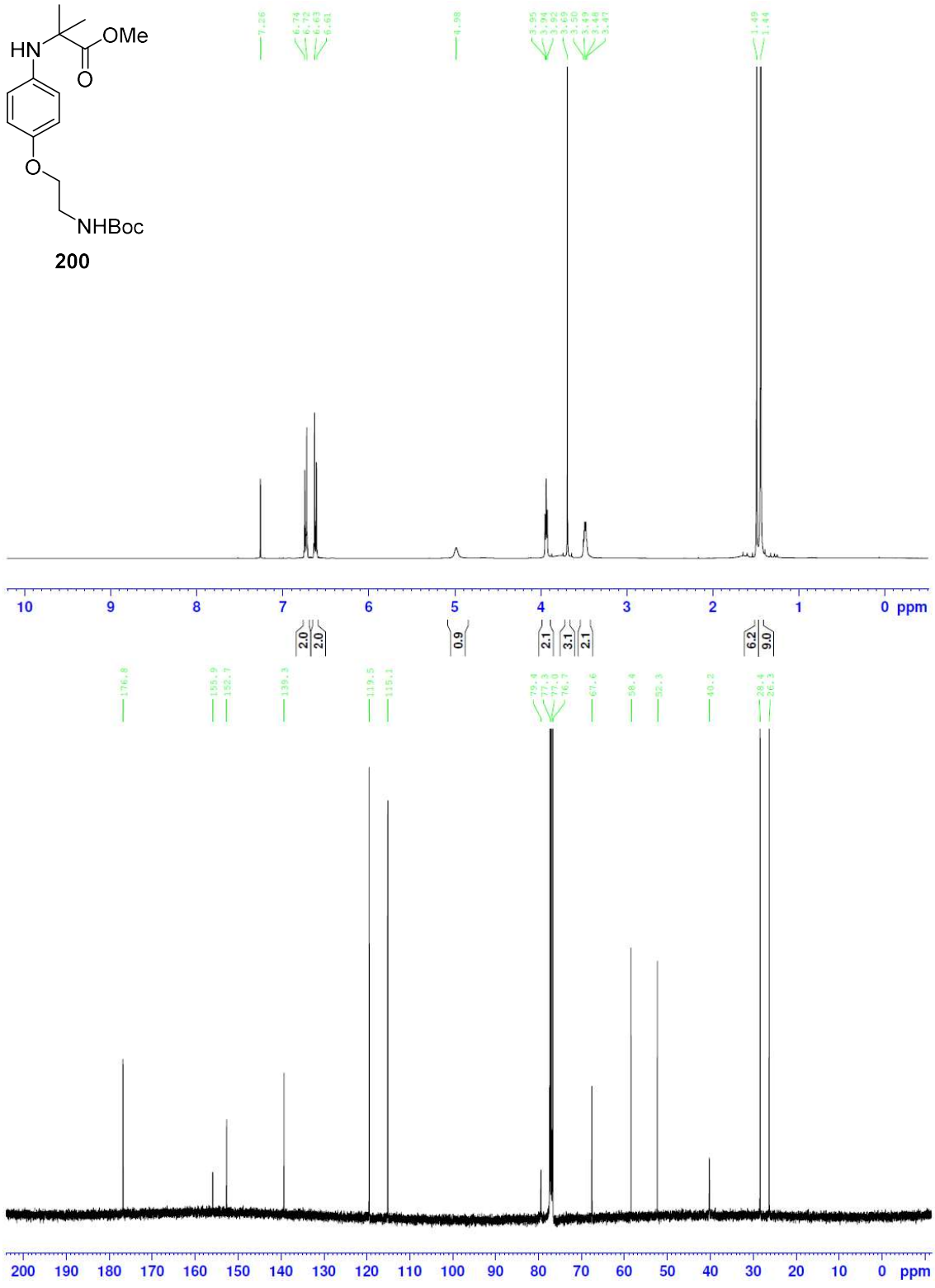
HN
OMe
O
O
NHBoc
200
7.26
6.74
6.72
6.63
6.61
4.98
3.95
3.94
3.92
3.69
3.50
3.49
3.48
3.47
1.49
1.44
10 9 8 7 6 5 4 3 2 1 0 ppm
2.0
2.0
0.9
2.1
3.1
2.1
6.2
9.0
176.8
155.9
152.7
139.3
119.5
115.1
79.4
77.3
77.0
76.7
67.6
58.4
52.3
40.2
28.4
26.3
200 190 180 170 160 150 140 130 120 110 100 90 80 70 60 50 40 30 20 10 0 ppm

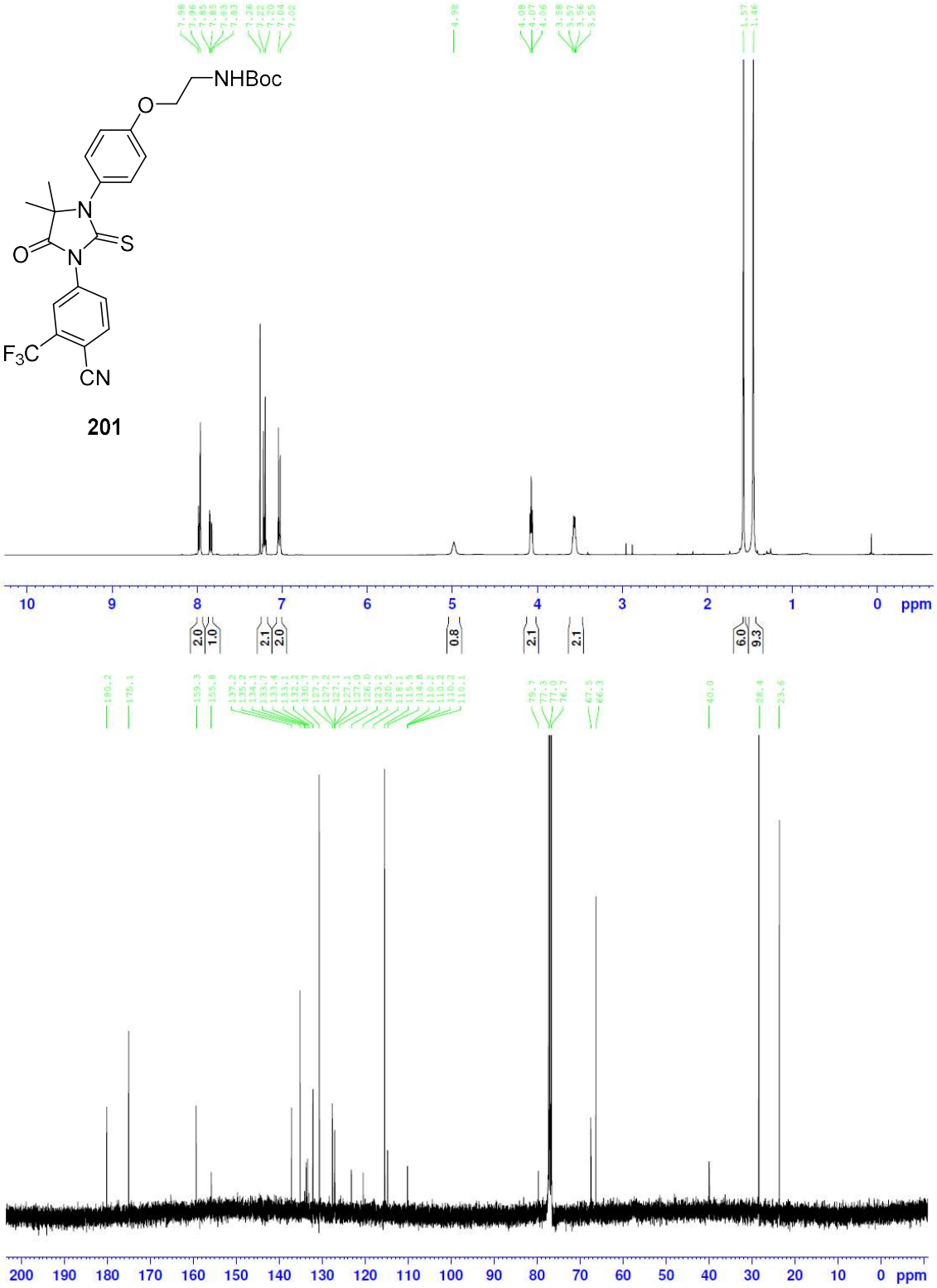
NHBoc
O
N
O
N
S
F3C
CN
201
ppm
ppm

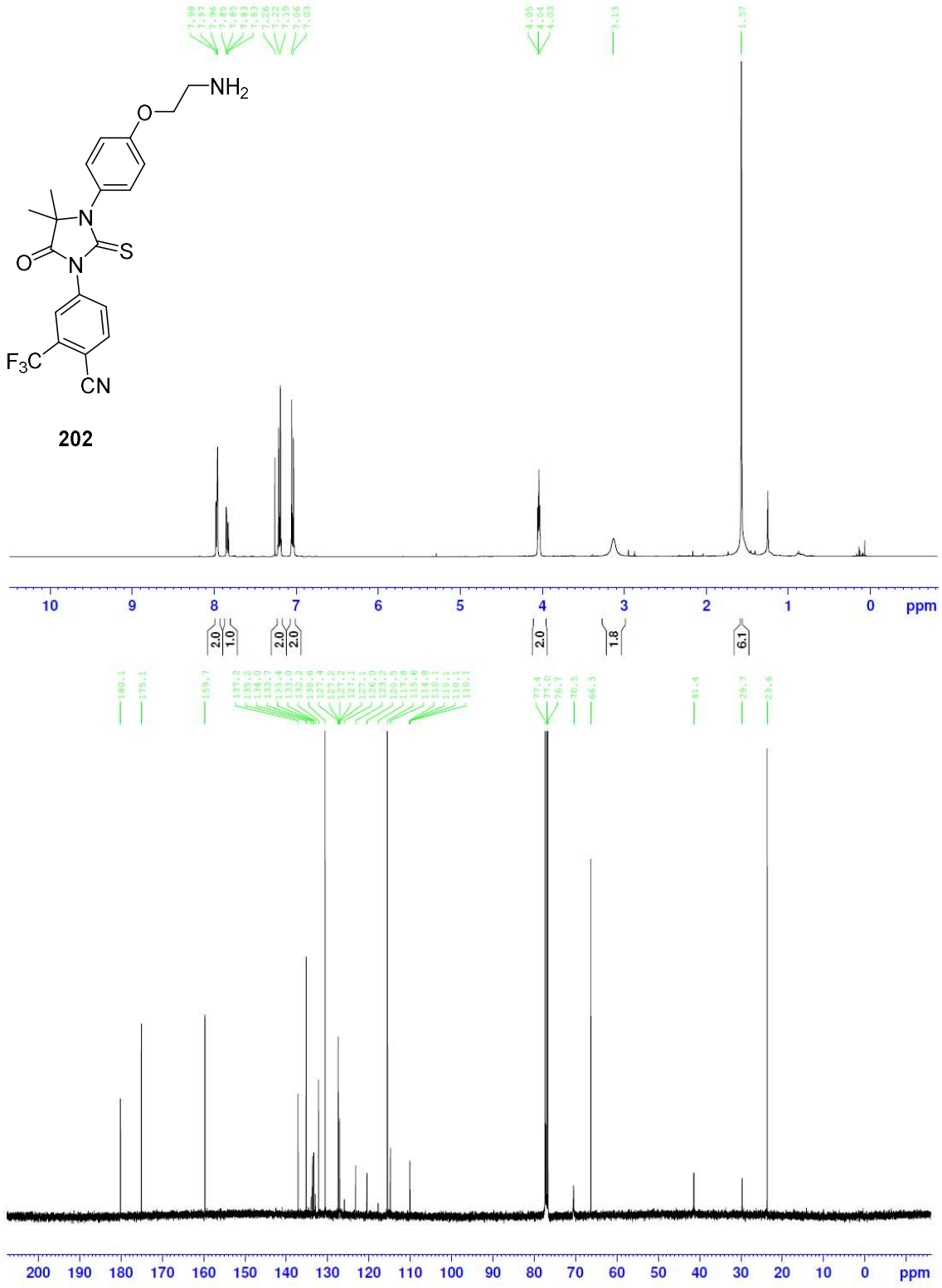
NH2
O
N
O
N
S
F3C
CN
202
ppm
ppm

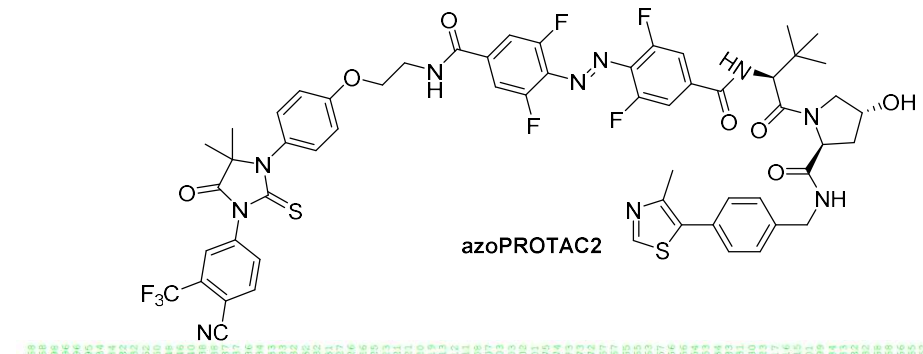
azoPROTAC2

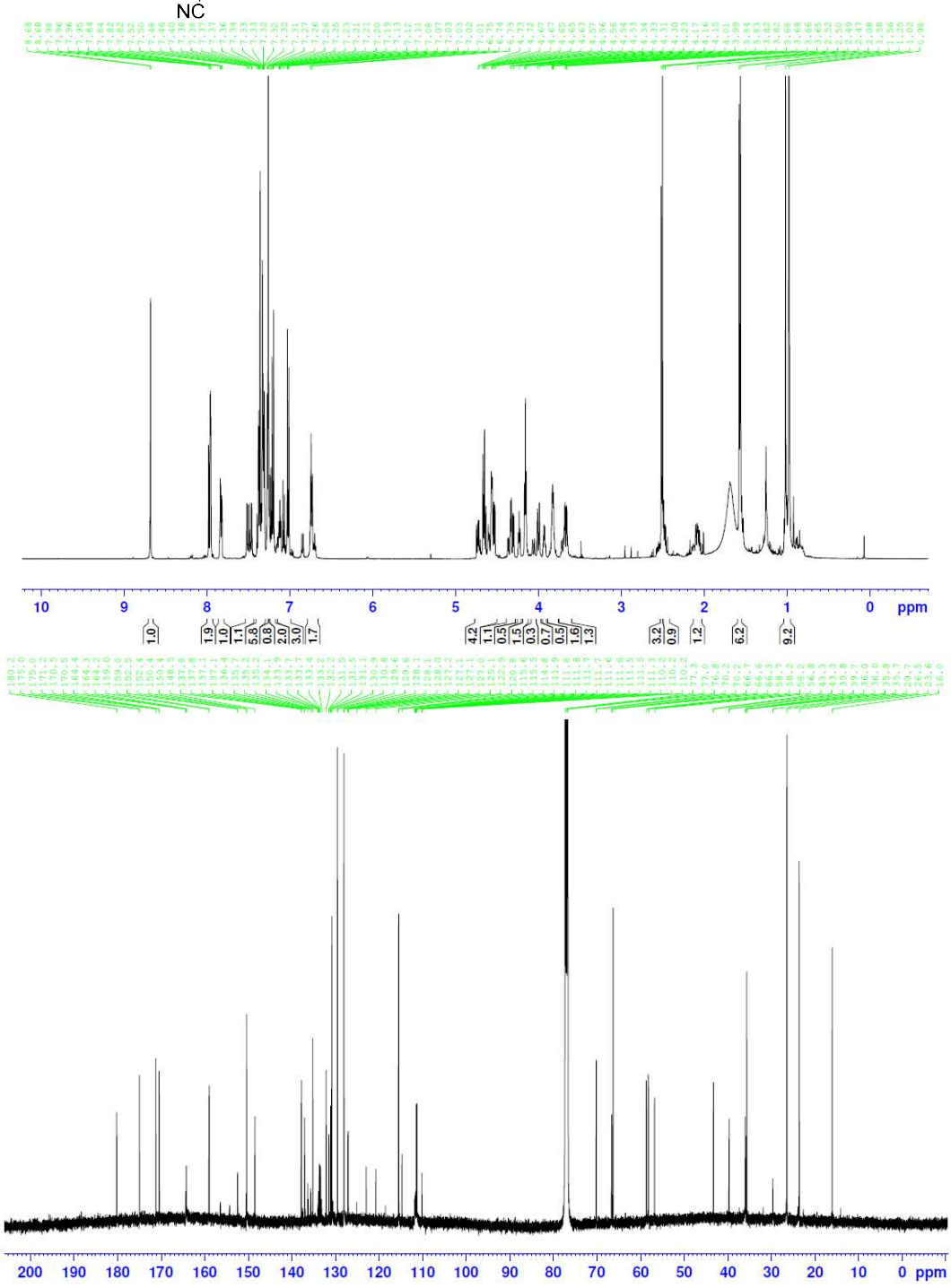
10 9 8 7 6 5 4 3 2 1 0 ppm
200 190 180 170 160 150 140 130 120 110 100 90 80 70 60 50 40 30 20 10 0 ppm

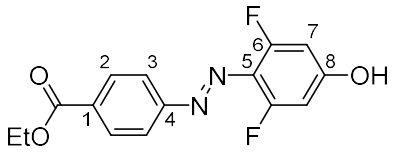
F
7
6
5
8
OH
2
3
O
N
N
1
4
EtO
F

209

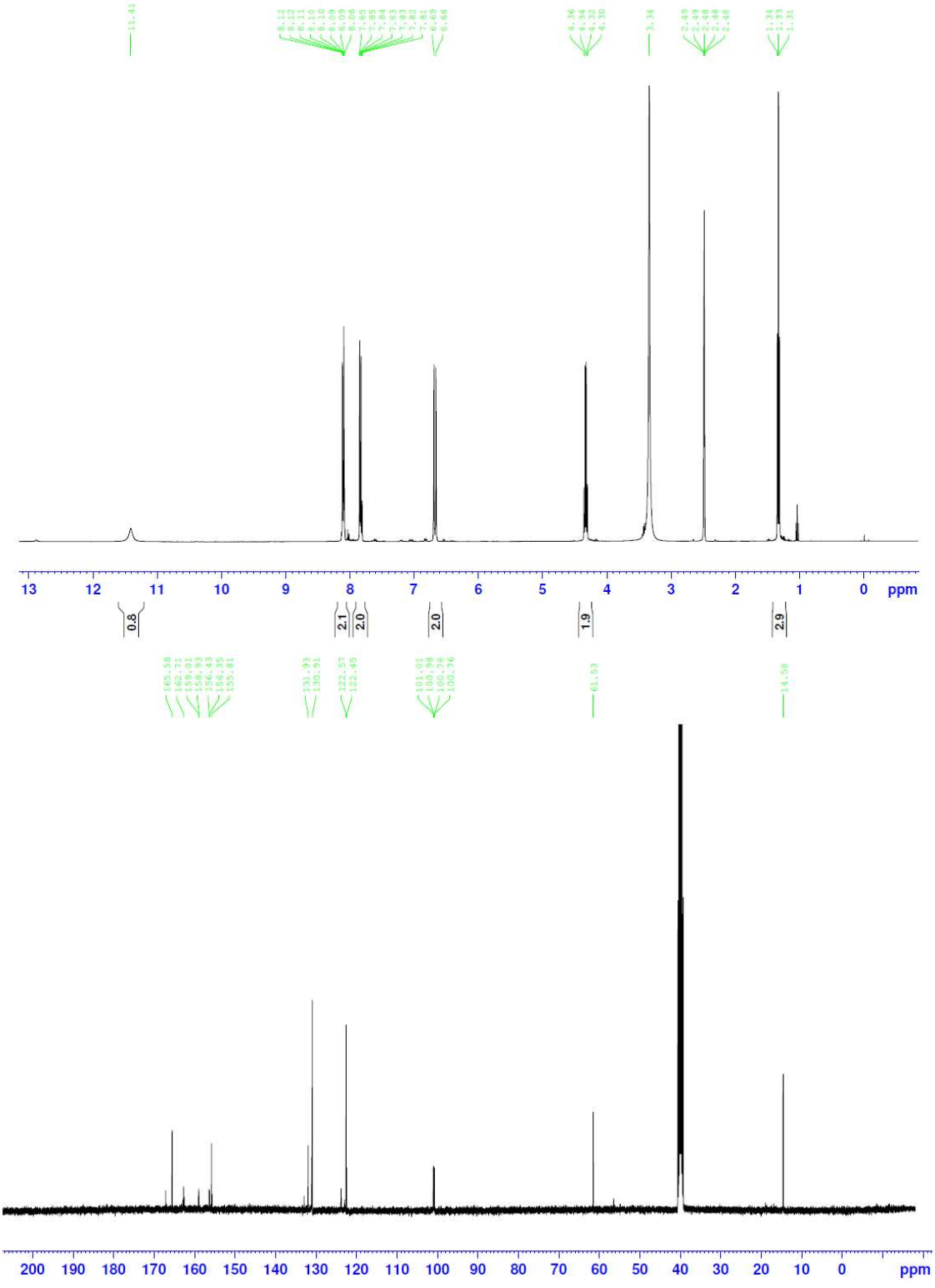
13
12
11
10
9
8
7
6
5
4
3
2
1
0
ppm
0.8
2.1
2.0
2.0
1.9
2.9
200
190
180
170
160
150
140
130
120
110
100
90
80
70
60
50
40
30
20
10
0
ppm

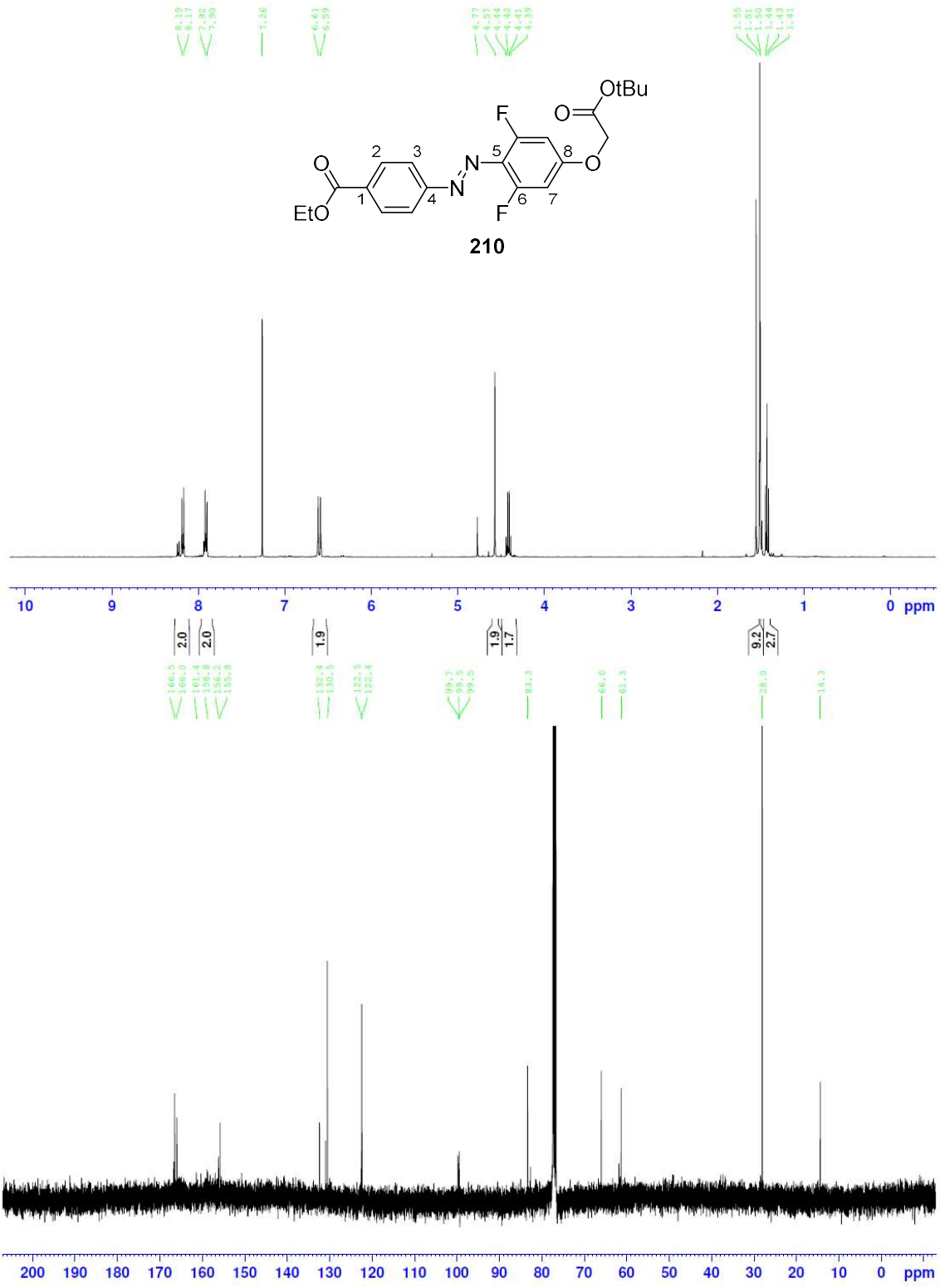

210

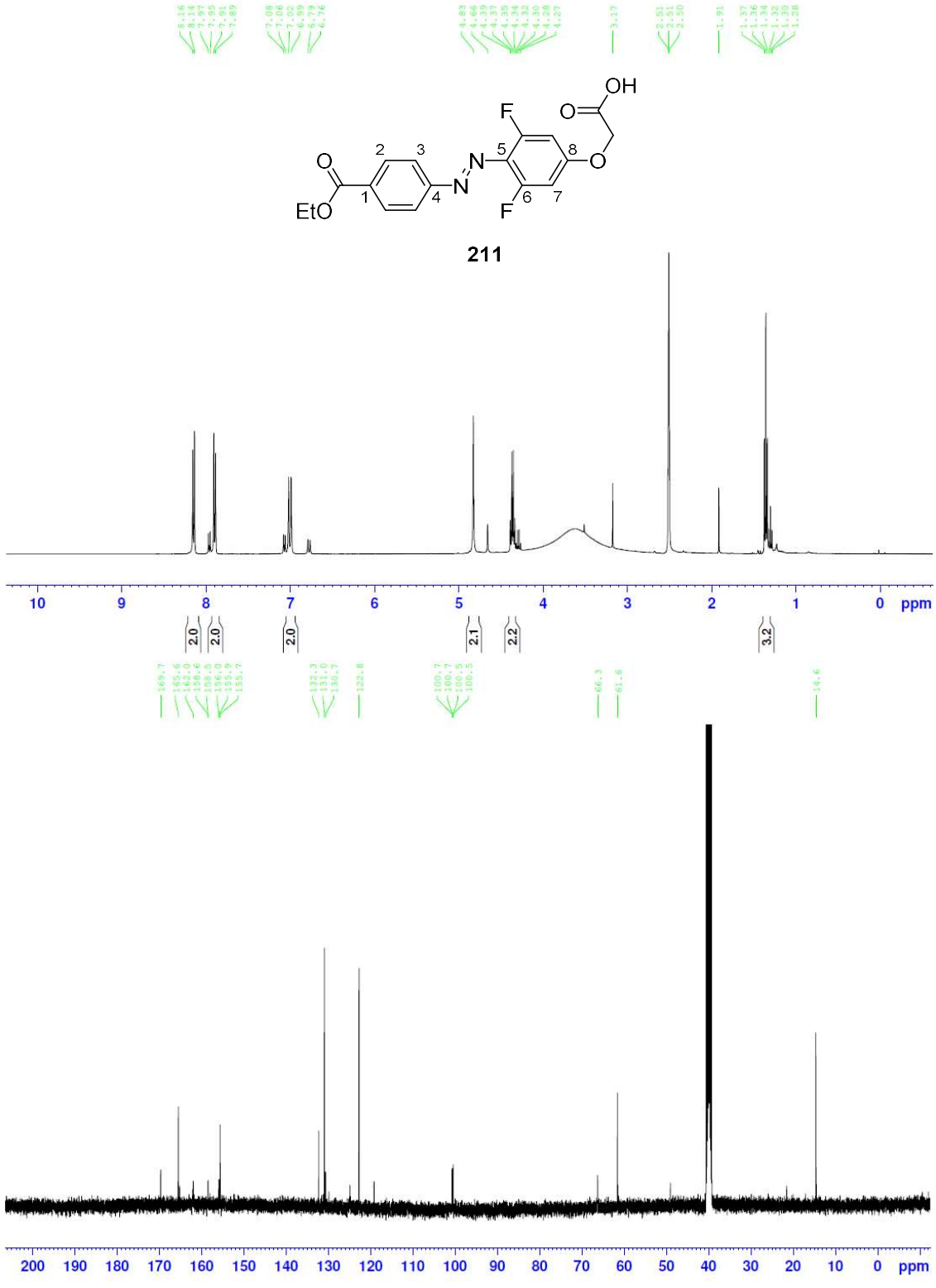
OH
O
F
O
2
3
5
8
O
N
N
O
1
4
6
7
EtO
F
211
10
9
8
7
6
5
4
3
2
1
0
ppm
2.0
2.0
2.0
2.1
2.2
3.2
200
190
180
170
160
150
140
130
120
110
100
90
80
70
60
50
40
30
20
10
0
ppm

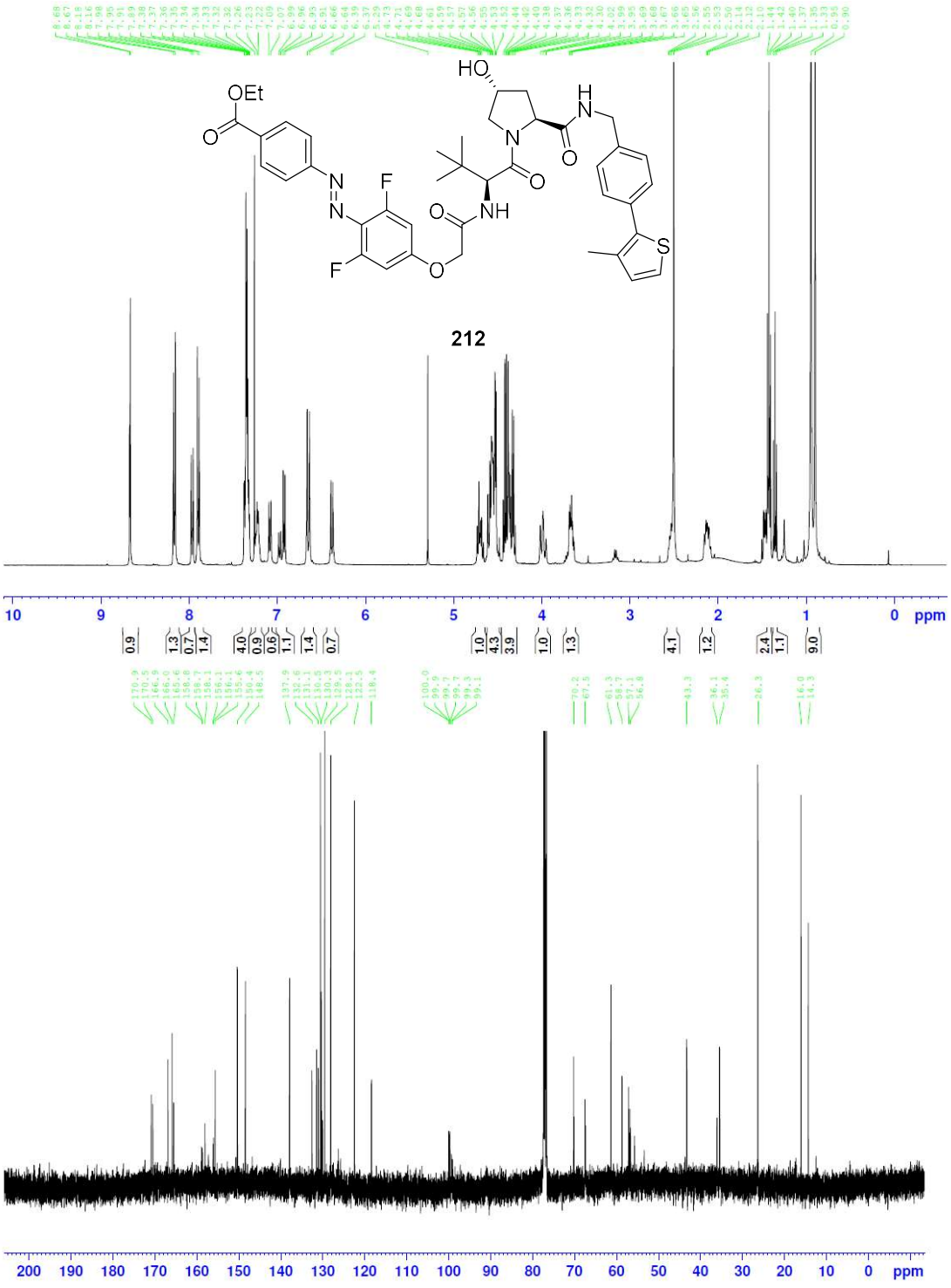
HO
OEt
O
N
F
H
N
O
N
O
O
NH
F
O
S
212
10 9 8 7 6 5 4 3 2 1 0 ppm
200 190 180 170 160 150 140 130 120 110 100 90 80 70 60 50 40 30 20 10 0 ppm

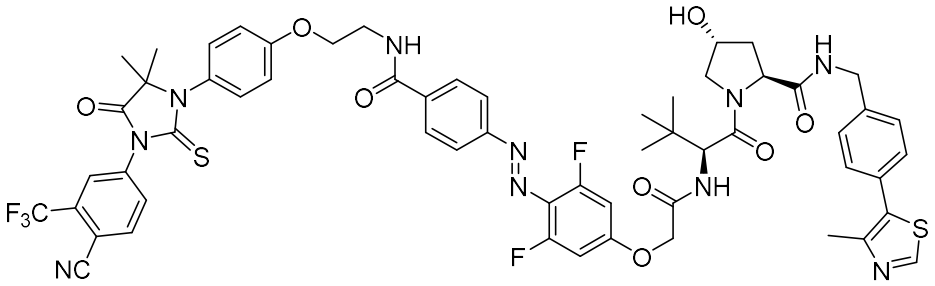
HO
H
N
O
NH
O
N
O
O
N
S
F3C
NC
N
N
F
F
O
O
NH
S
N

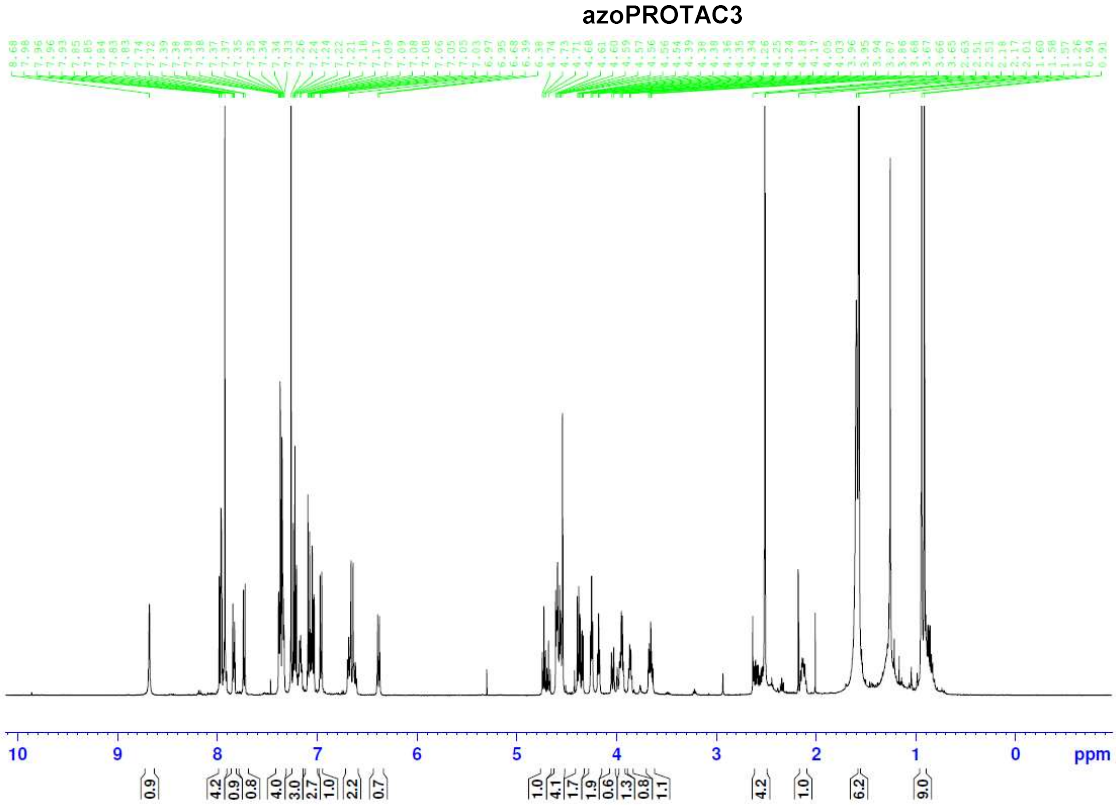
azoPROTAC3
10
9
8
7
6
5
4
3
2
1
0
ppm

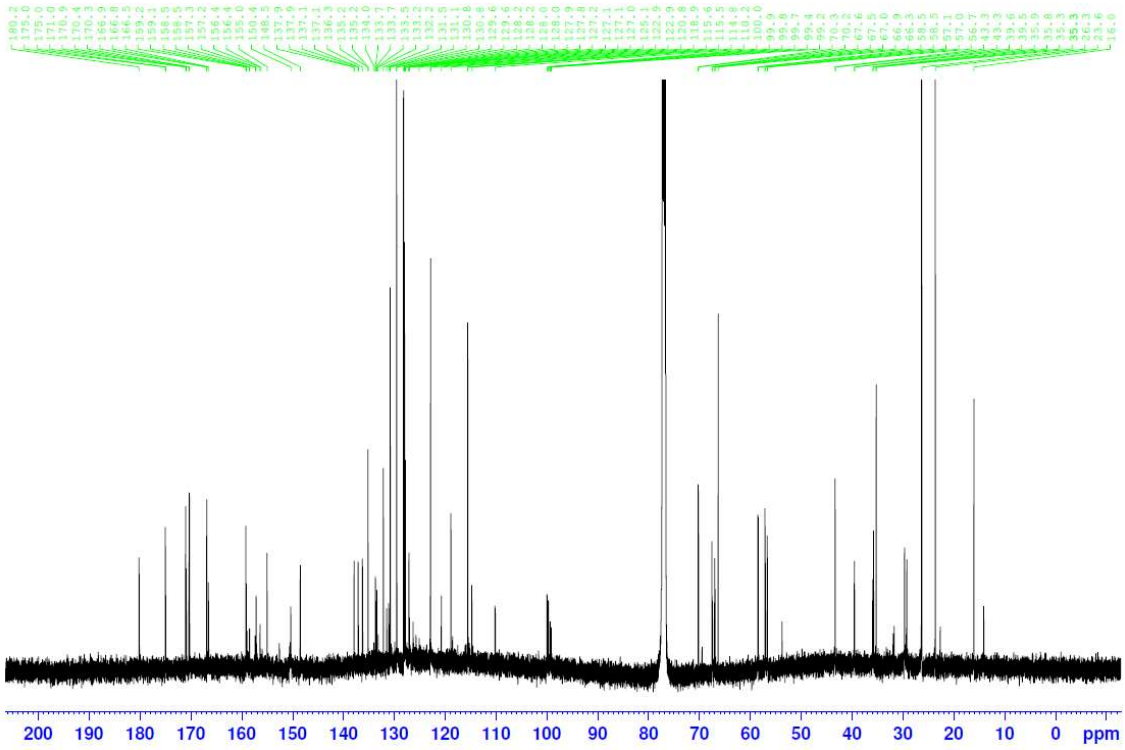
200 190 180 170 160 150 140 130 120 110 100 90 80 70 60 50 40 30 20 10 0 ppm

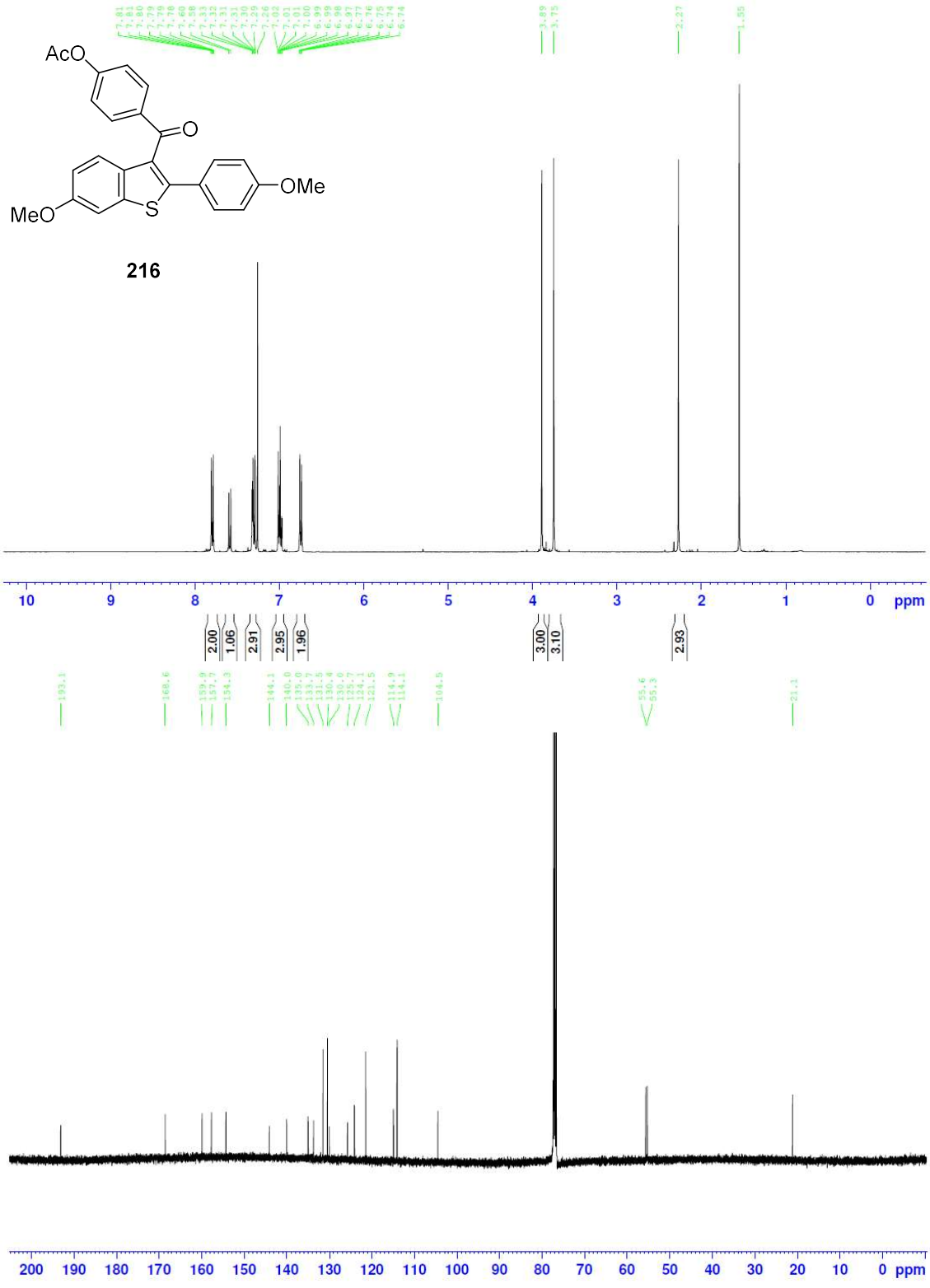
AcO
O
OMe
MeO
S
216
ppm
ppm

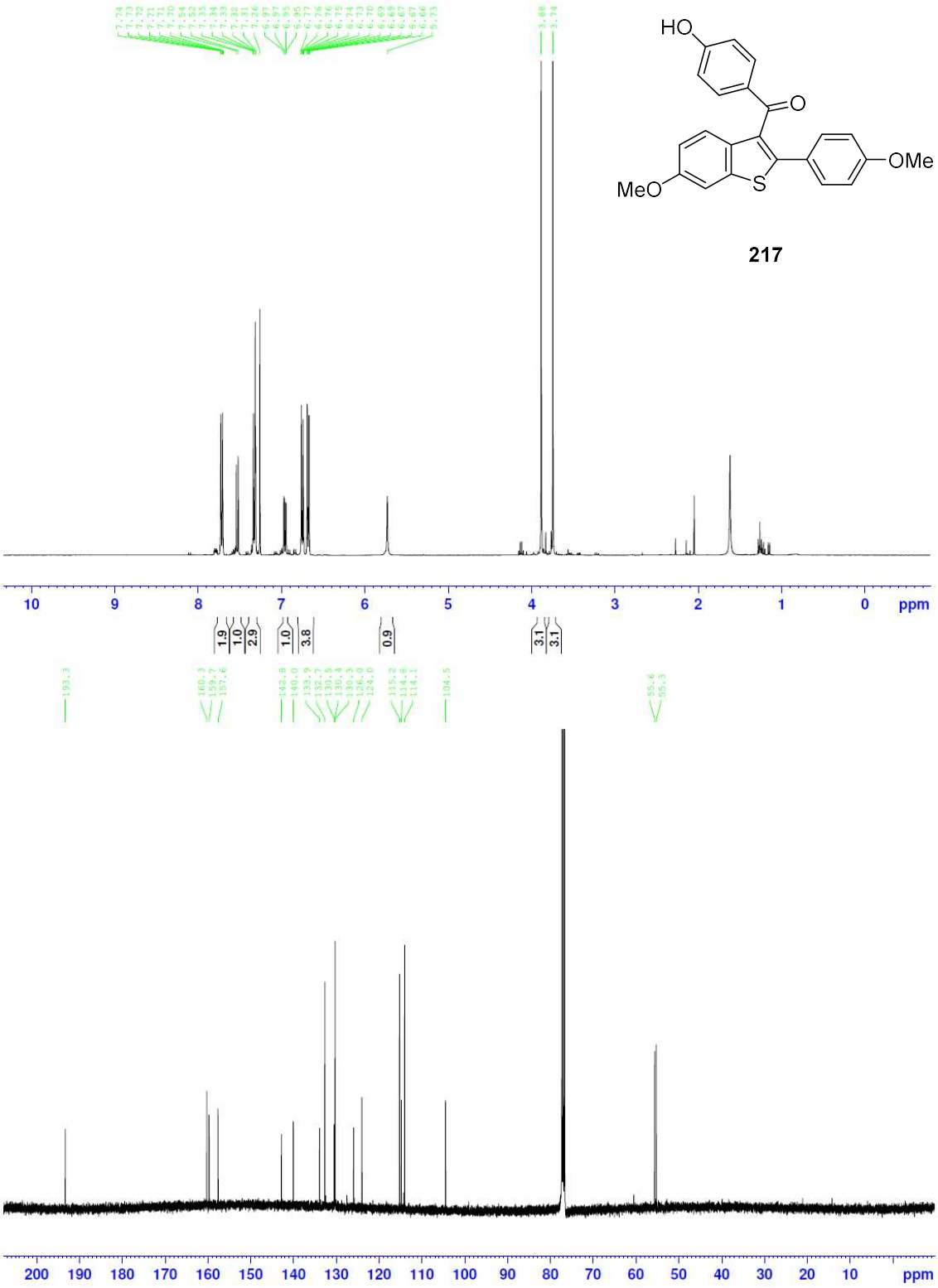
HO
O
OMe
MeO
S
217
ppm
ppm

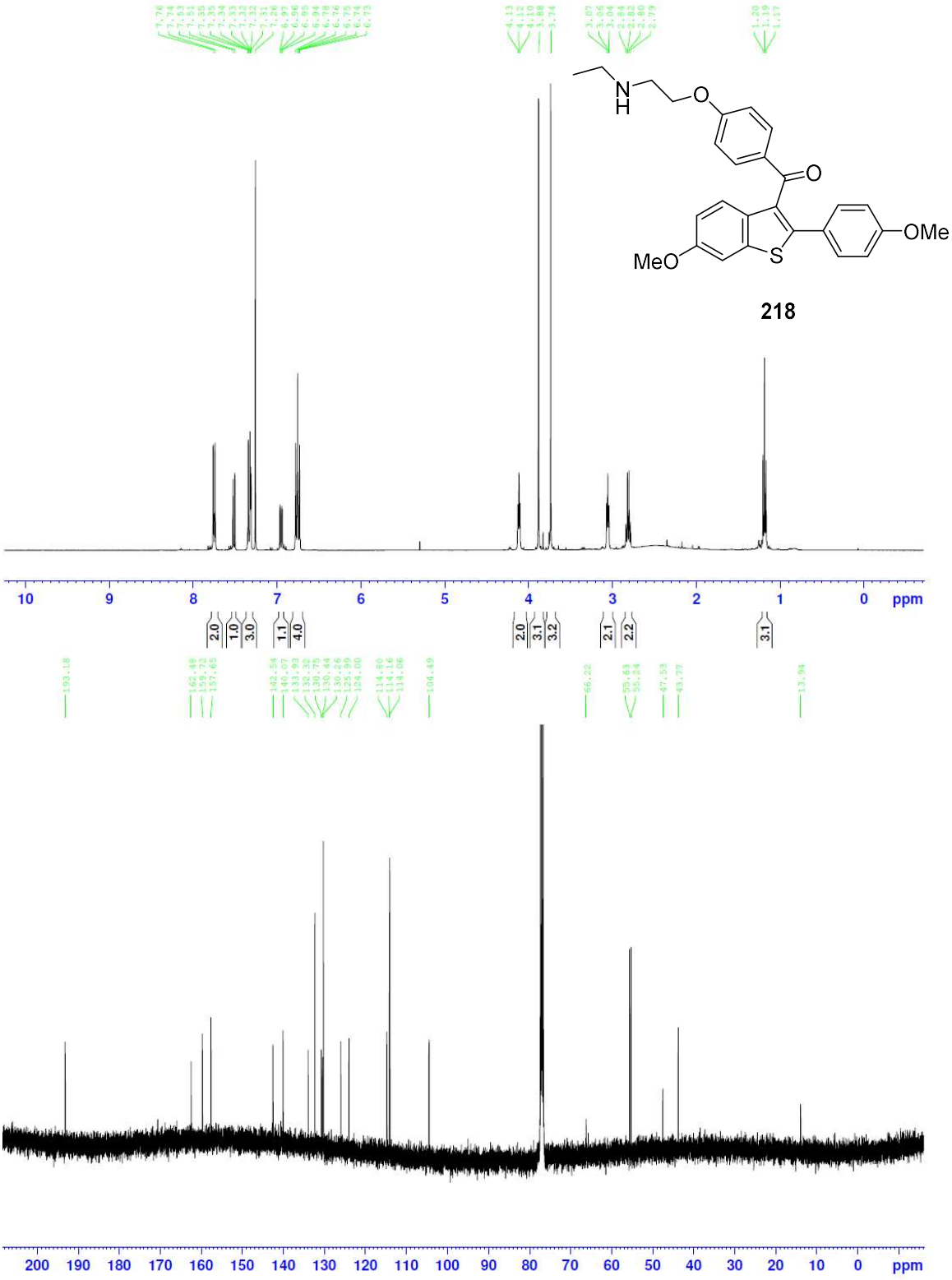
N
H
O
O
MeO
S
OMe
218
ppm
ppm

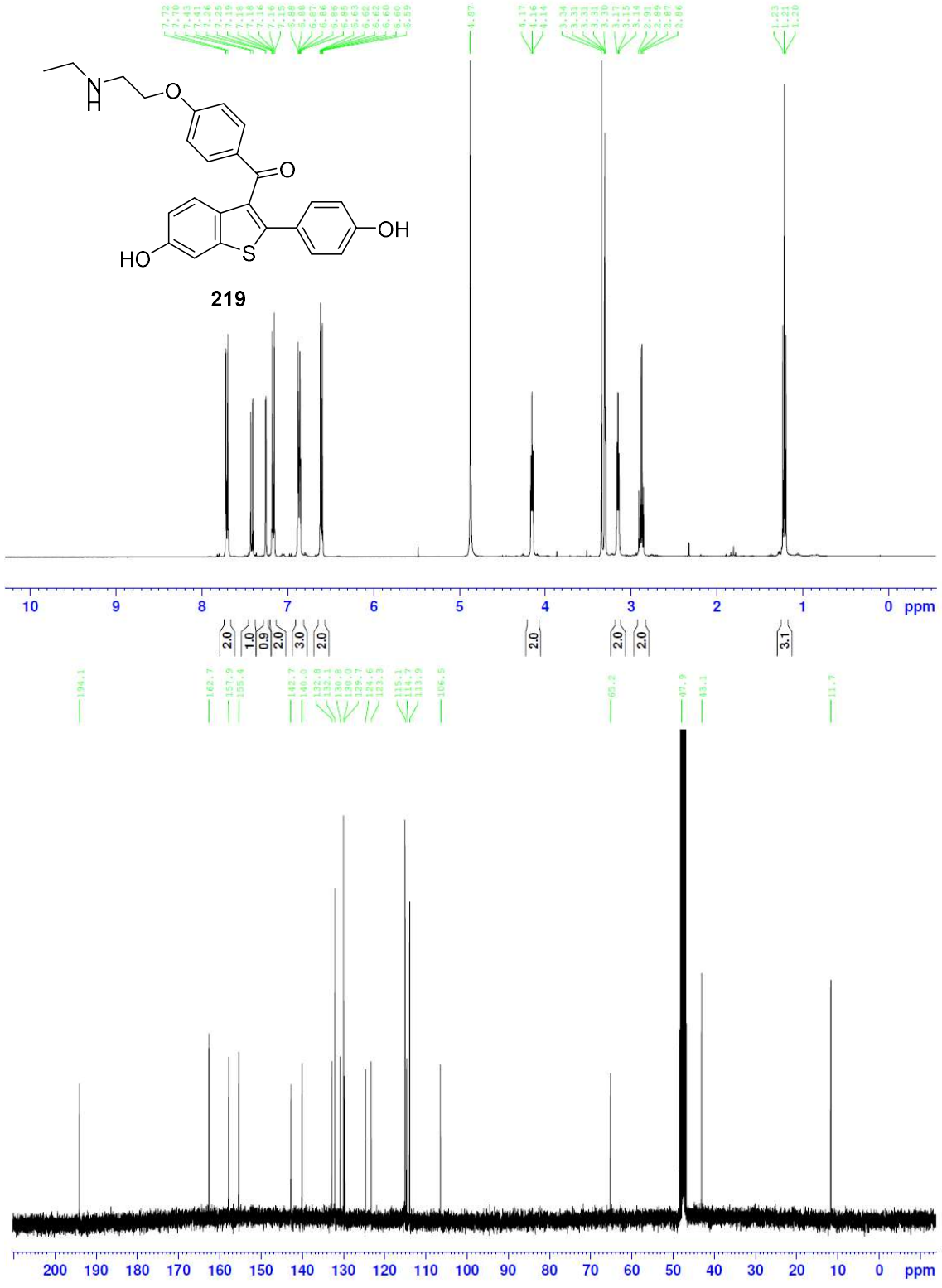
N
H
O
O
OH
HO
S
219
10 9 8 7 6 5 4 3 2 1 0 ppm
200 190 180 170 160 150 140 130 120 110 100 90 80 70 60 50 40 30 20 10 0 ppm

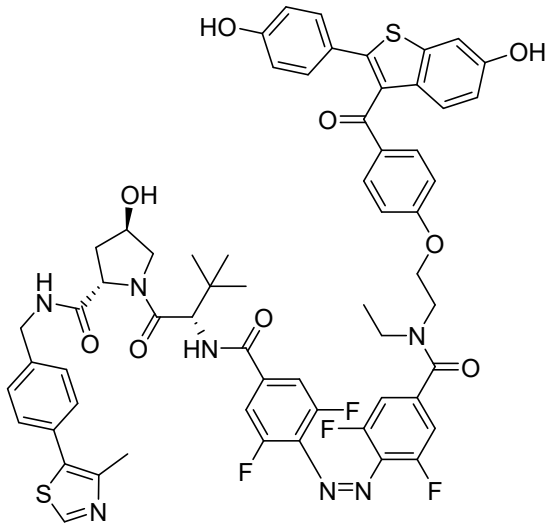
HO
S
OH
O
OH
O
H
N
N
O
O
HN
O
N
O
F
F
F
S
N
N=N
F

azoPROTAC4

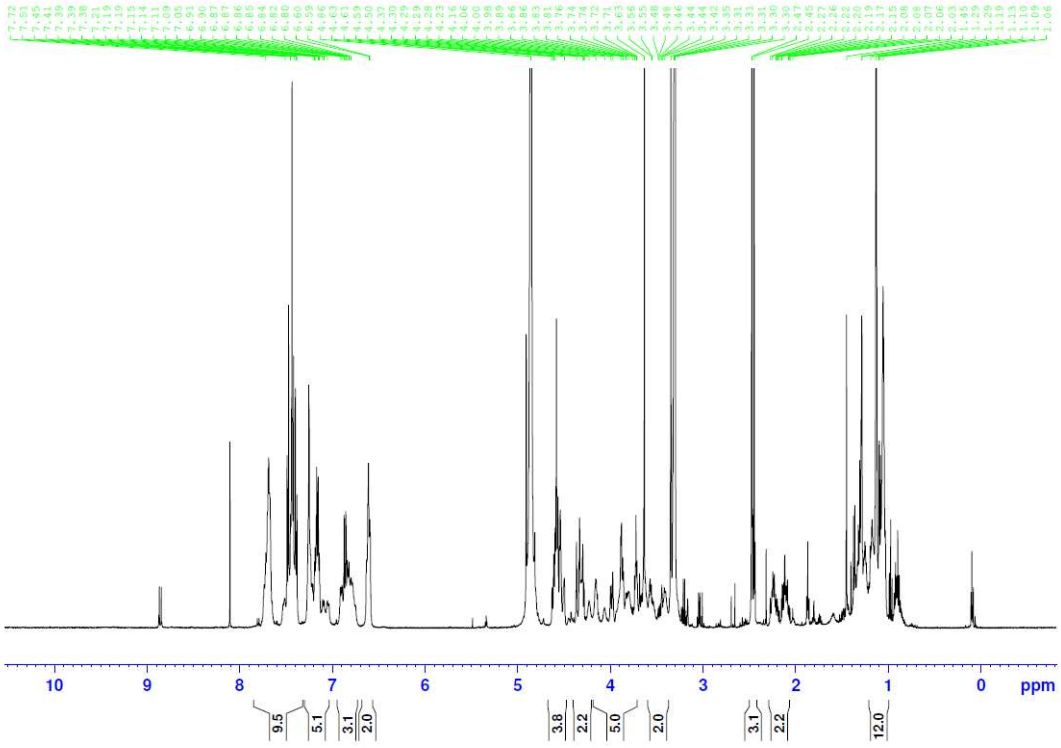
10
9
8
7
6
5
4
3
2
1
0
ppm
9.5
5.1
3.1
2.0
3.8
2.2
5.0
2.0
3.1
2.2
12.0

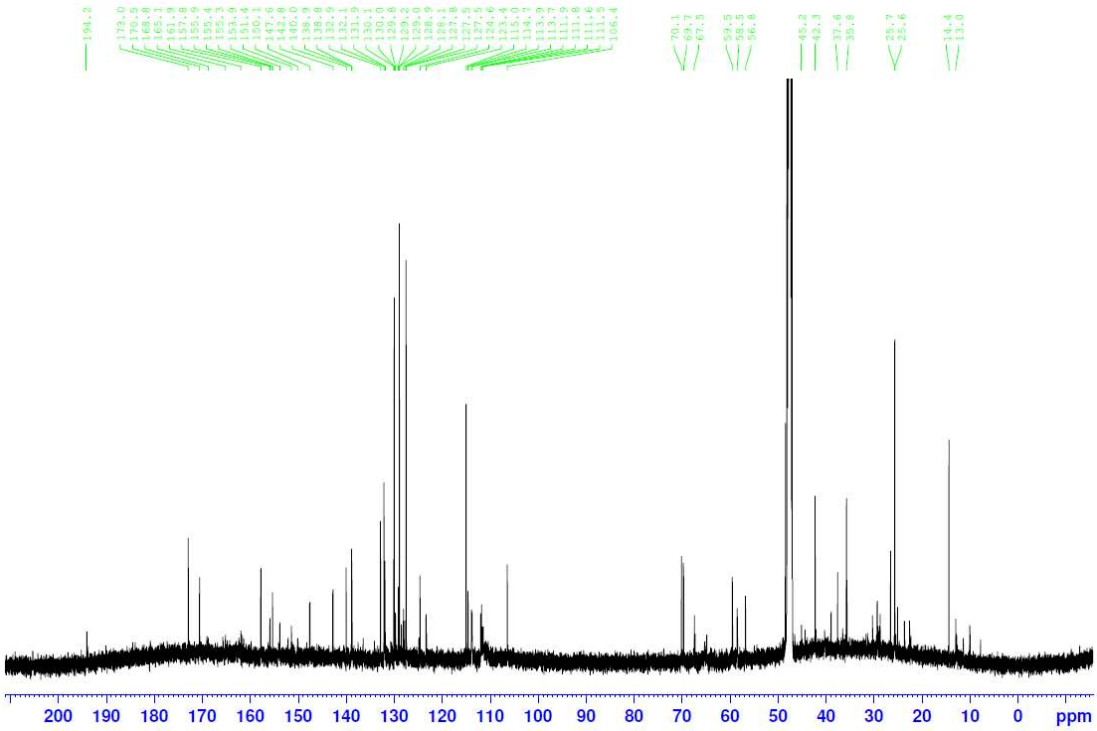
194.2
173.0
170.5
169.8
165.1
161.9
157.8
155.9
155.4
153.9
151.4
150.1
147.6
142.8
140.0
138.9
132.9
132.1
131.9
130.1
130.0
129.8
129.2
128.9
128.1
127.8
127.5
127.5
124.6
123.4
115.0
114.7
113.9
113.7
111.9
111.8
111.6
111.5
106.4
70.1
69.7
67.5
59.5
55.5
55.4
45.2
42.3
37.6
35.8
25.7
25.6
14.4
13.0
200 190 180 170 160 150 140 130 120 110 100 90 80 70 60 50 40 30 20 10 0 ppm

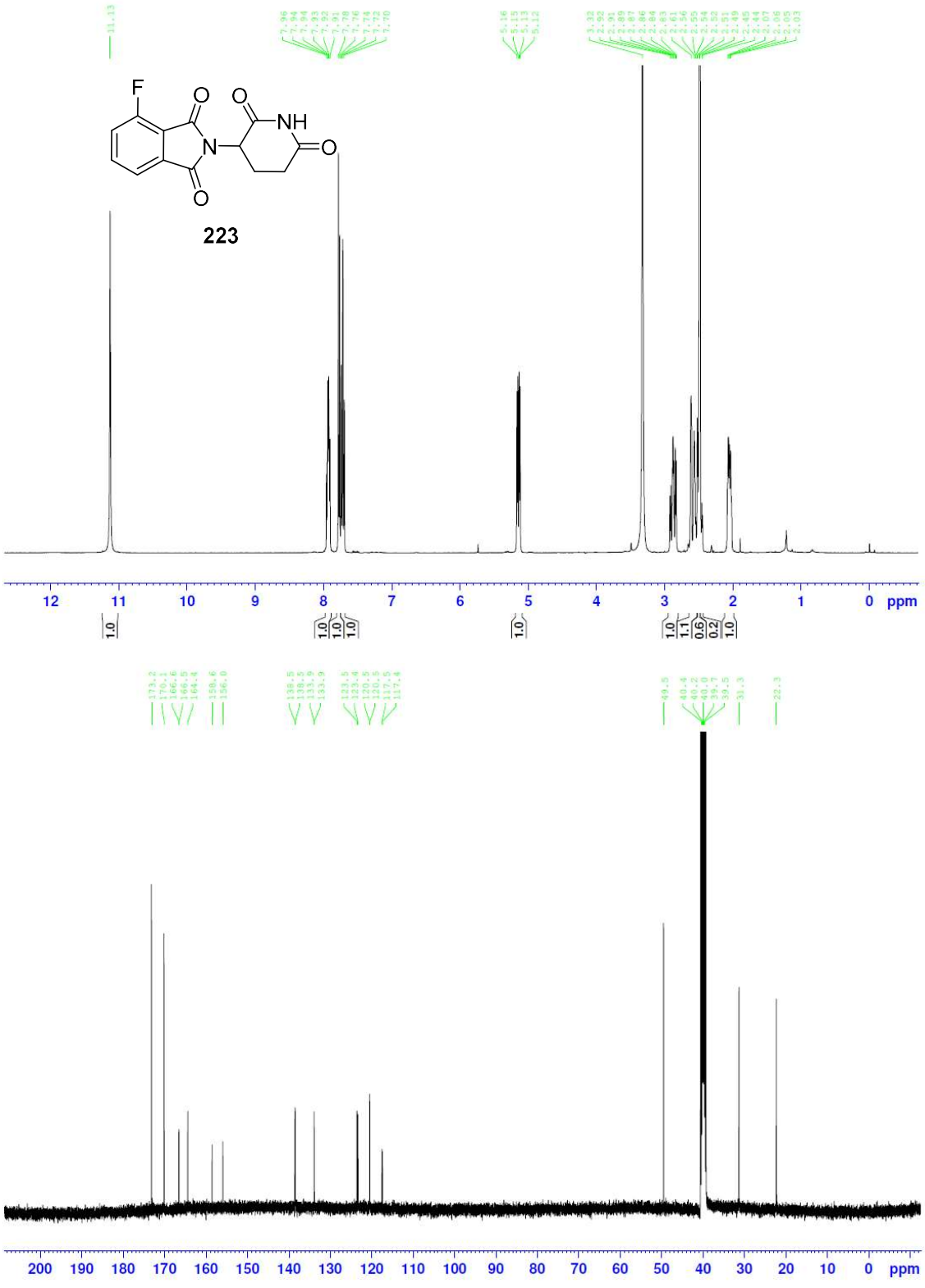
F
O
O
NH
N
O
O
223
11.13
7.96
7.94
7.84
7.83
7.92
7.91
7.78
7.76
7.74
7.72
7.70
5.16
5.15
5.13
5.12
3.32
2.92
2.91
2.89
2.87
2.86
2.84
2.83
2.61
2.56
2.55
2.54
2.52
2.51
2.49
2.45
2.44
2.07
2.06
2.05
2.03
12 11 10 9 8 7 6 5 4 3 2 1 0 ppm
1.0
1.0
1.0
1.0
1.0
1.0
1.1
0.6
0.2
1.0
173.2
170.1
166.6
166.5
164.4
158.6
156.0
136.5
136.5
133.9
133.9
123.5
123.4
120.5
120.5
117.5
117.4
49.5
40.4
40.2
40.0
39.7
39.5
31.3
22.3
200 190 180 170 160 150 140 130 120 110 100 90 80 70 60 50 40 30 20 10 0 ppm

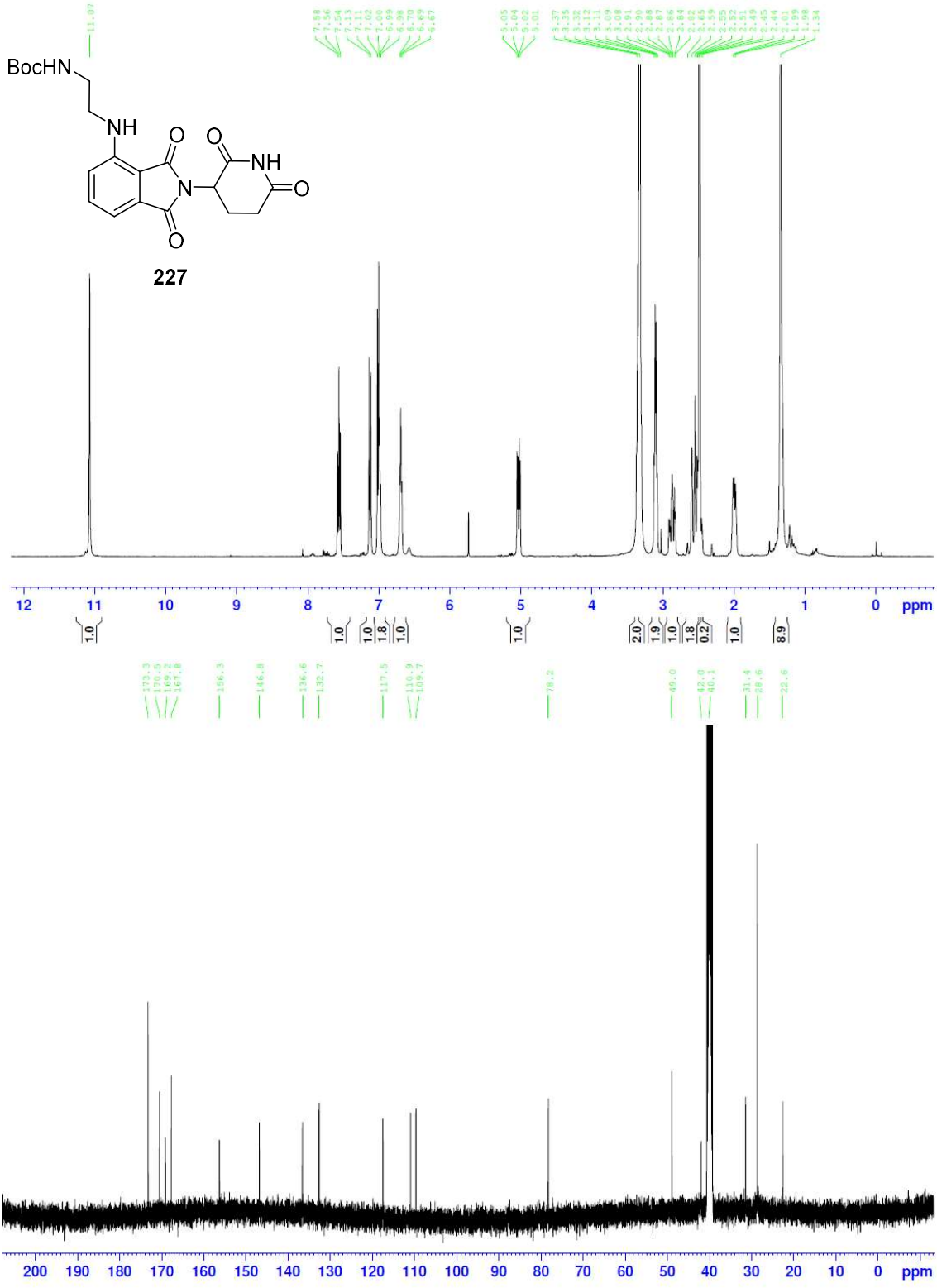
BocHN
NH
O
O
NH
N
O
O
227
ppm
ppm

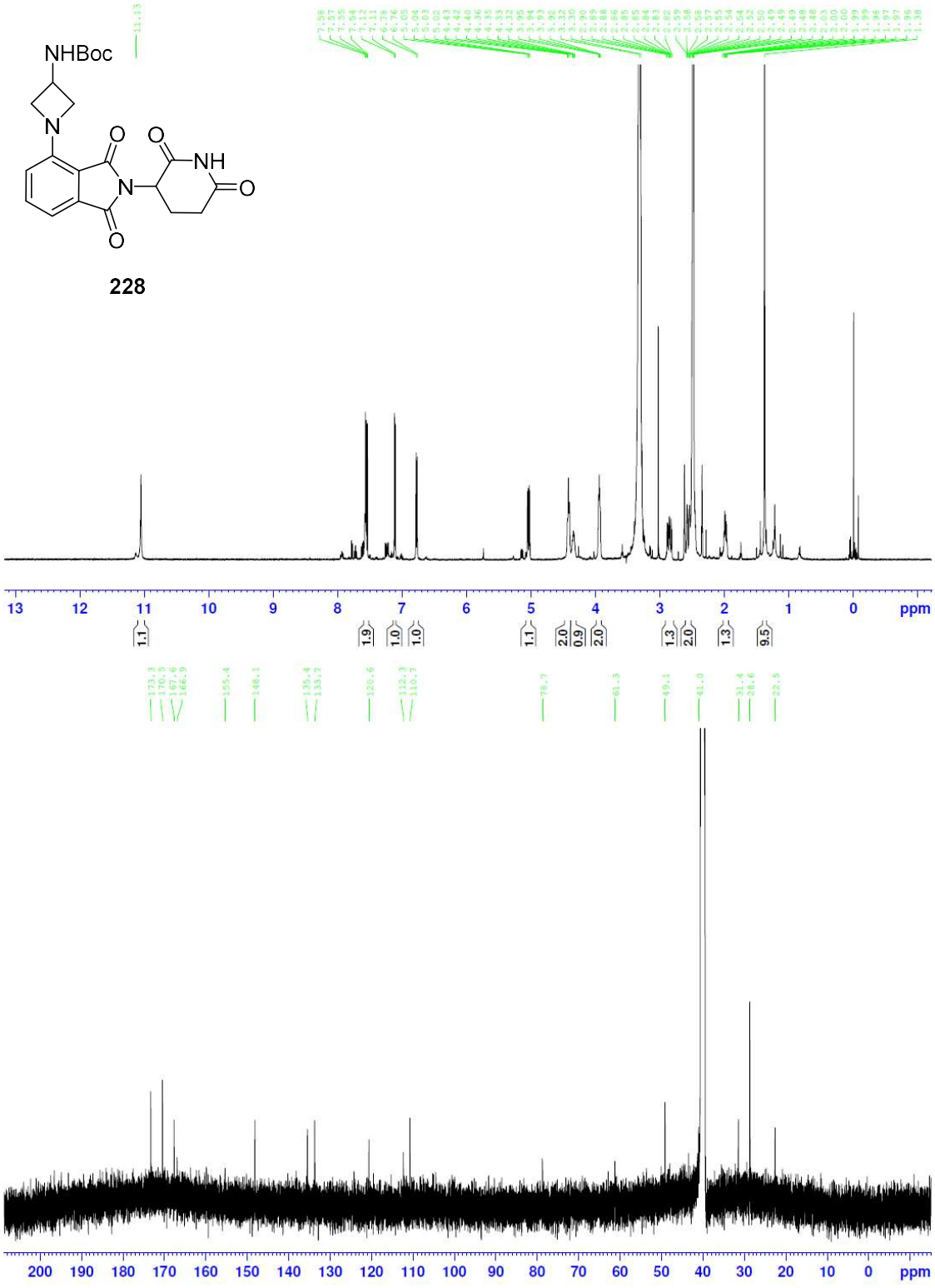
NHBoc
N
O
O
NH
N
O
O
228
13
12
11
10
9
8
7
6
5
4
3
2
1
0
ppm
200
190
180
170
160
150
140
130
120
110
100
90
80
70
60
50
40
30
20
10
0
ppm

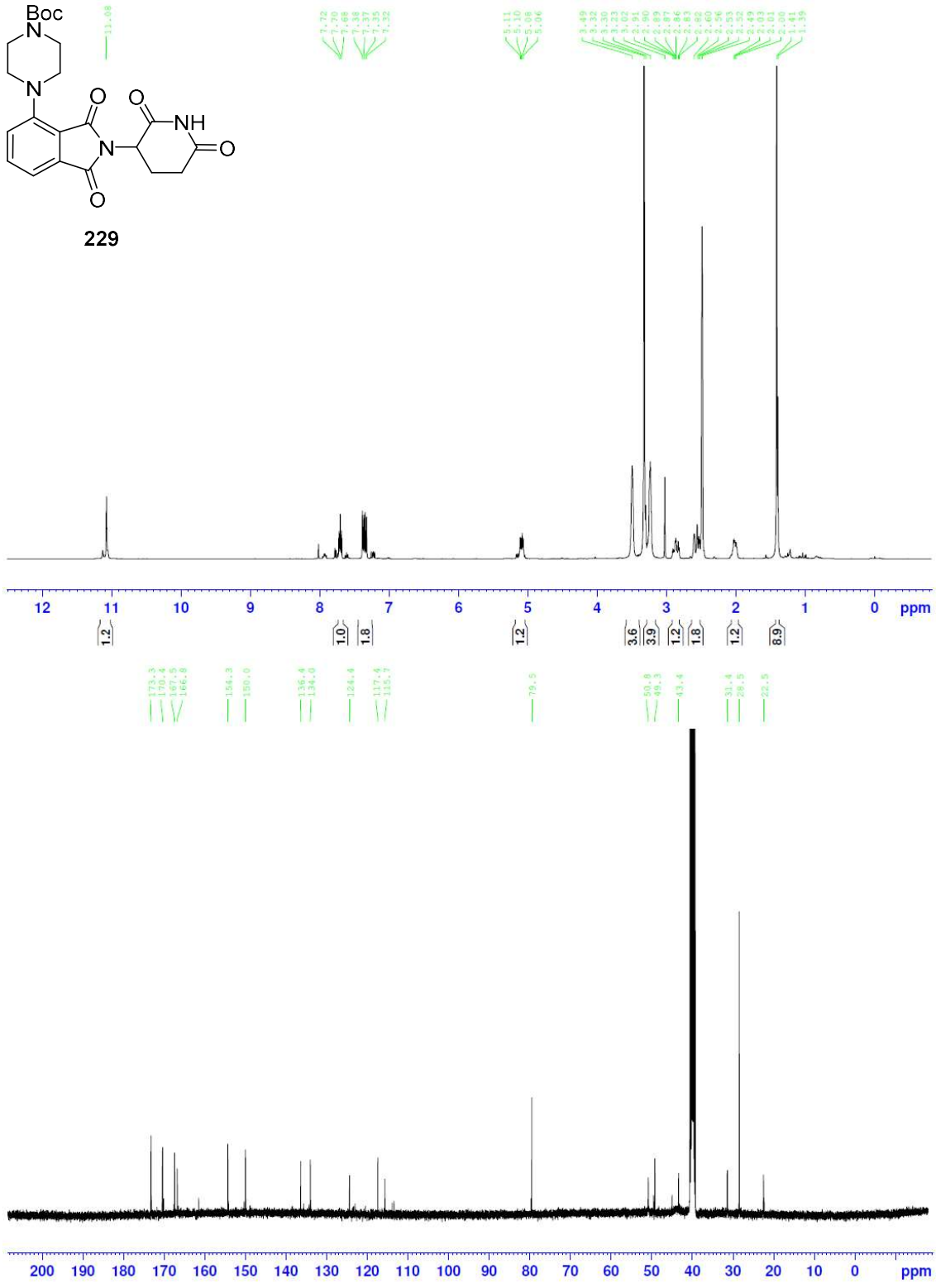
Boc
N
N
O
O
NH
N
O
O
O
229
11.08
7.72
7.70
7.68
7.38
7.37
7.35
7.32
5.11
5.10
5.08
5.06
3.49
3.32
3.30
3.23
3.02
2.91
2.90
2.89
2.87
2.86
2.83
2.82
2.60
2.56
2.53
2.52
2.49
2.03
2.01
2.00
1.44
1.39
12 11 10 9 8 7 6 5 4 3 2 1 0 ppm
1.2
1.0
1.8
1.2
3.6
3.9
1.2
1.8
1.2
8.9
173.3
170.4
167.5
166.8
154.3
150.0
136.4
134.0
124.4
117.4
115.7
79.5
50.8
49.3
43.4
31.4
28.5
22.5
200 190 180 170 160 150 140 130 120 110 100 90 80 70 60 50 40 30 20 10 0 ppm

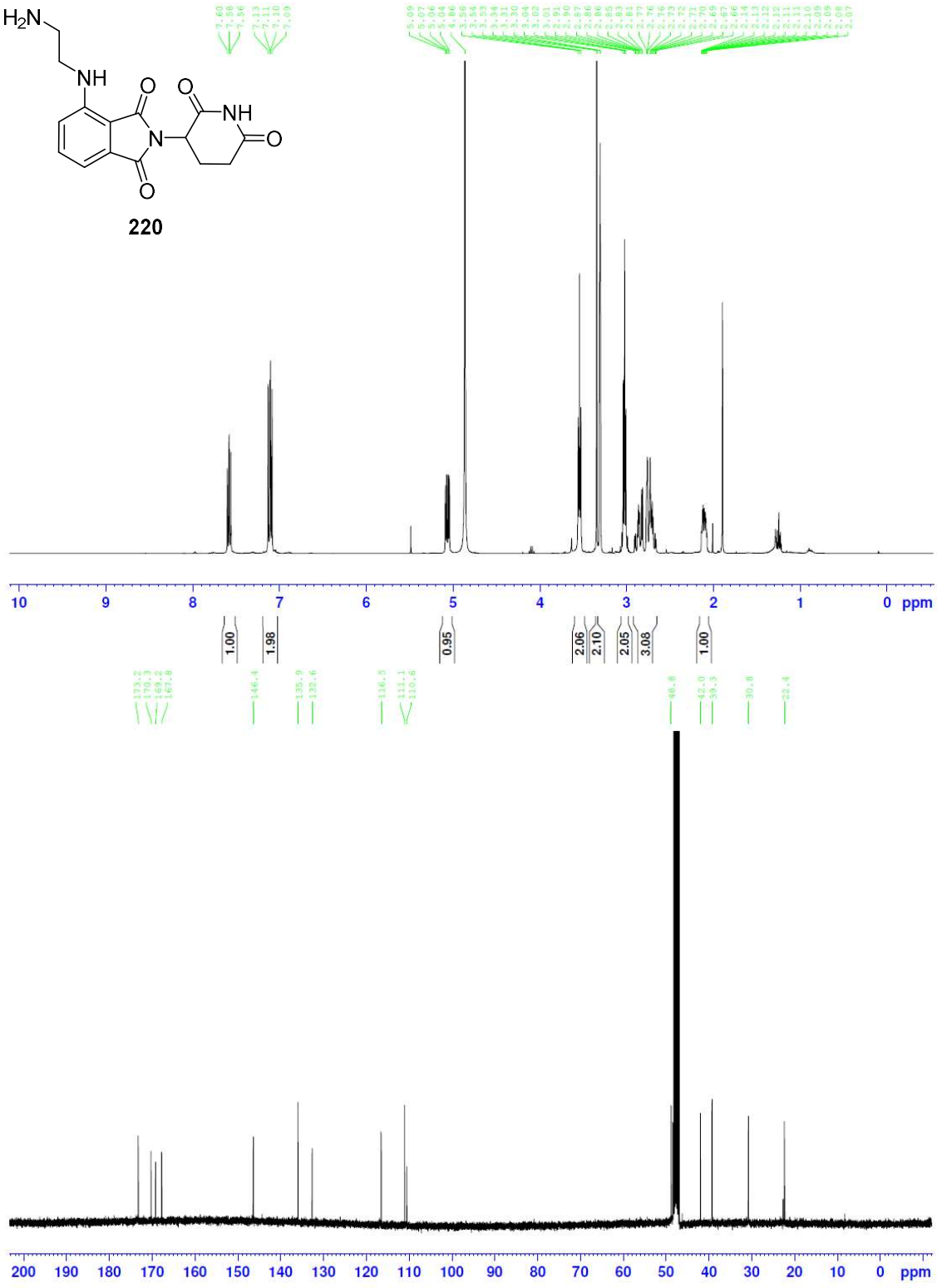
H2N
NH
O
O
NH
N
O
O
O
220
10 9 8 7 6 5 4 3 2 1 0 ppm
1.00 1.98 0.95 2.06 2.10 2.05 3.08 1.00
200 190 180 170 160 150 140 130 120 110 100 90 80 70 60 50 40 30 20 10 0 ppm

7.2. Publication List

Toolbox of Diverse Linkers for Navigating the Cellular Efficacy Landscape of Stapled Peptides, Wu Y, Kaur A, Fowler B, Wiedmann MM, Young R, Galloway WRJD, Olsen L, Sore HF, Chattopadhyay A, Kwan TT-L, Xu W, Walsh SJ, de Andrade P, Janecek M, Arumugam S, Itzhaki LS, Lau YH, Spring DR. *ACS Chem. Biol.*, 2019, **14**, 3, 526-533 DOI: 10.1021/acschembio.9b00063

Targeted covalent inhibitors of MDM2 using electrophile-bearing stapled peptides, Charoenpattarapreeda J, Tan Y, Iegre J, Walsh SJ, Fowler E, Eapen RS, Wu Y, Sore HF, Verma CS, Itzhaki L, Spring DR., *Chem. Commun.,* 2019, **55**, 7914-7917; DOI: 10.1039/C9CC04022F

Macrocyclisation and functionalisation of unprotected peptides *via* divinyltriazine cysteine stapling, Robertson N, Walsh S, Fowler E, Yoshida M, Rowe SM, Wu Y, Sore HF, Parker JS, Spring DR., *Chem. Commun.,* 2019, **55**, 9499-9502; DOI: 10.1039/C9CC05042F

Water-soluble, stable and azide-reactive strained dialkynes for biocompatible double strain-promoted click chemistry, Sharma K, Strizhak AV, Fowler E, Wang X, Xu W, Jensen CH, Wu Y, Sore HF, Lau YH, Hyvonen M, Itzhaki LS, Spring DR., *Org. Biomol. Chem.,* 2019, **17**, 8014-8018; DOI: 10.1039/C9OB01745C

Functionalized Double Strain-Promoted Stapled Peptides for Inhibiting the p53-MDM2 Interaction, Sharma K, Strizhak AV, Fowler E**,** Xu W, Chappell B, Sore HF, Galloway WRJD, Grayson MN, Lau YH, Itzhaki LS, Spring DR, *ACS Omega,* 2020, **5**, 2, 1157-1169; DOI: 10.1021/acsomega.9b03459

Diversity-Oriented Synthesis (DOS) assessment of biological space coverage and application to the *in silico* identification of novel MDM2 binders, Mervin LH, Fowler E, Kidd SL, Mateu N, Eapen RS, Sore HF, Itzhaki LS, Bender A, Spring DR, *Biorg. Med. Chem.*, 2020, submitted.